



Department of  
**Primary Industries and  
Regional Development**

# **Investigations of the potential for irrigated agriculture on the Bonaparte Plains:** hydrogeology, aquifer properties and groundwater chemistry



**Resource management technical report 425**





**Investigations of the potential for irrigated  
agriculture on the Bonaparte Plains:**  
hydrogeology, aquifer properties and groundwater  
chemistry

**Resource management technical report 425**

**Don Bennett, Paul Raper, Bob Paul, Tim Pope and Richard George**

© Western Australian Agriculture Authority ([Department of Primary Industries and Regional Development](#)) 2022

ISSN 1039-7205

Cover: Groundwater investigation site on the Bonaparte Plains



Unless otherwise indicated, 'Investigations of the potential for irrigated agriculture on the Bonaparte Plains: hydrogeology, aquifer properties and groundwater chemistry' by the Department of Primary Industries and Regional Development is licensed under a [Creative Commons Attribution 4.0 International Licence](#). This report is available at [dpird.wa.gov.au](http://dpird.wa.gov.au).

The Creative Commons licence does not apply to the State Crest or logos of organisations.

### **Recommended reference**

Bennett D, Raper GP, Paul R, Pope T and George R (2022) 'Investigations of the potential for irrigated agriculture on the Bonaparte Plains: hydrogeology, aquifer properties and groundwater chemistry', *Resource management technical report 425*, Department of Primary Industries and Regional Development, Western Australian Government.

### **Disclaimer**

The Chief Executive Officer of the Department of Primary Industries and Regional Development, and the State of Western Australia accept no liability whatsoever by reason of negligence or otherwise arising from the use or release of this information or any part of it.

Copies of this document are available in alternative formats upon request.

Department of Primary Industries and Regional Development

3 Baron-Hay Court, South Perth WA 6151

Telephone: +61 (0)8 9368 3333

Email: [enquiries@dpird.wa.gov.au](mailto:enquiries@dpird.wa.gov.au)

Website: [dpird.wa.gov.au](http://dpird.wa.gov.au)

# Contents

<b>Acknowledgements .....</b>	<b>v</b>
<b>Summary .....</b>	<b>vii</b>
<b>1 Introduction.....</b>	<b>1</b>
<b>2 Background.....</b>	<b>4</b>
2.1 Location, land use, surface water and physiography .....	4
2.2 Climate .....	8
2.3 Geology .....	10
2.4 Soils and vegetation .....	22
2.5 Groundwater sites .....	25
<b>3 Methods.....</b>	<b>27</b>
3.1 Heritage assessment for investigation works .....	27
3.2 Weather station .....	28
3.3 Groundwater inventory .....	28
3.4 Groundwater level monitoring.....	28
3.5 Bore, spring, lake and rainfall sampling .....	29
3.6 Sample analysis .....	32
3.7 Aquifer testing .....	33
3.8 Groundwater modelling .....	34
<b>4 Results .....</b>	<b>36</b>
4.1 Local climate at Bonaparte Plains .....	36
4.2 Groundwater depth, elevation, and occurrence .....	38
4.3 Groundwater level, spring discharge and lake level dynamics .....	45
4.4 Aquifer testing .....	57
4.5 Rainfall, groundwater, spring and lake water chemistry .....	59
<b>5 Discussion .....</b>	<b>70</b>
5.1 Local climate .....	70
5.2 Hydrostratigraphy .....	71
5.3 Groundwater within the Border Creek hydrostratigraphic unit.....	80
5.4 Groundwater modelling .....	90
5.5 Seawater interface .....	93
<b>6 Conclusions .....</b>	<b>95</b>



<b>Appendixes .....</b>	<b>97</b>
<b>Appendix A Seasonally wet land units adjacent to Bonaparte Plains .....</b>	<b>98</b>
<b>Appendix B Physicochemical analytes, abbreviations, LORs and methods</b>	<b>99</b>
<b>Appendix C ANSTO analysis of groundwater chemistry and isotope data..</b>	<b>104</b>
<b>Appendix D Suitability of groundwater for irrigation.....</b>	<b>145</b>
<b>Appendix E Test pumping method, results and analysis .....</b>	<b>147</b>
<b>Appendix F Water balance modelling report.....</b>	<b>172</b>
<b>Appendix G Irrigation development scenario models .....</b>	<b>255</b>
<b>Appendix H Monthly average climate data from Bonaparte climate station</b>	<b>274</b>
<b>Appendix I Locations of permanent groundwater discharge .....</b>	<b>275</b>
<b>Appendix J Groundwater, spring, lake and rainwater physicochemistry ....</b>	<b>277</b>
<b>Appendix K Hydrostratigraphic cross-sections .....</b>	<b>288</b>
<b>Appendix L Pumping cost assumptions.....</b>	<b>290</b>
<b>Shortened forms.....</b>	<b>291</b>
<b>References .....</b>	<b>293</b>

## Acknowledgements

This work by the Department of Primary Industries and Regional Development (DPIRD) was supported by the Bonaparte Plains Water for Food project.

Thank you to the senior men and women – Button Jones, Ronnie Carlton, Julie Bilminga, Kathleen Carlton and Eileen Huddleston (representing the traditional owners of the area) – for taking part in the heritage clearance surveys and providing us with their valued local knowledge of the area. Thank you also to Dominique Reeves and staff from the Yawoorroong Miriuwung Gajerrong Yirrgeb Noong Dawang Aboriginal Corporation (MG Corporation) and consultant anthropologists Kim Doohan and Joh Bornman for their management of the heritage clearance process.

Carlton Hill Station's manager, Glen Brooker, and his staff also provided valuable local knowledge and access to the area.

We acknowledge Karina Meredith and staff from the Australian Nuclear Science and Technology Organisation for their analysis of the groundwater hydrogeochemical and isotopic results and reporting their findings on the recharge and groundwater flow processes.

Thanks to Nicki Harrington (Innovative Groundwater Solutions) for her efforts in building the water balance model. During the modelling process, Nicki and Glenn Harrington were enthusiastic participants in discussions that improved their and our understanding of the groundwater system, and we thank them for this.

Jamie Bowyer, DPIRD's project manager, provided a rational and calming influence during negotiations with funding representatives.

DPIRD staff at the Frank Wise Institute of Tropical Agriculture – Noel Wilson, Mark Warmington, Gerard Morgan, Shayne Cullimore and Lorraine Hartle – provided guidance, logistical assistance and technical support. Russell Speed and Adele Killen collected downhole EM39 and gamma data from some drill holes.

Staff at Geoscience Australia provided the airborne electromagnetic (AEM) survey results and initial advice on AEM interpretation.

We gratefully extend our appreciation to Russell Speed and Penny Wallace-Bell for technical review and to Rhonda Bracey (Cybertext Consulting Pty Ltd) and Angela Rogerson for final edits.





## Summary

‘Cockatoo Sands’ is a common name for the Cockatoo Sands family of soils (comprising red to yellowish-red sands, sandy earths, and loamy earths) that have formed from quartz sandstone colluviums in relatively isolated patches throughout the East Kimberley region of Western Australia and the Northern Territory. Cockatoo Sands are recognised as potentially suitable for irrigated agriculture because they are generally well drained and not subject to waterlogging or inundation. These characteristics allow them to be cultivated and prepared for planting various crops during the wet and dry seasons of northern Australia.

Expanding agricultural production onto the Cockatoo Sands around Kununurra will increase opportunities by increasing the overall scale of agriculture, allowing year-round agricultural enterprise, and new crops and market opportunities.

In 2016, about 8,000 ha of suitable Cockatoo Sands soils were assessed close to Kununurra and the Ord River Irrigation Area. A further 34,947 ha of suitable Cockatoo Sands soils were identified on the Bonaparte Plains in 2019. However, because the Bonaparte Plains area is 50–100 km from the Ord River, irrigation water for any development here would need to come from groundwater or other water sources nearby.

This report describes the method, data, and analyses used to determine the hydrogeological and groundwater physicochemical conditions of the Bonaparte Plains area, in relation to the potential for irrigated agriculture development on the suitable Cockatoo Sands. Climate, watertable depth, shallow watertable extent, watertable dynamics, aquifer physical properties, groundwater chemistry and water balance data are reported in the context of the opportunities, potential hazards and generic risks to land and water resource conditions that may arise following irrigated agriculture development.

Underlying the Cockatoo Sands, the Point Spring Sandstone Formation aquifer is extensive and contains high quality groundwater. However, compared to the area of suitable soils, the aquifer has limited potential to provide a sustainable supply of groundwater for irrigation. Preliminary water balance modelling indicated that the net outflow to the ocean is 4.4 GL/y. This means that at the likely maximum allocation (50% of net outflow), the supply available for irrigation could be only 2.2 GL/y, equivalent to 150–300 ha of irrigation at application of 750–1,500 mm/y.

Scenario modelling forecast that suitable locations for irrigation were limited by the need to minimise depth to groundwater for economic reasons and the potential pumping could induce aquifer drawdowns that can extend to the wetlands fringing the Cockatoo Sands. Scenario modelling forecast that annual wet season cropping on Cockatoo Sands located above irrigation areas could reduce the extent of the aquifer drawdown by supplying additional recharge. The modelled application of this system was shown to minimise the potential head reduction impacts on wetlands at most of the locations modelled.

However, we stress that the investigation and modelling was not of a suitable scale and complexity as to be suitable for water allocation planning, support of a water

licence application, or for the detailed planning of pumping optimisation that will need to be undertaken by proponents of specific developments.

Generally, there is a low on-site risk of land and water resource degradation associated with irrigated agriculture development on Cockatoo Sands.

However, groundwater extraction for irrigation could pose site-specific off-site risks to the permanent wetlands and springs, which are biologically diverse and culturally significant. These off-site risks, which include eutrophication and reduction of the volume of groundwater discharge, could be mitigated by careful location of the development areas and the siting and design of any production bore fields. The modelled application of areas of dryland agriculture, to increase recharge above irrigated areas, was shown to minimise the potential head reduction impacts on wetlands at most locations modelled.

In addition, uncertainty remains regarding the location of the seawater interface. Therefore, the risks associated with seawater intrusion remain poorly defined.

Potential developers and environmental regulators can use the data reported here, in combination with the land capability report (Smolinski 2019), as a basis for further investigations of enterprise-specific opportunities and risks, and for developing specific management plans.

## 1 Introduction

Expanding irrigated agriculture within the state is a priority for the Western Australian Government, which has the goal of doubling food supply production for local consumption and export by 2025. The *Implementing Bonaparte Plains* project is the second stage of the Cockatoo Sands investigations (stage one in 2016 investigated the Victoria Highway and Carlton Hill areas of Cockatoo Sands near Kununurra). ‘Cockatoo Sands’ is a common name for the Cockatoo Sands family of soils comprising red, sandy soils of the East Kimberley (Western Australia [WA]) and Northern Territory (NT). The *Implementing Bonaparte Plains* project assessed land, water, and risk when investigating the potential for developing irrigated agriculture on the loamy sands (Cockatoo Sands) of the East Kimberley. Developing these areas with irrigated agriculture could potentially double the area of land suitable for production within 50–100 km of the Ord River Irrigation Area (Figure 1.1).

The need for scale is the biggest factor in providing investment opportunities to make northern Australia a resilient and productive agricultural region (Department of Regional Development and Lands 2009). Importantly, Cockatoo Sands are free-draining loamy soils that have the potential to support crops in both wet and dry seasons. During stage one, baseline conditions, irrigation suitability, and prefeasibility engineering and power requirements were assessed for about 8,000 ha of suitable Cockatoo Sands soils (Bennett et al. 2015; Bennett et al. 2016; Smolinski et al. 2015). DPIRD is working with local industry and the Yawoorroong Miriuwung Gajerrong Yirrgeb Noong Dawang Aboriginal Corporation (MG Corporation) to enable development of the Victoria Highway and Carlton Hill areas of Cockatoo Sands near Kununurra (Figure 1.1).

In 2010, an additional area of about 30,000 ha of Cockatoo Sands was identified during a broad reconnaissance soil survey on the Bonaparte Plains, north of Kununurra (Smolinski et al. 2010). This area is the focus for this second stage project. A more detailed soil survey has since been completed (Smolinski 2019) confirming the scale and suitability for irrigated agriculture of 34,947 ha of Cockatoo Sands in the Bonaparte Plains area.

However, because of the Bonaparte Plains’ landform and distance from the Ord River Dam, irrigation water for any development here would need to come from groundwater or other nearby water sources. Therefore, an important component of the *Implementing Bonaparte Plains* project was to undertake investigative drilling and to install monitoring and test pumping bores to help determine the potential for groundwater supply and to assess development risks in the area.

We commenced investigations in 2013 with desktop review and field reconnaissance of existing bores, mineral exploration drilling, outcrop geology and groundwater outcrop. Nested piezometers and a pumping test bore were then constructed and tested at one site in the approximate centre of the Bonaparte Plains area of Cockatoo Sands. The results from the initial review, drilling and pumping test indicated that additional investigations were warranted.

During 2015 and 2016, we undertook a more intensive census on existing operating and abandoned bores and installed 2 shallow monitoring bores and a climate station. An airborne electromagnetic (AEM) survey (SkyTEM312 system) of the area was



completed in December 2015, with interpretation products of an initial AEM data inversion provided by Geoscience Australia in March 2016 (Symington et al. 2016).

Using the information from the above investigations and guided by the location of conservation reserves and heritage information provided by traditional owners, we installed monitoring bores at 7 additional sites and pumping test bores at 2 sites in 2017. Bennett (2019) reports the results of the drilling programs undertaken in 2013, 2016 and 2017.

This report summarises the results of our investigations, including groundwater level monitoring, groundwater spring monitoring, geochemical and isotopic sampling and analysis, test pumping and water balance modelling activities, as they relate to information about available groundwater resources and risks associated with agricultural development on the Bonaparte Plains.

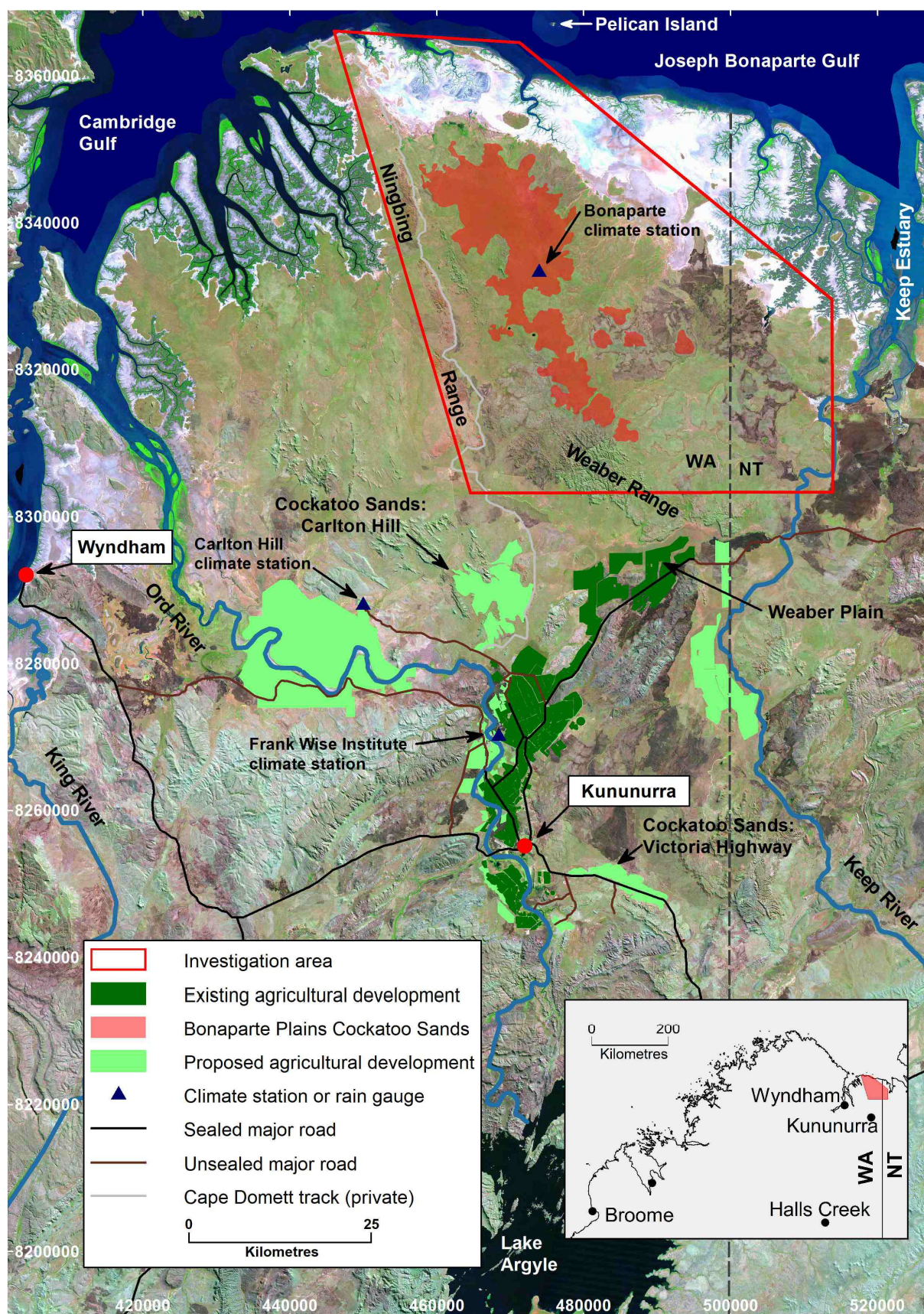


Figure 1.1: Major geographical features and existing and proposed agricultural developments near the Bonaparte Plains project area



## 2 Background

### 2.1 Location, land use, surface water and physiography

The Bonaparte Plains investigation area is in the north-east Kimberley region of WA, about 2,300 km north of Perth. It covers the central part of a peninsula that extends northwards into the Joseph Bonaparte Gulf, bordered by the Keep River and Keep River Estuary to the east, the limestone Ningbing Range and the Cambridge Gulf to the west, and the sandstone Weaber Range to the south (Figure 1.1).

The investigation area is about 2,600 km<sup>2</sup> and its centre is about 80 km north of Kununurra, the closest town. It is within the Carlton Hill Station pastoral lease, currently used for rangeland cattle grazing. For groundwater allocation purposes, the area lies within the extensive Canning–Kimberley groundwater area.

Extensive conservation reserves cover the Weaber Range to the south and the Ningbing Range to the west and other areas. Figure 2.1 shows the amalgamated outline of the numerous and extensive Aboriginal heritage listed areas that cover and surround the conservation reserves (Aboriginal Heritage Inquiry System 2021). Some of the listed heritage areas – such as those surrounding 2 intermittent lakes near the centre of the investigation area – have the highest classification of heritage protection and should not be visited without prior permission from the traditional owners.

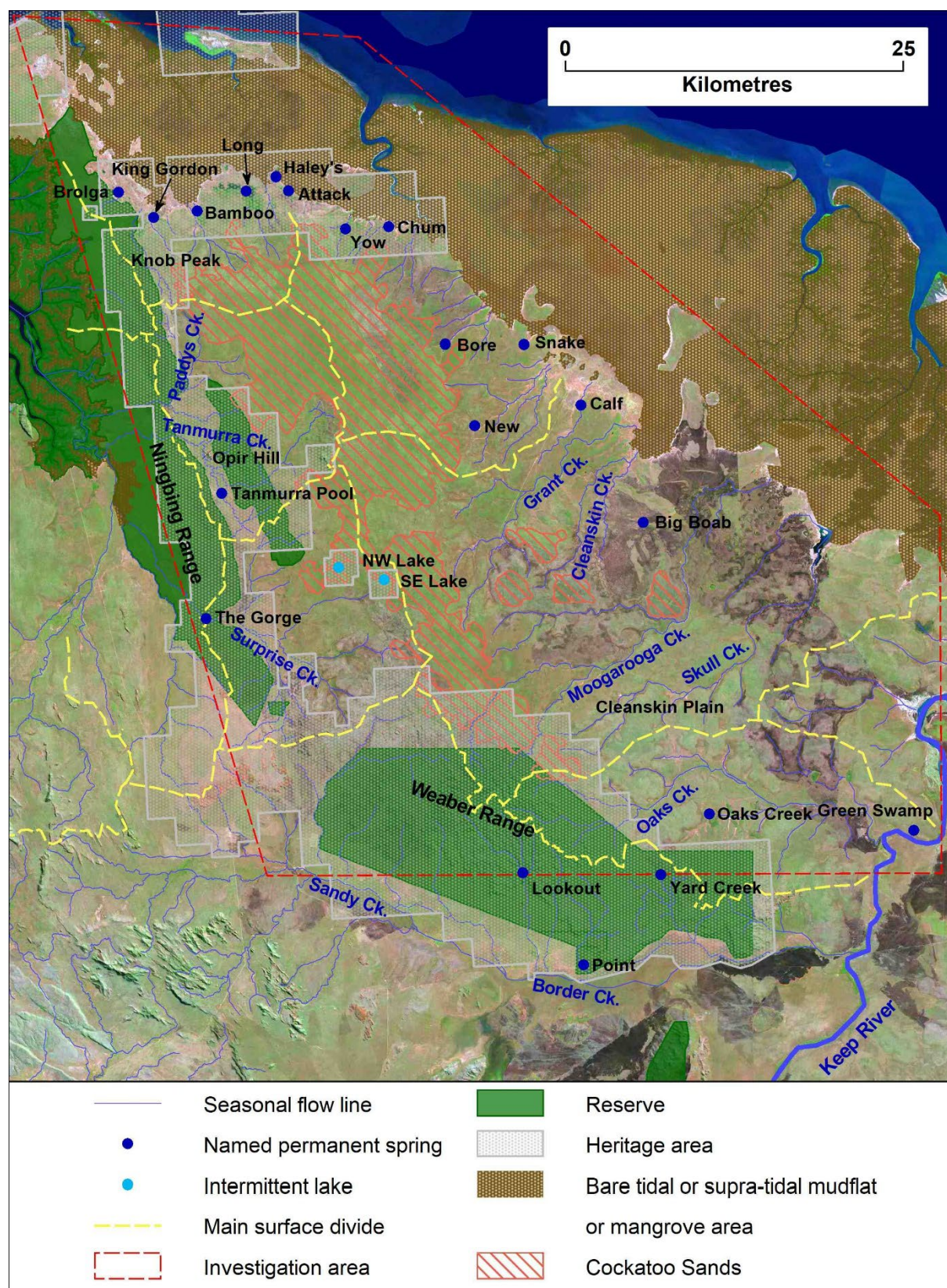
To the north, a large area of Aboriginal heritage also encompasses several large permanent groundwater springs located along the northern tidal mudflat margin.

The organic mound springs (Brolga, King Gordon, Attack and Long springs; Figure 2.1) are recorded as *Priority 1 Ecological Communities* in the Victoria–Bonaparte Bioregion, East Kimberley (DBCA 2021). Following vegetation and fauna surveys in 2017, the Department of Biodiversity, Conservation and Attractions recommended that a full nomination be presented to the *Western Australia Threatened Species Ecological Communities Scientific Committee* for formal assessment (DBCA 2020).

South-east of the central area of Cockatoo Sands lies the Cleanskin Plain, an extensive area of plains and broader drainage floors that continue to mudflats that extend to the mouth of the Keep River in the NT. Much of this area is seasonally wet (Schoknecht et al. 2004).

Tidal mudflats, as wide as 20 km, lie between the Bonaparte Plains and the ocean (Figure 2.1 and Figure 2.2). Although the mudflats support mangrove forest near the coast, plus samphire and some grasses on the plains, they are mainly bare. Level plains of loamy sands occur just above the mudflats or occasionally as islands on them. A low iron-stained ramp, 2–3 m high, often fringes the mudflat interface, indicating passive groundwater discharge over prolonged periods. Within the vegetated flats adjacent to the mudflats, some isolated small areas, which have localised internal drainage, are degrading naturally due to evaporated salt concentrations.





Sources: Carlton Hill Station map; Smolinski (2019); Payne and Schoknecht (2011); Landgate WA; Aboriginal Heritage Inquiry System (2021)

Figure 2.1: Location of named groundwater springs, seasonal creeklines, intermittent lakes, mudflat areas and the Cockatoo Sands in relation to the investigation area, reserves and listed Aboriginal heritage areas

West of the central area of Cockatoo Sands, the landscape dips gently westward to a north–south oriented, elongated depression (Figure 2.2). Geological mapping by Mory and Beere (1988) show that Milligans Formation (plus other shale formations of the Weaber Group) outcrops or subcrops along this feature. Steep, rocky sandstone scarps on the eastern side, and the craggy limestone Ningbing Range on the western side, bound most of this feature. Deeply incised north–south aligned surface drainages that capture headwater creeks from the east and west run along the depression before draining through gaps in the Ningbing Range and then across level or undulating plains and drainage floors on alluvium to the west. South of the Cockatoo Sands are the northern slopes of the well-consolidated sandstones of the Weaber Range.

Figure 2.1 shows an unusual feature of the Cockatoo Sands – no creeks start within it or pass through it. Instead, they start in either adjacent lower-lying areas, areas of sandstone outcrop or on limestone outcrop. Mory and Beere (1988, p155) also noted that sandplains in the area ‘often show a poorly developed internal drainage system’.

To the north and east most of the seasonally flowing creeks spill their water onto the mudflats. Creeks on the west side of the Cockatoo Sands initially flow to the west and are then captured by the north–south trending creeks that eventually drain westwards along Surprise, Tanmurra and Paddys creeks that flow through the 3 gaps in the Ningbing Range. To the south-east, Oaks Creek captures run-off from the north-eastern slopes of the Weaber Range, plus the adjacent seasonally wet plains, eventually discharging into the tidally influenced lower reaches of the Keep River (Bennett and George 2014). Southern-flowing creeks capture most of the run-off generated from the Weaber Range; this run-off is then captured by Border Creek, eventually discharging into the tidally influenced lower Keep River.

Two small, intermittent lakes are located high in the landscape on the south-western flank of the central area of Cockatoo Sands (Figure 2.1 and Figure 2.2).

Figure 2.2 shows the elevations across the investigation area. Areas of greatest elevation and slope correspond to areas of well-consolidated Point Spring Sandstone outcrop on the Weaber Range and along sections of the western margin of the Cockatoo Sands, plus the hard limestone rock of the Ningbing Range.

Surface elevations reach 240 mAHD on the Weaber Range and 120 mAHD on the sandstone ranges to the west and on the Ningbing Range.

The main area of Cockatoo Sands encompasses a gentle north–south trending ridge on which surface elevation reaches 120 mAHD in one area (Figure 2.2). However, the Cockatoo Sands occur mostly on undulating plain that has a ground surface between 40 mAHD and 100 mAHD. Slopes are generally 0–2%, although in some areas, usually bordering rock outcrop, slopes exceed 3% (Smolinski 2019).

The expansive plains and broad drainage floors of the Cleanskin Plain east of the central area of Cockatoo Sands have an elevation between about 10 mAHD and 40 mAHD. Localised ridges of sand occur frequently in this area and are elevated by up to about 20 m above the adjacent drainage swales. A veneer of Cockatoo Sands caps 4 of the ridges (Figure 2.2).



The elevation of the mudflats is about 3 mAHd, although it can vary between 0 and 5 mAHd.

Access to the general area is via the Cape Domett track, which is privately owned; permission must be obtained from Carlton Hill Station before travelling along it.

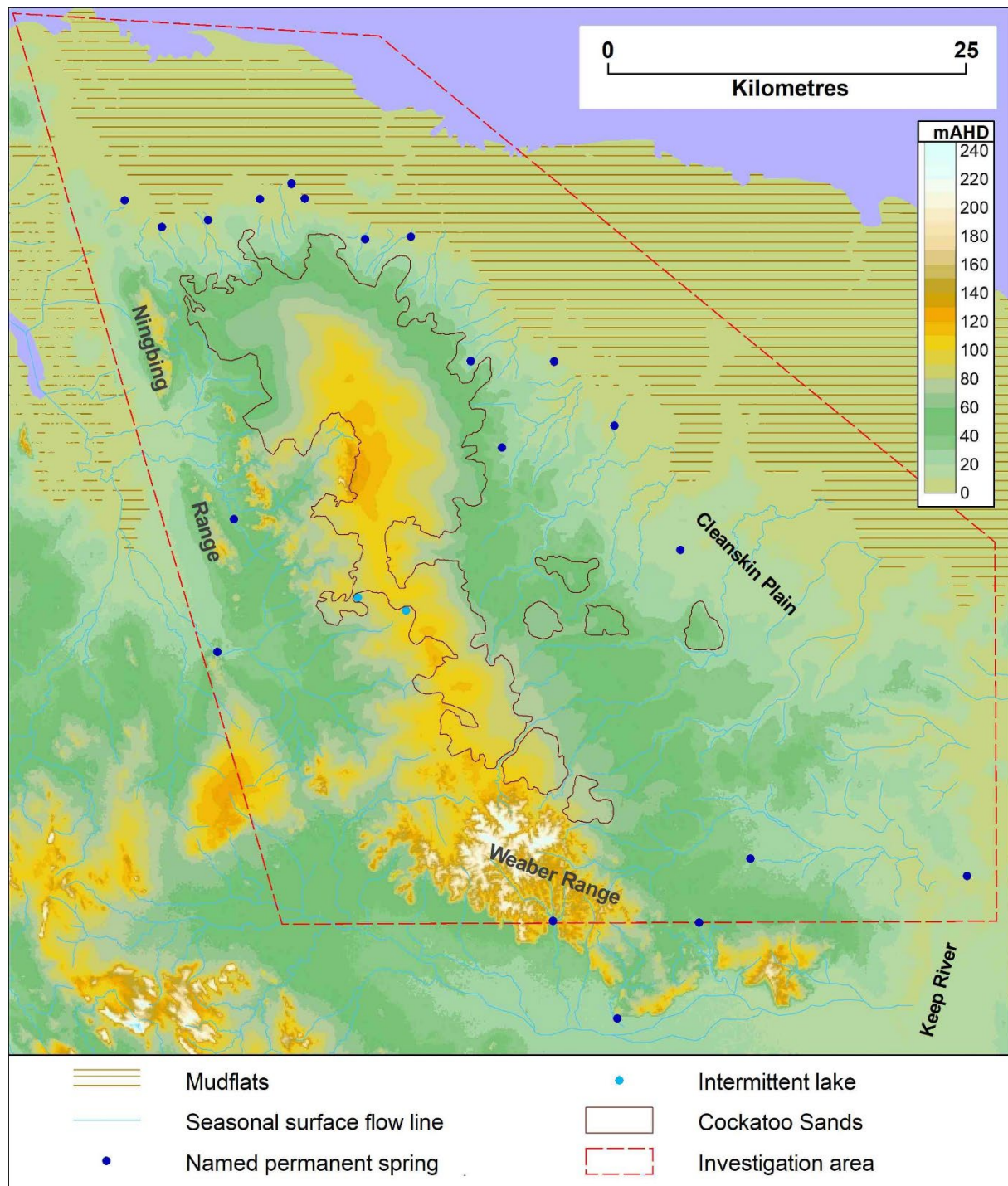


Figure 2.2: Land surface elevation

## 2.2 Climate

The climate around Kununurra is semi-arid, dry tropics. Rainfall is highly seasonal with about 90% of the annual total usually falling between November and March. The highest temperatures and accompanying highest rates of evaporation typically occur between September and December.

The closest climate stations to the Bonaparte Plains are at Frank Wise Institute (FWI) and Carlton Hill (Figure 1.1). Carlton Hill has recorded daily rainfall since 1907 and other climate variables since 1970. At FWI, daily rainfall has been recorded since 1945, with other climate variables recorded since 1965. Table 2.1 compares the mean annual rainfall for the period 1965–2018 and the mean annual pan evaporation for the period 1970–2018 for these climate stations.

Table 2.1: Mean annual rainfall and evaporation for the 2 closest climate stations to Bonaparte Plains for their coincidental periods of record

Site	Mean annual rainfall (mm)	Mean annual pan evaporation (mm)
Carlton Hill	911	2,679
Frank Wise Institute	883	2,712

Source: SILO (n.d.)

Rainfall occurs mainly between November and March, as shown in Figure 2.3. Mean monthly pan evaporation at Carlton Hill ranges from 183 mm in June and February to 296 mm in October. At FWI, pan evaporation ranges from 180 mm in February to 293 mm in October. On average, rainfall exceeds evaporation at both sites during February.

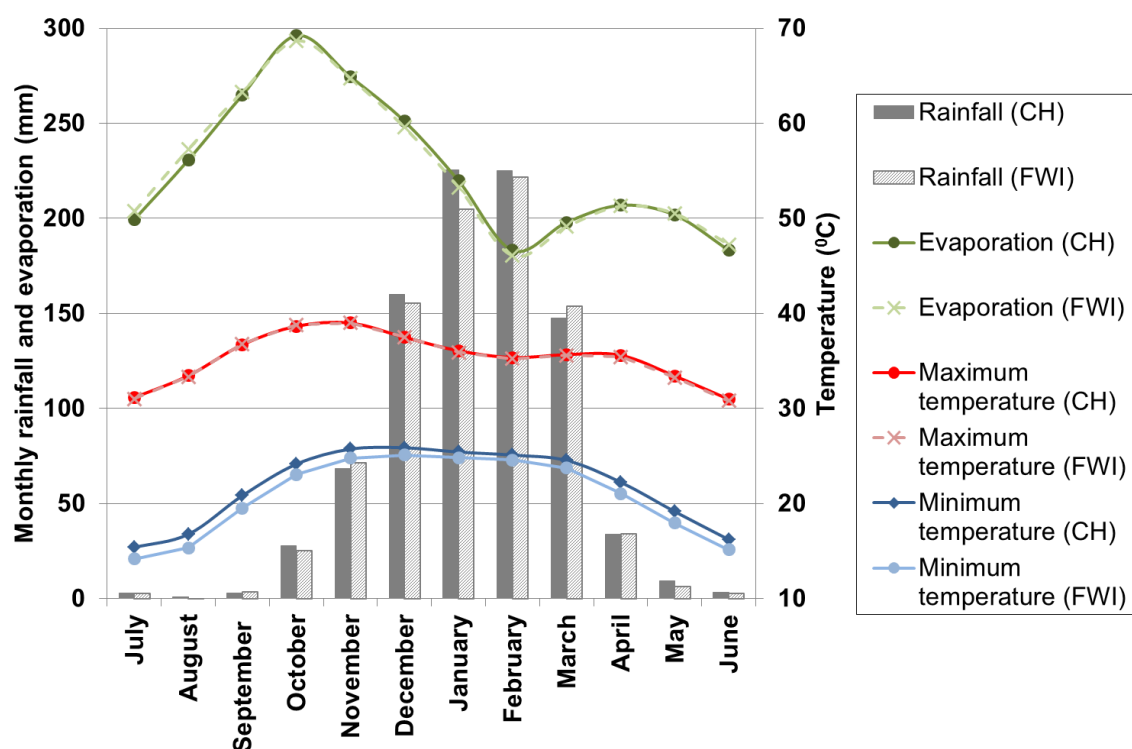
After 1993, annual rainfall at the FWI site increased, as shown by the 10-year moving average and accumulative annual residual rainfall (Figure 2.4).

Rainfall statistics for the FWI site include:

- the mean annual rainfall for 1993–2018 is 1,004 mm
- 1993–2018 was 33% wetter than 1945–1992 (99% confidence level)
- of the highest 10 rainfall years recorded since 1907, 7 occurred in the 1993–2018 period
- rainfall for the 2016–2017 year was the third highest on record (1,499 mm).

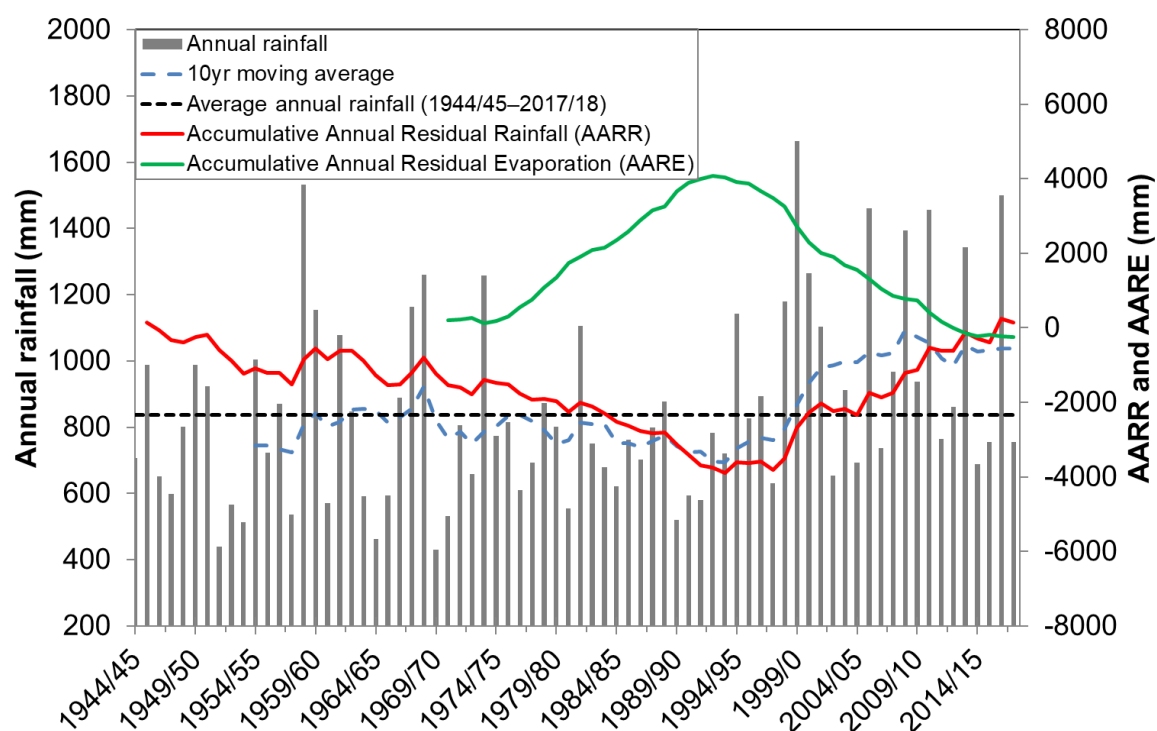
By contrast, the accumulative annual residual rainfall plot for pan evaporation shows a distinct decline in annual evaporation since 1993 (Figure 2.4). During the 1993–2018 period, the mean annual evaporation was 2,564 mm, which was 5% lower than the 1970–2018 period and 12% lower than the 1970–1992 period.

The mean monthly minimum temperature at FWI is about one degree cooler than at Carlton Hill for all months. Mean monthly maximum temperatures are similar.



Source: SILO (n.d.)

Figure 2.3: Mean monthly rainfall, pan evaporation, maximum and minimum temperatures at Carlton Hill (CH) and Frank Wise Institute (FWI)



Source: SILO (n.d.)

Figure 2.4: Total annual rainfall and evaporation (July to June) records from the FWI site

## 2.3 Geology

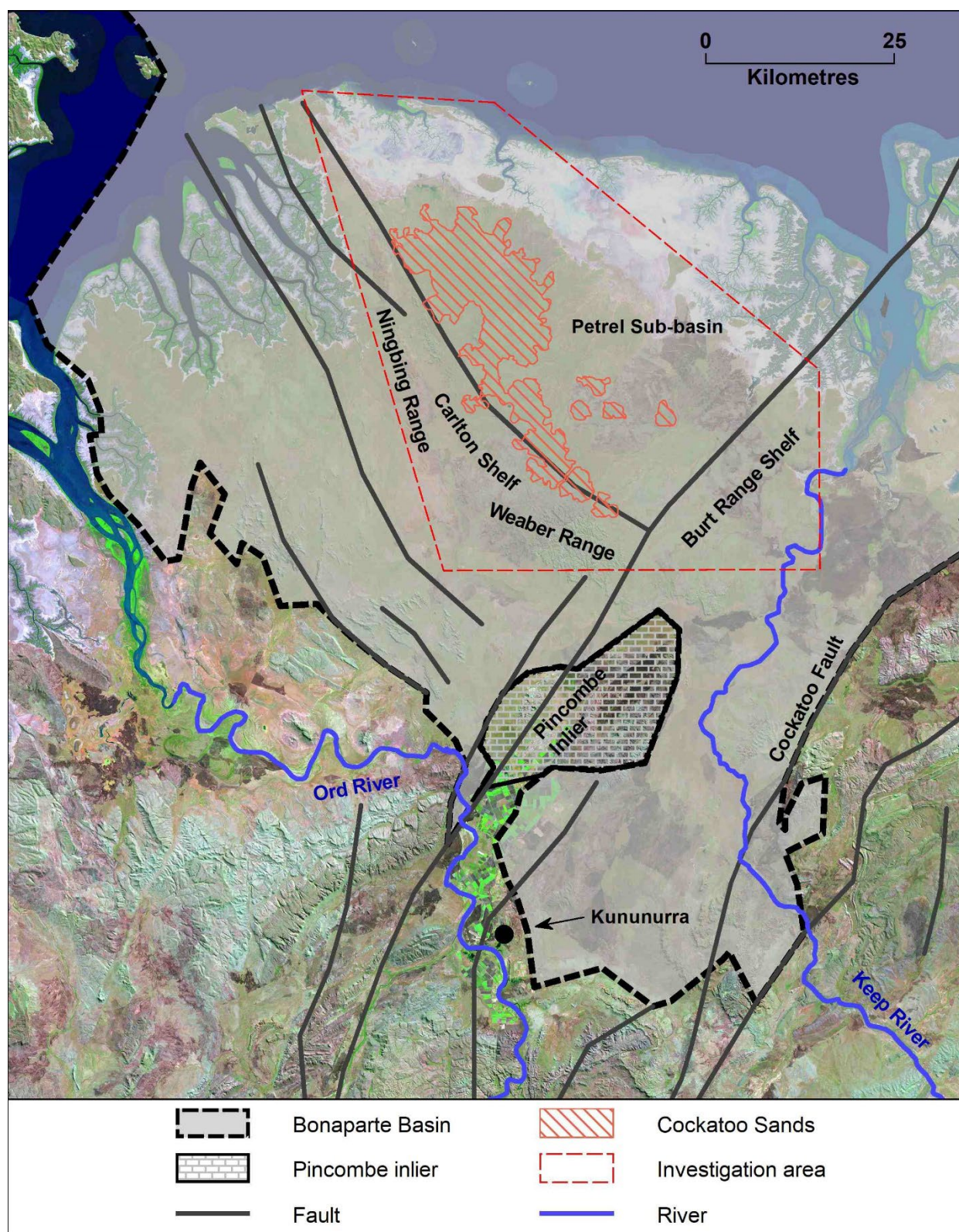
### 2.3.1 Regional setting

The investigation area sits within the 270,000 km<sup>2</sup> Bonaparte Basin, of which the onshore portion in WA covers 8,000 km<sup>2</sup>. The Bonaparte Basin contains moderate economic hydrocarbon accumulations onshore, where 2 gas flows and numerous bitumen shows are recorded (Geological Survey of Western Australia 2011). Some base metal deposits have also been discovered, such as the carbonate-hosted silver–lead–zinc deposit at Sorby Hills. Diamonds derived from the Argyle kimberlite pipe, which intrudes Proterozoic sediments south of the Ragged Range Outlier, are found in Cainozoic gravels in adjacent parts of the Bonaparte Basin.

The Bonaparte Basin contains a sedimentary succession that regionally dips to the north, with the oldest strata outcropping in the south (Mory and Beere 1988). The Carlton and Burt Range shelves and the Precambrian Pincombe Inlier occupy the southern margin. The Carlton Shelf deepens to the north-east and the Burt Range Shelf deepens to the north into the Petrel Sub-basin, which extends offshore from the approximate intersection of the Ningbing Range to the west and the Weaber Range to the south (Figure 2.5). The investigation area is mostly within the Petrel Sub-basin, which also makes up most of the onshore Bonaparte Basin and almost contains the area of Cockatoo Sands.

During the early to late Carboniferous period, the Weaber Group sediments were deposited in offshore to fluvial environments as a deltaic base-fill sequence on the Carlton and Burt Range shelves and in the Petrel Sub-basin. They unconformably overlie older faulted and folded sediments that were eroded because of uplift along the margins of the Bonaparte Basin. The Weaber Group sediments range in thickness from 600 m on the onshore shelves to 2,400 m in the offshore Petrel Sub-basin.





Source: Mory and Beere (1988)

Figure 2.5: Location of the Bonaparte Basin, its subdivisions and major faults in relation to the investigation area and Cockatoo Sands area

Broad folding of the Weaber and basal Kulshill Group sediments occurred before the glacial, continental, and shallow marine sediments of the Keep Inlet Formation (upper Kulshill Group) were deposited during the late Carboniferous and Permian periods. This occurred in response to movements along the regional Cockatoo Fault, which lies east of the Keep River and trends from the north-east to the south-west (Mory and Beere 1988).

### **2.3.2 Geology and nomenclature**

The geology within the investigation area is complex. Mory and Beere (1988) provide the most comprehensive published mapping and description of the geology for the onshore portion of the Bonaparte Basin. The following overview mainly focuses on published information relevant to the hydrogeology of the Kulshill and Weaber Group sandstones (Mory and Beere 1988) and the major underlying and overlying lithostratigraphic units within the Bonaparte Plains investigation area.

Gorter et al. (2005) reappraised Mory and Beere's stratigraphy of the Carboniferous formations of the south-eastern Bonaparte Basin using existing onshore and offshore oil well logs, seismic profiles and palaeontological information. They did not reappraise the surface geology.

Within the onshore location and to the depth of interest of our study, the most important differences between the Gorter et al. and Mory and Beere interpretations are that Gorter et al.:

- subdivided the Tanmurra Formation (194–497 m deep at Bonaparte1 oil well) into the Sunbird (new) and Tanmurra formations
- reassigned the Border Creek Member to the younger Border Creek Formation
- proposed the Kuriyippi Formation as the offshore depositional equivalent of the Border Creek Formation.

The differences in lithostratigraphic interpretations and naming conventions between the 2 reports has remained a source of uncertainty, particularly at the relatively shallow depths of our investigation, and is the subject of ongoing investigation (A Mory [Geological Survey of Western Australia], personal communication, 25 October 2018). As reported by Bennett (2019), palynological analysis of samples from recent drilling beneath the Cockatoo Sands showed that the age of the sediments, which Gorter et al. proposed to be Kuriyippi and Border Creek formations, were consistent with the original Point Spring Sandstone Formation classification of Mory and Beere (1988).

Furthermore, based on geology, Bennett (2019) speculated that the first hard rock formation that lies beneath the Cockatoo Sands area is most likely to be the Border Creek Member of the Point Spring Sandstone Formation.

In this report, we use the nomenclature of Mory and Beere (1988) to describe the Point Spring Sandstone Formation as containing the Border Creek Member. From recent palynological and lithological information gathered for the Bonaparte Plains area (Bennett 2019), we have not been able to distinguish the Sunbird Formation from the Tanmurra Formation. Therefore, we use the term Sunbird/Tanmurra Formation to describe either formation or a combination of both formations. Figure 2.6 provides a guide to compare the nomenclature proposed by the 2 groups of authors in terms of geologic age, period, formation and group.



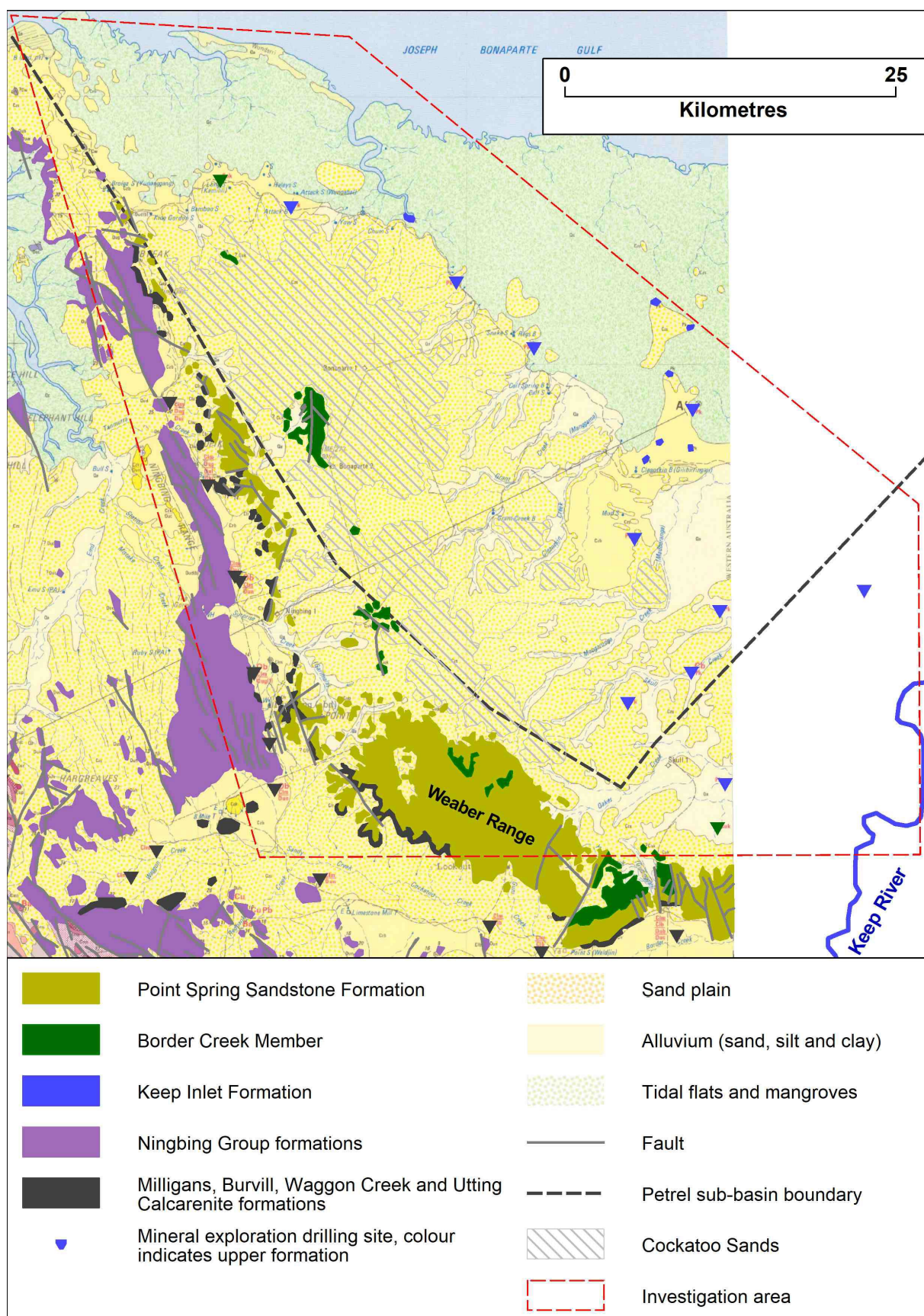
		Mory & Beere (1988)		Gorter et al. (2005)			
Ma	Period	Formation (Member)	Group	Formation	Group	Ma	
288	Permian	Keep Inlet	Kulshill	Keep Inlet	Kulshill	288	
295							295
299	Carboniferous	Keep Inlet	Kulshill	Border Creek and Kuriyippi	Kulshill	299	
307							
318		{ Border Creek	Weaber			318	
319						Point Spring Sandstone	
320				Point Spring Sandstone	Wadeye	320	
332		Tanmurra		Sunbird	Weaber	332	
333				Sandbar		333	
337		Burvill		Tanmurra		337	
339		Utting		Kingfisher Shale		339	
340		Calc. } Waggon Creek		Utting Calcarenite		340	
342				Yow Creek		342	
343		Milligans		Milligans		343	
347						347	
349		Bonaparte	Langfield		Langfield	349	
352				Bonaparte		352	
359	Devonian	Bonaparte	Ningbing		Ningbing	359	

Ma = million years before present

Figure 2.6: Generalised comparison of identified lithostratigraphic formations in the Petrel Sub-basin and Carlton Shelf

Figure 2.7 is a modified reproduction of Mory and Beere's (1988) mapping of outcrop and faulting in the area, together with the upper geological formations recognised from available mineral exploration drill holes. It shows the extensive sand plain, plus other alluvium, which blankets much of the investigation area. The Keep Inlet Formation is identified in the scattered, small areas of outcrop and as the upper formation in all drill holes within the extensive plain in the eastern half of the investigation area. Most of the Weaber Range to the south is Point Spring Sandstone Formation, along with the string of outcrop along the edge of the Petrel Sub-basin/Carlton Shelf boundary to the west. All outcrops that lie between the Point Spring Sandstone and Keep Inlet formations within the Petrel-Sub-basin are the Border Creek Member of the Point Springs Sandstone Formation.

In bedding located within the western belt and in the central part of the Weaber Range, the Point Spring Sandstone Formation has a 5–15° dip to the north-east (Mory and Beere 1988). In the eastern part of the Weaber Range the bedding dips north. Therefore, dip directions in the Point Spring Sandstone are consistently towards the Petrel Sub-basin.



Source of geology information: Mory and Beere (1988)

Figure 2.7: Outcrop geology and upper recognised formations from mineral exploration drilling programs (modified from Mory and Beere 1988)

For clarity of display, in Figure 2.7 we show an amalgamation of the many small, isolated outcrops of the Milligans, Burvill, Waggon Creek, and Utting Calcarenite formations that occur in a belt between the Ningbing Group limestones in the west and the Point Spring Sandstone Formation to the east. The Milligans Formation was identified as the uppermost hard rock stratigraphic unit in all exploration holes in this area, indicating that it is the predominant subcropping unit within the belt along this axis.

Mory and Beere (1988) also mapped faults that occur in all larger areas of outcrop. Outcrop of the Sunbird or Tanmurra Formations has not been mapped in the area.

### **2.3.3 Summary lithology**

#### **Weaber Group formations**

The shale-dominated Milligans Formation within the Weaber Group forms an impermeable boundary along the Ningbing Range to the west where it subcrops (Figure 2.7). Elsewhere onshore, the carbonaceous and sandy siltstones and sandstones of the Sunbird and Tanmurra formations may overlay the older shale units of the Weaber Group as it dips towards the north and the east.

Limestones and other carbonates of the Ningbing Group can underlie the Milligans Formation at depth and outcrop to form the Ningbing Range west of the Weaber Group subcrop.

#### **Sunbird and Tanmurra formations**

The Sunbird Formation comprises a massive, recrystallised, oolitic limestone that grades to grainstone and packstone. Locally, the matrix can also have white clay. The Sunbird Formation is thought to have been deposited in a relatively agitated shallow, probably shelfal, environment (Gorter et al. 2005).

The Tanmurra Formation comprises calcareous and dolomitic sandstone with significant calcareous re-cementation plus siltstone, shale and minor limestone. The Tanmurra Formation is thought to have been deposited as shelf carbonates, although the large clastic component observed in drill holes at current onshore locations may indicate a deltaic depositional environment.

#### **Point Spring Sandstone Formation**

The Point Spring Sandstone Formation comprises fine to coarse sandstone and pebbly sandstone with minor siltstone and shale. It is generally very well consolidated throughout the Weaber Range. Mory and Beere (1988) indicate that the Point Spring Sandstone Formation extends northwards from the Weaber Range, almost to the mudflats.

Mory and Beere (1988) identify the Border Creek Member within the Point Spring Sandstone Formation, describe its lithology and map its outcrop within the investigation area, as shown in Figure 2.7. The sandstones within the Border Creek Member are texturally similar to those of the Point Spring Sandstone Formation. However, the Border Creek Formation also contains thick sequences of conglomerate, siltstone, silty sandstone, and pebbly quartz sandstone (Mory and Beere 1988). Figure 2.8 contains photographs of typical porous sandstone, siltstone and conglomerate outcrop, taken at locations where Mory and Beere (1988) describe the outcrop as Border Creek Member.

The conglomerate comprises pebbles, cobbles and boulders of well-rounded quartzite. Bennett (2019) describes exposed remnant conglomerate beds occurring within or immediately adjacent to the area of Cockatoo Sands, and beds of pebble- to cobble-sized rounded quartzite occurring in most profiles drilled. Bennett (2019) also reported that all 8 deep locations drilled into the Point Spring Sandstone Formation had multiple layers of silty sandstone and siltstone.

A shale bed was intersected in 5 of the 8 sites drilled. This shale was identified as a layer situated at 142–152 m below ground level (mBGL) in Bennett's initial drill hole (13BP01D) and was the drilling depth target for most of the subsequent drilling for that investigation.

### **Keep Inlet Formation**

Deposited during the late Carboniferous to Permian period, the Keep Inlet Formation comprises sandstone, mudstone and shale-dominated units, plus minor conglomerate, deposited in continental, shallow marine and glaciomarine environments.

Onshore, the Keep Inlet Formation unconformably laps onto the Point Spring Sandstone Formation, thickening to up to 480 m thick at the most eastern location identified by drilling (Figure 2.7). The Keep Inlet Formation extends under the tidal mudflats to the north and east of Bonaparte Plains. Coal exploration drilling, undertaken around the inland margin of the mudflats (Williams 1982), shows that mudstone, shale, sandstone and minor coal beds make up the lithology of the upper Keep Inlet Formation. The finer-textured beds, described by Williams, likely form aquitards that cause the artesian heads in several of Williams' partially cased, abandoned drill holes along the northern mudflat margin. Coarse, friable sandstone beds within the mudstones and shales can occur at various intervals (Williams 1982, Cane 1969). Isolated zones of weakness in the aquitards, where they are relatively thin closer to the formation margin, are likely responsible for the locations of some of the permanent groundwater discharge springs that occur on the edge of the mudflats (Figure 2.7).

Variable but relatively thin Cainozoic alluvium, sandplains and coastal deposits, in turn, overlie the Keep Inlet Formation.



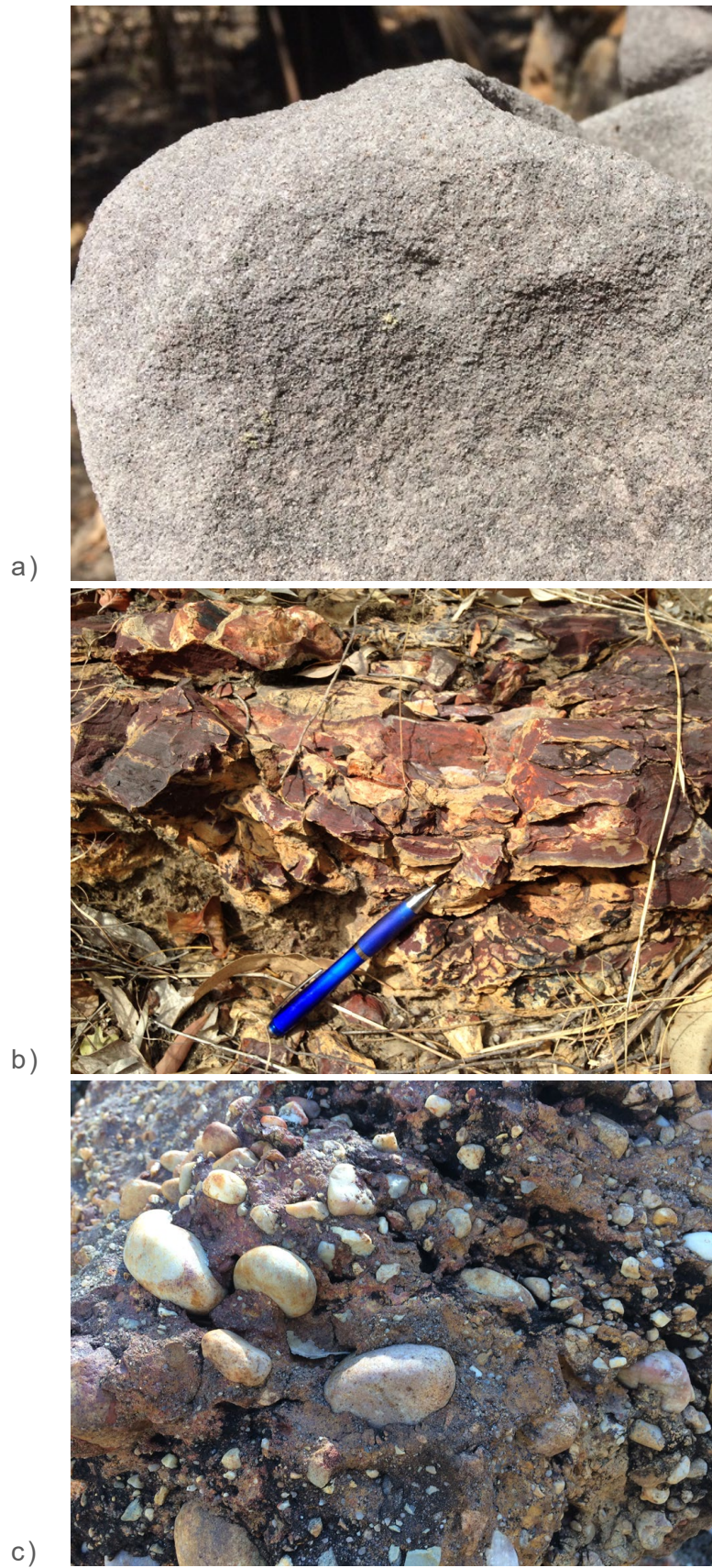


Figure 2.8: Photographs of a) sandstone; b) siltstone; and c) cobbly conglomerate beds, the major common lithological units found within Border Creek Member outcrop on the Bonaparte Plains

### 2.3.4 Airborne electromagnetic survey

An airborne electromagnetic (AEM) survey (SkyTEM312 system) was completed across much of the investigation area in December 2015. Initial interpretation products were provided by Geoscience Australia in March 2016, with a subsequent inversion completed in March 2018.

Figure 2.9 shows 3 one-dimensional AEM inversions, presented as cross-sections, located along 3 AEM flight lines (102401, 105401 and 109401). Their alignment is shown in Figure 2.10. The cross-sections show the belt of resistive Ningbing Group limestones of the Ningbing Range towards the west, and the Milligans Formation as a strong conductor east of the Ningbing Group.

The strong, near-surface conductor east of flight lines 102401 and 105401 and west of line 102401 corresponds to the mudflats. Features beneath these areas are largely masked by high near-surface conductivity.

West of the mudflats, all 3 AEM cross-sections have a weak, near-surface conductor that is contiguous with the mudflats. This feature indicates the mudstone and shale confining layers in the upper part of the Keep Inlet Formation. The other weak conductor, at about 100 m deep in the areas between the mudflats and the conductive Milligans Formation, is the shale unit described in drill holes by Bennett (2019). Discontinuities in the shale layer caused by faulting are most pronounced in flight line 105401 in Figure 2.9.

Below the shale, the next slightly conductive layer is likely to mark the Sunbird/Tanmurra Formation, but it is often poorly defined, even in the logarithmically stretched inversions shown in Figure 2.9.

Figure 2.10, in which the plan view of the area is overlain with the AEM cross-sections derived from the long flight lines, indicates the spatial extent of the AEM conductivity across the investigation area. The generally resistive (blue) central area corresponds to Point Spring Sandstone Formation and the area of Cockatoo Sands. The shale unit within this formation occurs over a relatively large area, although is absent around the margins and in the southern third. Generally, the shale appears to dip to the east. Faulting, which causes vertical offsets within the shale, is common. Offsets that are of larger magnitude than the shale thickness are visible in several locations, as are relatively short sections where the shale appears to be absent.

The very weak conductive layer of the Sunbird/Tanmurra is visible in some of the cross-sections beneath the Point Spring Sandstone Formation in Figure 2.10, although is not well differentiated by the AEM inversion in many areas.

To the west, the contact of the conductive shale-dominated Milligans Formation with the Point Spring Sandstone Formation is clearly visible, as is the increase in the contact angle from north to south.

The higher conductivity of mudstone and shale layers within the Keep Inlet Formation can be seen on-lapping the Point Spring Sandstone along its eastern flank.

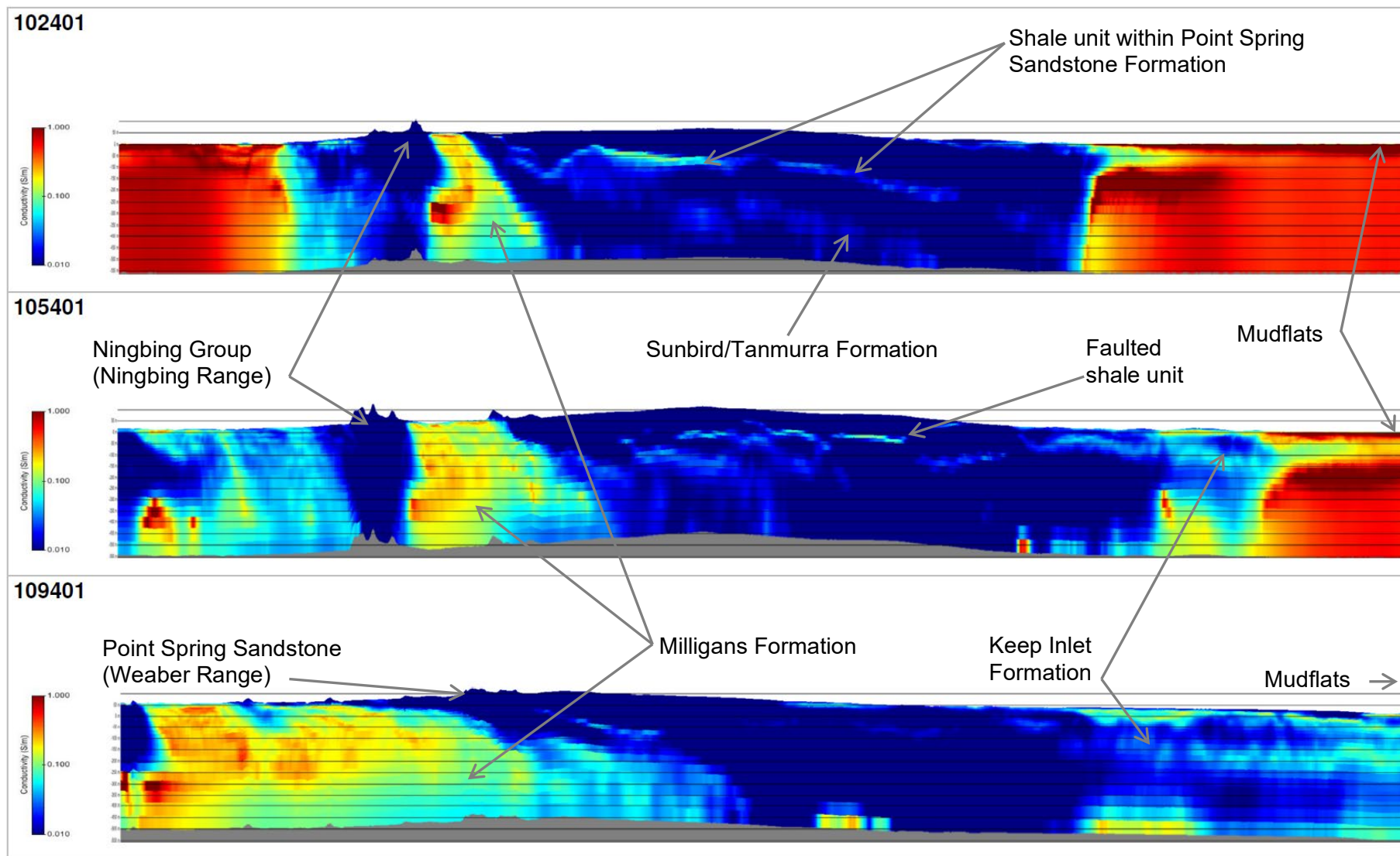


Figure 2.9: Airborne electromagnetic inversions as 550 m deep cross-sections for AEM flight lines 102401, 105401 and 109401



The high, near-surface conductivity beneath the mudflats in the north and east completely mask any deeper AEM response, making the deeper formations indistinguishable. The isolated, deep high-conductivity lobes apparent in southern cross-sections are likely to be artefacts of the inversion caused by the corresponding shallow high-conductivity areas above in the Keep Inlet Formation.

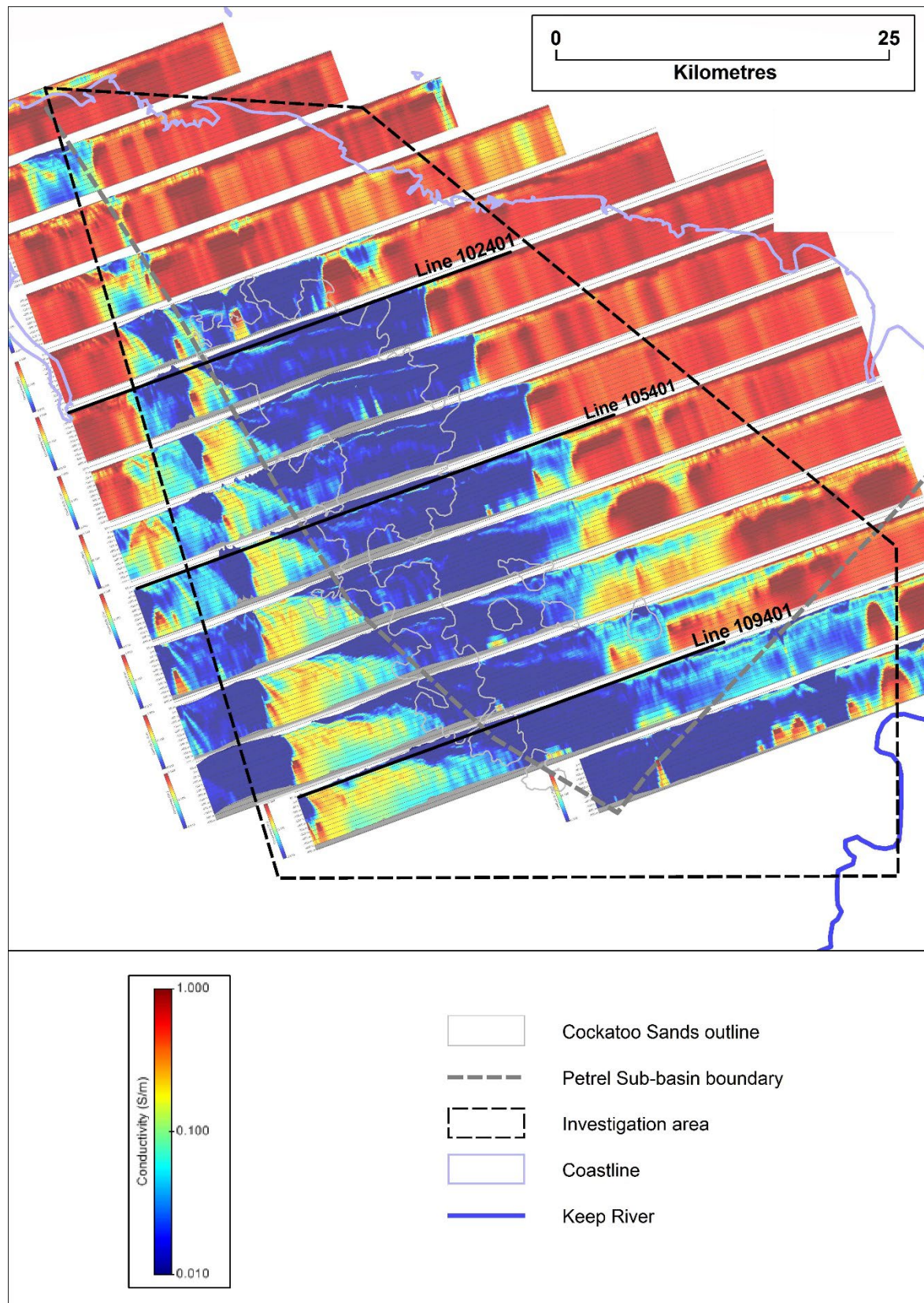
Tan et al. (2018) provides interpretations of hydrogeological features for the Bonaparte area, primarily based on the AEM inversion, plus surface nuclear magnetic resonance data that they collected. Together with the draft report, datasets of their 2- and 3-dimensional (2D and 3D) geospatial interpretations were provided to the Western Australian Government. These interpretations and data use the Gorter et al. (2005) nomenclature for formation names (see Figure 2.6).

During 3D analysis of the data provided by Tan et al., we found several major inconsistencies in the geometry for the hydrostratigraphic layers. For example, the upper and lower surfaces of the layer equivalent to the Point Spring Sandstone Formation did not align with the surfaces of the overlying or underlying formations in several key locations. We also found discrepancies between the interpreted AEM data used to construct the cross-sections and layers and borehole data.

Qualitative interpretations of recharge provided for the top 2 m of the profile was based on the AEM inversion for the top 5 m layer. These interpretations indicate that the topsoils directly overlying the Point Spring Sandstone Formation have a very high recharge potential (no units), while those overlying the Keep Inlet or Milligans formations were classified as very low and nil, respectively.

Tan et al. (2018) could not provide the anticipated 3D seawater intrusion interpretation from the AEM because the high conductivities of the mudflat surface masked the underlying conductivities in the AEM data.





Note: Each 500 m thickness cross-section image was laid flat on the map and positioned so that the ground surface in the image aligned with the position of the flight line.

Source of cross-section images: Geoscience Australia

Figure 2.10: Airborne electromagnetic survey cross-section images showing conductivity along the long flight lines of the 2015 survey

## 2.4 Soils and vegetation

### 2.4.1 Soils

Using land systems mapping by Stewart et al. (1970) as their basis, Schoknecht et al. (2004) mapped the land subsystems (land subdivisions based on landscape position, vegetation, and soils) in the Kununurra area. Payne and Schoknecht (2011) assembled revised land systems (areas of recurring patterns of landforms soils and vegetation) maps for the Kimberley region.

Within our investigation area, Schoknecht et al. (2004) identified the Cockatoo Plains land subsystem, which broadly contains the Cockatoo Sands, and adjacent subsystems. Appendix A contains a map of the seasonally wet subsystems identified by Schoknecht.

Smolinski et al. (2010) first assessed the agricultural potential of the Cockatoo Plains land subsystem during a broad reconnaissance soil survey of the Bonaparte Plains. Smolinski (2019) then undertook more intensive soils investigations on 55,000 ha of the area. Within this survey area, Smolinski (2019) identified 34,947 ha of the Cockatoo Sands family of soils, comprising Cockatoo sand normal phase and Cockatoo sand loamy phase soil map units (Figure 2.11). Smolinski (2019) classified these 2 map units as having a better than moderate-to-high capability for irrigated agriculture.

Cockatoo Sands generally have loamy sand to clayey sand topsoils that grade to compact sandy loam with depth. Subsoils grade to clay loam, sandy clay or, less commonly, to light clay. Clay content of the topsoil is within the range 4–10% and up to 36% in the subsoil. Cockatoo Sands are strongly weathered, with the clay fraction dominated by kaolin and quartz with minor haematite and goethite (Smolinski 2019). The Cockatoo Sands are likely to be colluvial sediments derived from siliceous siltstones and sandstones, or formed in situ from these sediments (Speck et al. 1964, Stewart et al. 1970, and Mory and Beere 1988: cited in Smolinski 2019).

Smolinski found that the depth to the parent rock was variable beneath the Cockatoo Sands, ranging from rarely being within 3 m to deeper than 5 m, which was the maximum depth of investigation at the 170 soil sites described. Where encountered, the parent rock often contained conglomerate that halted the penetration of the small drilling rig used (Smolinski pers comm., 25 September 2016). During a groundwater investigation Bennett (2019) found the depth to parent sandstone rock varied between 2 m and 28 m (mean 8.1 m,  $n = 9$ ). At 4 of the 9 sites where rock was encountered, Bennett (2019) classified the first parent rock encountered as conglomerate sandstone, containing pebble- to cobble-sized, hard and rounded quartzite.

The Cockatoo Sands soil profiles are well drained, highly permeable, and have very low electrical conductivity (EC) values. Smolinski (2019) also described and mapped the generally wetter Pago and Cadjeput soils, which occur downslope of, and mostly surround, the main Cockatoo Sands area (Figure 2.11).

Pago soils occur where underlying sandstone, ferruginous pans (bog iron ore), or clay layers are encountered within 3 m, or on lower positions in the landscape that receive run-on or seepage. In both scenarios, part of the subsoil becomes periodically saturated during the wet season and remains moist for a longer period than for Cockatoo Sands.

Watertables in Pago soils can be within 1 m of the surface in the wet season and remain within 2.5 m in lower slopes and depressions during dry seasons. Subsoil saturation and redox reactions result in the removal and illuviation of iron oxides and the formation of ironstone segregations and bog iron ore pans over the underlying clay or sandstone.

Cajeput soils are associated with lower slopes, flats and drainage depressions; they are highly variable in depth, soil texture and gravel content. They are invariably leached, showing pale soil horizons that remain saturated for several months during the wet season. Watertables are often within 2 m of the surface during the dry season and less than 1 m during the wet season.

#### 2.4.2 Vegetation

Most of the Cockatoo Sands vegetation is open woodland, 15–18 m tall, and has a *Eucalyptus tetradonta* (stringybark) to *E. miniata* (woolybutt) association. A layer of scattered acacia shrub (3–6 m tall), containing occasional *Erythrophleum chlorostachys* (ironwood), *Brachychiton tuberculatus* (large leaf kurrajong), and *Livistona eastonii* (fan palm), form the second stratum. Spinifex and low shrubs, particularly *Distichostemon hispidulus*, make up the understorey (Smolinski 2019).

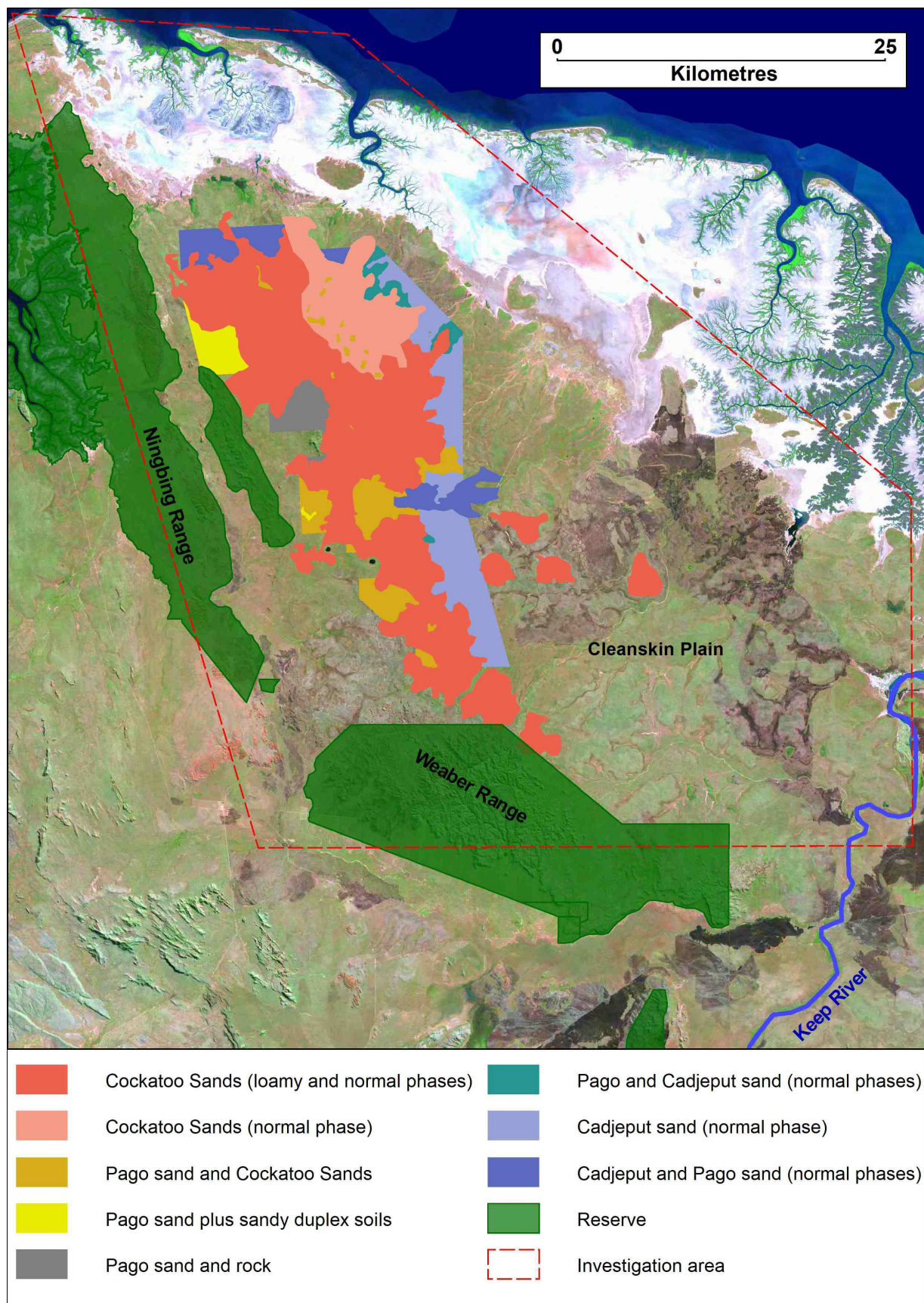
On the rocky ranges the vegetation cover is much lower and sparser, variably composed of sparse *Corymbia* spp. (stringy bark and bloodwood) and deciduous woodland, together with grasses (*Sorghum* spp. and *Triodia* spp.).

Downslope of the Cockatoo Sands, the vegetation of the transitional Pago and Cadjeput soil families and other sandy duplex soils can have a similar structure to the Cockatoo Sands (Smolinski 2019). However, the mainly *Eucalyptus tetradonta* and *Corymbia foelscheana* woodland is not as tall, can be more open, and has a denser and more diverse understory, including *Acacia* spp. (wattle) thickets and thick swards of tall grass species. The wetter areas, particularly on the Cadjeput soils, within this transition zone also usually have fewer *Eucalyptus* spp. and *Corymbia* spp., with scattered lower (less than 10 m tall) *Melaleuca* spp. often composing the dominant emergent vegetation, although these can also form dense copses. *Pandanus* spp. (pandanus palms) are also common.

The extensive plains and broad drainage floors of the Cleanskin Plain to the east support mostly short grass (*Xerochloa* spp.), patches of bluegrass (*Dichanthium* spp., *Eulalia* spp. and *Ophiuros* spp.) and scattered *Melaleuca* spp. (Payne and Schoknecht 2011).

The localised, low ridges of sand that often separate the drainage swales on the Cleanskin Plain contain sparse *Eucalyptus* spp., *Corymbia* spp. and *Acacia* spp., and often have dense, narrow belts of low *Melaleuca* spp. around their rim.





Source: Smolinski (2019)

Figure 2.11: The location of soil map units within the Cockatoo Sands family of soils plus the associated Pago, Cadjeput and duplex soils

## 2.5 Groundwater sites

Existing drilling sites (for mineral exploration, oil and gas exploration, and groundwater) are shown in Figure 2.12 (WA Department of Water 2013; NT Department of Environment Parks and Water Security 2017; WA Department of Mines, Industry Regulation and Safety 2015). Some of these sites do not have sufficiently detailed accompanying lithological and bore construction information available for the depth-interval of interest for this study. Most had no useful groundwater level or hydrogeochemical information, nor did they have information on whether they still existed as open casings or had been decommissioned after drilling or were otherwise lost or abandoned.

Additional drilling and bore installation programs were undertaken in 2013 and 2017 by DPIRD (formerly the Department of Agriculture and Food) to enable better hydrogeological data to be obtained in the Cockatoo Sands area (Bennett 2019). Drilling occurred within the mid-to-late Carboniferous Point Spring Sandstone Formation at most of the 10 sites (Figure 2.12), with drilled depths ranging from 4 to 172 m. At 6 of the sites where there was sufficient aquifer thickness, an adjacent shallow bore was installed so that piezometric pressure, isotopes and other geochemical attributes could be obtained from the top of the aquifer.

In 2018, Geoscience Australia completed drilling that targeted the deeper Sunbird/Tanmurra Formation next to 3 of the DPIRD-drilled sites (Figure 2.12). Although the lithological descriptions for these bores were not made available by Geoscience Australia at the time of writing, our later observations of the drilling cuttings remaining at the sites indicate that 2 of the sites intersected thick beds of calcareous siltstones, clays, and shales plus calcareous sandstones within the upper Sunbird/Tanmurra Formation. The third deep hole (18BP01DD) finished within the Point Springs Sandstone Formation.



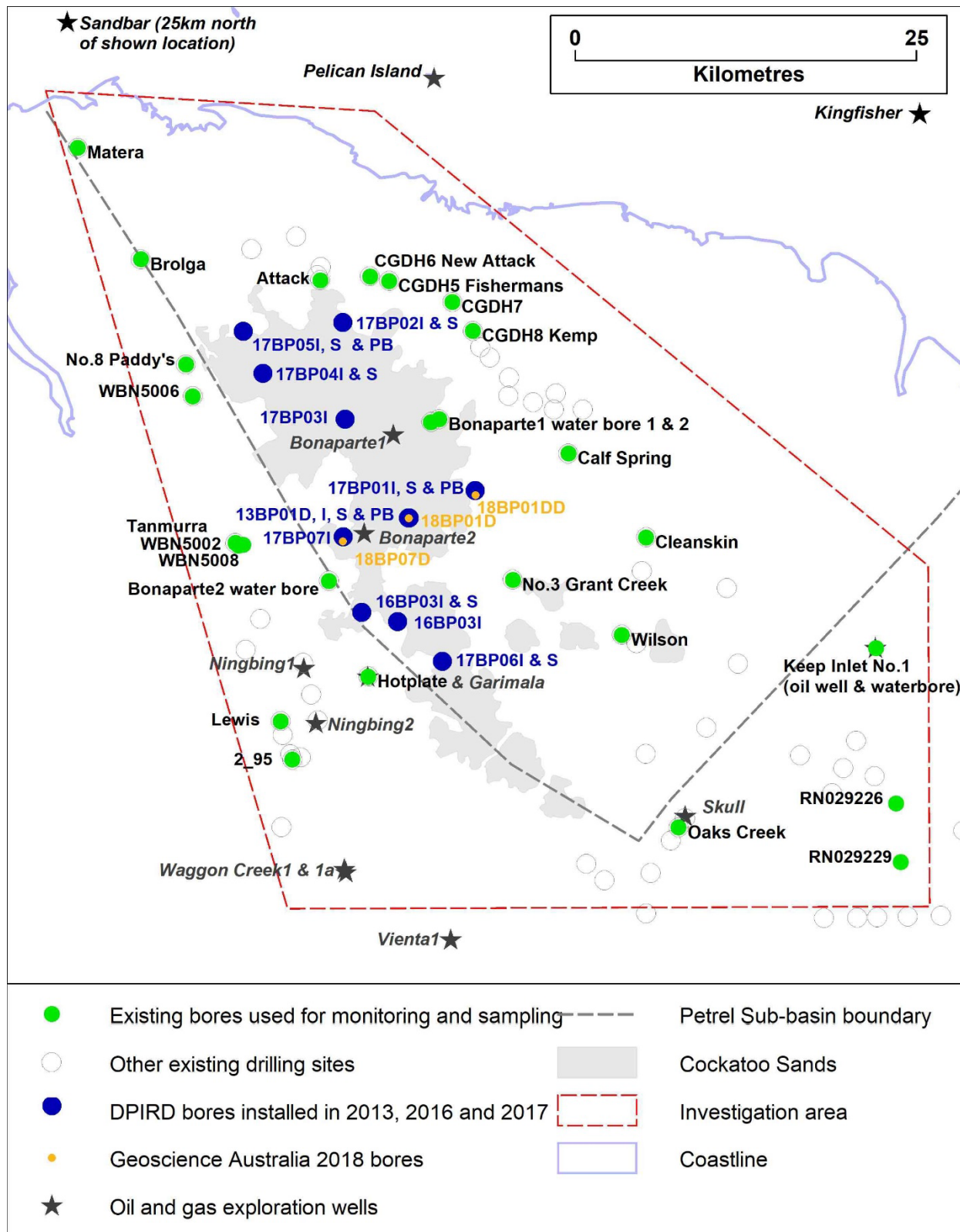


Figure 2.12: Location of DPIRD-installed bores, existing bores used for monitoring and sampling, existing other drilling and oil wells in the investigation area

## 3 Methods

### 3.1 Heritage assessment for investigation works

A site heritage assessment was undertaken on 10 April 2013 for drilling (at bore site 13BP01) and track upgrades to allow access for associated initial investigations. This was done by helicopter with Garralyel attendees Ronnie Carlton and Button Jones. A report summarising the heritage assessment indicated there were no areas of concern at the proposed work locations (MG Corporation 2013).

Ahead of the more intensive hydrogeological and soil investigations planned for 2016 and onwards, formal heritage clearance surveys were undertaken with senior representatives for the traditional owners of the area – Button Jones, Ronnie Carlton, Julie Bilminga, Kathleen Carlton and Eileen Huddleston (Figure 3.1). A heritage clearance survey report was then provided to DPIRD (Bornman and Doohan 2016), which described the culturally appropriate works and actions that we should follow during the investigations.



Figure 3.1: Participants in the Aboriginal heritage assessment surveys. From left to right: Don Bennett, Button Jones, Ronnie Carlton, Joh Bornman, Kim Doohan, Julie Bilminga, Kathleen Carlton and Eileen Huddleston

### 3.2 Weather station

In November 2015 we installed a Campbell Scientific® GRWS100 weather station in the approximate geographic centre of the Bonaparte Plains (Geocentric Datum of Australia 1994, Zone 52 coordinates: 8333255 mN and 473910 mE). The weather station is in the centre of an existing cleared 2,500 m<sup>2</sup> area within the surrounding open woodland. The unit was equipped with a Campbell Scientific® CR800 logger that recorded data at 15-minute intervals from the wind direction, wind speed, air temperature, relative humidity, soil temperature and solar radiation sensors. Two Hydrological Services® model TB3 tipping bucket rain gauges equipped with MiniLog ML-1® data loggers recorded 0.2 mm increments in rainfall, with one unit also sending rainfall data to the CR800 logger.

Potential evapotranspiration (pEt) was calculated from the relevant climatic factors recorded using Hydstra® software according to the FAO Penman-Monteith (Allen et al. 1998) method for calculating reference evapotranspiration.

### 3.3 Groundwater inventory

We undertook a bore census and groundwater inventory to prioritise the sites that were suitable for obtaining recent groundwater level and hydrogeochemical information.

In early 2013, we had undertaken a desktop review and field reconnaissance of existing bores, mineral exploration drilling, outcrop geology, groundwater outcrop and surface water within the area. However, the information was insufficient to determine if suitable groundwater resources existed beneath the Cockatoo Sands area.

During 2015 and 2016, we undertook a more intensive census on operating and abandoned bores providing water to livestock, cased mineral exploration holes and groundwater outcrops in the area. An assessment was also made of which lake, spring and existing bore sites were suitable for more detailed groundwater level observations and sampling. For the existing bores selected for monitoring and sampling that had poor bore casing and screen installation records, a submersible borehole camera connected to a depth encoder/recorder and video recorder was used to record visual information about the condition of the bore casings and to determine the inlet intervals.

### 3.4 Groundwater level monitoring

#### 3.4.1 Permanent and ephemeral springs

During site visits between 2013 and 2018, we made opportunistic visual estimates of the discharge rate of groundwater leaving the permanent spring areas, when conditions allowed. Most large springs near the mudflats had no obvious defined outflow in dry seasons. The area of the permanently damp swampy areas encompassing the springs was calculated from ortho-photographs using Geomedia® GIS software then verified or corrected using field observations. In 2017, we determined the elevations of highest occurrence of free water at each spring using real-time kinematic GPS survey methods.

Field observations during the early dry season of 2017 indicated there were significant areas of seasonal waterlogging and seepage around the margins of the Cockatoo Sands area. We used ortho-photographs and Geomedia® GIS software to map the extent of the ephemeral seepage areas.



### 3.4.2 Bores

We measured the initial groundwater level in all DPIRD-installed bores within one week of construction, then we manually measured groundwater levels twice a year until September 2018 – once in the early dry season and again in the late dry season.

Before 2016, we had opportunistically monitored suitable existing bores during site visits, and then only when conditions allowed vehicular access. From 2016, these bores were monitored at least twice a year, as for the DPIRD-installed bores.

In addition to the Insitu® non-vented data loggers installed in 2013 into the 2013-drilled DPIRD monitoring bores, similar loggers were installed in a selection of 10 existing bores in 2016 and all deep- and some shallow-drilled bores soon after drilling them in 2017. Data for barometric correction was obtained from Insitu® barometric loggers installed at 4 locations in the study area. Barometric correction was applied to the water level data using the Insitu® software. Groundwater level data were recorded at 4-hourly intervals, except for bore CGDH5 Fishermans. Because we considered that water levels in bore CGDH5 Fishermans were likely to be tidally influenced, we recorded water levels hourly to better define any tidal effects.

### 3.4.3 Groundwater elevation contours

Groundwater head elevation contours for the main aquifers within the investigation area were produced using a combination of data from:

- groundwater heads from bores observed in September 2018
- the most recent observations from other existing bores adjacent to the area
- locations of permanent or seasonal shallow groundwater discharge, identified in aerial photography and confirmed by field observation.

Site elevations were obtained using real-time kinematic GPS survey methods.

## 3.5 Bore, spring, lake and rainfall sampling

### 3.5.1 Sample collection from springs and intermittent lakes

We sampled the groundwater springs as close as possible to their source of discharge. Because most springs had a slightly dispersed source of discharge, it was not always possible to ensure that the sampled water had not been in contact with the atmosphere. Nonetheless, samples were collected from within a few metres of the point of strongest discharge to minimise the risk of atmospheric contamination.

The sample vessels were initially filled by placing them under the flowing water. A modified, hand-operated plastic vacuum pump and nylon tubing was then used to pump water from below the surface into the bottom of the sample vessel to flush it before taking the sample. The sample vessels were then capped while under water.

We obtained 2 samples – Bore Spring upper and Bore Spring lower – at the Bore Spring site. The upper site was a small, isolated spring of relatively low flow rate (about 0.1 L/s) about 100 m upslope of the more dispersed, elongated main spring area (Bore Spring lower), where the flow rate was about 30 L/s.

The general chemistry and metals samples collected from the 2 intermittent lakes comprised grab samples from about 0.5 m depth. At sample collection, elevations of the

lake water level, the lake high water mark, and the lake floor were surveyed using real-time kinematic GPS survey method.

### **3.5.2 Sample collection from bores**

All DPIRD-installed bores were developed and purged after drilling by airlifting until the water was free of sediment.

Existing station bores that were not equipped with regularly operating pumps and non-artesian cased exploration holes were purged by airlifting with a large compressor (7 cubic metres per minute of airflow) until the water was free of sediment.

We sampled the groundwater for chemical analysis within 2–6 weeks of bore development and purging. During the sampling procedure, water was first continuously pumped (or let flow in the case of artesian bores) until the field-measured water quality parameters had stabilised and a volume of water had been removed that was at least equivalent to 3 casing volumes. Once these conditions were met, we collected the water sample.

Bores that had a diameter of at least 100 mm nominal bore (NB), were pumped with a 240-volt electric, submersible, stainless steel Grundfos SQE 1-95<sup>®</sup> pump equipped with a 40 mm NB high-density polyethylene (HDPE) pipe riser extending to the surface. To ensure that the sampled water did not contact the non-inert HDPE pipe material, the riser had a 19 mm NB high-density nylon tube placed inside it so that the lower end of the nylon tube extended into the body of the stainless steel submersible pump, well past the lower end of the polyethylene pipe. The outlet of the riser, equipped with a specially designed nylon and brass fitting and valve assembly, allowed the water delivered through the nylon tube to remain isolated from the water delivered through the riser. The design allowed a single operation to purge the bore at relatively high pumping rates (0.5–1 L/s; depending on depth to water) and sample the water through the chemically inert nylon tube once the field parameters had stabilised.

Two chemically inert polytetrafluoroethylene tubes (3 mm and 9 mm NB) and a brass valve assembly were fitted to the sample-line outlet to facilitate sample collection into the various sample vessels at different flow rates without the sample having contact with the atmosphere. Figure 3.2 shows our sampling set-up in preparation for sampling groundwater from non-equipped, larger diameter bores.

Samples for dissolved inorganic radiocarbon (<sup>14</sup>C<sub>DIC</sub>), chlorofluorocarbons (CFCs comprising CFC-11, CFC-12 and CFC-113), sulfur hexafluoride (SF<sub>6</sub>), the stable isotope of oxygen (<sup>18</sup>O), deuterium (<sup>2</sup>H), and tritium (<sup>3</sup>H) were collected so that no air bubbles were introduced into the sample vessel and the sample did not contact the atmosphere during the process. We achieved this by adjusting the flow rate, putting the sample bottle in a stainless steel bucket, inserting the Teflon<sup>®</sup> tube to the bottom of the sample bottle, and filling from the bottom until the bucket filled above the level of the bottle's top. The vessel was capped underwater to prevent the sampled water from contacting the air.

Narrow (50 mm NB) bores were pumped and sampled with a plastic 12-volt electric pump (Proactive Environmental Products Mega-Monsoon<sup>®</sup>) connected to a 19 mm nylon riser tube and the flexible sample collection outlet, as described above.

At existing operating bores that were equipped with submersible pumps, we temporarily disconnected the water distribution pipes at the bore headworks. Then we inserted a 19 mm nylon tube inside the bore riser down to the pump. The samples were then collected using the flexible sample collection outlet and the procedure described above.



Figure 3.2: Pumping and sampling set-up in preparation for sampling from large diameter bores

### 3.5.3 Rainwater sample collection

We equipped one of the tipping bucket rain gauges at the Bonaparte climate station with a plastic 25 L rainfall collection drum that contained 2 L of paraffin oil to prevent evaporative loss of the collected rainwater. To reduce the volume of water collected, rainfall was collected from one side of the tipping bucket outflow, so that every second tip was directed into the sampling drum. On 5 occasions between November 2015 and June 2018, the rainwater was collected and analysed. The collection drum was emptied, and new paraffin added after each collection.

### 3.5.4 Sample handling and storage

Samples were collected into vessels, as specified or supplied by the laboratories. Water samples obtained for laboratory metal analyses were filtered, acidified and stored in acid-washed, 250 mL plastic containers, which were filled to exclude air and then kept cool (about 4 °C) in portable refrigerators. Samples for laboratory nutrient and general chemistry analyses were stored in acid-washed, 500 mL plastic bottles, filled and refrigerated until dispatched to the laboratory.

Samples collected for isotope and gas tracer analysis were also refrigerated until they were sent to GNS Science in New Zealand. Samples for analysis of:

- $^{14}\text{C}_{\text{DIC}}$  and tritium  $^3\text{H}$  were collected in new, 1,000 mL Nalgene® sample bottles
- $^2\text{H}$  and  $^{18}\text{O}$  were collected in 5 mL glass bottles
- CFCs were collected in 250 mL glass bottles supplied by GNS Science
- $\text{SF}_6$  was collected in 1,000 mL opaque glass bottles supplied by GNS Science.

Except for some rain samples and samples from bores 17BP05PB, 17BP02I, 18BP01D, 18BP01DD and 18BP07I, which we collected in 2018, all sampling was completed between August and November 2017.

### 3.6 Sample analysis

With minor exceptions, field, general and metals chemistry analyses were undertaken on all samples. Appendix B summarises the types of analysis undertaken on the various groundwater, surface water and rainfall samples collected.

Field measurements of pH, EC, temperature, dissolved oxygen, and oxidation–reduction potential were obtained from bore and spring water using a YSI Pro Plus® combination portable meter at the time the samples were collected. Field measurements of alkalinity were obtained by titration using a Hanna® HI3811 alkalinity test kit.

Laboratory analyses for general chemistry and metals were undertaken by the WA ChemCentre – a laboratory accredited by the National Association of Testing Authorities, Australia, and certified to ISO/IEC 17025:2005 standard.

Water Quality Australia (2019) recommends selecting chemical analytes based on prior knowledge of those that may pose a risk to the natural environment or, in the case of groundwater used for irrigation, a risk to potential crops. The suite of analytes we chose was comprehensive and encompassed all the stressors and metal toxicants listed in the Water Quality Australia (2019) surface water guidelines, or the ANZECC and ARMCANZ (2000) irrigation water guidelines. The list of laboratory analytes, their abbreviations, the analysis methods and the limits of reporting (LORs) are in Appendix B. Some of the LORs varied depending on the laboratory analysis method used.

Water dating analyses for  $^{14}\text{C}_{\text{DIC}}$ ,  $^2\text{H}$  and  $^{18}\text{O}$  was undertaken on groundwater samples from most bores and springs, while  $^3\text{H}$ , CFCs, and  $\text{SF}_6$  analyses were carried out on shallow groundwater and the discharge water at the source of most spring sites (Appendix B). The National Isotope Centre and Water Dating Laboratories of GNS Science in New Zealand performed these water dating analyses. The analysis methods and LORs of the isotopes and gas tracers are in Appendix B.

Of the 5 rainfall samples collected, 3 were analysed for general chemistry (Rain 2015–2016, Rain 2016–2017 and Rain 2017–2018 wet season). The Rain 2015–2016 and Rain 2016–2017 wet season samples were also analysed for metals chemistry. The Rain 2015–2016 wet season sample was collected during the entire 2015–2016 wet season (813 mm total rainfall), the Rain 2016–2017 wet season sample was collected during the November to March period of the 2016–2017 wet season (1542 mm), and the Rain 2017–2018 wet season sample was collected during the entire 2017–2018 wet

season (1,066 mm). The other 2 samples of rainfall collected but not analysed were from April to May (83 mm) and June to November (24 mm) in 2017.

### 3.6.1 Data analysis

Summary statistical analysis was performed on groundwater chemistry data using Microsoft Excel® and R Commander®. During data preparation for statistical analysis, concentrations that were below the LOR were assigned a value of half the LOR. Halving the LOR is one of the 3 suggested methods of dealing with LOR data during statistical analysis (ANZECC and ARMCANZ 2000). Alternatively, the LOR data can be excluded from the dataset, or a value equal to the LOR assigned during data analysis.

The results of the chemistry, isotope and gas tracer analyses, plus relevant details of the collection sites, were provided to the Australian Nuclear Science and Technology Organisation (ANSTO) for further analysis, modelling and reporting of the origin and rate of recharge, corrected groundwater ages and residence times spatially across the investigation area. ANSTO's method is described in their report (Meredith et al. 2018), which is included in Appendix C.

### 3.6.2 Chemical suitability of groundwater as a resource for agriculture

The suitability of the groundwater for direct irrigation was assessed by comparing it to the ANZECC and ARMCANZ (2000) irrigation guidelines. Additionally, we assessed salinity and sodium risk using the United States Department of Agriculture (USDA 1954) classification system. The relevant ANZECC and ARMCANZ (2000) guideline and USDA risk data we used are shown in Appendix D.

## 3.7 Aquifer testing

### 3.7.1 Slug tests

Slug addition and subtraction tests (Bouwer and Rice 1976) were undertaken in 2017 and 2018 on 13 selected bores screened within the Point Spring Sandstone Formation aquifer. Either a 1.5 m- or a 2 m-long slug displacement rod, constructed using 50 mm (60.02 mm outside diameter) PVC pipe filled with concrete, was used for the slug. Changes in water level during the slug tests were also recorded using Insitu® data loggers with barometric compensation applied at each site.

For bores with overdamped water level responses, the slug test data were analysed to calculate the hydraulic conductivity using a partially automated Microsoft Excel® spreadsheet that we developed to implement the calculations of Bouwer and Rice's (1976) method. For bores that have underdamped water level responses, we used a partially automated Microsoft Excel® spreadsheet developed by Butler and Garnett (2000) to implement the calculations of van der Kamp's (1976) method.



### **3.7.2 Test pumping**

Three production bores – 13BP01PB, 17BP01PB and 17BP05PB – were subjected to 3 continuous controlled pumping tests:

- a step test of three 100-minute steps for 17BP01PB and four 100-minute steps for 13BP01PB and 17BP05PB
- a constant rate test (CRT) of 48-hour duration for 17BP01PB and 17BP05PB, and 60-hour duration for 13BP01PB
- a recovery test when pumping ceased.

Each production bore had an accompanying piezometer, located at a distance equivalent to about half the thickness of the target aquifer, which were also monitored during the pumping tests. The construction of the production bores and accompanying piezometers is contained in Bennett (2019).

Appendix E contains more detail of the test pumping method and analysis.

## **3.8 Groundwater modelling**

### **3.8.1 Water balance model**

Using the results contained in this study and those from other reports, Bennett and Raper (unpublished) developed a conceptual model of the Point Spring Sandstone Formation groundwater system beneath the Bonaparte Plains. The conceptual model was used by Innovative Groundwater Solutions Pty Ltd (IGS 2019) to construct a numerical 3D, steady-state, calibrated water balance model of the Point Spring Sandstone aquifer at Bonaparte Plains. The numerical model, developed using the MODFLOW-2005 code (Harbaugh 2005) (MODFLOW) and built on a 200 m square grid, had 4 numerical layers that represented the major hydrostratigraphic units (HUs) (defined in Section 5.2). This model accounts for the evapotranspiration from the groundwater by vegetation in and surrounding the springs and wetlands fringing the Cockatoo Sands.

Further details of the method used and the calibration statistics of the water balance model are reported in IGS (2019), which is provided in Appendix F.

### **3.8.2 Seawater interface modelling**

IGS (2019) also forecast the position of the seawater interface (SWI) at 2 locations using 2D cross-section models. The cross-section models were constructed using the MODFLOW numerical model and the SEAWAT-2000 code (Langevin et al. 2008) (SEAWAT) to simulate density-dependent solute transport. The transient SEAWAT model couples MODFLOW and the solute transport code MT3DMS (Zheng and Wang 1999), iteratively calculating equivalent freshwater heads from solute concentrations provided by MT3DMS and using these in the calibrated MODFLOW model developed by IGS to simulate groundwater flow.

The IGS (2019) report (Appendix F) contains further details of the method used for the cross-section SWI models and their calibrations.



### 3.8.3 Irrigation development scenarios

A report containing the detailed methods and results for our scenario modelling of irrigation development is provided in Appendix G. In summary, we used the calibrated MODFLOW model to run hypothetical scenarios to forecast the effect on groundwater heads with abstraction for irrigation of 2.2 GL/y from the Point Spring Sandstone Formation at 11 locations. At each site, the modelled irrigation demand was 1,500 mm/y; applying the annual abstraction of 2.2 GL/y from a single bore resulted in irrigated areas of 147 ha, which were circular for ease of scenario construction.

A second round of scenarios was modelled that added areas of dryland agriculture upslope of sites 1–7 (Figure G2 in Appendix G). Semicircular dryland agriculture areas of about 1,000 ha were described immediately upslope of each irrigation area. The intention was to increase recharge to the Point Spring Sandstone aquifer and hence groundwater levels up gradient of pumping to reduce drawdowns at potentially sensitive wetlands down gradient. Dryland agriculture was not modelled above sites 8–11 as these are underlain by the low-permeability Keep Inlet Formation.

Three additional scenarios that combined irrigation sites were also modelled. The first combined sites 3 and 4 and doubled the area of upslope dryland agriculture to compensate (Figure G3 of Appendix G). In the other 2 scenarios, sites 8, 9, and 10 were combined and simulations undertaken for 2 different size areas of dryland agriculture on suitable Cockatoo Sands (Figure G3 of Appendix G).

## 4 Results

### 4.1 Local climate at Bonaparte Plains

Climate data were collected from the Bonaparte climate station from 2015 to 2018. Average monthly air temperature, soil temperature, rainfall, relative humidity, pEt, solar radiation, wind speed, and wind direction data are shown in Appendix H. The Bonaparte climate data were compared to climate data from a similar climate station operated by DPIRD at the Frank Wise Institute of Tropical Agriculture (FWI), about 15 km north-west of Kununurra (Figure 1.1).

The annual rainfall (July to June) for the 3 years at Bonaparte was 847 mm in 2015–2016, 1,696 mm in 2016–2017, and 1,091 mm in 2017–2018. Average annual rainfall was 1,212 mm for the 3-year period. On average, 205 mm/y more rainfall was recorded at Bonaparte than FWI over the same period. Average annual pEt at Bonaparte was 1,774 mm, 143 mm less than at FWI. Average monthly rainfall exceeded pEt on the Bonaparte Plains during December to March.

Average annual solar radiation at Bonaparte was 6,971 MJ/m<sup>2</sup>, which was 1,162 MJ/m<sup>2</sup> less than recorded at FWI.

Figure 4.1a shows monthly averages of total rainfall, pEt and solar radiation. Figure 4.1b and c show monthly averages of daily mean minimum and maximum air temperature and humidity recorded at Bonaparte and FWI. Higher rainfall during December to March accounts for the higher average annual rainfall at Bonaparte – this period also corresponded with a marked reduction in pEt at Bonaparte compared to FWI. Solar radiation was always lower at Bonaparte, with the largest difference during the wet season months (November to April).

Daily mean air temperature varied between 23 °C and 30 °C at Bonaparte and was about 1 °C lower than at FWI during the September to March period. Daily minimum temperature remained 1–2 °C higher throughout the year at Bonaparte (annual range 16–26 °C) compared to FWI. Daily maximum temperature (annual range 34–39 °C) was about 1 °C higher during April to August, about 1 °C lower from October to December, and similar during the other months.

Daily mean relative humidity at Bonaparte (range 53–83%) was between 4% and 13% higher than at FWI. Daily minimum relative humidity was also consistently higher (range 4–10%) at Bonaparte than FWI throughout the year, with the largest difference in the September to November period. Daily mean maximum relative humidity was similar or slightly higher at Bonaparte from September to April compared to FWI, but 5–8% lower from May to August at Bonaparte.

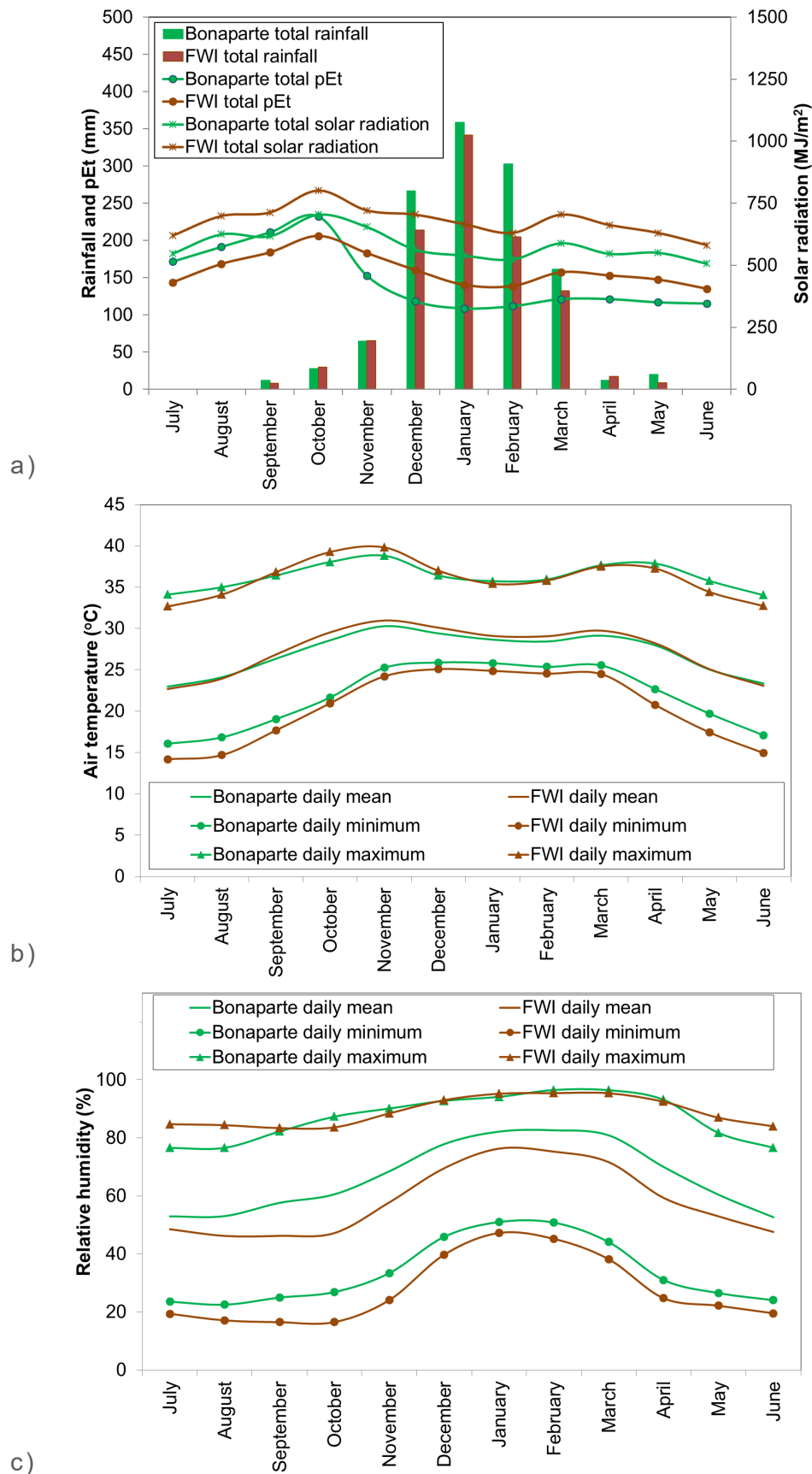


Figure 4.1: Annual dynamics of a) rainfall, potential evapo-transpiration (pEt), and solar radiation; b) air temperature; and c) relative humidity recorded at Bonaparte and FWI climate stations, 2015–2018

## 4.2 Groundwater depth, elevation, and occurrence

Table 4.1 and Table 4.2 show the groundwater heads in metres relative to ground level (mRGL) and the Australian Height Datum (mAHD) in the 2018 late dry season in each pre-existing bore and recent DPIRD-drilled bore, respectively.

Groundwater depths range from 46.71 mBGL in bore 13BP01D (in the elevated central area of Cockatoo Sands) to 13.39 m above ground at bore CDGH5 Fishermans (on the edge of the mudflats; Figure 2.12).

The artesian heads recorded at CGDH6 New Attack and CGDH8 Kemp bores, which have flowed freely for many years to provide stock water, may not be representative of those in the broader aquifer around those locations. This is because the aquifer may not have fully equilibrated during the 4-hour period when each bore was temporarily sealed to allow pressure observations to be made.

The elevations of the groundwater within the Point Spring Sandstone Formation range from 10.03 mAHD at the boundary of the northern mudflats to 62.23 mAHD at Hotplate bore on the south-eastern flank of the main area of the Cockatoo Sands. We believe that the 71.02 mAHD head at 17BP03I indicates a localised perched aquifer formed over a slightly concave section of the shale layer at this location, visible in the AEM inversion results. The relatively high EC of the groundwater of 34.5 mS/m in bore 13BP03I, which is almost 3 times the mean EC of all other sites in the Point Spring Sandstone aquifer (see Section 4.5), also indicates the groundwater there is not part of the main aquifer.

The water levels in the shallow bores at sites 16BP02 (near the intermittent NW Lake) and 16BP03 (near the intermittent SE Lake), and in bore 17BP02S reflect the heads of the perched aquifers at these locations.

Table 4.3 lists the vertical head difference and resultant vertical gradient (calculated from the ratio of the head difference to the distance between bore screens) between the watertable (shallowest bore) and the deeper bore within and between aquifers at locations where there are adjacent multiple depth bores. The vertical gradient is variably low in the upper Point Spring Sandstone aquifer, ranging from a downward gradient of 0.11% at site 17BP02, to an upward gradient of 0.37% at site 17BP05. There are upward gradients of 0.57% and 0.85% from the lower Point Spring Sandstone aquifer to the watertable at sites 17BP01 and 13BP01, respectively. There are also upward gradients from the Sunbird/Tanmurra aquifer to the watertable at sites 13BP01 (0.47%) and 17BP07 (0.78%). There is a stronger upward gradient of 2.14% from the Ningbing Group aquifer to the overlying Milligans Formation at the Tanmurra bore location. The large difference (14.78 m) between the watertable and deeper water level in bore 17BP06I is due to the locally perched watertable present at this location.

Groundwater elevations within the Keep Inlet Formation range from 8.05 mAHD near the Keep Inlet (RN029226) to 34.69 mAHD at the elevated Oaks Creek bore location. However, because Oaks Creek bore is screened at the Keep Inlet/Point Spring Sandstone Formation contact, we believe that the observed groundwater head indicates a combination of the heads in both formations.



Table 4.1: Summary drilling and water level data for existing bores

Bore name	Easting (GDA94 Z52)	Northing (GDA94 Z52)	Casing elevation (mAHD)	Ground elevation (mAHD)	Depth drilled (mBGL)	Inlet interval (mBGL)	Geological formation of inlet	Water level (mRGL)	Water level (mAHD)
2_95	464967	8314674	62.91	62.36	26	14.55–25.95	Ningbing Group/Milligans contact	–1.91	60.45
Attack	467111	8351526	21.54	21.24	Unknown	Unknown	Unknown	–3.42	16.09
Bonaparte1 water bore 1	475605	8340606	57.95	57.55	40	35.5–41.5	Point Spring Sandstone	–24.62	32.93
Bonaparte1 water bore 2	476256	8340827	47.52	47.12	28	22–28	Point Spring Sandstone	–15.23	31.70
Bonaparte2 water bore	467779	8328405	68.28	68.18	31	24.7–30.7	Point Spring Sandstone	–9.36	58.82
Brolga	453332	8353128	10.14	10.04	>10.5	>10.5–Unknown	Quaternary alluvium	–1.04	9.00
Calf Spring	486168	8338208	9.84	9.39	22	16.55–21.55	Keep Inlet	>0.45 <sup>a</sup>	14 <sup>b</sup>
CGDH5 Fishermans	472404	8351462	4.26	4.06	200	50–74 <sup>c</sup>	Point Spring Sandstone <sup>c</sup>	13.39	17.45
CGDH6 New Attack	470932	8351824	6.76	6.36	114	46–88 <sup>c</sup>	Point Spring Sandstone <sup>c</sup>	3.67 <sup>d</sup>	10.03 <sup>d</sup>
CGDH7	477332	8349855	4.24	4.09	134	76–134 <sup>c</sup>	Point Spring Sandstone <sup>c</sup>	>0.20 <sup>a</sup>	12 <sup>b</sup>
CGDH8 Kemp	478826	8347625	5.40	5.20	128	74–128 <sup>c</sup>	Point Spring Sandstone <sup>c</sup>	7.25 <sup>d</sup>	12.45 <sup>d</sup>
Cleanskin	492122	8331754	18.02	17.87	45.7	25.85–43.85	Keep Inlet	–3.14	14.73
Grant Creek	481902	8328502	32.70	32.10	22.25	Unknown–22.25	Keep Inlet	–1.44	30.66
Hotplate	470796	8321055	70.68	70.48	49.8	43.8–49.8	Point Spring Sandstone	–8.25	62.23
Lewis	464069	8317617	55.14	54.84	Unknown	157.6–Unknown	Ningbing Group	–1.64	56.48
Matera	448492	8361708	5.05	5.00	Unknown	Unknown	Quaternary alluvium	–1.21	3.79
No. 8 Paddys	456798	8345047	66.46	66.26	20.9	14.9–20.9	Ningbing Group	–7.41	58.85
Oaks Creek	494634	8309462	34.89	34.79	Unknown	40.6–46.6	Keep Inlet/Point Spring Sandstone	–0.10	34.69

(continued)

Table 4.1 (continued): Summary drilling and water level data for existing bores

Bore name	Easting (GDA94 Z52)	Northing (GDA94 Z52)	Casing elevation (mAHD)	Ground elevation (mAHD)	Depth drilled (mBGL)	Inlet interval (mBGL)	Geological formation of inlet	Water level (mRGL)	Water level (mAHD)
RN029226	511340	8311308	12.67	12.27	31	25–31	Keep Inlet	–4.42	8.05
RN029229	511700	8306778	10.16	9.96	16	10–16	Quaternary alluvium	–1.78	8.18
Tanmurra	460590	8331330	38.64	38.54	50.9	44.9–50.9	Milligans	–5.50	33.04
WBN5002	460693	8331232	38.46	38.36	410	>194.9–Unknown	Ningbing Group	–2.47	35.89
WBN5006	457323	8342589	45.66	45.36	301.5	>123–Unknown	Ningbing Group	–0.93	46.29
WBN5008	461184	8331204	35.04	34.94	443	>22.7–Unknown	Ningbing Group	–3.09	32.49
Wilson	490281	8324255	30.18	29.88	>75	>75–Unknown	Keep Inlet	–1.22	28.66

GDA94 Z52 = Geocentric Datum of Australia 1994 Zone 52; mRGL = metres relative to ground level

- a Flowing bore unable to be sealed.
- b Estimated because the flowing bore was unable to be sealed.
- c The bore hole was partially cased so an estimate of the inlet interval was made, based on the drilling log, of depth of the lithology that is most likely to contribute to the observed groundwater head.
- d Measurement was obtained by temporarily sealing a bore that has flowed for many years and so may have locally reduced the pressure in the aquifer at this location.

Table 4.2: Summary drilling and water level data for the 2013, 2016, 2017 and 2018 drilled bores

Site	Bore name	AWRC reference	Easting (GDA94 Z52)	Northing (GDA94 Z52)	Casing elevation (mAHD)	Ground elevation (mAHD)	Depth drilled (mBGL)	Screen interval (mBGL)	Geological formation screened	Water level (mRGL)	Water level (mAHD)
13BP01	13BP01D	81070023	473887	8333261	84.64	84.04	172	156–168	Point Spring Sandstone	–46.27	37.77
	13BP01I	81070024	473887	8333261	84.64	84.04	172	100–118	Point Spring Sandstone	–46.71	37.33
	13BP01S	81070026	473887	8333261	84.64	84.04	172	52–82	Point Spring Sandstone	–46.53	37.51
	13BP01PB	81070025	473925	8333272	84.56	83.96	83.3	35–83	Point Spring Sandstone	–46.42	37.54
	18BP01D <sup>a</sup>	ND	473912	8333233	84.63	84.03	303	248–254	Sunbird/Tanmurra	–44.31	39.92
16BP02	16BP02I	80970156	470297	8325993	88.507	87.707	7	5.2–6.2	Quaternary colluvium/Point Spring Sandstone	Dry	Dry
	16BP02S	80970157	470298	8325994	88.547	87.747	4	2.45–3.45	Quaternary colluvium	0.00 <sup>b</sup>	87.75 <sup>b</sup>
16BP03	16BP03I	80970158	473038	8325290	98.393	97.793	11.5	9.43–11.43	Quaternary colluvium	–9.75	88.05 <sup>c</sup>
17BP01	17BP01I	81070027	478993	8335027	42.55	41.75	126.5	112.75–124.75	Point Spring Sandstone	–5.9	35.85
	17BP01S	81070029	478984	8335023	42.763	41.963	15	12–15	Point Spring Sandstone	–6.06	35.90
	17BP01PB	81070028	479013	8335027	41.897	41.097	126.25	112.75–124.75	Point Spring Sandstone	–5.29	35.81
	18BP01DD <sup>a</sup>	ND	479020	8335002	41.714	41.114	250	214–220	Point Spring Sandstone	–4.72	36.39
17BP02	17BP02I	81070030	468839	8347946	44.989	44.489	131.68	102–114	Point Spring Sandstone	–24.35	20.14
	17BP02S	81070031	468830	8347942	45.08	44.58	34	30–33	Point Spring Sandstone	–24.54	20.04
17BP03	17BP03I	80970159	469012	8340499	110.125	109.525	52	44.7–47.7	Point Spring Sandstone	–38.5	71.02
17BP04	17BP04I	80970160	462706	8344019	67.074	66.474	62	45–57	Point Spring Sandstone	–38.24	28.23
	17BP04S	80970161	462707	8344008	66.995	66.395	49	45–48	Point Spring Sandstone	–38.11	28.28

(continued)

Table 4.3 (continued): Summary drilling and water level data for the 2013, 2016, 2017 and 2018 drilled bores

Site	Bore name	AWRC reference	Easting (GDA94 Z52)	Northing (GDA94 Z52)	Casing elevation (mAHD)	Ground elevation (mAHD)	Depth drilled (mBGL)	Screen interval (mBGL)	Geological formation screened	Water level (mRGL)	Water level (mAHD)
17BP05	17BP05I	81070032	461179	8347242	41.933	41.333	95.8	77.13–89.13	Point Spring Sandstone	–19.03	22.30
	17BP05S	81070034	461182	8347233	42.056	41.456	29.5	26–29	Point Spring Sandstone	–19.34	22.12
	17BP05PB	81070033	461173	8347265	41.474	40.874	93	76.97–88.97	Point Spring Sandstone	–18.64	22.23
17BP06	17BP06I	81070035	476482	8321900	95.217	94.617	107.65	85–91	Point Spring Sandstone	–38.75	55.87
17BP07	17BP06S	81070036	476484	8321891	95.202	94.602	34.5	31–34	Point Spring Sandstone	–23.59	71.01
	17BP07I	80970162	468860	8331473	93.747	93.147	83.77	50–56	Point Spring Sandstone	–44.49	48.66
	18BP07D <sup>a</sup>	ND	468826	8331456	93.347	92.747	300	268–274	Sunbird/Tanmurra	–41.97	50.78

AWRC = Australian Water Resources Council; GDA94 Z52 = Geographical Datum of Australia 1994 Zone 52; mBGL = metres below ground level; mRGL = metres relative to ground level; ND = no data

a Bore was drilled by Geoscience Australia in 2018.

b Bore was dry in September 2018; maximum water level recorded by logger on 11 February 2017 is shown from the perched aquifer

c The maximum water level recorded by logger was 95.55 mAHD on 14 March 2017.



The groundwater elevations within the Ningbing Group aquifer range from 32.49 mAHD at WBN5008 to 58.85 mAHD at No. 8 Paddys, which is located adjacent to an elevated and very steep section of the Ningbing Range.

Table 4.4: Groundwater head difference and calculated vertical gradient within and between aquifers at locations where there are multiple bores close to each other that are screened at different depths

Site	Within Point Spring Sandstone upper		Point Spring Sandstone lower to upper		Sunbird/Tanmurra to Point Spring Sandstone upper		Ningbing Group to Milligans Formation	
	Head difference (m)	Vertical gradient <sup>a</sup> (%)	Head difference (m)	Vertical gradient <sup>a</sup> (%)	Head difference (m)	Vertical gradient <sup>a</sup> (%)	Head difference (m)	Vertical gradient <sup>a</sup> (%)
13BP01	-0.02	-0.11	0.63	0.85	0.78	0.47	ND	ND
17BP01	-0.07	-0.07	1.14	0.57	ND	ND	ND	ND
17BP02	0.03	0.04	ND	ND	ND	ND	ND	ND
17BP05	0.18	0.37	ND	ND	ND	ND	ND	ND
17BP06	-14.78	ND	ND	ND	ND	ND	ND	ND
17BP07	ND	ND	ND	ND	1.65	0.78	ND	ND
Tanmurra bore	ND	ND	ND	ND	ND	ND	3.22	2.14

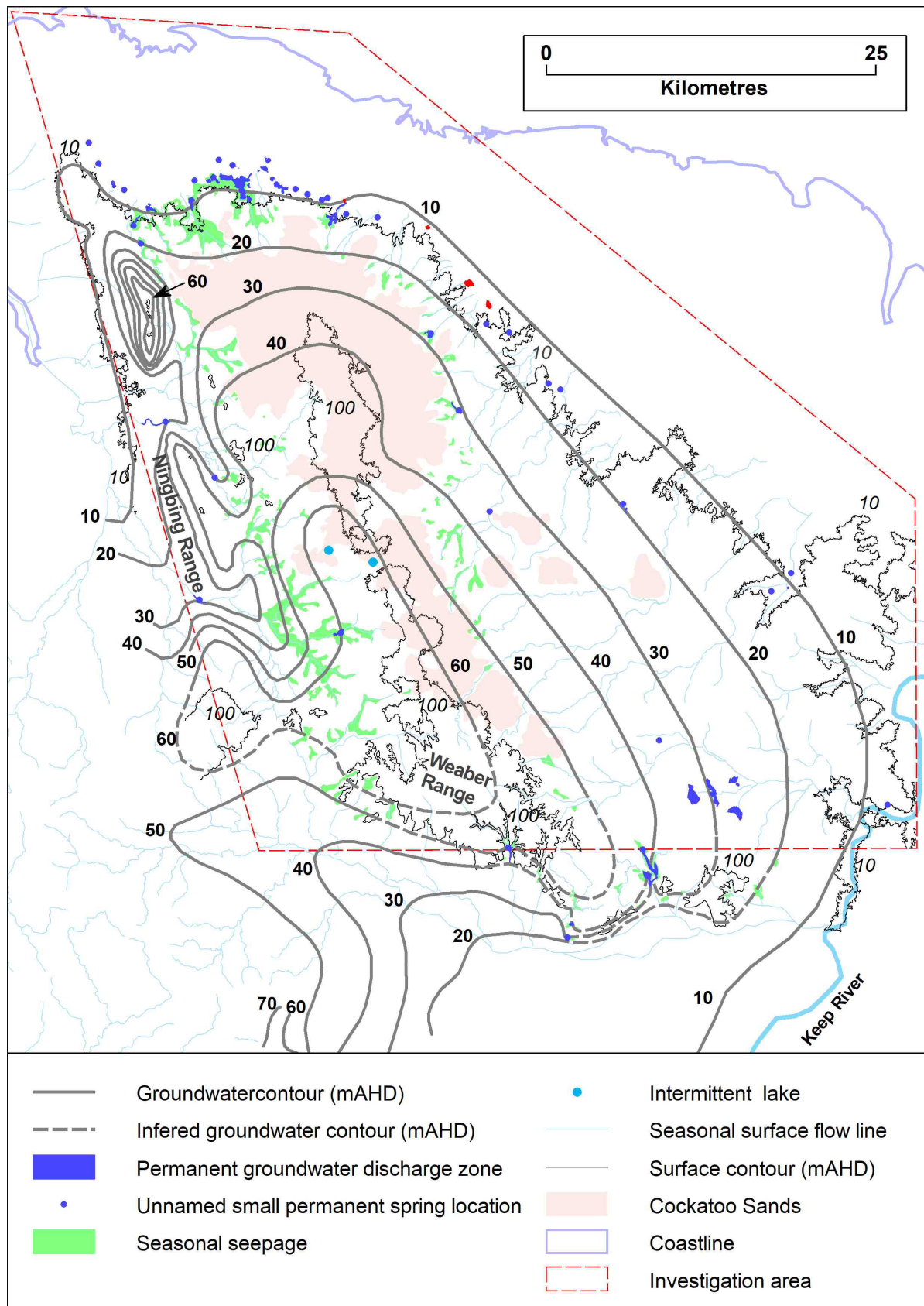
ND = no data for this parameter

a Ratio as a percentage of the head difference to the distance between the midpoint of bore screens.

Figure 4.2 shows the elevation contours, at 10 mAHD intervals, of the heads of the main aquifers within the investigation area. Much of the area of Cockatoo Sands straddles the north–south trending groundwater divide, which also approximates the local land surface divide.

Groundwater heads reduce eastwards towards the Keep River, Keep Estuary and north-east towards the ocean. There are small, isolated areas of permanent groundwater seepage within the extensive seasonally wet lowland areas of the Keep Inlet Formation (see Section 4.3 and Appendix I).

West of the groundwater divide, the groundwater heads generally reduce, and the hydraulic gradients steepen towards the north–south elongated depression underlain by shales of the Milligans Formation subcrop. Within the Milligans Formation subcrop, the groundwater heads approximate the ground surface elevation. West of the Milligans subcrop, groundwater heads in the Ningbing Group reduce towards the Cambridge Gulf, although are interrupted by significant elongated groundwater mounds underlying the more elevated sections of the Ningbing Range limestone.



Note: The 10 mAHd and 100 mAHd surface contours are shown for reference.

Figure 4.2: Contours of groundwater heads, locations of surface drainage lines, and mapped locations of permanent groundwater discharge and seasonal seepage

To the north, the groundwater heads reduce towards the ocean, becoming artesian at the terrestrial and supratidal interface. This zone also corresponds to the location of several permanent groundwater springs. Additional data collected on the permanent springs is provided in Section 4.3.

To the south, Figure 4.2 shows inferred groundwater head contours continuing through the Point Spring Sandstone Formation hard rock outcrop of the Weaber Range. Although we have no observations of groundwater heads within the Weaber Range, our observations of its surface outcrop indicate that it has very low permeability and high consolidation. Most groundwater within the Weaber Range is likely to exist within local zones of higher permeability caused by faults and variable weathering. Accordingly, we show the inferred groundwater heads sharply declining from north to south along the southern slopes of the Weaber Range, where Lookout Spring, Point Spring, and Yard Creek Spring (see Figure 2.1) permanently discharge groundwater at low rates from faulted zones.

### 4.3 Groundwater level, spring discharge and lake level dynamics

In this section, rainfall data after November 2015 was obtained from the Bonaparte climate station. Rainfall data shown prior to November 2015 was sourced from the FWI climate station.

#### 4.3.1 Groundwater level

Figure 4.3 and Figure 4.4 show logger and manually observed groundwater level responses for 17 of the 19 bores that were equipped with data loggers. Gaps in the logger data correspond to bad or missing data. Data corresponding to periods when station bores were pumping to provide stock water were removed from the hydrographs.

Figure 4.3a and Figure 4.3b show bore water level responses within the Point Spring Sandstone Formation grouped according to those with water levels above and below 40 mAHD, respectively. Except for CGDH5 Fishermans bore, groundwater levels have a rising trend over the observation period. For example, the groundwater level at site 13BP01, which has the longest record, has a consistent rising trend of 0.33 m/y (average of bores 13BP01D, 13BP01I, and 13BP01S) over the 5 years of observation. Most other bores follow a similar trend, although many have a much shorter record that also spans the 2016–2017 wet season, which had the highest rainfall on record in the region.

Water pressure in the artesian CGDH5 Fishermans bore reduced by 0.47 m between 2013 and 2018. The hourly interval logger recordings from CGDH5 Fishermans bore do not show any pressure response in the aquifer from tides up to 7.5 m. The maximum amplitude of diurnal responses observed was 0.02 m during spring tides greater than 8 m (Department of Transport, Fremantle, data accessed June 2018). We observed that tides within the 7.5–8.1 m range also correspond to widespread inundation of the mudflats adjacent to CGDH5 Fishermans bore.

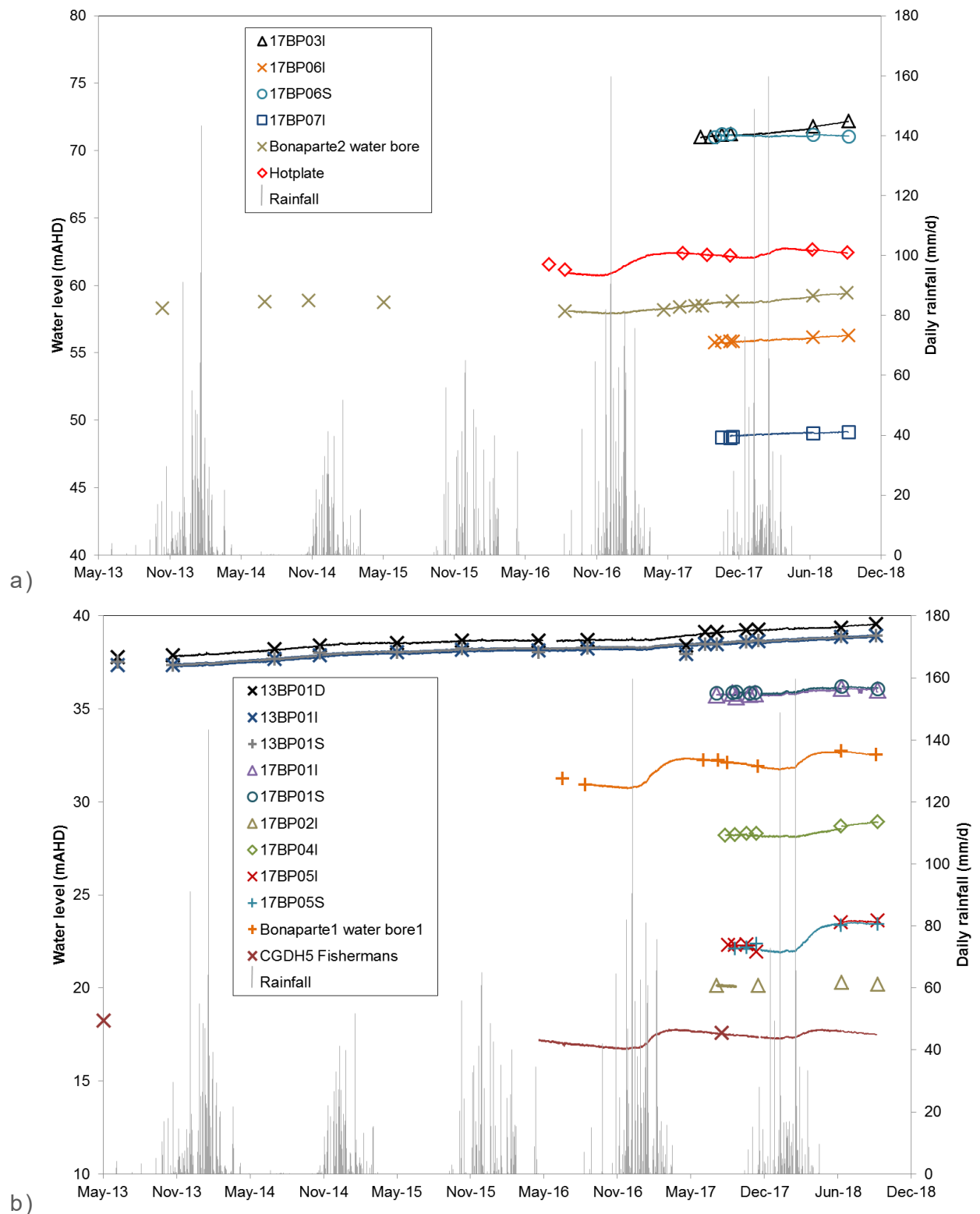
Bores within the Point Spring Sandstone aquifer that have a seasonal water level response are 17BP05I, 17BP05S, Bonaparte1 water bore 1, and Hotplate. Figure 4.3a and Figure 4.3b) show that the seasonal response is subdued and delayed, whereby

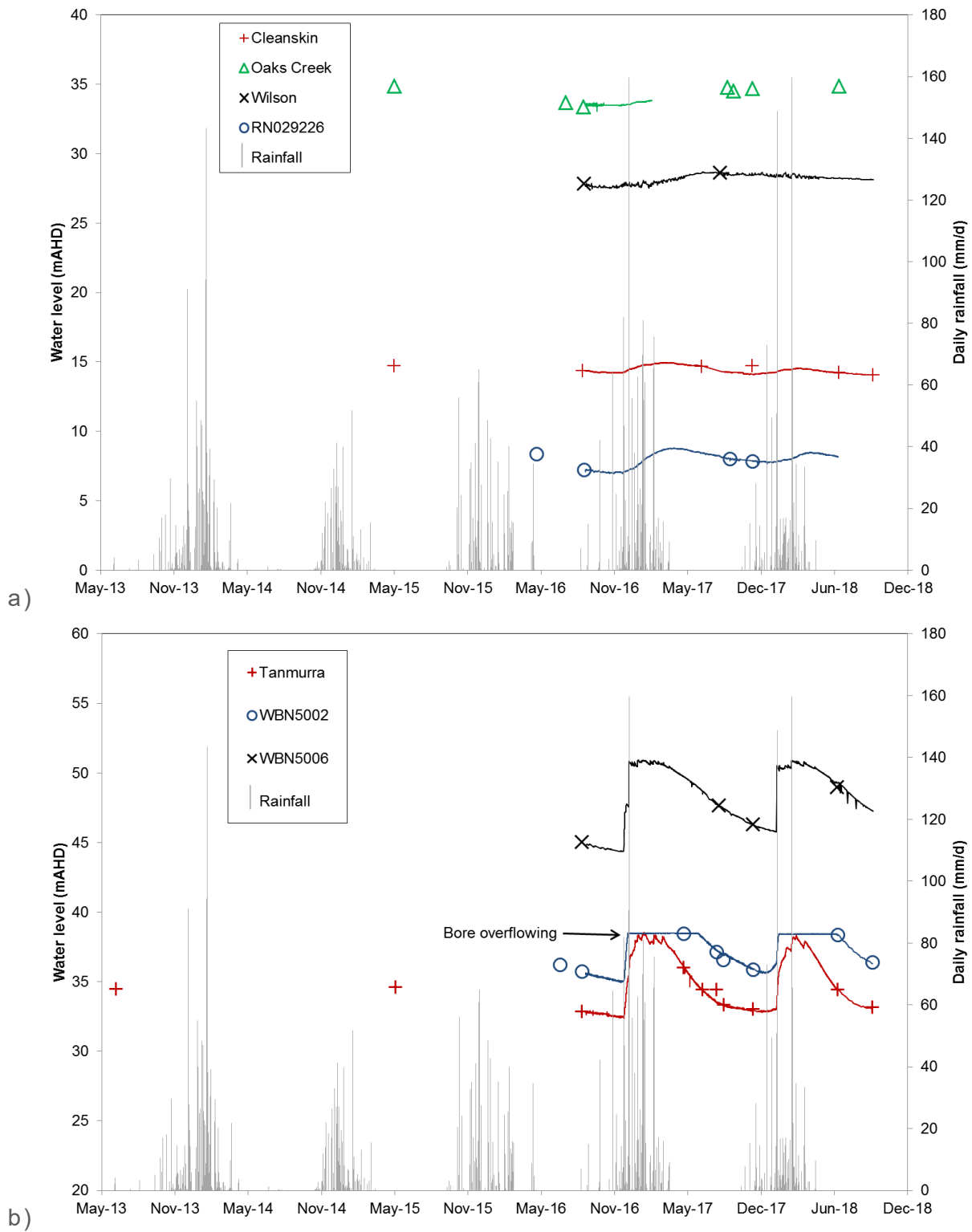
water levels continue to recede through the first half of the wet season and begin rising in the late wet season, often continuing to rise for varying periods even after rainfall ceases. Over the observation period, the rise in seasonal maximum water level was about 1.5 m each wet season. Water levels fell by a lesser amount in each subsequent dry season. The depth to water was less than 25 m in each of these seasonally responsive bores.

Except for CGDH5 Fishermans, water levels in all other bores screened within the Point Spring Sandstone Formation did not have a pronounced seasonal rise and fall cycle.

Groundwater heads in the Keep Inlet, Ningbing Group, and Milligans Group formations did not show any trend (Figure 4.4). Groundwater levels in the Keep Inlet Formation had subdued or minimal seasonal changes (Figure 4.4a). By contrast, groundwater heads within the Ningbing and Milligans Group formations were highly responsive to rainfall (Figure 4.4b). For example, water levels in bore WBN5006 rose 4.16 m on 9 September 2018 when 149 mm of rain was recorded at the Bonaparte weather station. The water levels in all bores within Ningbing and Milligans Group formations had large (about 6 m) seasonal cycles over the 2 years of observation.







Note: Short-term pumping drawdown effects are removed from Wilson and WBN5002 bores.  
 Figure 4.4: Groundwater elevation changes in bores with inlets within a) Keep Inlet Formation and b) the Milligans and Ningbing Group formations

### 4.3.2 Permanent and seasonal spring groundwater discharge

Figure 4.5 shows the location of the permanent springs that we identified within the investigation area. Some of these springs are either not named on maps or appear to have various local names – we assigned identification numbers to these for this report. Appendix I lists the coordinates and elevations of each named or numbered spring.

Table 4.4 summarises our observations of the elevation, area occupied, and the rate of outflow (where present) of natural permanent groundwater discharge spring areas. Table 4.4 also shows the surface geological formation at each location and the underlying formation that is the likely source of their discharge water. We mapped 510 ha of permanently wet areas caused by discharging groundwater within the investigation area.

Springs on low-lying and flat land adjacent to the mudflats near the boundary of the Keep Inlet Formation to the north (such as Long, Bamboo, King Gordon, and Brolga springs), have large, permanently wet areas but no off-site flow during dry seasons. However, they have zones within them where groundwater visibly upwells and then spreads out. In the absence of overall surface gradient, the discharging groundwater then eventually pools on the surface to create permanent swamps that can be up to 153 ha (Table 4.4, Figure 4.6; Long Spring). The swamps can contain organic mounds and support forests of *Melaleuca leucadendra* (paperbark) that are commonly about 30 m tall (Figure 4.6).

Except for Oaks Creek Spring, the permanent springs located within the Keep Inlet Formation – such as Big Boab, Legune, Calf, Snake, and the numbered springs in Figure 4.5 – are much smaller and often are present as small mound springs that have no outflow or little evidence of active flow. Calf Spring is a typical example of the small springs on flat land on the Keep Inlet Formation (Figure 4.7).

Oaks Creek Spring is relatively large (59 ha), lies within a gently sloping landscape and has a modest dry season outflow rate of about 5 L/s. Flow from this source was evident at a point about 5 km downstream but had dissipated or evaporated about 5 km further downstream. Although Oaks Creek Spring is on the Keep Inlet Formation outcrop, it is only about 3 km downslope of the margin with the Point Spring Sandstone Formation outcrop, the likely source of the discharge.

Permanent spring zones that occur on more elevated and sloping land, such as Yow, Bore, Garimala Creek and New springs, have defined outflow creeks (Figure 4.8) that have variable dry season outflow rates (Table 4.4). At Yow Spring we observed highly variable outflow rates during the 2017 dry season – the outflow was estimated to be 50 L/s on 19 August, 12 L/s on 11 September, and 400 L/s on 15 November. Humid wet season climatic conditions had commenced by 15 November with 21 mm of rain recorded in total from 3 events from 1–14 November 2017. We could not find evidence of any surface run-off around the spring margins from this event, indicating that increased groundwater discharge rather than surface run-off was responsible for the large increase in outflow. Outflow from Yow Creek is contained on the mudflats within a reed bed of about 15 ha.

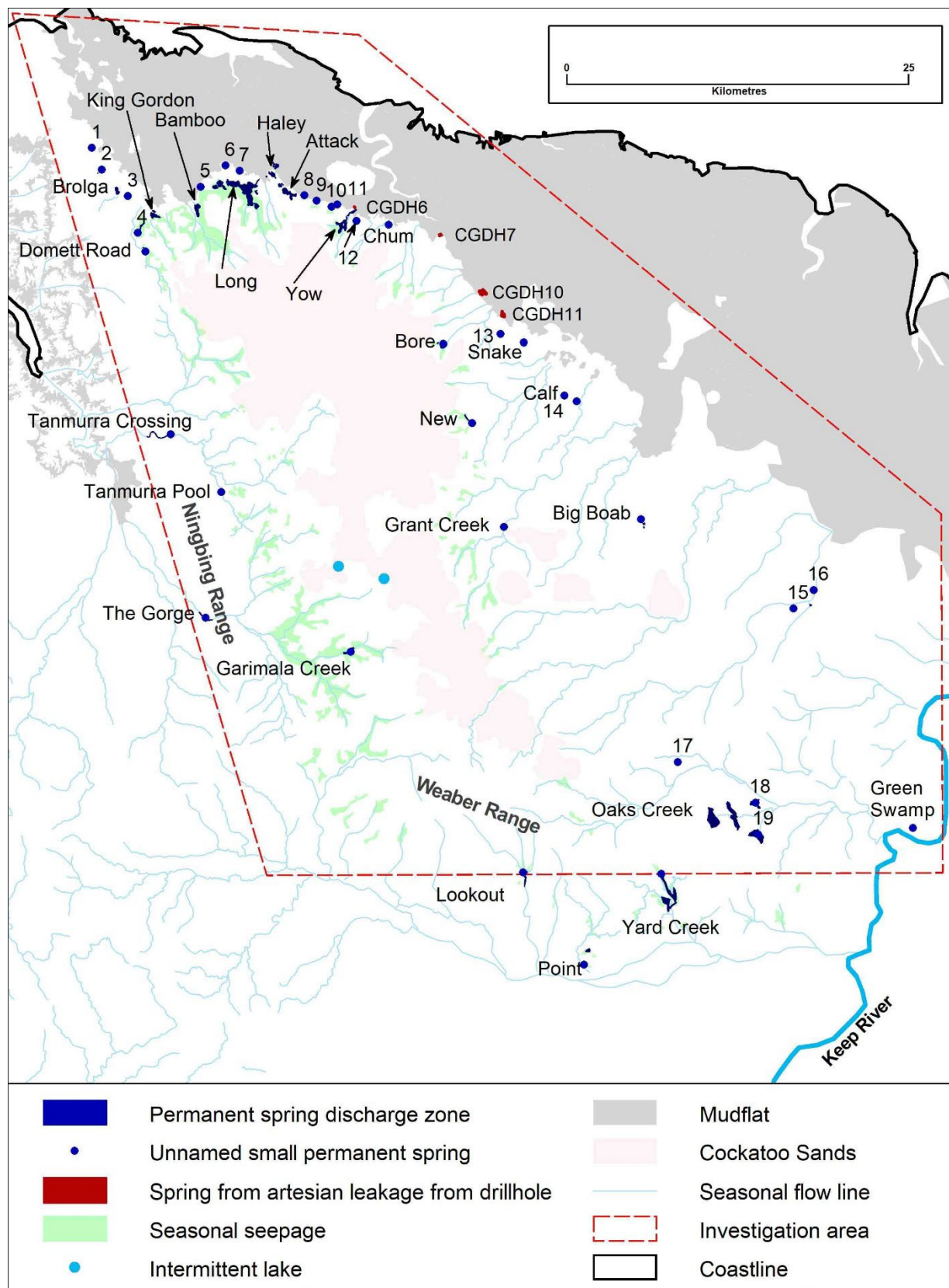
Figure 4.5 and Table 4.5 also show the location, elevation, and size of the permanently wet areas resulting from leakage of artesian water from the uncapped CGDH6 New

Attack bore, or through the annuluses of 3 (CGDH7, CGDH10 and CGDH11) of the 15 coal exploration bores that were drilled around the edge of the mudflats in 1981 (Williams 1982). These permanently wet areas have a total area of 43 ha. They also have forests of *M. leucadendra*, although the trees are markedly smaller, indicating that they are much younger than those in the naturally occurring springs. There are no outflows from these areas in dry seasons.

Including the springs resulting from bore leakage, discharge from the Point Spring Sandstone Formation is the likely source of water for 403 ha of permanently wet areas. The rate of dry season outflow away from the permanently wet areas at Bore, Garimala Creek, New, and Oaks Creek springs totals 62 L/s (Table 4.4), equivalent to about 2 GL/y. At all these locations, the dry season outflow evaporates or otherwise dissipates before reaching the ocean.

We found evidence that many of the larger springs have grown in recent years. For example, there is an apparent radial colonisation with younger paperbarks around the upper margins of most. Additionally, the centres of Yow and Oaks Creek springs contain areas of dead and dying mature paperbarks. These areas are becoming quite open, as there is no apparent succession of younger trees within these very sodden areas. The large, wet reed beds now colonising the mudflats immediately below Yow, Long, Bamboo, and King Gordon springs are not apparent on 2005 aerial photography, indicating that the rate of discharge has increased since 2005. Figure 4.9, a photograph taken in November 2017, shows the 15-ha reed bed that has colonised the mudflats immediately below Yow Spring since 2005. The *M. leucadendra* trees at Bore Spring are much smaller and appear to be much younger than those at the other major natural permanent springs, perhaps indicating that groundwater discharge there is comparatively recent.





Note: Mapping of seasonal groundwater discharge was undertaken only within or near Point Spring Sandstone Formation outcrop or subcrop.

Figure 4.5: Location of permanent springs and seasonal groundwater seepage zones in relation to seasonal surface flow lines, intermittent lakes and mudflats



Figure 4.6: Forest of large paperbarks at Long Spring



Figure 4.7: Calf Spring



Figure 4.8: The estimated 400 L/s outflow from Yow Spring on 15 November 2017





Figure 4.9: Reed bed colonising the mudflats in the area inundated by outflow from Yow Spring (November 2016)

Permanent discharge springs within the Ningbing Group limestones and the Milligans Formation subcrop are in incised parts of creek channels, forming small stagnant pools in deeper sections during dry seasons.

Figure 4.5 also shows the areas that we mapped as having seasonal seepage derived from either permanent or perched groundwater sources within the Point Spring Sandstone Formation. Photographed on 20 May 2017, Figure 4.10 shows active outflow from a perched seasonal seepage located about 20 m south of Bonaparte2 water bore. At that time, the water level in Bonaparte2 water bore was 10.01 mBGL. By 1 July 2017, the seepage area was dry.

The total area of the seasonal seepage zones that we mapped on or adjacent to the Point Spring Sandstone outcrop or subcrop is 4,816 ha. The emergent woody vegetation occupying seasonal seepage areas is usually sparse, with tall annual grasses and other herbaceous species occupying most of the area. Sparse *Melaleuca* spp. is the common emergent species in the wet areas and can form denser thickets towards the edges. *Acacia* spp. (wattle) shrub thickets usually make up the upslope, adjacent vegetation community, although this can vary depending on fire history.

We did not map the extensive seasonally wet areas away from the Point Spring Sandstone Formation subcrop or outcrop. Land unit mapping by Schoknecht et al. (2004) identifies seasonally wet land subsystems surrounding the Bonaparte Plains area (reproduced in Appendix A).



Figure 4.10: Outflow from a seasonal seepage area near Bonaparte2 water bore, 20 May 2017

Table 4.5: Elevation, area, estimated rate of outflow, surface formation and contributing aquifer of natural permanent springs located within the investigation area

Spring name	Ground elevation (mAHD)	Estimated dry season outflow (L/s)	Permanently wet area (ha) <sup>a</sup>	Surface formation	Likely aquifer water source	Date of outflow rate estimation
Attack	6	0	26	Keep Inlet	Point Spring Sandstone	16/05/2016
Bamboo	12	0	19	Point Spring Sandstone	Point Spring Sandstone	28/05/2015
Big Boab	15	0	2	Keep Inlet	Keep Inlet	04/07/2017
Bore (lower)	23	40 <sup>b</sup>	13	Keep Inlet	Point Spring Sandstone	13/07/2016 <sup>b</sup>
Bore (upper)	26	1	0.3	Keep Inlet	Keep Inlet	29/08/2017
Brolga	6	0	8	Quaternary colluvium	Quaternary colluvium	11/11/2017
Calf	7	0	0.2	Keep Inlet	Keep Inlet	09/11/2017
Chum	7	0	0.2	Keep Inlet	Keep Inlet	16/08/2017
Domett Road	21	1 <sup>e</sup>	2	Milligans	Ningbing Group	10/06/2016 <sup>e</sup>
Garimala Creek	55	2 <sup>c</sup>	10	Point Spring Sandstone	Point Spring Sandstone	8/06/2018 <sup>c</sup>
Grant Creek	32	0	1	Keep Inlet	Keep Inlet	09/11/2017
Haley	6	0	22	Keep Inlet	Point Spring Sandstone	16/05/2016
King Gordon	12	0	13	Point Spring Sandstone	Point Spring Sandstone	28/05/2015
Long Spring	6	0	153	Keep Inlet	Point Spring Sandstone	11/09/2017
New Spring	33	15 <sup>d</sup>	5	Keep Inlet	Point Spring Sandstone	15/11/2017 <sup>d</sup>
Oaks Creek	29	5	69	Keep Inlet	Point Spring Sandstone	07/09/2017
Snake	6	0	2	Keep Inlet	Keep Inlet	11/09/2017
Tanmurra Crossing	21	50	2	Ningbing Group	Ningbing Group	11/06/2018
Tanmurra Pool	31	2	2	Milligans	Milligans	11/06/2018
The Gorge	25	0	2	Ningbing Group	Ningbing Group	11/06/2018
Yow	14	200 <sup>f</sup>	31	Point Spring Sandstone	Point Spring Sandstone	30/06/2018 <sup>f</sup>
Unnamed other	Various	0	129	Mainly Keep Inlet	Mainly Keep Inlet	Various
<b>Total</b>	NA	<b>326</b>	<b>510</b>	NA	NA	NA

NA = not applicable

a Above outflow, if present

b Average outflow of 50 L/s on 13/07/2017 and 30 L/s on 29/08/2017

c Outflow of 2 L/s on 24/06/13 and 2 L/s on 9/06/2018

d Average outflow of 16 L/s on 30/08/2017 and 14 L/s on 15/11/2017

e Outflow of 1 L/s on 28/05/2015 and 1 L/s on 10/06/2016

f Average outflows of 200 L/s on 22/05/2013, 12 L/s on 27/05/2015, 50 L/s on 19/08/2017, 20 L/s on 11/09/2017, 400 L/s on 15/11/2017 and 100 L/s on 13/06/2018



Table 4.6: Location coordinates, elevation and the permanent wet areas caused by old leaking mineral investigation bores

Bore	Northing (GDA94 Z52)	Easting (GDA94 Z52)	Ground elevation (mAHD)	Permanently wet area (ha)	Surface formation	Contributing aquifer formation
CGDH6	8351966	470978	5	3	Keep Inlet	Point Spring Sandstone
CGDH7	8349943	477240	5	5	Keep Inlet	Point Spring Sandstone
CGDH10	8345800	480287	5	22	Keep Inlet	Point Spring Sandstone
CGDH11	8344183	487766	5	13	Keep Inlet	Point Spring Sandstone

GDA94 Z52 = Geographical Datum of Australia 1994 Zone 52

### 4.3.3 Intermittent lake water and groundwater level dynamics

Figure 4.11 shows the water levels observed in a) NW Lake and b) SE Lake in relation to groundwater level changes recorded by data loggers in the respective shallow bores (16BP02S and 16BP03I), together with the elevation of lake overflows, the lake bases and the elevation of the ground surface at the bores. The shallow bores are located up gradient of, and about 400 m distant from, the edge of each lake.

The lakes and the bores were dry in 2016, with lake and bore water levels rising during the 2016–2017 wet season. By mid-March 2017, the water in both lakes was just over 3 m deep, with NW Lake almost reaching its overflow level. Subsequently, we observed that water remained in both lakes until at least 7 September 2018, which was the last water level surveyed.

The perched groundwater levels near both lakes rose rapidly to be near the ground surface in early January 2017, then fluctuated with rainfall before steadily declining after the wet season rains ceased in mid-April 2017. The water level at bore 16BP02S, which is a shallower bore than 16BP03I, fell to below the casing by June 2017. The bore water levels also responded to the 2017–2018 wet season rains, although compared to the much wetter 2017–2018 wet season did not remain at the surface for as long in bore 16BP02S or rise as high in 16BP03I. We were unable to determine the maximum lake levels during the 2017–2018 wet season.

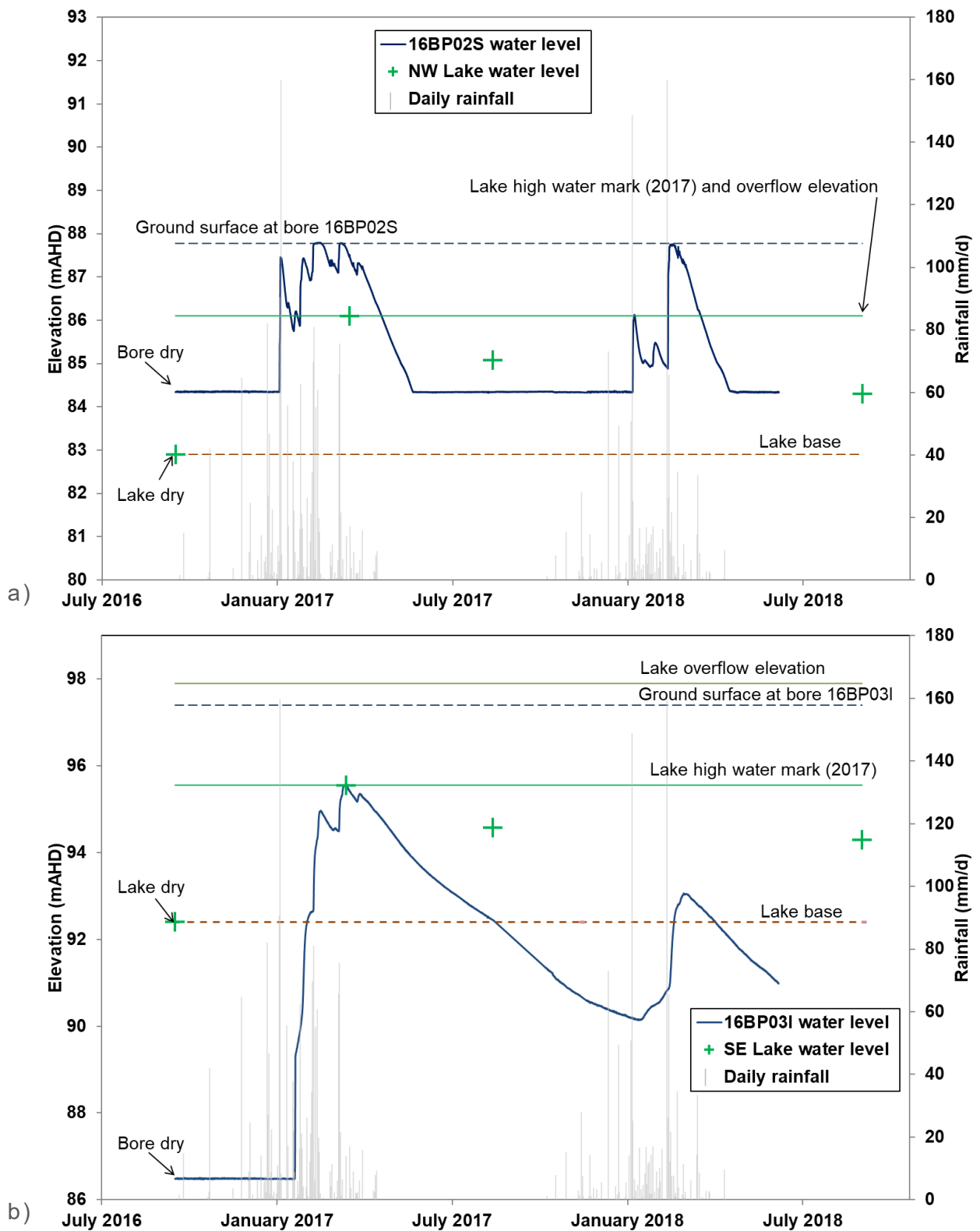


Figure 4.11: Lake water level and adjacent groundwater level changes relative to lake overflow level, lake base level and bore ground level for a) NW Lake; and b) SE Lake

## 4.4 Aquifer testing

Appendix E contains the groundwater response data, the analysis method and results obtained during the 3-step and constant rate tests (CRTs).

Table 4.6 summarises the aquifer properties of hydraulic conductivity (K), transmissivity (T), and specific yield ( $S_y$ ) derived from the analysis of groundwater responses observed during the slug and pumping tests of the Point Spring Sandstone Formation aquifer.

From Table 4.6, there is close agreement between the means of the K values derived from either the slug test method (11.5 m/d,  $n = 12$ ) or the pumping test method (11.2 m/d,  $n = 7$ ). However, the mean K values are influenced by the very high K value of 37.5 m/d in 17BP01S (CRT test) and 58.2 m/d in 18BP01DD (slug test). These 2 values are an order of magnitude higher than all other K values generally. The lithological description for the 15 m deep 17BP01S (Bennett 2019) does not indicate a lithology-related reason why the aquifer should have such a high K value. Our observations of the drilling cuttings at 18BP01DD indicate that the lithology at the screen interval depth is much coarser and less consolidated than observed at any other bore location and depth.

If the K values from bores 17BP01S (unreliable) and 18BP01DD (unrepresentative) are considered outliers, the mean K of the Point Spring Sandstone aquifer is 7.3 m/d calculated from slug tests, and 6.9 m/d calculated from pumping tests.

The derived aquifer transmissivity of 4,500 m<sup>2</sup>/d at 17BP01S is correspondingly very high, some 5–10 times greater than at other sites. Ignoring 17BP01S, transmissivities range from 387 m<sup>2</sup>/d at site 17BP01, to 939 m<sup>2</sup>/d at site 13BP01. Except for the results from 17BP01S, the mean transmissivity of bores within Point Spring Sandstone aquifer is 606 m<sup>2</sup>/d ( $n = 6$ ).

The mean of the calculated specific yield ( $S_y$ ) for the 6 bores where  $S_y$  data were able to be calculated (Table 4.6) is 0.004 ( $n = 6$ ).

Table 4.7 shows that derived estimates of sustained potential pumping rate for the 3 pumping test bores ranged between 22 and 46 L/s, with estimates of apparent long-term safe bore yields ranging from about 14 to 33 L/s (data in Appendix E).

Test pumping bore 17BP01BP had much lower sustained potential pumping rate and long-term safe bore yield than the similarly constructed 17BP05PB, which was able to be test pumped at more than double the rate. At completion of the CRT, the observed drawdown in 17BP01PB was 46.6 m, about double that at 17BP05D. The final drawdown in the fully screened, narrower diameter 13BP01PB was 6.66 m when pumped at the same rate and for the same duration as 17BP01PB.

Water was being drawn from about 50 mBGL in each of the pumping test bores by the end of the CRTs.

Table 4.7: The hydraulic conductivity, transmissivity and specific yield values of the Point Spring Sandstone aquifer derived from slug and pumping tests

Site	Bore	Screen midpoint (mBGL)	Screen length (m)	Slug test	Constant rate test (CRT)			
				K (m/d)	Q (L/s)	K (m/d)	T (m <sup>2</sup> /d)	S <sub>y</sub> value
13BP01	13BP01D	162	12	6.4	NA	ND	ND	ND
	13BP01I	109	18	ND	NA	ND	ND	ND
	13BP01S	67	30	ND	NA	9.4	939	0.0130
	13BP01PB	59	48	ND	16.1	4.3	430	ND
17BP01	17BP01I	119	12	3.5	NA	3.5	414	0.0010
	17BP01S	14	3	3.4	NA	37.5	4,500	0.0100
	17BP01PB	119	12	ND	16.1	3.2	387	ND
	18BP01DD	217	6	58.2	NA	ND	ND	ND
17BP02	17BP02I	108	12	ND	NA	ND	ND	ND
	17BP02S	32	3	14.0	NA	ND	ND	ND
17BP03	17BP03I	46	3	12.0	NA	ND	ND	ND
17BP04	17BP04I	51	12	8.7	NA	ND	ND	ND
	17BP04S	47	3	8.4	NA	ND	ND	ND
17BP05	17BP05I	83	12	7.5	NA	11.9	838	0.0006
	17BP05S	28	3	3.2	NA	ND	ND	ND
	17BP05PB	83	12	ND	36.0	8.9	628	0.0005
17BP06	17BP06S	33	3	7.2	NA	ND	ND	ND
17BP07	17BP07I	53	6	6.0	ND	ND	ND	ND

K = hydraulic conductivity; NA = not applicable; ND = no data; Q = pump discharge rate; S<sub>y</sub> = specific yield;  
T = transmissivity



Table 4.8. Summary discharge and drawdown data for the constant rate tests and the derived estimates of sustained potential pumping rate and apparent long-term safe bore yield

Bore	Pumping test discharge rate (L/s)	Drawdown at end of pumping test (m)	Available drawdown (m)	Sustained potential pumping rate (L/s)	Drawdown at sustained potential pumping rate (m)	Apparent safe long-term bore yield (L/s)	Drawdown at safe long-term yield (m)
13BP01PB	16.31	6.66	10	22	7.21	14.17	8.25
17BP01PB	16.31	46.67	80	32.4	50.2	22.04	51.7
17BP05PB	36.0	25	52	46.1	37.6	32.7	38.8

## 4.5 Rainfall, groundwater, spring and lake water chemistry

Appendix J contains the complete results of the field physicochemistry, the laboratory chemical analyses, and the isotope and gas tracer analyses from samples collected from rain, groundwater bore, spring and lake waters.

### 4.5.1 Rainfall physicochemistry

Wet season rainfall was very low in all major ion concentrations and extremely low (mostly below the LOR) in metals. The mean wet season EC, chloride (Cl), and sodium (Na) was 1 mS/m, 1.3 mg/L, and 1.7 mg/L, respectively. These parameters were highest during the high rainfall 2016–2017 wet season (2 mS/m, 2 mg/L, and 4.1 mg/L, respectively) and correspond to the high Na/Cl molar ratio of 3.3, indicating that sodium may have been contributed to rainfall from sources other than marine aerosols. Cyclones directly affected the area during the 2016–2017 wet season.

### 4.5.2 Bore groundwater physicochemistry

Appendix J contains the results of the field and laboratory physicochemical analyses from groundwater samples obtained from bores within the investigation area. Table 4.8 shows the mean, the number of samples analysed and the coefficient of variation for each of the physicochemical parameters grouped by geological formation for the Point Spring Sandstone Formation, Keep Inlet Formation, Ningbing Group formations and Sunbird/Tanmurra Formation. The means of the parameters from the shallow northern coastal Quaternary alluvium, represented by results from Matera and Brolga bores (Appendix J), are not included in Table 4.8. Similarly, results from Tanmurra bore, the only bore screened into the Milligans Group shales, are not included. The individual results from these 3 bores are provided in Appendix I.

Except for temperature, which increased with depth, there were no statistically significant trends in any parameter with depth within each aquifer represented in Table 4.8 (data not shown).

Overall, the groundwater in most aquifers and at most locations is fresh. The average EC of samples from all formations is 32.6 mS/m (range 2.8–413 mS/m). However, this value is influenced by the relatively high EC in Brolga (112 mS/m) and Matera

(413 mS/m) bores, which are located in coastal Quaternary alluvium. The mean EC of groundwater of all other bores is 20 mS/m.

Excluding the results from bores 17BP03I and 17BP05S that are screened into perched aquifers, the groundwater from the Point Spring Sandstone Formation has the lowest mean EC (12.3 mS/m, range 2.8–20.5 mS/m) of the main aquifers present in the 4 geological formations shown in Table 4.8. There is an excellent correlation ( $r^2 > 0.76$ ) between EC and the concentrations of sodium, chloride and sodium chloride. Sodium and chloride dominate the ionic concentration in the groundwater.

The relationship between EC and sodium chloride is poorer in the Ningbing, Keep Inlet, and Sunbird/Tanmurra aquifers, where calcium concentrations are more variable and make up a greater proportion of the ionic concentration (Appendix J).

The average pH of the Point Spring Sandstone aquifer is 6.5 and is slightly acidic in every bore except 18BP01DD (pH 7.6), which has a deep inlet (268–274 mBGL) located just above the calcareous Sunbird/Tanmurra Formation (Table 4.2). By contrast, the other aquifers are slightly to moderately alkaline, up to pH 8.1 in the groundwater in the Sunbird/Tanmurra Formation.

All groundwaters contained oxygen, with the Point Spring Sandstone aquifer having the highest mean dissolved oxygen (DO) content of 36%, with the most oxygenated water located beneath areas of Cockatoo Sands. Groundwaters from within the Keep Inlet Formation had the lowest DO (10%). The mean oxidation–reduction potential (ORP; expressed as Eh) of the Point Spring Sandstone aquifer was 300 millivolts (mV). For the other formations, mean Eh values followed a similar trend to DO, except for the very low mean Eh of the Sunbird/Tanmurra aquifer.

Nutrient concentrations were generally low in all aquifers, with many samples having concentrations of the various nutrient species below the LOR. Mean total nitrogen (TN), nitrate nitrogen, and total phosphorus (TP) concentrations were 0.13, 0.06, and 0.06 mg/L, respectively, in the Point Spring Sandstone Formation aquifer.

Various metal and other trace elements were usually in very low concentrations or below the LOR. Exceptions were iron in the sample from Hotplate (6.3 mg/L), and zinc from Bonaparte1 water bore 1 (3.2 mg/L) and Bonaparte2 water bore (2.6 mg/L). Hotplate bore has a rusting iron casing and contains an unused rusting iron pump and associated pipework that has not been operational for several years. The 2 bores that have high zinc levels also have galvanised steel casings and have not been used since they were installed in the 1960s. Therefore, the elevated iron or zinc concentration recorded from these old bores could be anomalies caused by long-term corrosion of their casings and pump equipment, resulting in contamination of the localised aquifer around them.

Table 4.9: The mean values of each of the physicochemical parameters analysed from groundwater bore samples grouped by hydrostratigraphy

Parameter	Point Spring Sandstone Formation			Keep Inlet Formation			Ningbing Group formations			Sunbird/Tanmurra Formation		
	Mean	n	COV	Mean	n	COV	Mean	n	COV	Mean	n	COV
<b>Field parameters</b>												
Alkalinity	40	22	0.5	106	5	0.5	349	4	0.1	205	2	0.2
DO (%)	36	22	0.5	10	5	1.1	32	4	0.7	26	2	0.2
Eh	300	22	0.2	128	5	0.8	257	4	0.4	30	2	0.2
Temp (°C)	32.3	22	0.02	32.5	5	0.05	34.8	4	0.02	34.5	2	0.01
<b>Laboratory general chemistry parameters</b>												
Acidity	27	25	0.4	11	5	0.9	16	4	0.7	11	2	0.5
HCO <sub>3</sub>	32	25	0.8	106	5	0.6	258	4	0.5	224	2	0.1
Br	0.09	25	0.7	0.12	5	0.8	0.04 <sup>b</sup>	4	0.9	0.02 <sup>b</sup>	2	0.7
CO <sub>3</sub>	0.5 <sup>a</sup>	25	0	0.5 <sup>a</sup>	5	0	1	4	0.5	1	2	0.5 <sup>a</sup>
Cl	24	25	0.7	26	5	0.9	10	4	0.6	11	2	0.2
EC	13.5	25	0.5	28.4	5	0.5	44.9	4	0.5	38.6	2	0.1
F	0.05	25	0.7	0.12	5	0.2	0.11	4	0.9	0.14	2	0.1
Hardness	27	25	0.6	56	5	0.5	280	4	0.4	107	2	0.3
OH	0.5 <sup>a</sup>	25	0	0.5 <sup>a</sup>	5	0	0.5 <sup>a</sup>	4	0	0.5 <sup>a</sup>	2	0.0
Ion balance	-5	25	-1.1	2	5	1.7	-5	4	-0.8	-3	2	-1.3
SO <sub>4</sub> S	5.5	25	0.7	15.3	5	0.5	26.6	4	1.8	11.3	2	0.2
TN	0.13	25	0.9	0.03	5	1.0	0.09 <sup>b</sup>	4	1.2	0.35	2	1.3
NH <sub>4</sub> N	0.01	25	1.3	0.01	5	1.3	0.01 <sup>b</sup>	4	0.4	0.22 <sup>b</sup>	2	1.4
NO <sub>3</sub> N	0.06	25	0.6	0.01	5	0.8	0.06 <sup>b</sup>	4	1.6	0.005 <sup>a</sup>	2	1.2
NO <sub>2</sub> N	0.01 <sup>a</sup>	25	0.5	0.005	5	0	0.01 <sup>b</sup>	4	1.3	0.005 <sup>a</sup>	2	0
pH	6.5	25	0.1	7.4	5	0.1	7.8	4	0.02	8.1	2	0
TP	0.06	25	2.7	0.05	5	0.3	0.03	4	1.3	0.08	2	1.0
SRP	0.03 <sup>b</sup>	25	3.5	0.02	5	0.9	0.01 <sup>b</sup>	4	0.4	0.0025 <sup>a</sup>	2	0
TDS Sum	73	25	0.5	160	5	0.5	250	4	0.5	220	2	0.2
<b>Laboratory metals</b>												
Al	0.055	25	1.5	0.028	5	0.3	0.024	4	0.6	0.018	2	0.4
Sb	0.0001 <sup>b</sup>	25	2.8	0.00005 <sup>a</sup>	5	0	0.00005 <sup>a</sup>	4	0	0.00005 <sup>a</sup>	2	0
As	0.001 <sup>b</sup>	25	1.4	0.0005 <sup>a</sup>	5	0	0.0005 <sup>a</sup>	4	0	0.0005 <sup>a</sup>	2	0
Ba	0.0540	25	0.9	0.0682	5	0.6	0.0270	4	0.3	0.1400	2	0.1
Be	0.0001 <sup>b</sup>	25	0.6	0.00005 <sup>a</sup>	5	0	0.00005 <sup>a</sup>	4	0	0.00005 <sup>a</sup>	2	0

(continued)

Table 4.8 (continued): The mean values of each of the physicochemical parameters analysed from groundwater bore samples grouped by hydrostratigraphy

Parameter	Point Spring Sandstone Formation			Keep Inlet Formation			Ningbing Group formations			Sunbird/Tanmurra Formation		
	Mean	n	COV	Mean	n	COV	Mean	n	COV	Mean	n	COV
Bi	0.00005 <sup>a</sup>	25	0	0.00005 <sup>a</sup>	5	0.0	0.0005 <sup>a</sup>	4	0	0.0005 <sup>a</sup>	2	0
B	0.067	25	0.5	0.022	5	0.2	0.026	4	0.7	0.041	2	0.1
Cd	0.0001 <sup>b</sup>	25	1.5	0.00005 <sup>a</sup>	5	0.0	0.0001 <sup>b</sup>	4	0.4	0.00005 <sup>a</sup>	2	0
Ca	5.0	25	1.0	13.2	5	0.7	58.2	4	0.7	27.6	2	0.4
Cr	0.0005 <sup>b</sup>	25	1.0	0.0003	5	0.4	0.00025 <sup>a</sup>	4	0	0.00025 <sup>a</sup>	2	0
Co	0.0014	25	1.6	0.0003	5	1.7	0.0001 <sup>b</sup>	4	0.4	0.0003	2	0.3
Cu	0.0057	25	1.7	0.0009	5	0.5	0.0018	4	1.5	0.0010	2	0.4
Ga	0.0001 <sup>b</sup>	25	1.3	0.00005 <sup>a</sup>	5	0	0.00005 <sup>a</sup>	4	0	0.00005 <sup>a</sup>	2	0
Fe	1.331	25	2.0	0.548	5	1.2	0.024	4	0.6	3.530	2	1.3
La	0.0025 <sup>a</sup>	25	0	0.0025 <sup>a</sup>	5	0	0.0025 <sup>a</sup>	4	0	0.0025 <sup>a</sup>	2	0
Pb	0.0018	25	2.4	0.0004	5	0.8	0.0004	4	0.6	0.0005	2	0.5
Li	0.0021	25	0.6	0.0128	5	0.4	0.0009	4	0.8	0.0051	2	0.7
Mg	3.3	25	0.8	5.6	5	0.3	16.5	4	0.4	9.4	2	0.2
Mn	0.0848	25	2.1	0.1418	5	0.8	0.0085	4	0.7	0.3300	2	0.0
Hg	0.000025 <sup>a</sup>	25	0	0.000025 <sup>a</sup>	5	0	0.000025 <sup>a</sup>	4	0	0.000025 <sup>a</sup>	2	0
Mo	0.001 <sup>b</sup>	25	0.7	0.0005 <sup>a</sup>	5	0	0.0005 <sup>a</sup>	4	0	0.0005 <sup>a</sup>	2	0
Ni	0.002	25	0.7	0.001	5	0.8	0.0005 <sup>a</sup>	4	0	0.001 <sup>b</sup>	2	0.5
K	1.9	25	1.4	11.8	5	0.3	1.3	4	0.9	12.9	2	0.2
Se	0.015 <sup>a</sup>	25	0.6	0.025 <sup>a</sup>	5	0	0.025 <sup>a</sup>	4	0	0.0005 <sup>a</sup>	2	0
Si	12.71	25	0.4	14.58	5	0.4	4.35	4	0.3	9.80	2	0.03
Ag	0.0001 <sup>b</sup>	25	2.4	0.00005 <sup>a</sup>	5	0	0.00005 <sup>a</sup>	4	0	0.00005 <sup>a</sup>	2	0
Na	16.1	25	0.6	35.8	5	0.9	7.5	4	0.9	35.4	2	1.0
Tl	0.0001 <sup>b</sup>	25	0.9	0.00005 <sup>a</sup>	5	0	0.0001 <sup>b</sup>	4	1.1	0.00005 <sup>a</sup>	2	0
Sn	0.0089	25	4.7	0.0012	5	1.4	0.0020	4	1.5	0.0030	2	0.8
Ti	0.0007 <sup>b</sup>	25	1.2	0.00025 <sup>a</sup>	5	0	0.00025 <sup>a</sup>	4	0	0.0011 <sup>b</sup>	2	1.1
U	0.0001 <sup>b</sup>	25	1.3	0.00005 <sup>a</sup>	5	0	0.0007	4	1.1	0.00005 <sup>a</sup>	2	0.0
V	0.0008 <sup>b</sup>	25	3.0	0.0002	5	0.7	0.0002	4	0.6	0.0001 <sup>b</sup>	2	0.8
Zn	0.274	25	2.9	0.176	5	1.9	0.097	4	0.6	0.060	2	1.2

n = number; COV = coefficient of variation

a All the results were below the LOR (these data were assigned a value equal to 50% of the LOR).

b At least half of the results were below the LOR (these data were assigned a value equal to 50% of the LOR).

Note: Appendix B shows the physicochemical parameters with their abbreviations, LORs and analysis methods.

### 4.5.3 Groundwater comparison to irrigation guidelines

Comparisons of the mean groundwater quality results from bores (Table 4.8) to the ANZECC and ARMCANZ (2000) and USDA (1954) guidelines for irrigation (Appendix D) shows that they easily meet the short- and long-term guidelines for irrigation with these exceptions:

- the USDA (1954) 'low' EC category for irrigation in the Keep Inlet, Ningbing, and Sunbird/Tanmurra aquifers
- iron for long-term irrigation in the Point Spring Sandstone and Keep Inlet aquifers
- TP in the Point Spring Sandstone and Sunbird/Tanmurra aquifers
- pH in the Ningbing and Sunbird/Tanmurra aquifers was close to the maximum guideline value.

Within the Point Spring Sandstone Formation, bore 17BP03I (EC = 35.5 mS/m), which is screened into a perched aquifer, was the only location where EC exceeded the USDA (1954) low-salinity water category (<25 mS/m).

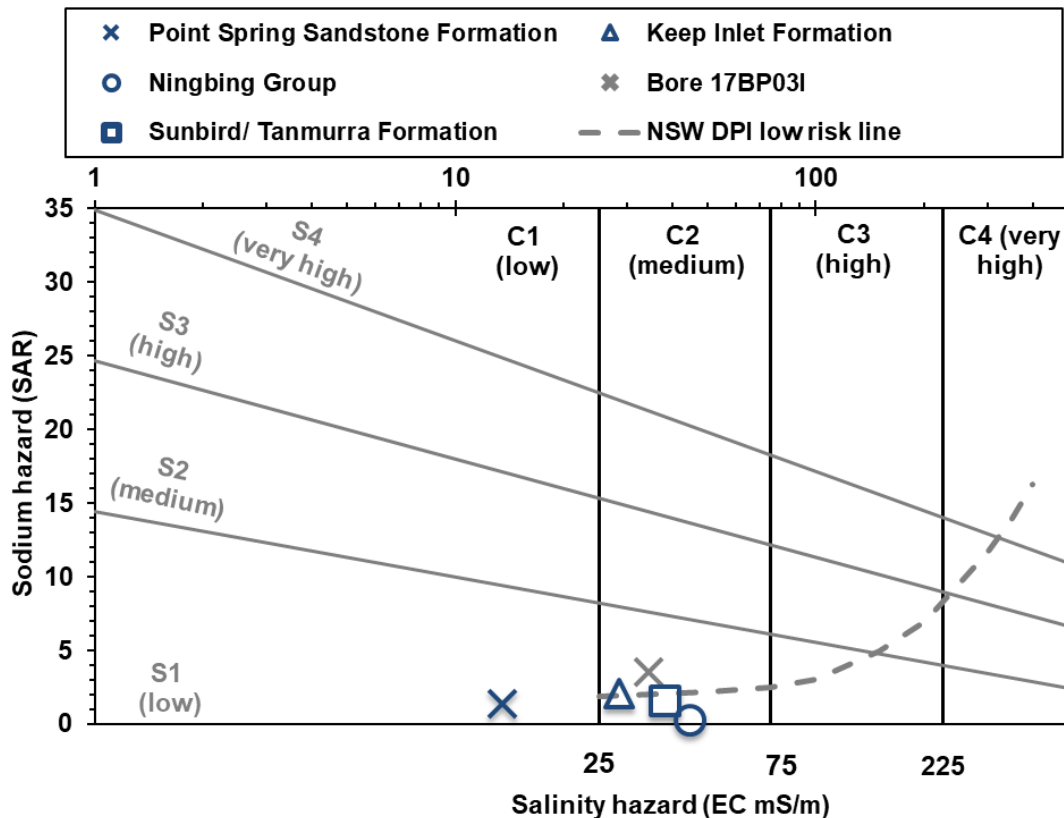
Associated with salinity hazard is the sodium hazard, which is the propensity of the sodium contained in irrigation water to replace calcium and magnesium anions adsorbed to clay colloids in the soil and cause deterioration of soil structure. Salinity and sodium hazard was assessed using a Wilcox diagram (USDA 1954), which classifies irrigation water according to its EC and calculated sodium adsorption ratio (SAR). Figure 4.12 shows the Wilcox diagram for the average salinity and sodium hazard of groundwater from each formation in the investigation area, together with results for the single bore 13BP03I. These are shown relative to the low-risk line for the relationship between EC and SAR for sandy loams (NSW Department of Primary Industry 2014) to further classify the groundwater in terms of soil structure hazard for irrigating Cockatoo Sands.

On average, the groundwater in the Point Spring Sandstone Formation has both a low salinity and sodium hazard classification and is of low risk for the salinity/sodium combination. Although groundwater from the other aquifers has a medium salinity hazard, on average it has a low sodium hazard and is of low risk for the salinity/sodium combination. The only groundwater tested within the Point Spring Sandstone Formation that does not have both low salinity and sodium hazard is from the perched aquifer at bore 17BP03I, which is also the only site that does not have a low risk for irrigation based on the salinity/sodium combination. In each of the other formations, there are individual sites that have a medium sodium or salinity hazard.

Iron concentrations were usually very low in samples obtained from most new PVC-cased bores screened within the Point Spring Sandstone Formation. However, iron concentrations did exceed the ANZECC and ARMCANZ (2000) irrigation guidelines in shallow bore 17BP01S (2.6 mg/L) and deep bores 13BP01D (1.4 mg/L) and 18BP01DD (11 mg/L), which are PVC-cased. Both deeper bores have their screens set deep in the Point Spring Sandstone aquifer, between the shale layer and the Sunbird/Tanmurra formation. If we ignore the excessive iron levels present in some existing older steel-cased water supply bores, the mean iron concentration of the Point Spring Sandstone aquifer is 0.13 mg/L, which is below the long-term irrigation guideline.



The mean TP concentration in the Point Spring Sandstone aquifer is elevated by a single extreme value of 0.8 mg/L, recorded in bore 18BP01DD. As phosphorus and iron are present in high levels in many drilling fluids, it is possible that the elevated TP and iron levels found 18BP01DD are a result of contamination resulting from inadequate bore development during bore completion operations. If we ignore the value in 18BP01DD, the mean TP concentration of the Point Spring Sandstone aquifer is 0.03 mg/L, which is less than the 0.05 mg/L long-term guideline.



Note: The 'NSW DPI low risk line' indicates the maximum EC/SAR combination of values that provide a low risk for irrigation water applied to well- to moderate-draining soils.

Data source: adapted from NSW Department of Primary Industry (2014)

Figure 4.12: Wilcox diagram showing the irrigation salinity and sodium hazard of groundwater for the average electrical conductivity (EC) and sodium adsorption ratio (SAR) of the formations and the results for bore 13BP03I

Selenium concentration was below the LOR in every groundwater sample. However, the LOR for selenium was 0.05 mg/L for most samples (from all aquifers), which was higher than the long-term irrigation guideline concentration of 0.02 mg/L.

#### 4.5.4 Spring water physicochemistry

The water quality results for the samples of groundwater collected directly from the spring discharges (contained in Appendix J) was compared to the Water Quality Australia (2019) guidelines for toxicants and chemical or physical stressors for high conservation or ecological value wetlands in tropical Australia.

Spring water samples were generally good quality, mostly within the guideline values for slightly disturbed wetland systems. Spring source waters had an average temperature of 23.1 °C. EC values were low (range 2.9–72.6 mS/m). The Tanmurra Creek and Tanmurra Pool spring sites, located over the calcareous Ningbing Group aquifers, had pH values of 8.1 and 8.0, respectively – slightly higher than or equal to the maximum recommended in the guidelines. Springs located over sandstone aquifers were generally more acidic (pH range 6.2–7.4), although were all within the guideline range.

Garimala Creek, Long, New, Yow and Domett Road springs had low DO levels (range 0.4–25.3%), consistent with their source being relatively deep groundwater. All springs had TP concentrations within 0.005–0.026 mg/L. These values are equal to, or exceed, the guideline value by factors of between 1.1 and 2.6, respectively. Soluble reactive phosphorus (SRP) was 4 times higher than the guideline value in Oaks Creek Spring and Long Spring (both 0.02 mg/L), and less than or equal to the guideline value elsewhere. TN concentration exceeded the guideline by a factor of 1.2 and 2.8 in New Spring (0.41 mg/L) and Long Spring (1.0 mg/L) respectively, while ammonium nitrogen ( $\text{NH}_4\text{N}$ ) was twice as high as the guideline concentration in Tanmurra Pool and Bore Spring Upper (both 0.02 mg/L).

Trace element and metal concentrations were very low or below the LOR in each of the springs sampled. No samples of spring discharge water contained metals in concentrations that exceeded the guideline toxicant values for the 99% level of species protection.

All springs also had water qualities that would be suitable for irrigation when compared to the ANZECC and ARMCANZ (2000) guidelines for long- and short-term irrigation.

#### 4.5.5 Major ion proportions

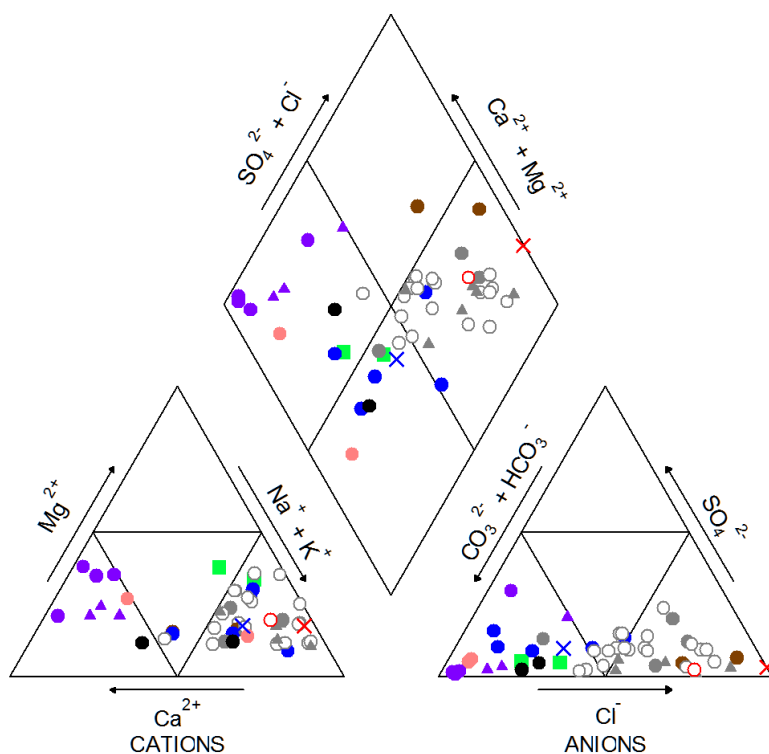
The Piper plot in Figure 4.13 classifies the rain, groundwater, spring and lake water samples in terms of major ion proportions from the different sample sources across the investigation area. Piper plots display the relative proportions of the major ion groups but not the absolute values – these are provided in Appendix J. For comparison, Figure 4.13 also shows the ionic proportion classification for local rainfall and seawater.

The rainfall samples are low in all major ions, having mixed cation and anion compositions and therefore plot near the centre of the trilinear plot. Because the collection site is relatively near the ocean, the absence of Na and Cl dominance is perhaps surprising and indicates that marine aerosols may not always be the major contributor to the ion balance of the rainfall (Meredith et al. 2018).

In combination, the major ion chemistry of all groundwater and spring sources plot across the trilinear plot. However, water types also group according to geologic formation.

Bores screened within the Ningbing Group formations and Sunbird/Tanmurra formations group as calcium + magnesium cation and carbonate anion dominated water types, as does the water from the springs located over Ningbing Group formations. Groundwater and spring water from within the Point Spring Sandstone Formation, although variable, have sodium + potassium and chloride-dominated water types with minor calcium, magnesium and carbonate. The single groundwater sample obtained from within the upper Milligans Formation (Tanmurra Bore, 70 m deep) also has similar major ion proportions to the Point Spring Sandstone Formation groundwater sources. Groundwater from within the Keep Inlet Formation tends to be sodium + potassium and carbonate dominant. Groundwater from the shallow northern coastal Quaternary alluvium is sodium and chloride dominant. Groundwater from the shallow northern coastal Quaternary alluvium is sodium and chloride dominant.

Samples from the 2 intermittent lakes have mixed cation and anion compositions. The lake waters plot very close to local rainwater, near the centre of the trilinear plots.



#### Legend

- Bore: inlet within upper Point Spring Sandstone Formation
- Bore: partially-cased artesian flow derived from underlying upper Point Spring Sandstone Formation
- ▲ Groundwater spring: Point Spring Sandstone Formation
- Bore: inlet within lower Point Spring Sandstone Formation
- Bore: inlet within Keep Inlet Formation
- Bore: inlet within Sunbird/Tanmurra Formation
- Bore: inlet within Ningbing Group
- ▲ Groundwater spring: Ningbing Group
- Bore: northern coastal alluvium
- Bore: Milligans Formation
- NW and SE lakes
- × Bonaparte rainfall
- × Seawater

Figure 4.13: Piper plot classifying groundwater according to major anion and cation composition for the bores, springs and lakes within the Bonaparte Plains investigation area

#### 4.5.6 Lake water physicochemistry

Water samples collected from the intermittent NW Lake and SE Lake had similar field- and laboratory-derived physicochemistry results (Appendix J). Both had temperatures around 27 °C, a near neutral pH of 6.9, and relatively high DO concentrations (91% in NW Lake and 80% in SE Lake) indicating an oxygenated, surface water environment.

NW Lake and SE Lake were very fresh, having an EC of 3.6 mS/m and 2.9 mS/m, respectively. The total dissolved solid (TDS) concentrations were accordingly also very low (21 mg/L and 16 mg/L), as were sodium (3.4 mg/L and 1.7 mg/L) and chloride (4 mg/L and 2 mg/L) concentrations. These salinity-related parameters are only marginally higher than those recorded in the local rainwater.

Some nutrient-related chemical parameters were elevated in both lakes when compared to the Water Quality Australia (2019) guidelines for aquatic stressors. TP was 0.017 mg/L in NW Lake and 0.026 mg/L in SE Lake, although both lakes had an SRP concentration that was below the LOR and the guideline value. TN was 0.82 mg/L in NW Lake and 0.87 mg/L in SE Lake – about 2.5 times the guideline concentration – while the ammonium nitrogen ( $\text{NH}_4\text{N}$ ) concentration of 0.02 mg/L in both lakes was twice the guideline concentration.

Trace element and metal concentrations in the lakes were very low, with most metals analysed as below the LOR and all below the Water Quality Australia (2019) guideline toxicant values for the 99% level of species protection.

#### 4.5.7 Isotope and gas tracer results

The results of the analysis for the water isotopes  $^{18}\text{O}$ ,  $^2\text{H}$  and  $^3\text{H}$  in the rainfall, spring and groundwater samples are shown in Appendix J. The stable isotope  $^{18}\text{O}$  and  $^2\text{H}$  ratios ( $\delta^{18}\text{O}$  and  $\delta^2\text{H}$ ) in the two 2017 dry season rainfall samples were 1.41 parts per thousand (‰) and  $-2.30\text{‰}$ , respectively. These values are much higher than the mean  $\delta^{18}\text{O}$  and  $\delta^2\text{H}$  values of  $-4.8\text{‰}$  and  $-26.3\text{‰}$ , respectively, recorded in the 2015–2016, 2016–2017 and 2017–2018 wet season samples. Considering relative rainfall quantity, it is unlikely that the dry season results represent much or any groundwater recharge.

The mean  $^3\text{H}$  activity was 1.61 TU (tritium unit; range 1.44–1.75,  $n = 4$ ) and was similar in wet and dry season rainfall samples.

For spring discharge water samples, the  $\delta^{18}\text{O}$  values range from  $-4.31\text{‰}$  (Yow Spring) to  $-7.48\text{‰}$  (New Spring) with an average of  $-6.52\text{‰}$  ( $n = 5$ ), and the  $\delta^2\text{H}$  values range from  $-34.3\text{‰}$  to  $49.6\text{‰}$  with a mean of  $-44.9\text{‰}$  for the same sites. The spring samples had relatively low  $^3\text{H}$  activities, ranging from 0.04 TU (Bore Spring) to 0.15 TU (Yow Spring) (mean = 0.05,  $n = 5$ ).

The  $\delta^{18}\text{O}$  values of the 35 groundwater samples obtained from bores range from  $-6.65\text{‰}$  (Lewis) to  $-9.02\text{‰}$  (17BP06S) with a mean of  $-7.73\text{‰}$ . The  $\delta^2\text{H}$  values range from  $-43.2\text{‰}$  to  $-61.8\text{‰}$  across the same samples. The  $^3\text{H}$  activities range from below quantification to 1.00 TU (17BP06S) with a mean of 0.23 TU ( $n = 24$ ), all much lower than the mean rainfall value of 1.6 TU.

The piston flow recharge dates, derived from the CFCs and  $\text{SF}_6$  analyses and based on the southern hemisphere atmospheric air concentrations, for the spring and shallower

groundwater samples are shown in Appendix J. Excluding the results for Yow and Bore Springs (which the staff at the ANSTO laboratory considered likely to be contaminated by atmospheric input), the range of resultant dates for the springs are 1970–1982 for CFC-11, 1975–1990 for CFC-12 and 1995–2018 for SF<sub>6</sub>. For the shallow groundwater samples, the range of piston flow recharge dates are 1958–1977 for CFC-11, 1959–1983 for CFC-12 and 1974–1997 for SF<sub>6</sub>.

The uncorrected results for the <sup>14</sup>C<sub>DIC</sub> analyses on spring and groundwater samples are in Appendix I. The <sup>13</sup>C ratios are also reported – as calculated from the concentration of <sup>13</sup>C measured in the sample analysed for <sup>14</sup>C<sub>DIC</sub> and normalised to a δ<sup>13</sup>C value of –25‰. Spring waters had high <sup>14</sup>C<sub>DIC</sub> values, ranging from 89.11 per cent modern carbon (pMC) at Long Spring to 94.4 pMC at Yow Spring, with the mean for all springs being 94.4 pMC (n = 5). The high proportions of modern carbon indicate that the spring waters are likely to be modern.

Groundwater <sup>14</sup>C<sub>DIC</sub> values sampled from bores were more variable. They ranged from a modern value of 115.16 pMC in 17BP02S (near the central part of the investigation area), to a palaeowater value of 4.2 pMC in Cleanskin bore (in the Keep Inlet Formation to the east). The mean groundwater <sup>14</sup>C<sub>DIC</sub> value of all bores and for all geologies is 75.75 pMC (n = 35).

The complete hydrochemistry data were provided to the ANSTO for further data analysis, modelling, and reporting of the origin and rate of recharge, corrected groundwater ages and residence times spatially across the investigation area. Appendix C contains ANSTO's reports of additional analyses of groundwater mean residence time, age and estimated recharge rates using CFC and SF<sub>6</sub> concentrations, <sup>3</sup>H activity and radiocarbon (Meredith et al. 2018).

#### 4.5.8 Recharge estimation

The chloride mass balance (CMB) method (Allison and Hughes 1978) uses meteoric chloride input as a conservative tracer for estimating the rate of recharge to an aquifer system, whereby the mean annual recharge rate is estimated by the calculation,  $Rr = P \times Clp/Clgw$ , where  $Rr$  = the annual rate of recharge (mm/y),  $P$  = the annual rainfall (mm),  $Clp$  = the concentration of chloride in rainfall (mg/L),  $Clgw$  = the chloride concentration (mg/L) in groundwater.

The average annual chloride concentration in the rainfall collected between 2015 and 2018 at the Bonaparte weather station was 1.3 mg/L. An annual rainfall of 1,209 mm was used for the CMB calculation, derived from the total of the medium term (1993–2018) average annual rainfall at FWI (1,004 mm; see Section 2.2) and the average difference between the annual rainfall recorded at FWI and at Bonaparte over the 3 years of observation (205 mm; see Section 4.1).

Table 4.9 lists the estimated recharge rates calculated from the chloride concentrations in the Point Spring Formation groundwater sampled from bores and permanent springs. The mean estimated rate of recharge within the Point Spring Sandstone Formation is 112 mm/y. There is large variability (18–393 mm/y) in the estimated recharge across the sample sites. There is also large variability in the estimated recharge between different depths, with most shallow bores having lower estimated recharge than their deeper counterparts. For example, the estimated recharge rate at site 17BP01 is



61 mm/y in the shallow bore (17BP01S) and 121 mm/y in the deeper bore (17BP01I). If the mean recharge is calculated using only the highest estimated rate at each site, the mean rate of recharge is 128 mm/y ( $n = 19$ ).

Table 4.10: Rates of recharge estimated using the CMB method on groundwater sampled from bores and springs containing Point Spring Formation groundwater

Site name	Estimated recharge (mm/y)
13BP01D	92
13BP01PB	54
17BP01I	121
17BP01S	63
17BP01PB	112
18BP01DD	83
17BP02I	87
17BP02S	54
17BP03I	18
17BP04I	45
17BP04S	48
17BP05I	48
17BP05S	40
17BP05PB	49
17BP06I	121
17BP06S	175
17BP07I	63
Bonaparte1 water bore 1	393
Bonaparte2 water bore	225
CGDH5 Fishermans	79
CGDH6 New Attack	92
CGDH7	87
CGDH8 Kemp	131
Hotplate	83
Oaks Creek	157
Bore Spring	175
Garimala Creek Spring	112
New Spring	196
Oaks Creek Spring	157

## 5 Discussion

### 5.1 Local climate

Based on the climate data collected, the Bonaparte Plains area has higher rainfall and humidity, and lower solar radiation and evaporation than the areas of established agriculture near Kununurra. Important seasonal climatic differences between the Bonaparte Plains and the Kununurra area include warmer minimum temperatures and higher humidity in the dry season, with a cooler, more humid wet season.

The observed differences are consistent with the Bonaparte Plains being north of Kununurra, closer to the tropics, and bounded by the Joseph Bonaparte Gulf on 3 sides. These geographical factors could contribute to the observed higher wet season rainfall, humidity and warmer dry season minimum daily temperatures.

Consistent with the higher wet season rainfall recorded is the general observation made by long-term residents of the Kununurra area that afternoon thunderstorms and associated cloud cover occur more consistently over the Bonaparte area during the September to December wet season 'build-up' period. When we stayed in the 2 areas from July to November 2017, we observed that early morning dews and mists occurred more regularly on the Bonaparte Plains than in the Kununurra area, consistent with the higher humidity recorded by the climate station.

The observed differences in climate will be important considerations for managing agricultural crops grown in the Bonaparte area. For example, higher daily minimum temperatures will be an advantage for the growth and seed set of some types of annual crops but a disadvantage for some types of perennial fruit species, while higher humidity will increase the risk of fungal disease in some crop types.

The observed higher wet season rainfall, combined with good drainage properties of the Cockatoo Sands, means that the area may be more suitable for dryland cropping than the established areas around Kununurra.

However, 3 years of data is a relatively short time for making reliable predictions about the long-term climate differences between Bonaparte Plains and Kununurra. For this reason, we recommend that climate monitoring continue in the area to more robustly assess the climatic factors that may affect the suitability of various prospective crops and growing systems.

Longer-term rainfall records collected at nearby locations show a distinct increasing trend in annual wet season rainfall in the area since the mid-1990s (Figure 2.4). The increasing rainfall correlates with the persistent rise in groundwater level recorded under the Cockatoo Sands, such as at site 13BP01 (Figure 4.3) over 5 years of observation. George et al. (2011) also found that that significant additional recharge since 1993 had caused the observed watertable rise under the nearby Weaber Plains area (Figure 1.1).

Our observations that the size of natural permanent springs have grown in recent years also indicate an increase in groundwater discharge, presumably driven by a corresponding increase in recharge to the Point Spring Sandstone Formation over several years.

CSIRO (2009) reports a statistically significant 26% average increase (range 10–60%) in annual rainfall across the Ord–Bonaparte region during the 1996–2005 period. CSIRO (2009) also modelled 3 sequences of future climate (to 2030) under high, medium and low global warming, which corresponded to wet (9% rainfall increase), mid (1% increase in rainfall) and dry (13% decrease in rainfall) scenarios.

## 5.2 Hydrostratigraphy

Tan et al. (2018) proposed a series of spatial layers of AEM-derived elevations corresponding to the upper surfaces of HUs in the area. As discussed in Section 2.3.4, we found several inconsistencies with these layers and thus reviewed them. Twelve representative cross-section alignments were selected, along which the AEM-derived layer elevation data were extracted. The layer elevation data were then reviewed and modified, as required, using a combination of the AEM data, lithology from drilling logs, hydrological and hydrogeochemical data, mapped geology of the area, and our hydrogeological experience. The modified cross-sections were then used to construct new hydrostratigraphic layers by interpolating layer elevation data between the revised cross-sections, including the consideration of mapped fault locations.

The high surface conductivity masked the AEM signal at depth beneath mudflat areas. Under the mudflats, the elevation of each hydrostratigraphic unit was extrapolated from its visible extent towards the elevation of its equivalent unit identified by Gorter et al. (2005) in the Sandbar, Pelican Island, and Kingfisher offshore petroleum exploration wells and by Cane (1969) in the Keep River1 onshore petroleum exploration well.

Table 5.1 summarises how our hydrostratigraphic units relate to the published names of the geological formations.

Table 5.1 The main geological formations and members within identified hydrostratigraphic units

Hydrostratigraphic unit	Geological formation and member
Keep Inlet	Keep Inlet Formation and thin Cainozoic alluvium, sandplains and coastal deposits
Border Creek	Border Creek Member of the Point Spring Sandstone Formation; may include some outcrop of hard rock Point Spring Sandstone Formation along the western edge
Shale	Shale unit within the Point Spring Sandstone Formation (Border Creek Member)
Sunbird/Tanmurra	Either, or a combination of, the Sunbird and Tanmurra Formations
Milligans	Milligans Formation, possibly with thin or remnant overlying Burvill, Waggon Creek, Utting Calcarenite and Yow Creek Formations
Ningbing Group	Ningbing Group Formation

Figure 5.1 shows an example of our hydrostratigraphic interpretation of the cross-sections along section 105401. The interpretations for each of the 12 cross-sections are contained in Appendix K, and their locations are shown in Figure 5.2. Layer elevation data extracted from the revised cross-sections were used to construct 3D HUs by computer interpolation, after cross-checking and adjusting some minor areas that had negative layer thickness (IGS 2019).

Figure 5.2 shows the spatial extent of the uppermost HU within the investigation area, plus the extent of the underlying Shale HU. The area of Cockatoo Sands is substantially located above areas where the Border Creek HU subcrops or outcrops and mostly coincides with the extent of the underlying Shale HU.

Our interpretation of the faulting alignment within the Border Creek HU is also shown as vertical projection to the ground surface in the cross-sections (Figure 5.1 and Appendix K). The alignment was derived by linking the locations where abrupt vertical displacements of layered conductivity features were evident across multiple AEM flight lines, guided by the alignment of linear features evident on aerial photography, plus the alignment of the faults mapped by Mory and Beere (1988) and Plumb and Veevers (1971). The locations of our interpreted faults are shown projected to the ground surface.

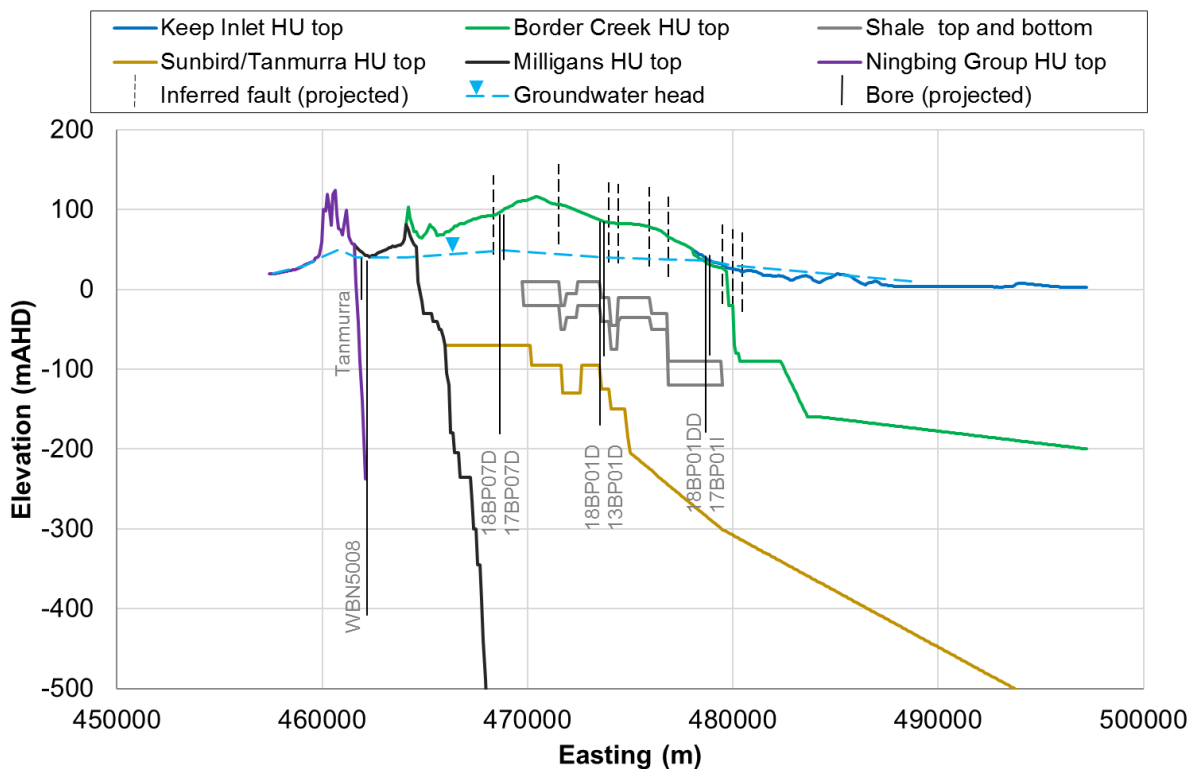


Figure 5.1: Hydrostratigraphic unit (HU) boundaries identified along cross-section 105401

### 5.2.1 Border Creek HU

The area of Border Creek HU outcrop or subcrop is about 60,000 ha. It abuts the Milligans HU along its western extent (Figure 5.2). Eastward from the margin, the saturated thickness of the Border Creek HU thickens with the dip in the Milligans HU until it overlays the Sunbird/Tanmurra HU. The saturated thickness then continues to increase eastwards and northwards where it is about 400 m and 600 m thick, respectively, at the edge of the investigation area.

Unsaturated profiles substantially occur wherever the Border Creek HU outcrops and these profiles vary in thickness from zero along the northern margin of outcrop to more than 100 m where there is elevated outcrop near the centre (Figure 5.3).

The average dip of the contact between the Border Creek HU and the Milligans HU is about 15% to the east. The contact between the Border Creek HU and the underlying Sunbird/Tanmurra HU dips 1.6% towards the east and 3.8% towards the north. The average dip in the contact between the upper surface of the Border Creek HU and the lower surface of the Keep Inlet HU, where present, is about 1.4% to the east and about 3% to the north.

Across the central part of the investigation area, the Border Creek HU appears to be divided into an upper unit and a lower unit, separated by the low-permeability Shale HU. The Shale HU is not present throughout the entire Border Creek HU, suggesting that the shale was deposited in a relatively localised low-energy environment, such as a terrestrial lake, swamp or small intertidal estuary of defined extent.

The shale is disrupted at regular intervals by faulting as it dips towards the east and north. The pattern of faulting, which has resulted in an average dip in the Shale HU of about 1.4% towards the east and north, suggests a series of displacements that may be associated with the late Carboniferous to early Permian period of broad folding of the Weaber Group sediments (Mory and Beere 1988). Palynology analysis of the Shale HU material indicates an age of 316–327 million years before present (Bennett 2019), which means it was deposited before the folding of the Weaber Group commenced.

Although not specifically tested in this investigation, there are indications that the Shale HU has a relatively minor influence on the hydrological properties of the Border Creek HU at the landscape scale. For example, the difference in head between bores screened above and below the shale at site 13BP01 is only 0.63 m of upward gradient across 74 m of vertical screen separation, while at 17BP01 there is only 1.14 m of upward head across 90 m of vertical separation. The age of the groundwater in the upper and lower sections of the aquifer are also similar (sub-modern; 100–500 y) at site 13BP01 (Meredith et al. 2018).

There is the potential for rainfall to directly recharge the lower sections of the aquifer across the substantial areas where the underlying shale is absent. Faults are common within the shale, often having offsets larger than the thickness of the shale and therefore providing zones that allow groundwater exchange between the upper and lower aquifers. Because broad folding events caused the faulting (Mory and Beere 1988), it is likely that even faults with smaller offsets contain a mixture of sandy and clastic lithologies derived from above or below the shale, and also provide conduits for groundwater flow. During calibration of their water balance model for the area, IGS



(2019) found that it was necessary to increase the hydraulic conductivity of the Shale HU, to equal that of the Border Creek HU, along some fault zones to improve model calibration. For example, without factoring an increase in hydraulic conductivity along a nearby fault zone, IGS found that modelling simulated several metres of downward hydraulic gradient, instead of the slight upward gradient, observed at site 13BP01.

Throughout the Border Creek HU, groundwater age was found to be modern (<100 y) to sub-modern (Figure 5.4), indicating active recharge is occurring in this unit. At all sites where there were shallow and deep bores installed, the age of the groundwater is modern, whether sampled from near the watertable surface or from deeper in the unit. The discharge from the springs near the boundary of the Border Creek HU and the Keep Inlet HU is all sub-modern age, slightly older than the modern aged groundwater in the nearest bore located higher up the groundwater gradient and screened within the Border Creek HU.

### 5.2.2 Keep Inlet HU

Most of the area of the Late Carboniferous to Permian aged Keep Inlet HU outcrop or subcrop (Figure 5.2) is fully saturated or has groundwater heads near the ground surface (Figure 5.3). Areas of higher elevation in the south-west of the unit plus isolated sandy rises of Cainozoic alluvium can have up to about 20 m of unsaturated material at their surface. The Keep Inlet HU unconformably laps onto the Border Creek HU along its western extent. On the margins of the investigation area the Keep Inlet HU can be up to 500 m thick.

The Keep Inlet HU comprises multiple and variable beds of sandstones, mudstones, shales, and conglomerate (Cane 1969, Barnes and Lee 1984, Williams 1982). As the beds were deposited in a combination of continental, shallow marine and glaciomarine environments, it is unlikely that unique layers are laterally extensive. Like Williams (1982), we also could not identify unique spatially consistent layers from the lithostratigraphy in the series of coal exploration bores along the northern mudflats.

All stock water bores within the Keep Inlet HU are low yielding. Higher-yielding layers could be present, although no formal aquifer testing has been done. For example, drilling data recorded on the *Water Information Recording* database (Department of Water 2013) indicate that airlift yields of about 25 L/s from sandy layers resulted in deep rotary-air blast exploration drilling being abandoned at 3 sites in the central area of the Keep Inlet HU (near Wilson bore; Figure 2.12).

Available drilling logs indicate that fine-textured beds of mudstone and siltstone always confine higher-yielding aquifer layers. As the groundwater heads are mainly equivalent to or above the ground surface and the low-permeability confining layers are likely to only allow insignificant rates of vertical leakage, there is limited potential for deep recharge to higher-yielding layers. Rates of recharge calculated from mean residence time and carbon-14 dating for groundwater from each bore screened within the Keep Inlet HU range between only 0.5 and 6 mm/y (Meredith et al. 2018; Appendix C). Groundwater is quite stagnant, having corrected  $^{14}\text{C}$  ages that range from 1,300 y at CGDH8 Kemp bore to 22,800 y at Cleanskin bore (Meredith et al. 2018; Appendix C). There is a general increase in groundwater age, with distance along the potentiometric gradient, away from the Border Creek HU subcrop and outcrop (Figure 5.4).

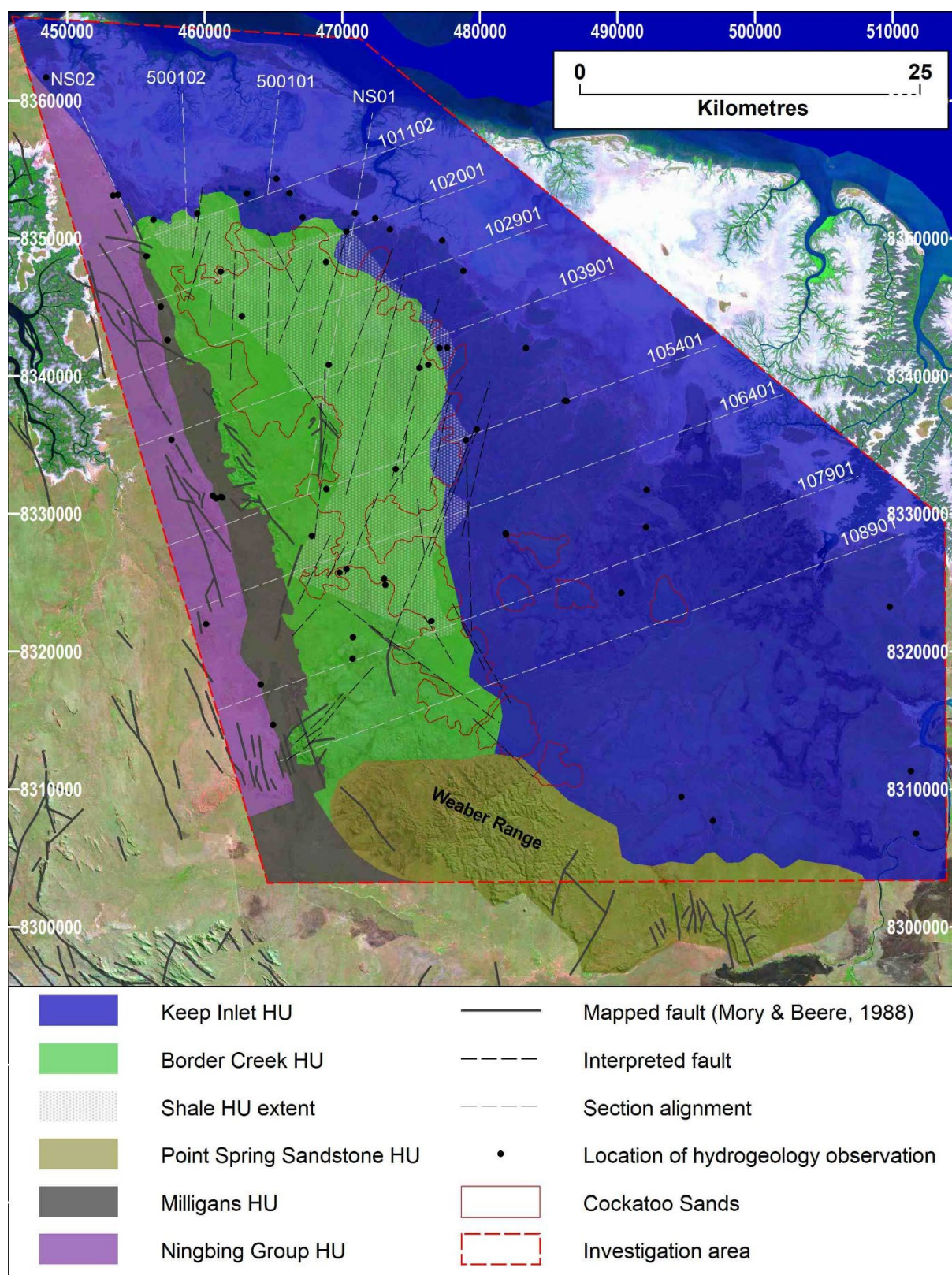


Figure 5.2: Extents of the uppermost HUs and the underlying Shale HU



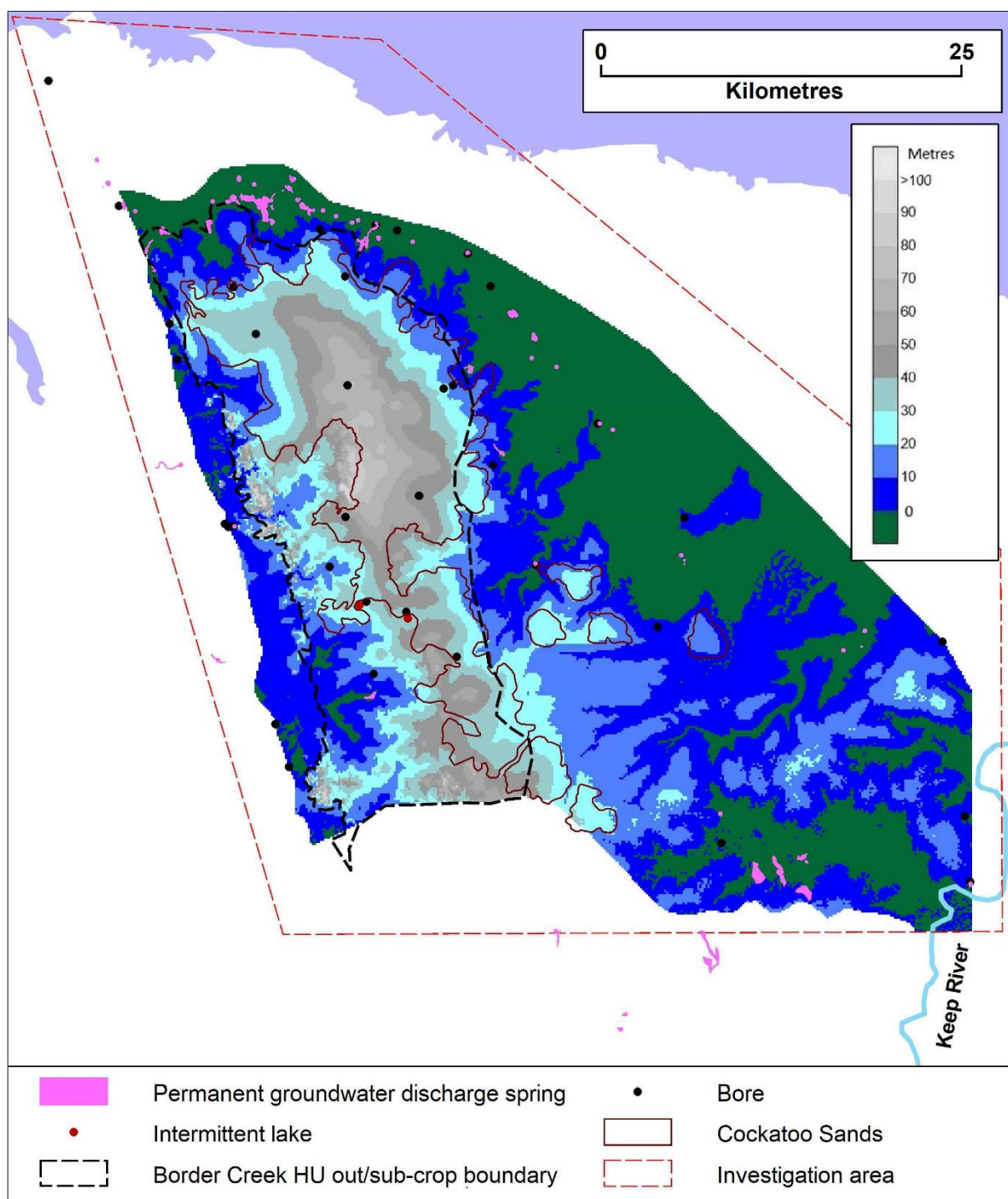


Figure 5.3: Groundwater head relative to ground surface

Although useful for obtaining small volumes of fresh groundwater, the higher-yielding sandstone layers in the Keep Inlet HU will generally have limited sustainable capacity to supply the high volumes of water required for long-term, broadscale irrigation developments. There is potential for sustainable higher yields from coarser layers within the Keep Inlet HU provided they have sufficient, continuous hydraulic connection with the Border Creek HU aquifer, through the interface of the 2 units. However, the probability of finding a bore site to intersect a suitable aquifer that is also well connected to the Border Creek HU is likely to markedly reduce with increasing distance from the interface and would require specific testing at any chosen location.

### 5.2.3 Sunbird/Tanmurra HU

Although Nugent (1989) indicates that the equivalent Tanmurra Formation outcrops at Garimala petroleum exploration well, we could not distinguish Tanmurra Formation in outcrop in the area or anywhere along the eastern edge of the Milligans subcrop. At the Garimala well site, Nugent attributes the upper 249 m of the profile to Tanmurra Formation, although did not report any palynology information to confirm its age. Nugent describes the upper 105 m of the profile at Garimala well site as fine- to very coarse-grained, unconsolidated sandstone, which is a description that aligns better with Point Spring Sandstone Formation than Tanmurra Formation. Nugent describes the 105–249 m interval as being mostly carbonaceous sandstone interbedded with siltstone, which aligns better with other descriptions of the lithology of the Tanmurra Formation.

We were not able to distinguish the Sunbird/Tanmurra HU in the AEM conductivity profiles near the Garimala site and therefore assigned the upper formation in this area to the Border Creek HU.

The equivalent Tanmurra Formation is 190 m thick at Bonaparte1 oil well (LeBlanc 1964) and 295 m thick at Bonaparte2 oil well (LeBlanc 1965). At both sites, LeBlanc describes the Tanmurra Formation as being a fine- to medium-grained calcareous, dolomitic or argillaceous sandstone unit. However, throughout the profile LeBlanc also describes it being regularly interbedded with various combinations of shale, siltstone, fine to silty limestone, recrystallised carbonate, arenaceous calcarenite, dolomite and oolite layers. Inferred and measured porosities appear highly variable in the various layers in the 2 oil wells. LeBlanc recorded that porosity was less than 4% in the finer-textured beds and was up to 30% in sandstone beds. However, in contrast to the high vertical and horizontal permeability within the Point Spring Sandstone Formation, LeBlanc noted that measurements of permeability from cores of Tanmurra Formation sandstones had up to 100 times less vertical and horizontal permeability. On this basis, he concluded that the common limestone-rich sandstone members in the Tanmurra Formation ‘are essentially tight’ (LeBlanc 1964:28).

Our observations of drilling cuttings from Sunbird/Tanmurra HU at the bore sites drilled by Geoscience Australia (18BP01D and 18BP07D) also indicate a generally low-permeability formation, given the thick sequences of calcareous clays, shales, and siltstones present within the 300 m depths reached. Groundwater heads in these bores, screened within the Sunbird/Tanmurra HU, also have upward gradients towards the Border Creek HU (Table 4.3). The modelled radiocarbon age of groundwater in the Sunbird/Tanmurra HU from bore 18BP01D is 4,600 y. This age is much older than the sub-modern age in the adjacent 13BP01D, screened within the Border Creek HU at 156–158 mBGL, and the modern to sub-modern age of groundwater generally in the Border Creek HU (Figure 5.4).

Based on lithology, groundwater head and groundwater age information, we conclude that the Sunbird/Tanmurra HU forms a low-permeability base to the Border Creek HU aquifer.

#### 5.2.4 Milligans and Ningbing Group HUs

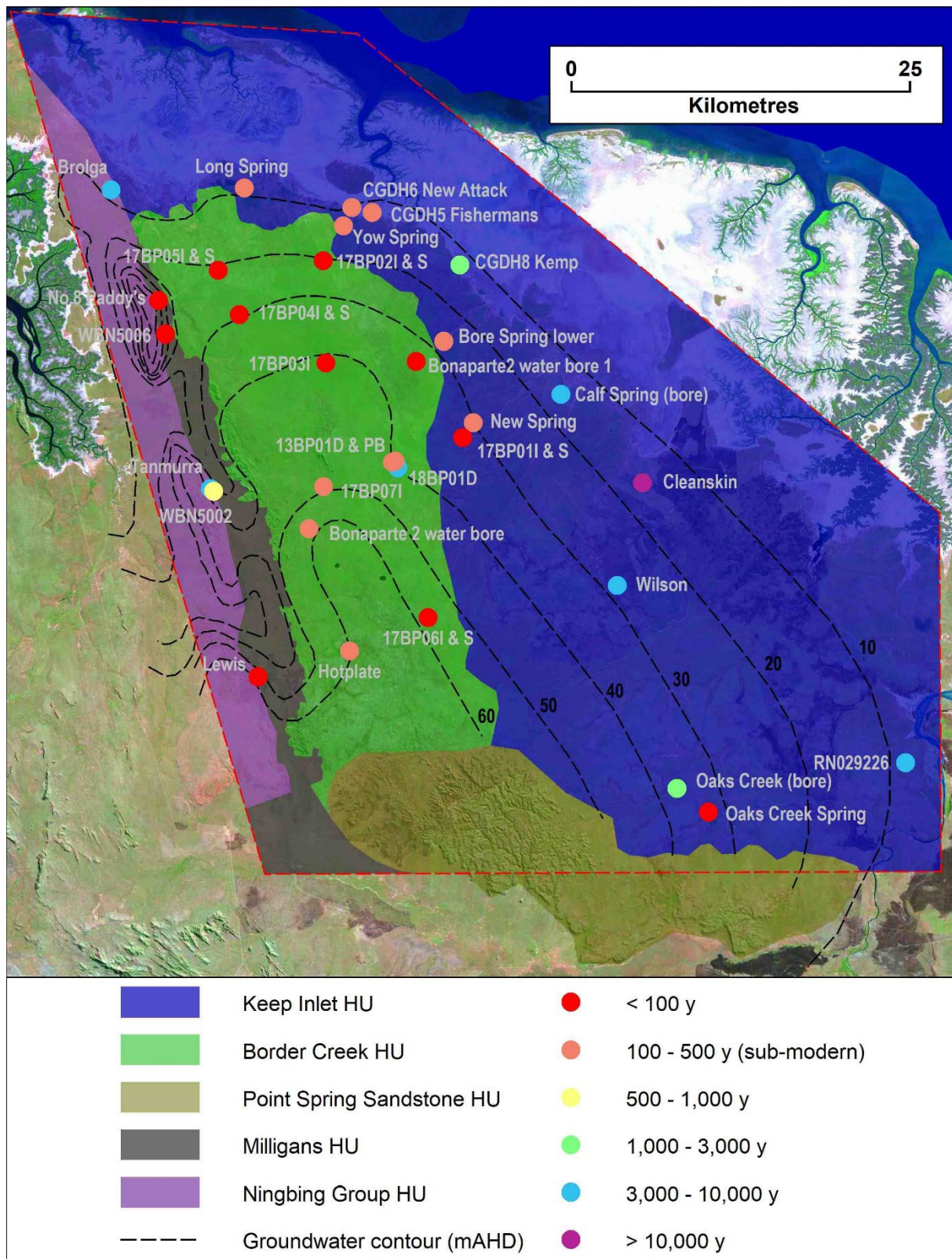
The fine-grained siltstones, mudstones, and shales of the Milligans Formation provide a substantial low-permeability barrier to groundwater flow out of the Border Creek HU to the west. Groundwater sampled from Tanmurra bore (Figure 5.4), a low yielding, 70 m deep, stock water supply bore screened in the Milligans Formation, had a corrected  $^{14}\text{C}$  age of 4,600 y and a very low estimated recharge rate of 3 mm/y (Meredith et al. 2018; Appendix C), indicating that groundwater within this unit is old and essentially stagnant. The Milligans HU subcrop has a vertical thickness of at least 500 m, the maximum depth to which the AEM data were processed (Figure 2.10). Under onshore areas east of the subcrop, petroleum exploration drilling logs show that the thickness of the Milligans Formation varies between 992 m (Garside 1982) and 2,142 m (Cane 1969).

The observed large and dynamic water level response to rainfall in bores screened deep within the Ningbing HU (Figure 4.4) indicates that the limestone aquifer has low storativity but relatively high hydraulic conductivity. The final corrected  $^{14}\text{C}$  age of Ningbing HU groundwater sampled from Lewis, No. 8 Paddys and WBN5006 bores is less than 100 y, indicating the aquifer has rapid turnover of groundwater at these locations. Groundwater from the Ningbing HU bore (WBN5002) has a  $^{14}\text{C}$  age of 900 y, much younger than the groundwater from the adjacent Milligans HU Tanmurra bore, even though it is substantially deeper.

The chemical composition and relative proportions of the major ions in Ningbing HU groundwater is quite different to those from the other HUs, providing further evidence that the Ningbing HU aquifer is a separate groundwater system.

It is unlikely that there is any significant groundwater flow from the Border Creek HU through the Milligans HU to the Ningbing HU. The steeper hydraulic gradient, different groundwater responses to rainfall, different geochemical signatures and opposing hydraulic gradients in some locations all show there is poor hydraulic connection across the boundary. Although some groundwater could flow across the Milligans HU in areas where there is a consistent small westward gradient through the shallow, coarser alluvium covering the Milligans Formation subcrop, the alluvium is thin and therefore would have low transmissivity. Along the Border Creek HU/Milligans HU boundary, nearly all groundwater flow from the Border Creek HU is likely to be captured as baseflow into the incised surface drainages that have their origins aligned to the contact between the 2 formations. This water is then transmitted across the Milligans and Ningbing HUs by the 3 creeks that flow west to the coast through the breaks in the Ningbing Range (Figure 2.1).





Source of groundwater ages: Meredith et al. (2018)

Figure 5.4: The spatial distribution of the corrected radiocarbon ages compared to hydrostratigraphic unit (HU) outcrop or subcrop and groundwater head contours

### 5.3 Groundwater within the Border Creek hydrostratigraphic unit

In terms of the likelihood of obtaining groundwater resources to supply irrigated agriculture on the Cockatoo Sands, the Border Creek HU is the prospective hydrostratigraphic unit within the investigation area. The Border Creek HU:

- is extensive, with a relatively large area that is exposed to direct recharge
- has very good quality water that is highly suitable for irrigation
- has a shallow watertable, particularly around the edge of the area of the agriculturally suitable Cockatoo Sands
- is a reasonably thick (>100 m) aquifer
- is mainly moderately to poorly consolidated sandstone from which reasonable pumping yields can be obtained.

#### 5.3.1 Rainfall recharge

Meredith et al. (2018) used the concentration of DO, silica and tritium in groundwater to confirm that the elongated central groundwater mound, largely corresponding to the area of Cockatoo Sands and the Border Creek HU outcrop (Figure 4.2), was the main source of recharge for the Border Creek HU. Due to the young age of most groundwater, reliable estimation of recharge using corrected groundwater age and mean residence time (MRT) data was not possible for most Border Creek HU groundwater samples.

Meredith et al. (2018) noted a general decrease in the rate of recharge occurring radially away from the area of Cockatoo Sands, although this was largely based on the recharge rates estimated from corrected groundwater age and MRT analysis of data obtained from the much older groundwater contained in the Keep Inlet HU.

Direct recharge is likely to occur over most of the area of Cockatoo Sands and Border Creek HU outcrop. Hydrographs of bores completed in the Border Creek HU indicate that the deep unsaturated zone located over the more elevated areas attenuates recharge responses in this area (Figure 4.3).

Recharge in the area is also likely to be spatially and temporally variable because of large annual rainfall variability and locally variable paths and intensities of the tropical storms that contribute most of the rainfall. The distribution of Cockatoo Sands can be considered an indication of an area of likely high groundwater recharge. However, its physical characteristics are variable across the study area (Smolinski 2019), as are the characteristics of the underlying material (Bennett 2019). Furthermore, areas of Border Creek HU outcrop that are outside the mapped Cockatoo Sands extent also have characteristics that are likely to allow significant recharge; these areas also have variable physical characteristics.

Recharge rate estimates based on CMB or other environmental tracer approaches provide a guide to the potential range in recharge rates. Using the CMB method estimations of recharge in the deepest bores (as listed in Table 4.9), combined with the spatial distribution of the major regolith characteristics that we consider likely to influence recharge rates, we conceptually defined 3 recharge zones over the Border Creek HU (Figure 5.5) and assigned rates of recharge to them (Table 5.2).

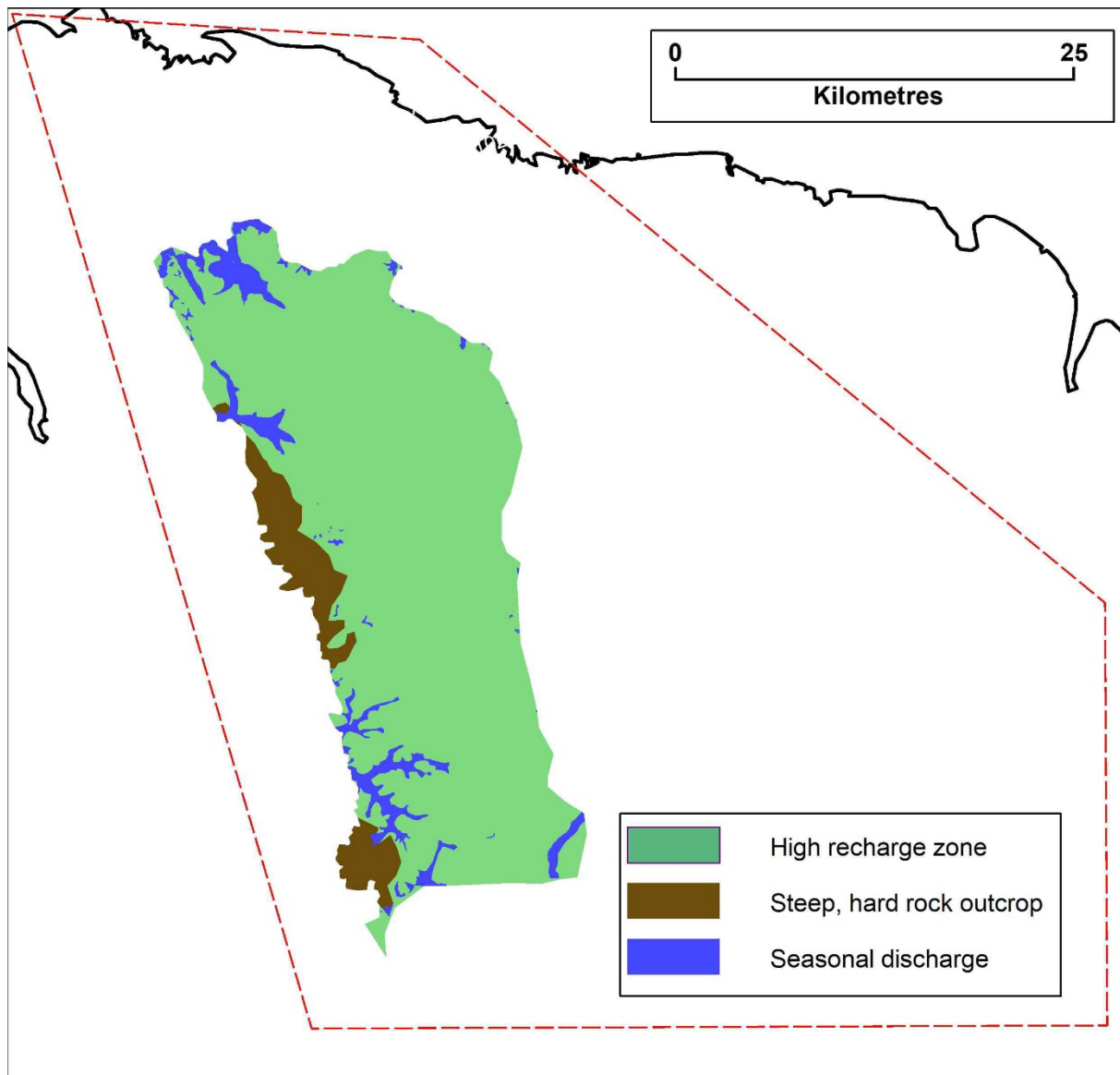


Figure 5.5: Conceptual rainfall recharge zones for the Border Creek HU aquifer

The high recharge zone encompasses the Cockatoo Sands and other sandy soils, such as the extensive areas of deep, dry Pago sands and other sandy to loamy textured soils (Smolinski 2019). In this zone, we estimate the mean rate of recharge to be 128 mm/y, calculated from the mean of the CMB results for deeper bores.

Limited published empirical data exists for rates of recharge for Cockatoo Sands under native vegetation. Using the CMB method, Bennett et al. (2016) estimated that recharge under areas of uncleared Cockatoo Sands close to Kununurra was 110 mm/y, based on the mean of values from 11 deep bores. The slightly higher recharge rate on the Bonaparte Plains is plausible given the higher annual rainfall recorded, compared to that recorded in the Kununurra area.

Over the area (about 50,330 ha), 128 mm/y equates to about 64 GL/y of recharge (Table 5.2).

Although there are no bores within the steep, hard rock outcrop areas to allow site-specific estimation of recharge beneath them, we assume they are likely to have a



lower rate of recharge than the rest of the Border Creek HU. Similarly, areas of seasonal seepage are likely to have a lower rate of recharge than the permanently unsaturated areas. We estimate that net recharge could be about 60 mm/y for the rocky or seasonally wet areas, which make up about 8,000 ha, equivalent to 14% of the Border Creek HU recharge area.

Because the Border Creek HU is confined under the Keep Inlet HU and the mudflats, we consider that recharge to the Border Creek HU is negligible.

Based on our recharge estimations, recharge likely contributes about 69 GL/y of groundwater to the Border Creek HU aquifer (Table 5.2).

Table 5.2: Details of conceptual rainfall recharge zones for the Border Creek HU

Recharge zone	Recharge rate (mm/y)	Area (ha)	Annual recharge (GL)
High	128	50,330	64
Steep, hard rock outcrop	60	4,275	3
Seasonal discharge	60	3,814	2
<b>Total</b>	NA	<b>58,292</b>	<b>69</b>

NA = not applicable

### 5.3.2 Discharge from springs

#### Permanent springs

To the north and east of the Cockatoo Sands, groundwater from the Border Creek HU aquifer discharges upslope of the tidal mudflats through well-defined permanent springs (Figure 4.5), otherwise it is confined by the mudstone layers of the upper Keep Inlet Formation around the lower slopes at Bonaparte Plains. No evidence of active or passive discharge was found on the tidal mudflats or along the low tide mark despite active efforts to do so.

Adjacent to the Milligans HU boundary to the west, the unconfined Garimala Creek Spring is the only permanent surface discharge from the Border Creek HU. The other western permanent springs discharge groundwater from the Ningbing HU aquifer or from the shallow alluvial sequences of the Milligans HU at very low rates.

The limited estimates made of discharge rates from the springs range from 0.5 to 400 L/s and appeared to vary with seasonal climatic conditions, presumably in response to changes in rainfall and evapotranspiration from their dense vegetation cover.

Evidence that some of the Border Creek HU springs had grown in recent years probably indicates a corresponding increase in their rate of discharge. This is likely to be in response to increased groundwater head within the aquifer, such as observed at site 13BP01, in response to increases in rainfall observed in the Kununurra area since 1993.

In addition to the estimated 2 GL/y (62 L/s from Table 4.4) combined dry season outflow from some springs, the permanent surface discharge from the Border Creek HU is

mostly contained within 403 ha of permanently wet areas during the dry season (Section 4.3.3).

If the rate of aquifer discharge to the spring zones is assumed constant during the year, we can approximate their combined total annual rate of discharge by multiplying the total area that is permanently wet by the annual pEt. Assuming a pEt of 1,774 mm/y (Section 4.1), the annual discharge required to maintain the permanently wet areas is about 7 GL. When combined with the outflow discharge, the estimated total surface discharge from the Border Creek HU is about 9 GL/y.

Although 9 GL/y of spring discharge is an estimate, it does indicate that the springs discharge a significant component of the estimated 69 GL/y of recharge to the Border Creek HU aquifer. Of the estimated total spring discharge, we estimate that discharge from the springs that have developed around the leaking old exploration bores (CGDH7, CGDH10, and CGDH11) accounts for about 1 GL/y.

Groundwater discharge from the Border Creek HU is the major contributor to flows sustaining the groundwater-dependent ecosystems that exist within the spring zones. The northern springs, such as King Gordon, Attack and Long springs (Figure 4.5), are *Priority 1 Ecological Communities* (DBCA 2021).

The larger northern springs, in particular, retain important Aboriginal cultural significance. They are associated with gender restricted knowledge and are important traditional food and water sources. They are considered potent and powerful 'living waters' (Bornman and Doohan 2016:14).

Pryde (2017) indicates that cattle have caused significant damage to the vegetation of those springs surveyed, by trampling, soil disturbance and nutrient accumulation. We also observed the impact of cattle at all springs, although within the larger springs the major cattle disturbance appeared to be mainly limited to the drier perimeters. The potential threat posed to the springs by bore water abstraction from their contributing aquifers is documented (Department of Biodiversity, Conservation and Attractions 2020).

Although we did not specifically test the water quality around the more stagnant and disturbed edges of the springs, our observation of physical disturbance and nutrient deposition via cattle dung and urine suggests water quality has likely deteriorated in these areas. However, water sampled from the source of each spring was generally of good quality and mainly within the Water Quality Australia (2019) guideline values for slightly disturbed wetland systems.

Proposals to increase groundwater extraction from the Border Creek HU for irrigation will need to consider and manage any impacts on the ecological and cultural values of the springs. The main potential effects of irrigation development include:

- change in groundwater head causing a change in discharge rate from the springs
- increase in nitrogen concentration in spring discharge resulting from leaching and then transport from developed areas.



### Seasonal springs

Of the 4,816 ha of seasonal seepage mapped on or adjacent to the Point Spring Sandstone Formation outcrop or subcrop (Section 4.3.2), about 2,600 ha is located over the Border Creek HU and therefore indicates direct seasonal discharge from either permanent or perched aquifers. GIS analysis was used to compare areas of seasonal seepage to the groundwater head relative to ground surface (Figure 5.3). There are about 370 ha, within 26 separate areas of seasonal seepage in locations where the groundwater head is at least 10 m below the ground, indicating discharge from perched watertables. Much of the remaining 2,230 ha of seasonal seepage is likely to be derived from discharge during seasonal or episodic periods that temporarily cause the aquifer to discharge in these areas.

Although it was not possible to quantify the groundwater outflow from the seasonal seepage areas, it is likely to be relatively small compared to loss through evapotranspiration over these areas.

#### 5.3.3 Intermittent lakes

The major ion balance signature of waters from NW Lake and SE Lake is very similar to that of local rainwater and is distinct from that of the Border Creek HU (Point Spring Sandstone Formation) (Figure 4.13). Although it was not possible to construct deeper bores to measure the comparative elevation of the groundwater heads in the Border Creek HU beneath each lake, projection indicates that the elevation of the NW Lake and SE Lake water is about 25 m and 35 m higher, respectively, than the groundwater head in the underlying Border Creek HU. Shallow drilling nearby confirmed the occurrence of clay layers just below the base elevation of the lakes at both sites that could support a perched aquifer.

Observations of the relative heads between the water level in SE Lake and the watertable in its nearby shallow bore (16BP03I) show that the lake water has the potential to drain into the surrounding perched aquifer during the entire observation period (Figure 4.11). Water in NW Lake has the potential to drain into the surrounding perched aquifer during dry seasons, while during some wet season periods the perched aquifer has the potential to contribute to the lake water.

In combination, the water chemistry, groundwater head and lithological observations indicate that the intermittent lakes may also be classified as hanging lakes – perched features that have accompanying localised perched aquifer systems.

The extremely low salinity ( $<3.9$  mS/m; Appendix J) of the water in both lakes shows that they do not accumulate salts as a result of evapotranspiration, as would be expected over time if there was no leakage through the underlying aquitards. To assess the likely magnitude of leakage through the aquitards, we undertook simple water balance modelling to compare net water inputs, calculated by the difference between daily rainfall and daily pEt, from the Bonaparte climate station to the observed lake levels.

The results of initial modelling scenarios indicated that to generate the maximum water levels observed in each lake (in March 2017), additional water (above that from rain falling directly on the lake surfaces) needed to be added to net water inputs in the water

balance. Most of the extra water required is likely contributed from run-off generated from localised surface catchments surrounding each lake. At NW Lake there is also the potential for seepage flow out of the perched aquifer during wet season periods to add to lake water, although this is likely a relatively small contribution and was ignored.

Figure 5.6a and Figure 5.6b show the output from final scenarios that resulted in the best match between modelled and observed water levels for NW Lake and SE Lake, respectively. In these scenarios, the extra water inputs via run-off from the small catchment areas occur when rainfall exceeds a threshold of 25 mm/d.

For the modelled water levels in the lakes to decline during the dry seasons and match the lake levels observed during August 2017 and September 2018, initial model scenarios showed that a net leakage factor was also required. In the final scenarios the corresponding leakage rates required to match the decline in lake water levels during the dry seasons was 5.1 mm/d at NW Lake and 3.3 mm/d at SE Lake.

Both lakes have very high Aboriginal cultural heritage significance, as indicated by them having the highest level of heritage protection. They are 'male access only' and are 'ceremonial/mythological water source' site type (Bornman and Doohan 2016:5–6).

Therefore, to protect the cultural significance of the lakes, any proposed irrigation development nearby should consider the potential effects on their water balance and water quality. The water chemistry results (Appendix J) indicate that, apart from slightly elevated nutrient levels caused by frequent visits by cattle, the lakes classify as being slightly modified according to the Water Quality Australia (2019) guidelines.

As the perched groundwater system associated with the lakes is a separate local system, it is unlikely that any future groundwater extraction from the Border Creek HU will affect the water balance of the lakes. However, changes associated with clearing and irrigation within their surface water catchments or within the extent of their local perched aquifers could affect their water balance, water nutrient concentrations and general chemistry. Therefore, clearing and development should be excluded from the surface catchment areas of both lakes and from the extent of the perched aquifer at NW Lake, because that aquifer has the potential to contribute to lake water. It is likely that the extent of the perched aquifers is also within the surface catchments of both lakes, although further investigation is needed to confirm this.

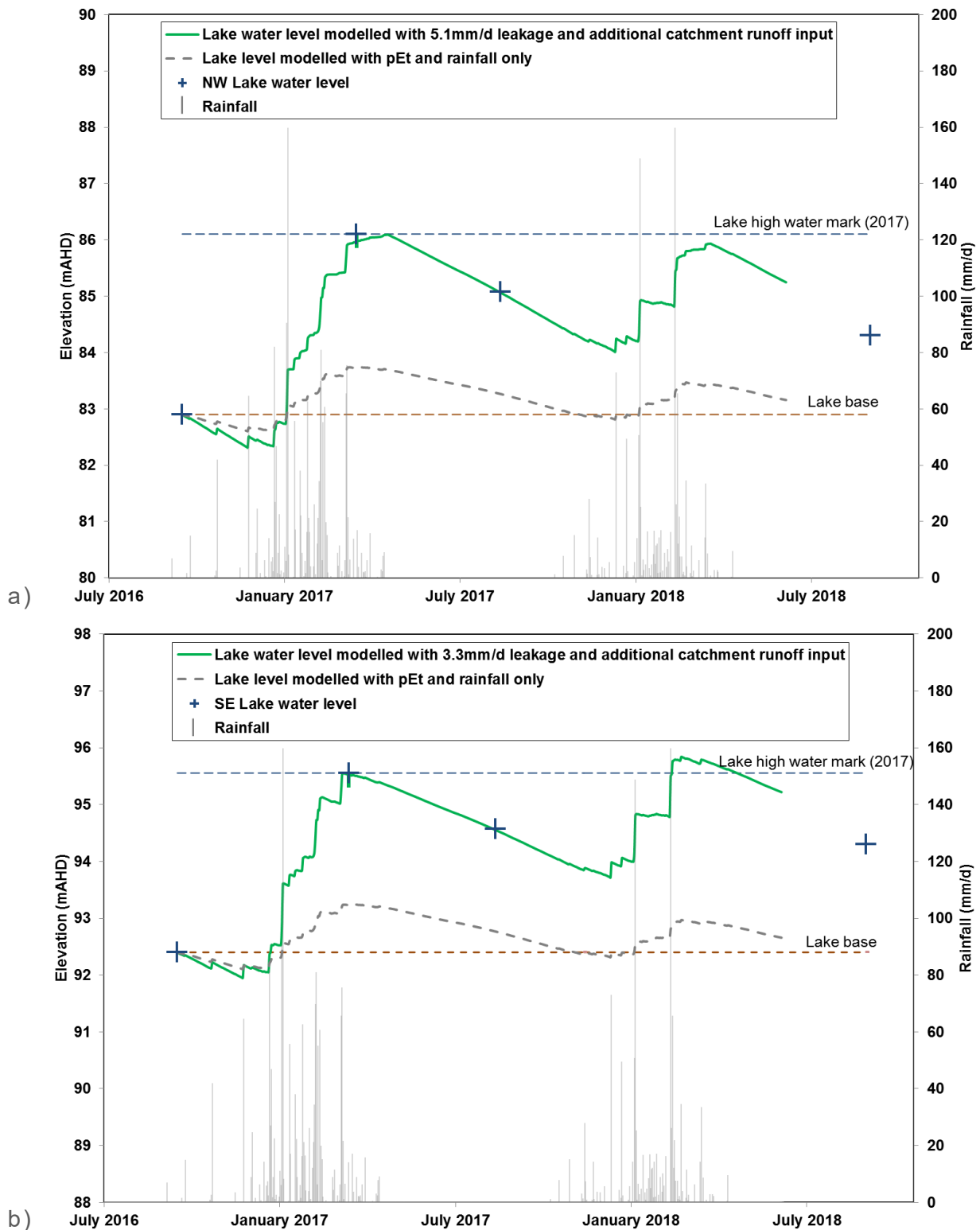


Figure 5.6: Results of water balance modelling of water levels for a) NW Lake; and b) SE Lake

### 5.3.4 Borefield design considerations

Lithological descriptions from various drilling programs (Barnes and Lee 1984; Bennett 2019; LeBlanc 1964; LeBlanc 1965) indicate that the Point Spring Sandstone Formation comprises sandstone layers having variable grain size, degree of consolidation, porosity and silt composition. In addition to the extensive shale layer, relatively thin siltstone layers and minor clay layers can also occur within the sandstone. The layered properties indicate that a degree of confinement or semiconfinement could exist between layers in the aquifer. However, at many locations faulting has substantially offset the layers thus disrupting their individual hydraulic integrity so that at the HU scale the aquifer is unlikely to be confined.

Localised perched aquifers identified at bore sites 17BP03, 17BP06, beneath the intermittent NW and SE lakes, plus the occurrence of localised seasonal springs show that semiconfined aquifer conditions exist at a local scale. Pumping test results (Appendix E) also indicate vertical heterogeneity and semiconfined aquifer conditions. The large drawdowns and the relatively low potential and safe long-term yield in bore 17BP01PB, in particular (Table 4.7), also suggests that the aquifer is locally semiconfined at the screen interval. By contrast, the fully screened 13BP01PB had much less drawdown at a similar test pumping rate, even though it has a narrower diameter bore.

Therefore, we suggest that to minimise drawdown and maximise bore yield within the Point Spring Sandstone aquifer, production bores should fully penetrate to at least the shale layer, where present, and be screened for as much of their saturated length as practicable. Large diameter, gravel-packed bores may be preferable.

If required, additional bore yield could be obtained by extending screen depths below the shale to the base of the Point Spring Sandstone Formation. However, limited drilling showed that the potential of this zone was variable and site-specific testing would be required. For example, about 20 m of poorly to very poorly consolidated sandstone was encountered below the shale at site 13BP01I, while at 18BP01DD there was about 50 m of coarse-grained, poorly consolidated sandstone below the shale.

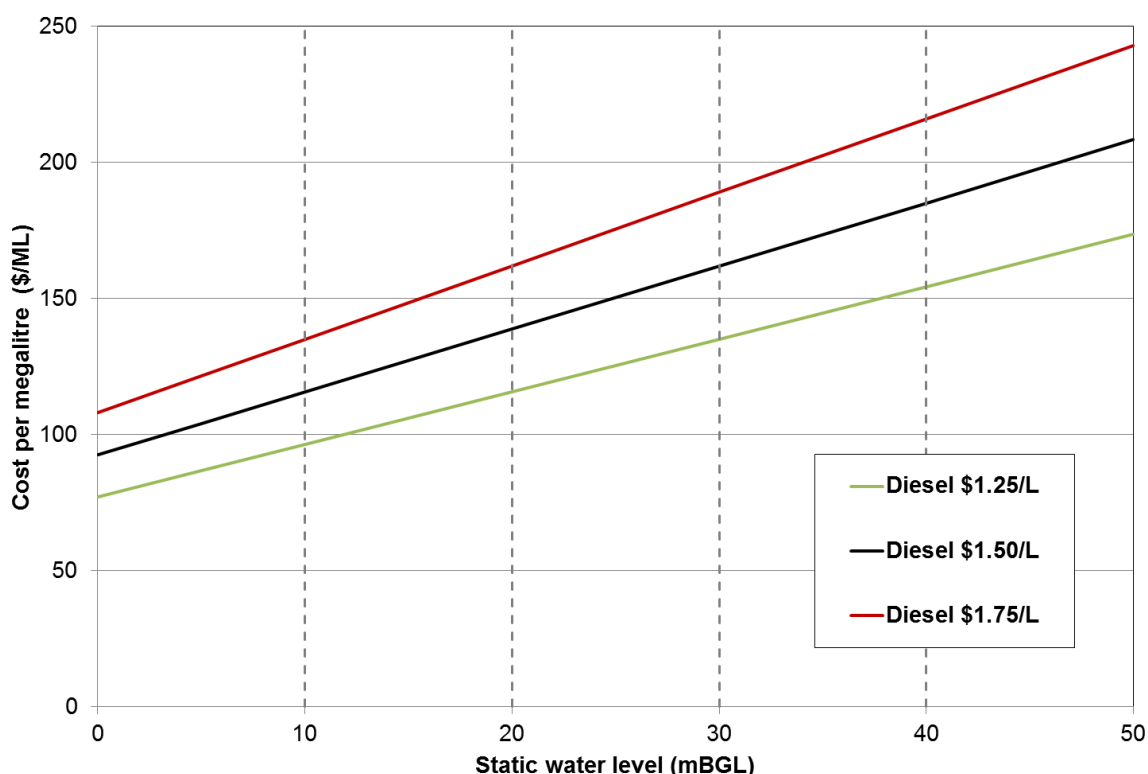
Even considering the above design principles, multiple bore sites for each irrigation area may be required, depending on its size, to minimise drawdown to reduce pumping costs.

In accordance with WA Department of Water and Environmental Regulation guidance, care should be taken to ensure that bores installed through perched aquifers, such as occurs at site 17BP06, are designed so that the perched aquifer remains hydraulically isolated from the underlying aquifer. Similarly, bores that are screened above and below the shale unit should have their annulus grouted across the shale interval.

Because the Bonaparte Plains area is remote and has no electricity supply, irrigated agriculture development must rely on diesel generators or alternative energy sources to supply pumping power. A major variable in the cost of pumping water is the total pumping head required. The total pumping head at any irrigated location is the sum of the depth to static water level (SWL) at that location, the drawdown in the pumping bore, the operating pressure of the irrigation equipment, plus any pressure loss caused by friction in the distribution pipelines.

Figure 5.7 shows indicative relationships between SWL and the cost (in Australian dollars) per megalitre (\$/ML) of using diesel power to apply irrigation through a centre pivot irrigator. The cost relationships to 3 different prices of diesel fuel are shown. Other variables include assumptions about generator, pump and bore efficiency and the flow rate required. Appendix L contains the assumptions and data used to generate the relationship shown in Figure 5.7.

Assuming a drawdown of 20 m and the equivalent of 20 m of head is required to overcome friction and pressurise a pivot irrigator, the minimum cost will be between about \$75/ML and \$110/ML using a diesel-powered irrigation system located where the SWL is at the ground surface under the irrigated area. The cost of pumping then increases by between \$2.00/ML and \$2.70/ML for each additional metre depth to the SWL. At a SWL of 40 mBGL, the pumping cost is in the range of \$154 /ML to \$216 /ML.



Source: C Ham (DPIRD), personal communication, 1 August 2016

Figure 5.7: Effect of static water level on centre pivot irrigation pumping costs using diesel power, assuming pump drawdown is 20 m and the head required to pressurise the system and overcome friction is 20 m

Figure 5.8 shows areas of Cockatoo Sands categorised by the SWL in 10 m increments, to a maximum of 40 mBGL. The groundwater beneath most of the area is relatively deep and will have a high pumping cost. For example, nearly 22,000 ha of Cockatoo Sands overlie groundwater that is more than 40 m deep. Pumping costs for this area would exceed about \$150/ML, based on the estimates shown in Figure 5.7.



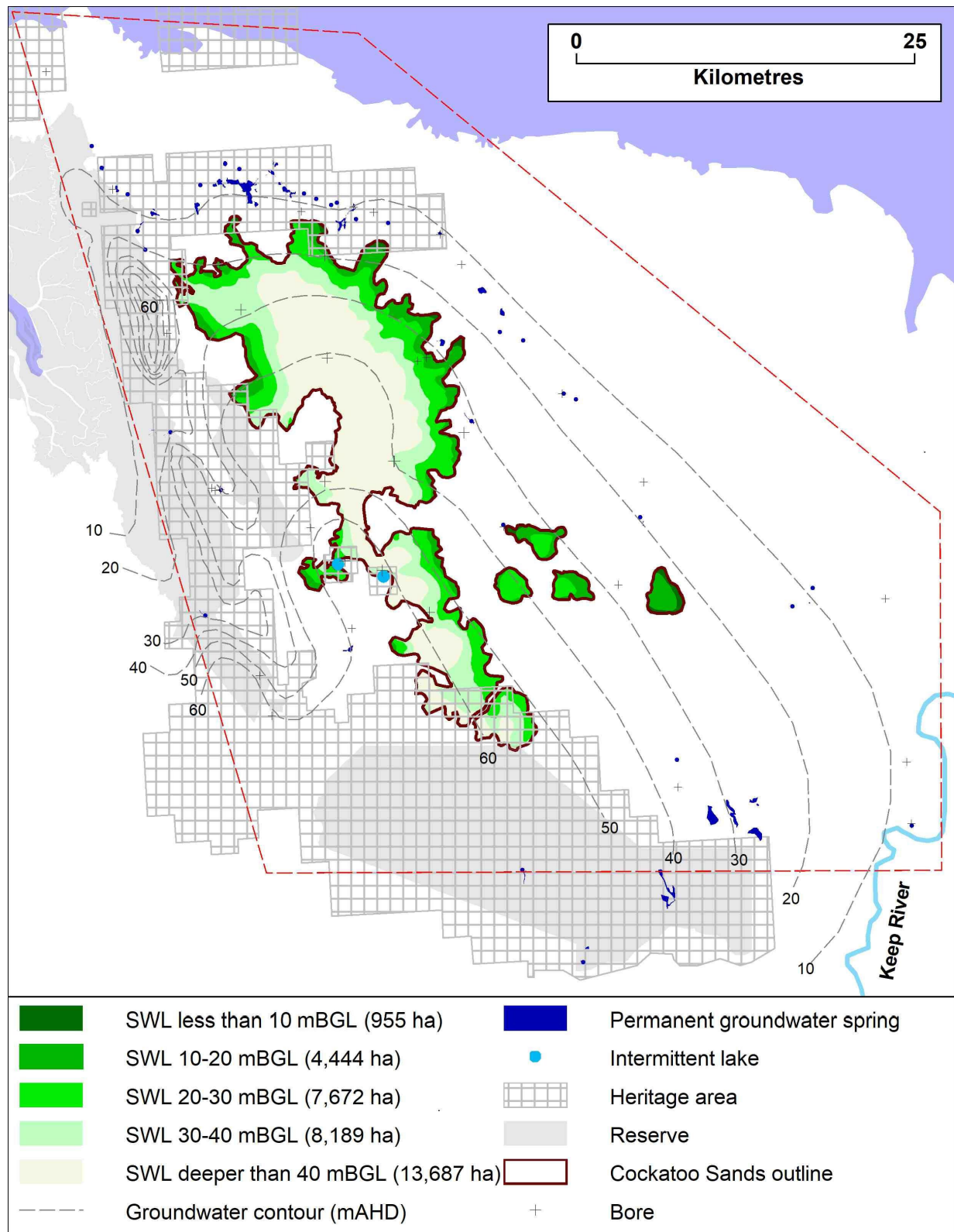


Figure 5.8: Sutable Cockatoo Sands subdivided by the depth to static water level (SWL) in relation to permanent springs, intermittent lakes, heritage areas, conservation reserves, groundwater contours and bores

Areas having an SWL within 10 m of the ground surface make up less than 1,000 ha of suitable Cockatoo Sands and occur in isolated and individually small areas. The 5,500 ha of suitable soils that have an SWL within 30 m is mainly located around the eastern rim and tends to occur in isolated patches as well. Much of the 13,000 ha with groundwater within 30 m is along the eastern rim of the main Cockatoo Sands area and within the 4, about 500 ha each, isolated patches to the east.

The 2,000 ha of suitable soils contained within the 4 eastern patches are furthest from the important heritage and conservation resources. Deeper bores would be required at these locations to draw from the Point Spring Sandstone Formation, which underlies the 200–250 m thick Keep Inlet Format.

Figure 5.8 shows that potential pumping and irrigation sites located in areas of shallower groundwater head along the eastern edge of the Cockatoo Sands are generally the most remote from the heritage areas, conservation reserves, intermittent lakes and most of the permanent wetlands. The forecast area and magnitude of long-term reduction in groundwater head surrounding various potential pumping locations is discussed in greater detail in Section 5.4.2.

Optimisation of borefield design will be critical in establishing new production bores so that they have high yields with the least drawdown to minimise energy costs. Other forms of power generation, such as solar, wind or gas, may reduce ongoing pumping costs, although these forms of energy may have a higher initial capital cost which will also increase with higher pumping head. Any bore and irrigation sites will need to be selected where there is the lowest risk of interaction with other bores, the SWI, wetlands and cultural assets.

## **5.4 Groundwater modelling**

The preceding analysis and discussion of data obtained during drilling (Bennett 2019) and subsequent field investigations form the basis of a conceptual model for the Point Spring Sandstone groundwater system beneath the Bonaparte Plains. The conceptual model was provided to IGS and formed the basis for the MODFLOW water balance model (IGS 2019; Appendix F), which enabled estimation of the magnitude of the components of the water balance and allowed us to estimate the effect of hypothetical irrigation development scenarios on groundwater levels.

We stress that this modelling is not of such scale and complexity as to be suitable for water allocation planning, support of a water licence application, or for the detailed planning of pumping optimisation that may be required by the proponent of a specific development.

### **5.4.1 Water balance model**

Table 5.3 shows the important components of the water balance for the Point Spring Sandstone aquifer at Bonaparte Plains estimated by the final (best calibrated), MODFLOW model (IGS 2019). This represents the status quo.

The final calibration was achieved using an aquifer K of 6 m/d, with a rate of recharge of 140 mm/y over most of the area. The modelled K was slightly less than the 6.9 m/d derived from aquifer testing (Section 4.4) and the modelled average recharge rate was

slightly greater than the 128 mm/y average rate derived from analysis of CMB (Section 5.3.2). The final calibration produces a hydraulic head distribution that is consistent with groundwater observations and simulates groundwater levels above ground surface at locations of mapped areas of seasonal and permanent groundwater discharge.

From Table 5.3, modelled total recharge to the aquifer is 69.4 GL/y. The 64.2 GL/y of evapotranspiration comprises about 93% of all net outflow from the system. Modelled evapotranspiration includes all outflow from spring zones, which evaporates or is transpired before it reaches the coastal boundary. The remaining outflow comprises about 1.1 GL/y of discharge along the western boundary and 4.4 GL/y discharge via the coastal boundary. Net outflow to the ocean represents about 6% of recharge.

Table 5.3: Water balance for the Point Spring Sandstone aquifer at Bonaparte Plains as estimated by the groundwater model; base case

Water balance term	Inflow (GL/y)	Outflow (GL/y)	Net outflow (GL/y)
Recharge	69.4	NA	NA
Coastal boundary	146.7	151.1	4.4
Evapotranspiration	NA	64.2	NA
Western boundary	NA	1.1	NA

NA = not applicable

Further details of the water balance model's calibration statistics and discussion of the effect of varying  $K$  and recharge rate on aquifer net outflow are reported in IGS (2019), provided in Appendix F. The limitations of the model, in terms of their potential impacts on the accuracy of the estimated water balance, have been clearly specified in IGS (2019).

#### 5.4.2 Irrigation development scenario modelling

Appendix G contains the report detailing methods and results for scenario modelling of irrigation development. In summary, we used the calibrated MODFLOW model to run hypothetical scenarios to forecast the effect on net aquifer outflow and groundwater drawdown, with abstraction from the Point Spring Sandstone aquifer for irrigation of Cockatoo Sands at 11 sites. Downslope irrigation sites (where groundwater is shallow) were selected to minimise the energy costs of pumping. Individual sites were then chosen to be as far as possible from environmentally sensitive wetlands to minimise the impact of potential aquifer drawdown on those wetlands.

At each site 2.2 GL/y was pumped, equivalent to 50% of the modelled net ocean outflow from the aquifer. This rate was based on the likely maximum volume that might be allocated by the WA Department of Water and Environmental Regulation (DWER), as the equivalent of half of the aquifer net outflow (for example, see Department of Water 2010, Appendix C). At each site, the modelled irrigation demand was 1,500 mm/y; applying the annual abstraction of 2.2 GL/y resulted in irrigated areas of 147 ha, which were circular for ease of scenario construction. The relatively high irrigation rate provided a conservative estimate of the area irrigated, which is

appropriate given the hypothetical nature of the scenarios. The type of crop likely to be grown and therefore its specific water requirement is unknown.

The modelling showed that net outflow to the ocean was the component of the water balance most affected, reducing by between 0.39 GL/y (–9%) and 1.00 GL/y (–24%) at the 11 sites. Changes in outflow through the western boundary were small in absolute terms ( $\leq 0.10$  GL/y) but significant in relation to the base case, up to a 10% reduction.

Despite the relatively small areas of irrigated land modelled, suitable locations were limited by the need to minimise depth to groundwater for economic reasons and the forecast drawdown impacts on the wetlands fringing the Cockatoo Sands.

Scenarios at 7 sites, which included a 1,000-ha area of annual dryland agriculture up slope of the irrigated areas, demonstrated that this strategy could successfully minimise the drawdown impacts on downslope wetlands. In these scenarios the increase in modelled recharge of 1.3–1.4 GL/y from the dryland areas reduced the net outflow across the coastal boundary by between 0.12 GL/y (3%) and 0.33 GL/y (8%). The addition of 1,000 ha sized areas of dryland annual agriculture provides greater flexibility in locating the irrigated areas, within the constraints of pumping depth and drawdown impacts.

Scenario modelling also showed that in one area it is possible to double the volume of water pumped, and therefore the area irrigated, by increasing the area of dryland agriculture to 2,000 ha without affecting wetlands. Under this scenario the net outflow to the coast is reduced by 0.67 GL/y (16% reduction) with minimal impact to outflow across the western boundary. It is uncertain whether abstraction that exceeds 2.2 GL/y, as required by this design, would be permitted by DWER.

The scenario modelling indicates that it is possible to irrigate up to about 150 ha (at the irrigation application rate of 1,500 mm/y) at a reasonable pumping cost without affecting wetlands. The modelling also indicates that including much larger areas of dryland agriculture (up to 5,000 ha modelled) to increase recharge to the aquifer can result in only relatively minor reductions in the magnitude and extent of the drawdown at the pumping location and result in the development of large-scale groundwater mounds, remote from the irrigation site.

The shale layer had a significant influence on the areal extent of groundwater level reductions in specific irrigation scenarios and had an equally significant role in determining the level of drawdown mitigation achieved in scenarios that included dryland agriculture (Appendix G). Where major faults were able to be mapped, IGS (2019) had to infer that the shale had a K equal to that of the sandstone for the MODFLOW modelled heads to match the observed heads. Therefore, the shale is likely to have a role in determining head responses, at least at the local scale. It is also likely that we did not identify all the faults nor obtain empirical data on their ability to conduct groundwater. Therefore, the degree to which faulting affects the shale continuity and how it controls groundwater heads and flow would need to be more precisely defined at an appropriate scale for specific development proposals.

## 5.5 Seawater interface

Due to the high near-surface conductivity of the coastal mudflats and parts of the Keep Inlet Formation under the Cleanskin Plain (Figure 2.10), it was not possible to precisely determine the location of the SWI from the AEM survey inversion data. However, we used the AEM profile data to locate the landward extent of sharp contrasts in conductivity (within a 50–500 m depth interval) to estimate the possible maximum landward extent of the SWI (Figure 5.9).

The very high surface conductivity variably masked any underlying resistive layers over much of the Cleanskin Plain. This meant that the SWI could be much further seaward than indicated by our interpretation of its maximum possible landward extent. Although not conclusive because of the variability in the AEM conductivity at depth, indications of the existence of an apparently resistive layer underlying the conductive surface layer under parts of the Cleanskin Plain suggests that the SWI may lie further east, possibly even under the mudflats in this area.

Close to the northern margin with the mudflats, the AEM section profiles tend to show more abrupt and consistent conductivity contrasts underlying resistive profiles. This may mean that our estimation of the maximum landward extent of the SWI may be close to the actual location of the SWI in this area.

The locations of the toe of the SWI predicted by the SEAWAT models are shown in Figure 5.9. The estimated depth of the toe was about 430 mBGL at NS01 and 450 mBGL at 103901, corresponding with the base of the Border Creek HU in both locations. IGS (2019) note that because the modelled SWI on section 103901 is close to the model boundary, the boundary condition may have forced the modelled SWI inland so that its actual location may be even further east.

The results of the cross-section models are consistent with our hypotheses, based on the AEM, that the SWI is likely to be near the estimated maximum inland extent along the northern mudflats and much closer to the coast, east of the Cleanskin Plain.

Simulation, under transient conditions, of the impact of pumping on the location and form of the SWI was not possible because of the short time series of groundwater head data available for model calibration. Therefore, we can only make qualitative judgements, based on the locations where drawdown was forecast, about the relative risks of inducing seawater intrusion by pumping at the selected irrigation areas.

The risk of inducing saltwater intrusion by pumping is apparently greatest at site 2 (Figure G5 in Appendix G). Except for irrigation site 11, this is the only scenario where the drawdown extends northward past the maximum possible landward extent of the SWI (Figure 5.9). However, the scenario for irrigation at site 11 was considered invalid because the predicted drawdown extended to the southern no-flow model boundary.

Although the risk of inducing saltwater intrusion appears low for much of the area at the pumping rates modelled, the risk of saltwater intrusion would need to be assessed on a site basis for any specific proposed development.



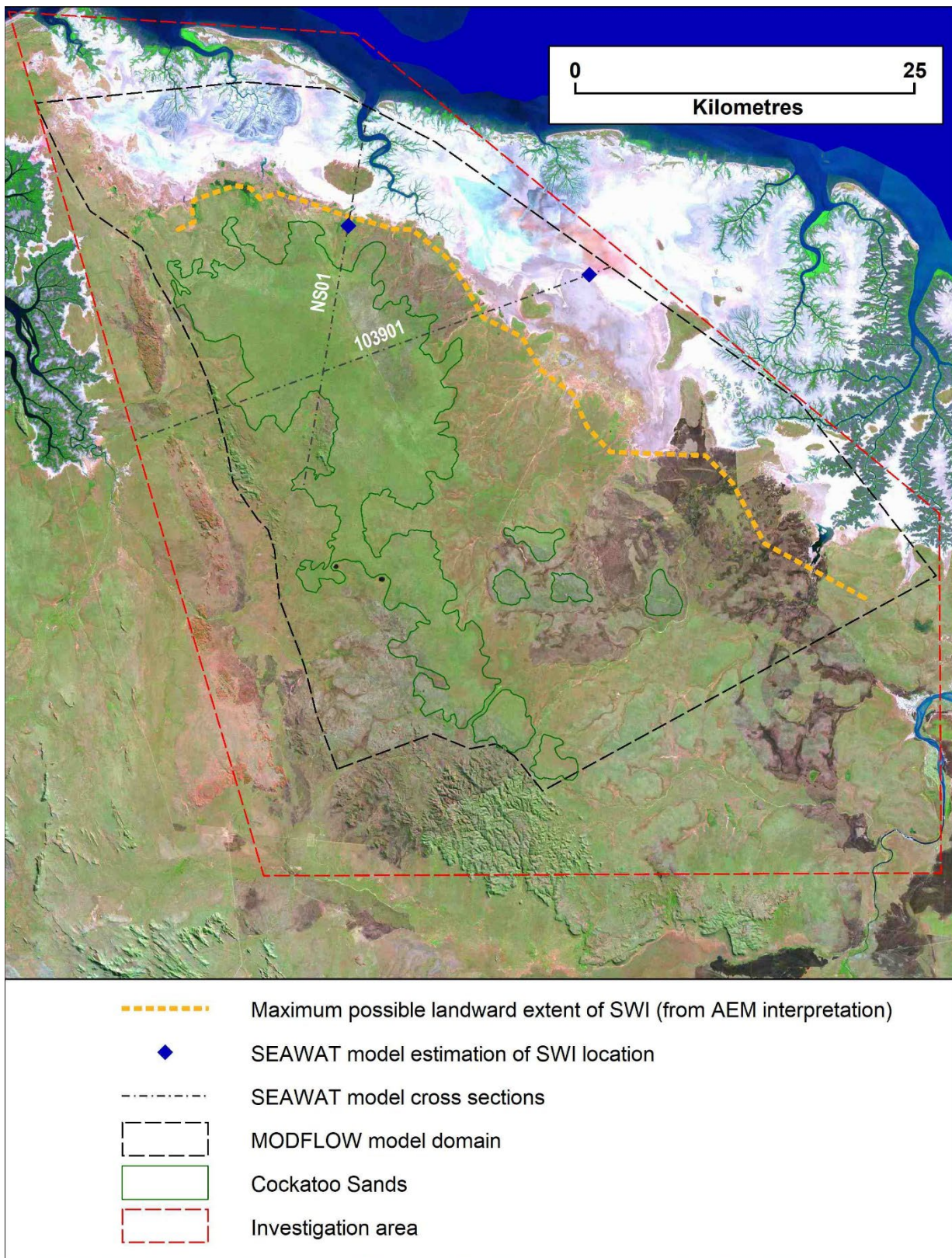


Figure 5.9: Maximum possible landward extent of the seawater interface (SWI), based on airborne electromagnetic (AEM) conductivity profiles, and the location of SWI estimated by SEAWAT modelling

## 6 Conclusions

This report describes the method, data, and analyses used to determine the hydrogeological and groundwater physical and physicochemical conditions of the Bonaparte Plains area, in relation to the potential for irrigated agriculture development on 34,947 ha of suitable Cockatoo Sands.

Climate, watertable depth, watertable dynamics, aquifer physical properties, groundwater chemistry and water balance data are reported in the context of the opportunities, potential hazards and generic risks to land and water resource conditions that may arise if developed for irrigated agriculture.

The Point Spring Sandstone Formation underlies the Cockatoo Sands and contains the prospective aquifer for obtaining groundwater supply for irrigation in the area. The aquifer is extensive and contains very good quality groundwater. However, it has limited potential as a sustainable water source for extensive irrigation. Based on the results of water balance modelling, up to 2.2 GL/y could be available for abstraction for irrigation (or other uses) from the aquifer. Depending on specific crop requirements, this supply may support about 150–300 ha of irrigated agriculture, a very small proportion of the area of suitable soils.

Another important constraint is the deep watertable beneath much of the Cockatoo Sands area. About two-thirds of the area overlies groundwater that is at least 30 m below the surface and will have a pumping cost exceeding \$150/ML, using current technology diesel-powered pumps.

Areas with shallower watertable, and therefore lower pumping costs, are mostly found around the northern and eastern margin of the suitable Cockatoo Sands. Much of this margin is next to culturally or environmentally sensitive locations containing groundwater-dependent, permanent wetlands. Even with relatively small areas of irrigation, scenario modelling forecast that suitable locations were limited by a combination of the need to minimise depth to groundwater for economic reasons and the potential pumping-induced aquifer drawdowns that can extend to the wetlands.

Leaching and transport of nitrogen in the aquifer beneath agriculturally developed areas poses an eventual site-specific risk of eutrophication to the biologically diverse and culturally significant ecosystems that depend on groundwater. Carefully planning the location of the development areas and the siting and design of production bore fields could mitigate these risks.

Scenario modelling forecast that annual wet season cropping on 1,000 ha areas located above irrigation areas could reduce the extent of the aquifer drawdown by supplying additional recharge. Modelling this system showed that the potential head reduction impacts on wetlands could be minimised at most of the locations modelled.

However, we stress that the investigation and modelling was not of a suitable scale and complexity as to be suitable for water allocation planning, support of a water licence application, or for the detailed planning of pumping optimisation that may be required by a proponent of a specific development. Estimations of the location of the seawater interface was only possible along 2 cross-sections by SEAWAT modelling and by

interpreting the AEM data. As uncertainty remains about the location of the seawater interface, the risks associated with seawater intrusion remain poorly defined.

Generally, there is a low on-site risk of land and water resource degradation associated with irrigated agriculture development on the Cockatoo Sands. Replacing existing vegetation with annual dryland or irrigation will increase on-site recharge but the associated risk of soil salinity is low due to the high permeability of the Cockatoo Sands.

Important seasonal climatic differences between the Bonaparte Plains and the Kununurra area include warmer minimum temperatures and higher humidity in the dry season, with a higher rainfall, cooler and more humid wet season. Although these differences are based on only 3 years of observation, they are consistent with the Bonaparte Plains being located further north and bordered by the Joseph Bonaparte Gulf on 3 sides. However, we recommend that climate data continue to be collected to enable a longer-term climate record on which to better assess the local climate.

Together with the land capability report (Smolinski 2019), potential developers can use the data reported here to further investigate site- and enterprise-specific opportunities and risks.

## Appendixes

**Appendix A Seasonally wet land units adjacent to Bonaparte Plains**

**Appendix B Physicochemical analytes, abbreviations, LORs and methods**

**Appendix C ANSTO analysis of groundwater chemistry and isotope data**

**Appendix D Suitability of groundwater for irrigation**

**Appendix E Test pumping method, results and analysis**

**Appendix F Water balance modelling report**

**Appendix G Irrigation development scenario models**

**Appendix H Monthly average climate data from Bonaparte climate station**

**Appendix I Locations of permanent groundwater discharge**

**Appendix J Groundwater, spring, lake and rainwater physicochemistry**

**Appendix K Hydrostratigraphic cross-sections**

**Appendix L Pumping cost assumptions**



## Appendix A Seasonally wet land units adjacent to Bonaparte Plains

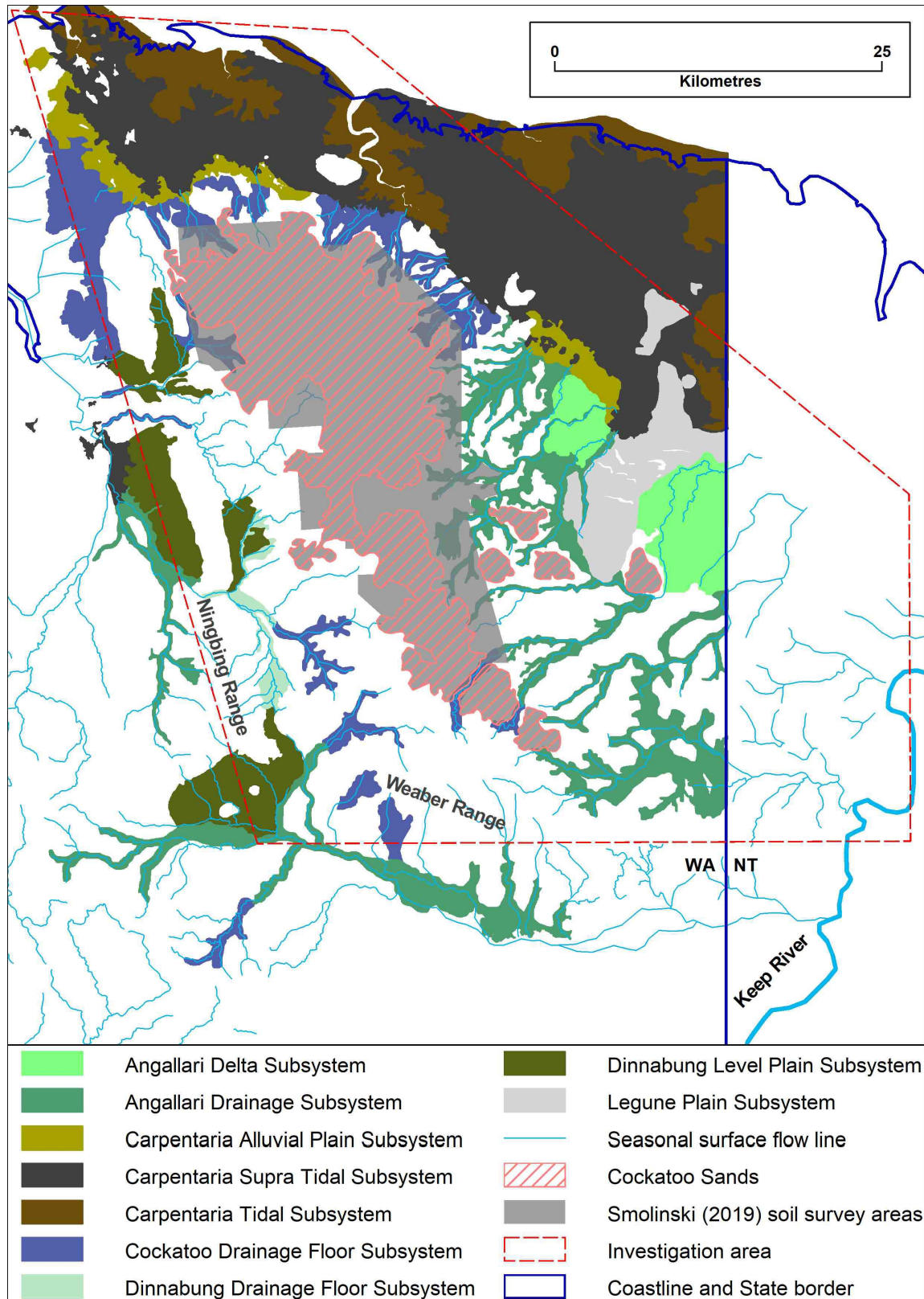


Figure A1: Map of the seasonally wet land units (subsystems) identified by Schoknecht et al. (2004) for the Bonaparte Plains area, shown in relation to the area of Cockatoo Sands and the Smolinski (2019) mapping boundaries



## Appendix B Physicochemical analytes, abbreviations, LORs and methods

Table B1: The types of analyses performed on samples collected from bore, spring, lake and rainfall sites

Site	Field chemistry	General chemistry	Metal chemistry	$^{14}\text{C}_{\text{DIC}}$	CFCs	$^2\text{H}$	$^3\text{H}$	$^{18}\text{O}$	$\text{SF}_6$
<b>Bores</b>									
13BP01D	Y	Y	Y	Y	N	Y	Y	Y	N
13BP01PB	Y	Y	Y	Y	N	Y	Y	Y	N
16BP03S	N	Y	Y	N	N	N	N	N	N
17BP01I	Y	Y	Y	Y	N	Y	N	Y	N
17BP01S	Y	Y	Y	Y	Y	Y	Y	Y	Y
17BP01PB	Y	Y	Y	N	N	N	N	N	N
17BP02I	Y	Y	Y	Y	N	Y	N	Y	N
17BP02S	Y	Y	Y	Y	Y	Y	Y	Y	Y
17BP03I	Y	Y	Y	Y	Y	Y	Y	Y	Y
17BP04I	Y	Y	Y	Y	N	Y	N	Y	N
17BP04S	Y	Y	Y	Y	Y	Y	Y	Y	Y
17BP05I	Y	Y	Y	Y	N	Y	N	Y	N
17BP05S	Y	Y	Y	Y	Y	Y	Y	Y	Y
17BP05PB	N	Y	Y	N	N	N	N	N	N
17BP06I	Y	Y	Y	Y	N	Y	N	Y	N
17BP06S	Y	Y	Y	Y	Y	Y	Y	Y	Y
17BP071	Y	Y	Y	Y	Y	Y	Y	Y	Y
18BP01D	Y	Y	Y	Y	N	Y	N	Y	N
18BP01DD	Y	Y	Y	Y	N	Y	N	Y	N
18BP07D	Y	Y	Y	Y	N	Y	N	Y	N
Bonaparte1 water bore 1	Y	Y	Y	Y	N	Y	Y	Y	N
Bonaparte2 water bore	Y	Y	Y	Y	N	Y	Y	Y	N
Brolga	Y	Y	Y	Y	Y	Y	Y	Y	Y
Calf spring bore	Y	Y	Y	Y	N	Y	Y	Y	N
CGDH5 (Fishermans)	Y	Y	Y	Y	N	Y	Y	Y	N
CGDH6 (New Attack)	Y	Y	Y	Y	N	Y	Y	Y	N
CGDH7	Y	Y	Y	Y	N	Y	Y	Y	N

(continued)

Table B1 (continued): The types of analyses performed on samples collected from bore, spring, lake and rainfall sites

Site	Field chemistry	General chemistry	Metal chemistry	$^{14}\text{C}_{\text{DIC}}$	CFCs	$^2\text{H}$	$^3\text{H}$	$^{18}\text{O}$	$\text{SF}_6$
CGDH8 (Kemp)	Y	Y	Y	Y	N	Y	Y	Y	N
Cleanskin	Y	Y	Y	Y	N	Y	Y	Y	N
Hotplate	Y	Y	Y	Y	N	Y	Y	Y	N
Lewis	Y	Y	Y	Y	N	Y	N	Y	N
Matera	N	Y	Y	N	N	N	N	N	N
No. 8 Paddys	Y	Y	Y	Y	Y	Y	Y	Y	Y
Oaks Creek bore	Y	Y	Y	Y	N	Y	Y	Y	N
RN029226	Y	Y	Y	Y	N	Y	Y	Y	N
WBN5002	Y	Y	Y	Y	N	Y	N	Y	N
WBN5006	Y	Y	Y	Y	N	Y	N	Y	N
Wilson	Y	Y	Y	Y	N	Y	Y	Y	N
<b>Lakes and springs</b>									
Bore Spring lower	Y	Y	Y	N	N	N	N	N	N
Bore Spring upper	Y	Y	Y	Y	Y	Y	Y	Y	Y
Domett Road	Y	Y	Y	N	N	N	N	N	N
Garimala Creek	Y	Y	Y	N	N	N	N	N	N
Long Spring	Y	Y	Y	Y	Y	Y	Y	Y	Y
New Spring	Y	Y	Y	Y	Y	Y	Y	Y	Y
NW Lake	Y	Y	Y	N	N	N	N	N	N
SE Lake	Y	Y	Y	N	N	N	N	N	N
Oaks Creek Spring	Y	Y	Y	Y	Y	Y	Y	Y	Y
Tanmurra Creek	Y	Y	Y	N	N	N	N	N	N
Tanmurra Pool	Y	Y	Y	N	N	N	N	N	N
Yow Spring	Y	Y	Y	Y	Y	Y	Y	Y	Y
<b>Rainfall</b>									
Rain 2015–2016 wet season	N	Y	Y	N	N	Y	Y	Y	N
Rain 2016–2017 wet season1	N	Y	Y	N	N	Y	Y	Y	N
Rain 2016–2017 wet season2	N	N	N	N	N	Y	Y	Y	N
Rain 2017 dry season	N	N	N	N	N	Y	Y	Y	N
Rain 2017–2018 wet season	N	Y	Y	N	N	Y	N	Y	N

Table B2: The field measurement suite of analytes with their abbreviations, LORs, units and analysis methods

Analyte	Symbol	LOR	Units	Analysis method
Alkalinity	Alk	1	mg/L	Titration
Electrical conductivity	EC	1	mS/m	Electronic probe at 25 °C
Dissolved oxygen (%)	DO	1	DO%	Galvanic electronic probe
Oxidation–reduction potential	Eh	0.1	mV	Electronic probe
pH	pH	0.1	NA	Electronic probe
Temperature	Temp	0.1	°C	Electronic probe

LOR = limit of reporting; NA = not applicable

Table B3: The general chemistry measurement suite of analytes with their abbreviations, LORs, units, laboratory analysis methods and filtration status before analysis

Analyte	Symbol	LOR	Units	Analysis method	Filtered
Acidity	Acidity	2	mg/L	Titration	N
Alkalinity	Alk	1	mg/L	Titration	Y
Bicarbonate	HCO <sub>3</sub>	1	mg/L	Titration	Y
Bromine	Br	0.01 or 0.02	mg/L	ICPAES	Y
Carbonate	CO <sub>3</sub>	1	mg/L	Titration	Y
Chloride	Cl	1	mg/L	Ion chromatography	Y
Electrical conductivity	EC	0.02	mS/m	Electronic probe at 25 °C	N
Fluoride	F	0.05	mg/L	Electrical probe	Y
Hardness	Hard.	1	mg/L	Calculation	Y
Hydroxide	OH	1	mg/L	Titration	Y
Ion balance	Ion bal.	–50	%	Calculation	Y
Sulfate	SO <sub>4</sub> S	0.1	mg/L	ICPAES	Y
Total nitrogen	TN	0.02	mg/L	PD, CaR, CR and AFIAC	N
Ammonium nitrogen	NH <sub>4</sub> N	0.01	mg/L	CR and AFIAC	Y
Nitrate nitrogen	NO <sub>3</sub> N	0.01	mg/L	CaR, CR and AFIAC	Y
Nitrite nitrogen	NO <sub>2</sub> N	0.01	mg/L	CR and AFIAC	Y
pH	pH	0.1	NA	Electronic probe	N
Total dissolved solids	TDS Sum	1	mg/L	Sum of anions/cations	Y
Total phosphorus	TP	0.01	mg/L	PD, CR and AFIAC	N
Soluble reactive phosphorus	SRP	0.01 or 0.005	mg/L	PO <sub>4</sub> P by CR and AFIAC	Y

AFIAC = automated flow injection analysis colorimeter; CaR = cadmium reduction; CIRD = combustion and infrared detection; CR = colorimetric reaction; ICPAES = inductively coupled plasma atomic emission spectroscopy; LOR = limit of reporting; NA = not applicable; PD = persulphate digestion

Table B4: The metals and chemical toxicant suite of analytes with their abbreviations, LORs, units, laboratory analysis methods and filtration status before analysis

Analyte	Symbol	LOR	Units	Analysis method	Filtered
Aluminium	Al	0.005	mg/L	ICPAES	Y
Antimony	Sb	0.0001	mg/L	CMS/ICPAES	Y
Arsenic	As	0.001	mg/L	CMS	Y
Barium	Ba	0.002	mg/L	ICPAES	Y
Beryllium	Be	0.0001	mg/L	CMS	Y
Bismuth	Bi	0.0001	mg/L	CMS	Y
Boron	B	0.02	mg/L	ICPAES	Y
Cadmium	Cd	0.0001	mg/L	CMS	Y
Calcium	Ca	0.01	mg/L	ICPAES	Y
Chromium	Cr	0.001	mg/L	ICPAES	Y
Cobalt	Co	0.0001 or 0.005	mg/L	CMS/ICPAES	Y
Copper	Cu	0.0001 or 0.002	mg/L	CMS/ICPAES	Y
Gallium	Ga	0.0001	mg/L	CMS	Y
Iron	Fe	0.005	mg/L	ICPAES	Y
Lanthanum	La	0.0001 or 0.005	mg/L	CMS/ICPAES	Y
Lead	Pb	0.0001	mg/L	CMS	Y
Lithium	Li	0.0001 or 0.005	mg/L	CMS/ICPAES	Y
Magnesium	Mg	0.1	mg/L	ICPAES	Y
Manganese	Mn	0.001	mg/L	ICPAES	Y
Mercury	Hg	0.0001	mg/L	CMS	Y
Molybdenum	Mo	0.001	mg/L	CMS	Y
Nickel	Ni	0.001	mg/L	CMS	Y
Potassium	K	0.1	mg/L	ICPAES	Y
Selenium	Se	0.001	mg/L	CMS	Y
Silicon	Si	0.05	mg/L	ICPAES	Y
Silver	Ag	0.0001	mg/L	CMS	Y
Sodium	Na	0.1	mg/L	ICPAES	Y
Thallium	Tl	0.0001 or 0.002	mg/L	CMS/ICPAES	Y
Tin	Sn	0.0001 or 0.02	mg/L	CMS/ICPAES	Y
Titanium	Ti	0.002	mg/L	ICPAES	Y
Uranium	U	0.0001	mg/L	CMS	Y
Vanadium	V	0.0001 or 0.005	mg/L	CMS/ICPAES	Y
Zinc	Zn	0.001 or 0.005	mg/L	CMS/ICPAES	Y

CMS = coupled mass spectroscopy; ICPAES = inductively coupled plasma atomic emission spectroscopy; LOR = limit of reporting

Table B5: The groundwater dating suite of analyses with their abbreviations, LORs, units, laboratory analysis methods and filtration status before analysis

Analyte	Symbol	LOR	Units	Analysis method
Carbon-13	$\delta^{13}\text{C}$	Individual error reported	‰	Accelerator mass spectrometry
Radiocarbon	$^{14}\text{C}_{\text{DIC}}$	Individual error reported	pMC	Accelerator mass spectrometry
Chlorofluorocarbons	CFC-11, CFC-12, CFC-13	Individual error reported	pmol/kg	Gas chromatography with electron capture detection
Deuterium	$\delta^2\text{H}$	2%	‰	Isoprime mass spectrometer
Tritium	$^3\text{H}$	0.02	TU	Radiometric detection with electrolytic enrichment and low-level scintillation detection
Oxygen stable isotope	$\delta^{18}\text{O}$	0.2%	‰	Isoprime mass spectrometer
Sulfur hexafluoride	$\text{SF}_6$	Individual error reported	fmol/kg	Electrolytic enrichment and gas chromatography with electron capture detection

$\delta$  = ratio of the isotope to the most common stable isotope;  $\delta^{13}\text{C}$  = ratio normalised to  $\delta^{13}\text{C}$  of  $-25\text{‰}$ ; ‰ = parts per thousand; LOR = limit of reporting; pMC = per cent modern carbon; TU = tritium unit, equal to  $^3\text{H}/^1\text{H}$  ratio of  $1 \times 10^{-18}$

Notes:

1.  $1 \text{ pmol/kg} = 10^{-12} \text{ mol/kg}$
2.  $1 \text{ fmol/kg} = 10^{-15} \text{ mol/kg}$



## **Appendix C ANSTO analysis of groundwater chemistry and isotope data**



Australian Government



Nuclear-based science benefiting all Australians

---

## **Analysis of Bonaparte Plains groundwater chemistry data.**

---

Prepared for	The Government of Western Australia, Department of Primary Industries and Regional Development.
Date of Issue	27 August 2018
Report No	ANSTO/C-1572
Security	Commercial In Confidence

---

**Dr Karina Meredith,  
Dr Stacey Priestley,  
Mr Stuart Hankin**

## Executive Summary

A groundwater investigation was designed and undertaken by the Government of Western Australia (WA), Department of Primary Industries and Regional Development (DPIRD). Water samples were collected from within and around the Bonaparte Plains during the dry season in 2017; including 34 groundwater wells, 5 springs and 2 lakes. Five bulk rainfall samples were also collected. Various hydrochemical (general field parameters, major and minor ions), isotopic ( $\delta^{18}\text{O}$ ,  $\delta^2\text{H}$ ,  $^3\text{H}$ ,  $^{14}\text{C}_{\text{DIC}}$ ) and age tracer ( $\text{SF}_6$ , CFC) measurements were undertaken. The target hydrogeological units were the late Carboniferous units of the Border Creek and Kuriyippi Formations and the Permian Keep Inlet Formation.

The primary objective of this project was to use the hydrochemical and isotopic results to provide a greater understanding of the Bonaparte Plains groundwater system with regards to (1) recharge processes (2) recharge rates, (3) groundwater flow paths and (4) groundwater residence times.

Groundwaters were found to have similar  $\delta^2\text{H}$  and  $\delta^{18}\text{O}$  compositions with very low averages of -7.73 ‰ and -51.64 ‰, respectively, implying they have a similar depleted meteoric origin. Groundwaters plot on the Darwin local meteoric water line and represent cyclonic or large monsoonal rainfall events that are recharging the aquifer. There is no evidence of evaporation prior to recharge suggesting that groundwater recharges fairly quickly through the unsaturated zone because the depleted  $\delta^2\text{H}$  and  $\delta^{18}\text{O}$  signal is retained in the groundwater.

The groundwater salinity was generally low with most containing less than  $3 \text{ mmol L}^{-1}$  of Cl and it was found that marine aerosols are the main source of Cl in this system, which is introduced via rainfall recharge. Elevated dissolved oxygen, silica concentrations and tritium values correlate with the location of two water level mounds in the centre of the site, suggesting the location of recharge areas. Carbonate dissolution was not found to be a dominant process in the younger target aquifers but was associated with the older carbonate-rich lithologies. The spatial distribution of the radiocarbon content of the dissolved inorganic carbon ( $^{14}\text{C}_{\text{DIC}}$ ) was found to be governed by the location of the groundwater wells with distance from the recharge areas. Groundwaters located close to the recharge mound (near 17BP03I) all have  $^{14}\text{C}_{\text{DIC}}$  contents greater than 70 pMC.

Groundwater residence times were calculated using five lumped parameter models and the mean residence time (MRT) values were calculated from combined tracer models using measured  $^3\text{H}$ ,  $\text{SF}_6$  and CFCs. Fourteen samples located within the Border Creek and Kuriyippi Formations were identified as less than 100 years old. These waters are found in the higher elevation areas of the site relating to higher water levels and various hydrochemical and isotopic indicators of recharge.

Of the 31 samples measured for  $^{14}\text{C}$ , 9 samples were within the  $^{14}\text{C}$  dating range. Older waters (1,000 to 23,000 years old) were found in the Keep Inlet Formation in the lower elevations. Groundwater recharge rates ranged from  $0.5\text{--}265 \text{ mm yr}^{-1}$  with the higher values generally found in the recharge areas.

# Table of Contents

<b>1</b>	<b>INTRODUCTION</b>	<b>4</b>
1.1	Objective	5
1.2	Scope of works	5
1.3	Limitations of the Assessment	5
<b>2</b>	<b>ENVIRONMENTAL SETTING</b>	<b>7</b>
2.1	Study site	7
2.2	Hydrogeology	9
<b>3</b>	<b>METHODOLOGY</b>	<b>11</b>
<b>4</b>	<b>RESULTS</b>	<b>13</b>
4.1	Rainfall	14
4.2	Lake water	14
4.3	Spring water	15
4.4	Groundwater	16
<b>5</b>	<b>DISCUSSION</b>	<b>19</b>
5.1	Origin of groundwater recharge	19
5.2	Source of salinity and location of recharge areas	20
5.3	Carbon evolution after recharge	21
5.4	Groundwater residence times	24
5.4.1	Lumped Parameter Models using $^3\text{H}$ , $\text{SF}_6$ and CFCs	24
5.4.2	Radiocarbon ( $^{14}\text{C}$ ) age	26
5.5	Groundwater recharge rate estimates	30
<b>6</b>	<b>CONCLUSIONS</b>	<b>31</b>
<b>7</b>	<b>RECOMMENDATIONS</b>	<b>33</b>
<b>8</b>	<b>ACKNOWLEDGEMENTS</b>	<b>33</b>
<b>9</b>	<b>REFERENCES</b>	<b>33</b>

## List of Figures

Figure 1 The location of Bonaparte Plains in Australia and the DPIRD groundwater study area in relation to Cockatoo Sands outcrop (in red) and transect lines (purple lines). .....	4
Figure 2 Location map of the study site with regards to the location of the Joseph Bonaparte Gulf showing the well locations, extent of Cockatoo Sands and state border locations. Map created by DPIRD.....	8
Figure 3 A piper diagram of all waters collected from the Bonaparte Plains 2017, showing the variation in all waters. ....	13
Figure 4 The spatial distribution of Cl (mg L <sup>-1</sup> ) in groundwaters for the study area compared with 10 m piezometric surface contours supplied by DPIRD.....	17
Figure 5 Bivariate plot of $\delta^2\text{H}$ vs. $\delta^{18}\text{O}$ compared with the Darwin LMWL ( $\delta^2\text{H} \text{‰} = 7.69\delta^{18}\text{O} + 9.75$ ) and an Evaporation Line (EL) ( $\delta^2\text{H} \text{‰} = 5.2\delta^{18}\text{O} - 14.4$ ) for the Pilbara. ....	19
Figure 6 Bivariate plot of Cl/Br vs. Na/Cl (molar concentration).....	20
Figure 7 The spatial distribution of $^3\text{H}$ (T.U.) in groundwaters for the study area compared with elevation (m AHD) and 10 m piezometric surface contours supplied by DPIRD. The 5 cross sections are initial depictions of the hydrogeology based on field information provided by DPIRD and require validation with geophysical survey information. ....	22
Figure 8 A bivariate plot of the saturation indices of calcite ( $\text{SI}_{\text{cc}}$ ) vs. log of Cl concentration for waters from the study site. ....	23
Figure 9 Bivariate plots of (a) DIC vs. $\delta^{13}\text{C}_{\text{DIC}}$ and (b) $\delta^{13}\text{C}_{\text{DIC}}$ vs. $^{14}\text{C}_{\text{DIC}}$ . ....	24
Figure 10 The spatial distribution of $^{14}\text{C}$ (pMC) in groundwaters for the study area compared with elevation (m AHD) and 10 m piezometric surface contours supplied by DPIRD. The 5 cross sections are initial depictions of the hydrogeology based on field information provided by DPIRD and require validation with geophysical survey information. ....	25
Figure 11 The spatial distribution of groundwater residence times for the study area compared with elevation (m AHD) and 10 m piezometric surface contours supplied by DPIRD. The 5 cross sections are initial depictions of the hydrogeology based on field information provided by DPIRD and require validation with geophysical survey information .....	29



# 1 Introduction

This report was prepared by Dr Karina Meredith, Dr Stacey Priestley and Mr Stuart Hankin from Australian Nuclear Science and Technology Organisation (ANSTO), for the Government of Western Australia (WA), Department of Primary Industries and Regional Development (DPIRD).

The Western Australian Government has the goal of doubling food production for local and international markets by 2025, within close proximity (50 to 100 km) of the Ord irrigation area (Figure 1). Considering this, the DPIRD have undertaken a large scale water and land investigation including a risk assessment of the Bonaparte Plains in the East Kimberley, North Kununurra, WA (Bennett and Raper, 2018).

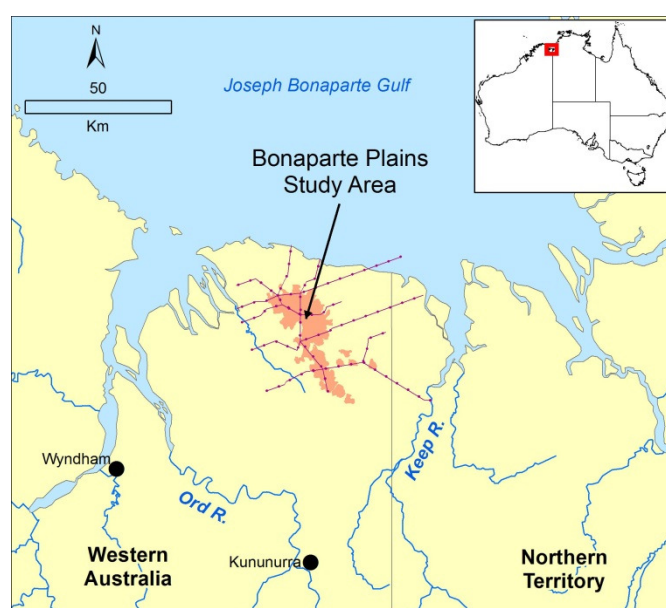


**Figure 1** The location of Bonaparte Plains in Australia and the DPIRD groundwater study area in relation to Cockatoo Sands outcrop (in red) and transect lines (purple lines).

The study undertaken by DPIRD involves using various geophysical investigations techniques to understand the aquifer lithology; such as nuclear magnetic resonance (NMR) and airborne electromagnetic (AEM) together with soil surveys. A groundwater investigation using hydrogeological methodologies including well drilling, installation and pump testing has also been undertaken. Groundwater samples were collected from 34 wells within and around the Bonaparte Plains (Figure 2). Water samples were collected by DPIRD from groundwater wells, springs and lakes during the dry season in 2017.

### **1.1 Objective**

The primary objective of this project was to use the hydrochemical and isotopic results of water samples collected by DPIRD to provide a greater understanding of the Bonaparte Plains groundwater system with regards to:

1. Recharge rates, processes and location of recharge areas;
2. Groundwater flow paths; and
3. Groundwater residence times.

The following samples were collected by DPIRD in 2017 and submitted to various laboratories in WA and New Zealand:

- General laboratory and field geochemistry for 34 groundwater samples, 5 spring samples, 2 lake samples and 2 rainwater samples;
- SF<sub>6</sub> and CFC data for 9 groundwater samples and 5 spring samples;
- Stable Isotope data ( $\delta^{18}\text{O}$  and  $\delta^2\text{H}$ ) for 31 bore samples, 5 spring samples and 5 rainwater samples;
- Radiocarbon data ( $^{14}\text{C}_{\text{DIC}}$ ) for 31 groundwater samples and 5 spring samples; and
- Tritium ( $^3\text{H}$ ) data for 24 groundwater samples, 5 spring samples and 4 rainwater samples.

Please note that  $\delta^{13}\text{C}$  was measured on the same sample container that was collected for  $^{14}\text{C}_{\text{DIC}}$ . This may differ from the  $\delta^{13}\text{C}$  of the DIC in the groundwater sample because  $\delta^{13}\text{C}_{\text{DIC}}$  measurements are generally undertaken on a sample that has been collected in a gas tight vial. This is done to minimise fractionation. Therefore the  $\delta^{13}\text{C}_{\text{DIC}}$  value in this study is used as a broad reference for the  $\delta^{13}\text{C}_{\text{DIC}}$  value in groundwater.

### **1.2 Scope of works**

To achieve the above stated objectives, the following scope of works was completed:

- Quality check of hydrochemical data;
- Interpretation of water samples using graphical and mass balance modelling techniques;
- Construction of cross-sections and spatial distribution maps for key parameters;
- Radiocarbon assessment and modelling;
- CFC, SF<sub>6</sub> and  $^3\text{H}$  assessment;
- Provided a draft report for review to DPIRD;
- A final report detailing the results.

### **1.3 Limitations of the Assessment**

The findings of this report are based on data obtained through the scope of work outlined above. The following general limitations apply:

- The physical hydrogeology (i.e. the water level, pump test data, including hydrogeology and geology summary) was not presented in

this report because it is beyond the scope of this project as outlined by the DPIRD;

- The interpretations and conclusions of this report are based solely on the hydrochemical and isotopic results obtained from the field study undertaken for this project;
- The validity of the hydrochemistry results are based on the assumption that the wells were sufficiently developed and purged after drilling; and
- Importantly, it was also assumed that the groundwater wells were sampled according to standard water quality sampling guidelines.

## 2 Environmental Setting

### 2.1 Study site

The study area is located in the Bonaparte Basin, which is 270,000 km<sup>2</sup> in total. The Western Australian onshore portion, which contains the area of interest for this study, is 8,000 km<sup>2</sup>. The Bonaparte Basin contains moderate economic hydrocarbon accumulations and various ore deposits. The Ord River and Keep River bound the region with the area located between the WA and Northern Territory border. The location of the study site and sample locations are provided in Figure 2.

Meteorological data is collected at Carlton Hill and Wyndham airport, with the recorded mean annual rainfall of 823 mm yr<sup>-1</sup> (1897-2016) and 807 mm yr<sup>-1</sup> (1951-2016), respectively. A meteorological station was established on the Bonaparte Plains in 2015 by DPIRD with an accumulating rain gauge. The two years of rainfall data collected at this station shows that the area received about 300 mm yr<sup>-1</sup> more rainfall than the Carlton Hill or Wyndham sites (Bennett and Raper, 2018).

The physiography of the study area is described in Bennett and Raper (2018). Briefly, the study area has wide tidal mud flats up to 20 km that lie between the Bonaparte Plains and the ocean. The mud flats support mangrove forest, samphire and some grasses but there are also large areas of bare grounds. Permanent fresh springs occur around the north and north-eastern interface between the tidal mud flats and sandy units. These springs are suggested to be discharging from the Border Creek and Kuriyippi Formation sandstone aquifers.

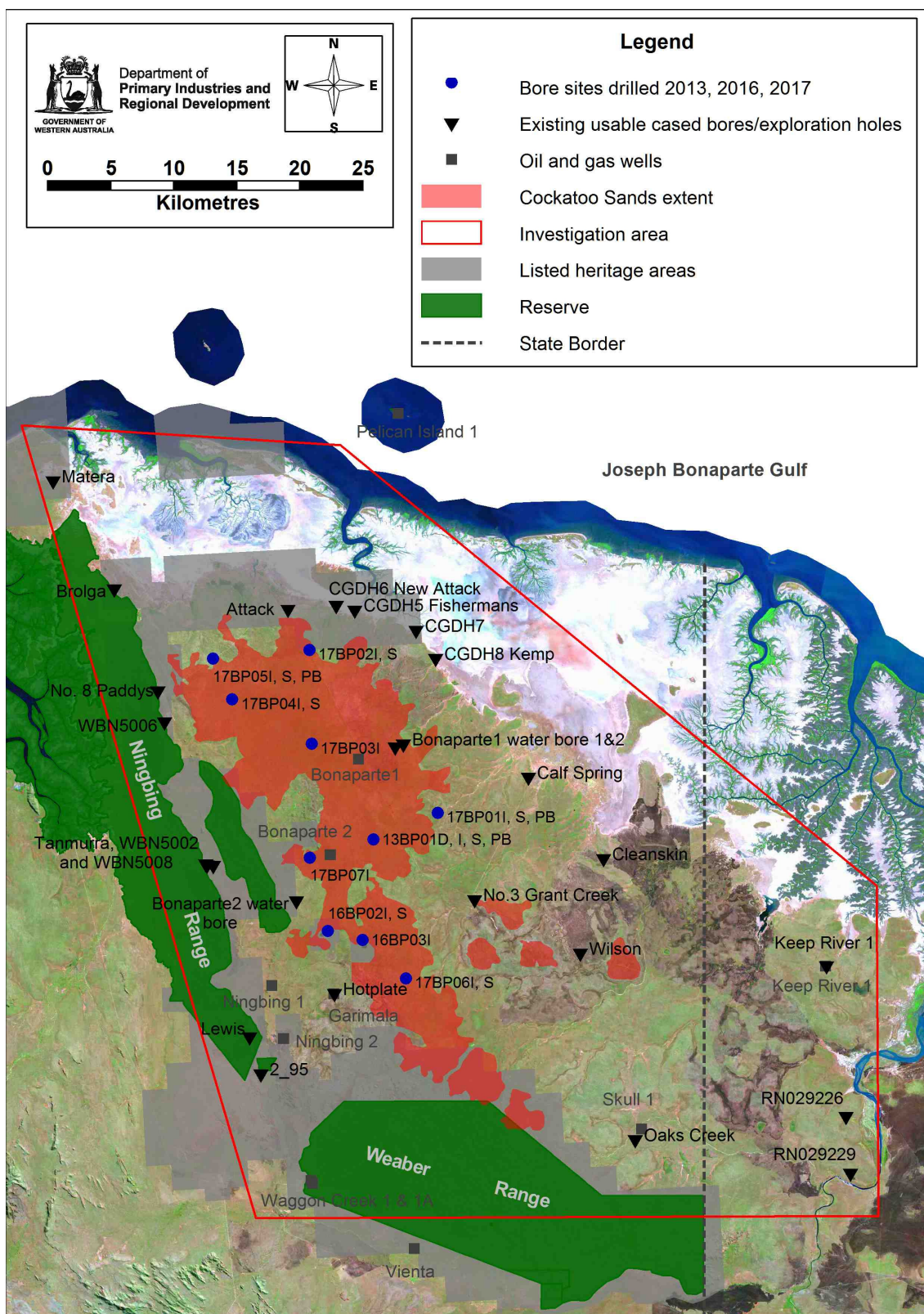


**Figure 2** Location map of the study site with regards to the location of the Joseph Bonaparte Gulf showing the well locations, extent of Cockatoo Sands and state border locations. Map created by DPIRD.



The central portion of Bonaparte Plains consists of the Cockatoo Sands (Figure 2), which include red to yellowish red sands, sandy earths and loamy earths that have formed from quartz sandstone colluviums. This unit is found throughout the East Kimberley and has been identified as suitable for irrigation. To the west of the central area of Cockatoo Sands, the landscape dips gently westward to a north-south elongated depression. Steep and rocky units occur either side of this feature with some surface water draining to the floors of the alluvium to the west. To the south are the northern slopes of the Weaber Range.

Two small ephemeral lakes are located high in the landscape, on the south-western flank of the central area of Cockatoo sands, they are believed to be maintained by a combination of direct rainfall and local perched groundwaters (Bennett and Raper, 2018).

## **2.2 Hydrogeology**

The geology and hydrogeology of the area has been described by Bennett and Raper (2018), this section aims to briefly summarise key findings. The geology within the investigation area is complex and has not been well defined. The Bonaparte Basin contains a Devonian-Carboniferous sedimentary succession that regionally dips to the north, with the oldest units outcropping in the south and the majority of the study area is overlain by Cockatoo Sands (Figure 2).

The target hydrogeological units in this study are the late Carboniferous units of the Border Creek and Kuriyippi Formations and the Permian Keep Inlet Formation. Older Carboniferous units that are shale-dominated such as the Milligans, Yow Creek and Kingfisher Formations form an impermeable boundary beneath the Border Creek and Kuriyippi Formations and where they sub-crop in the west which is – between them and the Devonian-aged Ningbing Range limestones (pers comms. Don Bennet Figure 2). Some carbonaceous units exist in these older sequences such as the calcareous and dolomitic sandstones of the Tanmurra Formation and oolitic limestone of the Sunbird Formation. The Point Spring Sandstone may overlies the Tanmurra and Sunbird Formations in the south of the study area. Here it outcrops as the hard rock of the Weaber Range (Figure 2). It consists of fine to coarse sandstone and pebbly sandstone with interbedded conglomerate, siltstone and shale.

The Border Creek and Kuriyippi Formations are mostly sandstones. They are texturally similar to those of the Point Spring Sandstone Formation. However, the Border Creek Formation also contains thick sequences of conglomerate, siltstone, silty sandstone and pebbly quartz sandstone. The Keep Inlet Formation is the youngest and consists of sandstone, mudstone and shale dominated units, plus minor conglomerate, that were deposited in continental, shallow marine and glaciomarine environments. The Keep Inlet Formation unconformably overlays the Border Creek, Kuriyippi and Point Spring Sandstone Formations. The Keep Inlet Formation extends under the tidal mud flats to the north and east of Bonaparte Plains. Zones of weakness in the

aquitards are likely responsible for the locations of the isolated groundwater discharge springs that occur on the edge of the mud flats. Thin Cainozoic alluvium, sand plains and coastal deposits overlie the Keep Inlet Formation.

The groundwater flow direction was assessed from wells within the Border Creek, Kuriyippi and Keep Inlet Formation sandstone aquifers at 10 m AHD intervals drawn from point groundwater observations for 2017 (Figure 4). Two groundwater mounds occur in these aquifers located under the Cockatoo Sands and are separated by a small saddle. Groundwater flow is directed away from the mounds in all directions except for the south where the Point Spring Sandstone Formation forms an impermeable boundary (Bennett and Raper, 2018).

Groundwater recharge is assumed to be via direct rainfall recharge, especially through the Cockatoo Sands. Groundwater discharge occurs as permanent and seasonal springs, plus it is likely to occur as sub-marine discharge, although this has not been verified.

### 3 Methodology

The water sampling protocol and analytical methods employed in this project were designed and undertaken by DPIRD. The water samples were collected by DPIRD and sent to the Chemcentre in WA and GNS Science in New Zealand for analysis. The data was then supplied to ANSTO in Excel format. The following is a summary of the interpretation methodology employed in this project.

Initially, the hydrochemical data was assessed for errors using charge balance error percentages (CBE%). The data was converted to mmol L<sup>-1</sup> for hydrochemical interpretation using bivariate plots. Descriptive statistics and correlation analysis was also undertaken. Saturation indices, the partial pressure of CO<sub>2</sub> (pCO<sub>2</sub>) and DIC concentrations were calculated using the WATEQ4F thermodynamic database in the PHREEQC 2.4.2 programme (Parkhurst and Appelo, 1999). Geographical information system spatial mapping in ArcGIS was undertaken to understand the spatial distribution of water chemistry and isotopes. The source of water was assessed using the stable isotope data in groundwater and rainfall for the site.

The measured <sup>14</sup>C values in percent modern carbon (pMC) for groundwaters were corrected for <sup>14</sup>C dilution using various correction models including: Vogel, Tamers (Tamers, 1975), Ingerson and Pearson, IAEA and Fontes-Garnier's (F-G) (Fontes and Garnier, 1979). For brevity, the Pearson and IAEA methods are reported here. These correction models use hydrochemical and isotopic data to calculate a *q* correction value based on the observed groundwater chemistry of a sample. This *q* value is then multiplied by *A*<sub>0</sub> and substituted into Equation 1 for a corrected age calculation:

$$t = -\frac{1}{\lambda} \ln\left(\frac{A}{A_0 \times q}\right) \quad \text{Equation 1}$$

where *t* is the groundwater age or time since recharge, *A* is the measured <sup>14</sup>C activity of the sample, *A*<sub>0</sub> is the natural background activity of carbon in equilibrium with the atmosphere (i.e. 100 pMC is used in these calculations) prior to radioactive decay and *q* is the calculated correction factor. Modelling assumptions for this study were that organic matter and soil CO<sub>2(g)</sub> were assigned a value of δ<sup>13</sup>C = -23 ‰ and <sup>14</sup>C activity of 100 pMC. Carbonates were assumed to be close to marine values with δ<sup>13</sup>C = 0 ‰ and <sup>14</sup>C = 0 pMC.

Groundwater age distributions were evaluated using environmental tracer data with lumped parameter models (LPMs), which are mathematical models of transport based on simplified aquifer geometry and flow configurations that account for effects of hydrodynamic dispersion or mixing within the aquifer, well, or discharge area. Groundwater ages were calculated using five LPMs: Piston-Flow Model (PFM), Exponential Mixing Model (EMM), Exponential Piston-Flow Model (EPM), Partial Exponential Model (PEM) and Dispersion Model (DM). For detailed methods on these models and the age equations refer to Jurgens et al. (2012). The modelling was completed using TracerLPM and the tritium input function was based on concentrations of tritium in rainfall

measured by the Global Network of Isotope in Precipitation (GNIP) and ANSTO on a monthly basis since the 1960s at Darwin, which is the closest observation dataset to the study site. Chloride mass balance and groundwater residence times were calculated and used to estimate recharge rates.

## 4 Results

Groundwater, spring, lake and rainfall water samples were collected by DPIRD in 2017. The analytical measurements undertaken on the samples are provided in Section 1.1. Work details for the wells sampled were supplied by DPIRD for this study and are included in Appendix A, Table A1. The data for field, hydrochemical and isotopic parameters are presented in Appendix A, Tables A2-A6.

Cations and anions were assessed for accuracy by evaluating the charge balance error percentage (CBE%) (Appendix A, Table A2). About a quarter of the samples had CBEs outside the acceptable limit of  $\pm 5\%$  (i.e. 13 of the 43 samples). A Piper plot of major ions highlights the differences in groundwater chemistry from across the site (Figure 3) with lake and rainfall samples plotting in the centre, and groundwaters and spring waters across the trilinear plot.

The groundwaters and spring waters are varied in chemistry suggesting a great deal of heterogeneity in the aquifer lithology of this region. Trace elements and metals were also analysed, with most found to be below detection limit or low in concentration (subset of data in Appendix A, Table A3). The hydrochemistry and environmental isotope character of water samples are described below according to rainfall, lake, spring and groundwater.

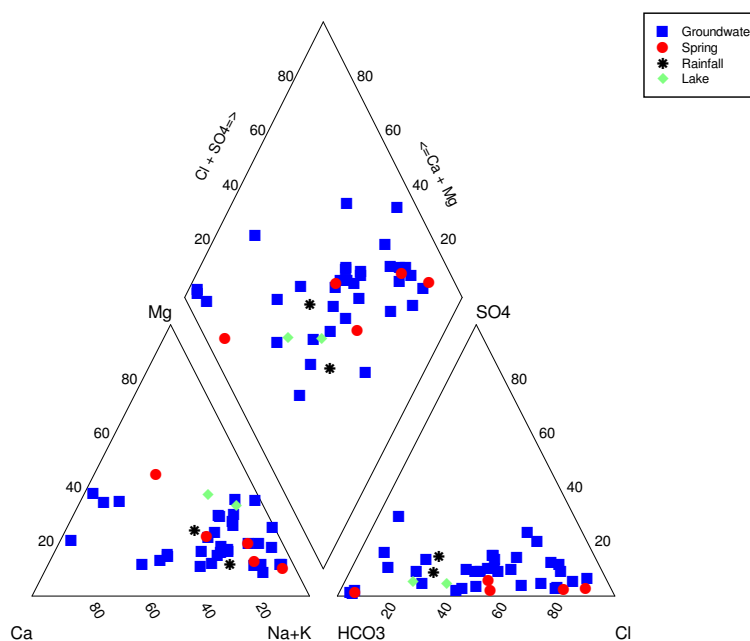


**Figure 3** A piper diagram of all waters collected from the Bonaparte Plains 2017, showing the variation in all waters.



## 4.1 Rainfall

Five rainfall samples were collected as part of this project including; Rain\_2015/16 wet season, Rain 1\_2016-17, Rain 2\_2016-17, Rain 3\_May-Nov 17 and Bonaparte Rain 12/6/18 (Appendix A, Tables A1-A4). Samples Rain 1\_2016/17 and Rain\_2015/16 were analysed for the complete hydrochemistry. Rainfall samples are low in major ion concentrations and have a mixed cation (Na-Ca-Mg) and anion composition ( $\text{HCO}_3\text{-Cl}$ ). Rainfall plots in the middle of the trilinear plot suggesting there is not a distinct end-member source such as marine aerosols (i.e. Na-Cl-rich) for these samples, which is surprising considering this is a coastal site (Figure 3). The degree in variation observed in this plot may be explained by the high CBEs (18 and 21%) of the rainfall samples.

The rainfall samples are low in all major ions with Cl concentrations below  $0.06 \text{ mmol L}^{-1}$  and Na/Cl ratios of 1.5 (Rain\_2015/16) and 3.2 (Rain 1\_2016/17). Elevated ratios above 1 could be due to analytical error or that Na is contributed to the rainfall from sources other than marine aerosols. If the latter was the case it is likely to be from terrestrial sourced aerosol with carbonate particulate material contributing Ca, Mg and  $\text{HCO}_3$ . These results could also indicate aerosol contamination of the rainfall sampler over time.

The water isotopes  $\delta^{18}\text{O}$ ,  $\delta^2\text{H}$  and  $^3\text{H}$  were measured on the 5 samples. The rainfall measured in May-Nov 17 had much higher  $\delta^{18}\text{O}$  and  $\delta^2\text{H}$  ratios (-1.41 ‰ and -2.3 ‰, respectively) compared to 2016/17 and 2018 (-7.12 ‰ and -43.2 ‰, respectively) with an average of -4.80 and -26.3 ‰, respectively ( $n = 5$ ). The higher sample was sampled during the dry season and is not likely to represent groundwater recharge. The  $^3\text{H}$  activities ranged from 1.7 TU in 2015/16 compared to 1.4 TU in 2016/17 with an average of 1.6 TU ( $n = 4$ ), which is what would be expected for  $^3\text{H}$  in rainfall for this region.

## 4.2 Lake water

The two perched lakes were sampled from the South East (94.5 m AHD) and North West (85.1 m AHD). Samples had mixed cation and anion compositions, with the SE lake being Mg-Na-K-Ca- $\text{HCO}_3$ -rich and the NW being Na-Mg-K- $\text{HCO}_3$ -Cl-rich water. The lake waters plot in the centre of the trilinear plot of the Piper plot near the rainfall samples (Figure 3). The CBEs for these samples are also high (12.8 and 14.1%).

The general parameters for the lake waters were fairly similar between sampling locations with temperature of around  $27^\circ\text{C}$ , pH around 6.9 and DO higher than  $6 \text{ mg L}^{-1}$ . The high DO concentration is indicative of an oxygenation surface water environment. Lake waters were low in salinity with Cl concentrations lower than  $0.1 \text{ mmol L}^{-1}$  and Na/Cl ratios (1.3) similar to the 2015 rainfall sample. DIC concentrations are low ( $<0.3 \text{ mmol L}^{-1}$ ) and are under-saturated with respect to calcite (-3.3). No environmental isotopes were measured on the lake samples.

### 4.3 Spring water

Five spring samples were collected from near the coast at 6 m AHD (Long Spring) to inland at 33 m AHD (New Spring). The spring waters were varied in chemistry and plot across the trilinear Piper plot and do not represent groundwater in the immediate localised areas directly adjacent the springs suggesting the waters come from other aquifers or they have undergone different hydrochemical processes. Yow and New Springs are Na-Cl-rich waters, Bore Spring is a Mg-Ca-HCO<sub>3</sub>-rich water, Long Spring is a Na-Ca-Mg-Cl-HCO<sub>3</sub>-rich water and Oaks Creek Spring Na-Cl-HCO<sub>3</sub>-rich.

The springs have an average temperature of 23.1 °C. The pH varies from acidic in New and Yow Springs (pH = 5.6) to a more neutral value (pH = 6.4±0.1) in the remaining samples. They all contain relatively high DO (1.9-3.7 mg L<sup>-1</sup>) indicating they have been in contact with the atmosphere or mixed with water containing oxygen.

Spring waters are relatively low in salinity with Cl concentrations ranging from 0.2 (New Spring) to 1.3 (Long Spring) mmol L<sup>-1</sup>. The Na/Cl ratios range from 1 (New Spring) to 3.3 (Bore Spring) with an average of 1.5. As with the lake and rainfall samples, this suggests a source of Na compared to Cl.

The spring waters have no detectable nitrate and low concentrations of phosphate (<0.02 mg L<sup>-1</sup>), Al (<0.07 mg L<sup>-1</sup>), Mn (<0.01 mg L<sup>-1</sup>) and Fe (<0.3 mg L<sup>-1</sup>). The Bore Spring sample had a Zn concentration of 0.1 mg L<sup>-1</sup> but the others were low (<0.04 mg L<sup>-1</sup>). DIC concentrations vary from low (<0.3 mmol L<sup>-1</sup>) in New Spring to fairly high in Bore Spring (7.3 mmol L<sup>-1</sup>) with an average of 2.1 mmol L<sup>-1</sup>. All spring waters are under-saturated with respect to calcite (less than -1.1) and contain low Si concentrations (0.18-0.3 mmol L<sup>-1</sup>).

The  $\delta^{18}\text{O}$  ratios range from -4.31 ‰ (Yow Spring) to -7.48 ‰ (New Spring) with an average of -6.52 ‰ (n = 5) and the  $\delta^2\text{H}$  ratios range from -34.3 ‰ to -49.6 ‰ with an average of -44.9 ‰ for the same samples. The values for  $\delta^{13}\text{C}_{\text{DIC}}$  range from -23.2 ‰ (Yow Spring) to -15.3 ‰ (Oaks Spring) [average of -18.4 ‰].

The <sup>3</sup>H activities were relatively low (less than 0.15 TU) with a minimum of 0.04 (Bore Spring) and maximum of 0.15 TU (Yow Spring). Uncorrected <sup>14</sup>C values are all high ranging from 89.1 (Long Spring) to 98.4 pMC (Yow Spring) with an average of 94.4 pMC. These results indicate the waters are likely to be modern from a <sup>14</sup>C perspective.

The piston flow recharge dates for CFCs and SF<sub>6</sub> are presented in Appendix A, Table A5 and A6 and are based on Southern Hemisphere atmospheric air concentrations. For CFC-11, they ranged from 1970 to 1982, for CFC-12 from 1975 to 1990 and for SF<sub>6</sub> they ranged from 1995 to 2018, excluding those that were considered by the laboratory (GNS) to be contaminated with atmospheric input for these tracers (i.e. Yow and Bore Springs). These recharge dates fall within the limits of using these age tracers, which is confirmed by low <sup>3</sup>H values.

#### 4.4 Groundwater

The elevation of the wells ranged from close to sea level at the coast (4 m AHD; CGDH\_5\_(FISHERMANS)) to 110 m AHD (17BP03I) inland (Figure 2). The shallowest sample was obtained from 10.4 m bgs (16BP03I) located in the southern half of the site and the deepest sample from 162 m bgs (13BP01D) located near the Ningbing Range. The average sample depth was 62 m bgs ( $n = 34$ ). However of these wells, six had very long inlets (18-54 m) and are considered not ideal for isotopic sampling but the majority of wells have an average screen thickness of 6 m ( $n = 22$ ).

Initially for hydrochemical interpretation, groundwater samples were divided according to the geological units that the mid-point of the well screen intersected. No trends were observed with depth in the aquifers. Groundwater types ranged from Na to Ca cation dominance and  $\text{Cl-HCO}_3$  being equally dominant anions (Figure 3). Samples from Border Creek, Kuriyippi and Keep Inlet Formations plot across the trilinear plot with no distinct end-member grouping, however 4 of the 5 spring waters did plot within the expanded data cloud produced by these groundwaters.

Groundwaters were mostly fresh throughout the study area and have an average EC of  $240 \mu\text{S cm}^{-1}$  ( $n = 32$ ) (Appendix A, Table A2). They Groundwaters were slightly acidic with an average pH of 6.11 ( $n = 32$ ) and had an average temperature of  $32.7^\circ\text{C}$  ( $n = 31$ ). Most groundwaters contained oxygen, with an average DO of  $2.1 \text{ mg L}^{-1}$  and only six samples measured below  $0.5 \text{ mg L}^{-1}$ . The most oxygenated water was found in the centre of the site at the highest elevation of  $\sim 110 \text{ m asl}$  (17BP03I =  $5.6 \text{ mg L}^{-1}$ ) and the lowest towards the northern coastline (CGDH\_7 =  $0.08 \text{ mg L}^{-1}$ ).

Silica concentrations ranged from  $0.04 \text{ mmol L}^{-1}$  (LEWIS) to  $0.47 \text{ mmol L}^{-1}$  (17BP03I), with an average of  $0.19 \text{ mmol L}^{-1}$ . The highest values were located in the centre of the site and lowest along the Ningbing Group limestone/Milligans Formation contact. Chloride concentrations were generally low but a large variation did occur ranging from 0.1 (BONAPARTE\_1\_Waterbore\_1) to  $33 \text{ mmol L}^{-1}$  (MATERA\_BORE) in the far northern section of the study area near the coast with an average of  $1.8 \text{ mmol L}^{-1}$  (Figure 4). The DIC concentrations were varied from very low  $0.2 \text{ mmol L}^{-1}$  (Tanmurra) to  $8.54 \text{ mmol L}^{-1}$  (WBN5006) were both are located in the Ningbing Range, with an average of  $2.4 \text{ mmol L}^{-1}$  ( $n = 34$ ). There was an excellent correlation (i.e.  $r^2 > 0.9$ ) between  $\text{Cl}^-$ ,  $\text{Na}^+$ ,  $\text{Br}^-$ ,  $\text{Ca}^{2+}$  and  $\text{Mg}^{2+}$  suggesting these ions originate from a similar source.

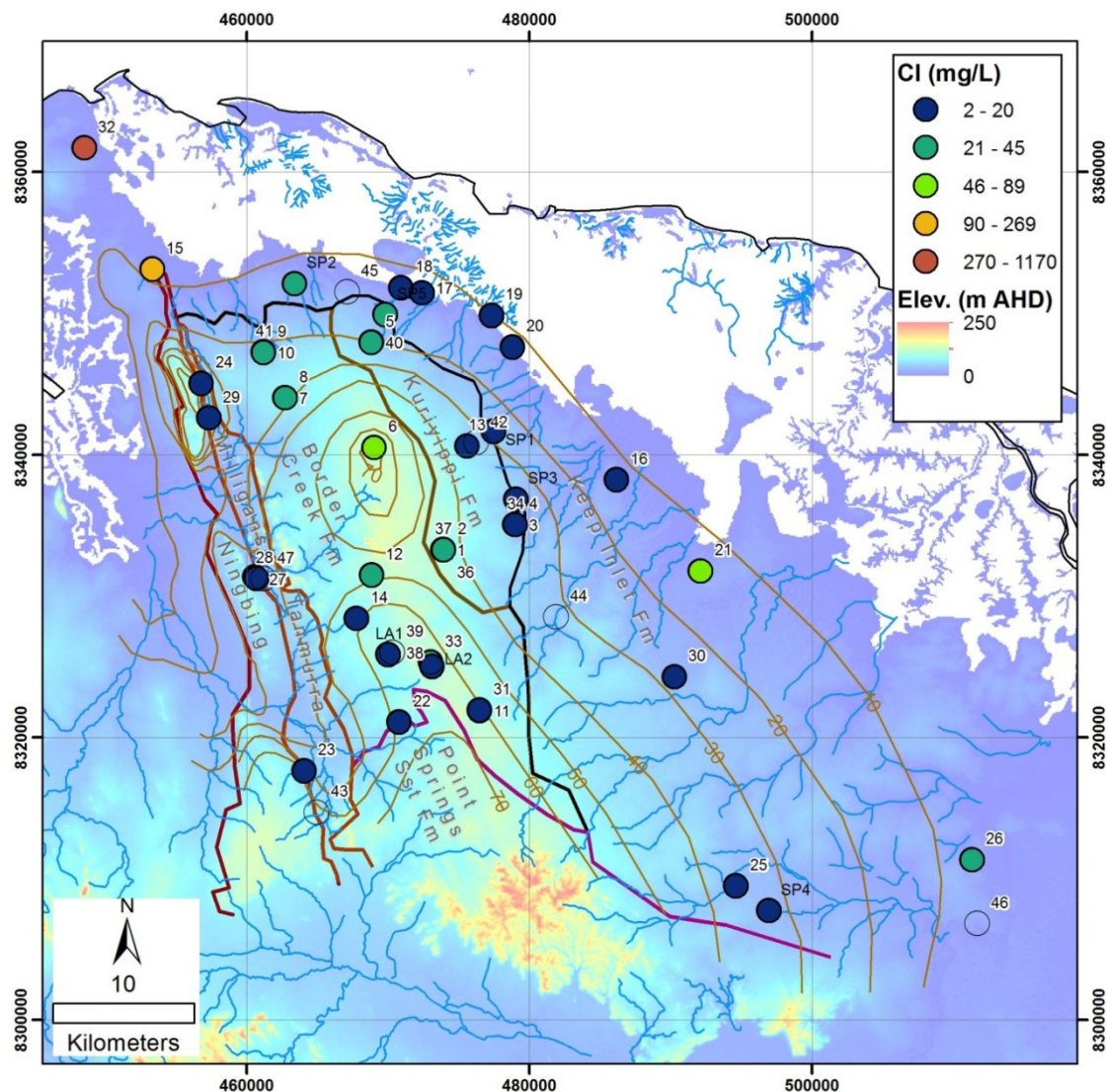


**Figure 4** The spatial distribution of Cl (mg L<sup>-1</sup>) in groundwaters for the study area compared with 10 m piezometric surface contours and sub-crop supplied by DPIRD.

Various trace elements and metals were analysed, with most found to be below detection limit or low in concentration (Appendix A, Table A3). Metal concentrations were all low. Analytes such as Al, B, Ba, Br, F, Li and Mn were all very low in concentration with average values of 0.05, 0.05, 0.05, 0.24, 0.11, 0.001 and 0.08 mg L<sup>-1</sup>, respectively. Nutrients such as nitrate, total nitrogen and total phosphorous were all very low with average values of 0.06, 0.13 and 0.04 mg L<sup>-1</sup>, respectively. Total Fe was generally low with an average value of 0.74 mg L<sup>-1</sup>. An elevated Fe concentration was observed in the HOTPLATE sample (6.30 mg L<sup>-1</sup>). Zinc concentrations were generally low with an average value of 0.24 mg L<sup>-1</sup>, except for BONAPARTE\_1\_Waterbore\_1 (3.2 mg L<sup>-1</sup>). The elevated concentrations may be due to the well construction material that was used in the older pre-existing wells located in the study site.

The  $\delta^{18}\text{O}$  ratios ranged from -6.65 ‰ (LEWIS) to -9.02 ‰ (17BP06S) with an average of -7.73 ‰ and the  $\delta^2\text{H}$  ratios from -43.17 ‰ to -61.82 ‰ with an average of -51.64 ‰ (n = 31) for the same samples. The values for  $\delta^{13}\text{C}_{\text{DIC}}$

ranged from -7.8 ‰ (TANMURRA) to -21.5 ‰ (17BP06S) with an average of -16.2 ‰ (n = 31).

The  $^3\text{H}$  activities ranged from below quantification limit to a high of 1.00 TU (17BP06S) with an average of 0.23 TU (n = 24). Of these samples, 11 contained  $^3\text{H}$  activities above 0.03 TU. These groundwater values are less than the average rainfall value of 1.6 TU. The piston flow recharge dates for CFCs and  $\text{SF}_6$  are presented in Appendix A, Tables A5 and A6. Uncorrected  $^{14}\text{C}$  values ranged from a 'bomb-pulse' signature of  $115.2 \pm 0.4$  pMC (17BP02S) in the central part of the site to a low palaeowater value of  $4.2 \pm 0.4$  pMC (CLEANSKIN) in the east with an average of 76.70 pMC (n = 31).



## 5 Discussion

### 5.1 Origin of groundwater recharge

The stable water isotopes (SWIs:  $\delta^{18}\text{O}$  and  $\delta^2\text{H}$ ) in groundwaters can provide information on the origin and evaporative effects that the water has undergone prior to recharge. Comparing the groundwater  $\delta^{18}\text{O}$  and  $\delta^2\text{H}$  values with rainfall can also provide information on the source of rainfall events contributing to the recharge, and therefore the origin of the groundwater.

The  $\delta^{18}\text{O}$  and  $\delta^2\text{H}$  values for groundwater, lakes, springs and rainfall samples were plotted on bivariate plots and are depleted relative to Vienna Standard Mean Ocean Water (V-SMOW) (Figure 5). Most waters plot on or close to the Darwin Local Meteoric Water Line ( $\delta^2\text{H} \text{‰} = 7.69\delta^{18}\text{O} + 9.75$ ; Hollins et al., 2018), except two spring water samples (Oaks Creek and Yow Spring) which plot to the right of this line suggesting that these samples have experienced evaporation. To explore this further these samples were compared to an Evaporation Line (EL) for the Pilbara Region ( $\delta^2\text{H} \text{‰} = 5.2\delta^{18}\text{O} - 14.4$ ; Dogramaci et al., 2012), which is considered the closest known EL that could potentially represent this study area. These relatively enriched samples plots close to this line suggesting evaporation in these two spring water samples.

Rainfall samples collected plot on or close to the Darwin LMWL but are generally significantly more enriched compared to groundwater. Two rainfall samples from 2016/17 and 2018 plot close to the groundwater samples. This suggests rainfall with very low  $\delta^{18}\text{O}$  and  $\delta^2\text{H}$  values are recharging the groundwater.

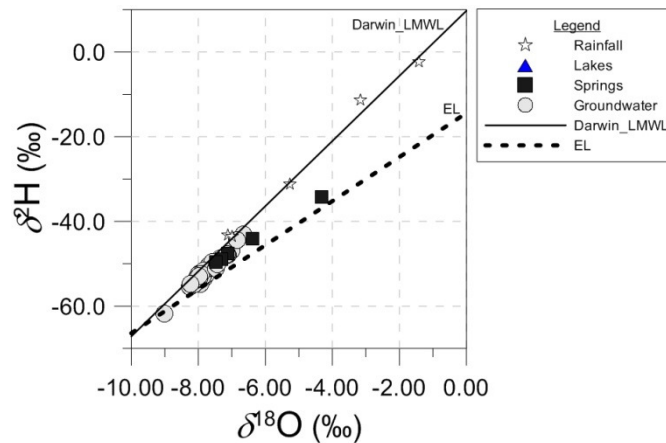


**Figure 5** Bivariate plot of  $\delta^2\text{H}$  vs.  $\delta^{18}\text{O}$  compared with the Darwin LMWL ( $\delta^2\text{H} \text{‰} = 7.69\delta^{18}\text{O} + 9.75$ ) and an Evaporation Line (EL) ( $\delta^2\text{H} \text{‰} = 5.2\delta^{18}\text{O} - 14.4$ ) for the Pilbara.

Groundwaters from this study site are low in  $\delta^{18}\text{O}$  and  $\delta^2\text{H}$  with an average of  $-7.73 \text{‰}$  and  $-51.64 \text{‰}$ , respectively, and are similar in composition for all aquifers implying they have a similar origin. Cyclonic or large monsoonal rainfall events are likely to be the dominant source of groundwater recharge to the system, which is similar to what is observed in the Pilbara where

groundwater also has very depleted compositions (average  $\delta^{18}\text{O}$  and  $\delta^2\text{H}$  values of -7.87 ‰ and -56.9 ‰, respectively) (Meredith et al., 2018). There is no evidence of evaporation prior to recharge suggesting that groundwater recharges quickly through the unsaturated zone because the depleted  $\delta^2\text{H}$  and  $\delta^{18}\text{O}$  signal is retained in the groundwater.

## 5.2 Source of salinity and location of recharge areas

The source of salinity and location of recharge areas were investigated using hydrochemical and isotopic techniques. This was done to provide a greater understanding of groundwater flow paths, the location of recharge areas and provide a means of validating calculated groundwater residence times.

The groundwater salinity is generally low with most containing less than 3 mmol L<sup>-1</sup> of Cl, with the exceptions being the two wells located in the northern corner of the study site closest to the coast (Matera\_bore and Brolga). These are likely to be influenced by seawater. There is no trend in Cl with depth in the aquifers, in fact the deeper samples tend to be lower in concentration.

The source of salinity was evaluated by using the Cl/Br and Na/Cl ratios in groundwater. Most Cl/Br ratios suggest that Cl is derived primarily from atmospheric accession with marine-like signatures close to the seawater value of 655 (Figure 6). Most groundwaters, lakes and spring waters have Na/Cl ratios close to unity implying NaCl dissolution or marine-derived aerosols (Figure 6). However, some waters (Wilson, Bore Spring, rain 2016/17, Calf Spring\_bore and Cleanskin) have Na/Cl ratios greater than 2 suggesting a source of Na. These samples are the exceptions and most samples have Na/Cl ratios similar to seawater. A strong correlation between major ions such as Na, Ca, Mg, K, Cl, SO<sub>4</sub> ( $r^2 = >0.9$ ) also suggests they are from a similar source. Therefore it can be interpreted that marine aerosols are the likely source of Cl in this system, which is introduced via rainfall recharge.

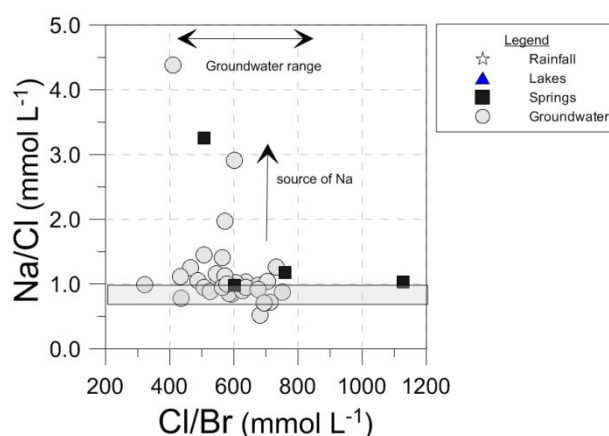


**Figure 6** Bivariate plot of Cl/Br vs. Na/Cl (molar concentration).

Key parameters such as DO, SiO<sub>2</sub> concentrations and  $^3\text{H}$  values were used as a guide for locating recharge areas. Higher values correspond with the two groundwater mounds also identified from the water levels data. The highest

SiO<sub>2</sub> concentration was observed in sample 16BP03I (0.47 mmol L<sup>-1</sup>) and a decrease in concentration occurred radially from this point. The two elevated DO concentrations in groundwater were also found in this area 16BP03I (5.59 mg L<sup>-1</sup>) and 17BP071 (4.9 mg L<sup>-1</sup>). Furthermore, elevated <sup>3</sup>H values in the Border Creek and Kuriyippi Formations are also associated with this region (Figure 7). Groundwater flow is directed away from the two mounds located in the centre of the site in all directions and the identification of elevated values for these parameters confirms the location of water that has been in contact with the atmosphere recently, and can therefore be interpreted as recharge areas.

### ***5.3 Carbon evolution after recharge***

In this coastal environment it would be expected that carbonate materials would be present in the form of marine carbonates or contained within the marine derived aquifer sediments. Carbonate dissolution processes are investigated to identify the relative contribution of carbon from these potential sources. This is important to consider when using radiocarbon to date groundwaters. We initially assess carbon processes by comparing the major ion chemistry and the saturation indices of carbonate minerals and then the carbon concentration and isotopes.

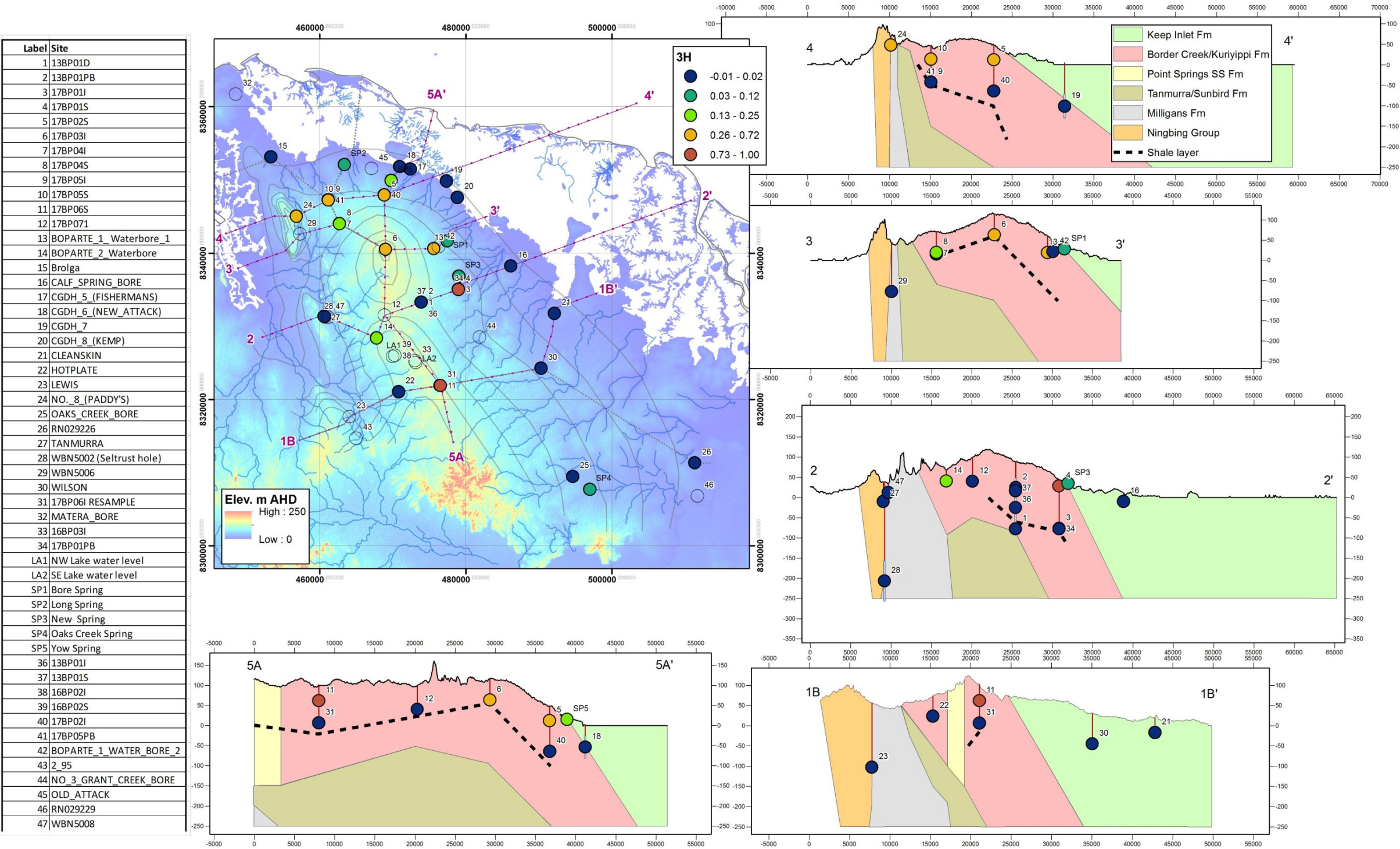


**Figure 7** The spatial distribution of  $^3\text{H}$  (T.U.) in groundwaters for the study area compared with elevation (m AHD) and 10 m piezometric surface contours supplied by DPIRD. The 5 cross sections are initial depictions of the hydrogeology based on field information provided by DPIRD and require validation with geophysical survey information.



All groundwaters are either undersaturated or in equilibrium with respect to common carbonates such as calcite, dolomite and siderite, implying that if these minerals are present within the aquifer then the groundwaters have the potential to dissolve them (Figure 8).

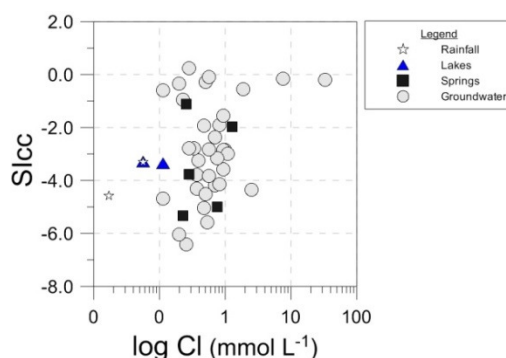


**Figure 8** A bivariate plot of the saturation indices of calcite ( $SI_{cc}$ ) vs. log of Cl concentration for waters from the study site.

The abundance of  $^{13}\text{C}$  in DIC ( $\delta^{13}\text{C}_{\text{DIC}}$ ) can indicate provenance and pathways in relation to fractionation by chemical changes, vegetation or microbial processes. The  $\delta^{13}\text{C}$  for this study was measured on the sample that was collected for  $^{14}\text{C}_{\text{DIC}}$ . This is not a true indication of the  $\delta^{13}\text{C}$  of the DIC and is used in this study as a broad reference for the  $\delta^{13}\text{C}_{\text{DIC}}$  value (see section 1.1 for explanation). Considering these limitations we can suggest that the  $\delta^{13}\text{C}_{\text{DIC}}$  values for groundwaters have an average of around -16 ‰ ( $n = 31$ ) and most are in the expected range for water that has been recharged through a  $\text{C}_3$  vegetation environment.

DIC concentrations showed no trend with depth but  $\delta^{13}\text{C}_{\text{DIC}}$  is highest in the WBN5002 (Seltrust hole) (-8.6 ‰) and Tanmurra (-7.8 ‰). These enriched values compared to other samples are most likely related to the carbonate aquifer material that the well is screened within. Other than these two samples, the relationship between  $^{14}\text{C}_{\text{DIC}}$  content and  $\delta^{13}\text{C}_{\text{DIC}}$  showed there is not a significant carbonate dilution trend (i.e.  $\delta^{13}\text{C}_{\text{DIC}}$  increase with  $^{14}\text{C}_{\text{DIC}}$  decrease) (Figure 9). This suggests that  $^{14}\text{C}_{\text{DIC}}$  is governed by decay.

The  $^{14}\text{C}_{\text{DIC}}$  content distribution appears to be governed by the location of the groundwater wells with distance from the recharge areas (Figure 10). Groundwaters located close to the recharge mound (near 17BP031) all had  $^{14}\text{C}_{\text{DIC}}$  contents greater than 70 pMC. There was no clear trend in  $^{14}\text{C}_{\text{DIC}}$  content along the groundwater flow path or with depth in the aquifer or distance from the coast. The lowest  $^{14}\text{C}_{\text{DIC}}$  values ranged between 4.2 and 19.5 pMC. They are associated with the Ningbing Range area and the Keep Inlet Formation located on the eastern side of the study area.



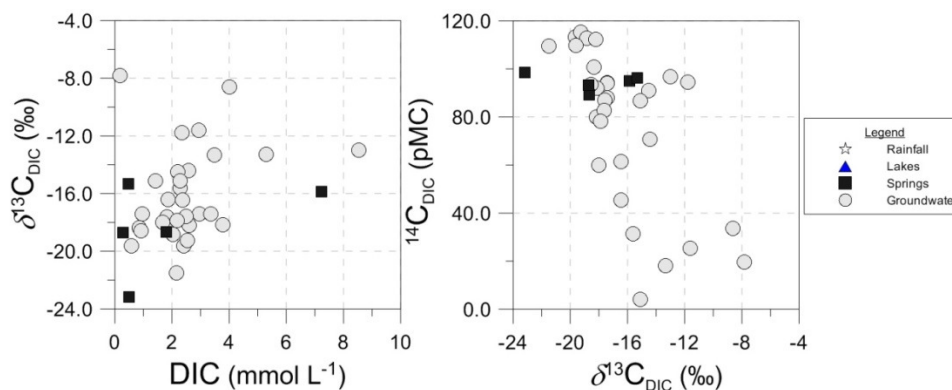


**Figure 9** Bivariate plots of (a) DIC vs.  $\delta^{13}\text{C}_{\text{DIC}}$  and (b)  $\delta^{13}\text{C}_{\text{DIC}}$  vs.  $^{14}\text{C}_{\text{DIC}}$ .

## 5.4 Groundwater residence times

Groundwater residence times or groundwater ‘ages’ were assessed using two radioisotopes ( $^3\text{H}$  and  $^{14}\text{C}_{\text{DIC}}$ ) and two chemical tracers (CFCs and  $\text{SF}_6$ ). The main isotopic age tracer employed for determining whether ‘modern’ recharge was happening in this study area was tritium ( $^3\text{H}$ ). It is a short-lived isotope of hydrogen with a half-life of 12.43 years. It is directly incorporated into the water molecule and therefore the only tracer that can be used to directly date water. Due to its short half-life,  $^3\text{H}$  is used to date groundwaters that are less than ~100 years old. The presence of  $^3\text{H}$  in a groundwater sample can also be used to qualitatively date the water sample, i.e. a measurable  $^3\text{H}$  activity in a water sample can be equated to a component of modern recharge.

CFCs are also used in this study with current estimates of the atmospheric lifetimes of CFC-11 and CFC-12 at  $45 \pm 7$  and  $87 \pm 17$  years, respectively (Plummer and Busenberg, 2000). CFCs are useful for dating waters that are less than 60 years old. Like  $^3\text{H}$  and CFCs, sulphur hexafluorides ( $\text{SF}_6$ ) can be used to date modern groundwaters and are useful for dating waters that are younger than 30 years old. Apparent ages can be very sensitive to excess air, so this needs to be accurately determined before calculating corresponding groundwater ages (Plummer and Busenberg, 2000).

### 5.4.1 Lumped Parameter Models using $^3\text{H}$ , $\text{SF}_6$ and CFCs

Groundwater residence times were calculated using five lumped parameter models (LPM): Piston-Flow Model (PFM), Exponential Mixing Model (EMM), Exponential Piston-Flow Model (EPM), Partial Exponential Model (PEM) and Dispersion Model (DM). The mean residence time (MRT) values were calculated from the combined tracer models using measured  $^3\text{H}$ ,  $\text{SF}_6$  and CFCs. The MRTs range from a minimum of 8 (17BP01S) to a maximum of 483 years (17BP071), which is outside the dating range for all of these tracers (Table 1).

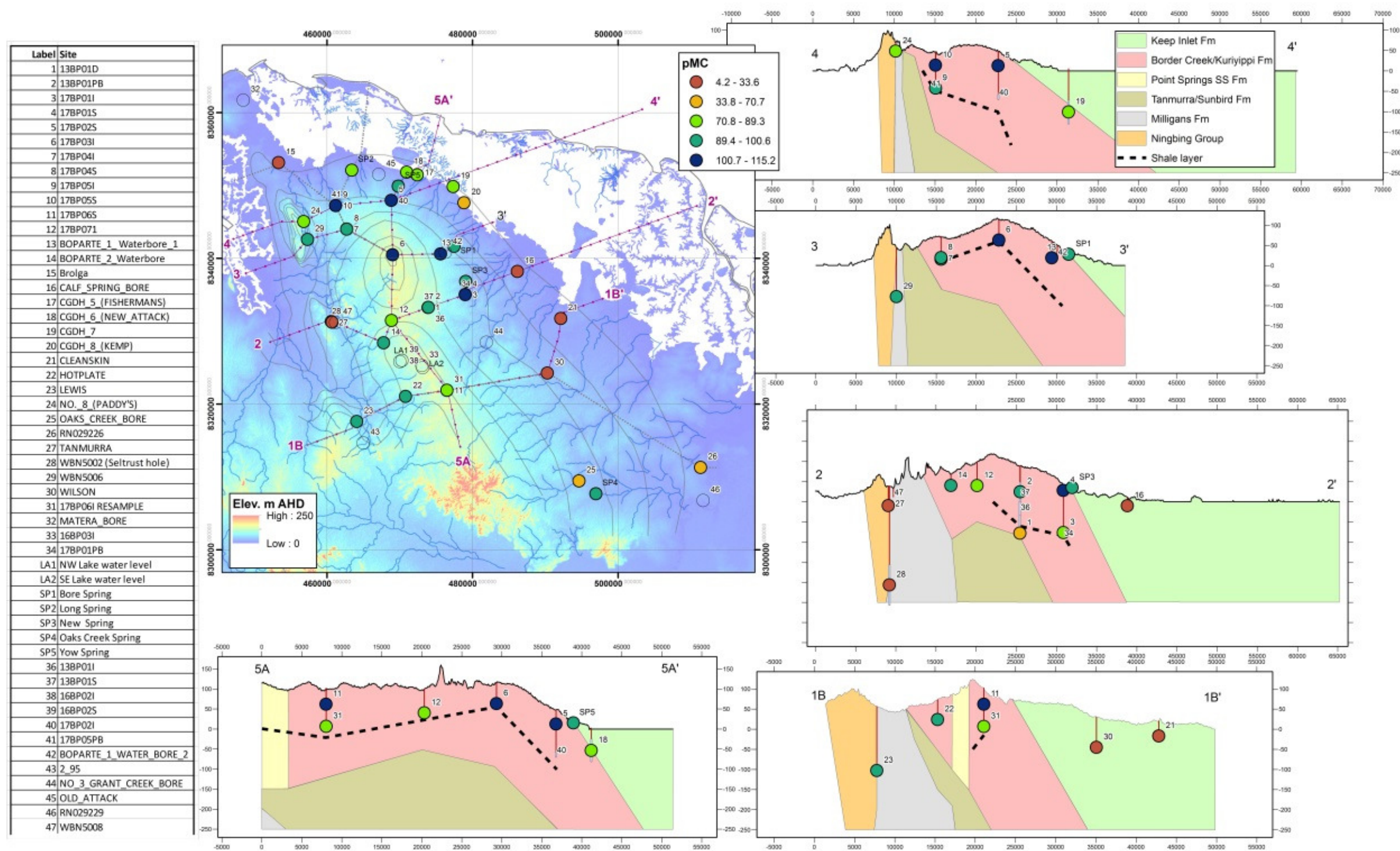


**Figure 10** The spatial distribution of  $^{14}\text{C}$  (pMC) in groundwaters for the study area compared with elevation (m AHD) and 10 m piezometric surface contours supplied by DPIRD. The 5 cross sections are initial depictions of the hydrogeology based on field information provided by DPIRD and require validation with geophysical survey information.

Excluding some EMM results, all the samples with these tracers present have MRTs less than 500 years, and several samples have MRTs of less than 100 years. The relatively large range of ages is due to the different assumptions in the LPMs. EMM results gave anomalously old groundwater ages for several samples. It was also identified that some of the samples may have been contaminated with atmospheric CFC or SF<sub>6</sub> based on results from the laboratory.

**Table 1** Groundwater residence time ranges calculated using Lumped Parameter Models with 3 tracers: <sup>3</sup>H, SF<sub>6</sub> and CFCs.

Well ID	Tracers in model	Age range (years)	MRT (years)	Comments
BONAPARTE_1_Waterbore_1	<sup>3</sup> H	53 – 64	56	
BONAPARTE_2_Waterbore	<sup>3</sup> H	55 – 205	139	
Brolga	CFC's	60 – 1390	202	EMM model excluded from MRT
17BP01S	<sup>3</sup> H, CFC's, SF <sub>6</sub> ( <sup>3</sup> H, SF <sub>6</sub> )	6 – 9 (12 – 20)	8 -18	CFC's possibly contaminated
17BP02S	<sup>3</sup> H, CFC's, SF <sub>6</sub>	43 – 145	102	
17BP03I	<sup>3</sup> H, CFC's, SF <sub>6</sub>	39 – 75	63	
17BP04S	<sup>3</sup> H, CFC's, SF <sub>6</sub>	56 – 612	135	EMM model excluded from MRT
17BP05S	<sup>3</sup> H, CFC's, SF <sub>6</sub>	40 - 98	82	
17BP06S	<sup>3</sup> H, CFC's, SF <sub>6</sub> ( <sup>3</sup> H, SF <sub>6</sub> )	34 – 64 (35 – 91)	48-66	CFC's possibly contaminated
17BP07I	<sup>3</sup> H, CFC's, SF <sub>6</sub>	72 - 17033	483	EMM model excluded from MRT
Bore Spring	<sup>3</sup> H, CFC's, SF <sub>6</sub>	68 - 1129	274	EMM model excluded from MRT
Long Spring	<sup>3</sup> H, CFC's, SF <sub>6</sub>	60 - 680	272	EMM model excluded from MRT
New Spring	<sup>3</sup> H, CFC's, SF <sub>6</sub>	65 - 946	385	EMM model excluded from MRT
NO._8_(PADDY'S)	<sup>3</sup> H, CFC's, SF <sub>6</sub> [ <sup>3</sup> H, CFC's]	33 – 53 [43 – 66]	43-66	SF <sub>6</sub> possibly contaminated
Oaks Creek Spring	<sup>3</sup> H, CFC's, SF <sub>6</sub>	56 - 393	260	CFC's possibly contaminated
Yow Spring	<sup>3</sup> H, CFC's, SF <sub>6</sub>	30 – 291	171	CFC's possibly contaminated

#### 5.4.2 Radiocarbon (<sup>14</sup>C) age

The <sup>14</sup>C age was corrected using the Pearson model age, the age calculated using the decay equation and rounded to the nearest 100 years for younger (sub-modern to 10,000 years old) and 1,000 years for older groundwaters (greater than 10,000 years old) (Table 2). Sub-modern waters were characterised as those ranging from 100-500 years old. Radiocarbon correction models use a variety of hydrochemical and isotopic data to calculate a correction value based on the observed groundwater chemistry of

a sample. The reader is to refer to Meredith et al., (2016 and 2018) for more detailed descriptions on radiocarbon correction methods. The Pearson correction model is more conservative method than the IAEA and is considered to be the more representative calculation based on the scope of the project. Refer to section 3 for a description on  $^{14}\text{C}$  methods.

Of the 31 samples measured for  $^{14}\text{C}$ , 9 samples were in the  $^{14}\text{C}$  dating range. The remaining samples are considered to be modern or sub-modern. Interestingly, 6 samples contain a 'bomb-pulse' value (i.e. greater than an atmospheric value of ~105 pMC) (Table 2). This seems reasonable when considering nuclear weapons testing occurred in the area on Monte Bello Islands, WA from 1952 to 1956.

The rate of groundwater movement from the recharge area to the wells with groundwater ages within the  $^{14}\text{C}$  age range could not be calculated for this study. This is because the actual recharge areas for 9 of those wells cannot be accurately determined from the available hydrogeological and geophysical data. Of the 9 wells:

- Six are likely to have their inlets within sandy lenses (or layers) of the Keep Inlet Formation (CGDH\_8\_[KEMP], OAKS\_CREEK\_BORE, RN029226, CALF\_SPRING\_BORE, WILSON and CLEANSKIN);
- Two have their inlets within the Milligans Formation or at the contact between the Milligans and the Ningbing Group limestones (WBN5002 [Seltrust hole] and Tanmurra);
- One has its inlet within Quaternary alluvium (Brolga).

A final age was assigned to each sample based on the  $^{14}\text{C}$  age and MRT calculations (Table 2). This value was determined by considering all 4 age tracers and noting that they have significantly different half-lives ranging from 10s to 1,000s of years which will influence the age calculations of the samples. Groundwater dating has inherent chemical and physical limitations associated with each tracer applied.  $^{14}\text{C}$  dating errors, depending on the groundwater environment can be as high as 1,000s of years.

Samples that had a 'bomb-pulse' were considered to be greater than 60 years due to the timing in nuclear activity in the region. Those that were modern or sub-modern are outside the  $^{14}\text{C}$  dating range, therefore the younger tracers were used to estimate the final age. As mentioned above, only 9 samples were within the  $^{14}\text{C}$  dating range. The  $^{14}\text{C}$  age was estimated from the Pearson correction model and the age was rounded up to the nearest 100 years. Please note the IAEA model was included to show the variation in age correction models. It is advised that further geochemical modelling is undertaken to refine the age for this particular groundwater environment.

The corrected model values of zero years indicate that the corrected value is outside of the  $^{14}\text{C}$  dating range for this groundwater environment. As most of these groundwaters are outside the  $^{14}\text{C}$  dating range, please refer to the final age in Table 2 for a more accurate groundwater residence time calculation. Fourteen samples located within the Border Creek and Kuriyippi Formations

were identified as less than 100 years old. These waters are found in the higher elevation areas of the site and relate to higher water levels. Generally, older waters (1,000 to 23,000 years old) are found in the Keep Inlet Formation (Figure 11).

**Table 2** Corrected radiocarbon ages using the Pearson and IAEA models (SM = sub-modern, BP = years before present) for groundwater samples with an assumed  $\delta^{13}\text{C}$  soil gas  $\text{CO}_2$  value of -23 ‰. The MRTs and a final water residence time are included. The  $^{14}\text{C}_{\text{uncorr}}$  is the uncorrected calculated age,  $^{14}\text{C}_{\text{pearson}}$  and  $^{14}\text{C}_{\text{IAEA}}$  are the modelled ages.

Site	Depth	$^{14}\text{C}_{\text{DIC}}$	$^{14}\text{C}_{\text{uncorr}}$	$^{14}\text{C}_{\text{pearson}}$	$^{14}\text{C}_{\text{IAEA}}$	$^{14}\text{C}$	MRT	Final
	M	pMC	years	years	years	years	years	years
17BP02S	32	115.16	0	0	990	bomb pulse	102	60-100
17BP01S	13.8	113.2	0	0	1289	bomb pulse	8 to 18	60-100
17BP03I	46.2	112.7	0	0	977	bomb pulse	63	60-100
17BP05S	27.62	112.2	0	0	737	bomb pulse	82	60-100
BONAPARTE_1_Waterbore_1	38.5	109.74	0	0	1537	bomb pulse	56	60-100
17BP06S	32.83	109.44	0	0	2316	bomb pulse	48 to 66	60-100
BONAPARTE_2_Waterbore	27.7	100.64	0	0	1704	modern	139	140
Yow Spring		98.44	130	194	3813	modern	171	170
WBN5006	123	96.65	282	0	0	modern		<100
Oaks Creek Spring		96.29	312	0	567	modern		<100
Bore Spring		94.89	433	0	985	sub-modern	274	270
LEWIS	157.55	94.44	473	0	0	modern		<100
17BP04I	51	94.29	486	0	1803	modern		<100
17BP04S	46.93	93.91	519	0	1846	modern	135	140
HOTPLATE	46.8	93.51	555	0	2405	sub-modern		100-500
New Spring		93.29	574	0	2495	sub-modern	385	390
17BP05I	83.82	91.9	698	0	2359	modern		<100
13BP01PB	59	90.89	789	0	595	sub-modern		100-500
NO_8_(PADDY'S)	17.90	89.27	938	0	30	modern	43	40
Long Spring		89.11	953	0	2843	sub-modern	272	270
17BP06I	88	87.92	1064	0	2377	modern		<100
CGDH_5_(FISHERMANS)	59.34	87.08	1143	0	2550	sub-modern		100-500
17BP07I	53	86.77	1173	0	1314	modern	483	480
CGDH_6_(NEW_ATTACK)	59.8	82.67	1573	0	2989	sub-modern		100-500
17BP01I	118	79.88	1857	0	3536	modern		<100
CGDH_7	105	78.17	2035	0	3568	modern		<100
13BP01D	162	70.67	2869	0	2635	sub-modern		100-500
CGDH_8_(KEMP)	101	61.47	4022	1252	4870	1300		1300
OAKS_CREEK_BORE	43.6	60.03	4218	2196	5815	2200	260	2200
RN029226	28	45.38	6530	3750	7368	3800		3800
WBN5002 (Seltrust hole)	123	33.65	9001	881	4499	900		900
CALF_SPRING_BORE	19.05	31.38	9579	6370	9989	6400		6400
Brolga	10.5	25.24	11378	5721	9340	5700	202	5700
TANMURRA	47.9	19.52	13502	4576	8194	4600		4600
WILSON	75	18.21	14076	9568	13186	9600		9600
CLEANSKIN	34.85	4.16	26278	22800	26419	22800		22800



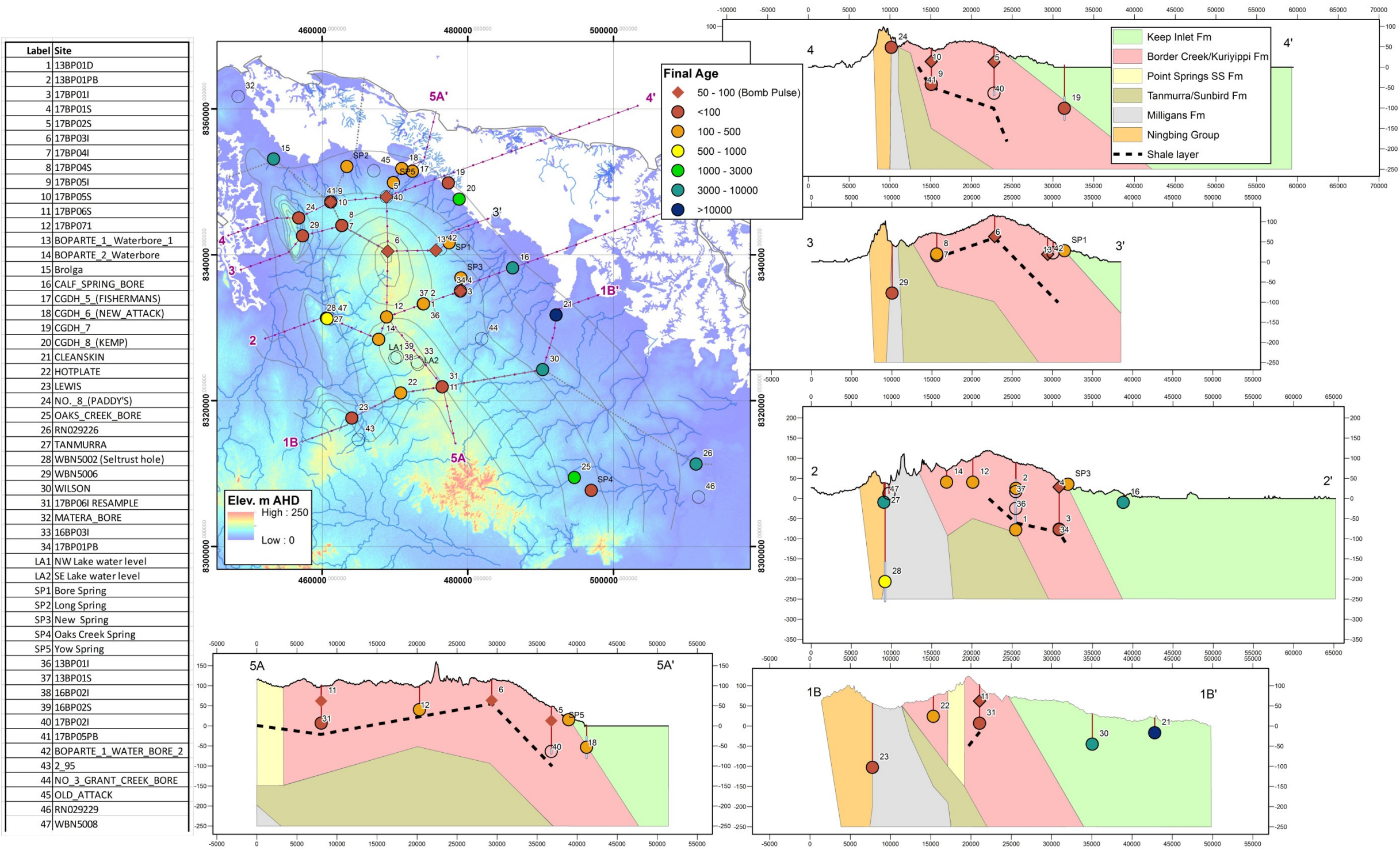


**Figure 11** The spatial distribution of groundwater residence times for the study area compared with elevation (m AHD) and 10 m piezometric surface contours supplied by DPIRD. The 5 cross sections are initial depictions of the hydrogeology based on field information provided by DPIRD and require validation with geophysical survey information

### 5.5 Groundwater recharge rate estimates

Tracers have been used to identify the location of recharge areas, groundwater residence times and infer the type of recharge processes leading to groundwater replenishment in this system. Here we use a variety of chemical and isotopic tracers to provide groundwater recharge rates for the system. We did this using Cl concentrations, corrected  $^{14}\text{C}$  'ages' and MRTs calculated using  $^3\text{H}$ , CFCs and  $\text{SF}_6$  data.

The chloride mass balance (CMB) method uses meteoric Cl input as a conservative tracer for determining water flux i.e. recharge rates into an aquifer system (Murphy et al., 1996). When applying the CMB technique, it is assumed that Cl is contributed from meteoric input, Cl is conservative, flow can be approximated by one dimensional piston flow and surface runoff is neglected.

The recharge rate,  $R$  to the aquifer is calculated using the following:

$$R = \frac{PC_P}{C_{gw}} \quad \text{Equation 2}$$

where  $P$  is the average yearly precipitation for the area,  $C_P$  is the  $\text{Cl}^-$  concentration of rainfall, and  $C_{gw}$  is the  $\text{Cl}^-$  concentration of groundwater.

Chloride in rainfall was measured from bulk rainfall samples collected between 2015 to 2017 yielding an average of  $1.3 \text{ mg L}^{-1}$  ( $n = 2$ ). Based on the average yearly precipitation rate of  $815 \text{ mm yr}^{-1}$  for the area, recharge rates ranged from 4 (Brolga) to  $265 \text{ mm yr}^{-1}$  (BONAPARTE\_1\_ Waterbore\_1 and Lewis) were calculated with an average of  $76 \text{ mm yr}^{-1}$  ( $n = 31$ ). This method suggests that between 0.5 to 33% of rainfall could potentially recharge the aquifer, considering the above stated assumptions. If we look at the samples with the highest  $^3\text{H}$  values i.e.  $>0.6 \text{ TUs}$  (17BP02S, 17BP05S, 17BP01S and 17BP06S) that ranged in depth from 13-32 m bgs, these samples generally had higher recharge rates ranging from 27 to  $118 \text{ mm yr}^{-1}$  (Table 3).

The MRTs and  $^{14}\text{C}$  ages were also used to calculate recharge rates, which were based on depth, groundwater age and porosity (0.3). These calculations yielded recharge rates ranging from  $0.5 \text{ mm yr}^{-1}$  (Cleanskin) to  $134 \text{ mm yr}^{-1}$  (NO.\_8\_(PADDY'S) with an average of  $31 \text{ mm yr}^{-1}$  ( $n = 13$ ) which equates to between 0.1 and 17% of rainfall being recharged into the aquifer each year. This average recharge rate is less than half of that calculated using the CMB method. Three samples located in the Border Creek Formation had recharge rates with an average of  $64 \text{ mm yr}^{-1}$ .

**Table 3** Groundwater recharge rates calculated using CMB technique and corrected ages (R).

<i>ID</i>	<i>CMB_mm/yr</i>	<i>R_mm/yr</i>
13BP01D	62	
13BP01PB	37	
17BP01I	82	
17BP01S	42	
17BP02S	37	
17BP03I	12	
17BP04I	30	
17BP04S	32	101
17BP05I	32	
17BP05S	27	
17BP06I	82	
17BP06S	118	
17BP07I	42	33
BONAPARTE_1_ Waterbore_1	265	
BONAPARTE_2_ Waterbore	151	59
Brolga	4	1
CALF_SPRING_BORE	132	1
CGDH_5_(FISHERMANS)	53	
CGDH_6_(NEW_ATTACK)	62	
CGDH_7	59	
CGDH_8_(KEMP)	88	23
CLEANSKIN	16	0
HOTPLATE	56	
LEWIS	265	
NO._8_(PADDY'S)	59	134
OAKS_CREEK_BORE	106	6
RN029226	39	2
TANMURRA	53	3
WBN5002 (Seltrust hole)	151	41
WBN5006	106	
WILSON	53	2

## 6 Conclusions

The isotopic and hydrochemical approach employed in this study has improved our understanding of the recharge sources, recharge locations and groundwater residence times for groundwaters in the Bonaparte Plains aquifers.

Groundwaters had similar  $\delta^2\text{H}$  and  $\delta^{18}\text{O}$  compositions with an average of -7.73 ‰ and -51.64 ‰, respectively implying they have a similar meteoric origin. Groundwaters plotted on the Darwin LMWL and represent cyclonic or large monsoonal rainfall events similar to other areas in WA such as the coastal Pilbara region. There was no evidence of evaporation prior to

recharge suggesting that groundwater recharges fairly quickly through the unsaturated zone.

The groundwater salinity was generally low with most containing less than 3 mmol L<sup>-1</sup> of Cl and it was found that marine aerosols are the source of Cl in this system, which is introduced via rainfall recharge. Elevated DO, SiO<sub>2</sub> concentrations and <sup>3</sup>H values correlate with the location of two water level mounds in the centre of the site. These parameters confirmed the location of water that has been in contact with the atmosphere recently i.e. recharge. Carbonate dissolution was not found to be a dominant process in the younger target aquifers. The spatial distribution of <sup>14</sup>C<sub>DIC</sub> content was found to be governed by the location of the groundwater wells with distance from the recharge areas. Groundwaters located close to the recharge mound (near 17BP03I) all had <sup>14</sup>C<sub>DIC</sub> contents greater than 70 pMC. There was no clear trend in <sup>14</sup>C<sub>DIC</sub> content along the groundwater flow path, with depth in the aquifer or distance from the coast.

Groundwater residence times were calculated and 14 samples located within the Border Creek and Kuriyippi Formations were identified as less than 100 years old. These waters are found in the higher elevation areas of the site and related well to the water level data. Generally, older waters (1,000 to 23,000 years old) were found in the Keep Inlet Formation in the lower elevations. Groundwater recharge rates ranged from 0.5-265 mm yr<sup>-1</sup> using the various methods but the average recharge rate calculated using the CMB method compared to those calculated from water residence times were up to 69% higher. Three samples located in the Border Creek aquifer had recharge rates with an average of 64 mm yr<sup>-1</sup>.

## 7 Recommendations

Recommendations for future works in the study area are as follows:

- Weekly or monthly rainfall collection and measurement;
- Should there be future significant groundwater abstraction in the area, monitoring for groundwater salinity changes on a regular basis to identify seawater intrusion in the northern sections of the aquifer;
- Undertake regular hydrochemical and isotopic sampling to identify whether changes occur in groundwater residence times due to cyclonic recharge events or changes in pumping scenarios; and
- Further research work into refining the  $^{14}\text{C}$  age, including bomb-pulse modelling.

## 8 Acknowledgements

The authors would like to thank the DPIRD for providing the funding and support for this project with special mention to Don Bennett. We would also like to thank Dr Dioni Cendon from ANSTO for providing the final review of the document.

## 9 References

Bennett, D., Raper, P. 2018, Conceptual hydrogeological model: Bonaparte Plains Kulshill Group sandstone aquifers. Department of Primary Industries and Regional Development, document. 10/3/2018

Dogramaci, S., Skrzypek, G., Dodson, W., Grierson, P.F. (2012). Stable isotope and hydrochemical evolution of groundwater in the semi-arid Hamersley Basin of subtropical northwest Australia. *Journal of Hydrology* 475, 281-293.

Hollins, S.E., Hughes, C.E., Crawford, J., Cendón, D.I. and Meredith, K.M. (2018) Rainfall isotope variations over the Australian continent – Implications for hydrology and isoscape applications. *Science of The Total Environment* 645, 630-645.

Jurgens, B.C., Böhlke, J.K., and Eberts, S.M., 2012, TracerLPM (Version 1): An Excel workbook for interpreting groundwater age distributions from environmental tracer data: U.S. Geological Survey Techniques and Methods Report 4-F3, 60 p.

Meredith, K.T., Han, L.F., Cendón, D.I., Crawford, J., Hankin, S., Peterson, M. and Hollins, S.E. (2018) Evolution of dissolved inorganic carbon in groundwater recharged by cyclones and groundwater age estimations using the  $^{14}\text{C}$  statistical approach. *Geochimica et Cosmochimica Acta* 220, 483-498.

Meredith, K.T., Han, L.F., Hollins, S.E., Cendón, D.I., Jacobsen, G.E. and Baker, A. (2016) Evolution of chemical and isotopic composition of inorganic



carbon in a complex semi-arid zone environment: Consequences for groundwater dating using radiocarbon. *Geochimica et Cosmochimica Acta* 188, 352-367.

Murphy, E., Ginn, T., Phillips, J. (1996). Geochemical estimates of paleorecharge in the Pasco basin: Evaluation of the chloride mass balance technique. *Water Resources Research*; 32(9), 2853-2868.

Parkhurst, D. and Appelo, C. (1999). User's guide to PHREEQC (version 2) – a computer program for speciation, batch-reaction, one dimensional transport, and inverse geochemical calculations. USGS Water Resources Investigations Report 99 4259.

**Table A1** Work details and locations for all water sampling locations. Please note values in italics under sample depth have been estimated because data was not available for these sample locations. All other data was supplied by DPIRD.

Site	Type	Geol at inlet	NORTHING	EASTING	ELEVATION	SWL_date	WL	screen_top	screen_bottom	sample depth	sample depth	screen thickness
			GDA_Z52	GDA_Z52	mAHD		mAHD	mAHD	mAHD	mAHD	m bgs	m
13BP01D	Groundwater	Kuriyippi Formation	8333260.730	473886.620	84.04	16/11/2017	39.25	-71.96	-83.96	-77.96	162.00	12.00
13BP01PB	Groundwater	Kuriyippi Formation	8333272.330	473925.070	83.96	16/11/2017	39.76	48.96	0.96	24.96	59.00	48.00
16BP03I	Groundwater	Quaternary colluvium	8325290.077	473038.289	97.793	15/11/2017	90.75	88.39	86.39	87.39	10.40	2.00
17BP01I	Groundwater	Kuriyippi Formation	8335027.204	478993.383	41.75	8/11/2017	35.84	-70.25	-82.25	-76.25	118.00	12.00
17BP01PB	Groundwater	Kuriyippi Formation	8335027.204	479003.939	41.097	8/11/2017	35.81	-71.65	-83.65	-77.65	118.75	12.00
17BP01S	Groundwater	Kuriyippi Formation	8335023.098	478983.939	41.963	8/11/2017	35.90	29.66	26.66	28.16	13.80	3.00
17BP02S	Groundwater	Kuriyippi Formation	8347942.353	468829.839	44.58	15/11/2017	20.12	14.08	11.08	12.58	32.00	3.00
17BP03I	Groundwater	Border Creek Formation	8340498.650	469012.153	109.525	10/11/2017	71.23	64.83	61.83	63.33	46.20	3.00
17BP04I	Groundwater	Border Creek Formation	8344019.122	462705.715	66.474	10/11/2017	28.31	21.47	9.47	15.47	51.00	12.00
17BP04S	Groundwater	Border Creek Formation	8344008.208	462707.263	66.395	10/11/2017	28.34	20.97	17.97	19.47	46.93	3.00
17BP05I	Groundwater	Border Creek Formation	8347241.926	461179.050	41.333	10/11/2017	21.95	-36.49	-48.49	-42.49	83.82	12.00
17BP05S	Groundwater	Border Creek Formation	8347232.544	461182.196	41.456	10/11/2017	22.40	15.34	12.34	13.84	27.62	3.00
17BP06I	Groundwater	Border Creek Formation	8321899.871	476482.346	94.617	16/11/2017	55.87	9.62	3.62	6.62	88.00	6.00
17BP06S	Groundwater	Border Creek Formation	8321890.871	476484.346	94.602	8/11/2017	71.22	63.27	60.27	61.77	32.83	3.00
17BP07I	Groundwater	Border Creek Formation	8331473.34	468859.889	93.147	14/11/2017	48.78	43.15	37.15	40.15	53.00	6.00
BONAPARTE_1_Waterbore_1	Groundwater	Border Creek	8340605.520	475605.004	57.553	15/11/2017	32.93	22.05	16.05	19.05	38.50	6.00
BONAPARTE_2_Waterbore	Groundwater	Border Creek	8328404.941	467779.058	68.181	15/11/2017	58.82	43.48	37.48	40.48	27.70	6.00
Brolga	Groundwater	Quaternary alluvium	8353128.053	453332.347	10.035	11/11/2017	9.00	<-0.46	ND	-0.46	10.50	
CALF_SPRING_BORE	Groundwater	Keep Inlet	8338208.236	486167.620	9.388	9/11/2017	14.00	-7.16	-12.16	-9.66	19.05	5.00
CGDH_5_(FISHERMANS)	Groundwater	Keep Inlet	8351461.647	472404.025	4.065	20/09/2017	17.45	-45.94		-55.27	59.34	18.68
CGDH_6_(NEW_ATTACK)	Groundwater	Keep Inlet	8351823.893	470932.215	6.363	15/11/2017	10.03	-25.24		-53.44	59.80	56.40
CGDH_7	Groundwater	Keep Inlet	8349855.258	477332.137	4.037	16/08/2017	12.00	-9.96		-38.96	105.00	58.00
CGDH_8_(KEMP)	Groundwater	Keep Inlet	8347624.734	478825.625	5.195	16/08/2017	12.45	-68.81	-122.81	-95.81	101.00	54.00
CLEANSKIN	Groundwater	Keep Inlet	8331754.046	492122.479	17.869	9/11/2017	14.73	-7.98	-25.98	-16.98	34.85	18.00
HOTPLATE	Groundwater	Border Creek	8321055.219	470795.535	70.48	8/11/2017	62.23	26.68	20.68	23.68	46.80	6.00
LEWIS	Groundwater	Ningbing Group	8317617.137	464069.415	54.836	23/08/2017	56.48	-102.76		-102.71	157.55	-0.10
MATERA_BORE	Groundwater	Unknown	8361708	448492	5	4/09/2017	3.79	ND	ND			
NO_8_(PADDY'S)	Groundwater	Ningbing Group	8345047.107	456797.598	66.262	11/11/2017	58.85	51.36	45.36	48.36	17.90	6.00
OAKS_CREEK_BORE	Groundwater	Point Spring	8309462.031	494634.026	34.786	9/11/2017	34.69	-5.81	-11.81	-8.81	43.60	6.00
RN029226	Groundwater	Keep Inlet	8311308.313	511340.479	12.467	9/11/2017	8.05	-12.53	-18.53	-15.53	28.00	6.00
TANMURRA	Groundwater	Milligans	8331329.644	460590.145	38.543	11/11/2017	33.04	-6.36	-12.36	-9.36	47.90	6.00
WBN5002 (Seltrust hole)	Groundwater	Ningbing Group/Milligans	8331231.636	460693.042	38.358	11/11/2017	35.89	-156.54	-156.54	-156.54	123.00	0.00
WBN5006	Groundwater	Ningbing Group	8342589.321	457322.695	45.358	11/11/2017	46.29	-77.64	ND	-77.64	123.00	
WILSON	Groundwater	Keep Inlet	8324255.210	490280.810	29.883	8/11/2017	28.66			-45.12	75.00	0.00
NW Lake water level	Lake		8325838.073	470004.553	85.075	15/08/2017	85.08	NA	NA	85.075	0.00	
SE Lake water level	Lake		8325001.546	473140.193	94.576	15/08/2017	94.58	NA	NA	94.576	0.00	
Bonaparte Rain 12/6/18	Rainfall											
Rain 2015/16	Rainfall											
Rain1 2016/17	Rainfall											
Rain2 2016/17	Rainfall											
Rain3 (May-Nov 17)	Rainfall											
Bore Spring	Spring		8341642.126	477448.584	25.951	24/09/2017	27.95	NA	NA	25.951		
Long Spring	Spring		8352098.751	463390.926	6.023	27/09/2017	10.02	NA	NA	6.023		
New Spring	Spring		8336838.653	479055.126	33.261	21/09/2017	35.26	NA	NA	33.261		
Oaks Creek Spring	Spring		8307699.379	496961.466	29.003	22/09/2017	32.00	NA	NA	29.003		
Yow Spring	Spring		8349904.014	469792.652	14.366	15/08/2017	15.37	NA	NA	14.366		

**Table A2** Field parameters, major ion chemistry and charge balance error percentage (CBE%). All data was supplied by DPIRD. CBE\_lab was the calculation supplied by the laboratory and CBE\_PHREEQC was calculated in PHREEQC using the supplied data.

Site	Sample_Date	T	pH	EC	DO	ORP as Eh	Field_Alkalinity	Ca	K	Mg	Na	Si	Cl	SO <sub>4</sub>	HCO <sub>3</sub>	CBE_lab	CBE_PHREEQC
		(°C)		mS/m @25	(mg/L)	mV	mg/L	mg/L	mg/L	mg/L	mg/L	mg/L	mg/L	mg/L	mg/L	%	%
13BP01D	4/8/2017	33.8	6.2	17.4	1.31	252	24	17.7	2	2.3	11.4	9.9	17	3.9	70	-3.9	-1.5
13BP01PB	16/11/2017	32.4	6.29	20.56	3.7	238	71	17.5	1.6	2.9	15.9	16	29	1.9	67	-4.3	-2.9
16BP03I								9.2	1.1	4.5	26.7	28	33	2.6	70	-4.1	-2.2
17BP01I	12/9/2017	32	5.56	8.91	2.46	332	31	4.3	2.2	1.4	7.2	7.3	13	5.4	17	-6.6	-3.2
17BP01PB			6.20	8.7				4.1	2.1	2.1	8.4	8.3	14	5.9	18	-3.8	-0.5
17BP01S	12/9/2017	32	5.35	14.62	2.6	277	40	3.4	3.4	1.6	18.1	15	25	14.1	15	-4.8	1.2
17BP02S	20/9/2017	32.4	5.77	17.1	1.9	307	36	0.6	1	6.6	21.7	14	29	6.8	35	-1.6	0.5
17BP03I	19/9/2017	32.2	5.78	35.4	5.59	308	35	0.5	1.8	9.4	51.4	28	89	14.5	30	-4.4	-3.3
17BP04I	18/9/2017	31.7	5.88	21.1	3.2	313	52	6.9	0.9	7	23.2	12	35	9.6	50	-2.5	-1.4
17BP04S	18/9/2017	31.8	5.83	20.8	2.97	311	59	7.4	1	7.4	24.1	13	33	8.6	53	0.7	2.1
17BP05I	18/9/2017	32.7	5.5	17.8	2.32	311	34	4.6	1.2	5	20.9	11	33	7.6	32	-2.8	-0.8
17BP05S	18/9/2017	34.2	5.95	23.7	2.7	316	54	3.9	0.8	9.2	26.7	12	39	10.2	50	-1	0.1
17BP06I	16/11/2017	32.5	5.67	7.34	2.99	280	27	1.5	1.1	0.9	10.6	13	13	4.3	11	-2.7	0.3
17BP06S	30/9/2017	32.1	4.75	4.7	2.85	351	22	0.3	0.4	0.7	5.5	14	9	1.9	3	-8.7	-1.4
17BP07I	18/11/2017	32.4	6.28	15.8	4.93	298	47	9.2	0.6	1.8	16.9	13	25	2.5	43	-3.4	-3.5
BONAPARTE_1_Waterbore_1	30/8/2017	32.3	5.72	9.27	2.05	278	36	0.8	0.2	0.4	2.6	9.2	4	1.1	7	-20	14.8
BONAPARTE_2_Waterbore	28/8/2017	31.1	5.24	6.88	2.52	351	15	0.2	0.1	0.3	4	9.4	7	0.4	3	-16	-6.2
Brolga	5/9/2017	32.0	7.12	117	0.31	128	165	86.6	6.7	18.6	90.1	5.4	269	23.7	159	-3.8	-3.6
CALF_SPRING_BORE	20/8/2017	31.0	6.95	24.7	0.54	102	115	22.5	16.1	4.6	15.1	11	8	19	114	0.5	2.4
CGDH_5_(FISHERMANS)	16/8/2017	32.4	5.41	10.43	2.89	377	30	5.6	1	1.4	12.3	9.2	20	1.6	17	1.1	4.3
CGDH_6_(NEW_ATTACK)	16/8/2017	31.4	5.18	8.53	3.25	375	18	1.3	3.7	1.8	10.4	9.9	17	4	7	1.6	5.4
CGDH_7	16/8/2017	32.8	5.16	9.54	0.08	279	30	3.9	2.4	1.8	11.7	8.9	18	7.9	9	2.8	6.1
CGDH_8_(KEMP)	16/8/2017	32.1	6.02	15.54	1.19	224	51	5.6	14.5	3.6	7.1	17	12	8.5	50	-4.8	3.3
CLEANSKIN	20/8/2017	34.0	7.55	45.8	0.1	-21	144	12.1	6.4	5.1	84.3	7.9	66	21	133	3.4	4.1
HOTPLATE	10/9/2017	31.0	5.32	8.74	2.45	291	28	0.4	0.9	0.7	8.9	9.2	19	1.7	5	-17	4.5
LEWIS	23/8/2017	34.5	7.17	53.3	2.48	296	285	23.7	0.2	9.2	1.3	2.7	4	0.9	128	-6.4	-5.5
MATERA_BORE								192	19.1	78.5	540	8.9	1170	115	160	2.7	2.6
NO_8_(PADDY'S)	5/9/2017	33.0	6.93	9.1	1.2	299	375	56.8	1.6	23.6	16.9	4.7	18	97.3	266	-11	-11.7
OAKS_CREEK_BORE	7/9/2017	31.2	6.26	12.5	0.54	198	61	3.3	14.8	4.9	9.1	13	10	5.1	48	4	7.6
RN029226	13/9/2017	32.1	5.93	17.4	0.38	238	44	4.2	11.1	5	13.6	19	27	9.9	34	-2.7	-0.8
TANMURRA	29/8/2017	33.3	7.12	6.65	0.42	56	345	1.8	0.2	1.7	11.3	5.8	20	0.9	9	-3.9	-1.1
WBN5002 (Seltrust hole)	28/8/2017	36	7.02	68.2	1.57	114	375	39.4	2.7	14.5	5.2	4.4	7	3.2	208	-3.7	-3.2
WBN5006	17/8/2017	35.5	6.92	66.5	1.8	318	360	113	0.5	18.6	6.4	5.6	10	5.1	431	-0.3	0.1
WILSON	20/8/2017	34.1	7.54	42.3	2.05	125	165	23.8	10.5	8.3	56.8	22	20	21.5	201	3.1	3.2
NW Lake water level		26.7	6.98	3.86	6.87	281	15	0.8	3	1.6	3.4	1.2	4	0.7	11	4.8	12.8
SE Lake water level		26.8	6.86	3	6.57	297	21	1.2	2.8	1.5	1.7	2.7	2	0.6	10	7.6	14.1
Rain 2015/16	15/16 wet season							0.4	0.2	0.2	0.6	0.2	0.6	0.4	2	-19	21.2
Rain1 2016/17	14/3/2017							1.3	0.2	0.4	4.1	1.7	2	0.8	7	11	18.8
Rain2 2016/17	20/5/2017																
Rain3 (May-Nov 17)	16/11/2017																
Bonaparte Rain 12/6/18	12/06/2018																
Bore Spring	29/8/2017	23.8	6.46	16.32	3.7	283	28	29.7	6.4	24.4	19	15	9	2.5	257	-0.8	-0.5
Long Spring	11/9/2017	19.9	6.53	26.5	1.87	304	70	13.4	0.2	6.8	30.1	14	45	6.7	65	0.2	1.1
New Spring	30/8/2017	24.4	5.58	11.1	1.88	346	15	0.9	0.7	0.5	5.1	14	8	0.3	3	0	9.8
Oaks Creek Spring	7/9/2017	22.8	6.28	4.74	3.46	305	21	1.4	3.2	1.3	6.8	11	10	0.5	14	-1.1	4.7
Yow Spring	19/8/2017	24.7	5.63	10.7	2.06	281	21	1	0.2	1.3	20.6	20	27	1.1	5	7.1	10.2

**Table A3** Minor ions, metals and nutrients. All data was supplied by DPIRD.

Site	Al	B	Ba	Br	F	Fe	Li	Mn	N_NO <sub>3</sub>	N_total	P_total	Zn
	mg/L	mg/L	mg/L	mg/L	mg/L	mg/L	mg/L	mg/L	mg/L	mg/L	mg/L	mg/L
13BP01D	0.023	0.051	0.067	0.06	<0.05	1.4	0.0052	0.23	0.04	0.08	0.016	0.04
13BP01PB	0.027	0.09	0.035	0.11	<0.05	0.022	0.0023	0.0042	0.07	0.13	0.053	0.09
16BP03I	0.44	0.13	0.091	0.16	0.14	0.48	0.0008	0.17	<0.01	0.62	0.07	0.25
17BP01I	0.036	0.036	0.051	0.05	<0.05	0.37	0.0021	0.064	0.03	0.1	0.025	0.039
17BP01PB	0.03	0.053	0.031	0.05	<0.05	0.37	0.0032	0.033	0.04	0.06	0.023	0.046
17BP01S	0.053	0.1	0.035	0.13	<0.05	2.6	0.0041	0.019	0.12	0.16	0.02	0.039
17BP02S	0.027	0.09	0.018	0.12	0.13	0.35	0.0007	0.0066	0.11	0.13	0.020	0.021
17BP03I	0.031	0.15	0.053	0.32	0.07	0.13	0.0022	0.014	0.06	0.08	<0.010	0.02
17BP04I	0.025	0.09	0.05	0.13	0.06	0.013	0.0014	0.004	0.1	0.11	<0.010	0.016
17BP04S	0.033	0.1	0.051	0.13	0.07	0.018	0.0014	0.0064	0.07	0.09	<0.010	0.03
17BP05I	0.027	0.08	0.05	0.11	0.07	0.063	0.0016	0.013	0.04	0.05	0.03	0.024
17BP05S	0.035	0.09	0.049	0.18	0.1	0.069	0.001	0.0069	0.06	0.09	0.038	0.025
17BP06I	0.15	0.05	0.022	0.04	<0.05	0.064	0.003	0.022	0.02	0.07	0.028	0.041
17BP06S	0.057	0.06	0.021	0.04	<0.05	0.041	0.0014	0.005	0.1	0.12	0.04	0.025
17BP07I	0.062	0.07	0.052	0.08	0.07	0.031	0.0023	0.026	0.06	0.09	0.025	0.044
BONAPARTE_1_ Waterbore_1	0.043	0.036	0.019	<0.02	<0.05	4.3	0.0007	0.048	0.03	0.22	0.047	3.2
BONAPARTE_2_ Waterbore	0.027	0.039	0.018	0.03	<0.05	0.64	0.0012	0.81	0.02	0.26	0.01	2.6
Brolga	0.013	0.013	0.085	0.89	0.13	0.11	0.0052	0.0032	<0.01	<0.02	0.011	0.014
CALF_SPRING_BORE	0.027	0.021	0.089	0.03	0.11	1.4	0.01	0.27	<0.01	0.07	0.064	0.02
CGDH_5_(FISHERMANS)	0.018	0.05	0.02	0.08	<0.05	0.046	0.001	0.0044	0.07	0.08	0.014	0.024
CGDH_6_(NEW_ATTACK)	0.027	0.037	0.055	0.06	<0.05	0.04	0.0016	0.01	0.06	0.07	<0.010	0.025
CGDH_7	0.048	0.046	0.027	0.07	<0.05	0.11	0.0009	0.02	<0.01	<0.02	0.039	0.043
CGDH_8_(KEMP)	0.035	0.034	0.22	0.04	0.07	4.7	0.0035	0.34	<0.01	0.04	0.11	0.039
CLEANSKIN	0.023	0.022	0.042	0.26	0.15	0.023	0.015	0.029	<0.01	<0.02	0.028	0.009
HOTPLATE	0.042	0.033	0.17	0.06	<0.05	6.3	0.0012	0.05	0.06	0.07	0.016	0.085
LEWIS	0.01	0.008	0.023	<0.02	<0.05	0.014	0.0001	0.0027	0.01	<0.02	0.02	0.027
MATERA_BORE	0.024	0.09	0.082	3.8	0.18	0.042	0.0043	0.017	<0.01	0.39	0.22	0.018
NO_8_(PADDY'S)	0.034	0.046	0.017	0.08	0.24	0.015	0.0014	0.0052	0.2	0.23	<0.01	0.16
OAKS_CREEK_BORE	0.026	0.023	0.13	0.04	0.1	1.1	0.0062	0.21	0.02	0.03	0.041	0.79
RN029226	0.023	0.027	0.055	0.14	0.13	0.18	0.012	0.01	<0.01	<0.02	0.048	0.024
TANMURRA	0.019	0.023	0.046	0.06	<0.05	0.012	0.0033	0.041	<0.01	0.14	0.021	0.12
WBN5002 (Seltrust hole)	0.013	0.011	0.032	<0.02	0.06	0.047	0.0016	0.009	<0.01	0.05	0.085	0.072
WBN5006	0.04	0.039	0.036	0.07	0.1	0.02	0.0004	0.017	0.02	0.05	<0.010	0.13
WILSON	0.04	0.016	0.025	0.11	0.11	0.035	0.021	0.19	<0.01	<0.02	0.053	0.039
NW Lake water level	0.032	0.028	0.004	<0.02	<0.05	0.043	0.0002	0.0023	<0.01	0.82	0.017	0.013
SE Lake water level	0.028	0.019	0.0095	<0.02	<0.05	0.052	0.0003	0.0022	<0.01	0.87	0.026	0.022
Rain 2015/16	0.035	0.009	0.003	<0.02	<0.05	0.061	<0.0001	0.005	<0.01		0.008	0.12
Rain1 2016/17	0.04	0.005	0.0023	<0.02	<0.05	0.029	<0.0001	0.0027	0.04	0.16	<0.010	0.04
Rain2 2016/17												
Rain3 (May-Nov 17)												
Bonaparte Rain 12/6/18												
Bore Spring	0.058	0.09	0.028	0.04	0.08	0.068	0.0019	0.013	<0.01	0.19	<0.010	0.1
Long Spring	0.035	0.1	0.031	0.09	<0.05	0.086	0.001	0.0073	<0.01	1	0.017	0.023
New Spring	0.069	0.055	0.024	0.03	<0.05	0.16	0.0039	0.013	<0.01	0.41	0.017	0.043
Oaks Creek Spring	0.045	0.03	0.018	<0.02	<0.05	0.25	0.0017	0.0096	<0.01	0.17	0.016	0.034
Yow Spring	0.042	0.08	0.0092	0.08	<0.05	0.11	0.0034	0.0074	<0.01	0.12	0.022	0.012

**Table A4** Isotopes and modelled output from PHREEQC such as partial pressure of CO<sub>2</sub>, Dissolved inorganic carbon and saturation indices of calcite and dolomite.

Site	δ <sup>2</sup> H	δ <sup>18</sup> O	<sup>3</sup> H	<sup>3</sup> H error	δ <sup>13</sup> C	<sup>14</sup> C <sub>DIC</sub>	<sup>14</sup> C <sub>DICerror</sub>	DIC	SI calcite	SI dolomite	pCO <sub>2</sub>
	‰	‰	TU	TU	‰	pMC	pMC	mmol/L			log atm
13BP01D	-53.4	-7.83	0.021	0.017	-14.43	70.67	0.27	2.58	-1.9	-4.3	-1.3
13BP01PB	-50.5	-7.69	0.043	0.014	-14.5	90.89	0.29	2.2	-1.9	-4.2	-1.4
16BP03I								1.38	-1.6	-3.1	-2.2
17BP01I	-52.7	-7.86			-18.19	79.88	0.27	1.85	-3.8	-7.6	-1.3
17BP01PB								0.71	-3.2	-6.4	-1.9
17BP01S	-48.8	-7.34	0.850	0.028	-19.64	113.2	0.35	2.42	-4.2	-8.3	-1.1
17BP02S	-55.5	-8.26	0.627	0.025	-19.27	115.16	0.36	2.53	-4.1	-6.8	-1.2
17BP03I	-46.9	-7.02	0.450	0.022	-18.83	112.7	0.35	2.03	-4.3	-7.0	-1.3
17BP04I	-53.4	-7.94			-17.41	94.29	0.3	2.96	-2.9	-5.3	-1.1
17BP04S	-54.7	-7.94	0.250	0.020	-17.43	93.91	0.3	3.37	-2.9	-5.3	-1.1
17BP05I	-52.5	-7.78			-18.15	91.9	0.29	3.78	-3.6	-6.7	-0.9
17BP05S	-52.3	-7.95	0.724	0.026	-18.21	112.2	0.34	2.6	-3.0	-5.2	-1.2
17BP06I	-53.8	-7.93			-17.4	87.92	0.29	0.97	-4.3	-8.4	-1.6
17BP06S	-61.8	-9.02	1.001	0.027	-21.5	109.44	0.34	2.17	-6.4	-12.0	-1.1
17BP07I	-52.6	-8.00	0.198	0.018	-15.1	86.77	0.28	1.43	-2.4	-5.0	-1.6
BONAPARTE_1_ Waterbore_1	-54.8	-8.10	0.542	0.021	-19.62	109.74	0.34	0.59	-4.7	-9.3	-1.8
BONAPARTE_2_Waterbore	-52.7	-7.85	0.227	0.018	-18.36	100.64	0.32	0.85	-6.1	-11.5	-1.6
Brolga	-53.7	-8.04	0.004	0.014	-11.6	25.24	0.34	2.95	-0.2	-0.6	-1.9
CALF_SPRING_BORE	-53.0	-7.87	0.013	0.014	-15.6	31.38	0.32	2.29	-1.0	-2.2	-1.8
CGDH_5_(FISHERMANS)	-49.6	-7.58	0.004	0.015	-17.6	87.08	0.28	2.49	-3.8	-7.8	-1.1
CGDH_6_(NEW_ATTACK)	-51.7	-7.83	-0.002	0.016	-17.6	82.67	0.29	1.83	-5.0	-9.5	-1.2
CGDH_7	-52.4	-7.91	0.014	0.015	-17.9	78.17	0.28	2.18	-4.5	-8.9	-1.1
CGDH_8_(KEMP)	-53.6	-7.97	0.011	0.014	-16.5	61.47	0.28	2.37	-2.8	-5.3	-1.3
CLEANSKIN	-51.1	-7.48	0.011	0.015	-15.1	4.16	0.42	2.28	-0.6	-1.0	-2.4
HOTPLATE	-53.7	-8.06	-0.004	0.014	-18.6	93.51	0.30	0.91	-5.6	-10.5	-1.6
LEWIS	-43.2	-6.65			-11.8	94.44	0.29	2.36	-0.6	-1.2	-2.0
MATERA_BORE								3.1	-0.2	-0.4	-1.9
NO_8_(PADDY'S)	-50.1	-7.44	0.584	0.022	-13.3	89.27	0.28	5.29	-0.3	-0.5	-1.5
OAKS_CREEK_BORE	-53.0	-7.98	0.006	0.015	-18.0	60.03	0.29	1.68	-2.8	-5.0	-1.5
RN029226	-47.9	-7.11	-0.007	0.015	-16.4	45.38	0.30	1.87	-3.2	-5.8	-1.3
TANMURRA	-44.4	-6.84	0.016	0.014	-7.8	19.52	0.37	0.18	-2.8	-5.3	-3.1
WBN5002 (Seltrust hole)	-44.4	-6.84			-8.6	33.65	0.32	4.01	-0.3	-0.7	-1.6
WBN5006	-54.9	-8.24			-13.0	96.65	0.31	8.54	0.2	0.2	-1.2
WILSON	-47.8	-7.14	0.001	0.016	-13.3	18.21	0.37	3.48	-0.1	-0.2	-2.2
NW Lake water level								0.22	-3.3	-6.0	-2.9
SE Lake water level								0.23	-3.3	-6.1	-2.8
Rain 2015/16	-11.3	-3.16	1.723	0.040				0.02	-4.6	-9.1	-3.9
Rain1 2016/17	-43.2	-7.12	1.441	0.037				0.15	-3.3	-6.8	-3.1
Rain2 2016/17	-31.3	-5.26	1.528	0.038							
Rain3 (May-Nov 17)	-2.3	-1.41	1.753	0.048							
Bonaparte Rain 12/6/18	-43.6	-6.99									
Bore Spring	-47.6	-7.11	0.043	0.015	-15.87	94.89	0.31	7.24	-1.1	-2.0	-1.1
Long Spring	-48.9	-7.30	0.070	0.016	-18.66	89.11	0.29	1.8	-2.0	-4.0	-1.7
New Spring	-49.6	-7.48	0.051	0.015	-18.73	93.29	0.3	0.29	-5.3	-10.6	-2.1
Oaks Creek Spring	-44.2	-6.38	0.117	0.019	-15.3	96.29	0.32	0.48	-3.8	-7.3	-2.1
Yow Spring	-34.3	-4.31	0.154	0.019	-23.18	98.44	0.31	0.5	-5.0	-9.5	-1.9



Table A5 Data for SF<sub>6</sub>. All data was supplied by DPIRD.

Site ID	Sampling Date	Measured conc SF6	Measured conc SF6 error	Calculated atmospheric partial pressure SF6	Calculated atmospheric partial pressure SF6 Error	SF6 Temperature	SF6 Temperature Error	SF6 Excess Air	SF6 Excess Air Error	SF6 Piston flow recharge year
17BP01S	12/09/2017	1.06	0.08	3.68	1.52	16.9	4.9	-0.3	2.6	1997
17BP02S	20/09/2017	0.53	0.08	0.84	0.19	15.5	3.9	7.2	2	1981
17BP03I	19/09/2017	1.22	0.09	2.18	0.23	11.1	1.6	4.1	0.8	1990
17BP04S	18/09/2017	0.21	0.08	0.33	0.13	13.8	2	6.7	1	1974
17BP06S	30/09/2017	0.82	0.09	0.94	0.17	24.7	4.6	14.6	1.9	1982
NO_8_(PADDY'S)	05/09/2017	1.51	0.09	3.18	0.39	18.9	2.5	4.4	1.1	1994
Long Spring	11/09/2017	2.77	0.10	8.15	0.73	18.9	1.6	1.4	0.5	2015
Bore Spring	29/08/2017	3.10	0.10	10.67	1.41	21.8	2	0.9	0.8	contaminated or 2018
New Spring	30/08/2017	0.92	0.07	3.37	0.45	21.6	1.8	0.4	0.6	1995.5
Oaks Creek Spring	07/09/2017	2.85	0.09	9.64	1.11	19.8	1.8	0.6	0.7	2017-2018
Yow Spring	19/08/2017	2.93	0.10	14.88	1.87	26.9	1.8	-0.4	0.6	contaminated
17BP071	18/11/2017	1.75	0.06	2.77	0.50	8.9	3.4	5.0	2.2	1993
17BP05S	10/11/2017	0.50	0.05	1.50	0.40					1986

Table A6 Data for CFCs. All data was supplied by DPIRD.

Site ID	Sampling Date	Measured conc CFC 11	Measured conc CFC 11 error	Measured conc CFC 12	Measured conc CFC 12 Error	Measured conc CFC 113	Measured conc CFC 113 Error	Calculated atmospheric partial pressure CFC 11	Calculated atmospheric partial pressure CFC 11 Error	Calculated atmospheric partial pressure CFC 12	Calculated atmospheric partial pressure CFC 12 Error	Calculated atmospheric partial pressure CFC 113	Calculated atmospheric partial pressure CFC 113 Error	Piston flow recharge year: CFC-11	Piston flow recharge year: CFC-12	Piston flow recharge year: CFC-113
17BP01S	12/09/2017	1.34	0.02	1.07	0.04	0.12	0.02	92.3	21.3	274	58	28.5	8.3	1975	1979	1984
17BP02S	20/09/2017	0.91	0.02	0.89	0.03	0.07	0.02	57.4	11.2	198	35	14.8	4.7	1971	1975	1979
17BP03I	19/09/2017	1.71	0.02	1.41	0.04	0.15	0.02	85.9	7.2	265	21	24.1	3.4	1974	1979	1982
17BP04S	18/09/2017	0.23	0.03	0.15	0.02	0.01	0.02	13.1	2.4	32	5.4	1.6	3.3	1963	1961	1968
17BP05S	18/09/2017	1.15	0.03	0.92	0.03	0.08	0.02	75.4	13.7	225	37	17	5.3	1973	1977	1980
17BP06S	30/09/2017	1.38	0.02	1.15	0.03	0.11	0.02	127	23	326	55	30.4	8.6	1977	1983	1984
Brolga	05/09/2017	0.06	0.03	0.08	0.02	0.02	0.02	5.9	2.7	26.1	6.1	5.4	5.2	1958	1959	1973
NO_8_(PADDY'S)	05/09/2017	1.06	0.02	1.14	0.03	0.14	0.02	78.5	9	299	32	33.3	5.9	1973	1981	1985
Long Spring	11/09/2017	0.62	0.49	1.46	0.04	0.09	0.04	46.6	37.3	398	29	23.4	9.1	1970	1987	1982
Bore Spring	29/08/2017	1.94	0.02	1.52	0.04	0.18	0.02	167	15	470	39	54.2	7	1982	1990	1989
New Spring	30/08/2017	0.77	0.02	0.61	0.02	0.07	0.02	66	5.3	187	14	20.9	5.1	1972	1975	1981
Oaks Creek Spring	07/09/2017	1.96	0.02	1.56	0.04	0.19	0.02	154	12	445	34	51.6	6.7	1980	1989	1988
Yow Spring	19/08/2017	1.26	0.05	1.17	0.04	0.13	0.02	135	11	445	31	48.7	7.2	1978	1989	1988
17BP071	18/11/2017	0.88	0.05	0.99	0.03	0.10	0.04	39.2	7.7	167	29	14.5	6.4	1969	1974	1979

## Appendix D Suitability of groundwater for irrigation

Table D1: Salinity classes of irrigation water from USDA (1954)

Salinity class	EC (mS/m)
Low	<25
Medium	75
High	225
Very high	550
Extremely high	>550

Table D2: Trigger values for sodium and chloride in irrigation water for variously sensitive crops from ANZECC and ARMCANZ (2000)

Class	Chloride (mg/L)	Sodium (mg/L)
Sensitive	<175	<115
Moderately sensitive	350	230
Moderately tolerant	700	460
Tolerant	1,000	800
Not suitable	>1,000	>800

Table D3: Trigger values for pH, based on corrosion and fouling potential of water delivery equipment, from ANZECC and ARMCANZ (2000)

Parameter	pH
Lower (high corrosion potential)	<5
Upper (increased fouling potential)	>8.5

Table D4: Trigger values for other elements in irrigation water from ANZECC and ARMCANZ (2000)

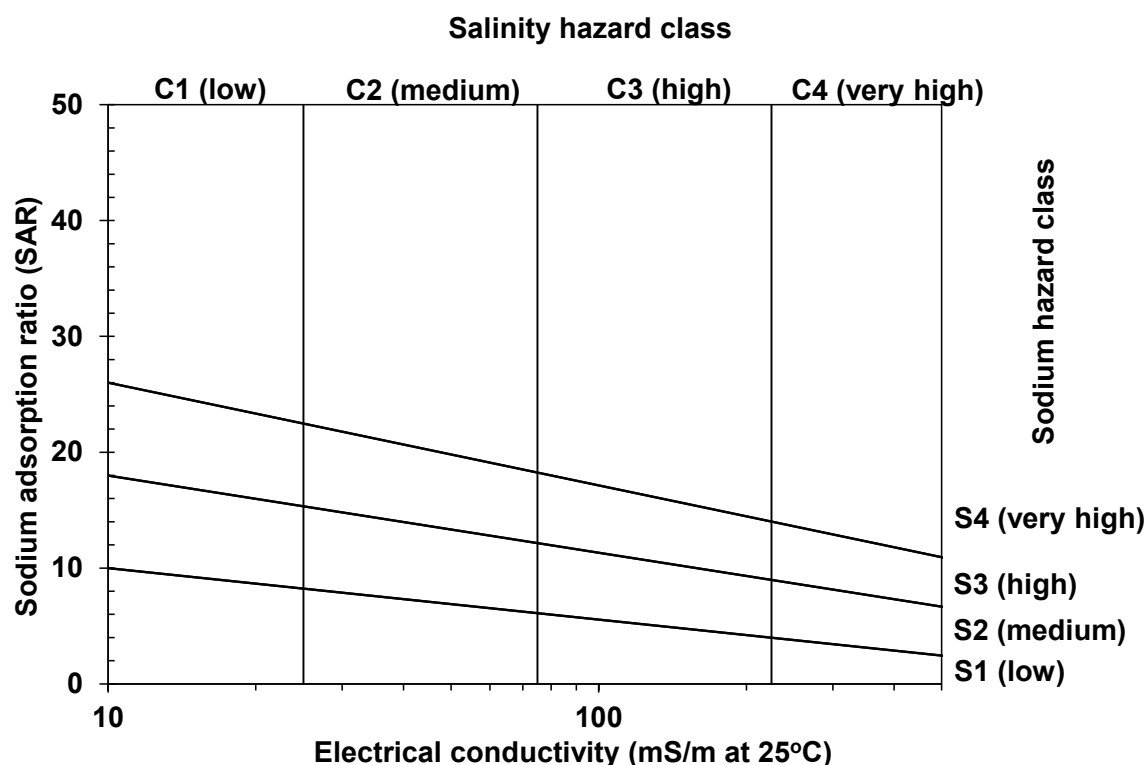
Parameter	Short-term trigger value (mg/L)	Long-term trigger value (mg/L)
Al	20	5
As	2	0.1
Be	0.5	0.1
B	Plant specific	0.5
Cd	0.05	0.01
Cr	1	0.1
Co	0.1	0.05
Cu	5	0.2

(continued)

Table D4 (continued): Trigger values for other elements in irrigation water from ANZECC and ARMCANZ (2000)

Parameter	Short-term trigger value (mg/L)	Long-term trigger value (mg/L)
F	2	1
Fe	10	0.2
Pb	5	2
Li	2.5	2.5
Li*	0.075	0.075
Mn	10	0.2
Hg	0.002	0.002
Mo	0.05	0.01
Ni	2	0.2
TN	12–125	5
TP	0.8–12	0.05
Se	0.05	0.02
U	0.1	0.01
V	0.5	0.1
Zn	5	2

\* Trigger values for lithium when irrigating citrus crops.



Source: USDA (1954)

Figure D1: The relationship between EC and SAR used to classify the sodicity hazard of the groundwater for irrigation use

## Appendix E Test pumping method, results and analysis

### Summary

Test pumping of Bonaparte Plains test production bores (17BP01PB, 13BP01PB, and 17BP05PB) was carried out in 2017 and 2018. Step tests and CRTs were undertaken at discharge rates between 6.2 and 36 L/s.

The test pumping results were analysed and returned K values in the range 2.4–3.3 m/d for 17BP01PB, 3.1–5.3 m/d for 13BP01PB, and 6.7–8.9 m/d for 17BP05PB.

The Point Spring Sandstone Formation aquifer has vertically heterogeneous aquifer properties, with some layers being semiconfined or confined, at least across localised scales. Generally, highest long-term safe yields will be obtained by maximising the length of the screened interval within the saturated zone.

### Introduction

The Bonaparte Plains area is being investigated to assess its suitability for irrigated agriculture. Three test pumping bores were drilled in the Bonaparte Plains area – bore 13BP01PB was drilled in 2013, with bores 17BP01PB and 17BP05PB drilled in 2017. Bennett (2019) shows the locations of the test pumping sites and contains the bore completion diagrams of the production bores and their associated observation bores.

The aim of the test pumping program was to estimate the aquifer properties of transmissivity and hydraulic conductivity, for a water balance model of the aquifer. The geology of the Bonaparte Plains is sand, alluvium and soil cover overlying the Upper Carboniferous Point Spring Sandstone Formation.

Two of the 3 production bores (13BP01PB and 17BP01PB) were test pumped in November 2017; bore 17BP05PB was test pumped in June 2018. There are 3 observation bores near 13BP01PB and 2 observation bores at each of the other test pumping sites. The distance from each test pumping bore to its observation bores is shown in Table E1 for each site. Summary details for the test pumping production and observation bores are shown in Table E2.

Table E1: Distance from test production bore to observation bores

Test production bore	Observation bore	Distance (m)
13BP01PB	13BP01S	40.25
	13BP01I	40.25
	13BP01D	40.25
17BP01PB	17BP01I	26.52
	17BP01S	36.80
17BP05PB	17BP05I	26.12
	17BP05S	35.90

Table E2: Test pumping bore and observation bore summary

Bore	Bore type	Easting (GDA94 Z52)	Northing (GDA94 Z52)	Drilled depth (mBGL)	Water level (mBGL)	Water level (date and time)	Casing internal diameter and type	Screen type and aperture	Screened interval (mBGL)
13BP01PB	Production	473925	8333272	83.3	45.12	17/11/2017 07:55	155 mm PN12 PVC	Slotted PVC 1 mm	35–83
13BP01S	Observation	473887	8333261	174*	45.39	07/11/2017 07:00	50 mm PN12 PVC	Slotted PVC 1 mm	52– 82
13BP01I	Observation	473887	8333261	174*	45.42	07/11/2017 07:02	50 mm PN12 PVC	Slotted PVC 1 mm	100–118
13BP01D	Observation	473887	8333261	174*	44.80	17/11/2017 06:58	50 mm PN18 PVC	Slotted PVC 1 mm	156–168
17BP01PB	Production	479013	8335027	126.25	5.61	09/11/2017 07:40	203 mm steel	Stainless steel wire wound screen 2 mm	112.75–124.75
17BP01I	Observation	478993	8335027	126.25	6.09	09/11/2017 07:15	100 mm PN12 PVC	Slotted PVC 1 mm	108–120
17BP01S	Observation	478984	8335023	15	5.95	09/11/2017 07:13	100 mm PN12 PVC	Slotted PVC 1 mm	12–15
17BP05PB	Production	461173	8347265	93	17.18	04/06/2018 11:50	203 mm steel	Stainless steel wire wound screen 2 mm	76.97–88.97
17BP05I	Observation	461179	8347242	95.8	17.73	04/06/2018 11:52	100 mm PN12 PVC	Slotted PVC 1 mm	77.13–89.13
17BP05S	Observation	461182	8347233	29.5	17.97	04/06/2018 11:55	100 mm PN12 PVC	Slotted PVC 1 mm	26–29

\* Nested piezometers

Note: Date format is day/month/year.



The test pumping program was carried out by the NT Department of Environment and Natural Resources (DENR). A Mono 820<sup>®</sup> pump, powered by a diesel engine coupled to a hydraulic pump, was used for the test pumping program. The discharge rate was maintained using an orifice plate and a manometer. Water was discharged into a tank and then flowed through plastic lay-flat hose to about 150 m from the test production bore. Figure E1 shows the set-up of the test pumping equipment at bore 17BP01PB. The test pumping data were analysed by Aqtesolv<sup>™</sup> Pro, which is industry-standard software used for interpreting aquifer tests.



Figure E1: The test pumping equipment and set-up used for all tests

### Test pumping 17BP01PB

At the start of test pumping 17BP01BP there was a strong smell of hydrogen sulfide ( $H_2S$ ) from the discharge water. This was possibly from the breakdown of the drilling mud. The  $H_2S$  smell persisted until the end of the CRT, but by the end it was barely detectable.

A 3-step step test of 17BP01PB was carried out on 9 November 2017. Table E3 summarises these step tests. A 4-step step test was proposed but the third step drew down to just above the pump top, so the fourth step was cancelled. The step test drawdown is shown in Figure E2. Steps 2 and 3 were corrected to derive the drawdown for the first 100 minutes of pumping. The first 100 minutes of the CRT is also included in Figure E2. It appears that the test production bore was still developing during the CRT as the rate of the CRT drawdown was less than during the third step test. The test pumping was analysed for both unconfined and confined conditions because the observation bores gave small storativity ( $S$ ) values for the unconfined analysis.

The drawdown,  $s$ , in a well can be expressed as the sum of a first-order (laminar) component and a second-order (turbulent) component:  $s = BQ + CQ^2$ .  $Q$  is the discharge rate,  $BQ$  is the laminar component, and  $CQ^2$  is the turbulent component. Bierschenk (1964) presented a simple graphical method for determining  $B$  and  $C$ .

Dividing  $s = BQ + CQ^2$  by  $Q$  and rearranging the terms yields  $s/Q = CQ + B$ . This is a linear equation in  $s/Q$  and  $Q$ , so if  $s/Q$  is plotted against  $Q$ , then the resultant graph is a straight line, with slope  $C$  and intercept  $B$ . The drawdown at 100 minutes was used to create a graph of  $s/Q$  plotted against  $Q$  for 17BP01PB (Figure E3). The calculated values of  $B$  and  $C$  were used to calculate the bore efficiency, and this returned figures of 96.5%, decreasing to 91.2% at the highest discharge rate (Table E4). The step test was analysed by the Theis (1935) method and returned a transmissivity ( $T$ ) value of 398 m<sup>2</sup>/d for unconfined conditions and 345 m<sup>2</sup>/d for confined conditions (Figure E4, Figure E5).

The CRT started on 10 November 2017 and was pumped for 2 days (2,880 minutes) at 16.31 L/s. The groundwater discharge was monitored by DENR personnel for EC and pH during the CRT. After the initial drawdown, when water was drawn from well storage, the drawdown stabilised to about 0.54 m per logged cycle. The drawdown was 47.85 m at 2,880 minutes (2 days). At the end of pumping, the bore almost completely recovered after 60 minutes (Figure E6). The observation bores (17BP01I and 17BP01S) responded during the test pumping, with 17BP01I drawing down 3.13 m and 17BP01S drawing down 0.11 m.

The CRT was analysed for both unconfined and confined conditions using the Theis method and Cooper-Jacob (1964) method. The Aqtesolv™ graphs are shown in Figure E7 and Figure E8 for the unconfined and confined Theis methods, respectively. The observation bores responses do not fit the theoretical curves – they are less than they theoretically should be. The plots for 17BP01I are shown in Figure E9 and Figure E10 for the unconfined and confined Theis methods, respectively. The graphs show that there is delayed yield in 17BP01I, which causes the drawdown curve to flatten out after about 8 minutes pumping. Because the drawdown curve is flattening out and the Cooper-Jacob method is a straight-line fit method, the transmissivity ( $T$ ) value is overestimated in the observation bores.

The calculated  $T$ , hydraulic conductivity ( $K$ ), and  $S$  are shown in Table E5. An aquifer thickness of 120 m was used to calculate  $K$ . The range of  $T$  values for the unconfined method is 375–414 and for the confined method is 240–385. The  $K$  values are calculated from the  $T$  values and the range of  $K$  values for the test production bore using the unconfined method is 3.1–3.3 and for the confined method is 2.4–2.9. The  $T$  and  $K$  values from the observation bore (17BP01I) for the unconfined method are 414 m<sup>2</sup>/d and 3.5 m/d, and for the confined method are 385 m<sup>2</sup>/d and 3.2 m/d. The  $S$  values cannot be calculated for the test production bore (17BP01PB) and the observation bore (17BP01I) gave an  $S$  value of 0.001 for the Theis method.

The analysis of data for 17BP01I observation bore showed there was delayed yield at the site, which caused the drawdown curve to flatten out so that it was almost flat after 10 minutes.

Table E3: 17BP01PB test pumping summary

Bore	Initial water level (m)	Test	Pump inlet depth (mBGL)	Discharge rate (L/s)	Discharge rate (m³/d)	Date and time started	Duration (minutes)	Drawdown at end of test (m)
17BP01PB	6.11	Step 1	51	6.21	536	09/11/2017 08:30	100	16.53
		Step 2	51	10.01	864	09/11/2017 10:10	100	26.96
		Step 3	51	15.08	1,303	09/11/2017 12:50	100	42.19
		CRT	87	16.31	1,409	10/11/2017 07:30	2,880	46.67

Note: Date format is day/month/year.

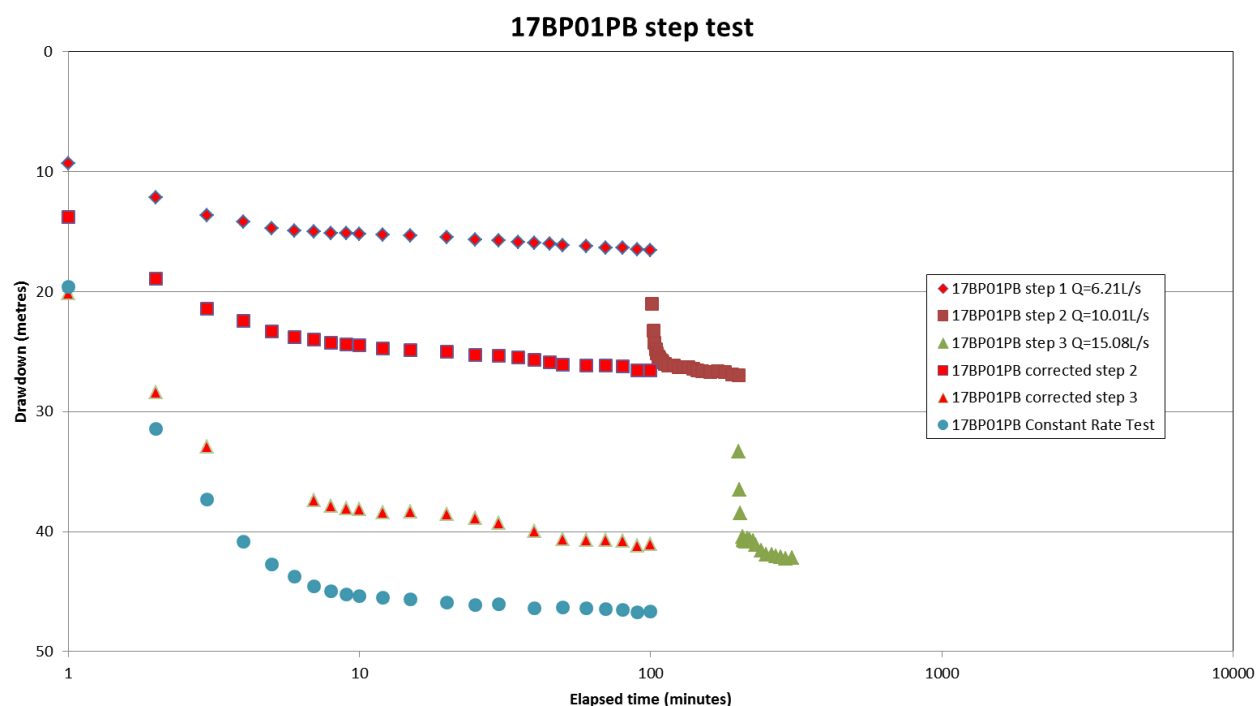


Figure E2: 17BP01PB step tests, corrected step tests and constant rate test

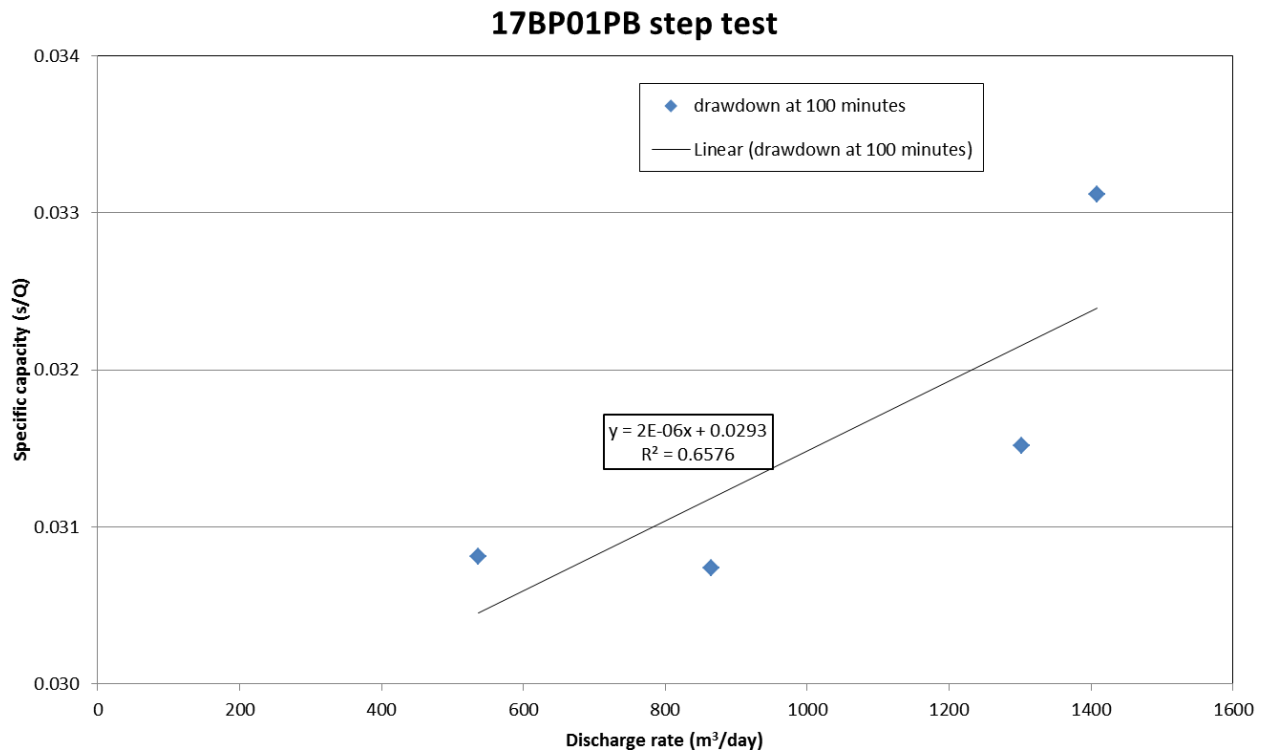


Figure E3: Relationship between specific capacity and discharge rate for 17BP01PB

Table E4: 17BP01PB bore efficiency

Q (m³/d)	S (m at 100 mins)	BQ (B = 0.0293)	CQ <sup>2</sup> (C = 0.000002)	BQ + CQ <sup>2</sup>	Actual drawdown (m)	Efficiency (%)
536.54	16.53	15.72	0.58	16.30	16.53	96.47
864.86	26.59	25.34	1.50	26.84	26.59	94.43
1,302.91	41.07	38.18	3.40	41.57	41.07	91.84
1,409.18	46.67	41.29	3.97	45.26	46.67	91.23

BQ = laminar component; CQ<sup>2</sup> = turbulent component; Q = discharge rate; s = drawdown

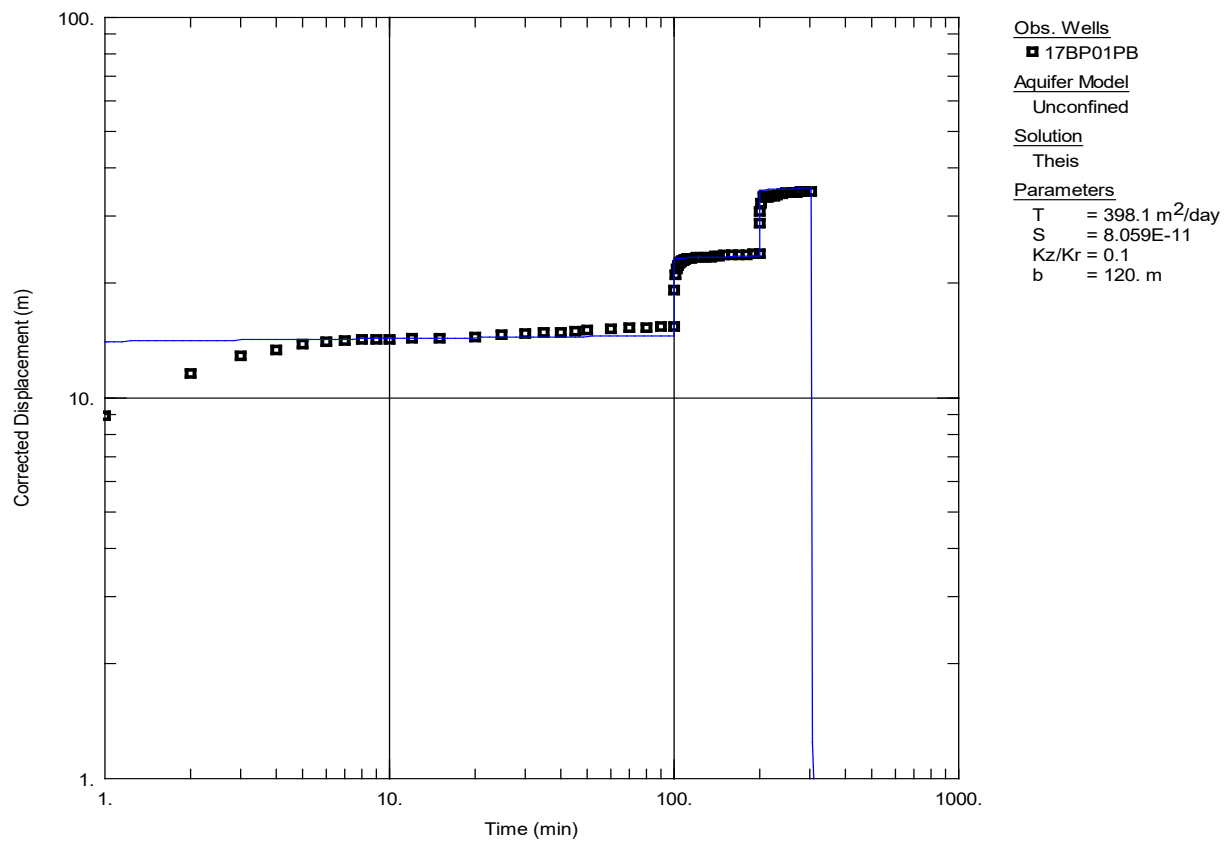


Figure E4: Step test unconfined analysis for 17BP01PB

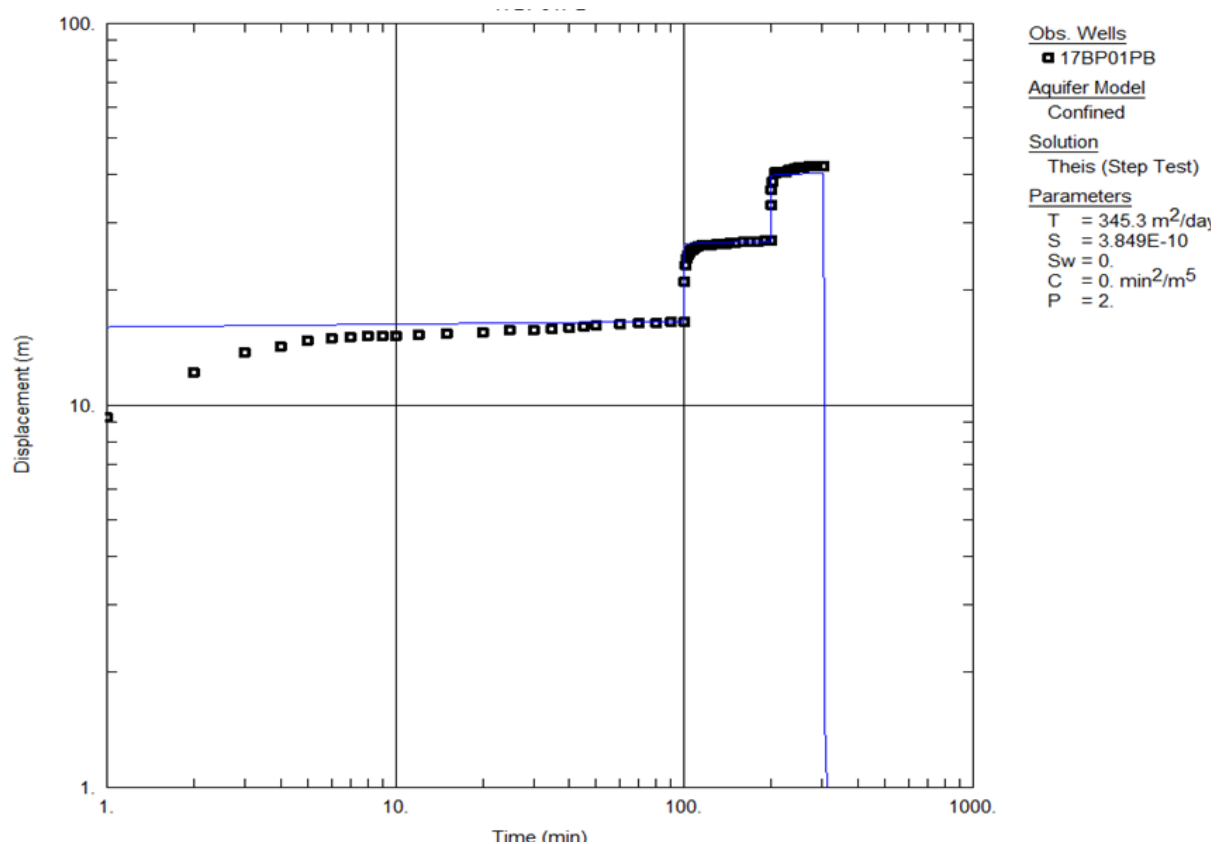


Figure E5: Step test confined analysis for 17BP01PB



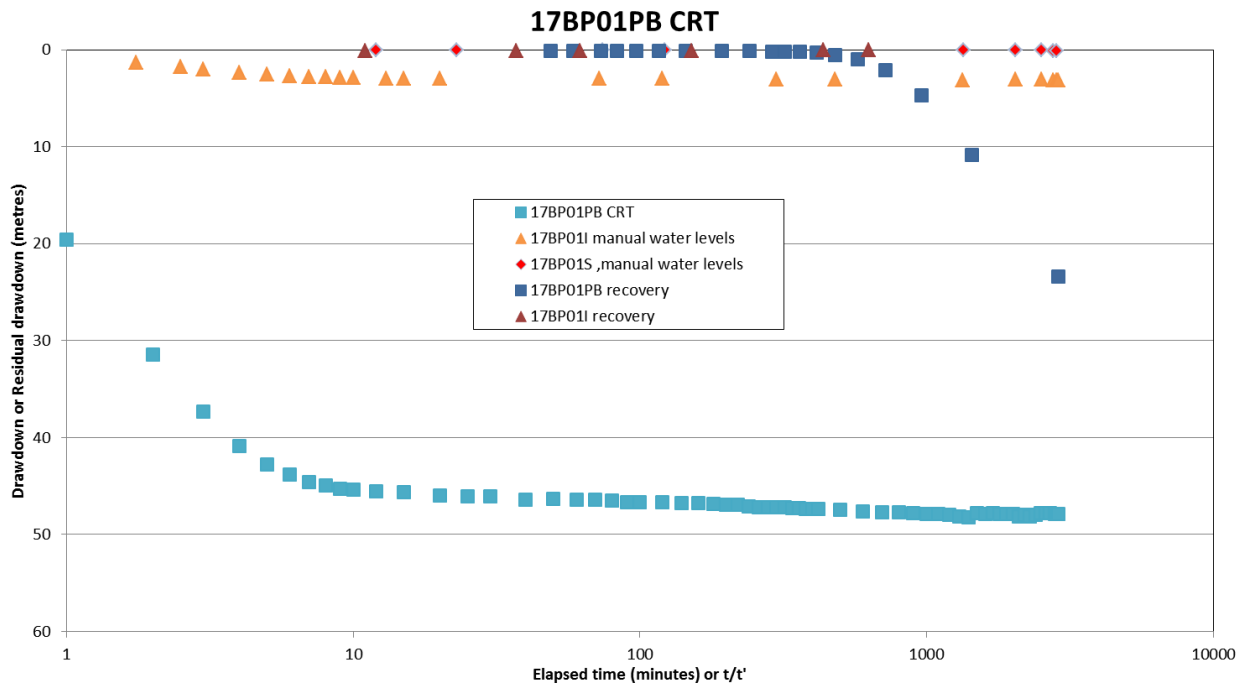


Figure E6: 17BP01PB constant rate test, recovery and observation bores

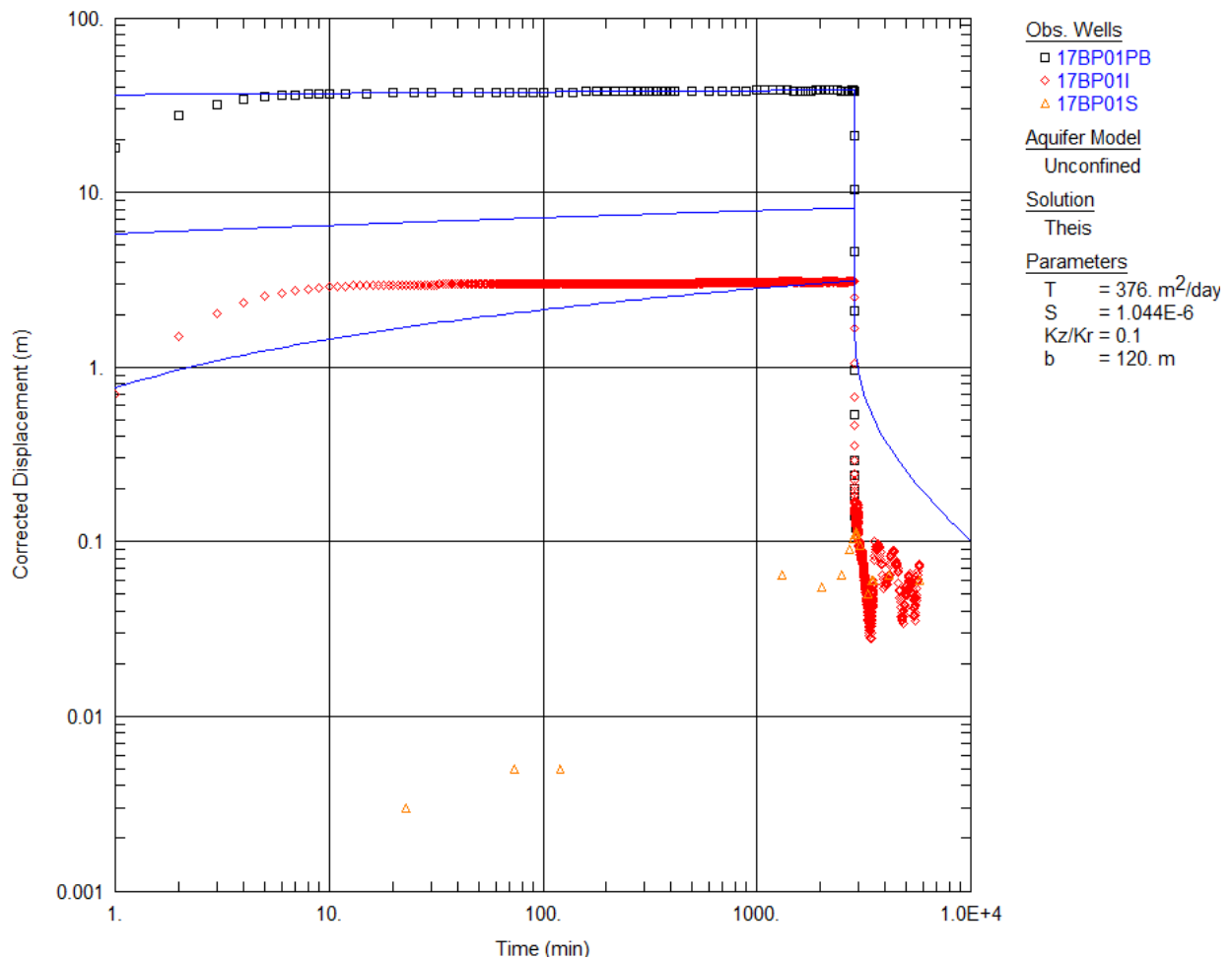


Figure E7: Constant rate test unconfined analysis for 17BP01PB

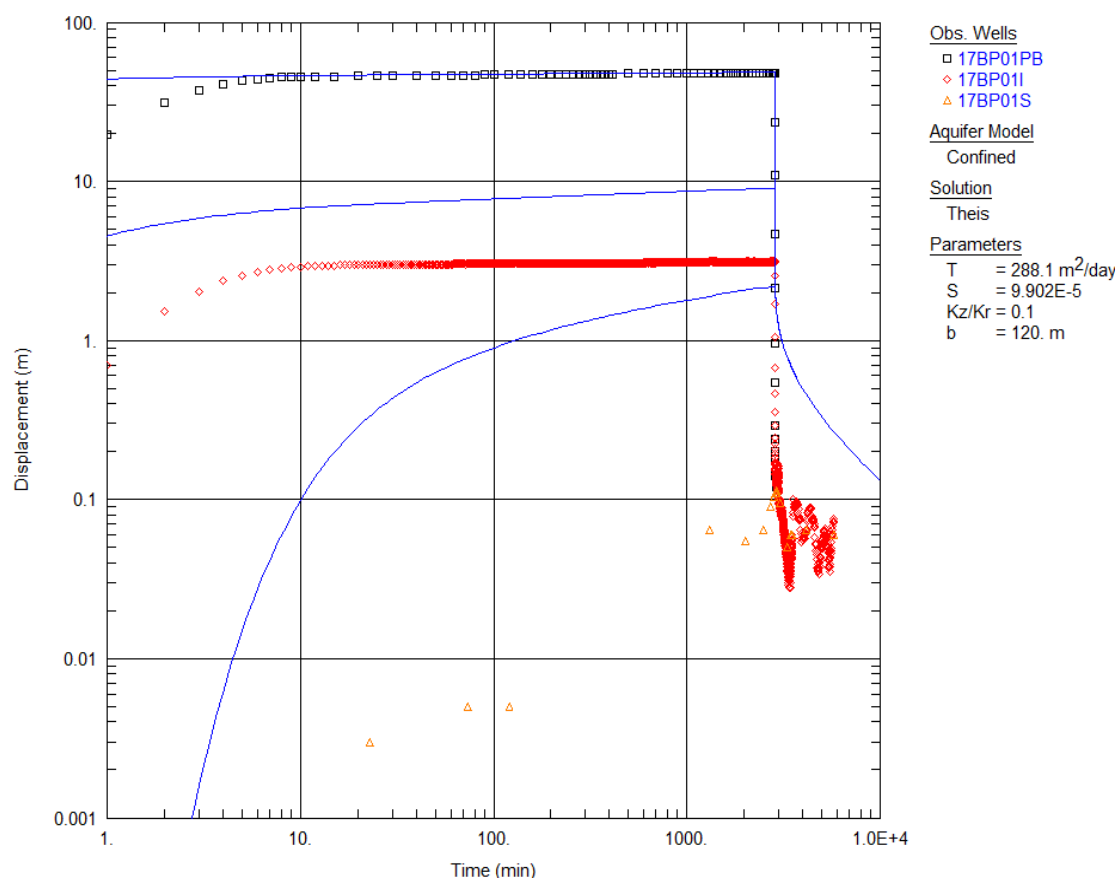


Figure E8: Constant rate test confined analysis for 17BP01PB

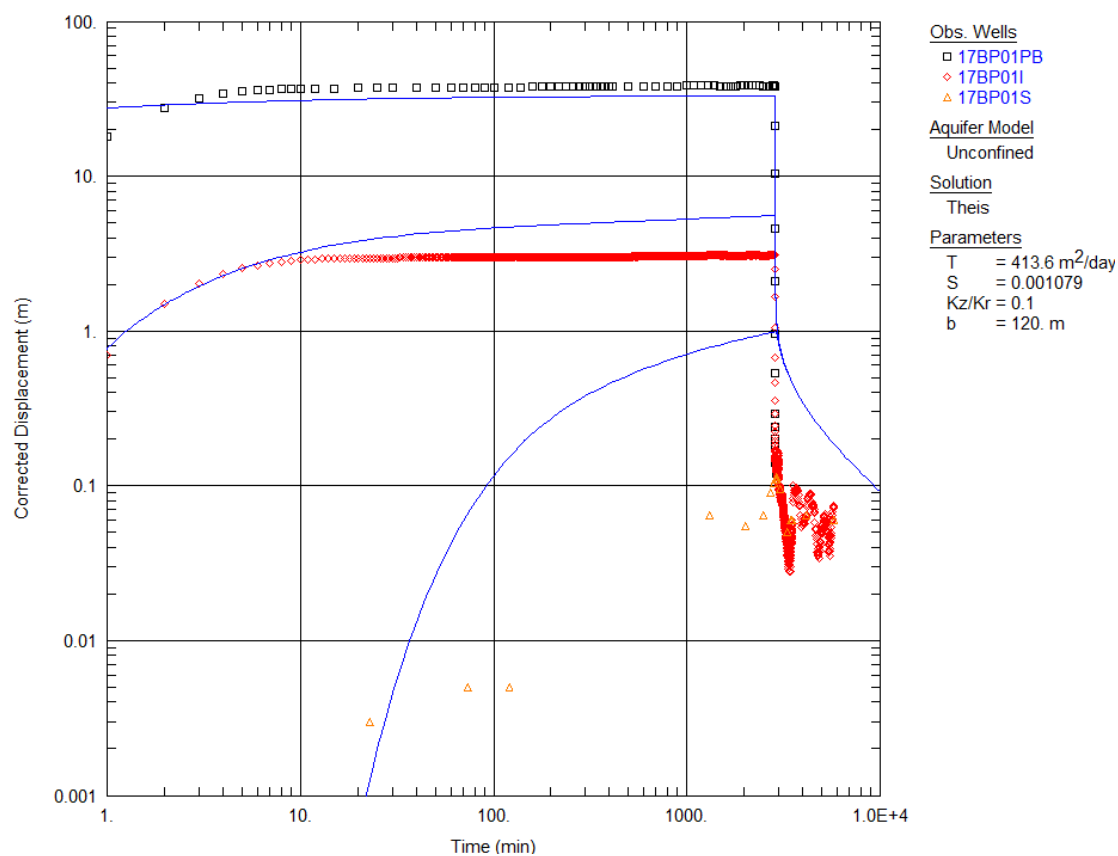


Figure E9: Observation bore 17BP01I Theis curve for unconfined aquifer model

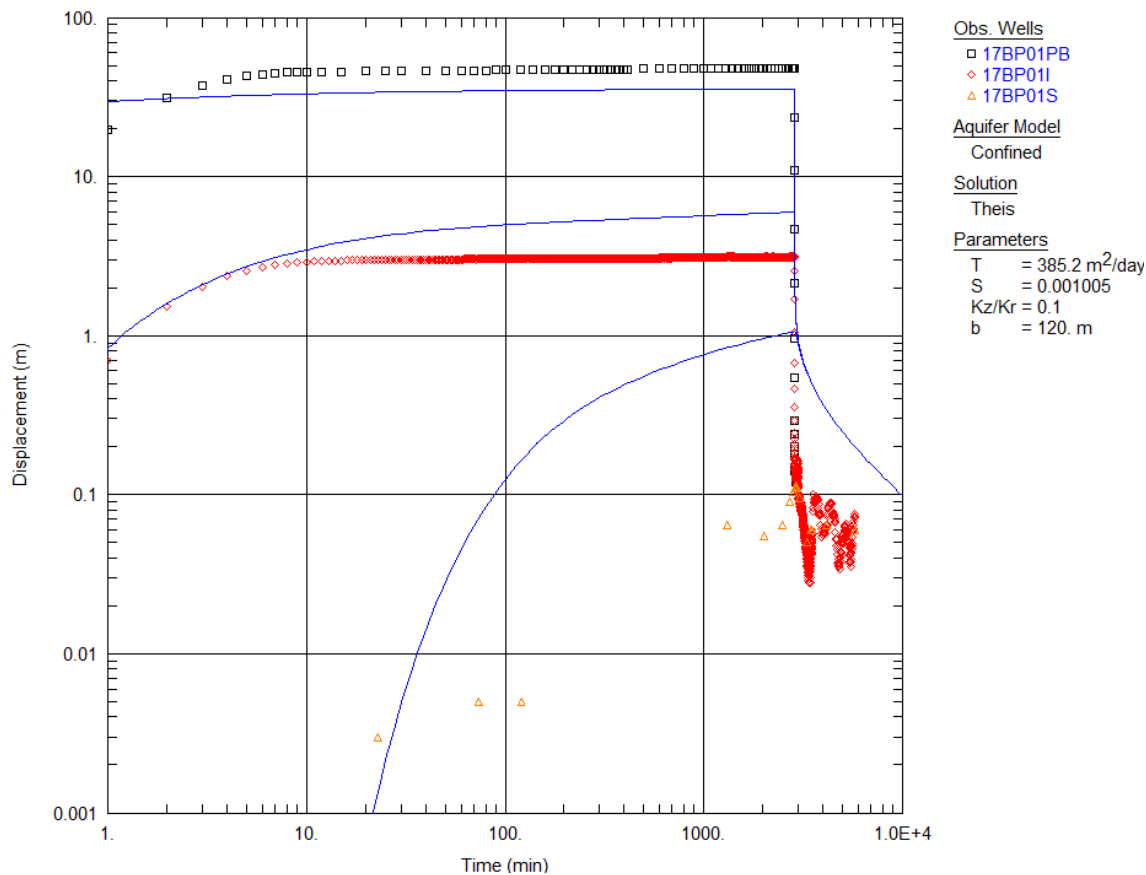


Figure E10: Observation bore 17BP01I Theis curve for confined aquifer model

Table E5: Analysis of 17BP01PB test pumping program

Bore	Analysis	T (m²/d)	K (m/d)	S
17BP01PB	Theis Step test Confined	345	2.9	NA
17BP01PB	Theis Step test Unconfined	398	3.3	NA
17BP01BP	Theis CRT Confined	288	2.4	NA
17BP01BP	Theis CRT Unconfined	376	3.1	NA
17BP01BP	Cooper-Jacob CRT Confined	240	2.0	NA
17BP01PB	Cooper-Jacob CRT Unconfined	375	3.1	NA
17BP01I	Cooper-Jacob CRT Confined	2,740	22.8	$2.2 \times 10^{-50}$
17BP01I	Cooper-Jacob CRT Unconfined	2,760	23.0	$1.4 \times 10^{-33}$
17BP01I	Theis CRT Confined	385	3.2	0.001
17BP01I	Theis CRT Unconfined	414	3.5	0.001
17BP01S	Cooper-Jacob CRT Confined	7,098	59.2	0.017
17BP01S	Cooper-Jacob Unconfined	4,020	33.5	0.0004
17BP01S	Theis CRT Confined	4,427	36.9	0.01
17BP01S	Theis CRT Unconfined	4,500	37.5	0.01

K = hydraulic conductivity; NA = not applicable; S = storativity; T = transmissivity

## Test pumping 13BP01PB

Before installing the test pump, the existing submersible pump was removed, and it was noticed that it had tree roots caught around its intake area. The bore was airlifted for several hours before test pumping to clean out any other roots that may have remained in the bore. It is likely that the roots had grown down inside the annulus, which is backfilled with gravel pack to about 6 mBGL, and entered the bore casing through the slotted section in the unsaturated zone. At the end of the pumping test the discharge drum contained a volume of about 1 L of gravel pack material, which may have entered the casing where there was some damage to the screen, perhaps caused by the tree roots expanding and opening up the slots where they entered. These issues are unlikely to have any effect on the pumping test results for 13BP01PB.

A 4-step step test was started on 17 November 2017 and the fourth step was extended into a 3,600-minute CRT. Table E6 summarises the step test parameters; Figure E11 shows the step test drawdown. In Figure E11, steps 2, 3, and 4 were corrected from the previous steps to derive the response during the first 100 minutes pumping of each subsequent step.

The drawdown at 100 minutes of steps 1, 2, 3, and 4 was used to create a graph of  $s/Q$  plotted against  $Q$  for 13BP01PB (Figure E12). B and C were not able to be calculated as the graph did not produce a straight line because the specific capacity during the first step was greater than the later steps. The step test was analysed by the Theis method and returned a  $T$  value of  $534 \text{ m}^2/\text{d}$  (Figure E13).

The CRT was an extension of the fourth step test. It started on 17 November 2017, and the bore was pumped for 2.5 days (3,600 minutes) at  $16.31 \text{ L/s}$ . The drawdown curve shows several boundary effects, one at 280 minutes and one at 1,400 minutes. The drawdown at 3,900 minutes, at the end of the CRT, was 6.66 m. After pumping finished the water level recovered by 90% after 70 minutes. The test pumping and recovery responses are shown in a semi-log plot in Figure E14. The observation bores (13BP01S and 13BP01I) responded during the test pumping, with 13BP01S drawing down 0.72 m and 13BP01I drawing down 0.49 m. The deep observation bore (13BP01D) showed no reaction to the test pumping program as it is screened in a lower formation (Figure E15).

The CRT was analysed for unconfined conditions. The Aqtesolv™ graphs of 13BP01PB and 13BP01S for the Theis method are shown in Figure E16 and Figure E17, respectively. The calculated  $T$ ,  $K$ , and  $S$  are shown in Table E7. An aquifer thickness of 100 m was used to calculate  $K$ . The calculated  $T$  range for 13BP01PB is  $321\text{--}534 \text{ m}^2/\text{d}$ , giving a  $K$  range of  $3.1\text{--}5.3 \text{ m/d}$ . The observation bore 13BP01S had a calculated  $T$  of  $939 \text{ m}^2/\text{d}$  and a calculated  $K$  of  $9.4 \text{ m/d}$ .

Table E6: 13BP01PB test pumping summary

Bore	Initial water level (m)	Test	Pump inlet depth (mBGL)	Discharge rate (L/s)	Discharge rate (m <sup>3</sup> /d)	Date and time started	Duration (minutes)	Drawdown at end of test (m)
13BP01PB	45.93	Step 1	70	3.28	283	17/11/2017 15:00	100	1.17
		Step 2	70	6.72	580	17/11/2017 16:40	100	2.15
		Step 3	70	11.11	959	17/11/2017 18:20	100	3.66
		Step 4 to CRT	70	16.31	1,409	17/11/2017 20:00	3,600	6.66

Note: Date format is day/month/year.

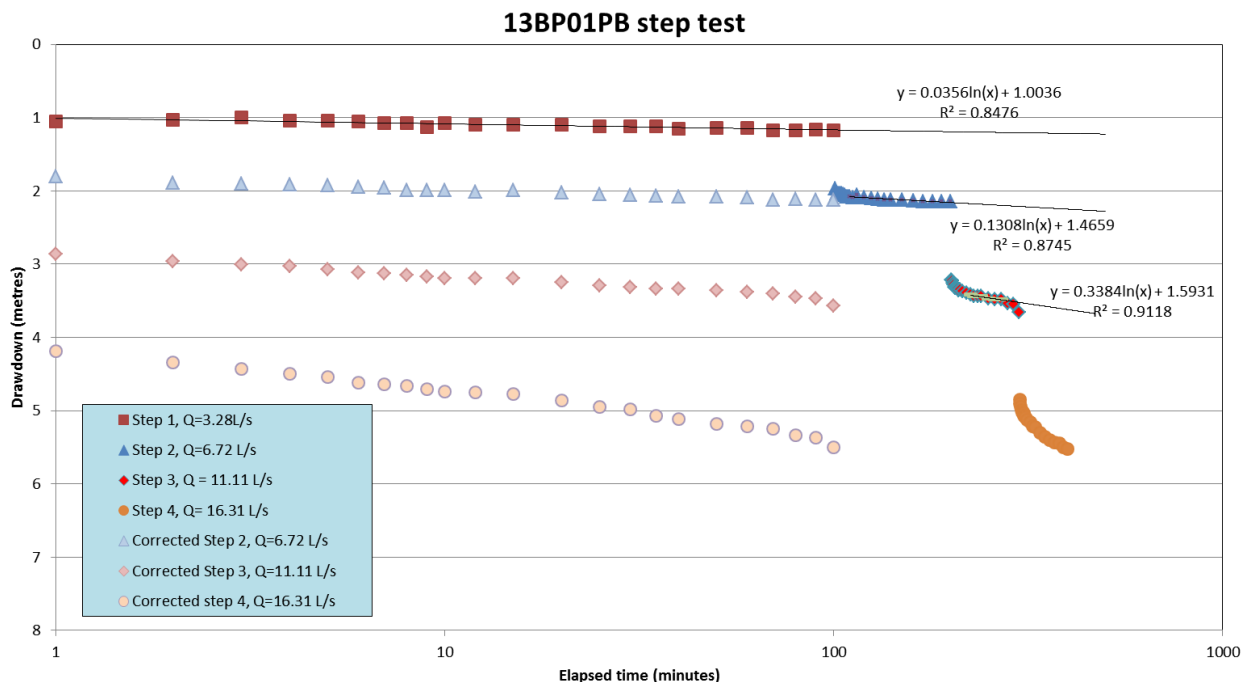


Figure E11: 13BP01PB step test



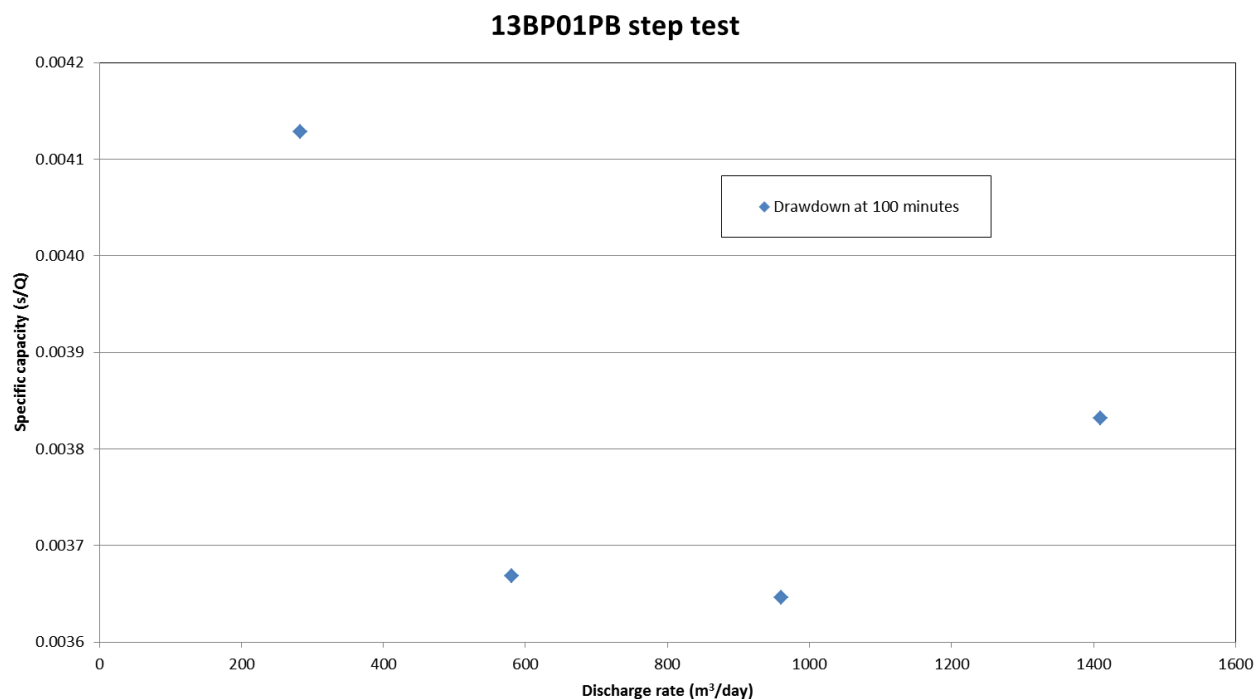


Figure E12: Relationship between specific capacity and discharge rate for 13BP01PB

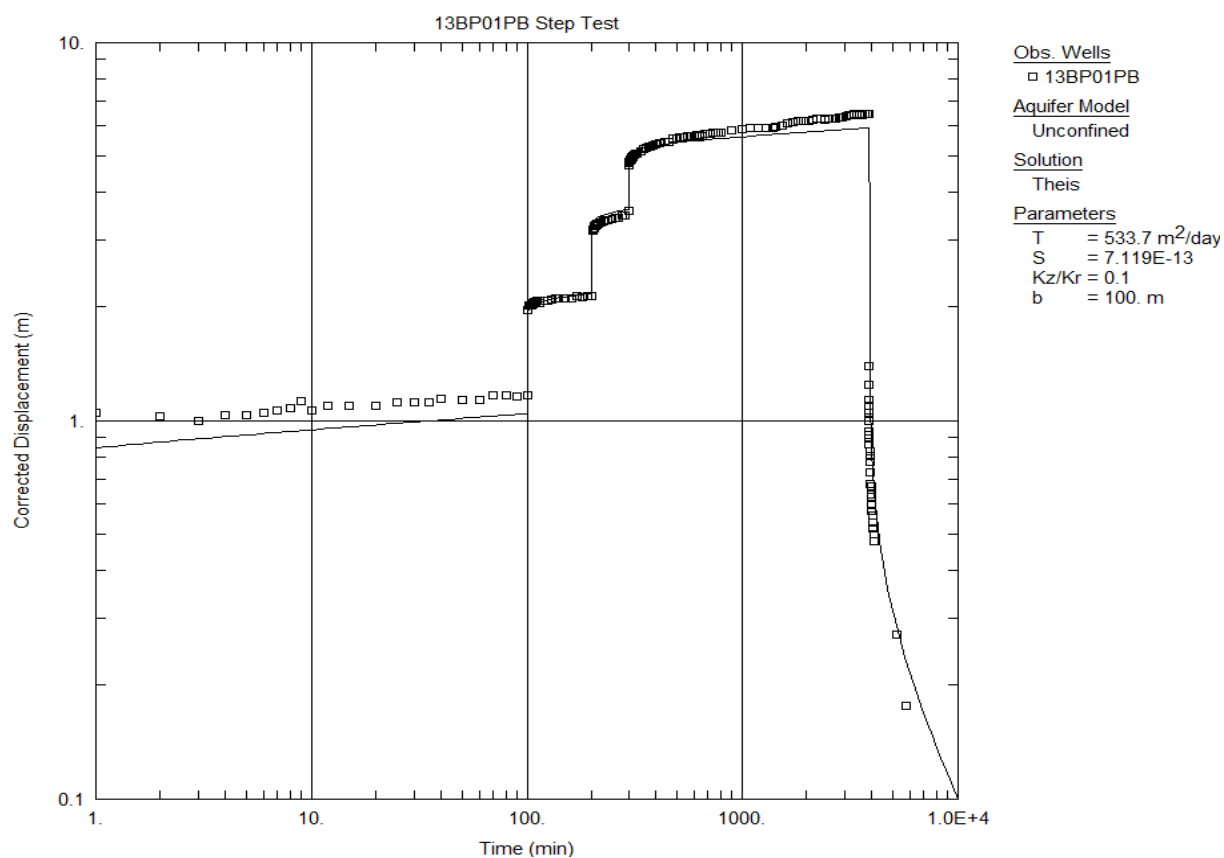


Figure E13: 13BP01PB step test analysis

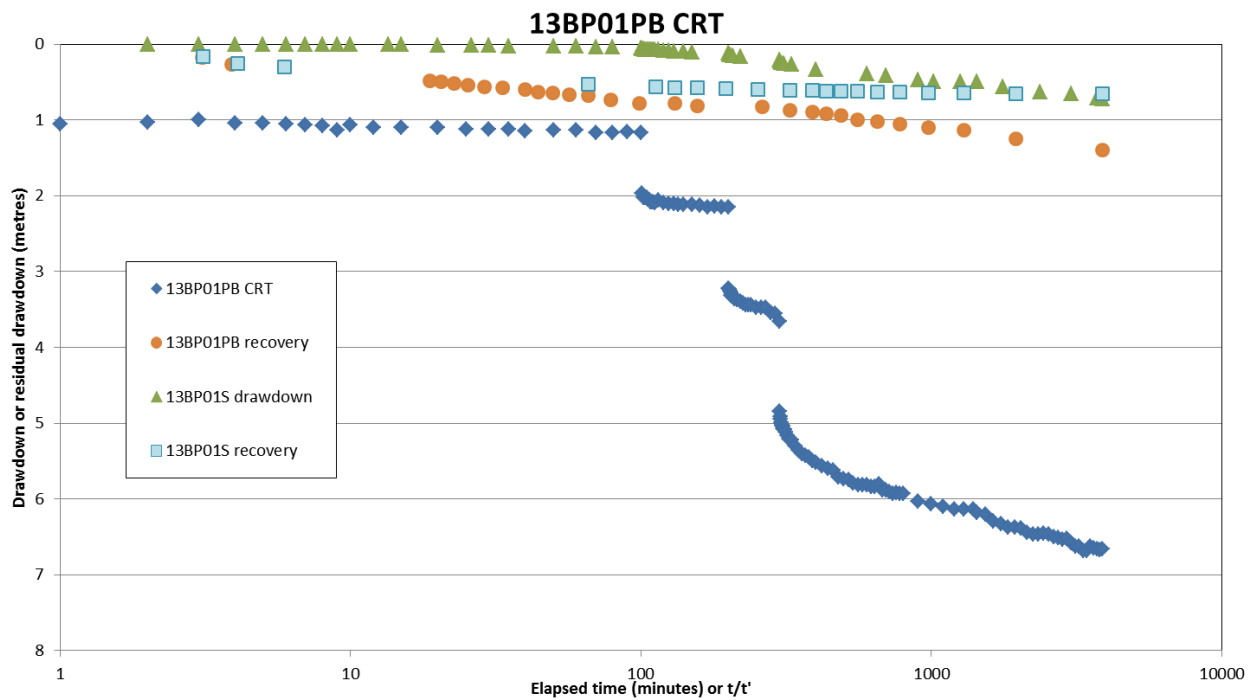


Figure E14: 13BP01PB constant rate test and recovery and observation bore 13BP01S

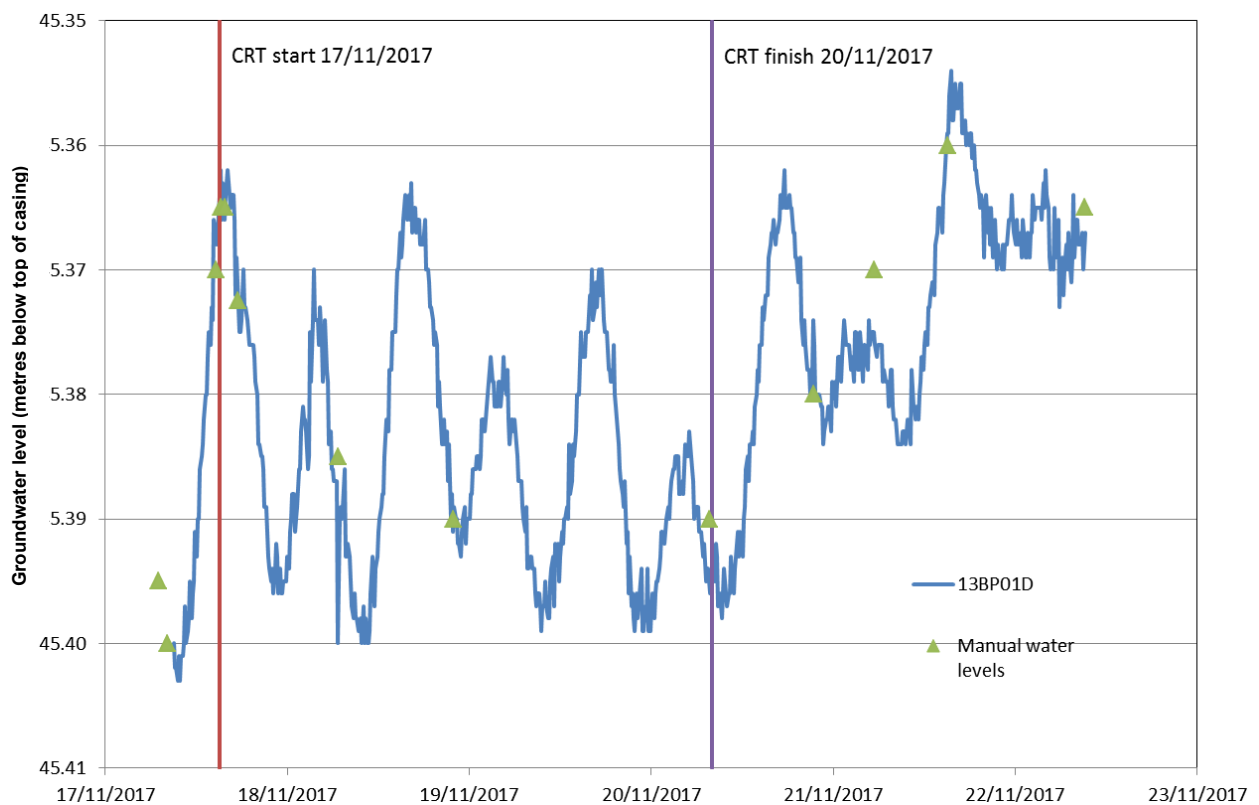


Figure E15: 13BP01D water level response during test pumping of 13BP01PB

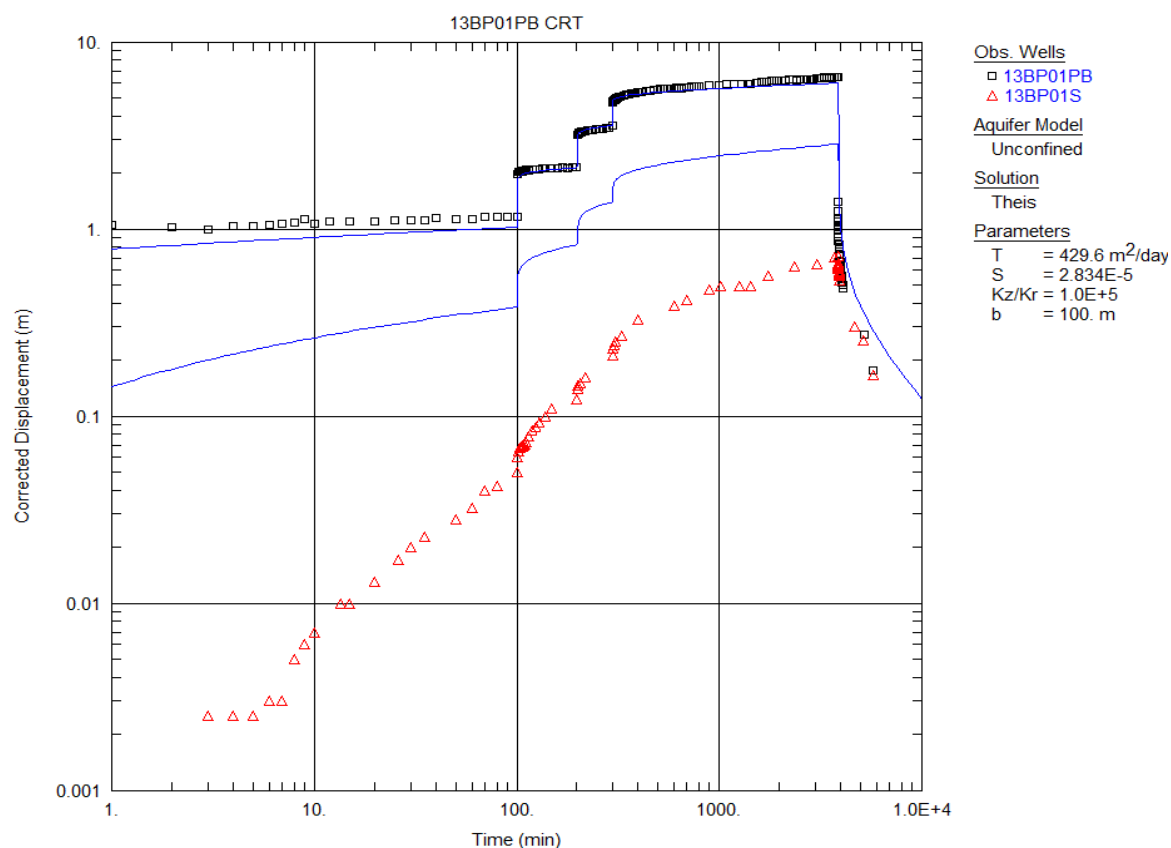


Figure E16: 13BP01PB constant rate test

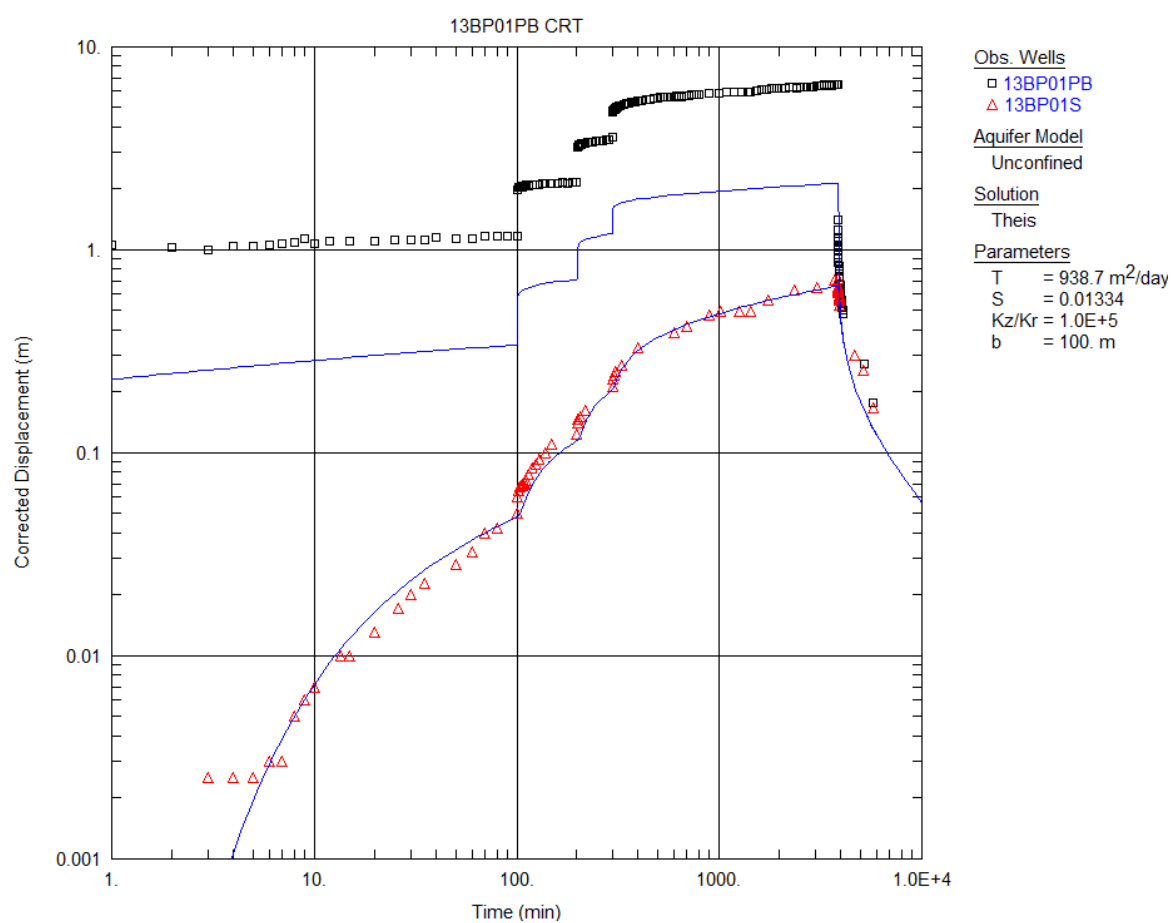


Figure E17: Observation bore 13BP01S constant rate test analysis

Table E7: Analysis of 13BP01PB test pumping program

Bore	Analysis	T (m <sup>2</sup> /d)	K (m/d)	S
13BP01PB	Theis step test	534	5.3	NA
13BP01PB	Theis CRT	430	4.3	NA
13PB01PB	Cooper-Jacob unconfined	321	3.1	NA
13BP01S	Theis CRT	939	9.4	0.013
13BP01S	Cooper-Jacob unconfined	939	9.4	0.013

K = hydraulic conductivity; NA = not applicable; S = storativity; T = transmissivity

### Test pumping 17BP05PB

A step test was carried out on 6 June 2018. The bore was test pumped over four 100-minute steps, as summarised in Table E8.

The step test was analysed using the Theis confined step test aquifer model (Figure E18). The step test data shows a good fit to the model except for during recovery, where the bore recovered faster than the model predicted. This suggests some leakage from the upper part of the aquifer.

The CRT was started on 7 June 2018 and went for 2 days (2,280 minutes). The bore was pumped at a rate of 34.8 L/s for 600 minutes, which was then increased to 36.0 L/s for the rest of the test. Water levels in the 2 monitoring bores were measured during the CRT. The shallow bore (17BP05S), screened at the top of the aquifer, only responded towards the end of the CRT. The response was minor and 17BP05S was not used in the CRT analysis. The CRT was analysed using the Theis method for confined conditions in the pump bore (19BP05PB) and the monitoring bore (17BP05I) (Figure E19, Figure E20), as well as for unconfined conditions (Figure E21, Figure E22).

Analysis of the CRT and step tests produced a T range of 471–777 m<sup>2</sup>/d, using a saturated thickness of 70.5 m (Table E9). The resultant K range was 6.7–11.6 m/d. Analysis using the Hantush-Jacob (Hantush and Jacob 1955) confined leaky method (Figure E23) resulted in a lower modelled T of 199.5 m<sup>2</sup>/d.

Table E8: 17BP05PB test pumping summary

Bore	Initial water level (m)	Test	Pump inlet depth (mBGL)	Discharge rate (L/s)	Discharge rate (m <sup>3</sup> /d)	Date and time started	Duration (minutes)	Drawdown at end of test (m)
17BP05PB	17.78	Step 1	70	10.3	890	06/06/2018 09:45	100	4
		Step 2	70	20.1	1,736	06/06/2018 11:25	100	10
		Step 3	70	30.0	2,592	06/06/2018 13:05	100	20
		Step 4	70	40.0	3,456	06/06/2018 14:45	100	30
		CRT	70	34.8	3,007	07/06/2018 06:30	600	24
		CRT	70	36.0	3,110	07/06/2018 16:30	2,280	25

Note: Date format is day/month/year.

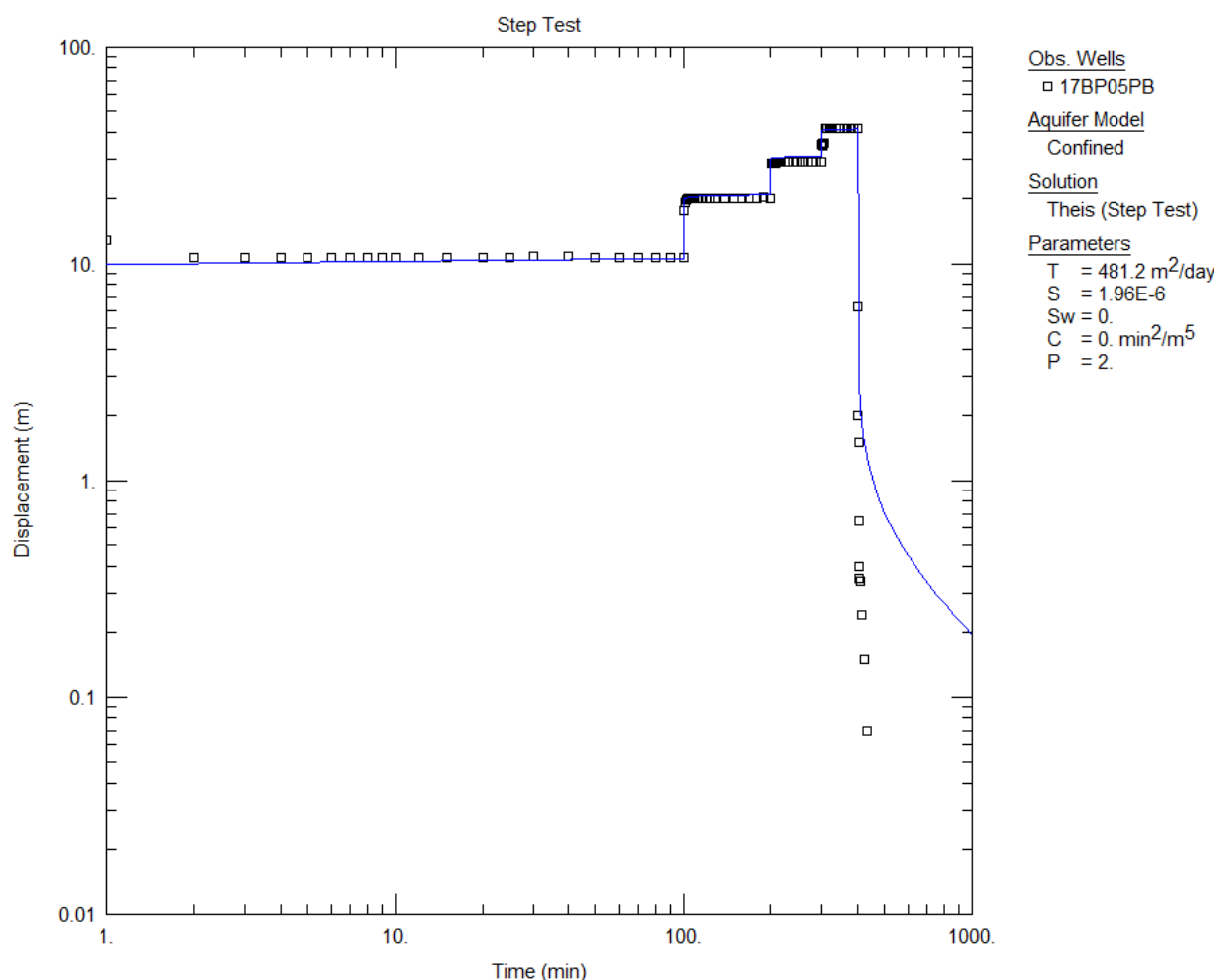


Figure E18: 17BP05PB step test analysis

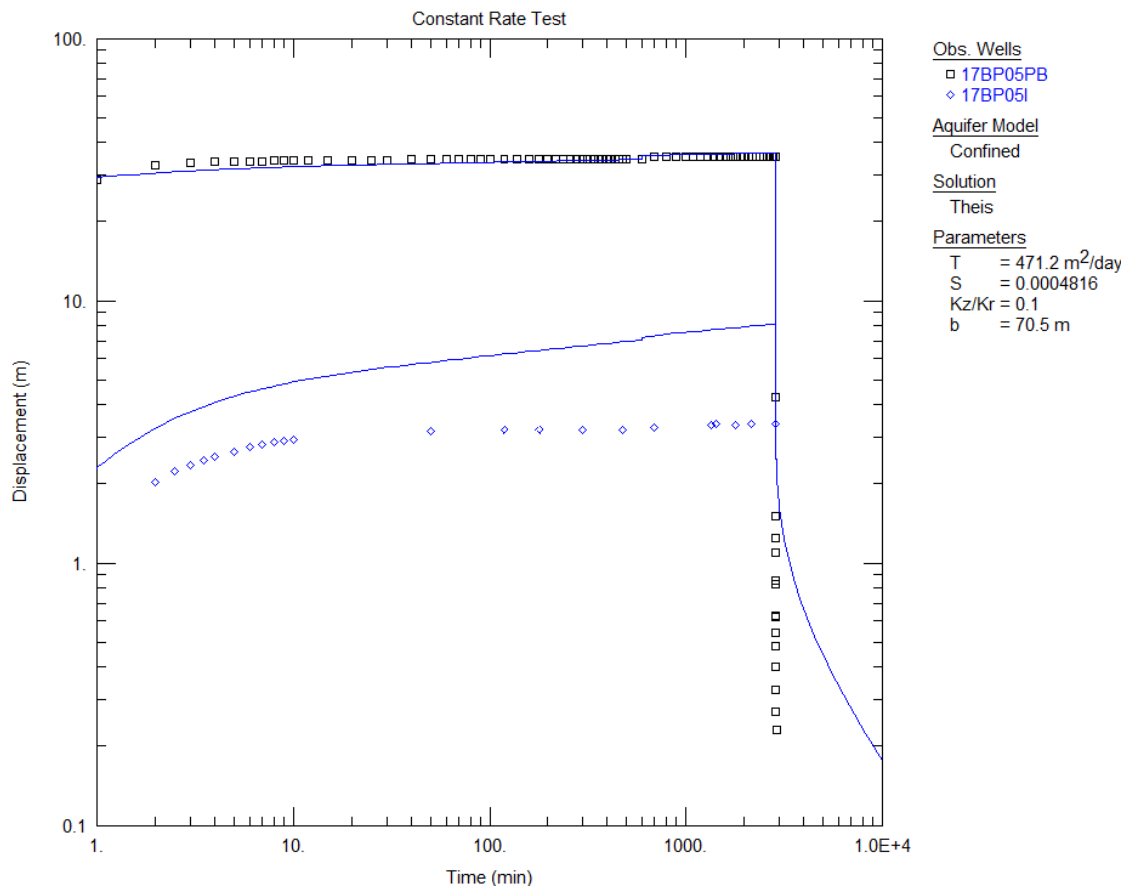


Figure E19: Theis confined constant rate test analysis of 17BP05PB

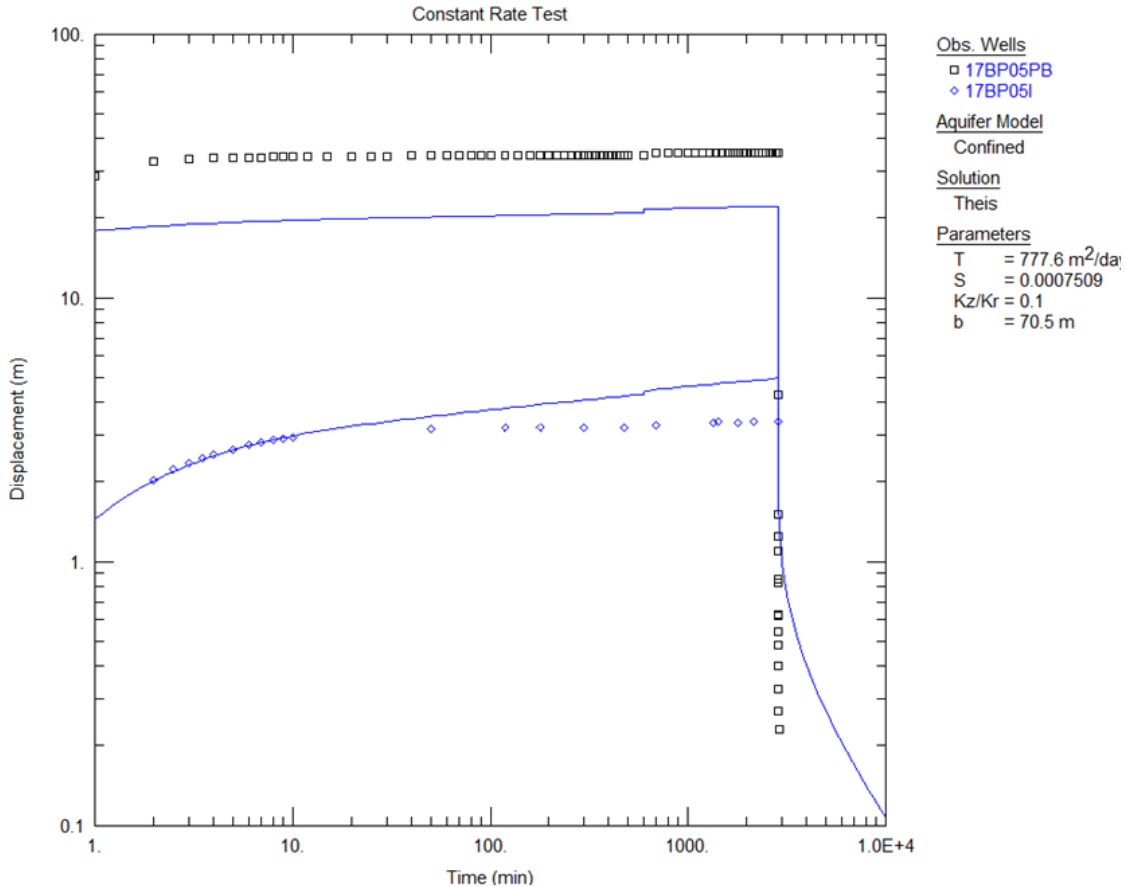


Figure E20: Theis confined constant rate test analysis of 17BP05I



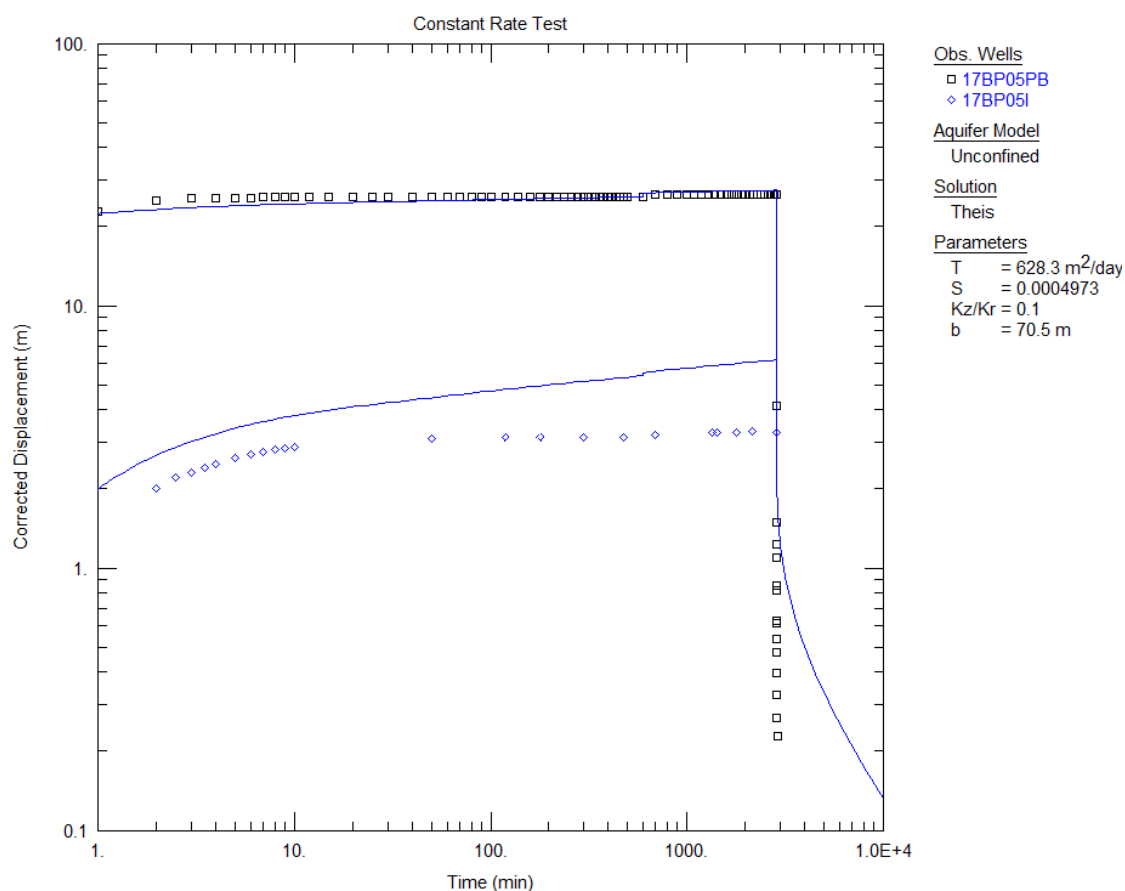


Figure E21: Theis unconfined constant rate test analysis of 17BP05PB

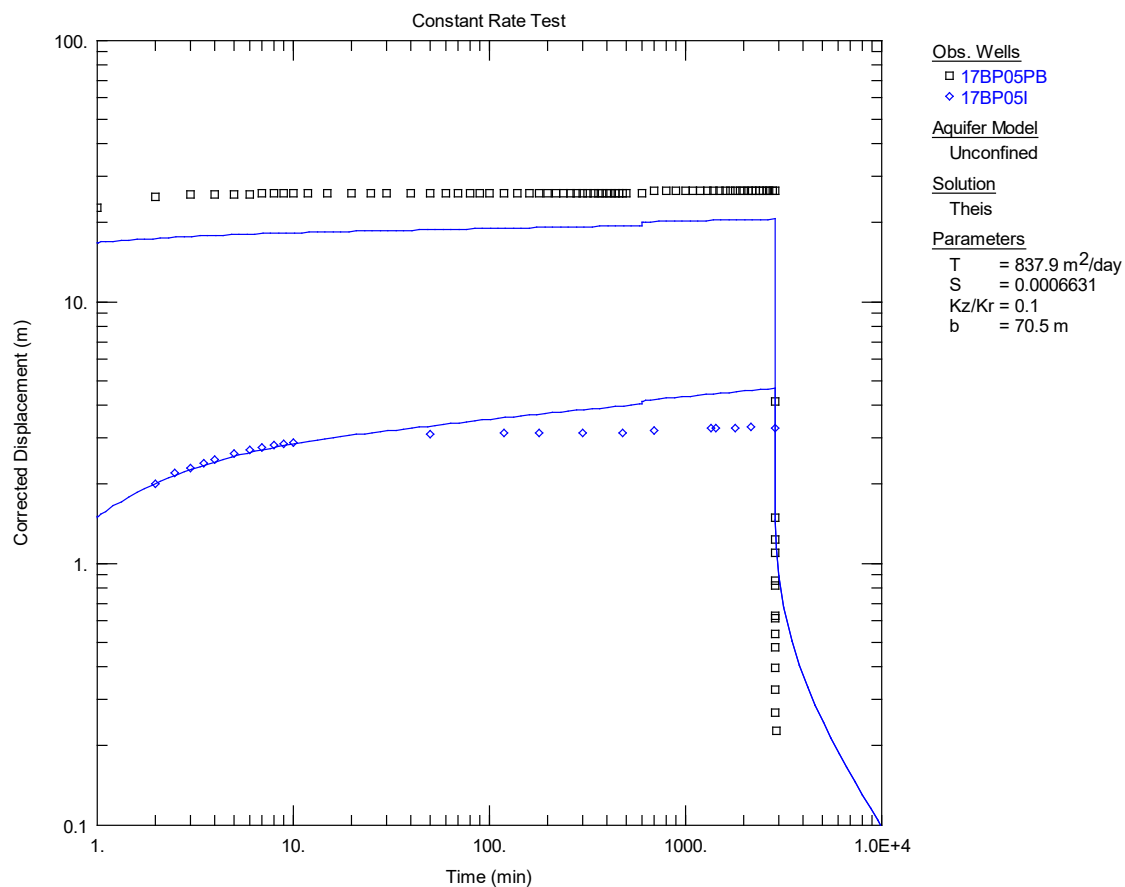


Figure E22: Theis unconfined constant rate test analysis of 17BP05I

Table E9: Analysis of 17BP05PB test pumping program

Bore	Analysis	T (m <sup>2</sup> /d)	K (m/d)	S
17BP05PB	Theis Step test Confined	481	6.8	NA
17BP05BP	Theis CRT Confined	471	6.7	0.0005
17BP05I	Theis CRT Confined	777	11.0	0.0008
17BP05BP	Theis CRT Unconfined	628	8.9	0.0005
17BP05I	Theis CRT Unconfined	838	11.9	0.0006
17BP05PB	Hantush-Jacob leaky confined	199	2.8	NA

K = hydraulic conductivity; NA = not applicable; S = storativity; T = transmissivity

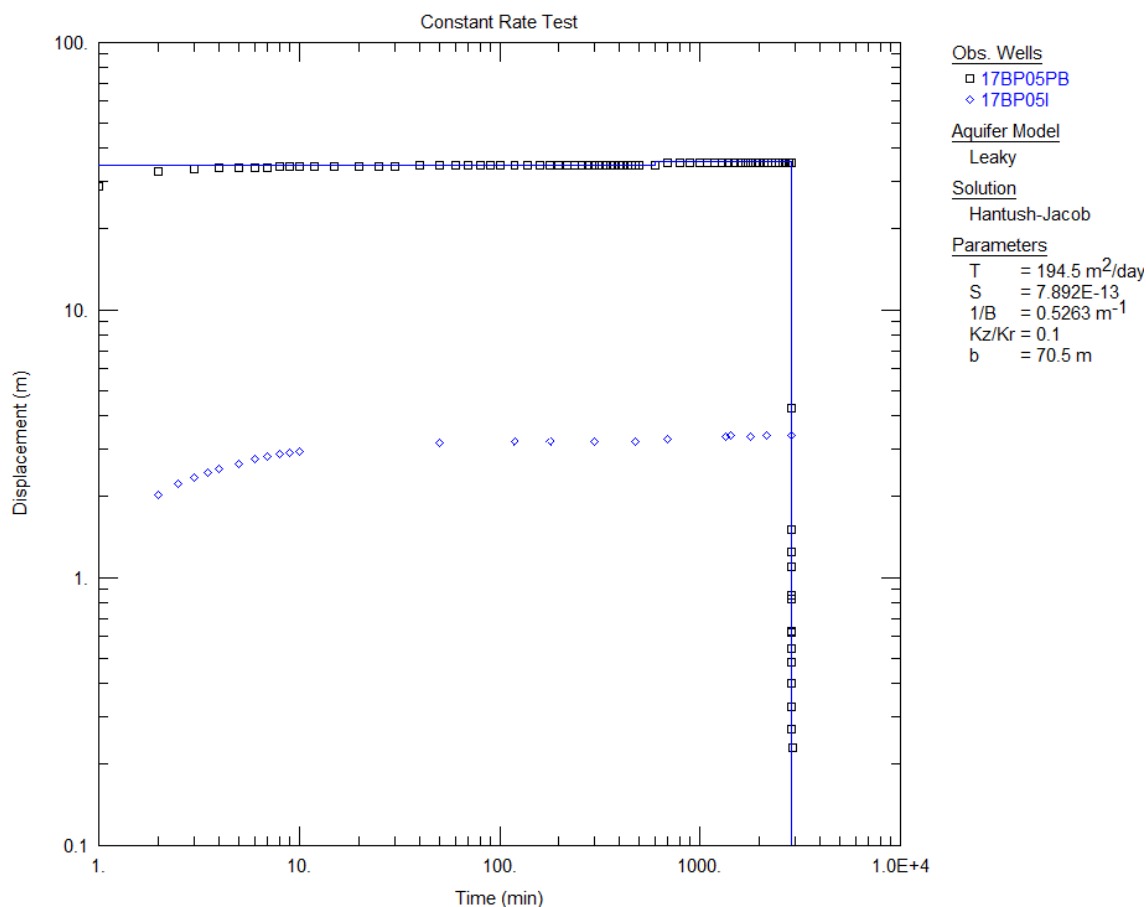


Figure E23: Hantush-Jacob confined leaky analysis of 17BP05PB

### Potential pumping rates and apparent safe yields

A theoretical, sustained potential pumping rate and apparent long-term safe bore yield analysis for the production bores was conducted using a Modified Non-Steady State flow equation (Hazel 2009) and the modified Moell Method (Maathuis and van der Kamp 2006), respectively.

The sustained (7 months) potential pumping rate was obtained by multiplying the CRT discharge rate by the ratio of the available drawdown (Table E10) to the extrapolated drawdown at 300,000 minutes during the CRT using equation 1.

$$Q_L = Q_{CRT} \times (S_a / S_{3E+5}) \quad (1)$$

Where:

$Q_L$  = long-term pump rate (L/s),

$Q_{CRT}$  = CRT pump rate (L/s),

$S_a$  = available drawdown (m),

$S_{3E+5}$  = extrapolated drawdown to 300,000 minutes (7 months).

The Maathuis and van der Kamp method was used to estimate the apparent long-term, safe bore yield by determining the maximum discharge rate that, after 20 years of pumping, would not result in the water level falling by more than the available drawdown (Table E10).

The apparent long-term safe bore yield was estimated by multiplying a safety factor, CRT discharge rate and available drawdown (Table E10) and dividing it by the sum of the measured drawdown after 100 minutes plus the predicted further drawdown from 100 minutes to 20 years (equation 2). A safety factor of 0.7 was also applied to offset overestimates of sustained yield resulting from well inefficiencies and losses that may increase over time due to incrustations and biofouling.

$$Q_{20} = 0.7 \times Q_{CRT} \times S_a / [S_{100} + (S_{e20yrs} - S_{e100min})] \quad [2]$$

Where:

$Q_{20}$  = apparent safe yield for a 20-year period (L/s),

0.7 = 70% safety factor,

$Q_{CRT}$  = CRT pump rate (L/s),

$S_a$  = available drawdown (m),

$S_{100}$  = measured drawdown at 100 minutes,

$S_{e20yrs}$  = estimated drawdown after 20 years of pumping at  $Q_{CRT}$ ,

$S_{e100min}$  = estimated drawdown at 100 minutes.

The calculated long term drawdown for bores 13BP01PB, 17BP01PB and 17BP05PB are shown in Figures E24, E25 and E26, respectively.

Table E10: Long-term discharge rates for Bonaparte bores

Bore	Static water level (mBGL)	Available drawdown (m)	Discharge rate (L/s)	Drawdown after 300,000 minutes (m)	Drawdown after 20 years (m)	Sustained potential pumping rate (L/s)	Apparent safe long-term bore yield (L/s)
13BP01PB	45.12	10	16.31	7.21	8.25	22.0	14.17
17BP01PB	6.11	80	16.31	50.20	51.70	32.4	22.04
17BP05PB	17.78	50	34.80	37.60	38.80	46.1	32.70

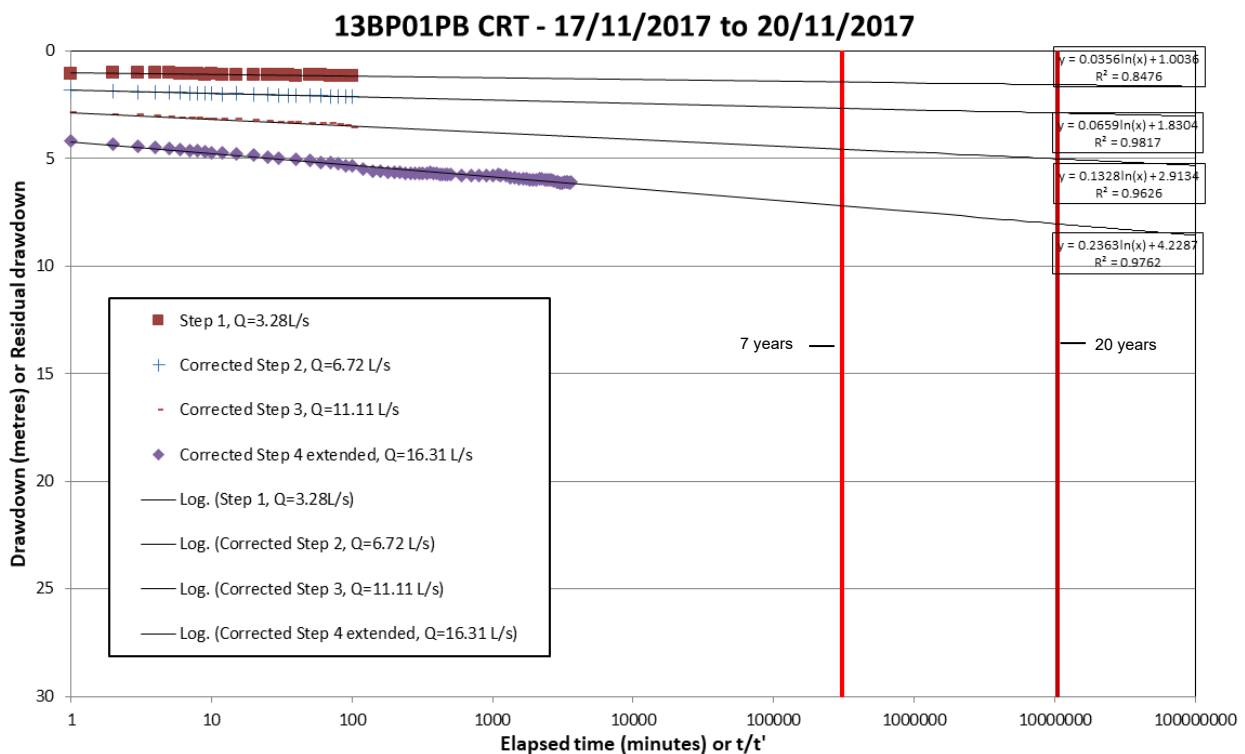


Figure E24: Calculated long-term drawdown for 13BP01PB

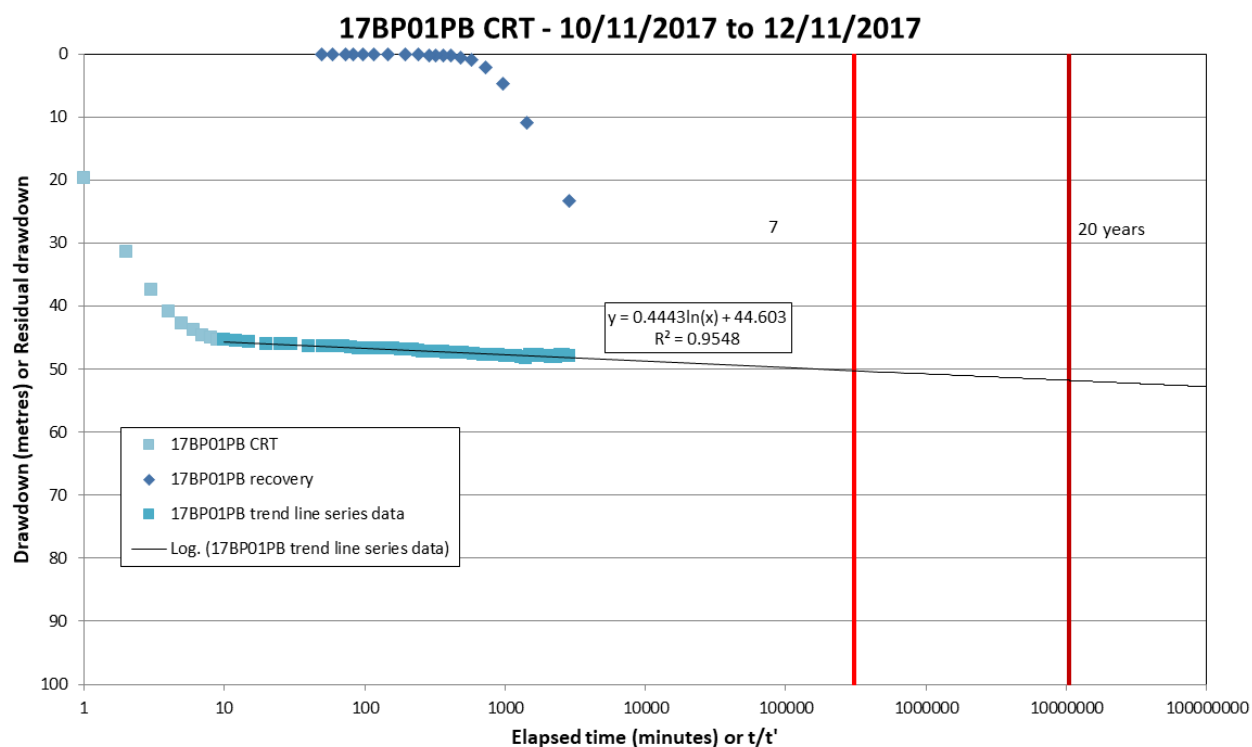


Figure E25: Calculated long-term drawdown for 17BP01PB

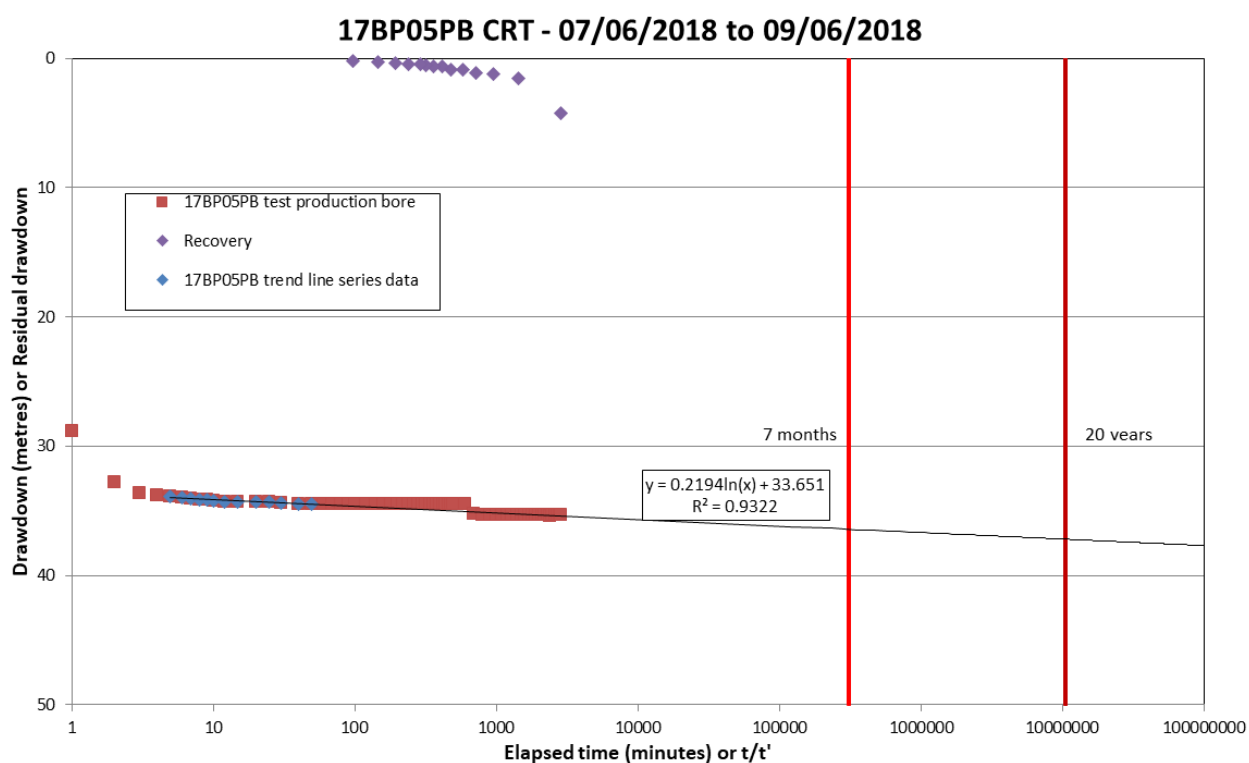


Figure E26: Calculated long-term drawdown for 17BP05PB

## Discussion

In general, the production bore test pumping drawdowns fit the type curves with reasonable accuracy; however, the responses in the observation bores fit the type curves with less accuracy. This suggests that there is imperfect connection between the observation and pumping bores at the sites.

Drilling logs and lithological descriptions at the 3 test pumping sites, plus 4 additional sites drilled during the same program (Bennett 2019) show that the Point Springs Sandstone Formation has a variable vertical lithology. Lithology also varies between drilling sites. Layers within the formation can be variably consolidated, indurated with iron oxides, silt and/or clay rich, shaly or porous.

The sandstone profile at bore 17BP01PB is generally well consolidated and indurated at depth, although porosity was visible in the rotary air hammered drilling cuttings to about 65 m depth. Below 65 m, the technique used was rotary mud drilling, which returned fine, ground-up samples from which it was not possible to assess porosity. Airlift water yields during drilling were up to about 50 L/s until 65 m depth.

The sandstone profile at 13BP01PB is generally poorly consolidated and less indurated with iron oxide. However, the sandstone generally contained more silt, with the silt content being variable in layers throughout the profile.

The sandstone profile at 17BP05PB also had fewer iron-indurated layers and is generally poorly consolidated. However, the profile also contains distinct layers of well-consolidated sandstone and siltstone. Porosity was apparent in rotary air hammered drilling cuttings from the poorly consolidated sandstone layers encountered to the full depth of 17BP05PB (Bennett 2019)

The derived K values align with those expected from the lithology at the 3 sites. Layering within the Point Spring Sandstone Formation apparent at each of the drilling sites (Bennett 2019), indicates the likelihood of layers of semiconfinement or confinement occurring throughout the aquifer. It is also probable that fractures, at various scales, occur throughout the formation.

Due to layering, the test pumping results at 17BP01PB and 17BP05PB likely reflect the aquifer properties of only the relatively thin sections of aquifer corresponding to their screened intervals. Large drawdowns of about 47 m and 25 m occurred in response to pumping rates of 16.31 L/s and 36 L/s, respectively. By contrast, the responses in the observation bores, screened similar depths to the test pumping bores, was delayed and less than predicted by the analyses models used, assuming unconfined conditions. In addition, the shallower observation bores had minor and delayed responses to pumping at both sites, indicating reduced connectivity between layers.

In contrast to 17BP01PB and 17BP05PB, there was modest drawdown of about 7 m in response to pumping (at a similar rate to 17BP01PB) in 13BP01PB, which, although it has a narrowed diameter bore, is screened from 35 to 83 m depth. Here, the response in the monitoring bore (13BP01S) installed to a similar depth was a reasonable fit to the Theis predicted response for an unconfined aquifer. Therefore, within the Point Springs Sandstone Formation aquifer, higher-yielding bores are likely to be achieved by maximising the length of screened aquifer and screening higher up in the aquifer.



Production bore 13BP01PB was constructed with the slotted casing from 35–83 m below ground level (mBGL) and the SWL in 2017 was 45.12 mBGL. This meant the pump was set in the slotted casing. The available drawdown was estimated to be the saturated thickness of the aquifer divided by 3 to give an approximate available drawdown of 10 m.

Using the Hazel method, the 3 production bores had an estimated sustained potential pumping rate ranging from 22–46 L/s. The estimated apparent long-term safe bore yield for the 3 production bores ranged from about 14–33 L/s, using the Maathuis and van der Kamp method.

All the production bores were drawing water from about 50 mBGL at the end of their CRTs.

## References

- Bierschenk W (1964) 'Determining well efficiency by multiple step drawdown tests', *International Association of Scientific Hydrology*, 64:493–507.
- Bennett D (2019) 'Investigations of the potential for irrigated agriculture on the Bonaparte Plains: bore completion report', 2nd edn, *Resource management technical report 414*, Department of Primary Industries and Regional Development, Western Australian Government.
- Cooper H and Jacob C (1946) 'A generalized graphical method for evaluating formation constants and summarizing well field history', *Am Geophys Union Trans*, 27:526–534.
- Hantush M and Jacob C (1955) 'Non-steady radial flow in an infinite leaky aquifer', *Am Geophys Union Trans*, 36:95–100.
- Hazel C (2009) *Groundwater hydraulics*, 2nd edn, The Irrigation and Water Supply Commission, Queensland, Lectures.
- Maathuis H and Kamp G (2006) 'The Q20 Concept: Sustainable well yield and sustainable aquifer yield', *Saskatchewan Research Council Publication No. 104717-4E06*, Saskatchewan Research Council, Canada.
- Theis C (1935) 'The relation between the lowering of the piezometric surface and the rate and duration of discharge of a well using groundwater storage', *Am Geophys Union Trans*, 16:519–524.

**Appendix F Water balance modelling report**



# **Water Balance Model for the Point Spring Sandstone Aquifer at Bonaparte Plains, Kimberley**



FINAL REPORT

July 2019





# Water Balance Model for the Point Spring Sandstone Aquifer at Bonaparte Plains, Kimberley

17 July 2019





## Document control

Version	Date Issued	Author	Reviewed by	Date Approved	Revision Required
1.4	12 <sup>th</sup> February 2019	N. Harrington	G. Harrington	13 <sup>th</sup> February 2019	Minor
1.5	13 <sup>th</sup> February 2019	N. Harrington	P. Raper, D. Bennett	28 <sup>th</sup> February 2019	Minor

## Distribution

Date	Version	Issued To
13 <sup>th</sup> February 2019	1.5 Final Draft	DPIRD (P. Raper, D. Bennett)
8 <sup>th</sup> March 2019	Final Report	DPIRD (P. Raper, D. Bennett)

## **SUGGESTED CITATION**

IGS (2019). Water Balance Model For the Point Spring Sandstone Aquifer at Bonaparte Plains, Kimberley. Final Report. 8 March 2019.

## **ACKNOWLEDGEMENTS**

We would like to thank Paul Raper and Don Bennett (DPIRD) for their feedback on draft project outputs, valuable insight into the study area and their overall contribution of experience in hydrogeology and groundwater modelling to the project.

## **DISCLAIMER**

This report is solely for the use of the Department of Primary Industries and Regional Development and may not contain sufficient information for purposes of other parties or for other uses. Any reliance on this report by third parties shall be at such parties' sole risk.

The information in this report is considered to be accurate with respect to information provided and conditions encountered at the site at the time of investigation. IGS has used the methodology and sources of information outlined within this report and have made no independent verification of this information beyond the agreed scope of works. IGS assumes no responsibility for any inaccuracies or omissions. No indications were found during our investigations that the information provided to IGS was false.

Innovative Groundwater Solutions Pty Ltd.

PO Box 2123, Victor Harbor SA 5211

Phone: 0458 636 988

ABN: 17 164 365 495 ACN: 164 365 495

Web: [www.innovativegroundwater.com.au](http://www.innovativegroundwater.com.au)

Email: [glenn@innovativegroundwater.com.au](mailto:glenn@innovativegroundwater.com.au)

## EXECUTIVE SUMMARY

A three-dimensional steady-state groundwater flow (water balance) model has been constructed of the coastal Point Spring Sandstone aquifer at Bonaparte Plains in the East Kimberley region. The model is intended to form a risk assessment tool to provide a basis for decisions around the release of land for dryland and irrigated agriculture. The groundwater flow model has been calibrated in steady-state to available hydraulic head data and used to assess the steady-state water balance of the Point Spring Sandstone aquifer.

The calibrated numerical model is based on the current conceptual model for the system, with a hydraulic conductivity of the Point Spring Sandstone of 6 m/day and an average annual recharge rate of 140 mm/yr across most of the recharge area. This model produces a hydraulic head distribution that is consistent with recent observation data.

The water balance of the calibrated numerical model suggests that total recharge amounts to 190 ML/day (69.4 GL/yr). Evapotranspiration accounts for more than 93% of the outflows from the system, with the remaining outflow consisting of approximately 6% discharging via the coastal boundary and 1% discharging at the western boundary of the model domain.

The model represents the current understanding of the Point Spring Sandstone aquifer groundwater system. However, the following limitations have been identified, with potential impacts of the accuracy of the estimated water balance:

1. Alternative conceptual models using combinations of lower hydraulic conductivity and lower recharge or higher hydraulic conductivity and higher recharge are also plausible, highlighting the non-uniqueness of the model. The results of testing of these scenarios indicates that different combinations of plausible recharge / hydraulic conductivity values can maintain model calibration but have a significant impact on the simulated water balance.
2. There is no data currently available on the vertical hydraulic conductivity of the Keep Inlet Formation. We tested the impact of using an order of magnitude lower value and found that it had a large impact on the water balance whilst maintaining a reasonable calibration.
3. The head observation dataset contains only one to two years of data, meaning that the selection of steady state head values for calibration of the steady state model based on the current dataset was uncertain.

Two cross-section models of the (density-dependent) freshwater-seawater interface within the study area have also been constructed to investigate the likely location of the seawater interface within the Point Spring Sandstone. The results of this exercise indicate that:

- The toe of the seawater interface lies below the mudflats at the location of Section 103901, approximately 1,500 m inland of the model boundary.
- The toe of the seawater interface at the location of Section NS01 is approximately 9 km inland of the model boundary, approximately at the location of Yow Spring.

## CONTENTS

<b>1. Introduction .....</b>	<b>1</b>
1.1. Background .....	1
<b>2. Site Description .....</b>	<b>1</b>
<b>3. Overview of Conceptual Model .....</b>	<b>5</b>
3.1. Hydrostratigraphy .....	5
3.2. Groundwater Flow and Hydraulic Heads .....	7
3.3. Aquifer Hydraulic Properties .....	11
3.4. Hydrogeological Boundaries .....	12
3.4.1. Western Boundary .....	12
3.4.2. Coastal Boundary .....	12
3.4.3. Southern Boundary .....	12
3.5. Recharge .....	12
3.6. Evapotranspiration .....	15
<b>4. Methodology .....</b>	<b>15</b>
4.1. Hydrostratigraphic Layer Development .....	15
4.2. Modelling Approach .....	16
4.3. Cross Section Model Design .....	17
4.4. Three-Dimensional Model Design .....	25
4.4.1. Modelling Platform and Domain .....	25
4.4.2. Model Grid and Layer Definition .....	25
4.4.3. Aquifer Properties .....	25
4.4.4. Simulating the Influence of Faults .....	26
4.4.5. Boundary Conditions .....	29
4.4.6. Recharge .....	29
4.4.7. Evapotranspiration .....	31
4.5. Calibration .....	33
4.5.1. Calibration Targets .....	33
4.5.2. Calibration Methodology .....	34
<b>5. Results .....</b>	<b>36</b>
5.1. Three-Dimensional Steady-State Groundwater Flow Model .....	36
5.1.1. Conceptual Model Version .....	36

5.1.1.	<i>Model Calibration</i> .....	36
5.2.	Two-Dimensional SEAWAT Models .....	43
<b>6.</b>	<b>Sensitivity Analysis and Alternative Models</b> .....	<b>45</b>
<b>7.</b>	<b>Conclusions</b> .....	<b>53</b>
<b>8.</b>	<b>Limitations</b> .....	<b>54</b>
<b>9.</b>	<b>References</b> .....	<b>55</b>
APPENDIX A. Hydrostratigraphic Cross-Sections.....		57
APPENDIX B. Model Calibration Data .....		63
APPENDIX C. Calibration Residuals for Conceptual Model and Calibrated Versions of the Three-Dimensional Model .....		64
APPENDIX D. Results Of Alternative Model Designs.....		65

## LIST OF FIGURES

Figure 1. Bonaparte Plains location map (from Bennett and Raper, 2018).....	2
Figure 2. Bonaparte Plains study area showing model domain, locations of cross-sections used to develop model layers and model calibration targets. The tidal mudflats can be identified as the light-coloured zones in the background image.....	3
Figure 3. Comparative summary of the lithostratigraphic formations identified by Mory and Beere (1988) and Gorter et al (2005) in the Petrel Sub-basin (from Bennett, 2019). ....	7
Figure 4. Groundwater elevation changes where they are (a) above 40m AHD and (b) below 40m AHD for bores with inlets within the Point Spring Sandstone Formation (Source: Bennett and Raper (2018)). ....	9
Figure 5. Groundwater elevation changes in bores with inlets within (a) Keep Inlet Formation and (b) the Weaber and Ningbing Group formations. Note short-term pumping drawdown (Source: Bennett and Raper (2018)). ....	10
Figure 6. Distribution of Cockatoo Sands and DPIRD's interpreted recharge zones.....	14
Figure 7. Hydrostratigraphic cross sections (a) 103901 and (b) NS01 plotted in Microsoft Excel format. Refer to Table 4 for names of hydrostratigraphic units.....	20
Figure 8. Cross sections (a) 103901 and (b) NS01 modified to provide continuous model layers. Vertical lines in upper figure indicate locations of inferred faults and extents of different hydrostratigraphic units, which would be defined in the groundwater flow model by zones of different hydraulic conductivity. ....	21
Figure 9. Model grid and hydraulic conductivity zones for two-dimensional models of Sections (a) 103901, and (b) NS01 (see Figure 2 for cross section locations).....	22
Figure 10. Model (a) evapotranspiration and (b) recharge zones for Cross Section 103901. Evapotranspiration rate = 1,775 mm/yr, with variable extinction depths as indicated in (a). Recharge rate (red zone) = 140 mm/yr. ....	23
Figure 11. Model (a) evapotranspiration and (b) recharge zones for Cross Section NS01. Evapotranspiration rate = 1,775 mm/yr, with variable extinction depths as shown in (a). Recharge rate (red zone) = 140 mm/yr. ....	24
Figure 12. Model domain for the three-dimensional model, showing the area designated as Keep Inlet Formation in Layer 1 (green area). Also shown are: coastal constant head boundary (blue cells), drain cells (yellow), mapped fault locations (red lines), mapped permanent groundwater discharge features (black lines) and locations of hydrostratigraphic cross sections used to create model layers (blue lines). Black cells represent the inactive portion of the model domain.....	27
Figure 13. Model grid for the three-dimensional model, showing the area designated as Bennett Shale in Layer 3 (red area) and the coastal constant head boundary (blue cells). Locations of inferred faults are indicated by straight lines. ....	27
Figure 14. Model cross sections at locations of (a) Section 101102, (b) Section 103901 and (c) Section 107901. White = Point Spring Sandstone, Red = Bennett Shale, Green = Keep Inlet Formation. Black cells = no flow, Blue/orange cells = constant head boundary. ....	28



Figure 15. Recharge zones used in the three-dimensional groundwater flow model. See Table 6 for recharge rates. Blue cells are constant head cells used to represent the coastal boundary, with constant head zones used for density correction indicated. Yellow cells at left hand edge of the model domain indicate the location of the drain boundary in Layer 1. Where these are absent, the drain boundary is located in Layer 2. ....	30
Figure 16. Evapotranspiration zones used in the three-dimensional groundwater flow model. Refer to Table 5 for zone descriptions. Yellow cells at left hand side of the model domain indicate the drain boundary in Layer 1. Where absent, the drain boundary is located in Layer 2. Dark blue cells represent constant head cells used to represent the coastal boundary. ..	32
Figure 17. Simulated equipotentials (Layer 2) and calibration residuals for Conceptual Model version of the three-dimensional groundwater flow model. ....	38
Figure 18. Simulated equipotentials (Layer 2) and calibration residuals for calibrated version of the three-dimensional groundwater flow model. ....	41
Figure 19. Distribution of dry cells (purple) and areas where simulated heads are above ground surface (light blue cells) compared with mapped areas of permanent groundwater discharge (black outline) and seasonal seepage (purple outline). Simulated equipotentials for Layer 1 are also shown (blue lines). ....	42
Figure 20. Simulated seawater wedge for cross section 103901. See Figure 2 for cross section location. ....	43
Figure 21. Simulated seawater wedge for cross section NS01. See Figure 2 for cross section location. ....	44
Figure 22. Calibration residuals and simulated equipotentials (Layer 2) for sensitivity test: Constant Head in Layer 1 = 0 m AHD. ....	47
Figure 23. Calibration residuals and simulated equipotentials (Layer 2) for sensitivity test: Keep Inlet Formation $K_v = 0.0001$ m/day. ....	48
Figure 24. Calibration residuals and simulated equipotentials (Layer 2) for sensitivity test: Low hydraulic conductivity, low recharge. ....	49
Figure 25. Calibration residuals and simulated equipotentials (Layer 2) for sensitivity test: High hydraulic conductivity, high recharge. ....	50

## LIST OF TABLES

Table 1. Mean annual rainfall and evaporation for the two closest climate stations to Bonaparte Plains for their coincidental periods of record.....	4
Table 2. Summary of hydraulic conductivity (K) and storativity (S) values for the Point Spring Sandstone aquifer made using data from either slug tests or constant rate pump tests. The mean and median values are calculated excluding data that is considered by DPIRD to be unreliable or unrepresentative.....	11
Table 3. Preliminary recharge rate estimates assigned to DPIRD's mapped recharge zones (Figure 6). .....	13
Table 4. Relationship between hydrostratigraphic layers and model layers.....	16
Table 5. Hydraulic conductivity values applied in the groundwater flow model. ....	26
Table 6. Recharge rates used in the initial <i>Conceptual Model version</i> of the groundwater flow model.....	31
Table 7. Evapotranspiration rates and extinction depths used in the groundwater flow model. ....	33
Table 8. Summary of calibration statistics for the <i>Conceptual Model</i> and <i>Calibrated</i> versions of the three-dimensional model. n=27. ....	39
Table 9. Summary of the model mass balances for the <i>Conceptual Model</i> and <i>Calibrated</i> versions of the three-dimensional model.....	39
Table 10. Recharge rates applied in the calibrated three-dimensional groundwater flow model (see Figure 15).....	40
Table 11. Comparison of calibration statistics for <i>Calibrated version</i> of the model and sensitivity test scenarios. ....	51
Table 12. Comparison of model water balances for <i>Calibrated version</i> and various sensitivity test scenarios.....	52

## 1. Introduction

### 1.1. BACKGROUND

Innovative Groundwater Solutions Pty Ltd (IGS) was contracted by the Department of Primary Industries and Regional Development (DPIRD) to construct a three-dimensional steady-state groundwater flow (water balance) model of the coastal Point Spring Sandstone aquifer at Bonaparte Plains in the East Kimberley region. The purpose of the model is to provide a risk assessment tool to inform decisions around the release of land for dryland and irrigated agriculture. The availability of a short time-series of observation bore data and a lack of significant existing groundwater development in the Bonaparte Plains area means that steady-state models are best suited to meet the project objectives. The groundwater flow model is calibrated in steady-state and used to assess the steady-state water balance of the aquifer. The model will be used by DPIRD to run a series of steady-state scenarios testing the impacts of (a) clearing of native vegetation, (b) application of irrigation, and (c) climate on groundwater levels and the water balance.

The project also included construction of up to three cross-section models of the (density-dependent) freshwater-seawater interface within the study area. The purpose of this is to determine the likely location of the seawater interface within the Point Spring Sandstone.

## 2. Site Description

The study area covers a large portion of the Petrel Sub-Basin of the Bonaparte Basin, which is located to the north of Kununurra in the north-east of Western Australia (Figure 1). The Ord River discharges to the west and the Keep River to the east. The loamy Cockatoo Sands that cover part of the study area are a focus for potential irrigated agriculture development under the Implementing Bonaparte Plains Project (Figure 1). Development of areas of loamy sands in the East Kimberley for irrigated agriculture could double the area of land available for production within 50 to 100 km of the Ord Irrigation Precinct (Bennett and Raper, 2018).

A large portion of the study area is covered by tidal mudflats up to 20 km wide, supporting mangroves, samphire and some grasses, with large areas of bare ground (Figure 2). Permanent and seasonal springs occur at the interface between the tidal mudflats and the more sandy units (Figure 2) and these are thought to be discharging from the Point Spring Sandstone aquifer (Bennett and Raper, 2018).

The central portion of the Bonaparte Plains is covered by the Cockatoo Sands, which include red/yellowish-red sands, and sandy loams that have formed from quartz sandstone colluviums (Smolinski et al., 2015 (in Bennett and Raper, 2018)). These areas are vegetated with dense Stringybark - bloodwood woodland (*Eucalyptus Sp.* and *Corymbia Sp.*) and tall grass (*Sorghum Sp.* and *Triodia Sp.*) (Bennett and Raper, 2018).

Lower-lying areas of sands inland of the tidal mudflats support Stringybark - bloodwood woodland, with paperbark (*Melaleuca*) and pandanus (*Pandanaceae*) with tall grass (*Sorghum Sp.*). Springs are extremely densely vegetated and larger springs support forests of large paperbark (*Melaleuca Sp.*), rushes and other aquatic vegetation (Bennett and

Raper, 2018). The plains and drainage floors support mostly short grass (*Xerochloa*), patches of bluegrass tall grass (*Dichanthium*, *Eulalia*, *Ophiuros*).

The landscape to the west of the Cockatoo Sands area dips gently towards a north-south elongated depression that runs along the base of the Ningbing Range. Steep and rocky features occur either side of this depression but some surface water drains to the west through gaps in the Ningbing Range (Bennett and Raper, 2018).

The northern slopes of the Weaber Range form the boundary at the southern margin of the Bonaparte Plains.

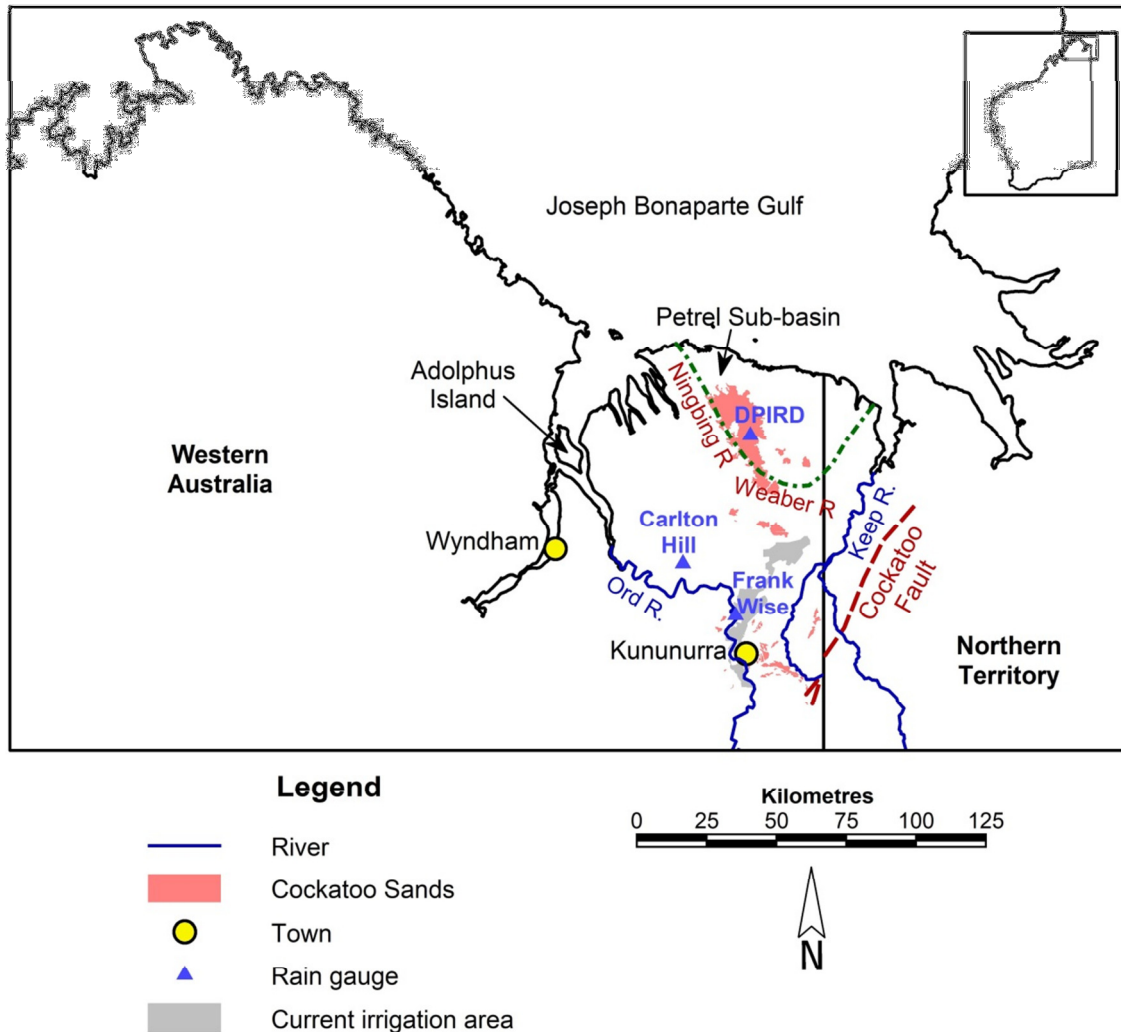


Figure 1. Bonaparte Plains location map (from Bennett and Raper, 2018).



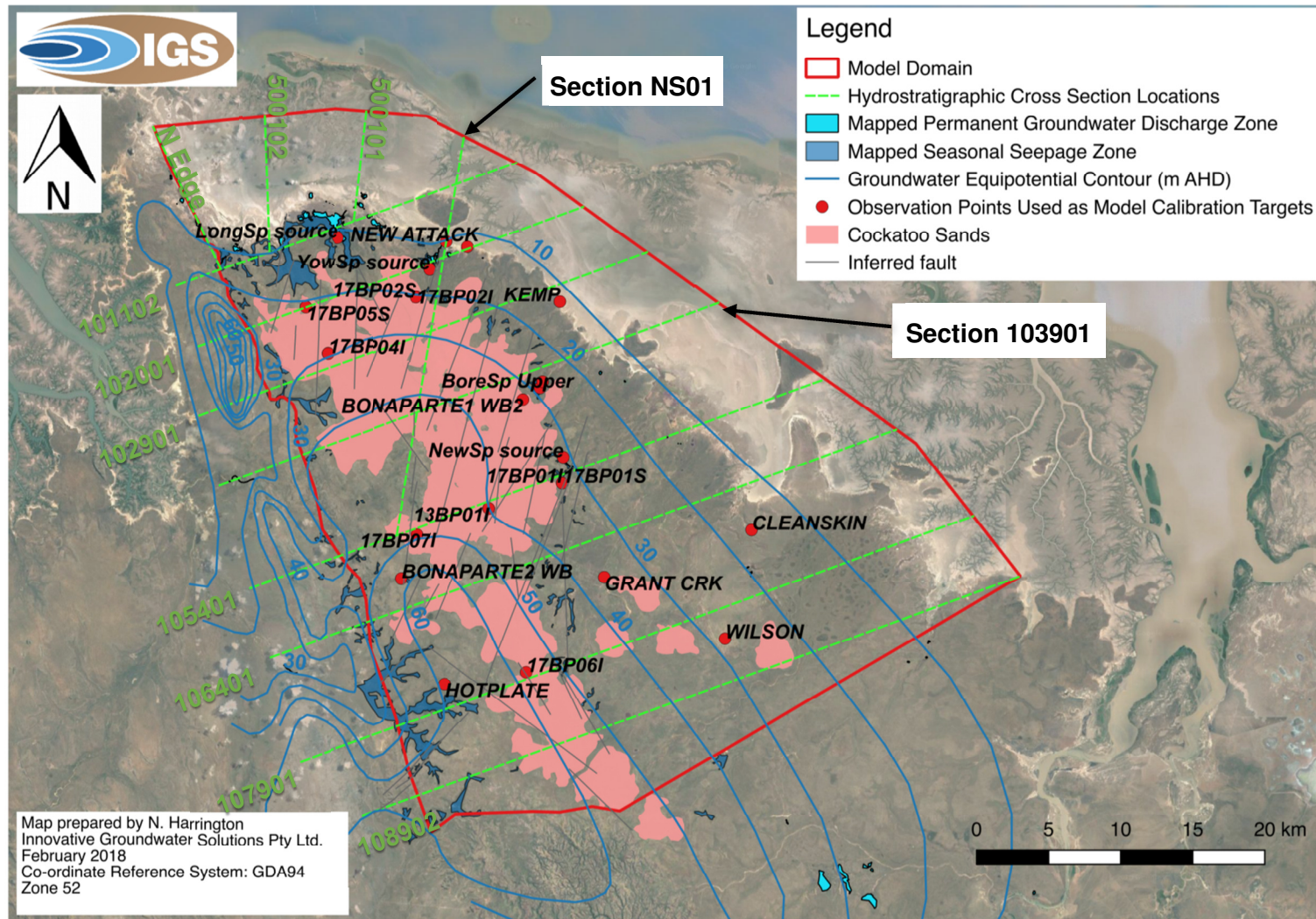


Figure 2. Bonaparte Plains study area showing model domain, locations of cross-sections used to develop model layers and model calibration targets. The tidal mudflats can be identified as the light-coloured zones in the background image.

Rainfall is highly seasonal with about 90% of the annual total usually falling between November and March. The highest temperatures and accompanying highest rates of evaporation typically occur within the September to December period.

The closest climate stations to the Bonaparte Plains are at Frank Wise Institute and Carlton Hill (Figure 1). Carlton Hill has daily rainfall records since 1907 and other climate variables since 1970. There have been daily rainfall and other climate variables recorded at Frank Wise Institute since 1965. Table 1 compares the mean annual rainfall for the period 1965–2018 and the mean annual pan evaporation for the period 1970–2018 for the above climate stations.

Table 1. Mean annual rainfall and evaporation for the two closest climate stations to Bonaparte Plains for their coincidental periods of record

Site	Mean annual rainfall (mm)	Mean annual pan evaporation (mm)
Carlton Hill	911	2679
Frank Wise Institute	883	2712

Source: Department of Science, Information Technology and Innovation 2018

The mean annual rainfall at Carlton Hill is 911 mm/yr and at Frank Wise Institute (FWI) it is 883 mm/yr (1965–2018), with annual pan evaporation of 2,679 mm/yr and 2,712 mm/yr (1970–2018), respectively (Table 1). The long-term (1907–2018) mean annual rainfall at Carlton Hill is 874 mm/yr.

Mean monthly pan evaporation at Carlton Hill ranges from 183 mm in June and February to 296 mm in October. At Frank Wise Institute, pan evaporation ranges from 180 mm in February to 293 mm in October. On average, rainfall exceeds evaporation at both sites in February.

Rainfall at Carlton Hill and Frank Wise Institute has increased since the early 1990s. Some informative rainfall statistics for the Carlton Hill site are:

- the mean annual rainfall for 1993–2018 is 1,036 mm
- 1993–2018 was 33% wetter than 1907–92 (99% confidence level)
- 1993–2018 was 33% wetter than 1968–92 (99% confidence level)
- of the highest ten rainfall years recorded since 1907, seven occurred in the 1993–2018 period
- rainfall for the 2016/17 year was the highest on record (1,649 mm).

Climate data was collected by DPIRD from 2015 to 2018 from a climate station installed on the Bonaparte Plains. The annual rainfall (July to June) for the three years at Bonaparte was 847 mm in 2015/16, 1,696 mm in 2016/17 and 1,091 mm in 2017/18. Average annual rainfall was 1,212 mm for the three-year period. On average, 203 mm/y more rainfall was recorded at Bonaparte than FWI over the same period. Average annual potential evapotranspiration (FAO Penman-Monteith) at Bonaparte was 1,774 mm, 143 mm less than at FWI. Average monthly rainfall exceeded pEt on the Bonaparte Plains during December to March (D. Bennett pers comm. 28 November 2018).



### 3. Overview of Conceptual Model

The current conceptual hydrogeological model for the Bonaparte Plains area is described in detail by Bennett and Raper (2018) and the reader is referred to that document for further information. Key features of the conceptual model that relate to the design of the numerical models have been summarised from that report below.

#### 3.1. HYDROSTRATIGRAPHY

The main publications that describe the geology of the study area are Mory and Beere (1988) and Gorter et al. (2005), with the latter providing a slightly revised stratigraphic interpretation for the south-eastern Bonaparte Basin (Figure 3). Examples of hydrostratigraphic cross-sections constructed for the study area based upon Airborne Electromagnetic (AEM) data (Tan et al., 2018) and drillhole data (Bennett, 2019) are presented in Section 4.1, with all cross-sections constructed to support model layer development provided in Appendix A.

A key feature of the hydrostratigraphy of the study area is a Devonian-Carboniferous sedimentary succession that dips to the north, with the oldest units outcropping in the south. The aquifer of main interest to the current study has been alternatively identified as the late-Carboniferous Point Spring Sandstone Formation (Morey and Beere, 1988) and the Border Creek / Kuriyippi Formation (e.g. Gorter et al., 2005). Figure 3 shows a comparison of the two lithostratigraphic interpretations from the two authors. However, recent palynological evidence suggests that this is predominantly Point Spring Sandstone Formation (Bennett, 2019) (Figure 3). The Point Spring Sandstone consists of fine to coarse sandstone and pebbly sandstone with interbedded conglomerate, siltstone and shale. The sandstone-dominated Border Creek Member of the Point Spring Sandstone Formation is texturally similar to the Point Spring Sandstone Formation. However, the Border Creek Member also contains thick sequences of conglomerate, siltstone, silty sandstone and pebbly quartz sandstone. Based on lithology, Bennett (2019) speculates that Border Creek Member sandstones are present in most of the seven profiles that they drilled and may therefore underlay most of the Cockatoo Sands area. The aquifer is divided into an upper unit and a lower unit, which are thought to have similar hydrogeological properties based upon drilling at two sites. Across the central part of the study area, the upper and lower aquifer units are separated by the low-permeability Bennett Shale.

The late Carboniferous to Permian Keep Inlet Formation consists of sandstones, mudstones and shales, with minor conglomerate, deposited in continental, shallow marine and glaciomarine environments. Onshore, the Keep Inlet Formation unconformably laps onto the Point Spring Sandstone Formation, thickening to the east where it is up to 480 m thick. The Keep Inlet Formation extends under the tidal mud flats to the north and east of Bonaparte Plains. Finer-textured beds are likely to form aquitards causing large artesian heads observed in several partially cased, abandoned coal exploration holes along the northern margin of the mudflats. Zones of weakness in these aquitards are likely to be responsible for isolated areas of groundwater discharge via springs on the edge of the mudflats. The Keep Inlet Formation is overlain by relatively thin Cainozoic alluvium, sand plains and coastal deposits.

Underlying the Point Spring Formation aquifer are the Tanmurra / Sunbird Formations. The Tanmurra Formation consists of calcareous and dolomitic sandstone, which have significant calcareous re-cementation and siltstone, shale and minor limestone units. The Sunbird Formation consists of a massive, re-crystallised, oolitic limestone that grades to grainstone and packstone. Locally, the matrix can also consist of white clay. Recent drilling and palynology was not able to determine which of these formations underlay the Point Spring Sandstone in the area and so it was assigned the name Sunbird/Tanmurra hydrostratigraphic unit in Bennett (2019). The Sunbird/Tanmurra unit is currently conceptualized to form an impermeable base to the aquifer.

The shale-dominated Milligans, Yow Creek and Kingfisher Formations within the Weaber Group form an impermeable boundary along the Ningbing Range to the west of Bonaparte Plains. Elsewhere onshore, the carbonaceous and sandy siltstones of the Sunbird and Tanmurra Formations, respectively, form the upper layers of the Gorter et al. (2005) interpretation of the Weaber Group as it dips towards the north and east. Limestones and other carbonates of the Ningbing Group underlay the Milligans Formation, and outcrop as the Ningbing Range, to the west of the Weaber Group sub-crop.

Folding of the Weaber and basal Kulshill Group sediments occurred as a result of movement on the regional Cockatoo Fault (Figure 1) prior to the deposition of the Keep Inlet Group. Significant faulting of the sedimentary units below the Keep Inlet Formation has been identified.

Ma	Period	Mory & Beere (1888)		Gorter et al (2005)		Ma
		Formation	Group	Formation	Group	
288	Permian	Keep Inlet	Kulshill	Keep Inlet	Kulshill	288
295						295
299	Carboniferous					299
307			Weaber	Border Creek and Kuriyippi	Weaber	307
318						318
319		Point Spring Sandstone				319
320					Wadeye	320
332				Point Spring Sandstone		332
333		Tanmurra (or Burvill)		Sunbird	Weaber	333
337				Sandbar		337
339				Tanmurra		339
340				Kingfisher Shale		340
342				Utting Calcarenite		342
343		Milligans		Yow Creek		343
347				Milligans		347
349		Bonaparte	Langfield		Langfield	349
352						352
359	Devonian	Bonaparte	Ningbing (equivalent)	Bonaparte	Ningbing (equivalent)	359

Figure 3. Comparative summary of the lithostratigraphic formations identified by Mory and Beere (1988) and Gorter et al (2005) in the Petrel Sub-basin (from Bennett, 2019).

### 3.2. GROUNDWATER FLOW AND HYDRAULIC HEADS

There are 21 dedicated observation bores located in the Bonaparte Plains area, along with 25 other water supply bores and 11 other water level elevation measuring points (spring outlets and perched groundwater lakes), which have been used to compile the current understanding of groundwater flow (Bennett and Raper, 2018). The subset of these bores used as calibration targets for the three-dimensional groundwater flow model is shown in Figure 2. Figure 2 also shows the equipotential contours developed for the Point Spring Sandstone Formation, Keep Inlet Formation, Milligans/Yow Creek/ Kingfisher Formation assemblage and Ningbing Group Formation based on observation well data, along with the mapped locations of seasonal and permanent springs / seepage zones. Groundwater flow is predominantly radially away from the central portion of the study area, which has a comparatively high elevation and includes the main area of Cockatoo Sands. Groundwater flows in all directions except to the south, where a well-consolidated area of Point Spring Sandstone Formation forms the Weaber Range and an impermeable boundary.

Most observation bores are screened in the upper unit of the Point Spring Sandstone or the Keep Inlet Formation. Only two groundwater observation bores are screened in the lower aquifer below the Bennett Shale (13BP01D and 18BP01DD), with two wells at the 13BP01 site screened above the Bennett Shale (13BP01S and 13BP01I). Here, a hydraulic head difference of 0.6 m between the lower bore and the two upper bores indicates a slight upward hydraulic gradient across the shale at this location.

Groundwater in the Point Spring Sandstone aquifer below the lower-lying areas of Bonaparte Plains is confined by the mudstone layers of the upper Keep Inlet Formation. Upward discharge is observed at some locations upslope of the Keep Inlet Formation through well-defined permanent springs. Estimates of dry season discharge rates from the springs range from 0.5 L/s to 200L/s, with higher rates thought to occur late in the wet season. Larger areas of seasonal groundwater discharge occur up-slope of these margin springs and in other areas. Some of the permanent springs occur within the boundary of the Keep Inlet Formation, probably due to localized weaknesses in the mudstone aquitard.

Two perched lakes have been identified in the central southern upland area and a shallow clayey colluvium perching layer that supports an ephemeral water table appears to be localized around these lakes (Bennett and Raper, 2018).

Monitoring of groundwater levels at Bonaparte Plains commenced in 2013, however, as most observation bores were installed in 2016 and 2017, a comprehensive time series of hydraulic head data is only available for the past one to two years (Figures 4 and 5).

Figure 4 and Figure 5 show water level responses in the Point Spring Sandstone Formation, Keep Inlet Formation, Ningbing Group and Milligans/Yow Creek/ Kingfisher Formation assemblage aquifers over the period of monitoring. The response to heavy rainfall in the 2016/17 wet season is most pronounced in the Ningbing Group and the Point Spring Sandstone bores that have shallower depths to water, with small or absent responses in the Keep Inlet bores. In many cases, a gentle and gradual rise in hydraulic heads in the Point Spring Sandstone aquifer is evident over the period of monitoring.

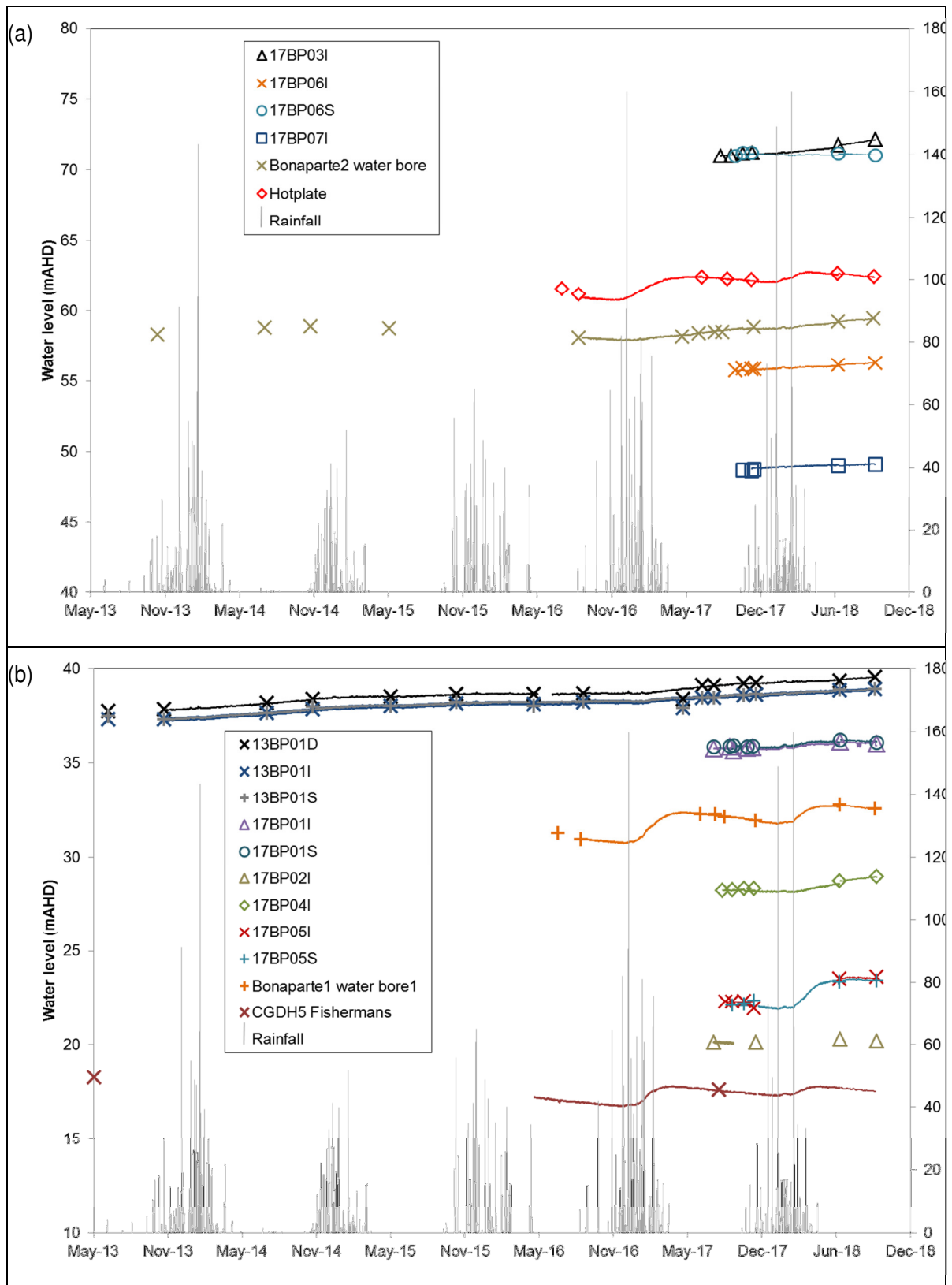


Figure 4. Groundwater elevation changes where they are (a) above 40m AHD and (b) below 40m AHD for bores with inlets within the Point Spring Sandstone Formation (Source: Bennett and Raper (2018)).

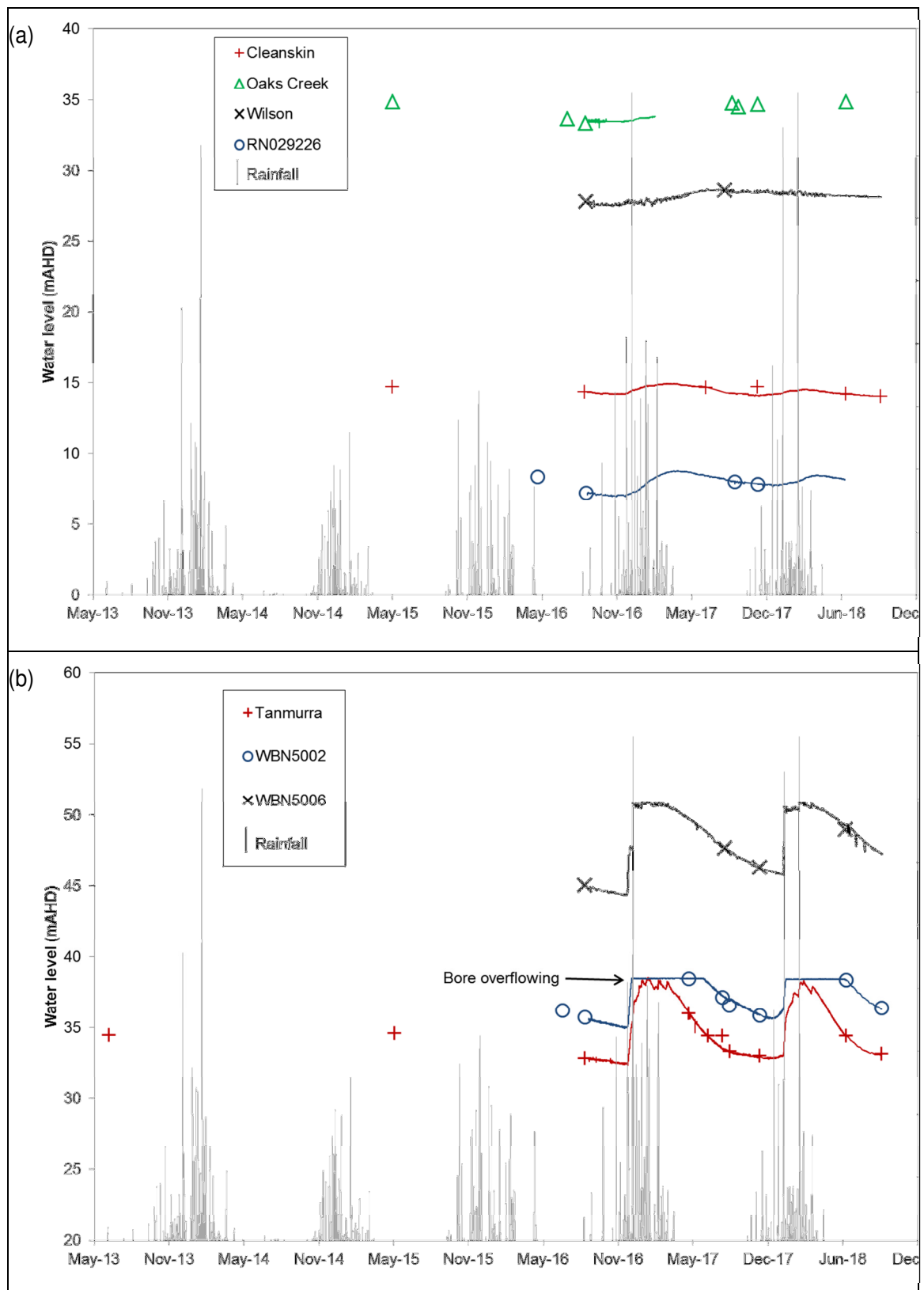


Figure 5. Groundwater elevation changes in bores with inlets within (a) Keep Inlet Formation and (b) the Weaber and Ningbing Group formations. Note short-term pumping drawdown (Source: Bennett and Raper (2018)).



### 3.3. AQUIFER HYDRAULIC PROPERTIES

Table 2 shows that estimates of hydraulic conductivity for the Point Spring Sandstone aquifer range between 3.2 m/day and 14 m/day, excluding data that was considered to be unreliable on analysis. Mean and median hydraulic conductivity values range between 6.6 m/day and 7.3 m/day. An intermediate value of 6.9 m/day was selected as a starting value for horizontal hydraulic conductivity of the Point Spring Sandstone for the purpose of groundwater flow model development.

A review of bore log data provided in Bennett and Raper (2018) suggests that the aquifer comprises mainly sandstone layers with varying grain size, sorting, degree of consolidation and silt composition. This variability in aquifer material may at least partially explain the variability in estimates of aquifer properties. Additionally, slug test results are likely to be representative of a small area immediately surrounding the bore screen whilst those from longer constant rate tests are likely to be more representative of the bulk characteristics of the aquifer.

Table 2. Summary of hydraulic conductivity (K) and storativity (S) values for the Point Spring Sandstone aquifer made using data from either slug tests or constant rate pump tests. The mean and median values are calculated excluding data that is considered by DPIRD to be unreliable or unrepresentative.

	Slug Test	Constant Rate Pump Test	
Bore	K (m/d)	K (m/d)	S (-)
Upper Aquifer			
13BP01S (2013)	-	21*	0.09*
13BP01PB (2013)	-	11*	-
13BP01S (2017)	-	9.4	0.013
13BP01PB (2017)	-	4.3	-
17BP01I	3.5	3.5	0.001
17BP01S	3.4	37.5*	0.01
17BP01PB	-	3.2	-
17BP02S	14.0	-	-
17BP03I	12.0	-	-
17BP04I	8.7	-	-
17BP04S	8.4	-	-
17BP05I	7.5	11.9	0.0006
17BP05S	3.2	-	-
17BP05PB	-	8.9	0.0005
17BP06S	7.2	-	-
17BP07I	6.0	-	-
Lower Aquifer			
13BP01D (2018)	6.4	-	-
18BP01DD	58.2**	-	-
Mean	7.3	6.9	0.019
Median	7.2	6.6	0.0055

\* Considered to be unreliable.

\*\* Screened in a very permeable feature – unlikely to be representative.

There is no data available on the hydraulic properties of the Bennett Shale or the Keep Inlet Formation, although these units are conceptualized as being aquitards of low to very low permeability. The Keep Inlet Formation may contain lenses of aquifer material, however the

presence of significant mudstone and shale units suggests that this formation is likely to be of low permeability at the regional scale.

### **3.4. HYDROGEOLOGICAL BOUNDARIES**

#### **3.4.1. Western Boundary**

Some seasonal groundwater discharge and flow is assumed to occur across the western boundary defined by the Ningbing Range and marked as the model boundary in Figure 2. However, the aquifer is thin and therefore of low transmissivity in this area and a poor hydraulic connection across the boundary is suggested by the steeper hydraulic gradient (Figure 2), different groundwater responses to rainfall and different geochemical signatures of groundwater (Bennett and Raper, 2018). The Point Spring Sandstone does contribute baseflow to surface drainage lines that flow to the west across the Ningbing Range (Bennett and Raper, 2018). Collector creeks for many of these drainage lines run parallel to the boundary before finding an outlet to the west through the Ningbing Range. The collector creeks are generally well-incised (up to 5m) and have gradients of about 0.5%. Westward flowing feeder creeks have a much higher gradient and often originate from swampy headwaters that exist above shale or other fine-textured layers.

#### **3.4.2. Coastal Boundary**

The Bonaparte Plains groundwater flow system is bounded to the north and the east by the coast, with groundwater assumed to be discharged via submarine groundwater discharge beyond the seaward extent of the tidal mud flats. No evidence of groundwater discharge along the low tide mark has been found despite active efforts to do so (Bennett and Raper, 2018).

#### **3.4.3. Southern Boundary**

At the southern extent of the Bonaparte Plains, a no-flow boundary is located parallel with the groundwater flow direction adjacent to the impermeable Weaber Range.

### **3.5. RECHARGE**

Direct recharge is assumed to occur over most of the area mapped as Cockatoo Sands in Figure 6. Hydrographs of bores completed in the Point Spring Sandstone indicate that the deep unsaturated zone over the upper portion of the Bonaparte Plains attenuates direct rainfall recharge in this area (Bennett and Raper, 2018).

The aquifer is confined under the Keep Inlet Formation in the lower parts of the landscape to the east of the Cockatoo Sands and recharge to the Point Spring Sandstone is assumed to be zero in this area and under the tidal mud flats.

Although the distribution of Cockatoo Sands can be considered a good first-pass indication of a likely high groundwater recharge area, its physical characteristics are variable across the study area, as are the characteristics of the underlying material. Furthermore, some of the soils outside the mapped Cockatoo Sands extent also have characteristics that are likely to provide significant recharge. DPIRD recently carried out an exercise to map potential high

and very high recharge areas across the Bonaparte Plains, based upon the spatial distribution of characteristics of the Cockatoo Sands and other soils likely to affect recharge rates (D. Bennett, pers. comm., 27 Nov. 2018). Five recharge areas were defined: Very High Recharge, High Recharge, Variable/Rocky zones, seepage zones and areas of hard sandstone (Figure 6). All other areas are considered to have negligible recharge as they are underlain by the low permeability Keep Inlet Formation.

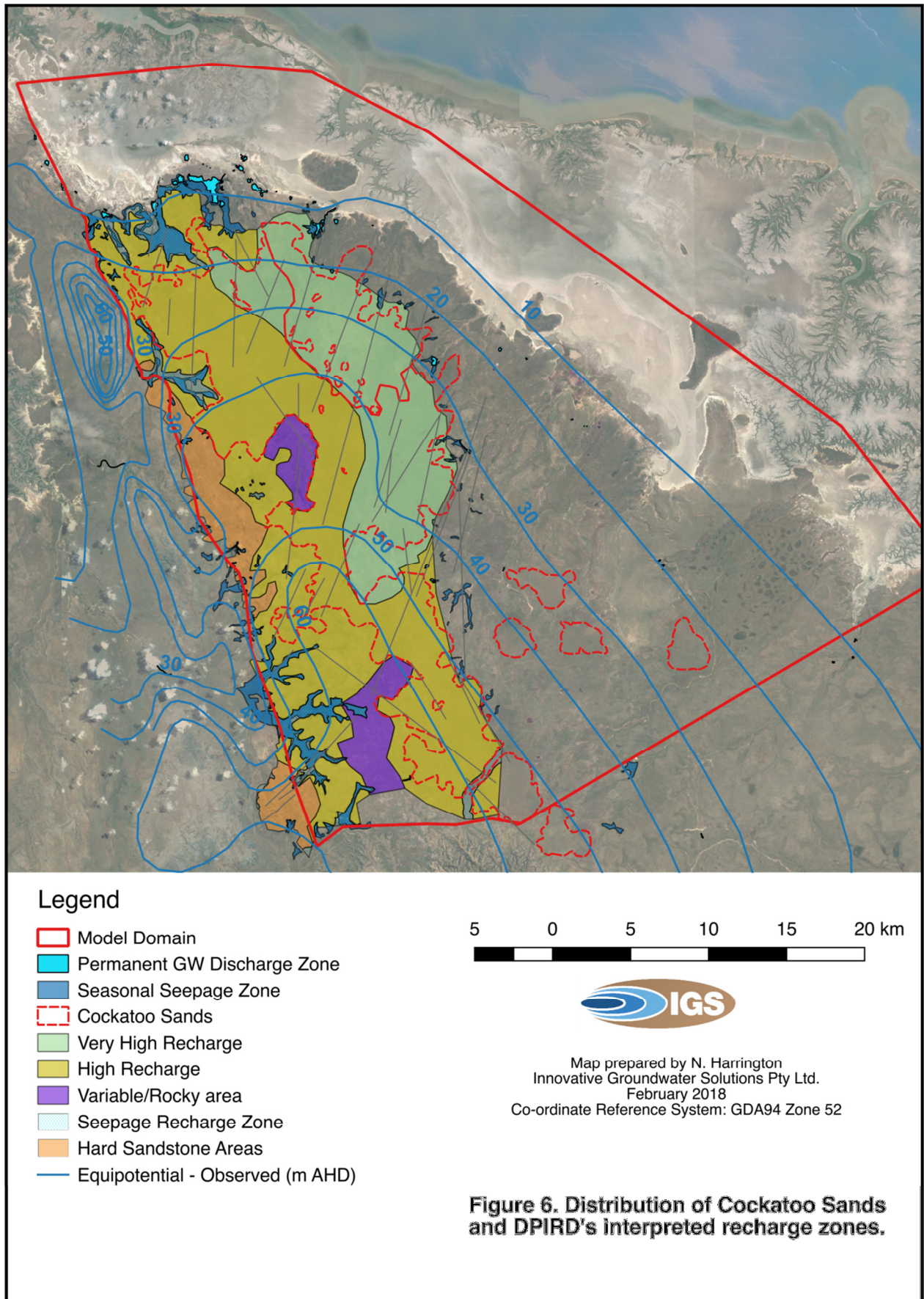
There is a small body of recharge data available for the study area, consisting of estimates made using chloride mass balance (CMB) and environmental tracer approaches ( $^{14}\text{C}$ ,  $^3\text{H}$ , CFCs and  $\text{SF}_6$ ) (Meredith et al., 2018; D. Bennett, pers. comm., 27 Nov. 2018). The CMB estimates for bores with suitably shallow screens to represent modern day recharge range between approximately 16 mm/yr and 350 mm/yr, with a mean of 107 mm/yr ( $n = 7$ ). Excluding the anomalously low value of 16 mm/yr at observation bore 17BP03I, the mean is 122 mm/yr ( $n = 6$ ). The bore locations for all but one of these values are in the area covered by Cockatoo Sands. The CMB estimates of recharge are based upon a mean rainfall chloride concentration of 1.3 mg/L ( $n = 2$ ) and an assumed average rainfall value of 1,077 mm/yr (long-term mean annual rainfall at Carlton Hill plus 203mm, see Section 2).

Estimates of recharge derived from environmental tracers range from less than 10 mm/yr (often from deeper sampling points outside the main recharge area) to 134 mm/yr (western margin of the model domain). The values for sampling points within and around the main recharge area range between 33 mm/yr and 101 mm/yr ( $n = 3$ ). Based upon these estimates, DPIRD have assigned preliminary recharge rates to the mapped recharge zones shown in Figure 6, with comments based upon data coverage and field observations (Table 3).

Table 3. Preliminary recharge rate estimates assigned to DPIRD's mapped recharge zones (Figure 6).

Zone	Recharge Rate (mm/yr)	Comment
Very High Recharge	134	Mean of relevant estimates.
High Recharge	72	Mean of estimates from within this zone.
Variable / Rocky Zones	72	Uncertain. Could be lower.
Seepage Zones	30	Uncertain. Could be lower.
Hard Sandstone Areas	0	Uncertain. Could be up to 50 mm/yr.
Remaining Area	0	Highly likely to be negligible due to presence of Keep Inlet Formation.





### 3.6. EVAPOTRANSPIRATION

Active seasonal groundwater discharge is observed at some springs at Bonaparte Plains and the vegetation types and density in the vicinity of springs suggest that it is supported by direct access to groundwater (Bennett and Raper, 2018). It is therefore thought that evapotranspiration is a major component of the groundwater balance for Bonaparte Plains, especially across the lower elevation areas immediately inland of the tidal mud flats.

Artesian groundwater heads are observed under the tidal mud flats and over large sections of the extensive vegetated flats to the west of the mudflats, suggesting a potential for evaporative discharge of groundwater from those areas. However, it is thought that the mudstone and fine textured layers of the upper Keep Inlet Formation may limit evapotranspiration losses from deeper in the aquifer. It has been suggested that evaporative discharge from the Point Spring Sandstone through the mud flats and Keep Inlet Formation is a trivial component of the water balance compared to that occurring up gradient (Bennett and Raper, 2018).

As described in Section 2, annual pan evaporation is 2,679 mm/yr and 2,712 mm/yr at Carlton Hill and Frank Wise Institute respectively. The average annual potential evapotranspiration (FAO Penman-Monteith) for Bonaparte Plains is calculated based on DPIRD Bonaparte Plains weather station data to be 1,775 mm/yr (Section 2). Extinction depths are likely to vary between less than a metre on the mudflats and several metres in the woodland areas where larger trees and shrubs with root systems that may extract groundwater from these depths exist.

## 4. Methodology

### 4.1. HYDROSTRATIGRAPHIC LAYER DEVELOPMENT

A series of spatial layers of AEM-derived elevations of tops of hydrostratigraphic units have been provided by Tan et al. (2018), along with representative hydrostratigraphic cross-sections constructed using the same AEM data. However, the stratigraphy and nomenclature for the aquifers used by Tan et al. (2018), based on Gorter et al. (2005) was subsequently found to be inconsistent with the results of recent drilling and palynological analysis (Bennett, 2019). Also, several discrepancies between the interpretation of the AEM data to construct the layers and cross-sections and existing borehole data were identified by DPIRD. Revised hydrostratigraphic layers were therefore constructed by DPIRD and IGS (Table 4) using the following methodology:

1. Identification of the most representative AEM sections for use in creating revised hydrostratigraphic layers (DPIRD).
2. Use of a GIS methodology (QGIS; [www.qgis.org](http://www.qgis.org)) to extract the AEM-derived layer elevation data along the selected cross sections and provision of these to DPIRD as Microsoft Excel cross section graphs (IGS).
3. Review of preliminary cross section graphs in the context of the original cross sections constructed from AEM data, as well as drillhole information and hydrogeological experience, with modifications made as required (DPIRD). During this process it was also decided to divide the Point Spring Sandstone hydrostratigraphic layer into an upper and lower unit, to expedite the assignment of

different aquifer properties to each unit, should this have been required during the modelling process. The division between the upper and lower units coincided with the bottom of the Bennett Shale layer (where it was present) and extended into adjacent areas using modified geometry based on layers proposed by Tan et al. (2018).

4. Construction of new hydrostratigraphic layers using *Surfer® 15* ([www.goldensoftware.com](http://www.goldensoftware.com)) and QGIS by interpolating layer elevation data between the revised cross sections, including the consideration of mapped fault locations provided by DPIRD (IGS).

The grids produced for each layer were then clipped to layer extent shapefiles that were developed based upon a combination of data coverage (cross sections) and layer extents provided by the AEM project (Tan et al., 2018). In some cases, the interpreted layer extents were further revised as part of the layer checking process when small areas of negative layer thickness were encountered at layer edges due to layers pinching out in areas between cross-section datasets.

5. Testing of the new hydrostratigraphic layers for negative layer thicknesses (i.e. no cross-over) via layer difference calculations in Surfer with amendments made accordingly (IGS).

An extensive and iterative layer checking and validation process was carried out by DPIRD and IGS during which interpolation anomalies around cross-section intersections and other features / layer thicknesses that were not consistent with DPIRD's conceptual understanding of the hydrostratigraphy were rectified.

Table 4. Relationship between hydrostratigraphic layers and model layers.

Geological Formation	Hydrostratigraphic layer	Abbreviation used in this report	Model layer occurrence
Keep Inlet Formation	Keep Inlet	Pk	1
Point Spring Sandstone	Point Spring Sandstone upper	Cup1	1, 2, 3
	Point Spring Sandstone Bennett Shale	Cup2	3
	Point Spring Sandstone lower	Cup3	4
Sunbird/Tanmurra Formations	Sunbird/Tanmurra	Cut	NA
Milligans/Yow Creek/Kingfisher assemblage	Milligans	Clm	NA
Ningbing Group	Ningbing	Dun	NA

## 4.2. MODELLING APPROACH

The overall modelling approach taken for the development of the two-dimensional and three-dimensional models for this project can be summarized as follows:

1. Two cross-section models were developed first in order to test the applicability of the model design / conceptual model, model sensitivity to different parameters and to provide guidance in selecting model parameters and boundary conditions for the three-dimensional model. The two cross-sections selected as priorities for modelling



of the seawater interface were Sections 103901 and NS01 (see Figure 2 for locations). Development of the cross-section models is outlined in Section 4.3. The two models were (a) loosely calibrated to point observation data (where available) or equipotential contours, (b) used to provide summary water balances for review by the project team, and then (c) converted into SEAWAT models for a preliminary analysis of the likely location of the seawater interface. This process identified appropriate values of hydraulic conductivity of the Bennett Shale and Keep Inlet Formation to simulate the observed patterns in hydraulic head. The need to implement zones of different recharge was also identified, leading to the development of the recharge zones described in Section 3.5.

2. The three-dimensional model was constructed using the hydrostratigraphic layers described in Section 4.1 and the boundary conditions and aquifer parameters selected through loose calibration of the two-dimensional models. The recharge zones and preliminary recharge rates, and the intermediate estimate of hydraulic conductivity of the Point Spring Sandstone ( $K_H = 6.9$  m/day), were considered to represent the best conceptual model for the aquifer system at commencement of the modelling exercise. These parameters were fixed, with other more uncertain parameters varied manually to obtain the best possible match to observed hydraulic head data (see Section 4.5.2 for details of calibration methodology). This version of the model is referred to as the '*Conceptual Model version*'.
3. The best possible fit to observed head data using the *Conceptual Model version* of the three-dimensional model resulted in a poor fit to observation well data (Scaled Root Mean Square Error = 14.6%), suggesting that modifications to the conceptual model (i.e. recharge rates and aquifer hydraulic conductivity) were required. Manual calibration was therefore carried out by varying recharge and hydraulic conductivity of the Point Spring Sandstone within their observed ranges (Section 4.5.2) to obtain a '*Calibrated version*' of the model.
4. The two cross-section models were updated with parameters from the *Calibrated version* of the three-dimensional model and used to run SEAWAT to identify the position of the seawater interface.
5. The process of calibration of the two-dimensional and three-dimensional models identified the parameters that the three dimensional water balance model is most sensitive to. A sensitivity analysis was carried out to quantify the influence of varying these parameters on key model outputs.

### 4.3. CROSS SECTION MODEL DESIGN

The two-dimensional cross-section models were constructed using the MODFLOW-2005 code for groundwater flow (Harbaugh, 2005) and the SEAWAT-2000 code (v4; Langevin et al., 2008) to simulate density-dependent solute transport. SEAWAT couples MODFLOW and the solute transport code MT3DMS (Zheng and Wang, 1999), iteratively calculating equivalent freshwater heads from solute concentrations provided by MT3DMS and using these in MODFLOW to simulate groundwater flow. Groundwater Vistas 7 (Environmental Simulations, Inc.; [www.groundwatermodels.com](http://www.groundwatermodels.com)) was used as the graphical user interface.

Top and bottom elevations of the four layers required to simulate the groundwater flow system for Cross Sections 103901 and NS01 were extracted from the Microsoft Excel cross-

sections constructed as described in Section 4.1 (Figure 7). The hydrostratigraphic layers were then converted to continuous model layers as shown in (b)

Figure 8. Model Layer 1 was set as unconfined, whilst Layers 2-4 were set as confined.

The model grids for Sections 103901 and NS01 originally comprised one row and (a) 210 columns (b) 98 columns respectively of cells that are 200 m x 200 m. However, the grid for Section 103901 was refined during the SEAWAT modelling in order to better resolve the position of the seawater interface, resulting in 312 columns (Figure 9).

Steady-state flow models were used to provide initial heads for the transient SEAWAT models (NB. SEAWAT simulations are run in transient mode, however all stresses are held constant). For the steady-state models, constant head boundaries representing the coast (located at eastern model domain boundary shown in Figure 2) were density-corrected, assuming that seawater is present at this boundary in all units. In Section 103901, a drain cell was implemented at the left hand (western) end of the model, with a drain elevation of 50 m, 5 m below ground surface, as described in Section 3.4.1.

Prior to converting them to layer structures appropriate for solute transport modelling, the steady-state flow models were used to test the influences of different aquifer properties and boundary conditions on the simulated model water balance and to obtain an approximate calibration to observed hydraulic heads as described in Section 4.2.

To convert the steady-state flow models to solute transport models, Layers 1, 2 and 4 were each divided into four layers of equal thickness and the new layers assigned the aquifer properties, layer types and boundary conditions of their parent layers. Layer three (Bennett Shale) remained as in the steady-state flow model. This resulted in a 13-layer model structure for solute transport (Figure 9).

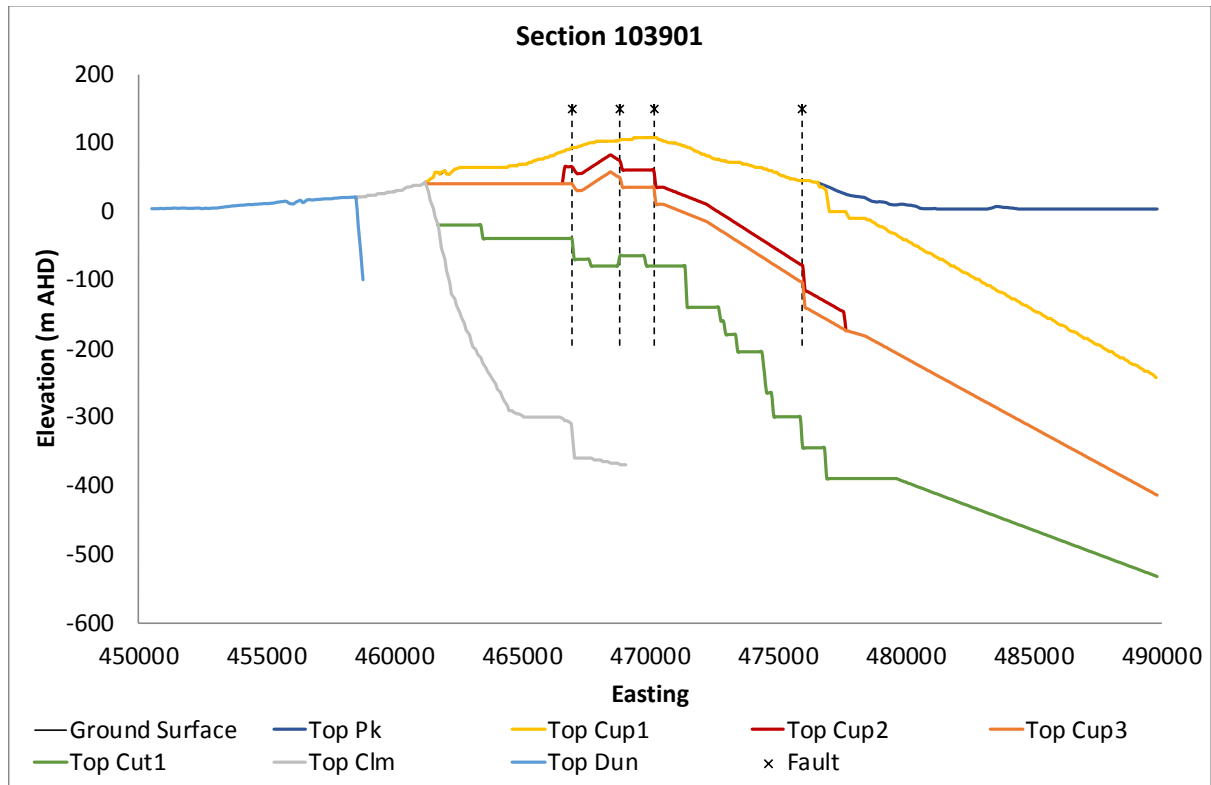
Figure 9 to Figure 11 show the final hydraulic conductivity, recharge and evapotranspiration values obtained from the calibrated three-dimensional flow model (Section 5.1.1) for use in the final versions of the cross section models. The 13-layer cross section flow models were run in steady state to provide initial heads for the transient SEAWAT models.

For the SEAWAT modelling, pure seawater was assumed to be present at the constant head boundaries in both models and a constant concentration boundary of  $35 \text{ kg/m}^3$  was implemented in all layers at this boundary. IGS has previously carried out a study to determine the effects of different constant head / constant concentration boundary designs on the simulated position of the seawater interface in a similar environment (IGS, 2018). The boundary conditions tested included (a) a vertical constant head / constant concentration boundary as employed in this project, (b) horizontal constant head / constant concentration boundaries extending both 10 km and 20 km offshore and (c) a horizontal constant head / constant concentration boundary extending 10 km offshore with an increased seafloor gradient. The study found that the boundary condition design has little influence over the simulated position of the toe of the seawater interface, with those boundaries set further offshore simply taking longer to reach steady state.

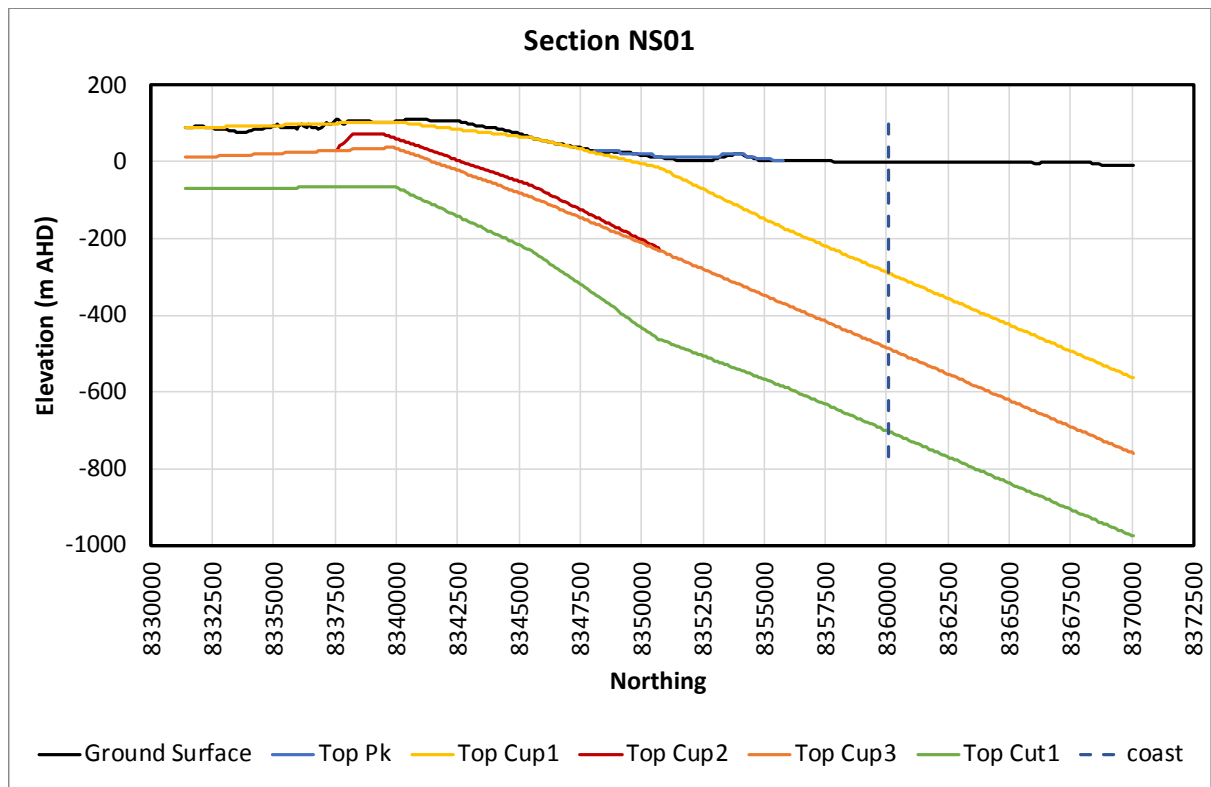
Initial concentrations were set at  $0.1 \text{ kg/m}^3$  throughout the model domain and a recharge concentration of  $0.01 \text{ kg/m}^3$  was applied across the recharge area. Specific storage and specific yield were set at  $1 \times 10^{-5}$  and 0.01 respectively, with a porosity of 0.2. NB. The storage parameters used were tested and found to have no influence over the simulated position of the seawater interface. Dispersion and diffusion were excluded from the

simulations, as density-driven flow is expected to dominate the effects of these solute transport processes in this system. To confirm this, a test was carried out with a dispersivity of 100 m, resulting in a seawater interface that is more diffuse over a distance of a few hundred metres, but at the same location.

SEAWAT was run in transient mode for a time period of 5,000 years. This period was divided into 1,000 flow time steps with a multiplier of 1. The PCG2 solver was used to solve the flow equations. The solute transport model (MT3DMS) was run with an initial transport step size of 0.5 days, a multiplier of 1.05 and a maximum time step size of 100 days. The GCG solver is used by MT3MS to solve the transport equations. Checks were made to ensure that the simulated position of the seawater interface had reached a steady state by the end of the simulations in both models, i.e. that there was no change in position of the interface between flow time steps.

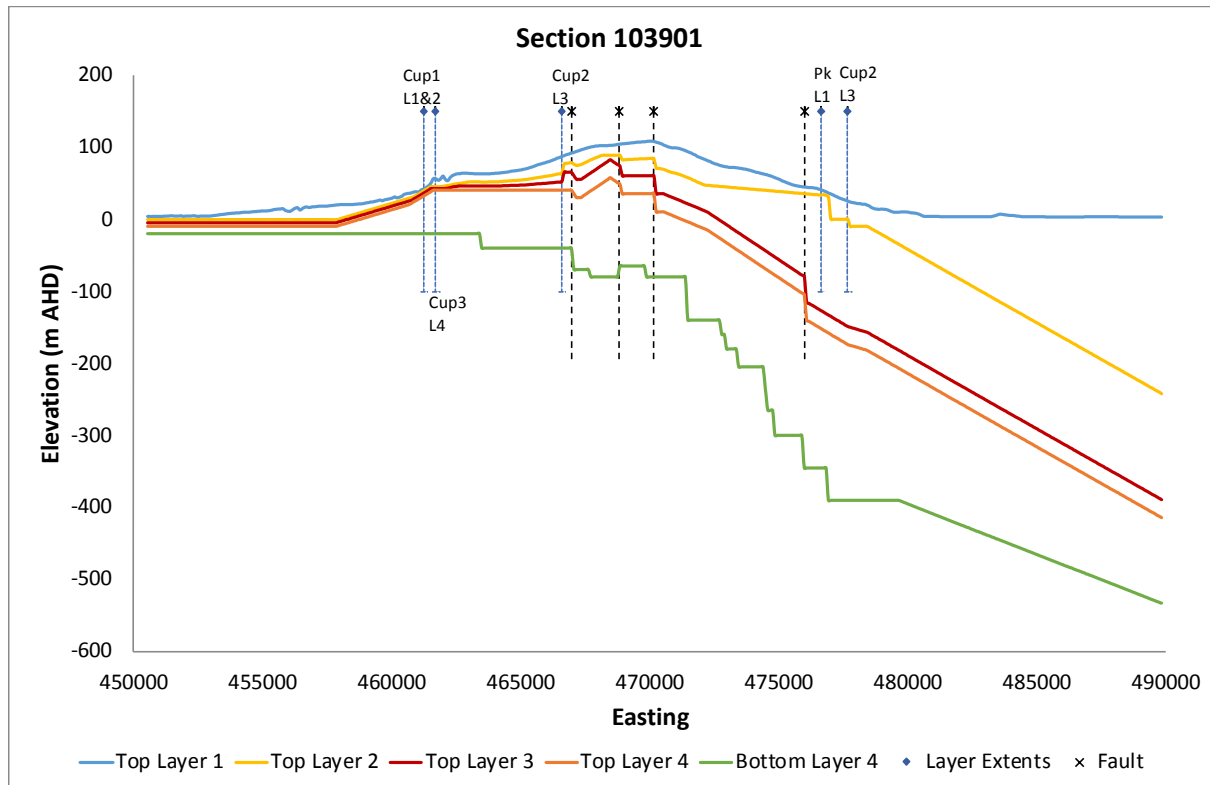


(a)

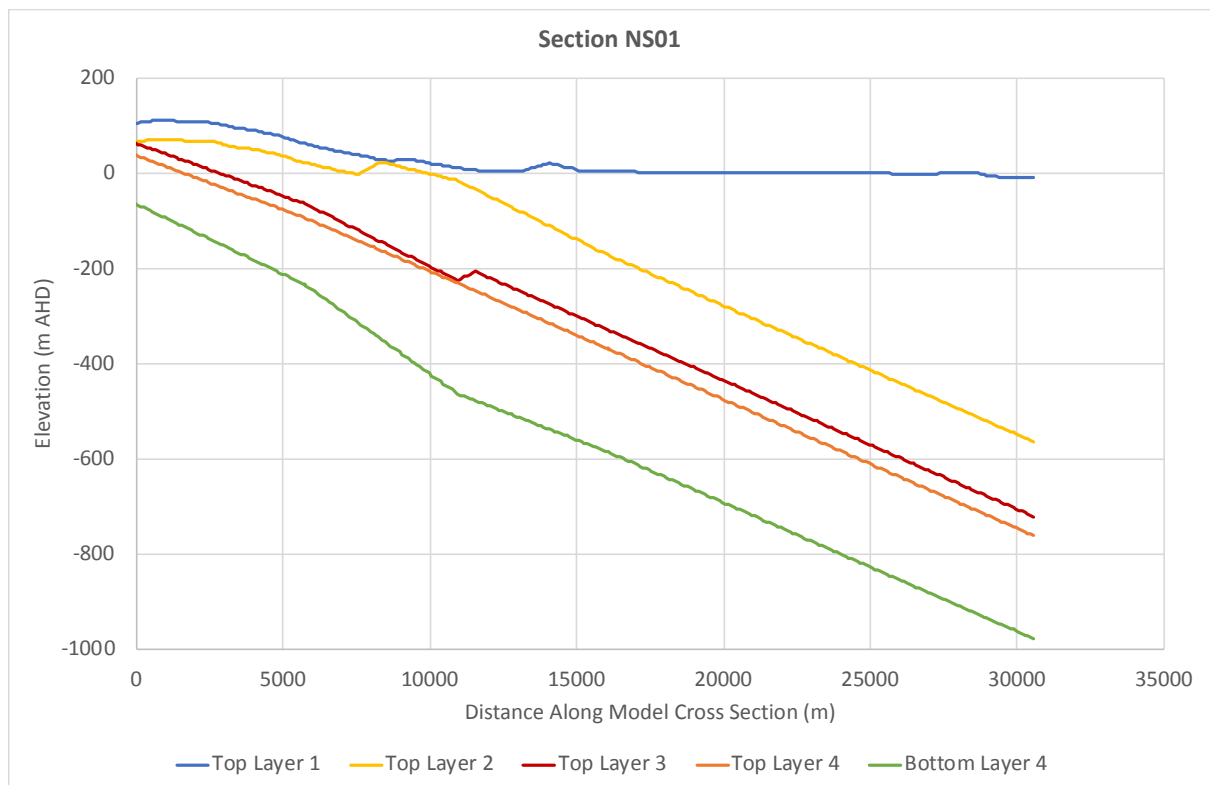


(b)

Figure 7. Hydrostratigraphic cross sections (a) 103901 and (b) NS01 plotted in Microsoft Excel format. Refer to Table 4 for names of hydrostratigraphic units.

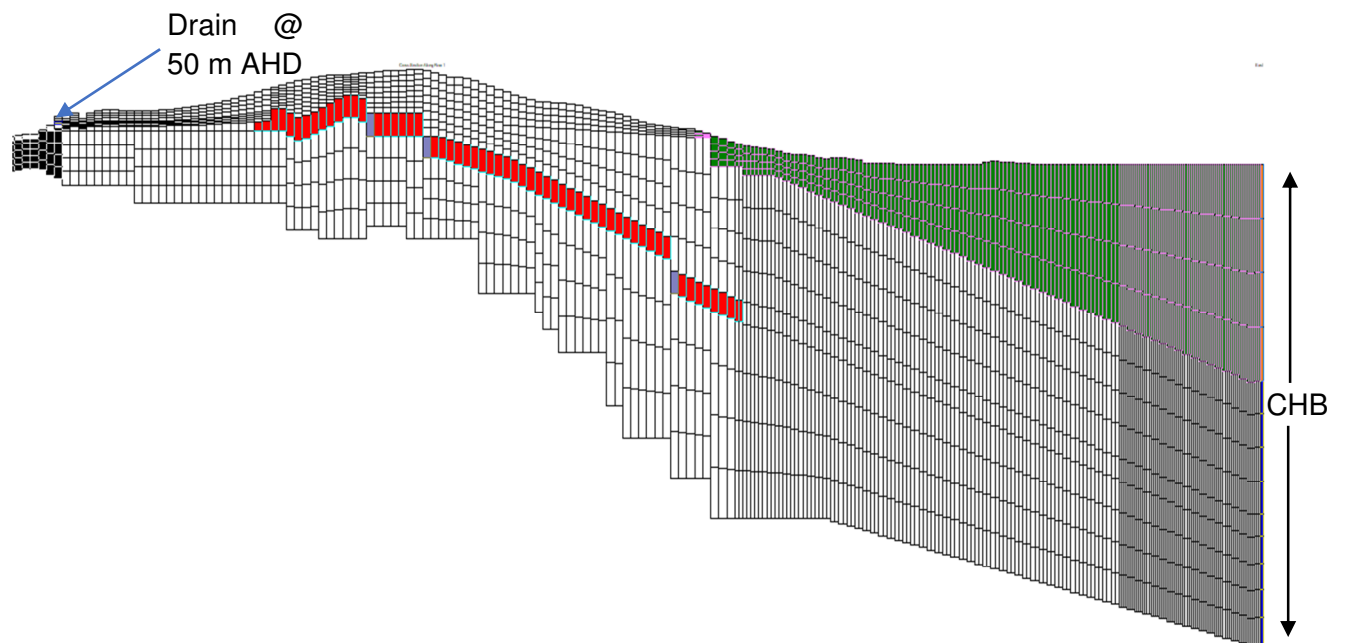


(a)

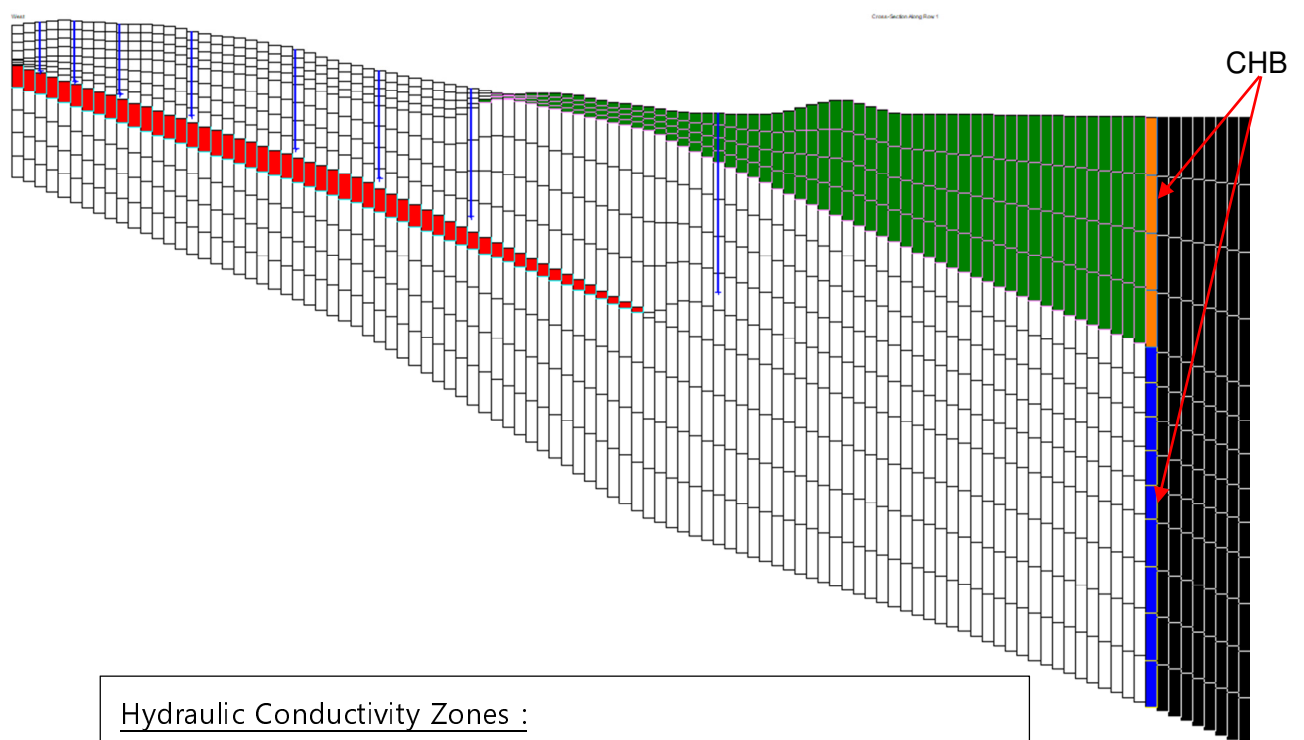


(b)

Figure 8. Cross sections (a) 103901 and (b) NS01 modified to provide continuous model layers. Vertical lines in upper figure indicate locations of inferred faults and extents of different hydrostratigraphic units, which would be defined in the groundwater flow model by zones of different hydraulic conductivity.



(a)



(b)

## Hydraulic Conductivity Zones :

White = Point Spring Sandstone (upper and lower);  $K_H = 6.0$  m/day,  $K_V = 0.6$  m/day.

Green = Keep Inlet Formation;  $K_H = 0.001$  m/day,  $K_V = 0.001$

Figure 9. Model grid and hydraulic conductivity zones for two-dimensional models of Sections (a) 103901, and (b) NS01 (see Figure 2 for cross section locations).



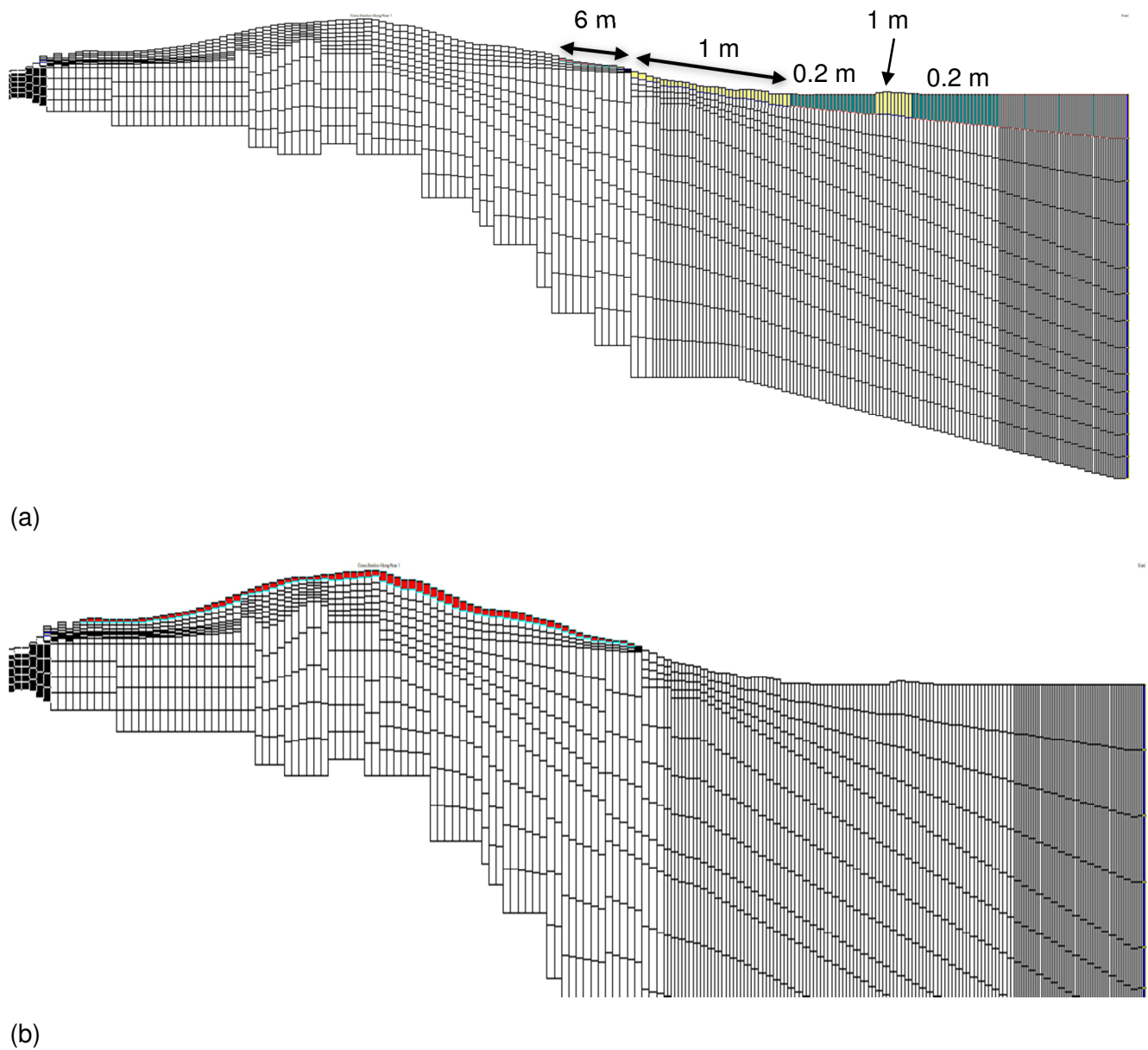


Figure 10. Model (a) evapotranspiration and (b) recharge zones for Cross Section 103901. Evapotranspiration rate = 1,775 mm/yr, with variable extinction depths as indicated in (a). Recharge rate (red zone) = 140 mm/yr.

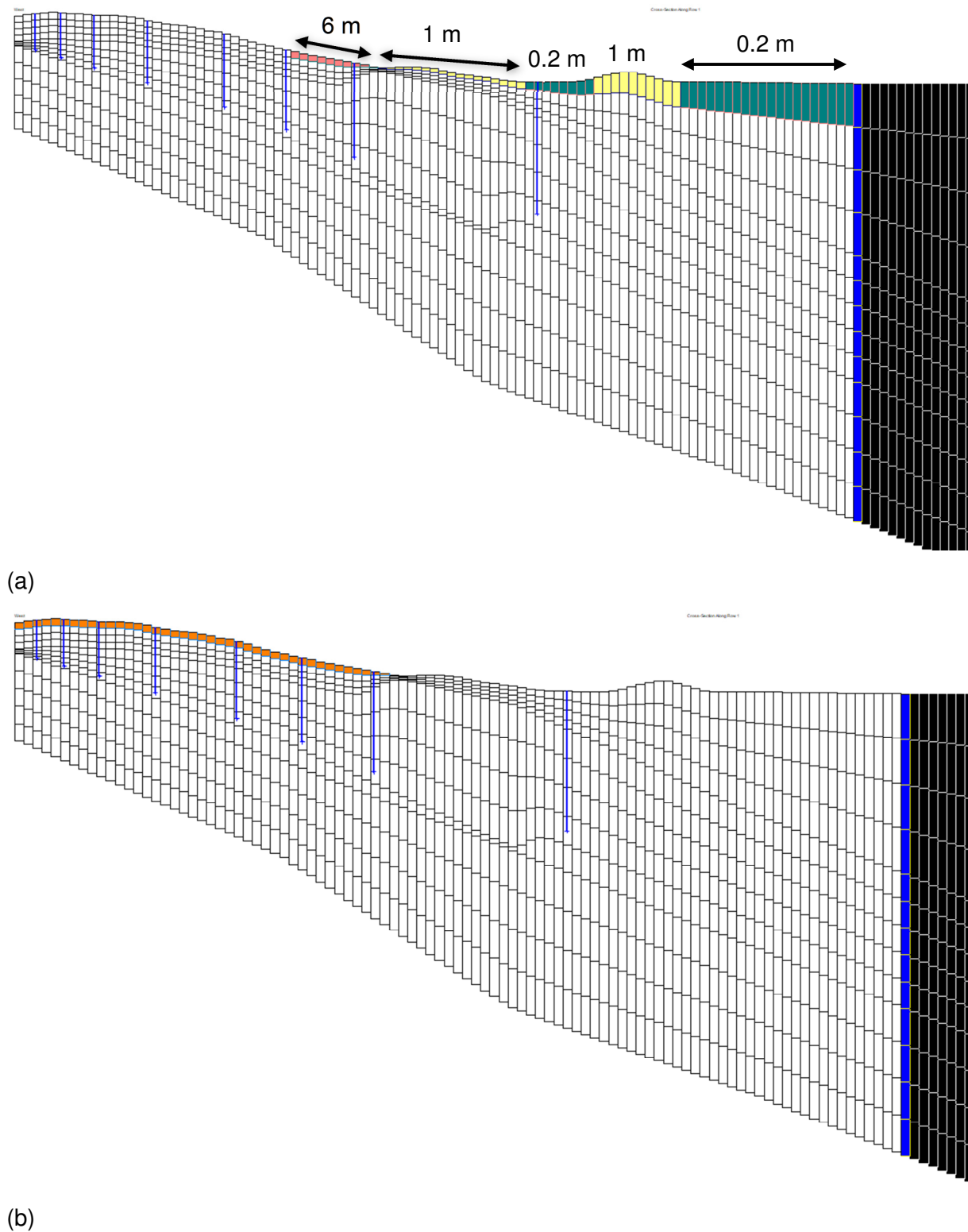


Figure 11. Model (a) evapotranspiration and (b) recharge zones for Cross Section NS01. Evapotranspiration rate = 1,775 mm/yr, with variable extinction depths as shown in (a). Recharge rate (red zone) = 140 mm/yr.

## **4.4. THREE-DIMENSIONAL MODEL DESIGN**

### **4.4.1. Modelling Platform and Domain**

The three-dimensional groundwater flow model was constructed using the MODFLOW-2005 code (Harbaugh, 2005) and the Groundwater Vistas 7 graphical user interface (Environmental Simulations, Inc.; [www.groundwatermodels.com](http://www.groundwatermodels.com)). The NWT solver (Niswonger et al., 2011) was used to facilitate convergence of the model, which contains numerous cells that iterate between wet and dry during the model run. The original model domain was defined as shown in Figure 2. The western boundary was refined within Groundwater Vistas for each model layer based on the interpreted extents of each aquifer unit. This slight modification resulted in a change of no more than three model cells (600 m) at any location from the original model domain shown in Figure 2.

### **4.4.2. Model Grid and Layer Definition**

The model grid comprises 200 m x 200 m cells with four layers based on the hydrostratigraphic layers constructed as described in Section 4.1. To develop continuous model layers, the cross section layers representing the Point Spring Sandstone, Keep Inlet Formation and Bennett Shale were made continuous. The layer top data from the cross sections was then re-interpolated using the previously defined methodology (Section 4.1) to form spatially continuous layer top datasets. The relationships between the model layers and the different hydrostratigraphic units are shown in Table 4.

The extents of the Keep Inlet Formation in Layer 1 and the Bennett Shale in Layer 3 are defined in the model using different aquifer property zones (Figure 12 and Figure 13). Figure 14 shows some examples of model cross-sections selected to compare with the original Microsoft Excel cross sections (Appendix A).

Layer 1 was simulated as unconfined, whilst Layers 2 to 4 were simulated as confined. The Keep Inlet Formation, Bennett Shale and other low-permeability shale and mudstone layers are expected to result in predominantly confined aquifer conditions for Layers 2 to 4.

### **4.4.3. Aquifer Properties**

The hydraulic conductivity (K) values initially applied to the hydraulic conductivity zones representing each hydrostratigraphic unit in the model are shown in Table 5. The horizontal hydraulic conductivity value applied to the Point Spring Sandstone aquifer was selected as described in Section 3.3. The hydraulic conductivity values assigned to the Bennett Shale and the Keep Inlet Formation were determined during the early phases of manual model calibration / testing of both the preliminary two-dimensional models and the three-dimensional model.

Table 5. Hydraulic conductivity values applied in the groundwater flow model.

Hydrostratigraphic Unit (s)	$K_H$ (m/day)	$K_v$ (m/day)
Point Spring Sandstone (upper and lower)	6.9	0.69
Bennett Shale	$1 \times 10^{-8}$	$1 \times 10^{-9}$
Keep Inlet Formation	0.001	0.001

#### 4.4.4. Simulating the Influence of Faults

The influences of faults are observed in the structure of the model layers, particularly as vertical offsets in the Bennett Shale (model Layer 3). Inferred fault locations were used in the interpolation of layer top data as described in Section 4.1. In some areas this offset is large, resulting in a discontinuous layer and in others it is less pronounced. It has been hypothesized that faults may act as conduits for groundwater flow through the Bennett Shale. However, as there is little hydraulic head data for the Point Spring Sandstone below the Bennett Shale, this is unconfirmed. It was found during model calibration that it was necessary to implement a higher hydraulic conductivity zone in the Bennett Shale (Layer 3) at the position of observation bores 13BP01S / 13BP01I / 13BP01D. Here, a head difference of only 0.6 m (upward gradient) is observed between the deep bore and the shallower ones. However, without a higher conductivity conduit through the Bennett Shale, the model simulates a head difference of several metres (downward hydraulic gradient). Observation bores 13BP01S/I/D are located at an intersection of faults and a location where there is a large vertical offset in the Bennett Shale. The hydraulic conductivity of the zone representing the Bennett Shale was set at the value of the Point Spring Sandstone along the fault lines at this location and at the few others where fault occurrence has resulted in large offsets in the elevation of the Bennett Shale layer (Figure 13). This significantly improved the model fit to head data in both the shallow and deep observation bores at 13BP01. A higher hydraulic conductivity zone was also implemented in the Keep Inlet Formation at a location where mapped faults coincide with a mapped area of permanent groundwater discharge. This was also found to improve model calibration in this area. It is possible that future additional evidence (i.e. head observations in the lower Point Spring Sandstone) may suggest that this approach should be used to represent faults at other locations.

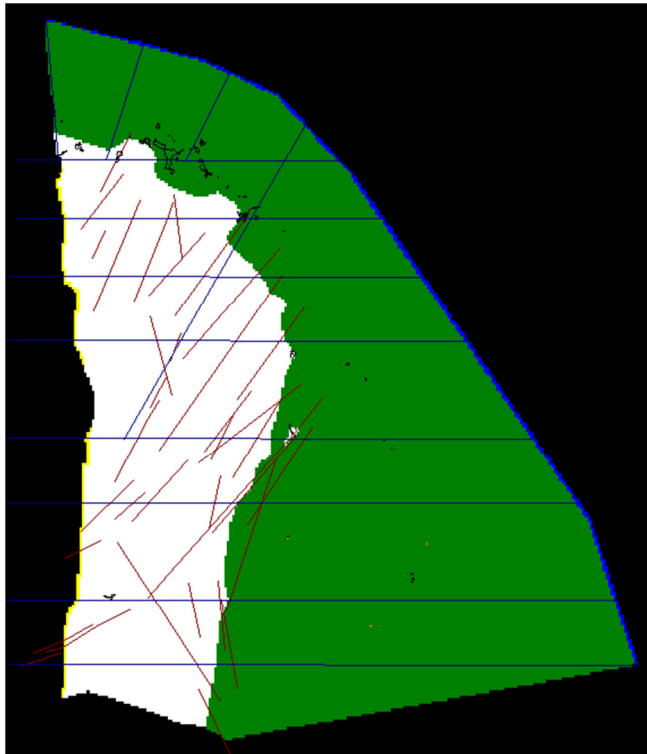


Figure 12. Model domain for the three-dimensional model, showing the area designated as Keep Inlet Formation in Layer 1 (green area). Also shown are: coastal constant head boundary (blue cells), drain cells (yellow), mapped fault locations (red lines), mapped permanent groundwater discharge features (black lines) and locations of hydrostratigraphic cross sections used to create model layers (blue lines). Black cells represent the inactive portion of the model domain.

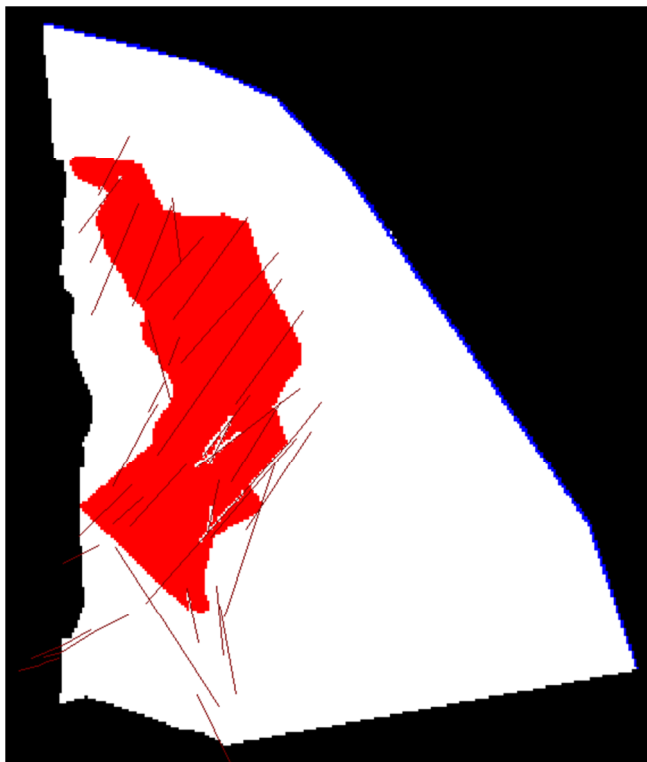
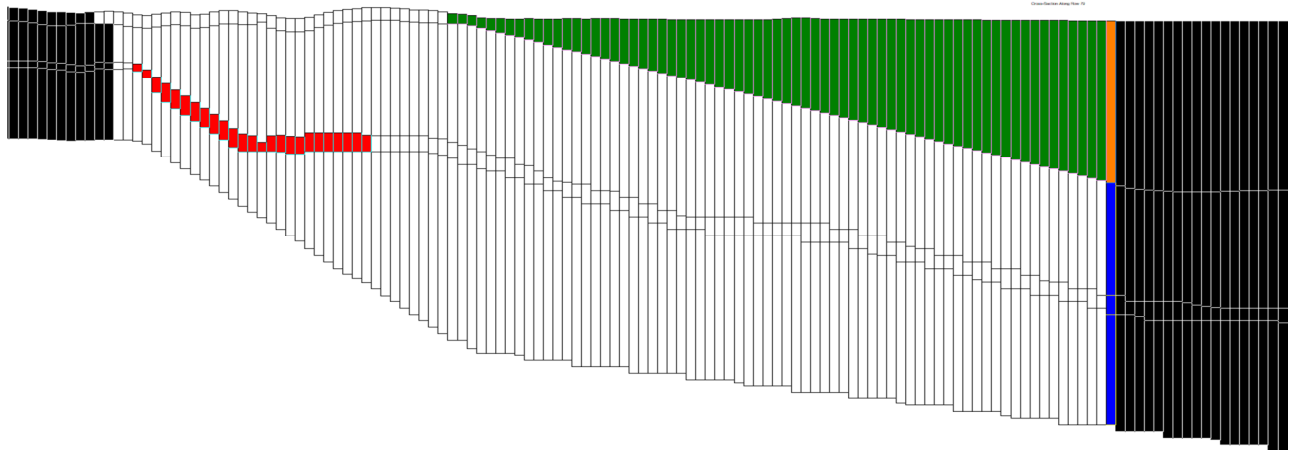
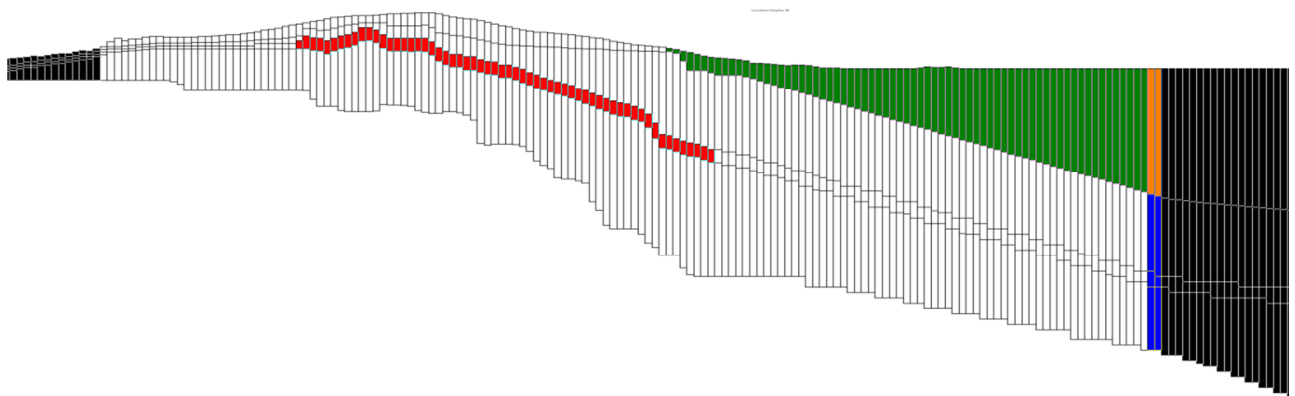


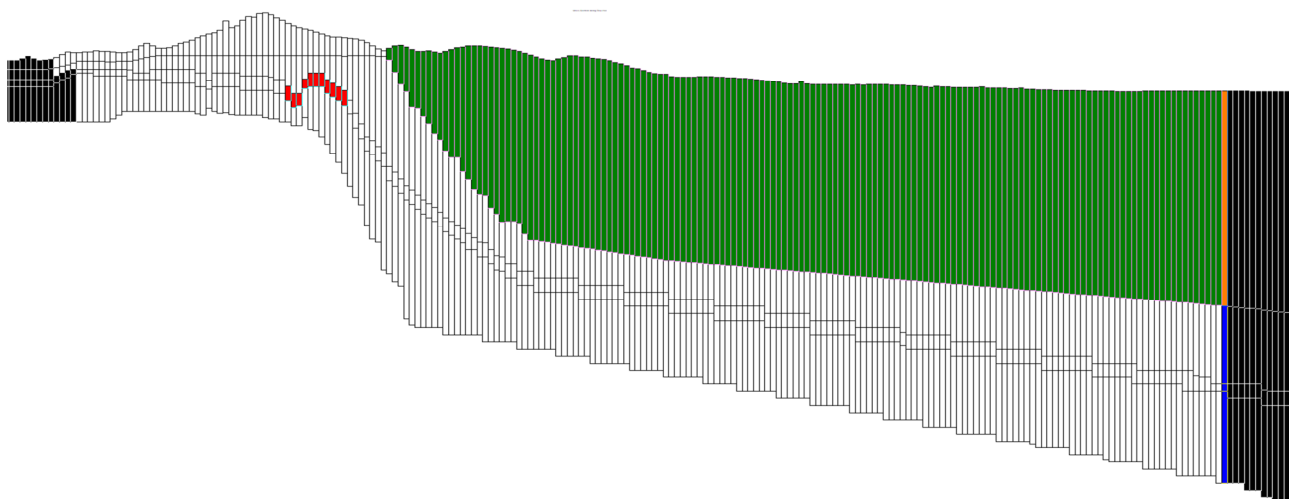
Figure 13. Model grid for the three-dimensional model, showing the area designated as Bennett Shale in Layer 3 (red area) and the coastal constant head boundary (blue cells). Locations of inferred faults are indicated by straight lines.



(a)



(b)



(c)

Figure 14. Model cross sections at locations of (a) Section 101102, (b) Section 103901 and (c) Section 107901. White = Point Spring Sandstone, Red = Bennett Shale, Green = Keep Inlet Formation. Black cells = no flow, Blue/orange cells = constant head boundary.



#### 4.4.5. Boundary Conditions

A drain boundary was applied along the western edge of the model domain (excluding the mudflats at northern end) (see Figure 12 and Figure 15). The drain elevation was set at 5 m below ground elevation. The SURFER grid file of the digital elevation model (DEM) for the study area, provided by DPIRD, was used as the basis for this. Contours of  $DEM - 5\text{ m}$  were created in SURFER and used in Groundwater Vistas as the guide for adding drain reaches, with the stages of the reaches set as linear gradients between the contours. The drain conductance value of  $6\text{ m}^2/\text{day}$  was selected during the model calibration process (Section 5.1.1).

The southern boundary of the model domain was designated a no-flow boundary (Section 3.4.3).

The northern and eastern boundaries of the model domain were set as a constant head boundary (CHB) representing the coast. This boundary is located on the mudflats at the approximate 0 m AHD groundwater equipotential (Figure 2). The CHB was density-corrected in all layers, under the assumption that seawater is present at the boundary in all layers and to represent groundwater interactions with seawater at the coast. To set the constant head elevations, the boundary length was divided into five zones (Figure 15). The density-corrected head applied to cells along each linear zone in each layer was calculated based on the (approximate) average depth of the cell mid-points below sea level in that zone. This resulted in five constant head zones for each layer. The ranges of density-corrected constant heads for each layer were as follows:

Layer 1: 2.25 m to 3.4 m

Layer 2: 7.8 m to 9.5 m

Layer 3: 9.8 m to 14.6 m

Layer 4: 12.0 m to 17.3 m

Results of the final SEAWAT cross section models suggest that seawater may be located seaward of the model boundary in Layer 1 (Keep Inlet Formation; see Section 5.2). As a result, a test of the sensitivity of model outputs to the application of a density-corrected boundary in Layer 1 was included as part of the Sensitivity Analysis presented in Section 6. The analysis showed that the application of a density correction in Layer 1 has no influence over the simulated heads or water balance.

#### 4.4.6. Recharge

Rainfall recharge in the study area is likely to be highly variable both spatially and temporally due to:

- Large inter-annual variability in rainfall.
- Variable paths and intensities of the tropical storms that contribute the majority of the rainfall recharge.

Recharge rate estimates based on chloride mass balance and environmental tracer approaches are therefore considered to provide a guide to the potential range in recharge rates, rather than precise estimates or averages.

For the preliminary three-dimensional model, recharge zones and rates were applied as outlined in the conceptual model described in Section 3.5 (Figure 15, Table 6), except for the areas of ‘Seepage’ and ‘Hard Sandstone’, which were assigned recharge rates of 0 mm/yr. Assigning recharge to these zones did not benefit model calibration and it is likely that recharge in these areas is negligible. An evapotranspiration rate of 1,775 mm/yr was applied to the seepage zones (Section 4.4.7), meaning that such a small recharge rate is negligible compared with the influence of evapotranspiration.

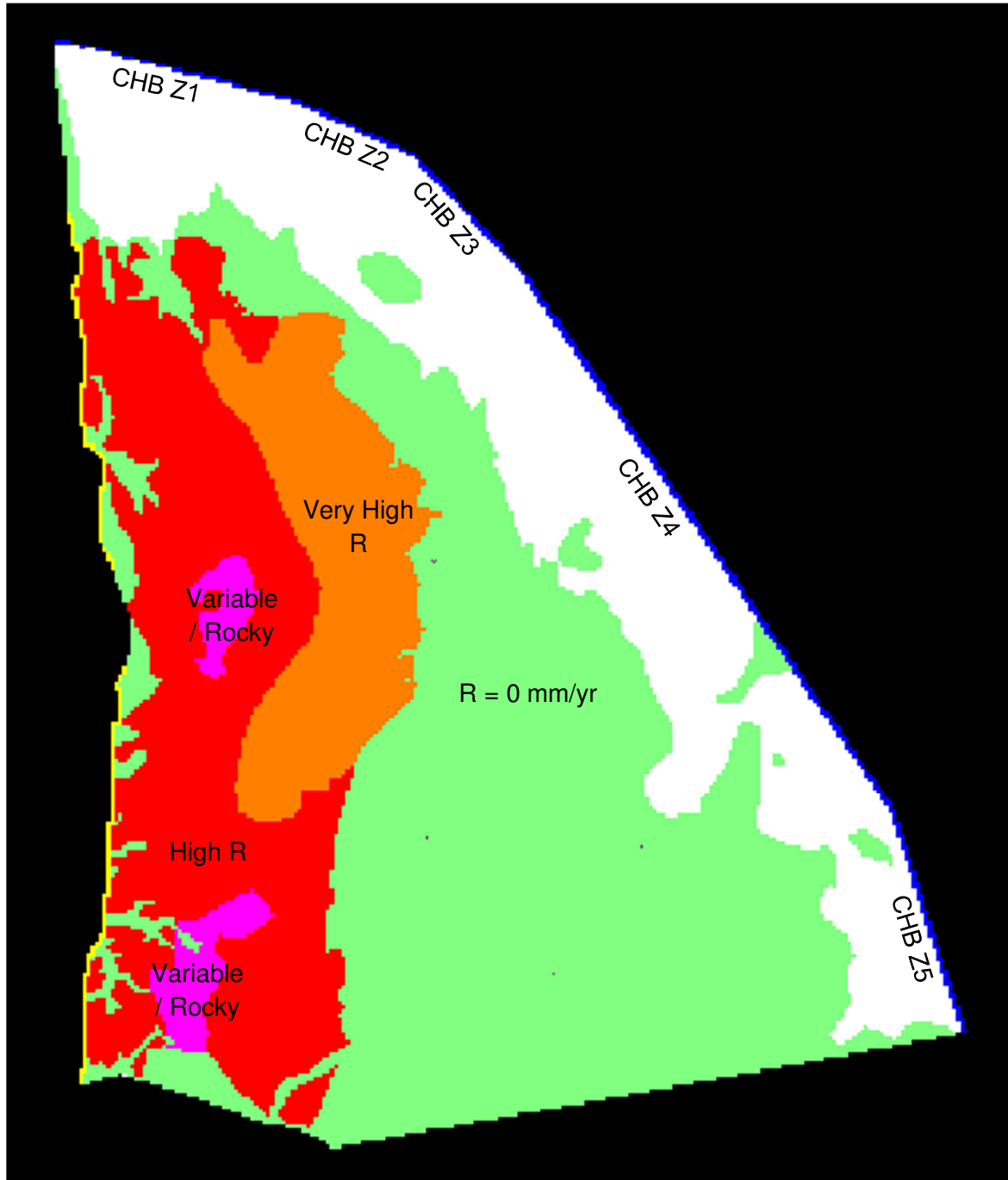


Figure 15. Recharge zones used in the three-dimensional groundwater flow model. See Table 6 for recharge rates. Blue cells are constant head cells used to represent the coastal boundary, with constant head zones used for density correction indicated. Yellow cells at left hand edge of the model domain indicate the location of the drain boundary in Layer 1. Where these are absent, the drain boundary is located in Layer 2.

Table 6. Recharge rates used in the initial *Conceptual Model version* of the groundwater flow model.

Zone No.	Colour in Figure 14	Description	Conceptual Model Recharge Rate (mm/yr)
1	Orange	Very High Recharge	134
2	White	Mudflat	0
3	Red	High Recharge	72
4	Green	Other	0
5	Pink	Variable / Rocky areas	72

#### 4.4.7. Evapotranspiration

The spatial distributions of the evapotranspiration zones used in the three-dimensional model are shown in Figure 16. Separate zones were assigned to (1) the mudflats (white), (2) non-mudflat areas underlain by Keep Inlet Formation (blue), (3) lower-lying areas just inland of the Keep Inlet Formation boundary (pale pink), (4) permanent groundwater discharge zones (blue and hot pink) seasonal seepage zones (green and purple) A large number of evapotranspiration zones was used initially to allow evapotranspiration rates and extinction depths to be varied as required for model calibration. For example, it was considered that lower rates may be appropriate for seasonal discharge zones and areas up-gradient of the western extent of the Keep Inlet Formation. However, early in the model testing and calibration process, it was determined that the maximum evapotranspiration rate was required for all zones, with variable extinction depths applied as shown in Table 7. The evapotranspiration rate was set at 1,775 mm/yr, which is based on the 3 years of climate data from the Bonaparte climate station, is considered to be the average potential evapotranspiration rate for the study area (Section 3.6).

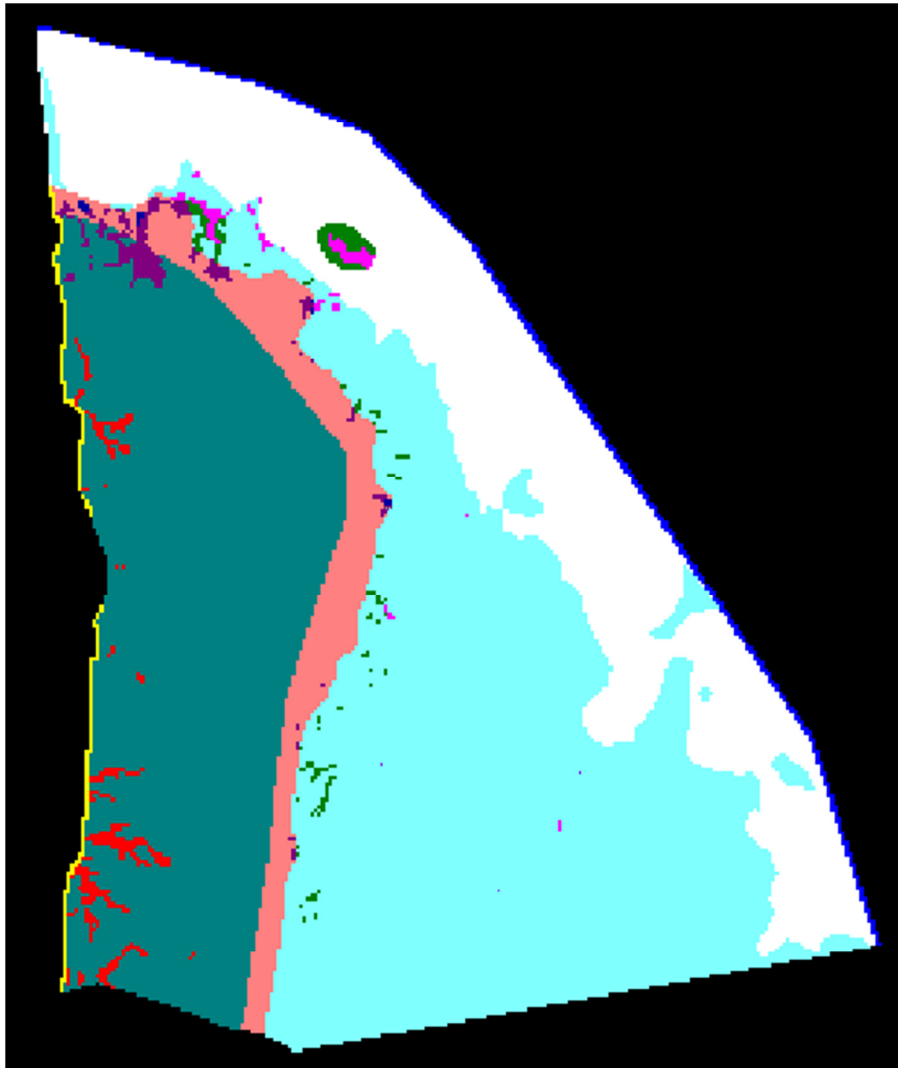


Figure 16. Evapotranspiration zones used in the three-dimensional groundwater flow model. Refer to Table 5 for zone descriptions. Yellow cells at left hand side of the model domain indicate the drain boundary in Layer 1. Where absent, the drain boundary is located in Layer 2. Dark blue cells represent constant head cells used to represent the coastal boundary.

Table 7. Evapotranspiration rates and extinction depths used in the groundwater flow model.

Zone Number	Colour	Description	Evapotranspiration Rate (mm/yr)	Extinction Depth (m)
1	White	Mudflats	1,775	0.2
2	Pale blue	Keep Inlet Non-mudflat	1,775	1
3	Pale Pink	Non-Keep Inlet low-lying	1,775	6
4	Hot Pink	Keep Inlet Permanent GW discharge	1,775	1
5	Blue	Non-Keep Inlet Permanent GW Discharge	1,775	2
6	Green	Keep Inlet Seasonal Seepage	1,775	1
7	Purple	Non Keep Inlet Seasonal Seepage	1,775	2
8	Teal	Zero ET (deep water tables)	0	0
9	Red	Inland Seasonal Seepage	1,775	1

## 4.5. CALIBRATION

### 4.5.1. Calibration Targets

The focus of model calibration of both the three-dimensional model and the cross-section models was (a) obtaining a good match between simulated and observed heads, and hence a good representation of the observed groundwater flow pattern, and (b) ensuring that the model mass balances were sensible and consistent with observations and the conceptual model.

The head calibration dataset is provided in Appendix B. As described in Section 3.2, the hydraulic head observation record mainly consists of approximately one to two years of monitoring data (Figure 4 and Figure 5). Despite the short record, much of this data is from loggers, providing a good indication of seasonal variability. Heads have risen slightly in many of the observation bores over the monitoring period, with several bores showing obvious responses to the comparatively wet 2016/17 wet season. Selection of head values from observation bore records for use as steady state calibration targets was based upon an assessment of the trends observed. Where a rising trend has been observed, the latest head value was selected, considering that the groundwater system may be approaching a new steady state in response to higher average rainfall over the past 25 years. The table of

calibration data provided in Appendix B includes comments about the temporal trends in observed heads that were taken into consideration during selection of values to best represent steady state. In recognition of the uncertainty in selecting steady state head values, a residual value (observed head – simulated head) between – 1 m and + 1 m was considered to indicate a good match during model calibration. Less importance was placed on calibration residuals relating to head estimates at artesian springs and for pressure observations made of artesian New Attack and Kemp bores. These bores have been discharging for many years (stock water supply) and the aquifer is likely to have localized reduced heads. The pressure observations that were made were done over a period of about 2 hours which is unlikely to have been long enough for the aquifer to equilibrate to the no flow conditions.

#### 4.5.2. Calibration Methodology

As described in Section 4.2, model calibration involved an iterative process, using both the two-dimensional cross-section models and different versions of the three-dimensional model. Due to large areas of uncertainty in the conceptual model, a step-wise approach was taken, which recognized the model parameters that could be relatively well-constrained by data and those that could not. Initially, the best-constrained parameters were held constant at their ‘conceptual model’ values, i.e. recharge as shown in Table 4 and the best estimate of  $K_H$  for the Point Spring Sandstone aquifer ( $K_H = 6.9$  m/day). Other more uncertain parameters were then varied systematically to build up knowledge of model sensitivity to these parameters and their influence on model calibration. These parameters were:

- $K_V$  of the Point Spring Sandstone aquifer,
- $K_H$  and  $K_V$  of the Bennett Shale (where  $K_V$  was set at  $0.1 \times K_H$ ),
- $K_H$  and  $K_V$  of the Keep Inlet Formation ( $K_H$  and  $K_V$  were varied independently),
- evapotranspiration rates and extinction depths for the evapotranspiration zones shown in Figure 16, and
- conductance of the drain boundary implemented along the western edge of the model domain.

These model parameters were refined through a process of trial and error, whilst considering the processes simulated by the model and the influence of each parameter on simulated groundwater heads and fluxes. This manual calibration approach was used in preference to an automated approach (e.g. PEST; Doherty and Hunt (2010)) due to (a) the varying degrees of uncertainty in different areas of the conceptual model, (b) the large number of parameters available to be modified and (c) the observed sensitivity of the simulated heads and water balance to some model parameters.

Elevations of the drain boundary and coastal constant head boundary were not varied during model calibration. These boundary elevations were based upon the conceptual understanding of the system and there was no basis for varying them.

This initial model calibration process resulted in the best calibrated model using the recharge rates shown in Table 6 and a  $K_H$  of the Point Spring Sandstone aquifer of 6.9 m/day. This model is referred to as the ‘*Conceptual Model version*’. In general, simulated heads for this model were well below observed heads (see Section 5.1.1), indicating a need to increase recharge rates and/or decrease the hydraulic conductivity of the Point Spring Sandstone aquifer.



The second stage of calibration of the three-dimensional model involved maintaining all of the more uncertain parameters at the optimum values obtained by calibrating the *Conceptual Model* version and varying recharge and  $K_H$  of the Point Spring Sandstone aquifer within their observed ranges. This resulted in a '*Calibrated version*' of the model.

Results of both the *Conceptual Model* and *Calibrated* versions of the three-dimensional model are presented in Section 5.1

## 5. Results

As described in Section 4.2, the modelling approach for this project involved development of preliminary two-dimensional models, followed by development and calibration of the three-dimensional model. The parameters from the calibrated three-dimensional model were then used to finalize the two-dimensional models. Based on this process, the results of the three-dimensional model are presented first, followed by the results of the final two-dimensional models.

### 5.1. THREE-DIMENSIONAL STEADY-STATE GROUNDWATER FLOW MODEL

#### 5.1.1. Conceptual Model Version

Figure 17 shows the calibration residuals and simulated Layer 2 equipotentials (upper Point Spring Sandstone) for the *Conceptual Model* version of the three-dimensional groundwater flow model (see Section 4.5.2). For this model version, the model boundaries, aquifer properties, recharge zones and rates and evapotranspiration zones and rates are as described in Section 4.4. Figure 17 shows that this version of the model generally underestimates heads across the study area, which is reflected in the calibration statistics for the model scenario (Table 8).

The model mass balance indicates inflows comprising recharge of 125 ML/day, and a net inflow of 6 ML/day across the coastal boundary; all of this water is discharged via evapotranspiration (Table 9). The lack of simulated flow to the natural drainage line along the western model boundary is not consistent with field observations.

#### 5.1.1. Model Calibration

Manual calibration of the three-dimensional model (see Section 4.5) resulted in a reduction in the hydraulic conductivity of the Point Spring Sandstone aquifer from  $K_H = 6.9$  m/day and  $K_V = 0.69$  m/day to  $K_H = 6$  m/day and  $K_V = 0.6$  m/day. Recharge was increased in the High and Very High recharge zones to 140 mm/yr as shown in Table 10. On reviewing preliminary model outputs from this simulation, DPIRD also recommended that the recharge rate associated with the southern Variable / Rocky recharge zone (see Figure 15 for location) be increased to that of the High Recharge zone. This was due to the fact that the soils in this area are more sandy than the other Variable / Rocky zone and this change improved the match between simulated and observed heads in this area of the model by up to 0.5 m. Figure 18 shows that a good match between simulated and observed heads is achieved by the *Calibrated version* of the model and this is reflected in improved calibration statistics for the simulation (Table 8). Figure 19 shows the locations where the simulated groundwater level is above ground surface and these areas correspond to the mapped locations of seasonal or permanent seepage zones. The calibration residuals for each observation point for both the *Conceptual Model* and *Calibrated* versions of the model are provided in Appendix C.

Figure 18 shows that the best matches between simulated and observed heads are in the central southern area of the model domain and in the north of the main recharge area. A residual value of -3.9 m (overestimate) near the northern mudflat boundary relates to a head estimate at a spring, which should be considered to be of low reliability. Likewise, the values

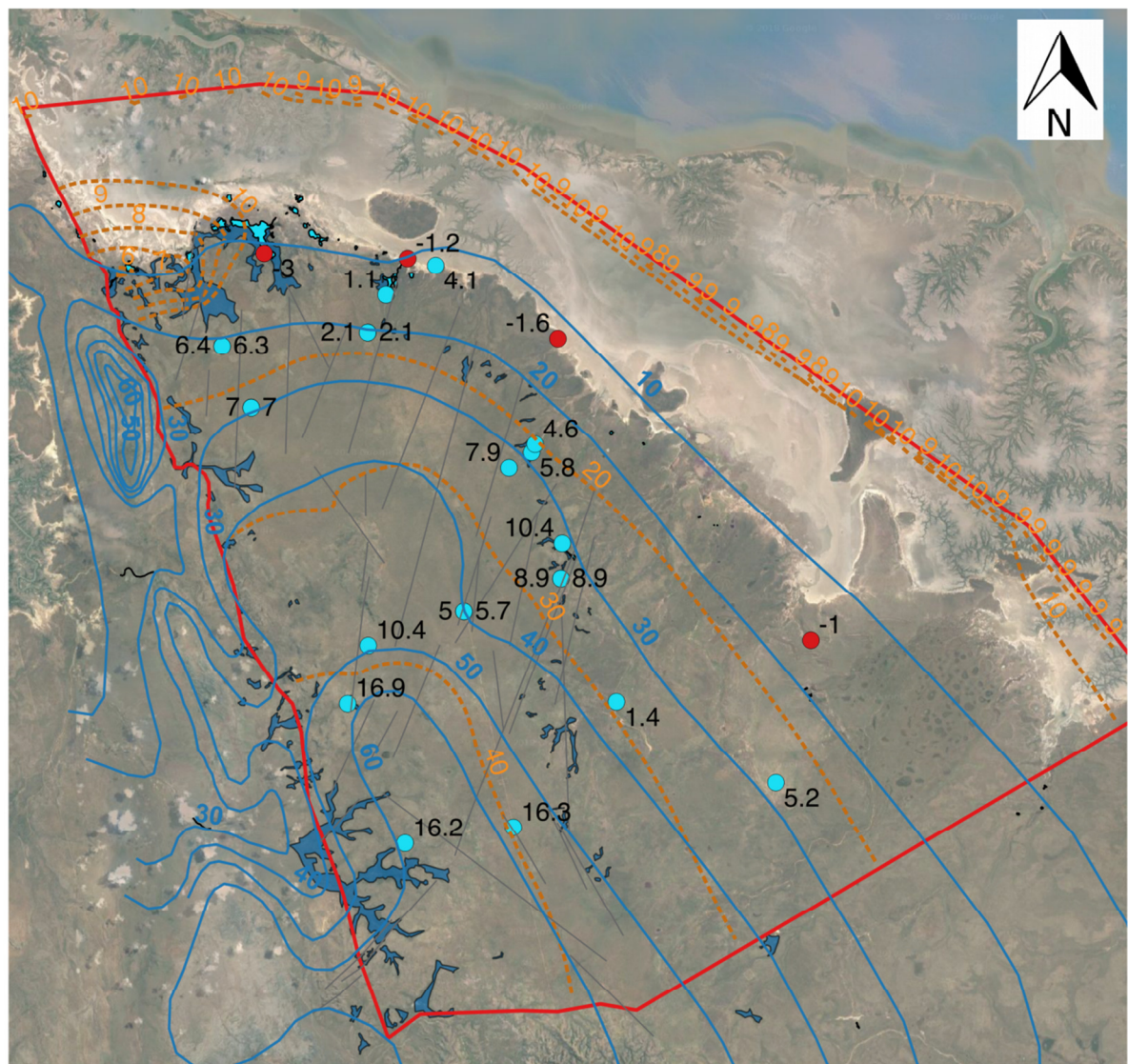
of -2.3 m and -3 m in the north-east of the model domain relate to head measurements made on artesian bores that have been flowing for long time periods. The residual of +2.9 m located between these bores relates to Fisherman's bore, which has been permanently sealed for many years and is therefore considered to be of greater reliability.

Figure 18 suggests that the model underestimates heads in the central-eastern and south-western portions of the model domain, whilst overestimating heads at two bores near the middle of the model domain. Applying a slight increase to the recharge rate across the High and Very High recharge zones would improve the model-observed match in the areas where heads are currently underestimated. However, this would also further increase heads through the centre of the model domain, where heads are currently overestimated. The reason for this pattern of mismatch is currently unknown, but could include:

- A zone of lower recharge in the central portion of the model domain that is not captured in the current conceptual model.
- A higher hydraulic conductivity through the central zone or preferential flow along faults.

The recharge scenario applied in the current *Calibrated version* of the model provides the best balance between overestimating heads in the central zone and underestimating heads in the north-east and south-west and is consistent with the current conceptual model.

The water balance of the *Calibrated version* of the model indicates that evapotranspiration accounts for 93% of groundwater outflows, whilst 6 % discharges to the marine environment via the constant head boundary and 1% discharges to the drain applied along the western boundary of the model domain (Table 9). The groundwater discharge of 3 ML/day simulated to the western drain boundary (equivalent to approximately 7 kL per 100 m length of drain) is more consistent with field observations of groundwater occurrence than the Conceptual Model version, which indicated no discharge to the drain. Note that evapotranspiration is only applied to mapped areas of permanent or seasonal groundwater seepage in this area of the model. The drain is the only other discharge mechanism modelled for the western boundary. Therefore, groundwater that flows into the drain boundary may account for groundwater that (a) enters the creeks, (b) is intercepted by evapotranspiration from shallow water tables or (c) flows as groundwater west through the Milligans/Yow Creek/ Kingfisher shale subcrop assemblage to the west of the drain location. However, westward flow through the shales is considered to be trivial given the lithology of this unit, and the occurrence of an opposing (eastward) groundwater gradient from the Ningbing Range (Ningbing Group) along much of this axis.



### Legend

— Equipotential - Observed (m AHD)

--- Equipotential - Modelled (m AHD)

Calibration Residuals (m)

● Too High

● Good

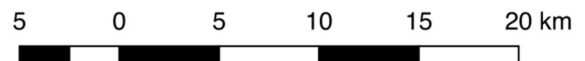
● Too Low

— Interpreted Fault

□ Model Domain

■ Permanent GW Discharge Zone

■ Seasonal Seepage Zone



Map prepared by N. Harrington  
Innovative Groundwater Solutions Pty Ltd.  
February 2018  
Co-ordinate Reference System: GDA94 Zone 52

**Figure 17. Simulated equipotentials (Layer 2) and calibration residuals for Conceptual Model version of the three-dimensional groundwater flow model.**

Table 8. Summary of calibration statistics for the *Conceptual Model* and *Calibrated* versions of the three-dimensional model. n=27.

	Conceptual Model	Calibrated Model
Residual Mean (m)	5.85	-0.32
Residual Standard Deviation (m)	5.14	2.87
Absolute Residual Mean (m)	6.36	2.38
RMS Error (m)	7.79	2.89
Minimum Residual (m)	-3.04	-5.9
Maximum Residual (m)	16.93	4.65
Range of Observations (m)	53.5	53.5
Scaled Residual Standard Deviation (%)	9.6	5.4
Scaled Absolute Mean (%)	11.9	4.5
Scaled RMS (%)	14.6	5.4
Mass Balance Error (%)	0.045	0.029

Table 9. Summary of the model mass balances for the *Conceptual Model* and *Calibrated* versions of the three-dimensional model.

	Conceptual Model	Calibrated Model
<b>Inflows (ML/day)</b>		
Recharge	125	190
Coastal Boundary	474	402
<b>Outflows (ML/day)</b>		
Evapotranspiration	130 (100%)	176 (93%)
Drains	0	3 (1%)
Coastal Boundary	468	414
(Coastal Boundary Net Outflow)	-6 (0%)	12 (6%)



Table 10. Recharge rates applied in the calibrated three-dimensional groundwater flow model (see Figure 15).

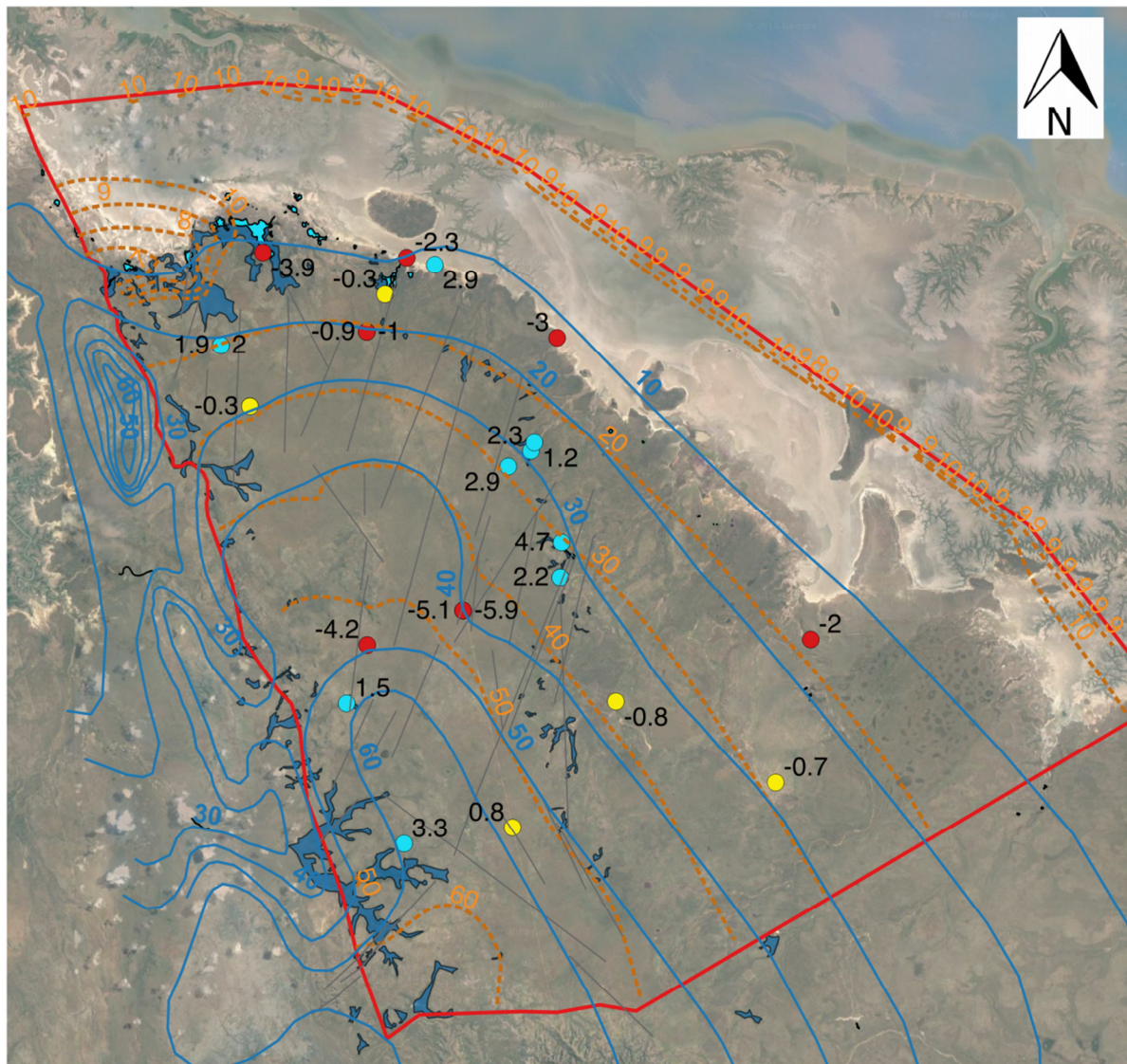
Zone No.	Colour	Zone Description	Calibrated Model Recharge Rate (mm/yr)
1	Orange	Very High Recharge	140
2	White	Mudflat	0
3	Red	High Recharge	140
4	Green	Other	0
5	Pink	Variable/Rocky areas*	72

\*Note: southern Variable/Rocky area (see Figure 15) increased to High recharge rate following review of recharge zone by DPIRD.

Both Figure 17 and Figure 18 show an area in the north of the model domain where simulated groundwater flow in model Layer 2 (upper Point Spring Sandstone) appears to converge near the intersection between the inland mudflat boundary and the western model boundary. This is observed as an apparent depression in the simulated equipotential contours for Layer 2. A review of the simulated water balance and groundwater flow vectors in cross section for this area indicates that it corresponds to a localized area of net groundwater inflow across the coastal boundary. Here, the Point Spring Sandstone aquifer extends to the greatest depths (approximately 800 m) at the coastal boundary compared with other areas of the model domain. Hence, the equivalent freshwater head applied at the coastal Constant Head Boundary (CHB) in Layer 4 is 17.31 m AHD to account for the weight of seawater above it. In Layer 2, the CHB is set at 9.46 m. This area is located in CHB zone 1 as shown in Figure 15). As a comparison, in CHB zone 3 (see Figure 15), the Layer 4 CHB is set at 14.1 m AHD and the Layer 2 CHB is set at 8.6 m AHD. The larger heads applied in CHB zone 1, to account for the large mass of seawater in the aquifer, result in groundwater discharge being focused further inland, at the inland extent of the Keep Inlet Formation where discharge from a shallow water table occurs via ET. The occurrence of this groundwater discharge adjacent a no-flow boundary may exacerbate the depression in the potentiometric surface, as there is no radial inflow available from the west.

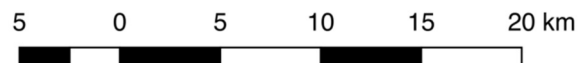
The simulated convergence of groundwater flow in this northern part of the model domain is not consistent with equipotentials mapped based on observation bore data (Figure 17 and 18). However, this may be due to a lack of head observation data in this area. If future work identifies that aquifer depths are not as great at the model boundary as those incorporated into the current model design, the resulting modifications may allow groundwater discharge to occur at the coastal boundary and eliminate this apparent depression in the potentiometric surface.





### Legend

- Equipotential - Observed (m AHD)
- - - Equipotential - Modelled (m AHD)
- Calibration Residuals (m)
  - Too High
  - Good
  - Too Low
- Interpreted Fault
- ▭ Model Domain
- ▭ Permanent GW Discharge Zone
- ▭ Seasonal Seepage Zone



Map prepared by N. Harrington  
Innovative Groundwater Solutions Pty Ltd.  
February 2018  
Co-ordinate Reference System: GDA94 Zone 52

**Figure 18. Simulated equipotentials (Layer 2) and calibration residuals for calibrated version of the three-dimensional groundwater flow model.**

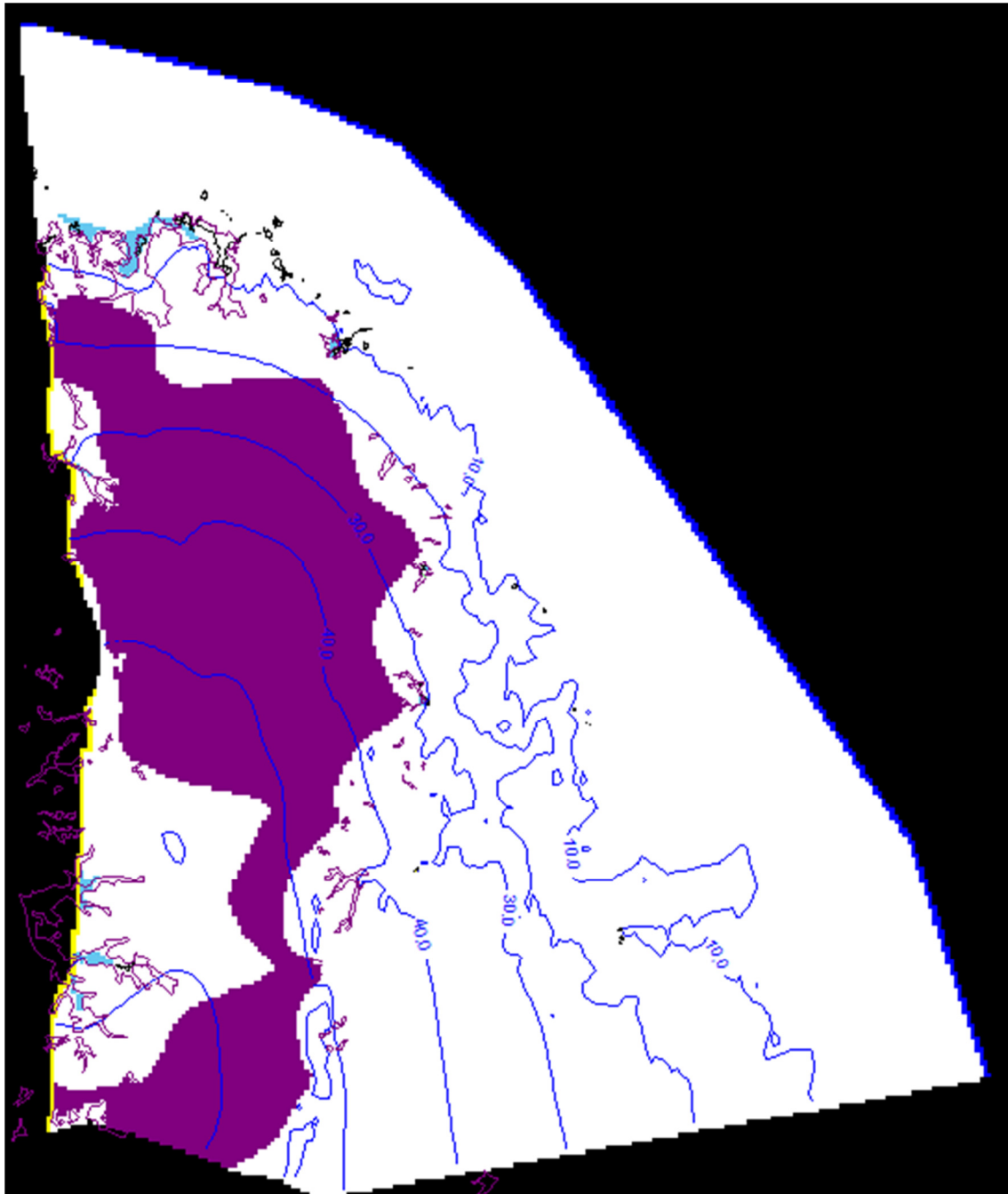


Figure 19. Distribution of dry cells (purple) and areas where simulated heads are above ground surface (light blue cells) compared with mapped areas of permanent groundwater discharge (black outline) and seasonal seepage (purple outline). Simulated equipotentials for Layer 1 are also shown (blue lines).

## 5.2. TWO-DIMENSIONAL SEAWAT MODELS

Figure 20 shows that the SEAWAT model of cross section 103901 estimates the position of the toe of the seawater wedge to be approximately 1,500 m inland of the model boundary in model layer 4, which represents the base of the Point Spring Sandstone aquifer. The simulated seawater / freshwater interface is very sharp, with a salt concentration of  $17 \text{ kg/m}^3$  in the model cell at the interface, and groundwater salinity decreasing from seawater concentration to background concentration over approximately 400 m. The simulated seawater wedge does not penetrate far into the aquifer in model layer 1, which represents the Keep Inlet Formation at this location. This may suggest that the seawater / freshwater interface is actually located seaward of the model boundary in the Keep Inlet Formation in this part of the model domain as the concentrations here are only maintained by the presence of the constant concentration boundary.

Figure 21 shows that the simulated position of the toe of the seawater / freshwater interface for cross section NS01 is approximately 9 km inland of the model boundary, which is approximately level with Yow Spring (but 430 m below ground level). This simulated interface is more diffuse, with groundwater salinity decreasing from seawater concentration to background concentration over approximately 1 km. A more inland-penetrating seawater interface in Layer 1 of section NS01 suggests that the seawater interface penetrates as far as the model boundary in the Keep Inlet Formation at this location.

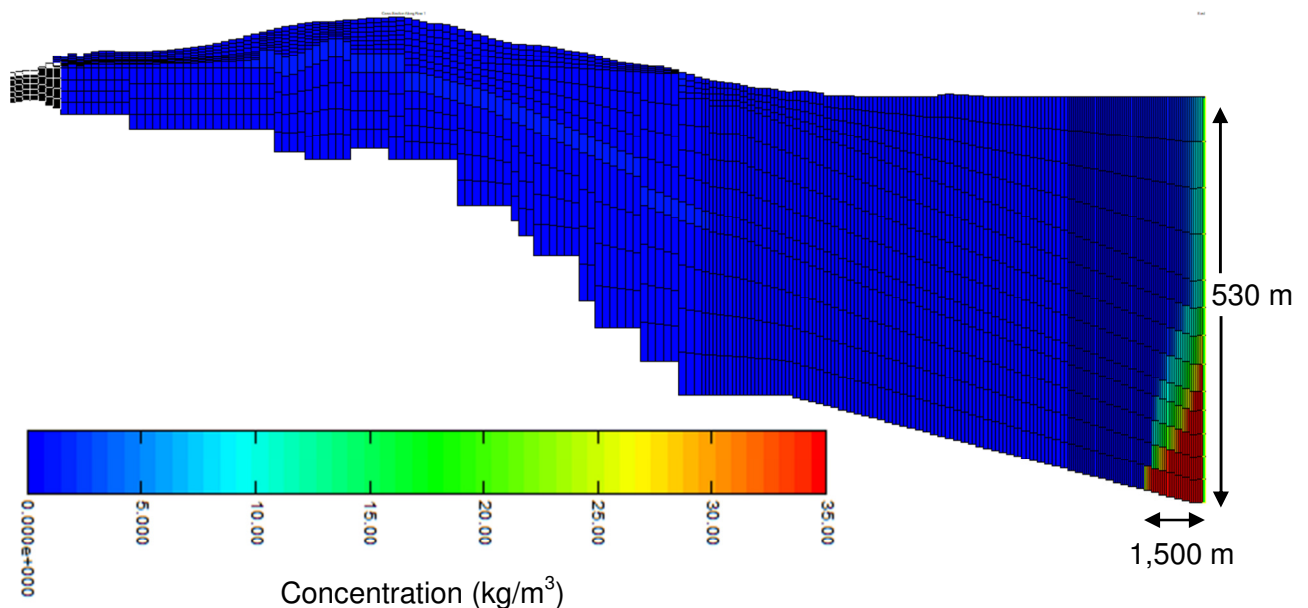


Figure 20. Simulated seawater wedge for cross section 103901. See Figure 2 for cross section location.

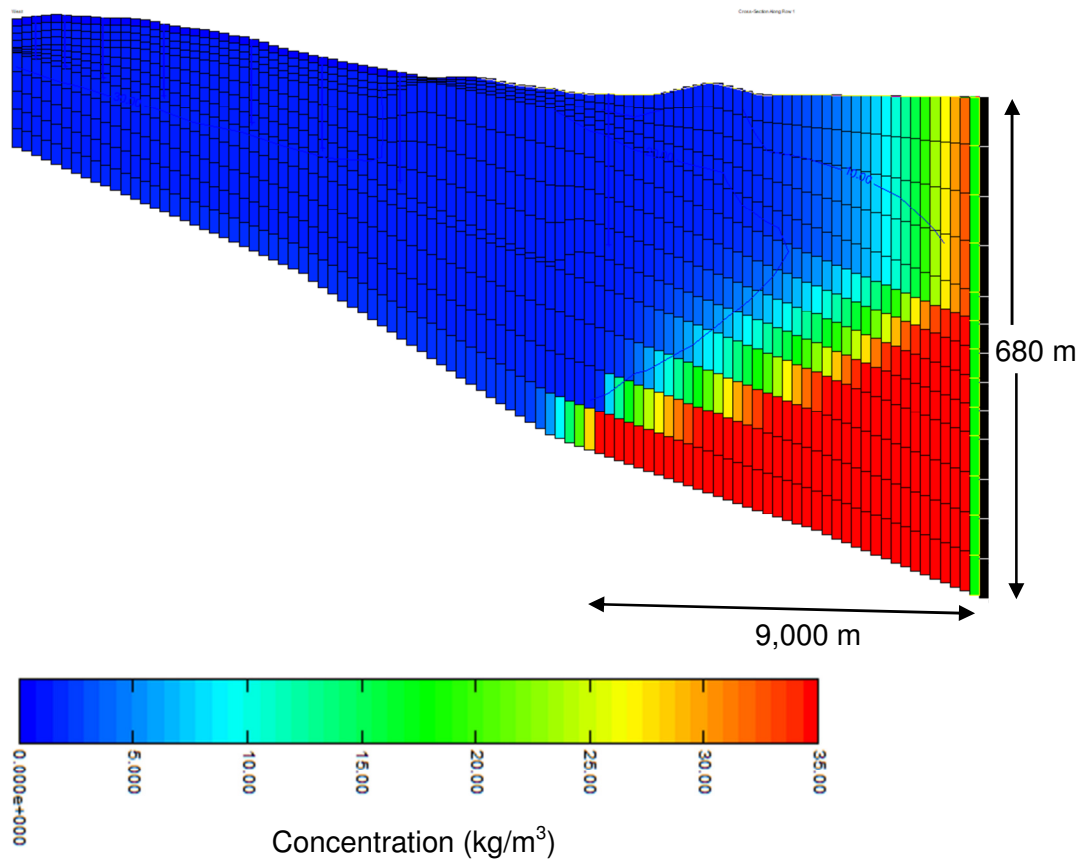


Figure 21. Simulated seawater wedge for cross section NS01. See Figure 2 for cross section location.



## 6. Sensitivity Analysis and Alternative Models

The final SEAWAT models identified that the original assumption that seawater is present at the model boundary in all hydrostratigraphic layers may not be true for Layer 1 (the Keep Inlet Formation) (Section 5.2). The effect of not applying a density correction for seawater density in Layer 1 was tested as part of the model sensitivity analysis.

Additionally, the model calibration process identified the following model parameters as having the most influence over key model outputs (simulated heads and/or water balance):

- $K_v$  of the Keep Inlet Formation,
- Hydraulic conductivity of the Point Spring Sandstone aquifer,
- Recharge

The model sensitivity analysis therefore included the following tests carried out individually on the *Calibrated version* of the three-dimensional model:

1. Set the constant head boundary values to 0 m in Layer 1.
2. Reduce the  $K_v$  of the Keep Inlet Formation by one order of magnitude.
3. Reduce the hydraulic conductivity of the Point Spring Sandstone to half its original value ( $K_H = 3$  m/day and  $K_v = 0.3$  m/day). Halve the recharge rates in all recharge zones to maintain approximate calibration.
4. Increase the hydraulic conductivity of the Point Spring Sandstone to double its original value ( $K_H = 12$  m/day and  $K_v = 1.2$  m/day). Double the recharge rates in all recharge zones to maintain approximate calibration.

The variations made in steps 3 and 4 approximately cover the ranges of independent estimates for hydraulic conductivity and recharge (see Sections 3.3 and 3.5).

Figures 22 to 25 show the resulting equipotential distributions for model Layer 2 and the distributions of calibration residuals. Table 11 and Table 12 provide summaries of the calibration statistics and model water balances for each of the scenarios.

Setting the elevations of the coastal constant head cells in Layer 1 to 0 m AHD (i.e. assuming that seawater is not present at this boundary in Layer 1) had no influence on any of the model outputs (Figure 22, Table 11 and Table 12).

Reducing the  $K_v$  of the Keep Inlet Formation slightly modified the position of the simulated equipotential contours compared with the *Calibrated version* and therefore had a slight influence over simulated heads, as observed in the distribution of calibration residuals and calibration statistics for the scenario (Figure 23, Table 11). The largest effect of reducing the  $K_v$  of the Keep Inlet Formation was a reduction in evapotranspiration as a percentage of total outflows (Table 12). In this scenario, evapotranspiration represents 57% of outflows compared with 93 % for the *Calibrated version*. This reduces inflows at the coastal boundary and increases net discharge at the coast.

The low hydraulic conductivity / low recharge and high hydraulic conductivity / high recharge scenarios were designed to maintain simulated heads that are similar to the *Calibrated version* of the model (Figure 24 and 25). However, the influence of these modifications is seen in the model water balance, with evapotranspiration for the high K/high R and low K/low R scenarios ranging between 67% and 98% of the total outflows respectively and,

conversely, coastal discharge ranging between 32% and 0% respectively (Table 12). Outflows at the western (drain) boundary ranged between 1% and 2% of total outflows.

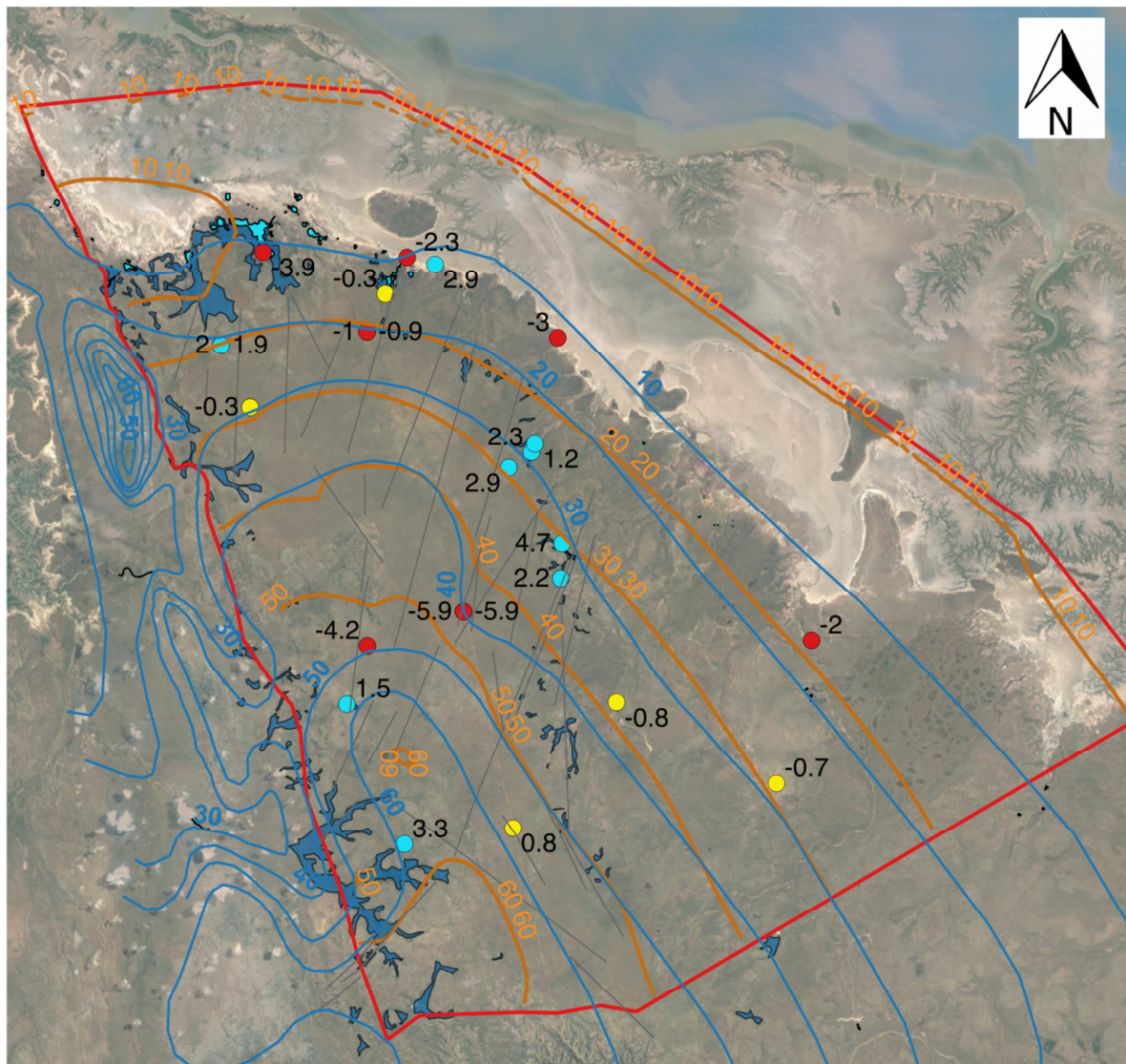
Modifications to the coastal constant head boundary (Scenario 1) had little influence over model outputs. Each of the remaining scenarios represent alternative conceptual models, with alternative water balances, as they each provide a reasonable match to observed hydraulic head data and have model parameters within the plausible ranges. However, the high K/high R and low K/low R scenarios represent extremes in the estimates for hydraulic conductivity and recharge. The current data set suggests that the values for these parameters used in the *Calibrated version* of the model represent the most plausible estimates for application at the regional scale.

As the vertical hydraulic conductivity of the Keep Inlet Formation is unknown and this parameter has a large influence over the simulated water balance, this represents one of the largest limitations to estimating a water balance for the Bonaparte Plains.

Initial attempts to calibrate the two-dimensional and three-dimensional models included data from observation bore 17BP03I, which suggested the occurrence of groundwater heads of approximately 71 m AHD in the central portion of the model domain. The current conceptual model for recharge and hydraulic conductivity does not facilitate the simulation of such high heads in this region. A review of the hydrogeological log for this bore and discussions with DPIRD resulted in the decision that bore 17BP03I is probably screened in a pocket of groundwater that is separated from the regional system by, for example, slight folding or faulting of the Bennett Shale, which the AEM indicates has minimal general slope in the immediate vicinity of 13BP03I. This is also supported by (a) the hydrogeological log of the bore, which indicates that it is screened in a thin zone of saturated aquifer immediately above the Bennett Shale, and (b) the chloride concentration of this groundwater, which is much higher than groundwater from the remainder of the system. As a result, this observation bore was removed from the calibration dataset for this project.

However, the above hypothesis relating to observation bore 17BP03I is unconfirmed, as there are no other observation bores in the Upper Point Spring Sandstone aquifer in the vicinity of 17BP03I and there is no information available on groundwater occurrence below the screened interval of this bore. For this reason, the results of models using alternative conceptual models, which were constructed in an attempt to calibrate to the original dataset that included 17BP03I, are included in Appendix D of this report. The outcomes of these exercises may be of use if additional data indicates that 17BP03I is in fact connected to the regional system.





### Legend

- Equipotential - Observed (m AHD)
- Equipotential - Calibrated version (m AHD)
- Equipotential - Sensitivity Test (m AHD)
- Calibration Residuals (m)
  - Too High
  - Good
  - Too Low
- Interpreted Fault
- Model Domain
- Permanent GW Discharge Zone
- Seasonal Seepage Zone

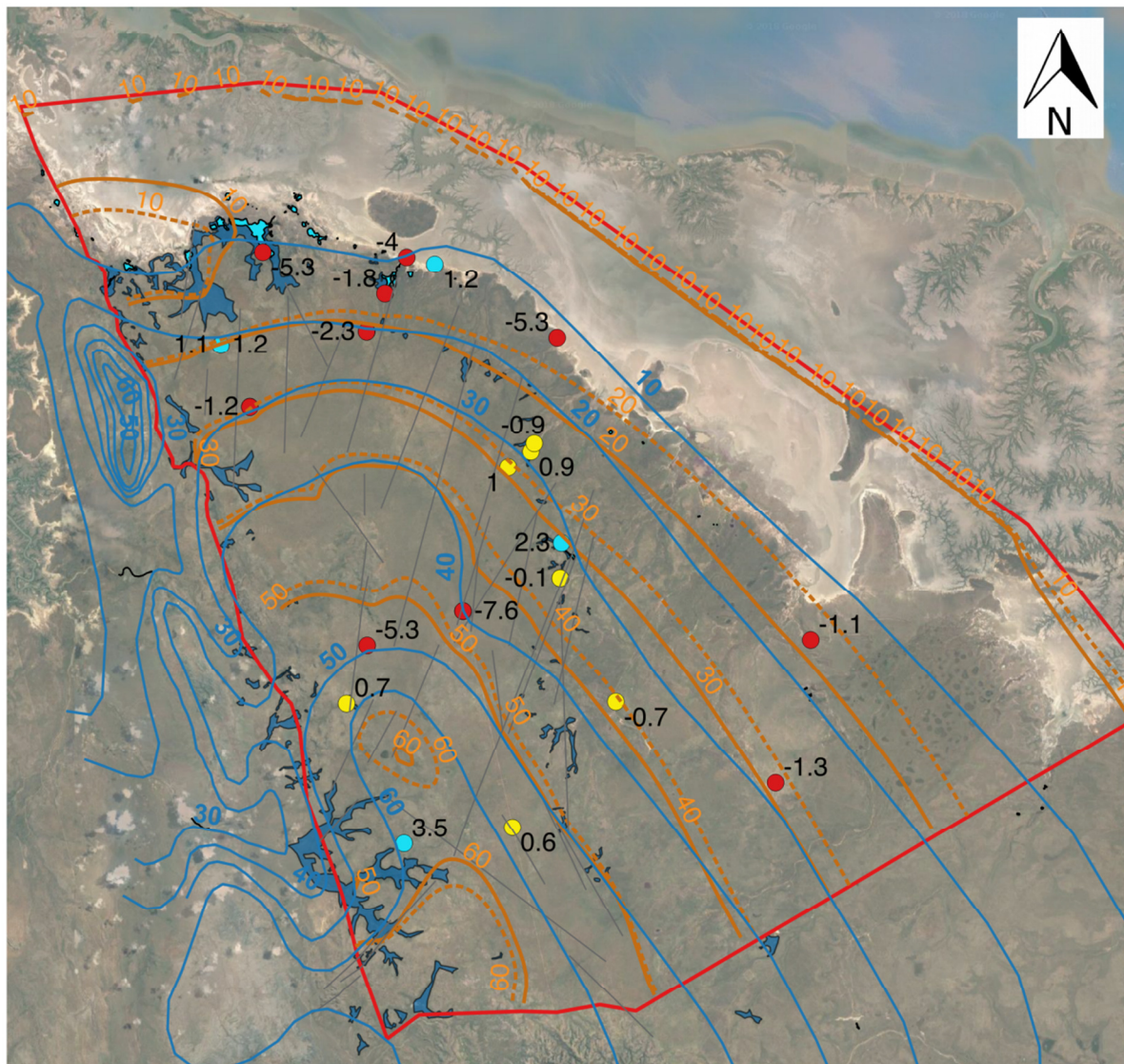
5 0 5 10 15 20 km



Map prepared by N. Harrington  
Innovative Groundwater Solutions Pty Ltd.  
February 2018  
Co-ordinate Reference System: GDA94 Zone 52

**Figure 22. Calibration residuals and simulated equipotentials (Layer 2) for sensitivity test: Constant Head in Layer 1 = 0 m AHD.**





### Legend

- Equipotential - Observed (m AHD)
- Equipotential - Calibrated version ( AHD)
- - - Equipotential - Sensitivity Test (m AHD)
- Calibration Residuals (m)
  - Too High
  - Good
  - Too Low
- Interpreted Fault
- Model Domain
- Permanent GW Discharge Zone
- Seasonal Seepage Zone

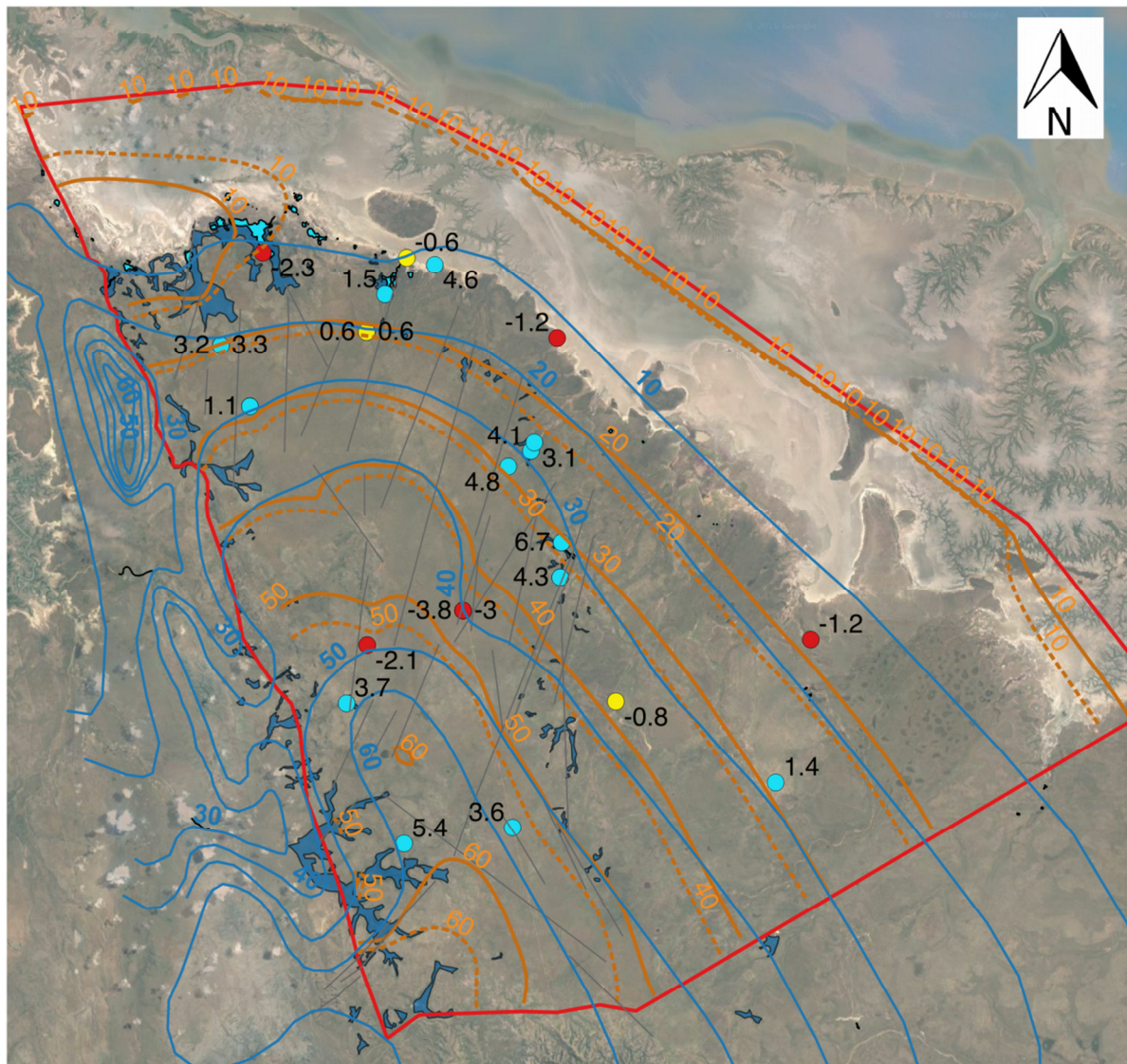
5 0 5 10 15 20 km



Map prepared by N. Harrington  
Innovative Groundwater Solutions Pty Ltd.  
February 2018  
Co-ordinate Reference System: GDA94 Zone 52

**Figure 23. Calibration residuals and simulated equipotentials (Layer 2) for sensitivity test:**  
Keep Inlet Formation  $K_v = 0.0001$  m/day.





### Legend

- Equipotential - Observed (m AHD)
- Equipotential - Calibrated version (AHD)
- - - Equipotential - Sensitivity Test (m AHD)
- Calibration Residuals (m)
  - Too High
  - Good
  - Too Low
- Interpreted Fault
- Model Domain
- Permanent GW Discharge Zone
- Seasonal Seepage Zone

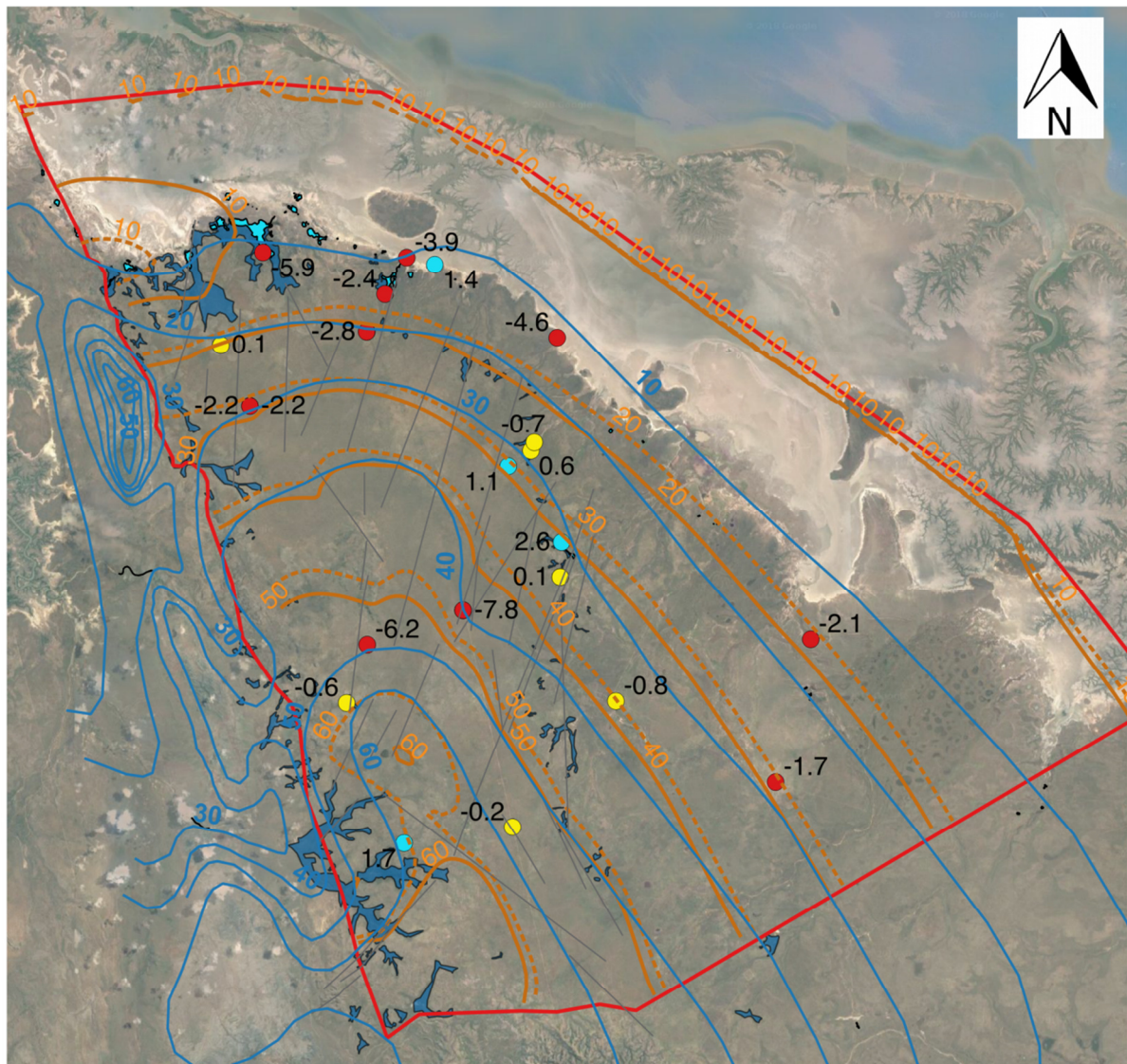
5 0 5 10 15 20 km



Map prepared by N. Harrington  
Innovative Groundwater Solutions Pty Ltd.  
February 2018  
Co-ordinate Reference System: GDA94 Zone  
52

**Figure 24. Calibration residuals and simulated equipotentials (Layer 2) for sensitivity test: Low hydraulic conductivity, low recharge.**





### Legend

- Equipotential - Observed (m AHD)
- Equipotential - Calibrated version (AHD)
- - - Equipotential - Sensitivity Test (m AHD)
- Calibration Residuals (m)
  - Too High
  - Good
  - Too Low
- Interpreted Fault
- ▭ Model Domain
- ▭ Permanent GW Discharge Zone
- ▭ Seasonal Seepage Zone

5 0 5 10 15 20 km



Map prepared by N. Harrington  
Innovative Groundwater Solutions Pty Ltd.  
February 2018  
Co-ordinate Reference System: GDA94  
Zone 52

**Figure 25. Calibration residuals and simulated equipotentials (Layer 2) for sensitivity test: High hydraulic conductivity, high recharge.**

Table 11. Comparison of calibration statistics for *Calibrated version* of the model and sensitivity test scenarios.

	<b>Calibrated version</b>	<b>L1 CHB = 0m</b>	<b>Kv Keep Inlet = 0.0001 m/d</b>	<b>Low K, Low R</b>	<b>High K, High R</b>
Residual Mean (m)	-0.32	-0.32	-1.57	1.44	2.00
Residual Standard Deviation (m)	2.87	2.87	2.98	2.93	2.89
Absolute Residual Mean (m)	2.38	2.38	2.49	2.81	2.57
RMS Error (m)	2.89	2.89	3.36	3.26	3.51
Minimum Residual (m)	-5.9	-5.9	-7.58	-3.79	-7.81
Maximum Residual (m)	4.65	4.65	3.48	6.72	2.56
Range of Observations (m)	53.5	53.5	53.5	53.5	53.5
Scaled Residual Standard Deviation (%)	5.4	5.4	5.6	5.5	5.4
Scaled Absolute Mean (%)	4.5	4.5	4.6	5.3	4.8
Scaled RMS (%)	5.4	5.4	6.3	6.1	6.6
Mass Balance Error (%)	0.029	0.029	0.0043	0.021	0.015

Table 12. Comparison of model water balances for *Calibrated version* and various sensitivity test scenarios.

	Calibrated Model	Layer 1 CHB = 0 m	Kv Keep Inlet = 0.0001 m/d	Low K, Low R	High K, High R
<b>Inflows (ML/day)</b>					
Recharge	190	190	186	93	373
Coastal Boundary	402	402	367	217	754
<b>Outflows (ML/day)</b>					
Evapotranspiration	176 (93%)	176 (93%)	106 (57%)	116 (98%)	248 (67%)
Drains	3.0 (1%)	2.6 (1%)	3.0 (2%)	1.5 (2%)	4.4 (1%)
Coastal Boundary	414	414	444	193	873
(Coastal Boundary Net Outflow)	12 (6%)	12 (6%)	77 (41%)	-24.3 (0%)	120 (32%)



## 7. Conclusions

Construction and calibration of the three-dimensional groundwater flow model, and assessment of the simulated model water balance, has led to the following conclusions about the Point Spring Sandstone aquifer groundwater system beneath Bonaparte Plains:

1. The calibrated numerical model is based on the current conceptual model for the system, with a hydraulic conductivity of the Point Spring Sandstone of 6 m/day ( $K_v = 0.6$  m/day) and a recharge rate of 140 mm/yr across most of the recharge area. This model produces a hydraulic head distribution that is consistent with recent observation data. The model also simulates groundwater levels above ground surface at locations of mapped areas of seasonal and permanent groundwater discharge, providing additional confidence.
2. An overestimation of heads in the central portion of the model domain by 4.2 m to 5.1 m, coupled with underestimation of heads in the central eastern and south western portion of the model domain by 1.2 m to 4.7 m suggests that some feature contributing to lower heads in the former area is not captured by the current conceptual model. Examples of this may be an area of higher hydraulic conductivity or faults acting as conduits for vertical groundwater flow. If such a feature/s were included in the model, improved calibration may be achieved using a slightly higher recharge rate.
3. The water balance of the calibrated numerical model suggests that total recharge amounts to 190 ML/day (69.4 GL/yr). Evapotranspiration accounts for more than 93% of the outflows from the system, with the remaining outflow consisting of approximately 6% discharging via the coastal boundary and 1% discharging at the western boundary of the model domain.
4. The vertical hydraulic conductivity of the Keep Inlet Formation is unknown, although it is expected to be low based on the observed characteristics of the unit. A good calibration is achieved using a  $K_v$  for this unit of 0.001 m/day and this value was required to allow evapotranspiration at the edges of the mudflats to remove water from the underlying Point Spring Sandstone and maintain heads at observed levels. However, the model sensitivity analysis indicated that, if the  $K_v$  of the Keep Inlet Formation was reduced by an order of magnitude, this would have a large impact on the simulated water balance whilst maintaining approximate calibration to observed hydraulic heads (Table 12). Estimation of  $K_v$  of the Keep Inlet formation should therefore be a priority for future work in order to better constrain the water balance of the Point Spring Aquifer.
5. Alternative conceptual models using combinations of lower hydraulic conductivity and lower recharge or higher hydraulic conductivity and higher recharge are also plausible, highlighting the non-uniqueness of the model. The results of testing of these scenarios indicates that small variations in recharge / hydraulic conductivity can maintain model calibration but have a significant impact on the simulated water balance. Additional independent estimates of these water balance parameters could improve the accuracy and certainty of the estimates of those parameters for the aquifer, or provide a basis for improved model calibration through zoning of recharge and hydraulic conductivity.

6. Density-dependent solute transport modelling of the interface between seawater and fresh groundwater along two cross sections indicate that:
  - a. The toe of the seawater interface lies below the mudflats at the location of Section 103901, approximately 1,500 m inland of the model boundary.
  - b. The toe of the seawater interface at the location of Section NS01 is approximately 9 km inland of the model boundary, corresponding to the location of Yow Spring but at a depth of 430 m below ground level.

## 8. Limitations

Groundwater models are simplified representations of complex natural systems. As such, they include a range of standard assumptions about the systems they represent, and their outputs are limited by the level of understanding of the system and amount of input data available. Key limitations of the current models that have been identified through the modelling process are:

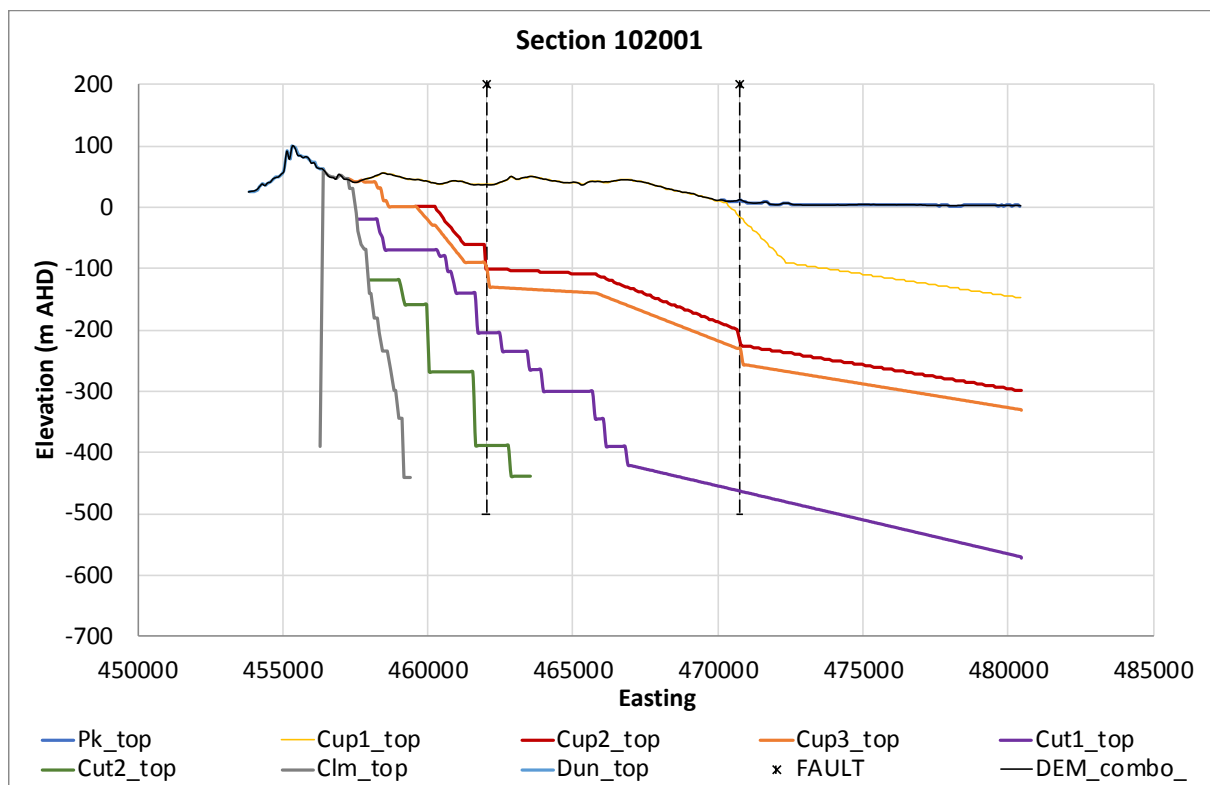
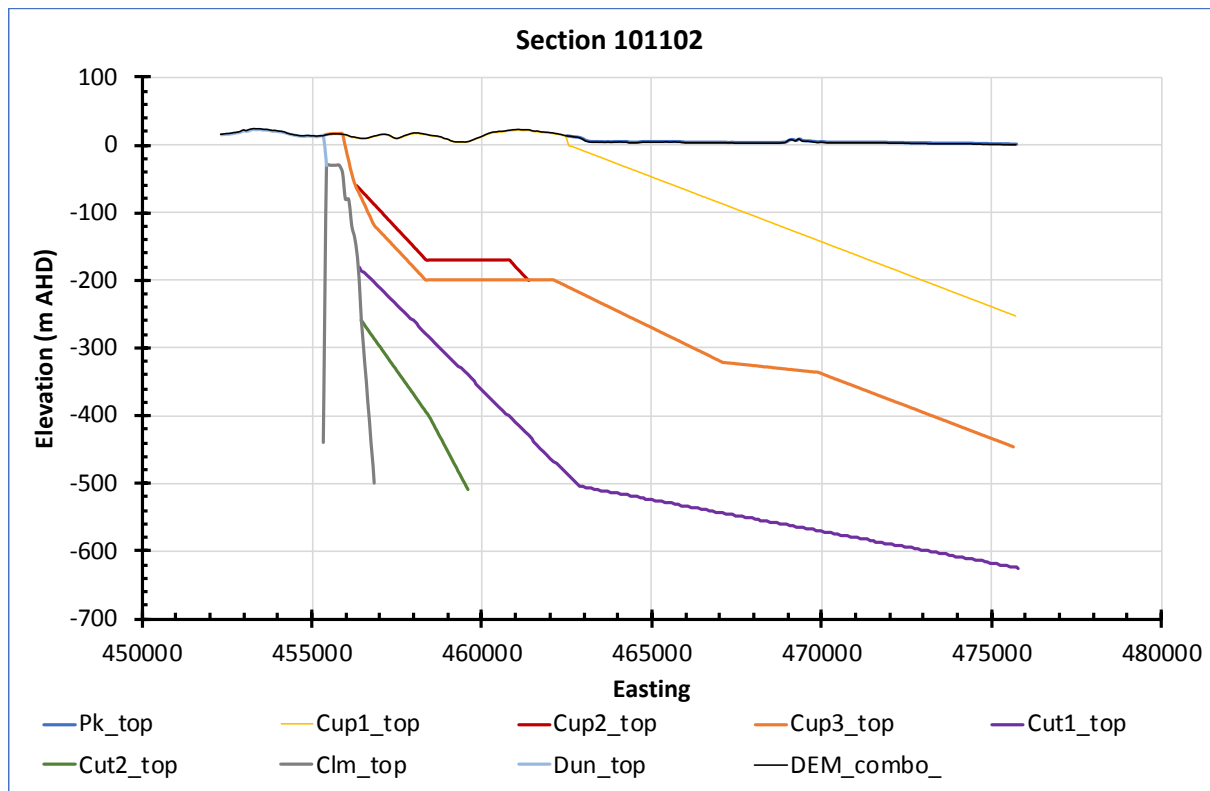
1. The currently available data on the hydraulic conductivity (K) of the Point Spring Sandstone and recharge rates provides values that range between 3 m/day and 14 m/day, and between 30 mm/yr and 350 mm/yr, respectively. The current models employ values that are reasonable intermediates within these ranges. However, the model is non-unique with combinations of K and recharge rates within these ranges providing a satisfactory calibration to head data but different water balance results.
2. There is no data currently available on the vertical hydraulic conductivity of the Keep Inlet Formation. A value of 0.001 m/day has been selected as this provides the best calibration to observed head data and is a reasonable value based upon the properties of the unit.
3. The head observation dataset contains only one to two years of time series data, albeit much of this is from loggers providing a good indication of seasonal variability. Heads are observed to be gradually rising in some bores meaning that the selection of steady state head values for calibration of the steady state model based on the current dataset is uncertain.

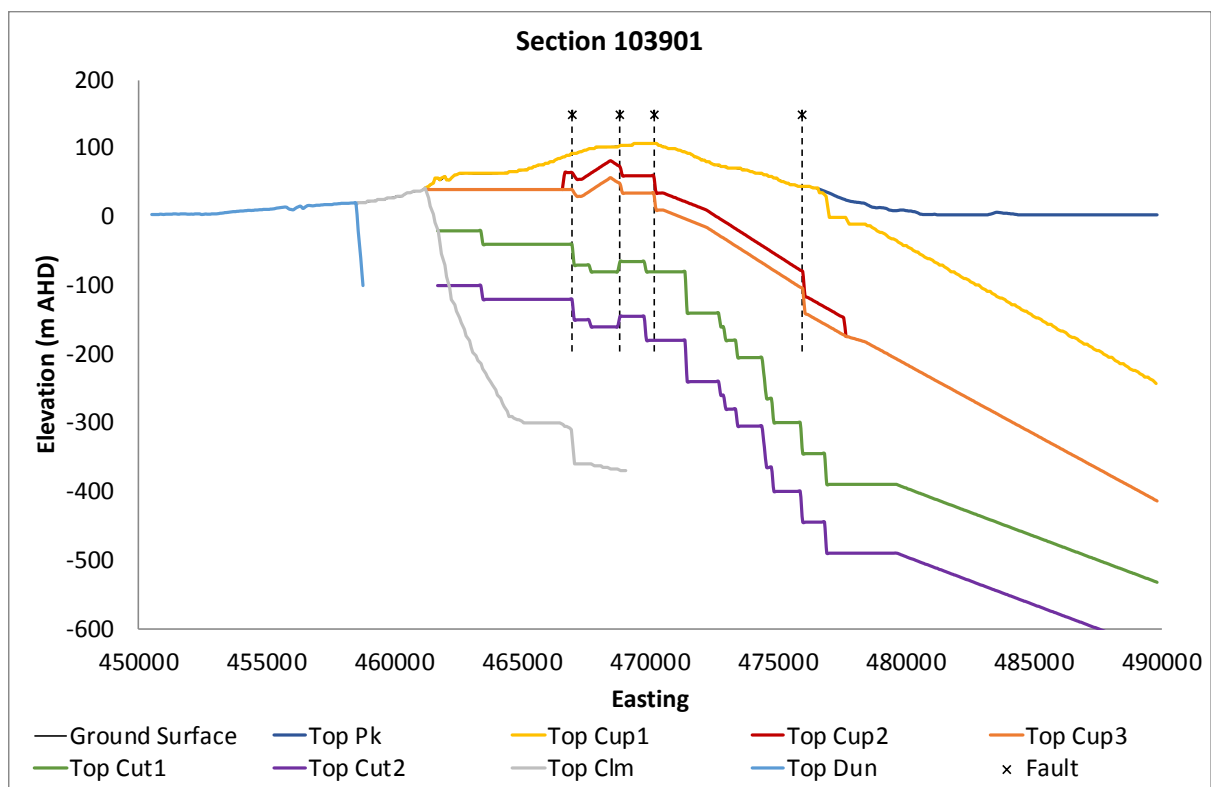
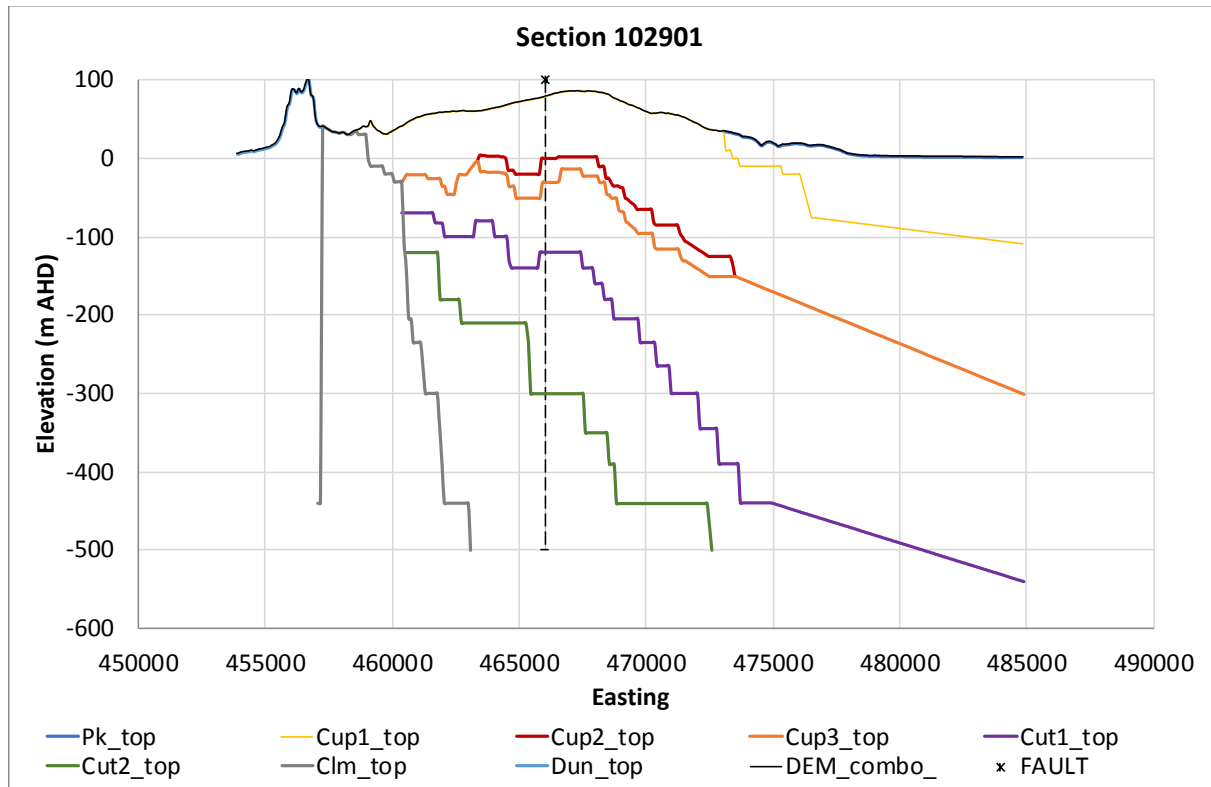
## 9. References

- Bennett, D 2019, 'Investigations of the potential for irrigated agriculture on the Bonaparte Plains: bore completion report', 2nd edn, Resource management technical report 414, Department of Primary Industries and Regional Development, Perth.
- Bennett, D. and Raper, P. (2018). Conceptual hydrogeological model: Bonaparte Plains Kulshill Group sandstone aquifers. Unpublished report.
- Doherty, J.E., and Hunt, R.J., 2010, Approaches to highly parameterized inversion—A guide to using PEST for groundwater-model calibration: U.S. Geological Survey Scientific Investigations Report 2010–5169, 59 p.
- Gorter, J, Jones, P & Nicoll, R 2005, 'A reappraisal of the Carboniferous stratigraphy and the petroleum potential of the southeastern Bonaparte Basin (Petrel Sub-basin), northwestern Australia', *The APPEA Journal*, vol. 45, no. 1, pp. 275–296.
- Harbaugh, A.W., 2005, MODFLOW-2005, the U.S. Geological Survey modular ground-water model—The ground-water flow process: U.S. Geological Survey Techniques and Methods 6–A16, variously paged. <http://pubs.er.usgs.gov/publication/tm6A16>
- IGS (2018). SEAWAT: 2D Cross Section Model. Setup, Results and Useful Tips in Groundwater Vistas. Unpublished Internal Draft Report.
- Langevin, C.D., Thorne, D.T., Jr., Dausman, A.M., Sukop, M.C., and Guo, Weixing, 2008, SEAWAT Version 4: A Computer Program for Simulation of Multi-Species Solute and Heat Transport: U.S. Geological Survey Techniques and Methods Book 6, Chapter A22, 39 p
- Meredith, K., Priestley, S. and Hankin, S. (2018). Analysis of Bonaparte Plains groundwater chemistry data. Report prepared for the Government of Western Australia, Department of Primary Industries and Regional Development. ANSTO Report ANSTO/C-1572. 27 August 2018.
- Mory, AJ & Beere, GM 1988, 'Geology of the onshore Bonaparte and Ord Basins in Western Australia', *Geological Survey of Western Australia Bulletin 134*, Department of Mines Western Australia, Perth.
- Niswonger, R.G., Panday, Sorab, and Ibaraki, Motomu, 2011, MODFLOW-NWT, A Newton formulation for MODFLOW-2005: U.S. Geological Survey Techniques and Methods 6-A37, 44 p.
- Smolinski, H., Pathan, S., Galloway, P., Kuswardiyanto, K. and Laycock, J. (2015). Cockatoo Sands in the Victoria Highway and Carlton Hill areas, East Kimberley: land capability assessment for developing irrigated agriculture. *Resource management technical report 391*, Department of Agriculture and Food, Western Australia, Perth.
- Tan, K. P., Symington, N. J., Halas, L., Christensen, N.B., Harris-Pascal, C., McPherson, A. A., Lawrie, K. C., Cathro, D. L., McMillan, M. & Halas, V. 2018. *Ord-Bonaparte Groundwater Investigations – East Kimberley region, Western Australia*. Draft Professional Opinion 2018/xx. Geoscience Australia, Canberra.
- Zheng C., Wang P.P. MT3DMS: A modular three-dimensional multispecies transport model for simulation of advection, dispersion, and chemical reactions of contaminants in

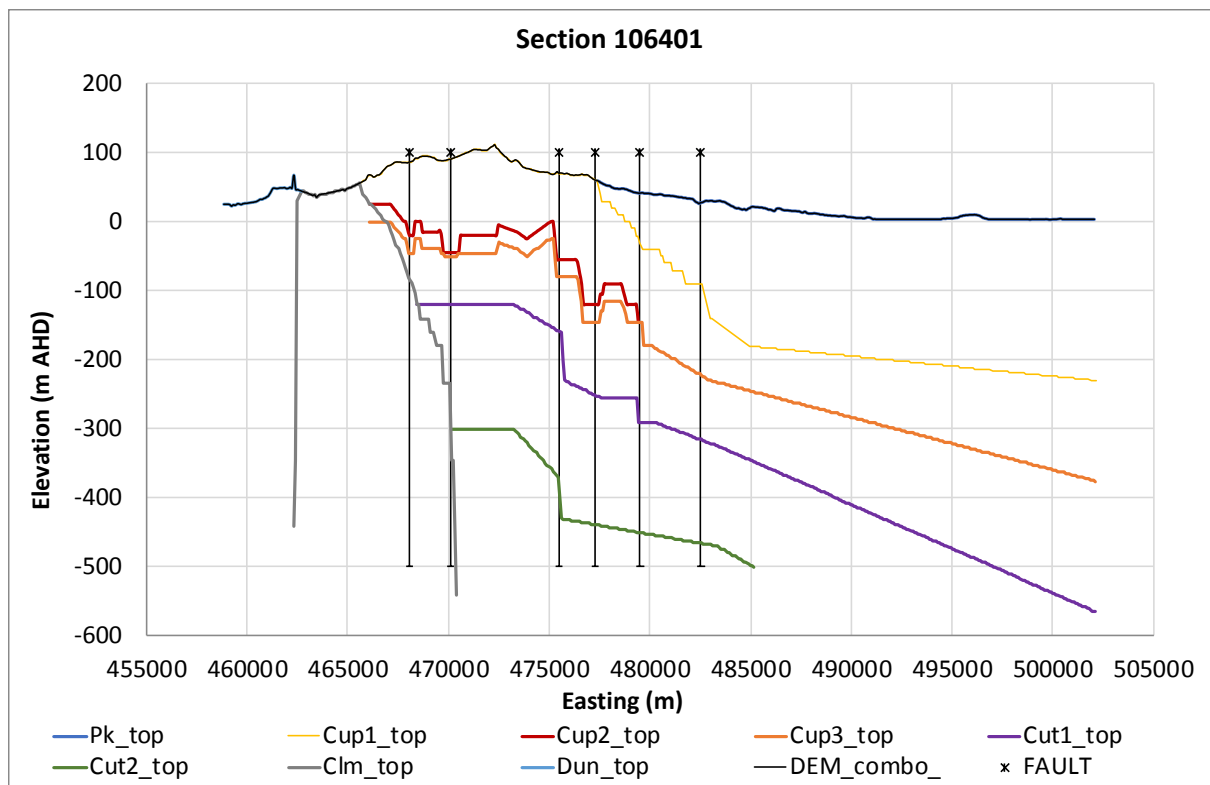
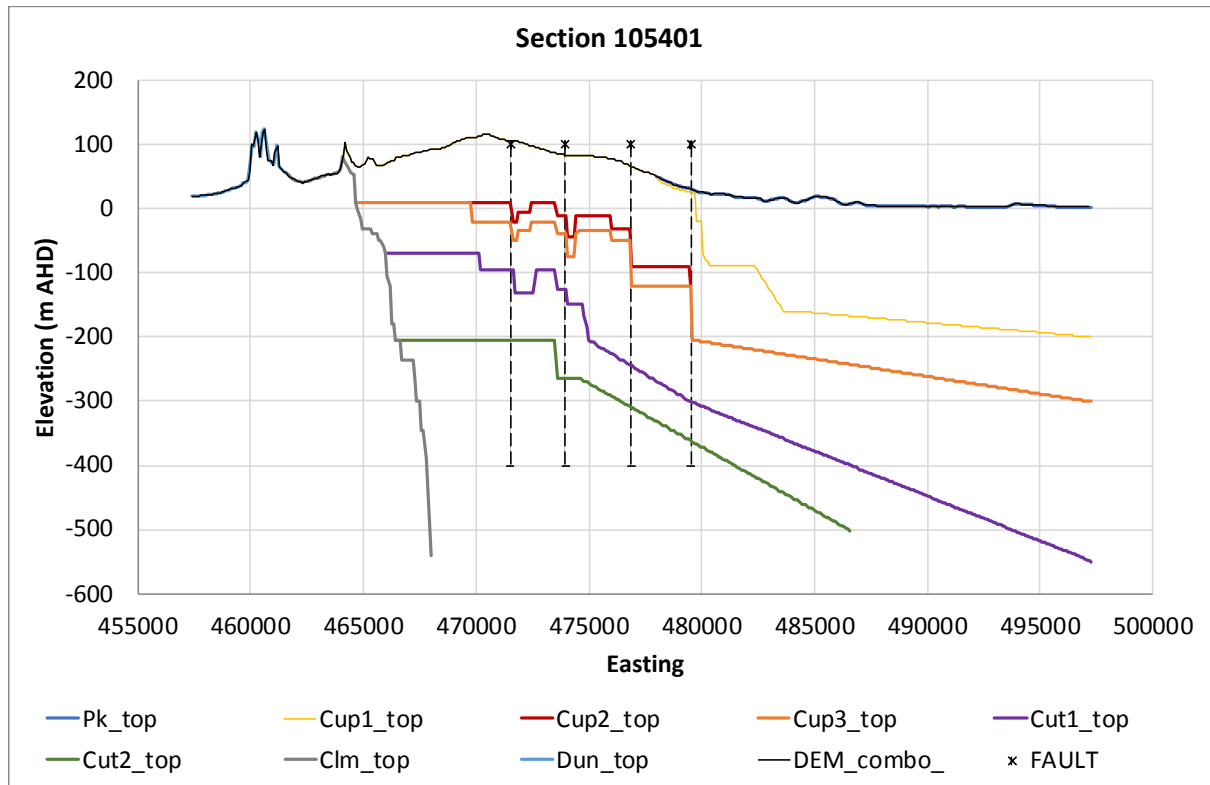
groundwater systems; documentation and user's guide. Am. J. Roentgenol. 1999;169:1196–1197.

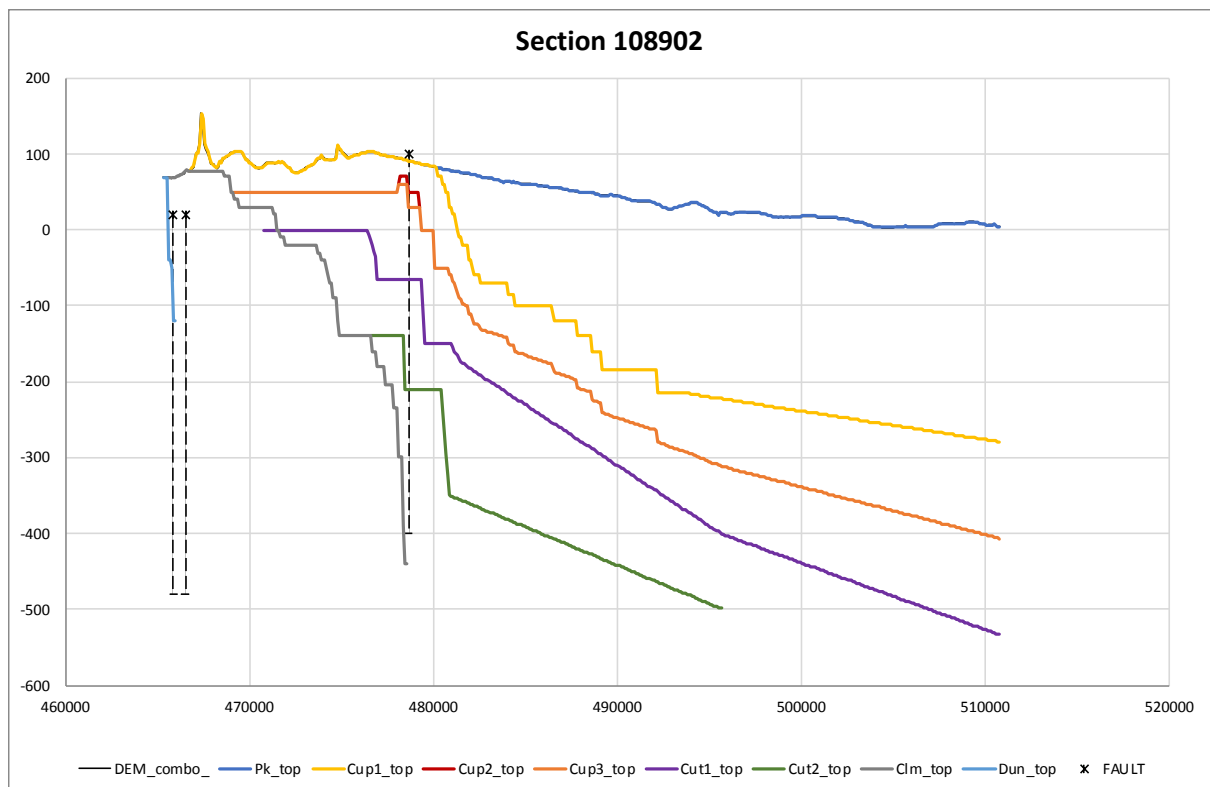
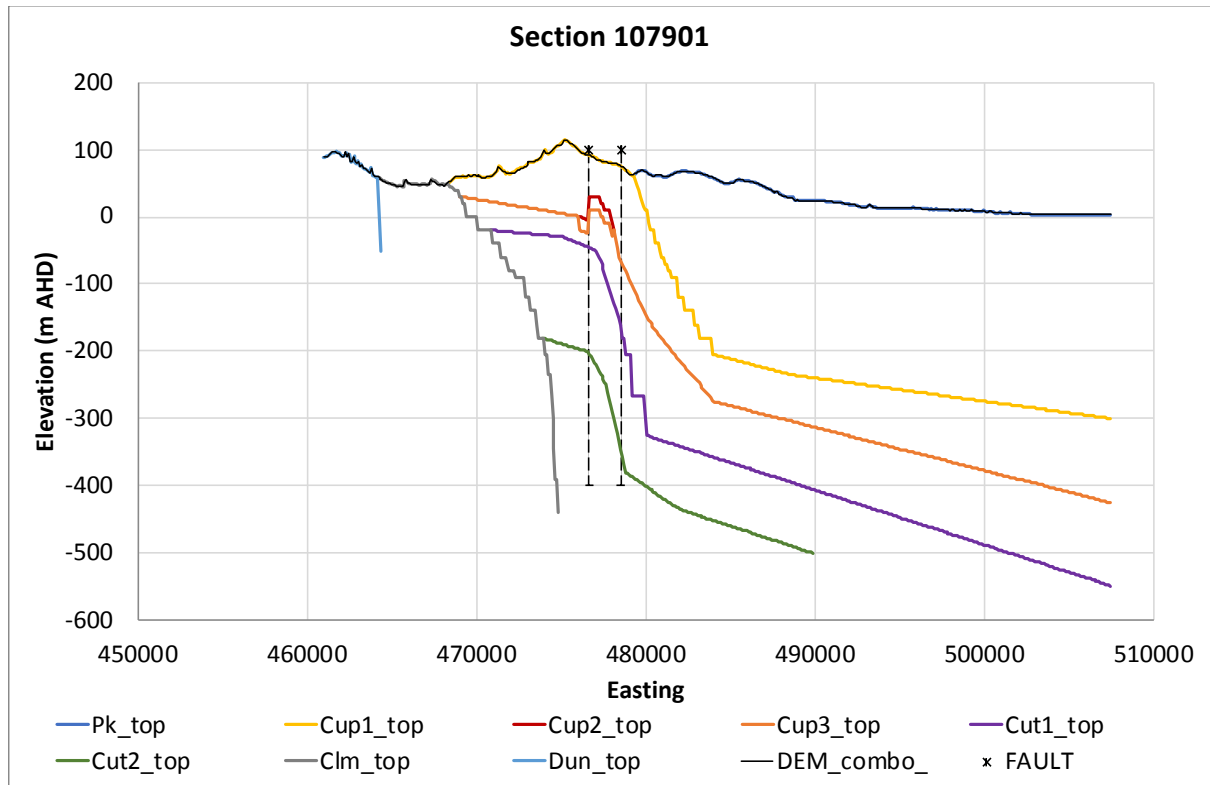
## APPENDIX A. HYDROSTRATIGRAPHIC CROSS-SECTIONS

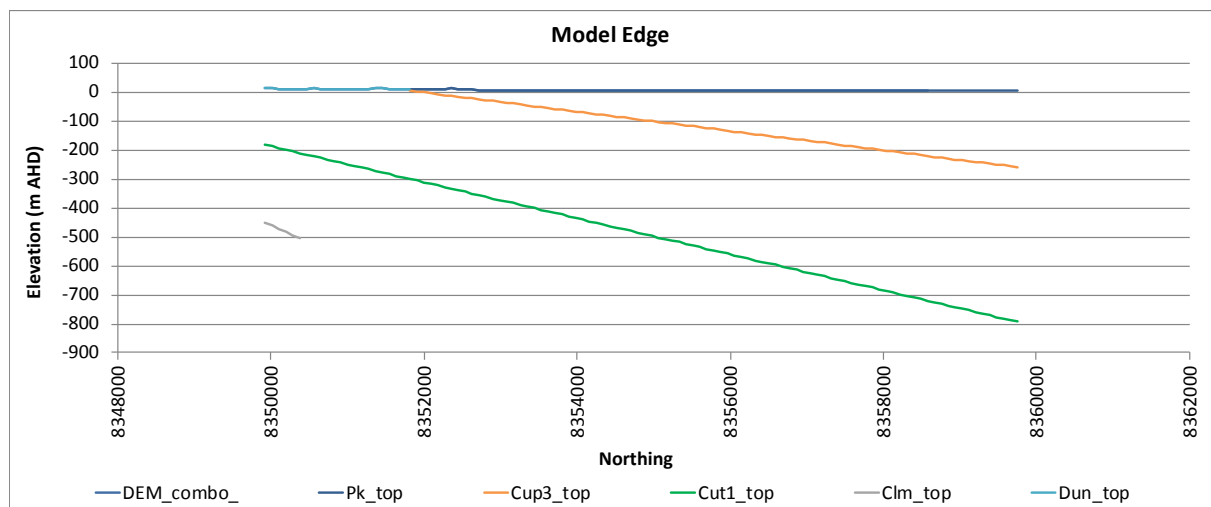
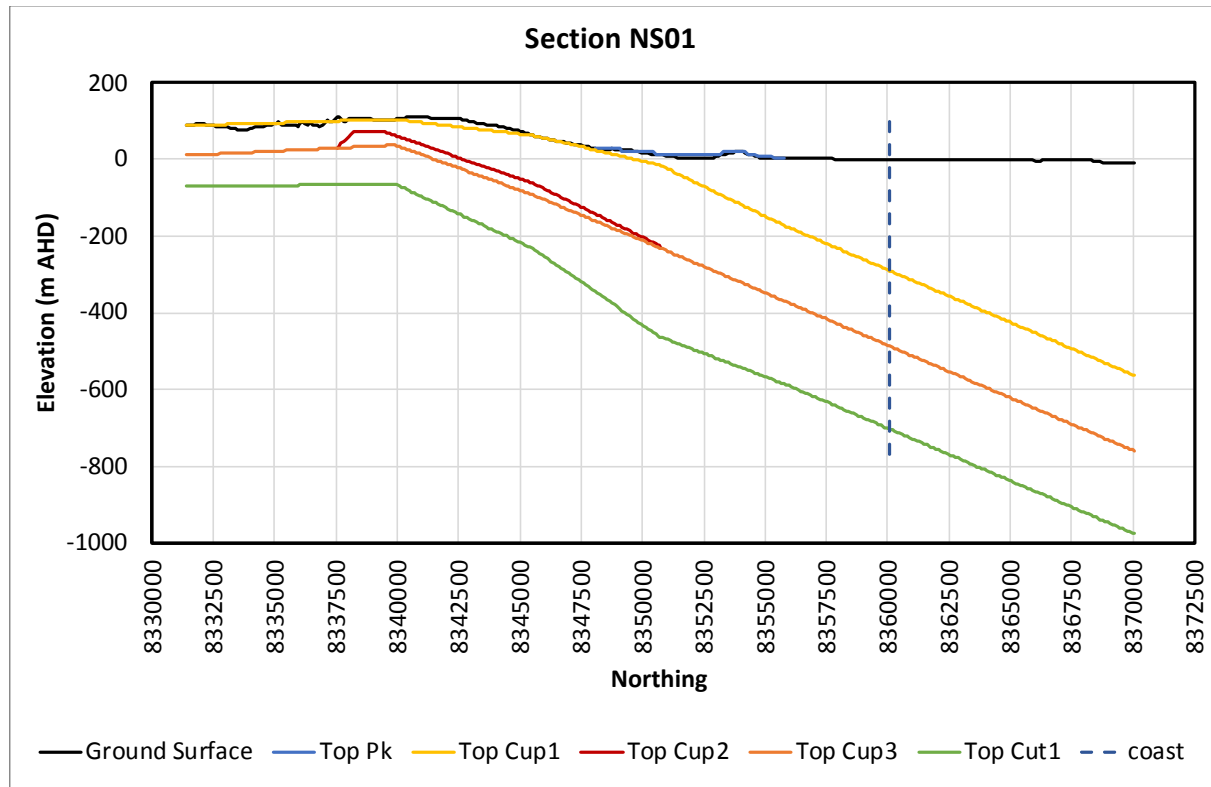


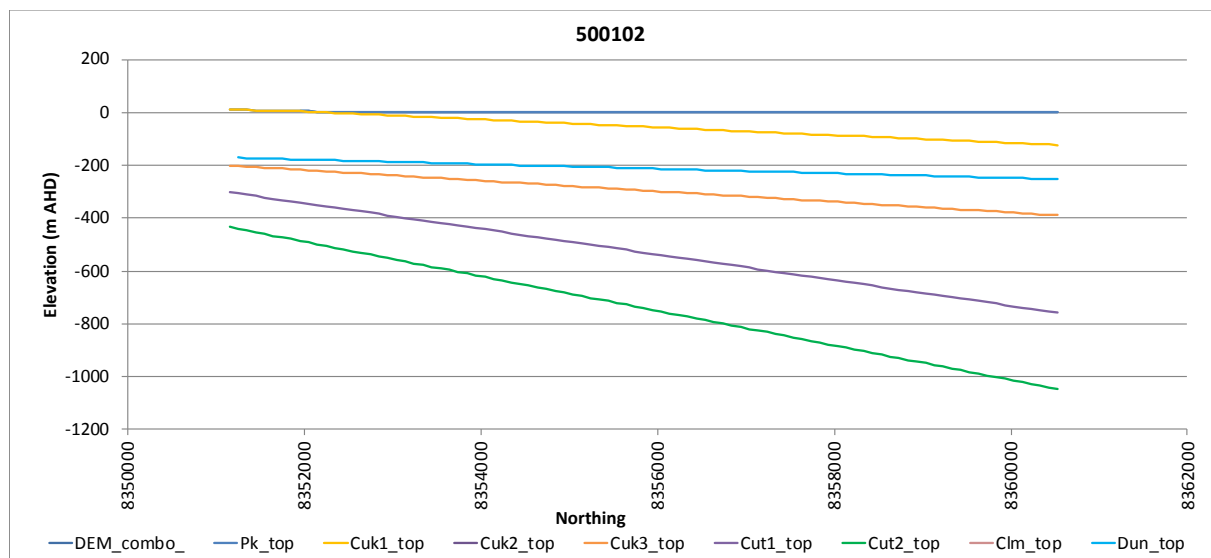
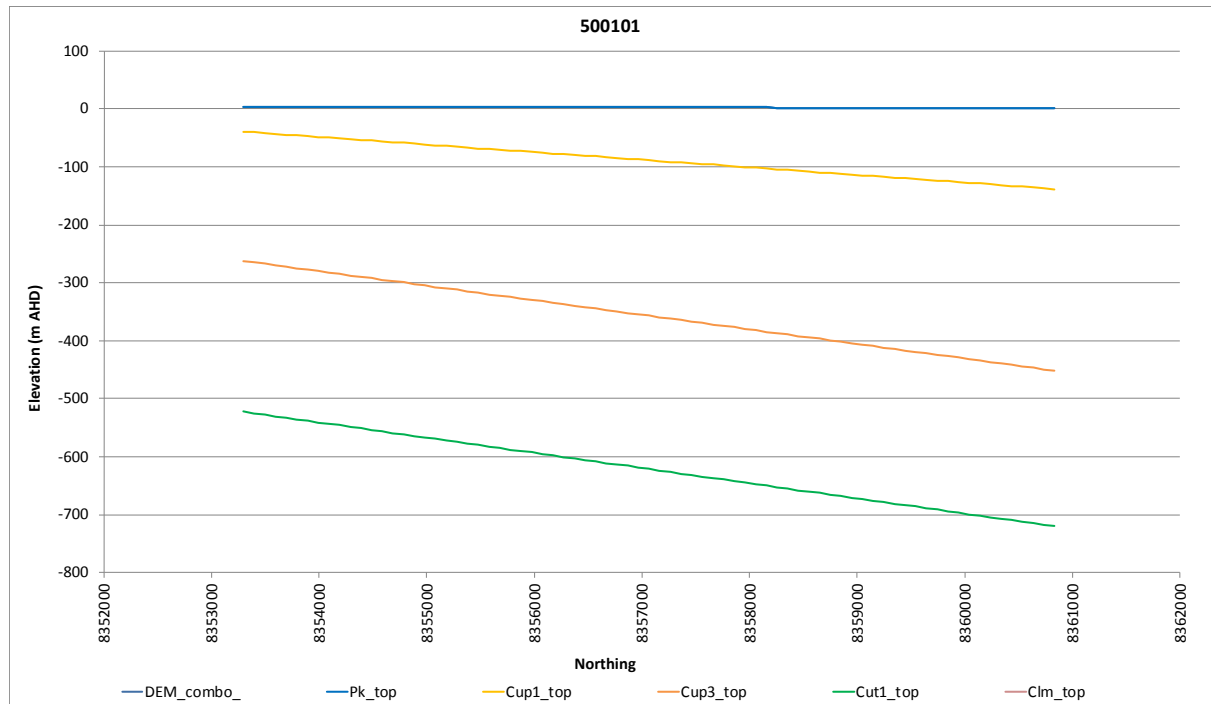












## APPENDIX B. MODEL CALIBRATION DATA

Observation Point	X	Y	Model Layer	Observed Head (m AHD)	Comment
13BP01D	473886.6	8333260.7	4	39.35	Rising. Highest observed value.
13BP01I	473886.6	8333260.7	2	38.9	Rising. Highest observed value.
13BP01S	473886.6	8333260.7	2	38.9	Rising. Highest observed value.
17BP01I	478993.4	8335027.2	2	35.9	Steady
17BP01S	478983.9	8335023.1	2	35.9	Steady
17BP02I	468839.0	8347946.3	2	20.1	V. short record
17BP02S	468829.8	8347942.3	2	20.1	V. short record
17BP03I	469012.2	8340498.6	2	71.3	Rising slightly but short record.
17BP04I	462705.7	8344019.1	2	28.7	Fluctuates by 0.6 m
17BP04S	462707.3	8344008.2	2	28.7	Short record but rising.
17BP05I	461179.0	8347241.9	2	22.2	
17BP05S	461182.2	8347232.5	2	22.1	
17BP06I	476482.4	8321899.9	2	55.9	Short record but rising slightly.
17BP07I	468859.9	8331473.3	2	48.9	
BONAPARTE1 WB2	476256.0	8340826.6	2	31.8	
BONAPARTE2 WB	467779.1	8328404.9	2	58.5	Recent slight rise.
FISHERMANS	472404.0	8351461.6	2	17.3	Pressure taken at tap.
NEW ATTACK	470932.2	8351823.9	2	11.8	Flowing – pressure taken. May underestimate actual head?
KEMP	478825.6	8347624.7	2	12.4	Flowing – pressure taken. May underestimate actual head?
CLEANSKIN	492122.5	8331754.1	1	14.7	Keep Inlet Fm. Steady.
HOTPLATE	470795.5	8321055.2	4	61.5	Fluctuates between 60.8 and 62.4 m.
GRANT CREEK	481901.8	8328501.7	1	30.7	
WILSON	490280.8	8324255.2	1	27.9	Keep Inlet Fm. Fluctuates between 27.9 and 28.7 m.
Bore Spring Upper	477448.0	8341642.0	1	27	Spring. Head estimate only.
Bore Spring Lower	477624.0	8342072.0	2	25	Spring. Head estimate only.
Long Spring Source	463391.0	8352099.0	2	8	Spring. Head estimate only.
New Spring Source	479055.0	8336839.0	2	35.3	Spring. Head estimate only.
Yow Spring Source	469793.0	8349904.0	2	15.4	Spring. Head estimate only.

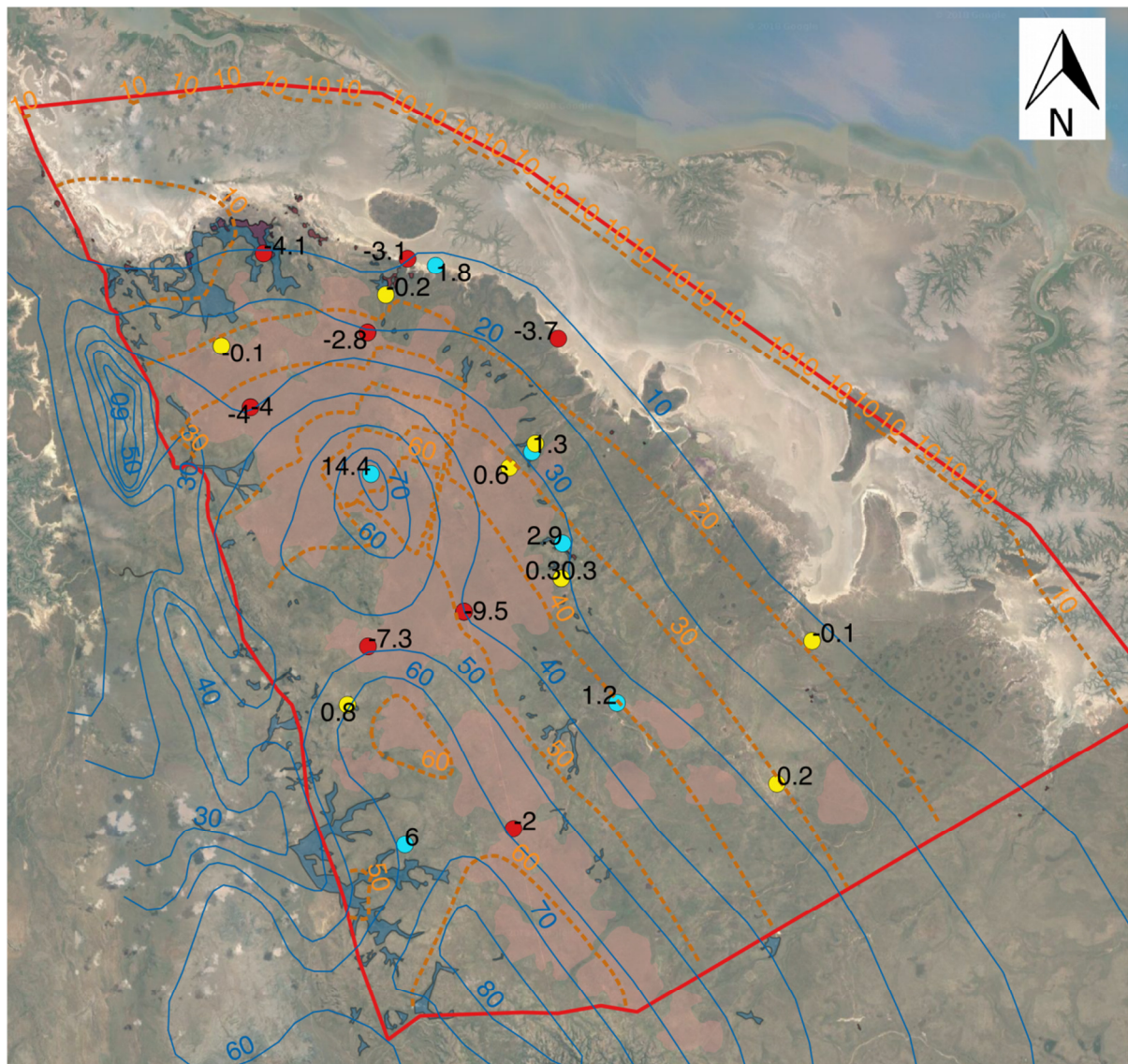
## APPENDIX C. CALIBRATION RESIDUALS FOR CONCEPTUAL MODEL AND CALIBRATED VERSIONS OF THE THREE-DIMENSIONAL MODEL

Observation Point	X	Y	Residual (m)	
			Conceptual Model	Calibrated
13BP01D	473886.6	8333260.7	5.7	-5.1
13BP01I	473886.6	8333260.7	5	-5.9
13BP01S	473886.6	8333260.7	5	-5.9
17BP01I	478993.4	8335027.2	8.9	2.2
17BP01S	478983.9	8335023.1	8.9	2.2
17BP02I	468839.0	8347946.3	2.1	-0.9
17BP02S	468829.8	8347942.3	2.1	-1
17BP03I	469012.2	8340498.6	7	-0.3
17BP04I	462705.7	8344019.1	7	-0.3
17BP04S	462707.3	8344008.2	6.4	2
17BP05I	461179.0	8347241.9	6.3	1.9
17BP05S	461182.2	8347232.5	16.3	0.8
17BP06I	476482.4	8321899.9	10.4	-4.2
17BP07I	468859.9	8331473.3	7.9	2.9
BONAPARTE1 WB2	476256.0	8340826.6	16.9	1.5
BONAPARTE2 WB	467779.1	8328404.9	4.1	2.9
FISHERMANS	472404.0	8351461.6	-1.2	-2.3
NEW ATTACK	470932.2	8351823.9	-1.6	-3
KEMP	478825.6	8347624.7	-1	-2
CLEANSKIN	492122.5	8331754.1	16.2	3.3
HOTPLATE	470795.5	8321055.2	1.4	-0.8
GRANT CREEK	481901.8	8328501.7	5.2	-0.7
WILSON	490280.8	8324255.2	5.8	2.3
Bore Spring Upper	477448.0	8341642.0	4.6	1.2
Bore Spring Lower	477624.0	8342072.0	-3	-3.9
Long Spring Source	463391.0	8352099.0	10.4	4.7
New Spring Source	479055.0	8336839.0	1.1	-0.3



## **APPENDIX D. RESULTS OF ALTERNATIVE MODEL DESIGNS**

The figures presented in this Appendix relate to initial calibration exercises that included bore 17BP03I in the calibration dataset. Inclusion of this bore resulted in an apparent groundwater mound of approximately 71 m AHD in the central part of the model domain. Figures D1 to D4 present the results of alternative conceptual models, which included (a) implementing walls along the mapped fault lines in these locations to investigate the effect of simulating the faults as barriers to flow, and (b) implementation of a zone of higher recharge associated with the higher elevation areas of Cockatoo Sands (DEM elevation > 90 m AHD). Note that there is currently no justification for implementation of such a zone. The mapped extent of the Cockatoo Sands was used as the main basis for higher recharge in these models. This was superseded by revised recharge zones constructed by DPIRD, as described in Section 3.5. The scenarios presented in Figures D1 to D4 were those that provided the best calibration to the dataset that included BP03I prior to removal of this bore from the calibration dataset.



### Legend

- Equipotential - Observed (m AHD)
- - - Equipotential - Modelled (m AHD)
- Target Residuals (m)
- Too High
- Good
- Too Low
- Interpreted Fault
- Model Domain
- Coastline
- Permanent GW Discharge Zone
- Seasonal Seepage Zone

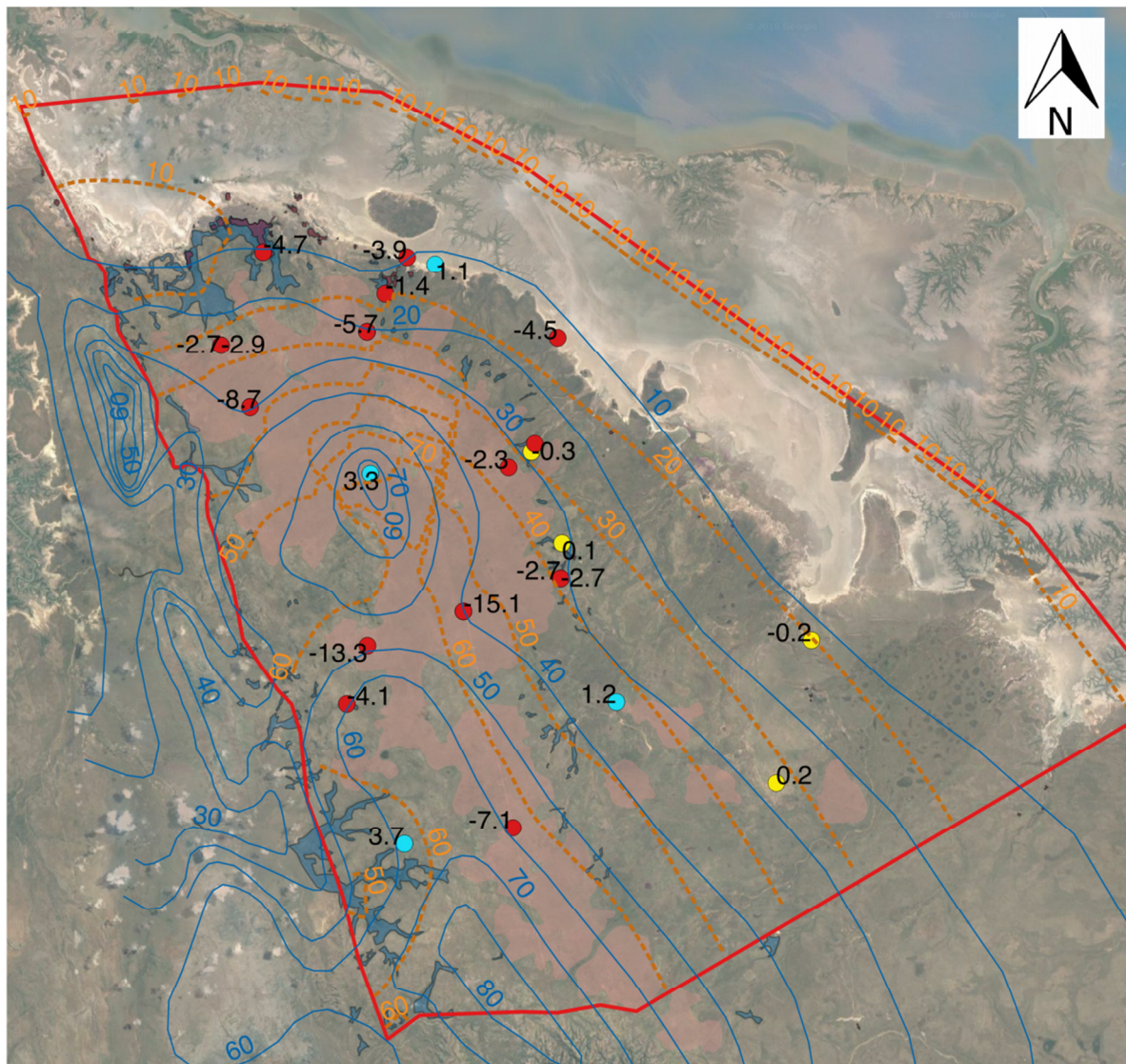
5 0 5 10 15 20 km



Map prepared by N. Harrington  
Innovative Groundwater Solutions Pty Ltd.  
February 2018  
Co-ordinate Reference System: GDA94 Zone 52

**Figure D1. Scenario 14c.1. Cockatoo Sands Recharge = 225 mm/yr. Faults implemented as barriers to flow. SRMSE = 7.6%**





### Legend

- Equipotential - Observed (m AHD)
- - - Equipotential - Modelled (m AHD)
- Target Residuals (m)
- Too High
- Good
- Too Low
- Interpreted Fault
- Model Domain
- Coastline
- Permanent GW Discharge Zone
- Seasonal Seepage Zone

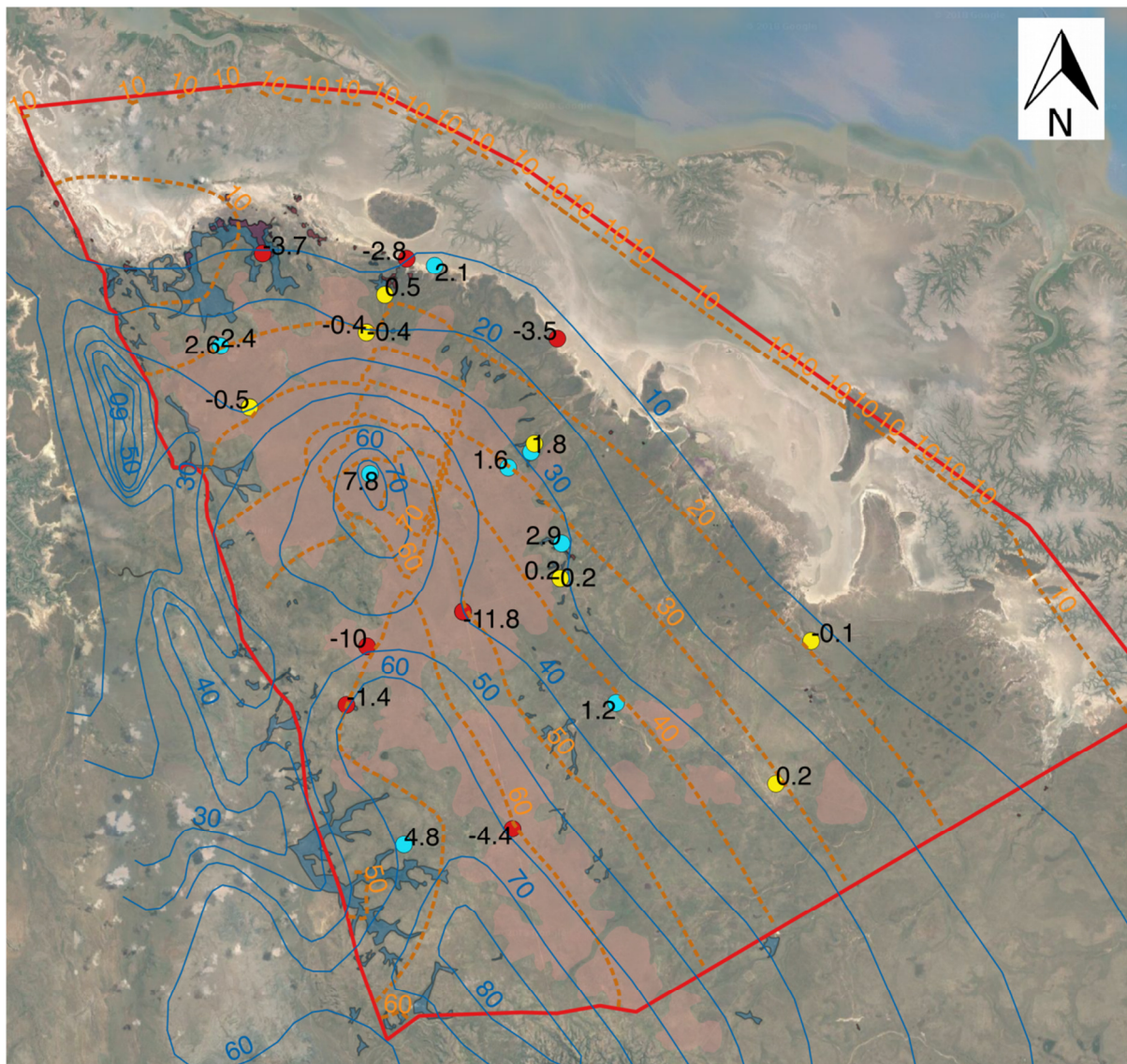
5 0 5 10 15 20 km



Map prepared by N. Harrington  
Innovative Groundwater Solutions Pty Ltd.  
February 2018  
Co-ordinate Reference System: GDA94 Zone 52

**Figure D2. Scenario 14c.2. Cockatoo Sands Recharge = 300 mm/yr. Faults implemented as barriers to flow. SRMSE = 10.5%**





### Legend

- Equipotential - Observed (m AHD)
- - - Equipotential - Modelled (m AHD)
- Target Residuals (m)
- Too High
- Good
- Too Low
- Interpreted Fault
- Model Domain
- Coastline
- Permanent GW Discharge Zone
- Seasonal Seepage Zone

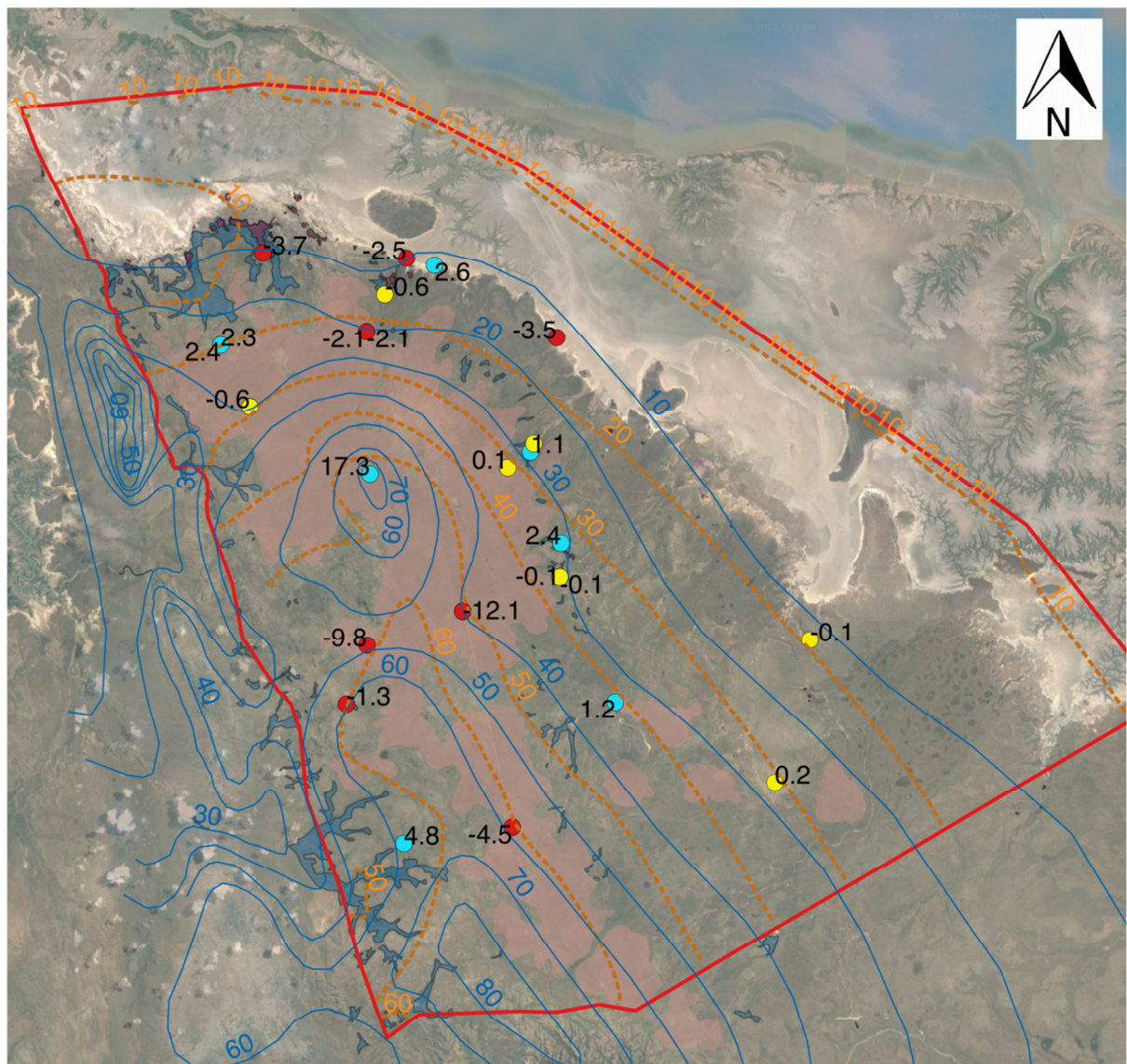
5 0 5 10 15 20 km



Map prepared by N. Harrington  
Innovative Groundwater Solutions Pty Ltd.  
February 2018  
Co-ordinate Reference System: GDA94 Zone 52

**Figure D3. Scenario 14d. High elevation recharge = 350 mm/yr. Other Cockatoo Sands Recharge = 140 mm/yr. Other high R zone = 72 mm/yr. Faults implemented as barriers to flow. SRMSE = 7.7%**





### Legend

- Equipotential - Observed (m AHD)
- - - Equipotential - Modelled (m AHD)
- Target Residuals (m)
- Too High
- Good
- Too Low
- Interpreted Fault
- Model Domain
- Coastline
- Permanent GW Discharge Zone
- Seasonal Seepage Zone

5 0 5 10 15 20 km



Map prepared by N. Harrington  
Innovative Groundwater Solutions Pty Ltd.  
February 2018  
Co-ordinate Reference System: GDA94 Zone 52

**Figure D4. Scenario 14e. High elevation recharge = 350 mm/yr. Other Cockatoo Sands Recharge = 140 mm/yr. Other High R zone = 72 mm/yr. No barriers to flow. SRMSE = 9.1%**

## Appendix G Irrigation development scenario models

### Introduction

A 3D steady-state groundwater model of the Point Spring Sandstone aquifer (Border Creek HU) at Bonaparte Plains was constructed and calibrated by Innovative Groundwater Solutions (IGS 2019).

The model was developed using the MODFLOW-2005 code (Harbaugh 2005) and constructed on a 200 m square grid. Four numerical layers were used to represent the major HUs.

The model domain is bounded to the north and east by the boundary with a groundwater head fixed at 0 mAHD, which controls outflow from the aquifer to the ocean (Figure G1). This boundary assumes aquifer outflow maintains the saltwater interface (SWI) at its current location.

The southern boundary is a no-flow boundary aligned along the Weaber Range in its western third. The remainder of the southern boundary is along an inferred groundwater flow line.

Along the western boundary, IGS used the MODFLOW drain package to simulate aquifer outflow. This was done to account for the aquifer discharge that occurs against the low-permeability Milligans HU, expressed as westward surface flow in creeks that flow across the Milligans HU and through the Ningbing Range.

The model also accounts for the evapotranspiration from the groundwater by vegetation in and surrounding the springs and wetlands fringing the Cockatoo Sands.

Table G1 shows the important components of the water balance for the Border Creek and Keep Inlet HUs at Bonaparte Plains as estimated by the 3D groundwater model (IGS 2019). This represents the status quo and is referred to as the base case. The model calculated that the net outflow to the ocean is 4.4 GL/y.

Table G1: Water balance for the Border Creek and Keep Inlet HUs at Bonaparte Plains as estimated by the groundwater model; base case

Water balance term	Inflow (GL/y)	Outflow (GL/y)	Net outflow (GL/y)
Recharge	69.4	NA	NA
Coastal boundary	146.7	151.1	4.4
Evapotranspiration	NA	64.2	NA
Western boundary	NA	1.1	NA

NA = not applicable



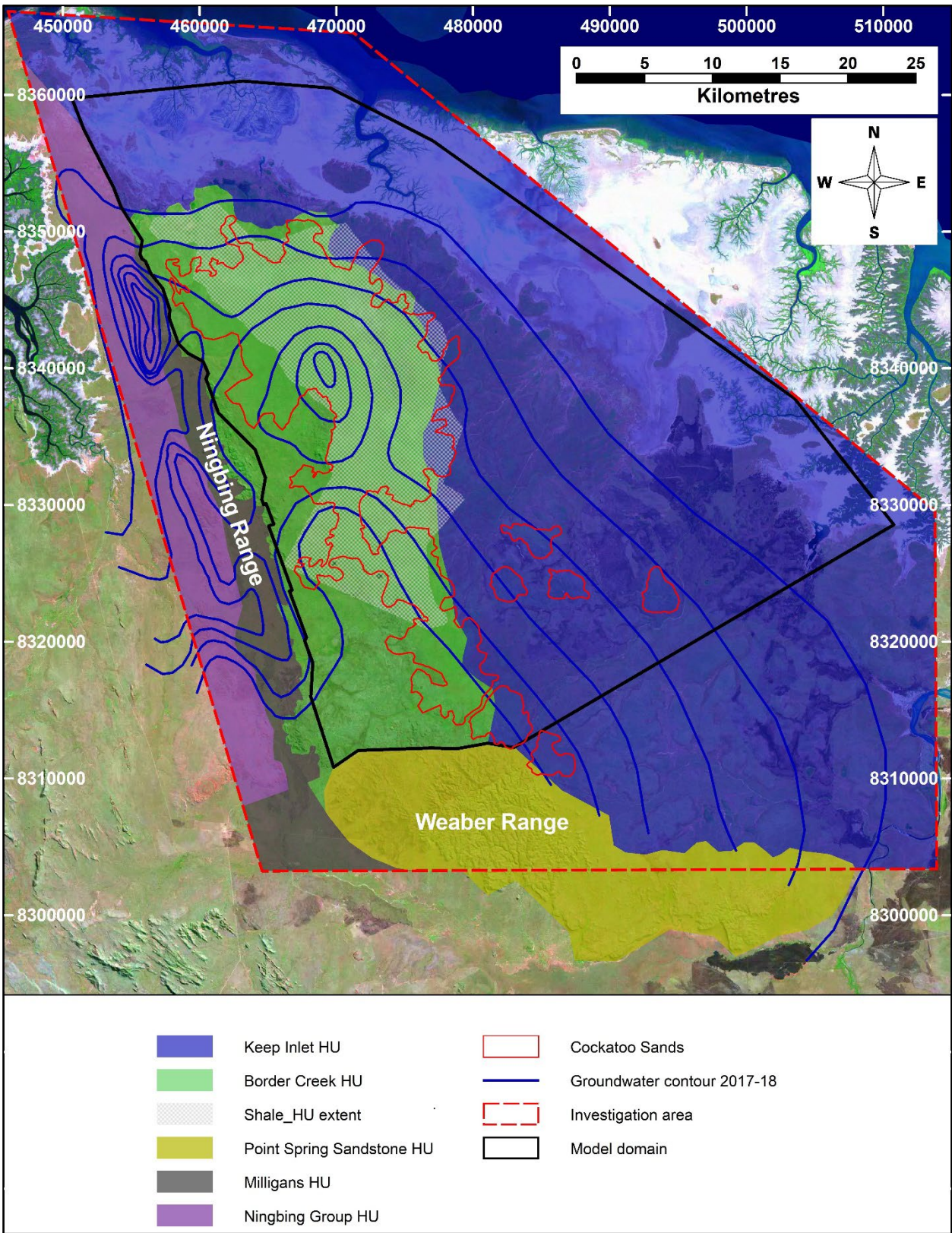


Figure G1: Model domain for the 3D groundwater flow model

This report details the results of scenarios that were run, using the IGS model, to inform the hydrological resource risk assessment for the potential development of dryland and irrigated agriculture at Bonaparte Plains.

The resource risk assessment is required to:

- alert the Commissioner of Soil and Land Conservation of the likely risks to land and water resources from clearing native vegetation at Bonaparte Plains for irrigated and dryland agriculture
- inform prospective proponents of the likely level of investigation into land and water resource impacts that will be required to gain development approval from the relevant state and federal bodies.

To meet these objectives, the model and scenarios chosen are hypothetical and regional. The model is not of such scale and complexity as to be suitable for water allocation planning, support of a water licence application, or for the detailed planning of pumping optimisation that may be required by the proponent of a specific development.

## Methods

The scenarios were modelled using the MODFLOW-2005 code (Harbaugh 2005) used to generate the base case by IGS (2019). Calibrated recharge rates were used; these were determined by IGS and are indicative of the current climate.

In each of the initial 11 scenarios modelled, 2.2 GL/y was pumped for irrigation. This is about 50% of the modelled net ocean outflow from the aquifer. This volume was chosen because it represents the maximum volume likely to be allocated by DWER for an aquifer for which limited hydrogeological data is available (for example, see Department of Water 2010, Appendix C).

### Irrigation-only scenarios

Eleven potential pumping and associated irrigation sites were selected towards the downslope extent of the area of suitable Cockatoo Sands. Downslope sites were selected because groundwater is shallowest at such sites, which minimises the energy costs of pumping. Individual sites were then chosen to be as far as possible from environmentally sensitive wetlands. Depths to groundwater ranged from 14 to 18 m for bore sites 1 to 7. For sites 8 to 11, situated on discrete elevated mounds of Cockatoo Sands overlaying the Border Creek HU (in turn underlain by the Keep Inlet HU), heads ranged between 5 and 30 mBGL.

Figure G2 shows the location of the 11 sites. At each site, the modelled irrigation demand was 1,500 mm/y; applying the annual abstraction of 2.2 GL/y resulted in irrigated areas of 147 ha, which were circular for ease of scenario construction.

Pumping was simulated from the Border Creek HU, within model layers 2 and 4 for most irrigation scenarios. Model layer 1 is unsaturated over most of the model domain. Model layer 3 represents the Shale HU, which has insignificant yield. One-third of the total pumped volume was extracted from layer 2 and two-thirds from layer 4. Exceptions to this arrangement were areas 2 and 7 to 11, where the Shale HU is not present. In these scenarios, pumping was equally distributed between model layers 2 and 4.

The only model parameter that was varied from the IGS (2019) calibrated 3D model was an increase in recharge to 280 mm/y under irrigation sites 1 to 7. Recharge was not increased for irrigation sites 8 to 11 because they are underlain by the low-permeability Keep Inlet HU – return flow to the Border Creek HU would be minimal at those locations.

### **Addition of dryland agriculture scenarios**

Once the modelled results were obtained for the scenarios detailed above, a second round of scenarios was undertaken that incorporated areas of dryland agriculture upslope of sites 1 to 7. The intention was to increase recharge in those areas and hence groundwater levels up gradient of pumping to reduce drawdowns at potentially sensitive wetlands down gradient.

Semicircular dryland agriculture areas of about 1,000 ha were described above each irrigation site (Figure G2). The dryland agricultural areas were roughly aligned on the centre of each irrigation area. Dryland agriculture areas upslope of irrigation sites 2 and 7 were not semicircular to conform to the irregular boundary of the suitable Cockatoo Sands in those locations. Annual recharge under dryland agriculture was assumed to be 280 mm/y, double that of the base case. Dryland agriculture was not modelled for irrigation sites 8 to 11 that are underlain by the low-permeability Keep Inlet HU.

Three additional scenarios were modelled that combined irrigation sites. The first combined irrigation sites 3 and 4 and doubled the area of upslope dryland agriculture to compensate.

In the other scenarios, sites 8, 9 and 10 were irrigated together with areas of dryland agriculture simulated on the suitable Cockatoo Sands upslope of the point at which the low-permeability Keep Inlet HU overlies the Border Creek HU. This configuration was chosen because it allows recharge under the dryland agriculture area upslope of pumping for irrigation. Two areas of dryland agriculture were simulated – one of 3,000 ha and one of 5,000 ha.

Recharge on dryland agriculture areas was 280 mm/y for the 3 additional scenarios. The configurations of irrigation sites and dryland agriculture areas are shown in Figure G3.



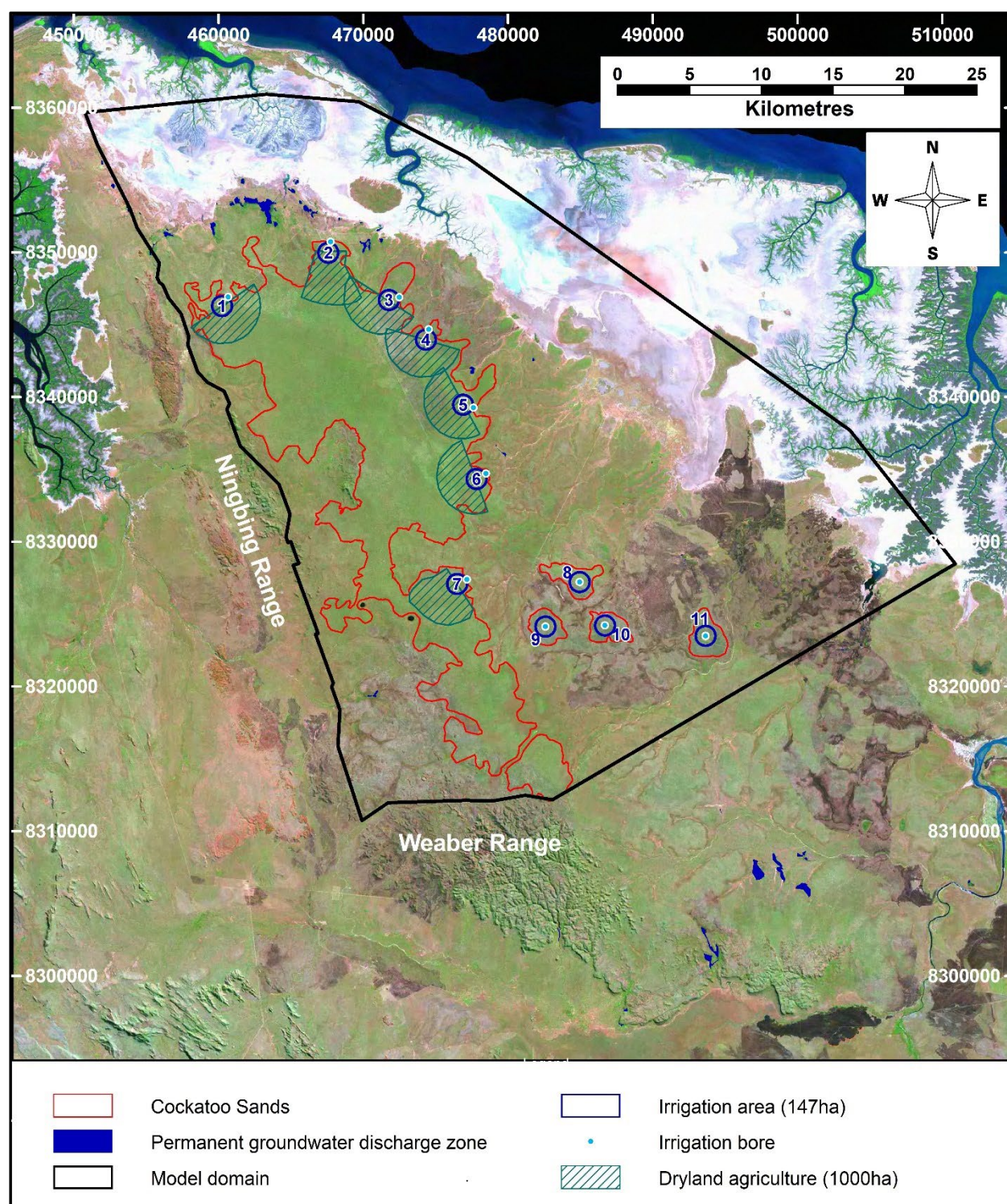


Figure G2: Potential pumping and associated irrigation sites and areas of modelled dryland agriculture



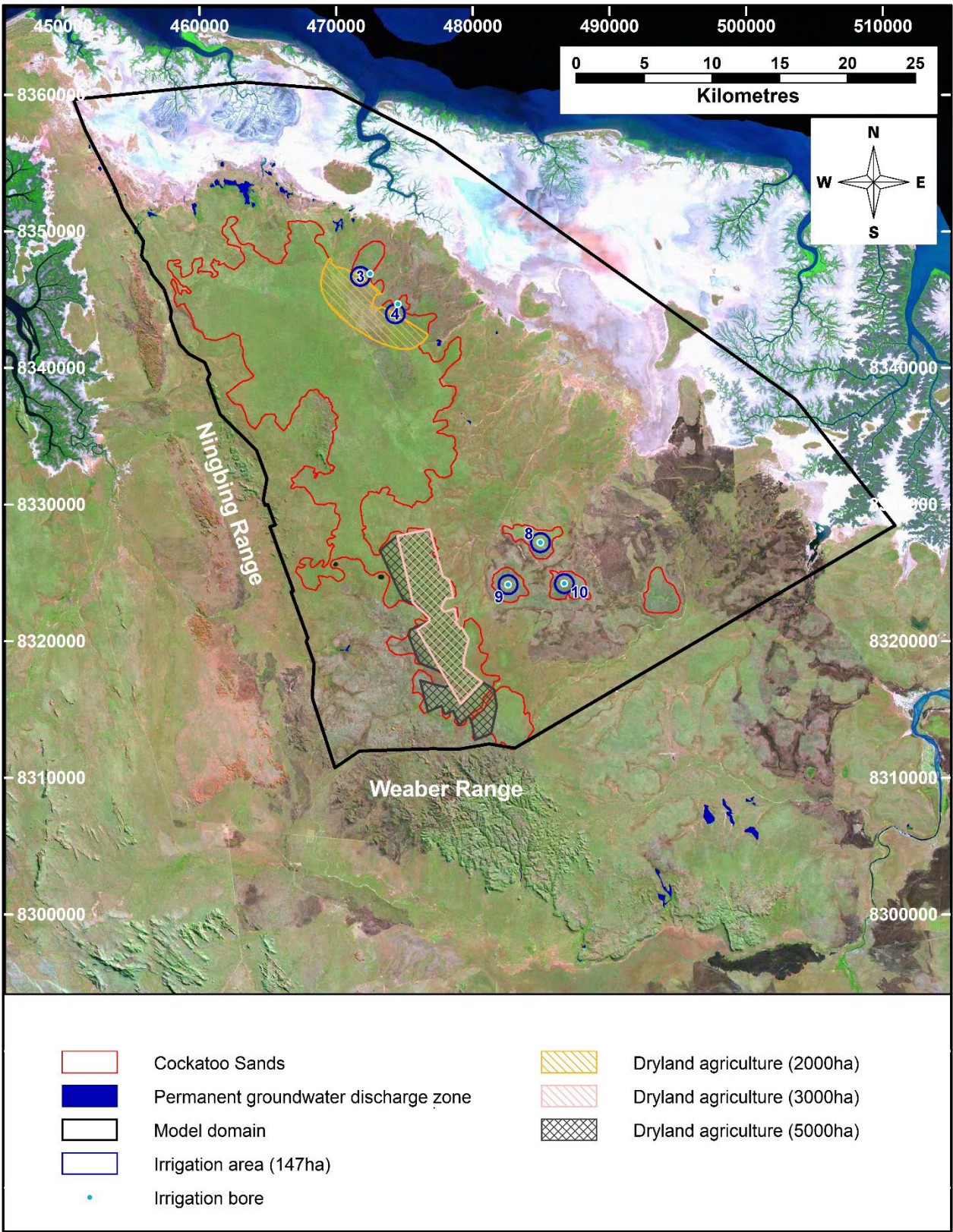


Figure G3: Irrigation scenarios that include multiple sites with large areas of dryland agriculture

## Results

### Irrigation-only scenarios

The important water balance terms for each irrigation area were compared to the base case values in Table G2. The table shows that:

- total recharge increased by about 0.2 GL/y for scenarios 1 to 7 – this increase is trivial in relation to the overall water balance of the aquifer
- recharge remained unchanged for scenarios 8 to 11 because of the influence of the Keep Inlet HU
- total evapotranspiration from the aquifer decreased by about 2% in all irrigation scenarios
- net outflow to the ocean was the component of the water balance most affected, in relative terms – it reduced by between 0.39 GL/y (–9%) and 1.00 GL/y (–24%)
- changes in outflow through the western boundary were small in absolute terms ( $\leq 0.10$  GL/y) but significant in relation to the base case; up to a 10% reduction.

Table G2: Predicted changes to water balance components for irrigation of 2.2 GL/y over 147 ha on each of 11 sites

Site	Recharge		Evapotranspiration		Western boundary		Coastal boundary		Bores
	Base +/- (GL/y)	% base	Base +/- (GL/y)	% base	Base +/- (GL/y)	% base	Base +/- (GL/y)	% base	Base +/- (GL/y)
1	+0.23	100	–1.40	98	–0.02	98	–0.39	91	+2.2
2	+0.22	100	–1.17	98	–0.01	99	–0.72	83	+2.2
3	+0.21	100	–1.02	98	–0.02	97	–0.89	79	+2.2
4	+0.23	100	–0.99	98	–0.03	97	–0.85	79	+2.2
5	+0.22	100	–1.09	98	–0.05	95	–0.71	83	+2.2
6	+0.21	100	–1.26	98	–0.06	93	–0.57	86	+2.2
7	+0.21	100	–1.31	98	–0.10	90	–0.50	88	+2.2
8	0.00	100	–1.32	98	–0.06	94	–0.71	83	+2.2
9	0.00	100	–1.41	98	–0.07	92	–0.64	85	+2.2
10	0.00	100	–1.29	98	–0.05	94	–0.77	82	+2.2
11	0.00	100	–1.10	98	–0.03	97	–1.00	76	+2.2

Note: Changes relative to the base case are expressed as a variation (+/–) from the base case (GL/y) and as a percentage of the base case value.

Maps showing contours of changes in groundwater level for the Border Creek HU at the 11 sites are shown in Figure G4 to Figure G14. Changes in groundwater level are presented rather than drawdowns because increases in groundwater levels were predicted in later scenarios and the concept of negative drawdown (increase in groundwater level) is counterintuitive.

As the 3D groundwater model is run in steady state, the predicted reductions in groundwater levels do not represent the maximum reductions to be expected during pumping; rather, they may be inferred to represent the long-term average change in



groundwater levels resulting from all changes to the aquifer water balance. Contours are presented with a uniform colour scale, in 0.5 m increments starting from  $\pm 0.5$  m.

Figure G4 shows the groundwater level reductions predicted for irrigating 147 ha at 2.2 GL/y at site 1. The  $-0.5$  m contour extends to the model's western boundary indicating that groundwater and surface water flows across that boundary would be impacted. Table G2 indicates that flow across the boundary is reduced to 98% of that predicted in the base case; however, flow across this boundary is impacted to a higher degree in some of the other irrigation-only scenarios.

Figure G5 shows that the extent of the  $-0.5$  m contour for irrigation at site 2 is considerably less than for site 1; however, it does extend to include a small wetland about 1.7 km north of the irrigation area.

Figure G6 and Figure G7 show that the  $-0.5$  m contours predicted for scenarios with irrigation at sites 3 and 4 do not extend to any of the mapped wetlands despite the total area impacted being greater than for irrigation on sites 1 and 2.

The extent of the  $-0.5$  m contour for scenario 5 (Figure G8) is considerably larger than for the earlier scenarios and reaches 2 permanent wetlands. Irrigation at site 6 also impacts a large area (Figure G9), including a wetland north-east of the pumping site.

Figure G10 to Figure G14 show the effects of pumping and irrigation at sites 7 to 11. In all cases the  $-0.5$  m contour extends to the model's southern boundary. The southern boundary is no flow and was chosen on an inferred groundwater flow line over two-thirds of its length. That the groundwater level reductions reach this boundary invalidates these scenarios because groundwater that would flow to the north-west towards the pumping is artificially restricted. Therefore, even though the maps may broadly indicate what might be expected from pumping and irrigation on these areas, the water balance figures reported in Table G2 should not be relied upon.

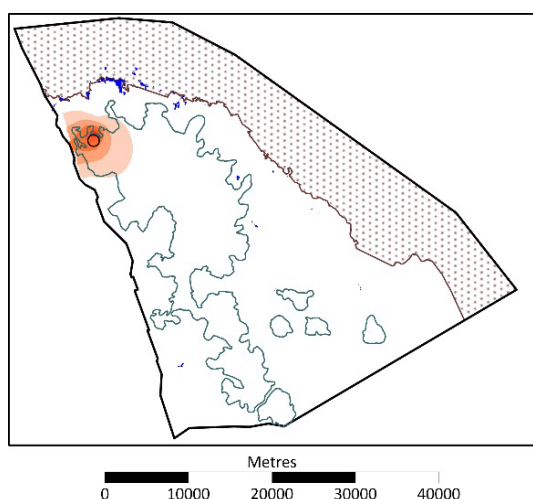


Figure G4: Contours of change in groundwater level for irrigation of 147 ha with 2.2 GL/y at site 1

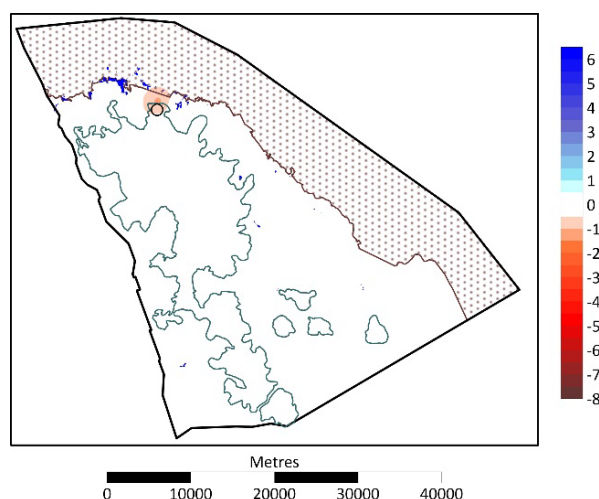


Figure G5: Contours of change in groundwater level for irrigation of 147 ha with 2.2 GL/y at site 2

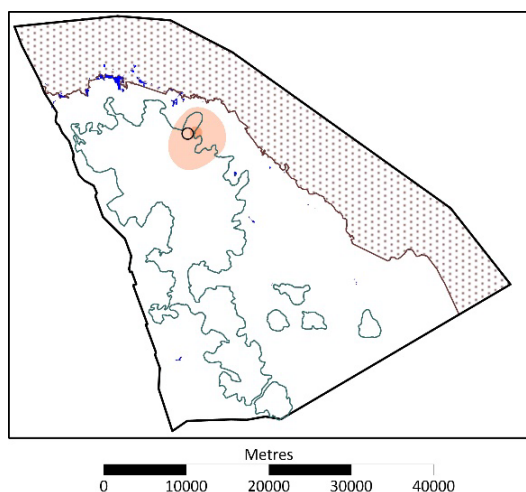


Figure G6: Contours of change in groundwater level for irrigation of 147 ha with 2.2 GL/y at site 3

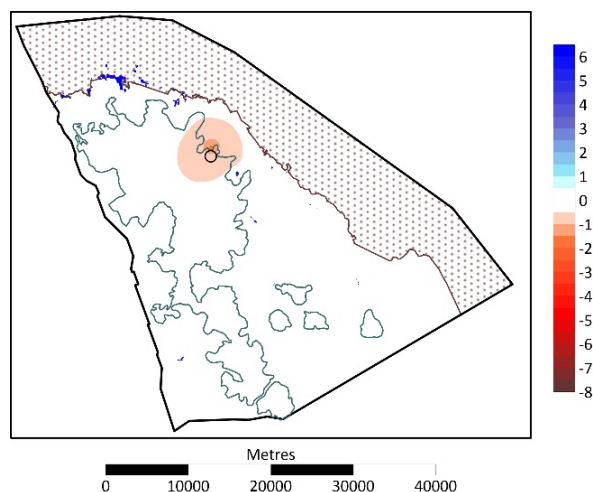


Figure G7: Contours of change in groundwater level for irrigation of 147 ha with 2.2 GL/y at site 4

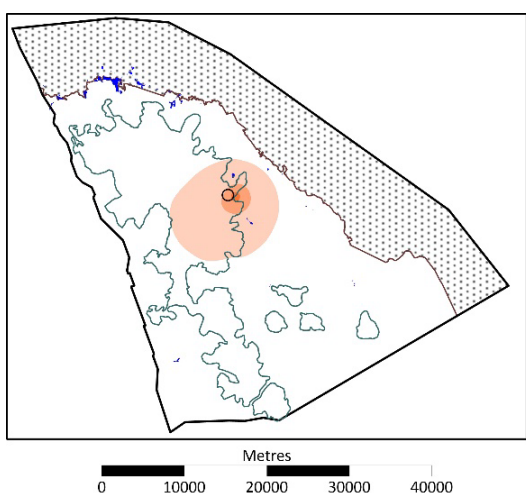


Figure G8: Contours of change in groundwater level for irrigation of 147 ha with 2.2 GL/y at site 5

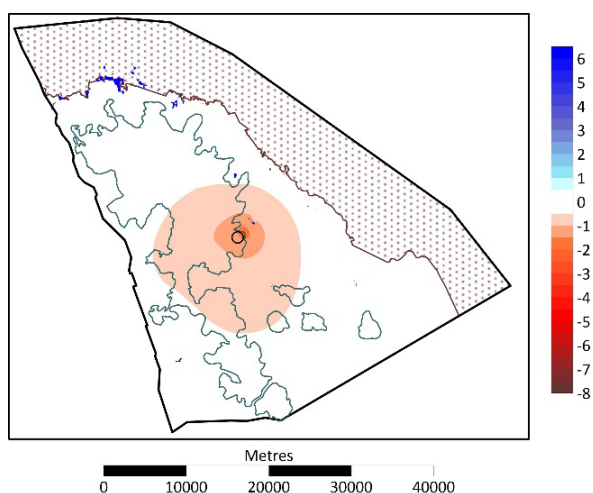


Figure G9: Contours of change in groundwater level for irrigation of 147 ha with 2.2 GL/y at site 6

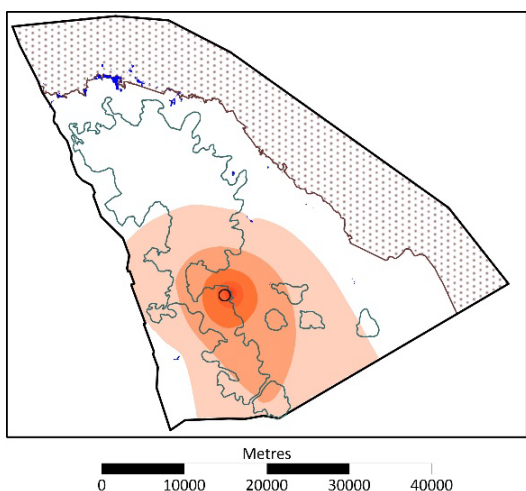


Figure G10: Contours of change in groundwater level for irrigation of 147 ha with 2.2 GL/y at site 7

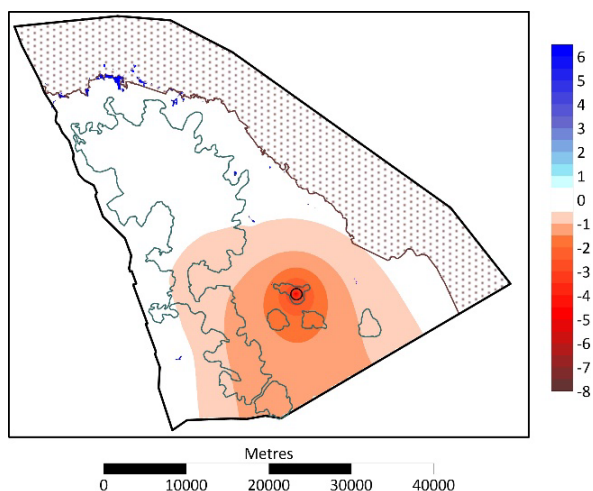


Figure G11: Contours of change in groundwater level for irrigation of 147 ha with 2.2 GL/y at site 8

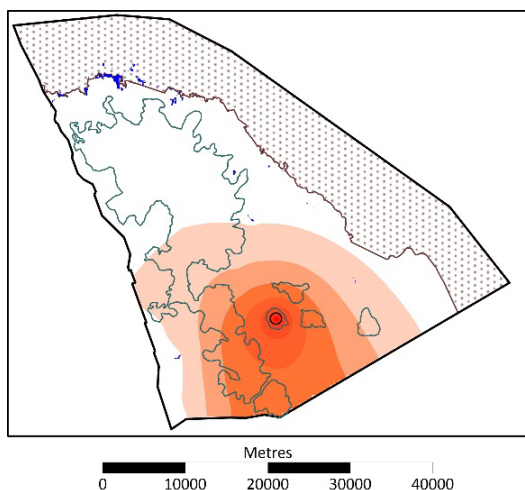


Figure G12: Contours of change in groundwater level for irrigation of 147 ha with 2.2 GL/y at site 9

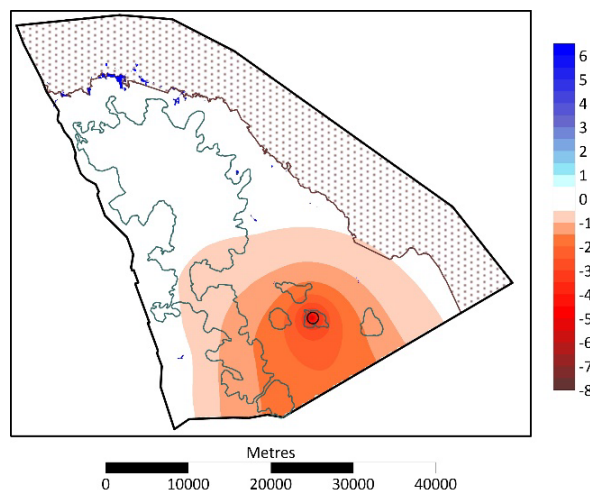


Figure G13: Contours of change in groundwater level for irrigation of 147 ha with 2.2 GL/y at site 10

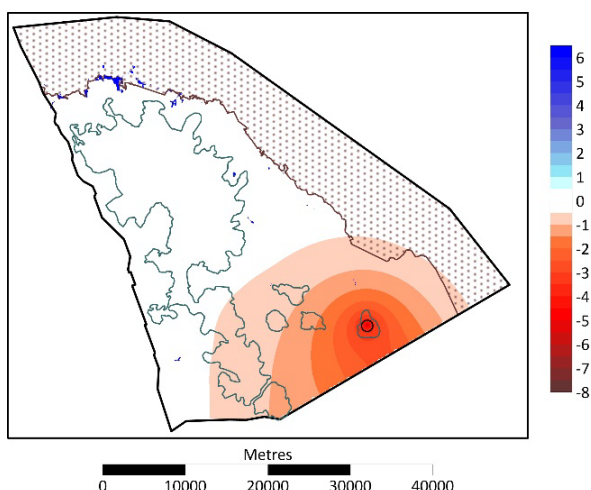


Figure G14: Contours of change in groundwater level for irrigation of 147 ha with 2.2 GL/y at site 11

### Irrigation plus dryland agriculture scenarios

The important water balance terms for scenarios that included areas of dryland agriculture as well as irrigation at single sites were compared to the base case values in Table G3. The table shows that:

- total recharge increased by 2% for all scenarios
- total evapotranspiration from the aquifer varied from 99% to 100% of the base case value
- net outflow to the ocean was again the component of the water balance most affected in relative terms – it reduced by between 0.12 GL/y (–3%) and 0.33 GL/y (–8%)
- changes in outflow through the western boundary were small in absolute terms ( $\pm 0.01$  GL/y) and relative to the base case;  $\pm 1\%$ .

A comparison of changes to the water balance for irrigation on individual areas, with and without dryland agriculture, is presented in Table G4; changes are expressed

relative to the base case values. Changes in recharge and evapotranspiration are small and show little variation with spatial location.

Changes to outflow through the western boundary are smaller ( $\pm 1\%$ ) when areas of dryland agriculture are included. Without dryland agriculture, changes were  $-1\%$  to  $-10\%$ . There is also much less variation in water balance changes with spatial location when dryland agriculture was included in the scenarios. Changes to net coastal outflow are similar – without dryland agriculture, reductions range from  $-9\%$  to  $-21\%$ ; with areas of dryland agriculture included, reductions in net coastal outflow range from  $-3\%$  to  $-8\%$ .

Maps showing contours of modelled changes in groundwater levels for scenarios with irrigation on sites 1 to 7 and including areas of dryland agriculture for the Border Creek HU are shown in Figure G15 to Figure G21. In all scenarios, other than irrigation at site 6 (Figure G20), the addition of 1,000 ha of dryland agriculture resulted in no wetlands being impacted by the  $-0.5$  m change contour. There is also an area of increased groundwater levels within and/or up slope of the dryland agriculture in all cases except the site 6 scenario. Maximum increases in groundwater level are less than 1 m, other than for dryland agriculture at sites 3 and 4 (Figure G17, Figure G18).

Comparison of Figure G20 with Figure G9, for site 6, shows that the area within the  $-0.5$  m contour has been reduced to about 3% of the area impacted for the scenario without dryland agriculture. However, the  $-0.5$  m change contour still extends beyond the wetland 1.7 km north-east of the irrigated area.

The water balance changes for the 3 scenarios that combine irrigation on multiple sites with larger areas of dryland agriculture are shown in Table G5. The areas under dryland agriculture range from 2,000 to 5,000 ha, resulting in 5–11% increases in recharge relative to the base case. Total evapotranspiration is reduced except in the scenario with 5,000 ha of dryland agriculture, where it increased by 2%.

Changes in outflow through the western boundary were close to zero for the scenarios with 2,000 and 3,000 ha of dryland agriculture but increased by 11% for the scenario with 5,000 ha of dryland agriculture. Net outflow to the ocean decreased by 10–27%.

Table G3: Predicted changes to water balance components for irrigation of 2.2 GL/y over 147 ha plus 1,000 ha of dryland agriculture on single areas

Site	Recharge		Evapotranspiration		Western boundary		Coastal boundary		Bores
	Base +/- (GL/y)	% base	Base +/- (GL/y)	% base	Base +/- (GL/y)	% base	Base +/- (GL/y)	% base	Base +/- (GL/y)
1	+1.49	102	-0.40	99	0.00	100	-0.12	97	+2.2
2	+1.61	102	-0.25	100	+0.01	101	-0.25	94	+2.2
3	+1.59	102	-0.16	100	0.00	99	-0.33	92	+2.2
4	+1.63	102	-0.23	100	0.00	100	-0.29	93	+2.2
5	+1.60	102	-0.25	100	-0.01	99	-0.21	95	+2.2
6	+1.53	102	-0.34	99	-0.01	99	-0.18	96	+2.2
7	+1.62	102	-0.39	99	-0.01	99	-0.14	97	+2.2

Note: Changes relative to the base case are expressed as a variation (+/-) from the base case (GL/y) and as a percentage of the base case value.

Table G4: Relative changes to water balance components for irrigation of 2.2 GL/y over 147 ha with and without 1,000 ha of dryland agriculture on selected areas

Site	Recharge		Evapotranspiration		Western boundary		Coastal boundary	
	No dryland	Dryland	No dryland	Dryland	No dryland	Dryland	No dryland	Dryland
1	100%	102%	98%	99%	98%	100%	91%	97%
2	100%	102%	98%	100%	99%	101%	83%	94%
3	100%	102%	98%	100%	97%	99%	79%	92%
4	100%	102%	98%	100%	97%	100%	79%	93%
5	100%	102%	98%	100%	95%	99%	83%	95%
6	100%	102%	98%	99%	93%	99%	86%	96%
7	100%	102%	98%	99%	90%	99%	88%	97%

Maps of changes in groundwater levels for these scenarios are shown in Figure G22 to Figure G24. Figure G22 shows that simultaneous irrigation of sites 3 and 4 at 2.2 GL/y each could be achieved without impacting wetlands with the addition of a 2,000-ha area of dryland agriculture.

Figure G23 and Figure G24 show the watertable impacts of irrigation at sites 8, 9 and 10 at 2.2 GL/y supplemented with 3,000 or 5,000 ha of dryland agriculture. Reductions in groundwater levels reach the southern, no-flow boundary in both cases, invalidating the water balance numbers reported in Table G5. For the scenario including 5,000 ha of dryland agriculture, increases in groundwater levels exceed 5.5 m and the +0.5 m contour reaches the model's western boundary, significantly increasing aquifer outflow across that boundary (Table G5).

Table G5: Predicted changes to water balance components for irrigation of 2.2 GL/y over 147 ha on multiple sites plus dryland agriculture of varying extent

Site*	Recharge		Evapotranspiration		Western boundary		Coastal boundary		Bores
	Base +/- (GL/y)	% base	Base +/- (GL/y)	% base	Base +/- (GL/y)	% base	Base +/- (GL/y)	% base	Base +/- (GL/y)
3 and 4 (2,000 ha)	+3.27	105%	-0.31	100%	-0.01	99%	-0.67	84%	+4.4
8, 9 and 10 (3,000 ha)	+4.24	106%	-1.10	98%	0.00	100%	-1.13	73%	+6.6
8, 9 and 10 (5,000 ha)	+7.36	111%	+1.15	102%	+0.11	111%	-0.41	90%	+6.6

\* The area of dryland agriculture is shown in parentheses in column 1.

Note: Changes relative to the base case are expressed as a variation (+/-) from the base case (GL/y) and as a percentage of the base case value.



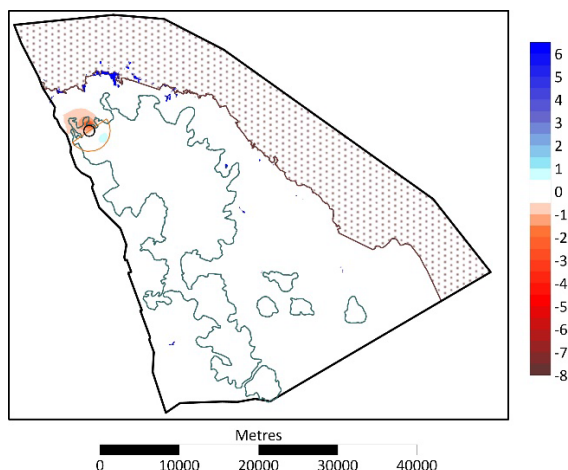


Figure G15: Contours of change in groundwater level for irrigation of 147 ha with 2.2 GL/y plus 1,000 ha of dryland agriculture at site 1

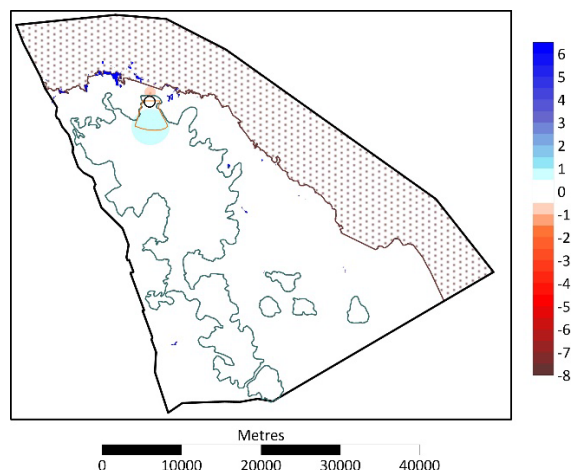


Figure G16: Contours of change in groundwater level for irrigation of 147 ha with 2.2 GL/y plus 1,000 ha of dryland agriculture at site 2

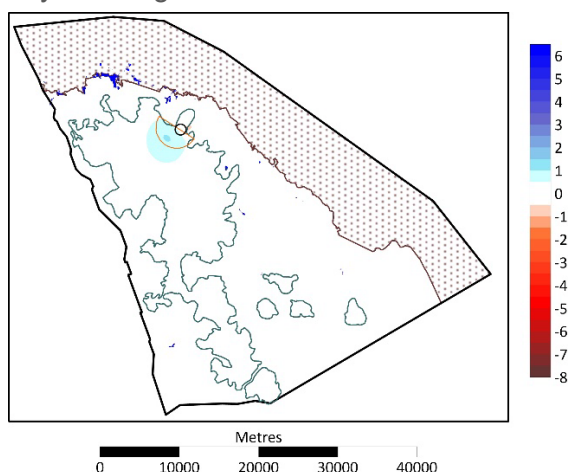


Figure G17: Contours of change in groundwater level for irrigation of 147 ha with 2.2 GL/y plus 1,000 ha of dryland agriculture at site 3

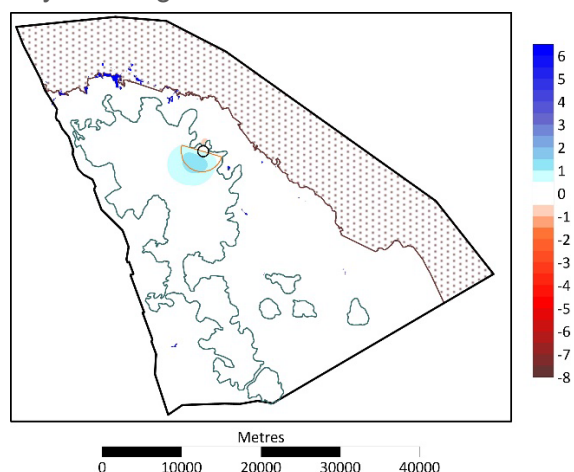


Figure G18: Contours of change in groundwater level for irrigation of 147 ha with 2.2 GL/y plus 1,000 ha of dryland agriculture at site 4

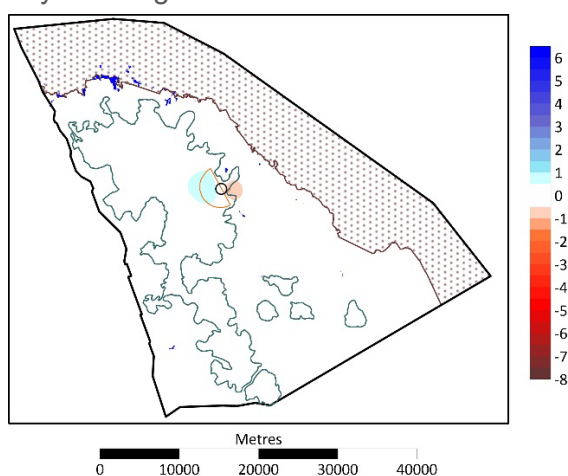


Figure G19: Contours of change in groundwater level for irrigation of 147 ha with 2.2 GL/y plus 1,000 ha of dryland agriculture at site 5

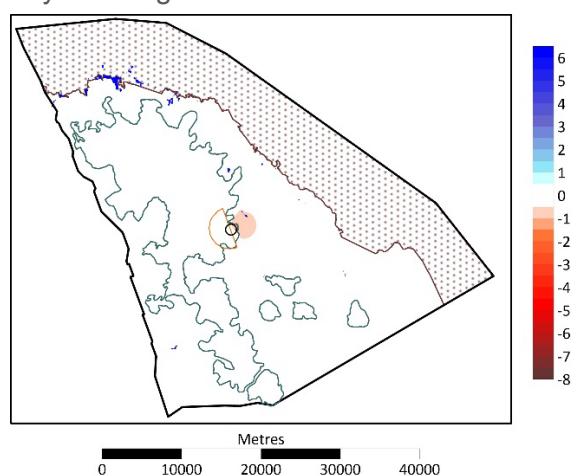


Figure G20: Contours of change in groundwater level for irrigation of 147 ha with 2.2 GL/y plus 1,000 ha of dryland agriculture at site 6

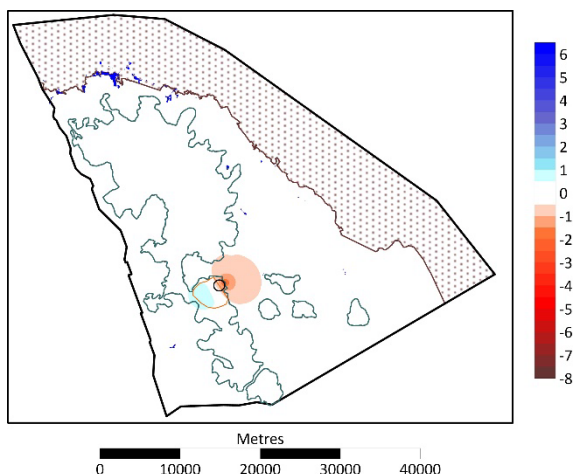


Figure G21: Contours of change in groundwater level for irrigation of 147 ha with 2.2 GL/y plus 1,000 ha of dryland agriculture at site 7

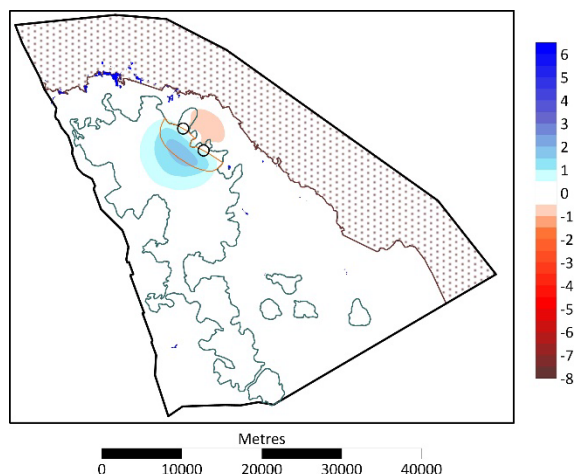


Figure G22: Contours of change in groundwater level for irrigation of 147 ha with 2.2 GL/y at sites 3 and 4 plus 2,000 ha of dryland agriculture

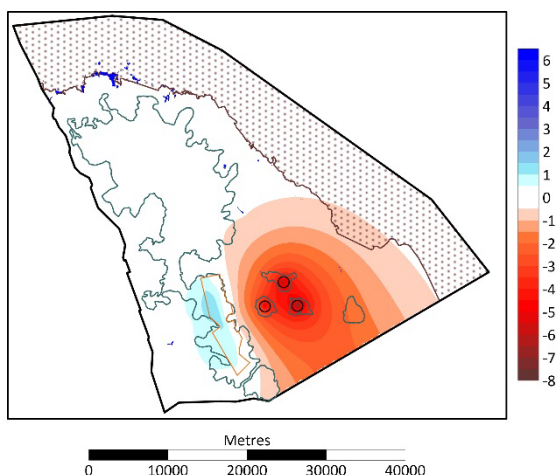


Figure G23: Contours of change in groundwater level for irrigation of 147 ha with 2.2 GL/y at sites 8, 9 and 10 plus 3,000 ha of dryland agriculture

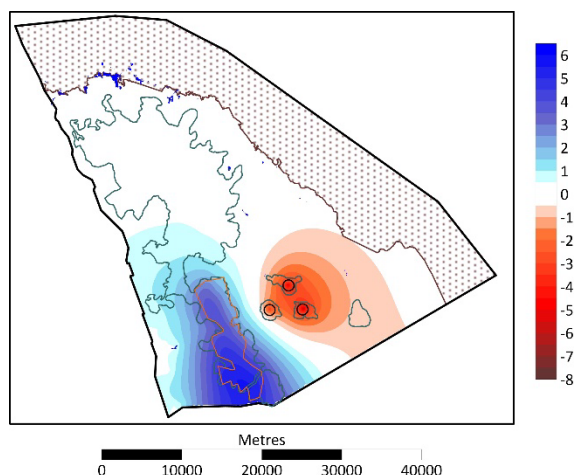


Figure G24: Contours of change in groundwater level for irrigation of 147 ha with 2.2 GL/y at sites 8, 9 and 10 plus 5,000 ha of dryland agriculture

## Discussion

### Recharge under irrigated and dryland agricultural areas

Recharge under the irrigated areas and areas cleared for dryland agriculture was modelled at 280 mm/y. The only published experimental findings we could locate that compared the water balance under perennial grasses and tropical woodland on a similar soil type and climate to Bonaparte Plains was a study carried out in the Upper Burdekin catchment in north Queensland (Williams et al. 1997). This study used SWIM (Soil and Water Integrated Model; Krysanova and Wechsung 2000) to estimate the water balance components from the results of water balance monitoring carried out for adjacent woodland and grassland sites over a 185-day period. Williams et al. (1997) determined that deep drainage past 0.36 m depth under perennial grasses was about twice that under native woodland in the Upper Burdekin catchment. Therefore, recharge

under irrigated and cleared areas for the Bonaparte Plains irrigation scenarios was set at 280 mm/y – twice the value assigned to native vegetation in the calibrated 3D model (IGS 2019).

Under irrigated areas, we should assume a dense vegetation cover with a leaf area greater than that of a perennial grass grown under dryland conditions. This would lead to higher evaporation from the irrigated vegetation. Irrigation bypass still needs to be considered so the simplest assumption is to apply the same recharge rate to both dryland and irrigated areas.

### **Irrigation-only scenarios**

Initial irrigation scenarios were based on the annual abstraction for irrigation at any point of 2.2 GL/y. This is 50% of the net annual ocean outflow from the Border Creek HU of 4.4 GL/y (Table G1). We then assumed an annual irrigation water demand of 1,500 mm/y; the abstraction rate of 2.2 GL/y applied at 1,500 mm/y results in an irrigated area of about 147 ha.

The relatively high irrigation rate provided a conservative estimate of the area irrigated, which is appropriate given the hypothetical nature of the scenarios. The type of crop likely to be grown and therefore its specific water requirement is unknown. The irrigated areas modelled were circular for ease of scenario construction. Circular irrigation areas would use a centre pivot irrigation system, although the size of the area (147 ha) is larger than would normally be used in practice for an efficient irrigation system.

Table G2 shows that irrigation at sites 5 and 6 resulted in the most significant reductions in aquifer outflow across the model's western boundary other than sites 7 and 9, for which groundwater level reductions reached the model's western and southern boundaries. The reductions in flow across the boundary were –5% relative to the base case for area 5 and –7% for site 6; for comparison, the reduction for site 1, in which the pumped bore is only 3.3 km from the model boundary, was 2%. Figure G8 and Figure G9 also show that the spatial extent of the –0.5 m change contour was greater for irrigation at sites 5 and 6 than for all other scenarios other than those for which groundwater level reductions reached the model's southern boundary.

Figure G25 shows the saturated thickness of the Border Creek HU above the Shale HU for the base case. The figure goes some way to explaining why the impact of pumping for irrigation at sites 5 and 6 is significantly greater than for sites 1 to 4. There are large areas up gradient of sites 5 and 6 of limited saturation above the shale, and there is also an area east of site 5 where the whole profile above the shale is unsaturated. Limited saturation above the shale will restrict groundwater flow in model layer 2, thus increasing the area over which head reductions will spread and contribute to lower heads at the western boundary. The figure also explains why the area of groundwater reduction is so extensive for scenarios for irrigation at sites 7 to 11.

The small, saturated thickness of the Border Creek HU above the shale in the area up slope of sites 5 and 6 also explains why the addition of areas of dryland agriculture at these locations causes significant reductions in the areal extent of the –0.5 m contour shown in Figure G19 and Figure G20. The thin saturated thickness in this area also explains the increase in aquifer outflow through the model's western boundary relative to irrigation-only scenarios shown in Table G4. Increased recharge maintains saturation

above the shale (in layer 2), increasing aquifer flow to the west while reducing drawdowns to the east.

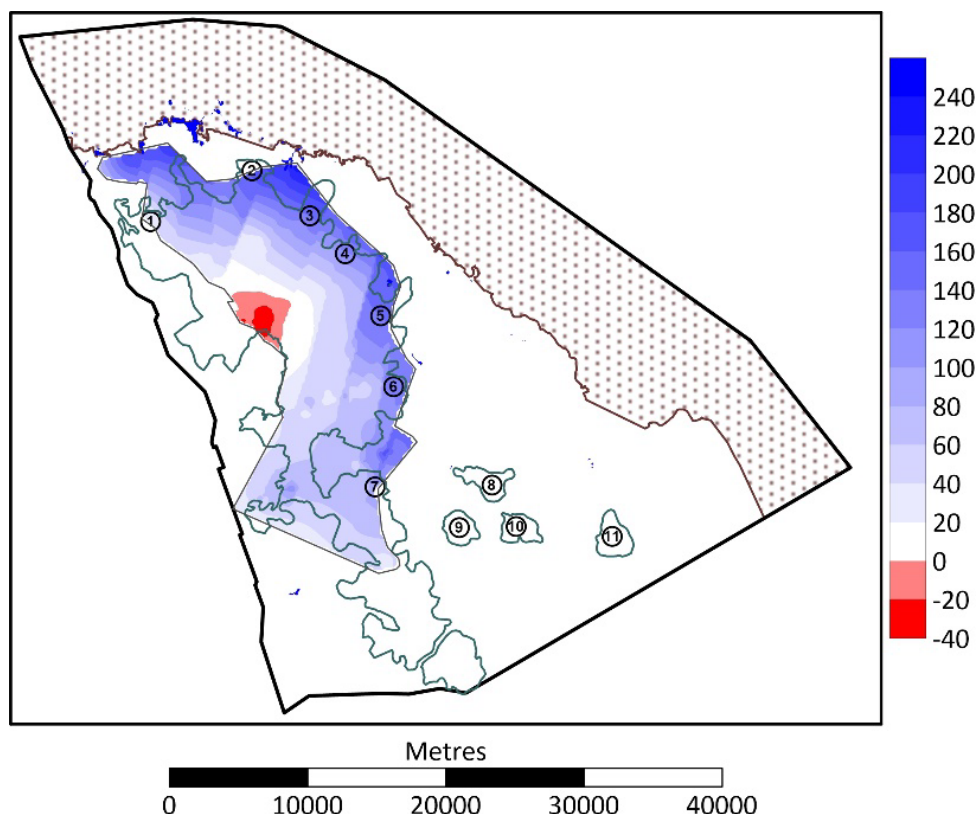


Figure G25: Border Creek HU saturated thickness above shale

Two main factors contribute to the large and widespread groundwater level reductions for scenarios depicting irrigation at sites 7 to 11:

- the limited saturation of the Border Creek HU above the shale layer, as discussed above
- the lack of direct recharge to the Border Creek HU under areas 8 to 11 because of the presence of the Keep Inlet HU.

Therefore, even though the areas impacted by groundwater level reductions intersect the southern no-flow boundary, invalidating the scenario results, the outcome of large, widespread drawdowns for these scenarios is a valid result.

The scenario results for irrigation of individual sites show that sites 3 (Figure G6) and 4 (Figure G7) in the central portion of the eastern boundary of the Cockatoo Sands have the best prospects because they are:

- within areas of shallow groundwater and therefore would have low pumping costs
- down gradient of the widest expanse of Cockatoo Sands through which the aquifer is recharged
- in areas with significant depths of saturation above the shale
- furthest from potentially sensitive wetlands.

## **Irrigation and dryland scenarios**

Modelling shows that only small areas are available for irrigation (based on 2.2 GL/y) compared to the area of suitable Cockatoo Sands at Bonaparte Plains. Irrigation potential is limited due to the proximity of potentially sensitive wetlands and the need to maintain aquifer outflow across both the western and coastal boundaries.

Scenarios were run for sites 1 to 7; these scenarios included areas of dryland agriculture as a mechanism to increase aquifer recharge up slope of irrigated areas. It was expected that increasing recharge up slope of irrigated areas would minimise drawdown impacts on wetlands and possibly increase pumping volumes and therefore the area available for irrigation.

The introduction of 1,000 ha areas of dryland agriculture up slope of irrigated areas was very effective at mitigating groundwater level reductions at potentially sensitive wetlands. The impact was most notable at sites 5, 6 and 7, which overlie areas of limited saturation above the shale (Figure G25). Groundwater level reductions at wetlands were eliminated in all scenarios run with dryland agriculture, except for site 6 (Figure G20) where the -0.5 m contour extended to a wetland but not much beyond it.

The addition of 1,000 ha of dryland agriculture resulted in small groundwater mounds for irrigated areas other than site 6. However, increases in groundwater levels were less than 1.5 m in all cases.

Several scenarios were run in which an area of dryland agriculture of more than 1,000 ha was located up slope of multiple irrigation sites. The most prospective of these was the scenario for sites 3 and 4 with 2,000 ha of dryland agriculture. Figure G22 shows that the -0.5 m contour did not approach any wetlands and that a significant groundwater mound was generated up slope. Changes in groundwater level ranged from +1.5 to -1.1 m. Table G5 shows that aquifer outflow to the west reduced by only 1% but outflow to the ocean was reduced by 16%. These results indicate that the strategy may be successful in maximising aquifer yield and the area irrigated; however, the relatively large decrease in outflow to the coast may be of concern as the SWI is assumed (but not confirmed) to be at or near the coast.

The other scenarios in which multiple irrigation areas were combined with a large area of dryland agriculture involved sites 8, 9, and 10 (Figure G23 and Figure G24). The results of these scenarios suggest that, even with the inclusion of dryland agriculture, the southern portion of the Cockatoo Sands is less prospective for irrigated agriculture than the north. Even with 5,000 ha of dryland agriculture, which generated an extensive groundwater mound of more than 5.5 m, head reductions down gradient still exceeded 6 m. Aquifer outflow to the west also increased by 11%, which may produce unexpected environmental consequences.



## Conclusion

The scenarios presented here suggest that the total area available for irrigated agriculture is several hundred hectares, only a tiny proportion of the 35,000 ha of suitable Cockatoo Sands at Bonaparte Plains.

We assumed that the annual allocation limit for the Border Creek HU would be 2.2 GL/y, some 50% of the net ocean outflow determined by the water balance model (IGS 2019). On this basis, the total irrigation area would be limited to about 147 ha. Despite the relatively small areas of irrigation modelled, suitable locations were limited by the need to minimise depth to groundwater for economic reasons and the potential drawdown impacts on wetlands fringing the Cockatoo Sands.

Scenarios, which included 1,000 ha areas of dryland agriculture up slope of irrigated areas, demonstrated that this strategy could successfully minimise the drawdown impacts on wetlands.

In some areas it may be possible to double the volume of water, and therefore the area irrigated, by increasing the area of dryland agriculture to 2,000 ha. Scenarios in which the irrigated area was further increased, together with an increase in the area of dryland agriculture, were not attempted. It is uncertain whether abstraction exceeding 2.2 GL/y would be permitted by DWER.

The shale layer had a major impact on the areal extent of groundwater level reductions in irrigation scenarios. It played an equally significant role in determining the level of drawdown mitigation achieved in scenarios that included dryland agriculture. Therefore, it would be imperative that any development proposal more precisely define the physical extent of the shale layer and the degree to which faulting affects the shale continuity and how it controls groundwater heads and flow.

The model used to generate these results is not of such scale and complexity as to be suitable for water allocation planning, support of a water licence application, or for the detailed planning of pumping optimisation that may be required by the proponent of a specific development. Therefore, these results should be considered only as a guide to the level of irrigated development that may be possible at Bonaparte Plains. Any proponent would need to undertake further resource assessment work to prove that a proposed development was economically viable and likely to be environmentally acceptable.

## References

- Department of Water (2010), *La Grange groundwater allocation plan*, Water Resources Planning and Allocation Series 25, Department of Water, Perth, Western Australia.
- Harbaugh AW (2005) *MODFLOW-2005, The US Geological Survey modular groundwater model – the groundwater flow process*, Techniques and Methods Book 6, Chapter A16, United States Geological Survey, Reston, Virginia.
- IGS (Innovative Groundwater Solutions) (2019) *Water balance model for the Point Spring Sandstone aquifer at Bonaparte Plains, Kimberley*, final report, IGS, Adelaide.

Krysanova V and Wechsungenet F (2000) *SWIM (Soil and Water Integrated Model): user manual*, PIK Report no. 69, Potsdam Institute for Climate Impact Research, Potsdam, Brandenburg.

Williams J, Bui EN, Gardner EA, Littleboy M and Probert ME (1997) 'Tree clearing and dryland salinity hazard in the Upper Burdekin Catchment of North Queensland', *Australian Journal of Soil Research*, 35(4):785–801.

## Appendix H Monthly average climate data from Bonaparte climate station

Table H1: Monthly average climate recorded at Bonaparte climate station, 2015–2018

Month	Total rainfall	Total potential evapo-transpiration	Total solar radiation	Average daily air temperature (°C)			Daily relative humidity (%)			Daily soil temperature at 5 cm (°C)			Daily wind speed* (ms <sup>-1</sup> )		Daily wind direction* (°)
	(mm)	(mm)	(MJ/m <sup>2</sup> )	mean	min	max	mean	min	max	mean	min	max	mean	max	mean
July	0	172	548	23	16	34	53	24	77	30	23	39	0.48	4.41	231
August	0	192	625	24	17	35	53	23	77	32	24	42	0.50	4.48	247
September	12	211	618	26	19	36	58	25	82	34	27	45	0.58	4.66	262
October	28	232	704	29	22	38	61	27	87	37	30	47	0.65	4.94	248
November	65	153	655	30	25	39	69	33	90	37	32	47	0.64	4.95	269
December	267	118	563	29	26	36	78	46	93	34	30	41	0.52	4.69	239
January	359	109	540	29	26	36	82	51	94	33	30	39	0.41	4.03	245
February	303	112	524	28	25	36	83	51	97	32	29	38	0.33	4.13	240
March	161	121	589	29	26	38	81	44	96	32	29	38	0.29	4.11	234
April	12	121	547	28	23	38	70	31	93	33	29	39	0.31	4.01	236
May	20	117	551	25	20	36	60	27	82	30	26	37	0.39	4.23	228
June	0	115	507	23	17	34	53	24	77	29	24	38	0.48	4.44	220

max = maximum; min = minimum

\* Wind speed and direction data were observed to be affected by wind eddies caused by the forest surrounding the available 50 m × 50 m square area of existing cleared area.

## Appendix I Locations of permanent groundwater discharge

Table I1: Location and elevation of observed areas of permanent groundwater discharge

Name or identifier	Northing (GDA94 Z52)	Easting (GDA94 Z52)	Ground elevation (mAHD)
<b>Named springs</b>			
Attack Spring	8352732	466353	6
Bamboo Spring	8352043	459316	12
Big Boab Spring	8328968	491844	15
Bore Spring lower	8342072	477624	23
Bore Spring upper	8341642	477449	26
Brolga Spring	8352929	453686	6
Calf Spring	8338201	486313	7
Chum Spring	8350671	473472	7
Domett Road	8348999	455525	21
Garimala Creek	8319497	469088	55
Green Swamp	8306651	511713	8
Haley Spring	8354338	465008	6
King Gordon Spring	8351498	456176	12
Long Spring	8352099	463391	6
New Spring	8336839	479055	33
Oaks Creek Spring	8307699	496961	29
Point Spring	8296698	487670	40
Lookout Spring	8303308	483321	42
Snake Spring	8342057	483363	10
Tanmurra Crossing	8335333	457909	21
Tanmurra Pool	8331182	461210	31
The Gorge	8321886	460264	25
Yard Creek	8300715	494062	30
Yow Spring	8349904	469793	14
<b>Unnamed springs</b>			
1	8356278	451830	3
2	8354700	452553	6
3	8352760	454459	3

(continued)

Table I1 (continued): Location and elevation of observed areas of permanent groundwater discharge

Name or identifier	Northing (GDA94 Z52)	Easting (GDA94 Z52)	Ground elevation (mAHD)
4	8350065	455174	11
5	8353434	459760	5
6	8354996	461560	4
7	8354593	462595	4
8	8352810	467329	5
9	8352424	468233	3
10	8351988	469301	6
11	8352136	469737	7
12	8350944	471134	6
13	8342693	481644	9
14	8337779	487208	11
15	8322668	503012	6
16	8324021	504491	4
17	8311475	494586	29
18	8308511	500247	20
19	8306199	500455	24



## Appendix J Groundwater, spring, lake and rainwater physicochemistry

Table J1: Field chemistry data obtained from bores, springs and lakes

Site name	Date	Temp (°C)	pH	EC (mS/m)	DO (%)	Eh	Alk (mg/L)
<b>Bores</b>							
13BP01D	04/08/2017	33.8	6.2	17.4	18.5	252	24
18BP01D	07/09/2018	34.6	7.2	34.4	29.5	35	180
13BP01PB	12/11/2017	32.4	6.3	20.6	53.0	238	71
17BP01I	12/09/2017	32.0	5.6	8.9	34.0	332	31
17BP01S	12/09/2017	32.0	5.4	14.6	35.9	277	40
17BP01PB	12/11/2017	32.1	6.2	8.7	ND	ND	ND
18BP01DD	07/09/2018	32.7	5.9	24.3	5.1	101	111
17BP02I	08/09/2018	32.8	4.8	8.1	55.0	421	29
17BP02S	20/09/2017	32.4	5.8	17.1	26.3	307	36
17BP03I	19/09/2017	32.2	5.8	35.4	77.4	308	35
17BP04I	18/09/2017	31.7	5.9	21.1	43.9	313	52
17BP04S	18/09/2017	31.8	5.8	20.8	40.8	311	59
17BP05I	18/09/2017	32.7	5.5	17.8	31.4	311	34
17BP05S	18/09/2017	34.2	6.0	23.7	38.4	316	54
17BP05PB	20/11/2017	32.7	7.1	15.5	ND	ND	ND
17BP06I	16/11/2017	32.5	5.7	7.3	43.8	280	27
17BP06S	30/09/2017	32.1	4.8	4.7	32.7	351	22
17BP07I	08/11/2017	32.4	6.3	15.8	68.4	298	47
18BP07D	06/09/2018	34.3	6.8	48.7	23.3	25	230
Bonaparte1 water bore 1	30/08/2017	32.3	5.7	9.3	28.0	278	36
Bonaparte2 water bore	28/08/2017	31.1	5.2	6.9	34.3	351	15
Brolga	05/09/2017	32.0	7.1	117.0	4.1	128	165
Calf Spring	20/08/2017	31.0	7.0	24.7	7.6	102	115
CGDH5 Fishermans	16/08/2017	32.4	5.4	10.4	39.8	377	30
CGDH6 New Attack	16/08/2017	31.4	5.2	8.5	44.7	375	18
CGDH7	16/08/2017	32.8	5.2	9.5	1.1	279	30

(continued)

Table J1 (continued): Field chemistry data obtained from bores, springs and lakes

Site name	Date	Temp (°C)	pH	EC (mS/m)	DO (%)	Eh	Alk (mg/L)
CGDH8 Kemp	16/08/2017	32.1	6.0	15.5	16.6	224	51
Hotplate	10/09/2017	31.0	5.3	8.7	33.1	291	28
Lewis	23/08/2017	34.5	7.2	53.3	63.2	296	285
No. 8 Paddys	05/09/2017	33.0	6.9	9.1	16.9	299	375
Oaks Creek	07/09/2017	31.2	6.3	12.5	7.3	198	61
RN029226	13/09/2017	32.1	5.9	17.4	5.1	238	44
Tanmurra	29/08/2017	33.3	7.1	6.6	6.0	56	345
WBN5002	28/08/2017	36.0	7.0	68.2	23.1	114	375
WBN5006	17/08/2017	35.5	6.9	66.5	23.1	318	360
Wilson	20/08/2017	34.1	7.5	42.3	29.2	125	165
<b>Springs</b>							
Bore Spring (lower)	13/07/2017	22.4	7.1	15.1	87.5	255	ND
Bore Spring (upper)	29/08/2017	23.8	6.5	16.3	43.6	283	28
Garimala Creek	09/06/2018	22.8	6.7	6.6	0.4	390	ND
Long Spring	11/09/2017	19.9	6.5	26.5	20.1	304	70
New Spring	30/08/2017	24.4	5.6	11.1	22.5	346	15
Oaks Creek	07/09/2017	22.8	6.3	4.7	40.4	305	21
Tanmurra Creek	11/06/2018	22.8	8.7	46.9	100.5	299.4	ND
Tanmurra pool	11/06/2018	20.2	8.7	70.6	72.0	330	ND
Domett Road	10/06/2018	27.0	7.8	76.0	1.2	207.5	ND
Yow Spring	19/08/2017	24.7	5.6	10.7	25.3	281	21
<b>Lakes</b>							
NW Lake	15/08/2017	26.7	7.0	3.9	91.1	281	15
SE Lake	15/08/2017	26.8	6.9	3.0	80.5	297	21

ND = no data available

Note: Date format is day/month/year

Table J2: General chemistry laboratory data obtained from bores, springs and lakes. All units are mg/L, unless otherwise stated

Site	Date	Acidity	Alk	HCO <sub>3</sub>	Br	Ca	CO <sub>3</sub>	Cl	EC (mS/m)	F	Hard.	OH	Ion bal. (%)	K	Mg	TN	NH <sub>4</sub> N	NO <sub>3</sub> N	NO <sub>2</sub> N	pH	TP	SRP	Na	SO <sub>4</sub> S	TDS sum
Bores																									
13BP01D	04/08/2017	20	58	70	0.06	17.7	<1	17	17.3	<0.05	54	<1	-3.9	2	2.3	0.08	<0.01	0.04	<0.01	6.9	0.016	<0.01	11.4	3.9	90
18BP01D	07/09/2018	7	165	202	0.03	34.8	<1	9	34.9	0.13	130	<1	-5.9	11.4	11	0.04	<0.01	<0.01	<0.01	8.1	0.025	<0.005	10.4	9.6	190
13BP01PB	12/11/2017	21	55	67	0.11	17.5	<1	29	19.9	<0.05	56	<1	-4.3	1.6	2.9	0.13	<0.01	0.07	<0.01	7.1	0.053	0.02	15.9	1.9	100
16BP03I	15/08/2017	18	57	70	0.16	9.2	<1	33	16.9	0.14	41	<1	-4.1	1.1	4.5	0.62	0.05	<0.01	<0.01	6.9	0.07	0.01	26.7	2.6	110
17BP01I	12/09/2017	42	14	17	0.05	4.3	<1	13	8.5	<0.05	17	<1	-6.6	2.2	1.4	0.1	<0.01	0.03	<0.01	6.2	0.025	0.02	7.2	5.4	43
17BP01S	12/09/2017	53	12	15	0.13	3.4	<1	25	14.0	<0.05	15	<1	-4.8	3.4	1.6	0.16	<0.01	0.12	<0.01	6	0.02	0.02	18.1	14.1	75
17BP01PB	12/11/2017	18	15	18	0.05	4.1	<1	14	8.5	<0.05	19	<1	-3.8	2.1	2.1	0.06	<0.01	0.04	<0.01	6.9	0.023	<0.01	8.4	5.9	47
18BP01DD	07/09/2018	27	81	98	0.05	10.9	<1	19	20.6	0.14	39	<1	-5.5	2.4	2.9	0.16	0.06	0.02	0.03	7.6	0.8	0.58	26.7	2.3	110
17BP02I	08/09/2018	26	5	6	0.04	0.5	<1	18	7.7	<0.05	7	<1	-7.1	0.5	1.4	0.13	<0.01	<0.01	0.11	6.5	<0.005	<0.005	10.8	3	39
17BP02S	20/09/2017	41	29	35	0.12	0.6	<1	29	16.3	0.13	29	<1	-1.6	1	6.6	0.13	<0.01	0.11	<0.01	6.4	0.020	0.01	21.7	6.8	85
17BP03I	19/09/2017	32	24	30	0.32	0.5	<1	89	34.4	0.07	40	<1	-4.4	1.8	9.4	0.08	0.01	0.06	<0.01	6.3	<0.010	<0.01	51.4	14.5	180
17BP04I	18/09/2017	41	41	50	0.13	6.9	<1	35	20.5	0.06	46	<1	-2.5	0.9	7	0.11	<0.01	0.1	<0.01	6.5	<0.010	<0.01	23.2	9.6	110
17BP04S	18/09/2017	33	43	53	0.13	7.4	<1	33	19.9	0.07	49	<1	0.7	1	7.4	0.09	<0.01	0.07	<0.01	6.6	<0.010	<0.01	24.1	8.6	110
17BP05I	18/09/2017	30	26	32	0.11	4.6	<1	33	17.0	0.07	32	<1	-2.8	1.2	5	0.05	<0.01	0.04	<0.01	6.4	0.03	<0.01	20.9	7.6	90
17BP05S	18/09/2017	38	41	50	0.18	3.9	<1	39	21.5	0.1	48	<1	-1	0.8	9.2	0.09	<0.01	0.06	<0.01	6.5	0.038	<0.01	26.7	10.2	120
17BP05PB	08/06/2018	22	25	30	0.11	4.4	<1	32	16.8	0.07	31	<1	-3.5	1.1	4.9	0.28	0.03	0.12	<0.01	6.8	0.015	<0.01	19	6.4	85
17BP06I	16/11/2017	22	9	11	0.04	1.5	<1	13	6.4	<0.05	7	<1	-2.7	1.1	0.9	0.07	<0.01	0.02	<0.01	6.4	0.028	0.02	10.6	4.3	38
17BP06S	30/09/2017	29	2	3	0.04	0.3	<1	9	4.0	<0.05	4	<1	-8.7	0.4	0.7	0.12	<0.01	0.1	<0.01	5.3	0.04	<0.01	5.5	1.9	21
17BP07I	08/11/2017	22	35	43	0.08	9.2	<1	25	14.6	0.07	30	<1	-3.4	0.6	1.8	0.09	<0.01	0.06	<0.01	6.8	0.025	0.02	16.9	2.5	77
18BP07D	06/09/2018	15	201	246	<0.02	20.4	<1	12	42.2	0.14	83	<1	-0.2	14.3	7.8	0.65	0.44	<0.01	<0.01	8.1	0.13	<0.005	60.4	12.9	250
Bonaparte1 water bore 1	30/08/2017	12	6	7	<0.02	0.8	<1	4	2.8	<0.05	12	<1	-20	0.2	0.4	0.22	<0.01	0.03	<0.01	6.7	0.047	0.01	2.6	1.1	14

(continued)

Table J2 (continued): General chemistry laboratory data obtained from bores, springs and lakes. All units are mg/L, unless otherwise stated

Site	Date	Acidity	Alk	HCO <sub>3</sub>	Br	Ca	CO <sub>3</sub>	Cl	EC (mS/m)	F	Hard.	OH	Ion bal. (%)	K	Mg	TN	NH <sub>4</sub> N	NO <sub>3</sub> N	NO <sub>2</sub> N	pH	TP	SRP	Na	SO <sub>4</sub> S	TDS sum
Bonaparte2 water bore	28/08/2017	9	3	3	0.03	0.2	<1	7	3.1	<0.05	8	<1	-16	0.1	0.3	0.26	<0.01	0.02	<0.01	6.5	0.01	0.01	4	0.4	15
Brolga	05/09/2017	11	130	159	0.89	86.6	<1	269	112.0	0.13	240	<1	-3.8	6.7	18.6	<0.02	<0.01	<0.01	<0.01	7.7	0.011	0.01	90.1	23.7	570
Calf Spring	20/08/2017	7	94	114	0.03	22.5	<1	8	24.5	0.11	75	<1	0.5	16.1	4.6	0.07	0.04	<0.01	<0.01	7.6	0.064	<0.01	15.1	19	140
CGDH5 Fishermans	16/08/2017	25	14	17	0.08	5.6	<1	20	10.1	<0.05	20	<1	1.1	1	1.4	0.08	<0.01	0.07	<0.01	6.3	0.014	<0.01	12.3	1.6	52
CGDH6 New Attack	16/08/2017	22	6	7	0.06	1.3	<1	17	8.1	<0.05	11	<1	1.6	3.7	1.8	0.07	<0.01	0.06	<0.01	5.9	<0.010	<0.01	10.4	4	43
CGDH7	16/08/2017	24	7	9	0.07	3.9	<1	18	9.3	<0.05	17	<1	2.8	2.4	1.8	<0.02	<0.01	<0.01	<0.01	5.9	0.039	<0.01	11.7	7.9	51
CGDH8 Kemp	16/08/2017	21	41	50	0.04	5.6	<1	12	13.6	0.07	29	<1	-4.8	14.5	3.6	0.04	0.04	<0.01	<0.01	6.8	0.11	<0.01	7.1	8.5	77
Cleanskin	09/08/2017	3	109	133	0.26	12.1	<1	66	47.1	0.15	51	<1	3.4	6.4	5.1	<0.02	<0.01	<0.01	<0.01	7.9	0.028	<0.01	84.3	21	260
Hotplate	10/09/2017	38	4	5	0.06	0.4	<1	19	6.8	<0.05	5	<1	-17	0.9	0.7	0.07	<0.01	0.06	<0.01	6.3	0.016	0.02	8.9	1.7	35
Lewis	23/08/2017	6	105	128	<0.02	23.7	<1	4	19.8	<0.05	190	<1	-6.4	0.2	9.2	<0.02	<0.01	0.01	<0.01	7.7	0.02	0.01	1.3	0.9	100
Matera	11/11/2017	8	132	160	3.8	192	<1	1170	413.0	0.18	800	<1	2.7	19.1	78.5	0.39	0.06	<0.01	<0.01	7.9	0.22	<0.01	540	115	2,200
No. 8 Paddys	05/09/2017	28	218	266	0.08	56.8	<1	18	62.4	0.24	410	<1	-11	1.6	23.6	0.23	<0.01	0.2	0.04	8	<0.01	<0.01	16.9	97.3	350
Oaks Creek	07/09/2017	15	40	48	0.04	3.3	<1	10	12.1	0.1	29	<1	4	14.8	4.9	0.03	<0.01	0.02	<0.01	7	0.041	0.02	9.1	5.1	73
RN029226	13/09/2017	25	28	34	0.14	4.2	<1	27	16.9	0.13	31	<1	-2.7	11.1	5	<0.02	<0.01	<0.01	<0.01	6.8	0.048	0.05	13.6	9.9	89
Tanmurra	29/08/2017	3	8	9	0.06	1.8	<1	20	8.5	<0.05	12	<1	-3.9	0.2	1.7	0.14	<0.01	<0.01	<0.01	7	0.021	0.01	11.3	0.9	42
WBN5002	28/08/2017	6	171	208	<0.02	39.4	<1	7	33.3	0.06	160	<1	-3.7	2.7	14.5	0.05	0.01	<0.01	<0.01	7.9	0.085	<0.01	5.2	3.2	180
WBN5006	17/08/2017	25	353	431	0.07	113	<1	10	63.9	0.1	360	<1	-0.3	0.5	18.6	0.05	<0.01	0.02	<0.01	7.6	<0.010	<0.01	6.4	5.1	370
Wilson	20/08/2017	4	166	201	0.11	23.8	<1	20	41.3	0.11	94	<1	3.1	10.5	8.3	<0.02	<0.01	<0.01	<0.01	7.9	0.053	0.04	56.8	21.5	240

(continued)

Table J2 (continued): General chemistry laboratory data obtained from bores, springs and lakes. All units are mg/L, unless otherwise stated

Site	Date	Acidity	Alk	HCO <sub>3</sub>	Br	Ca	CO <sub>3</sub>	Cl	EC (mS/m)	F	Hard.	OH	Ion bal. (%)	K	Mg	TN	NH <sub>4</sub> N	NO <sub>3</sub> N	NO <sub>2</sub> N	pH	TP	SRP	Na	SO <sub>4</sub> S	TDS sum
<b>Springs</b>																									
Bore Spring lower	13/07/2017	2	14	17	0.1	3.1	<1	36	14.9	<0.05	19	<1	-2.1	0.5	2.7	0.23	<0.01	<0.01	<0.01	7.4	0.024	0.005	21.1	0.7	74
Bore Spring upper	29/08/2017	14	211	257	0.04	29.7	<1	9	40.6	0.08	24	<1	-0.8	6.4	24.4	0.19	0.02	<0.01	<0.01	7.7	<0.010	<0.01	19	2.5	220
Domett Road	10/06/2018	17	341	416	0.18	104	<1	39	72.6	0.2	340	<1	-1.4	0.4	19.9	0.04	<0.01	<0.01	<0.01	8	0.012	<0.01	24.5	9.9	400
Garimala Creek	09/06/2018	2	8	10	<0.02	1.2	<1	14	6.6	<0.05	8	<1	-2.6	0.9	1.3	0.22	0.01	<0.01	<0.01	7.1	0.016	<0.01	9.4	1.4	34
Long Spring	11/09/2017	15	54	65	0.09	13.4	<1	45	26.3	<0.05	62	<1	0.2	0.2	6.8	1	<0.01	<0.01	<0.01	7.1	0.017	0.02	30.1	6.7	140
New Spring	30/08/2017	7	2	3	0.03	0.9	<1	8	3.5	<0.05	15	<1	0	0.7	0.5	0.41	<0.01	<0.01	0.01	6.4	0.017	<0.01	5.1	0.3	18
Oaks Creek	07/09/2017	8	11	14	<0.02	1.4	<1	10	5.5	<0.05	9	<1	-1.1	3.2	1.3	0.17	<0.01	<0.01	0.01	6.7	0.016	0.02	6.8	0.5	31
Tanmurra Creek	11/06/2018	3	212	258	0.09	60	<1	33	46.4	0.12	210	<1	-4.2	1	14.5	0.05	<0.01	<0.01	<0.01	8.1	0.014	<0.01	16.7	8	260
Tanmurra Pool	11/06/2018	3	178	217	0.22	78.5	<1	71	69.2	0.17	270	<1	-0.9	1	17.4	0.17	0.02	0.01	<0.01	8	0.011	<0.01	35	67.6	380
Yow Spring	19/08/2017	8	4	5	0.08	1	<1	27	10.5	<0.05	8	<1	7.1	0.2	1.3	0.12	<0.01	<0.01	<0.01	6.2	0.022	0.01	20.6	1.1	55
<b>Lakes</b>																									
NW Lake	15/08/2017	<2	9	11	<0.02	0.8	<1	4	3.6	<0.05	9	<1	4.8	3	1.6	0.82	0.02	<0.01	<0.01	6.9	0.017	<0.01	3.4	0.7	21
SE Lake	15/08/2017	3	9	10	<0.02	1.2	<1	2	2.9	<0.05	9	<1	7.6	2.8	1.5	0.87	0.02	<0.01	<0.01	6.9	0.026	<0.01	1.7	0.6	16
<b>Rain</b>																									
Rain 2015–2016 wet season	16/05/2016	2	1	2	<0.02	0.4	<1	0.6	0.5	<0.05	2	<1	-19	0.2	0.2		<0.01	<0.01	<0.01	6.2	0.008	<0.005	0.6	0.4	5
Rain 2016–2017 wet season	14/03/2017	<2	6	7	<0.02	1.3	<1	2	2.0	<0.05	5	<1	11	0.2	0.4	0.16	<0.01	0.04	<0.01	7.2	<0.010	<0.01	4.1	0.8	13
Rain 2017–2018 wet season	12/06/2018	<2	<1	<1	<0.02	0.1	<1	<1	0.5	<0.05	<1	<1	-47	<0.1	<0.1	0.2	0.01	0.01	<0.01	6.1	0.013	<0.01	0.3	0.2	3

Note: Date format is day/month/year



Table J3: Metals chemistry laboratory data obtained from groundwater bores, springs, lakes and rainwater. All units are mg/L, unless otherwise stated

Site	Date	Al	Sb	As	Ba	Be	Bi	B	Cd	Cr	Co	Cu	Ga	Fe	La	Pb	Li	Mn	Hg	Mo	Ni	Se	Si	Ag	Tl	Sn	Ti	U	V	Zn	
Bores																															
13BP01D	04/08/2017	0.023	0.0001	0.002	0.067	<0.0001	<0.0001	0.051	<0.0001	<0.0005	0.0027	0.006	<0.0001	1.4	<0.005	0.0053	0.0052	0.23	<0.00005	<0.001	0.005	<0.05	9.9	<0.0001	0.0003	0.0002	<0.0005	<0.0001	0.0003	0.04	
18BP01D	07/09/2018	0.022	<0.0001	<0.001	0.13	<0.0001	<0.0001	0.043	<0.0001	<0.0005	0.0002	0.0007	<0.0001	0.36	<0.005	0.0003	0.0026	0.34	<0.00005	<0.001	<0.001	<0.001	9.6	<0.0001	<0.0001	0.0012	<0.0005	<0.0001	<0.0001	0.01	
13BP01PB	12/11/2017	0.027	<0.0001	<0.001	0.035	<0.0001	<0.0001	0.09	<0.0001	<0.0005	0.0004	0.0095	<0.0001	0.022	<0.005	0.0014	0.0023	0.0042	<0.00005	<0.001	0.001	<0.001	16	<0.0001	<0.0001	0.0011	<0.0005	<0.0001	0.0004	0.09	
16BP03I	15/08/2017	0.44	0.0021	<0.001	0.091	0.0002	<0.0001	0.13	0.0007	0.002	0.0015	0.049	0.0005	0.48	<0.005	0.022	0.0008	0.17	<0.00005	<0.001	0.004	<0.05	28	<0.0001	<0.0001	0.21	0.0034	0.0007	0.012	0.25	
17BP01I	12/09/2017	0.036	<0.0001	<0.001	0.051	<0.0001	<0.0001	0.036	<0.0001	<0.0005	0.0018	0.0028	<0.0001	0.37	<0.005	0.001	0.0021	0.064	<0.00005	<0.001	0.002	<0.05	7.3	<0.0001	<0.0001	0.0004	0.0009	<0.0001	0.0004	0.039	
17BP01S	12/09/2017	0.053	<0.0001	<0.001	0.035	0.0001	<0.0001	0.1	<0.0001	0.0005	0.0008	0.0024	<0.0001	2.6	<0.005	0.001	0.0041	0.019	<0.00005	0.002	0.002	<0.05	15	<0.0001	<0.0001	0.0003	0.001	<0.0001	0.001	0.039	
17BP01PB	12/11/2017	0.03	<0.0001	<0.001	0.031	0.0001	<0.0001	0.053	<0.0001	0.0014	0.0013	0.0013	<0.0001	0.37	<0.005	0.0005	0.0032	0.033	<0.00005	<0.001	0.002	<0.001	8.3	0.0003	<0.0001	0.0009	<0.0005	0.0001	0.0006	0.046	
18BP01DD	07/09/2018	0.037	<0.0001	0.006	0.1	<0.0001	<0.0001	0.045	<0.0001	<0.0005	0.012	0.0007	<0.0001	11	<0.005	0.0004	0.0048	0.2	<0.00005	0.002	0.003	<0.001	11	<0.0001	<0.0001	0.0004	0.0007	0.0001	0.0003	0.026	
17BP02I	08/09/2018	0.032	<0.0001	<0.001	0.015	0.0002	<0.0001	0.054	<0.0001	<0.0005	0.0006	0.011	<0.0001	0.038	<0.005	0.0011	0.0028	0.011	<0.00005	<0.001	0.001	<0.001	9.5	<0.0001	<0.0001	<0.0001	<0.0005	<0.0001	<0.0001	0.024	
17BP02S	20/09/2017	0.027	<0.0001	<0.001	0.018	<0.0001	<0.0001	0.09	<0.0001	<0.0005	0.0002	0.0027	<0.0001	0.35	<0.005	0.0003	0.0007	0.0066	<0.00005	<0.001	<0.001	<0.05	14	<0.0001	<0.0001	0.0006	<0.0005	<0.0001	0.0001	0.021	
17BP03I	19/09/2017	0.031	<0.0001	<0.001	0.053	<0.0001	<0.0001	0.15	<0.0001	<0.0005	0.0005	0.004	<0.0001	0.13	<0.005	0.0004	0.0022	0.014	<0.00005	<0.001	<0.001	<0.05	28	<0.0001	<0.0001	0.0003	<0.0005	<0.0001	0.0003	0.02	
17BP04I	18/09/2017	0.025	<0.0001	<0.001	0.05	<0.0001	<0.0001	0.09	<0.0001	<0.0005	0.0004	0.0005	<0.0001	0.013	<0.005	0.0002	0.0014	0.004	<0.00005	<0.001	<0.001	<0.05	12	<0.0001	<0.0001	0.0003	<0.0005	<0.0001	0.0002	0.016	
17BP04S	18/09/2017	0.033	<0.0001	<0.001	0.051	<0.0001	<0.0001	0.1	<0.0001	<0.0005	0.0003	0.0006	<0.0001	0.018	<0.005	0.0003	0.0014	0.0064	<0.00005	<0.001	<0.001	<0.05	13	<0.0001	<0.0001	0.0006	<0.0005	<0.0001	0.0002	0.03	
17BP05I	18/09/2017	0.027	<0.0001	<0.001	0.05	<0.0001	<0.0001	0.08	<0.0001	<0.0005	0.001	0.0024	<0.0001	0.063	<0.005	0.0004	0.0016	0.013	<0.00005	<0.001	0.001	<0.05	11	<0.0001	<0.0001	0.0002	<0.0005	<0.0001	0.0002	0.024	
17BP05S	18/09/2017	0.035	<0.0001	<0.001	0.049	<0.0001	<0.0001	0.09	<0.0001	0.0012	0.0003	0.0056	<0.0001	0.069	<0.005	0.0007	0.001	0.0069	<0.00005	<0.001	<0.001	<0.05	12	<0.0001	<0.0001	0.0003	<0.0005	<0.0001	0.0007	0.025	
17BP05PB	08/06/2018	0.017	<0.0001	<0.001	0.03	<0.0001	<0.0001	0.07	<0.0001	<0.0005	0.0006	0.0018	<0.0001	0.087	<0.005	0.0003	0.0019	0.0037	<0.00005	<0.001	0.001	<0.001	10	0.0015	<0.0001	0.0018	0.001	0.0001	0.0001	0.035	
17BP06I	16/11/2017	0.15	0.0001	<0.001	0.022	0.0001	<0.0001	0.05	0.0001	0.0011	0.0012	0.0059	<0.0001	0.064	<0.005	0.001	0.003	0.022	<0.00005	<0.001	0.004	<0.001	13	0.0001	<0.0001	0.001	0.0027	0.0001	0.0005	0.041	
17BP06S	30/09/2017	0.057	<0.0001	<0.001	0.021	0.0001	<0.0001	0.06	<0.0001	0.0005	0.0009	0.013	<0.0001	0.041	<0.005	0.0022	0.0014	0.005	<0.00005	<0.001	0.001	<0.05	14	<0.0001	<0.0001	0.0004	0.0005	<0.0001	0.0001	0.025	
17BP07I	08/11/2017	0.062	<0.0001	<0.001	0.052	<0.0001	<0.0001	0.07	0.0001	<0.0005	0.0006	0.0052	<0.0001	0.031	<0.005	0.0005	0.0023	0.026	<0.00005	<0.001	0.002	<0.001	13	<0.0001	<0.0001	0.0009	0.0009	0.0002	0.0007	0.044	
18BP07D	06/09/2018	0.013	<0.0001	<0.001	0.15	<0.0001	<0.0001	0.038	<0.0001	<0.0005	0.0003	0.0013	<0.0001	6.7	<0.005	0.0006	0.0076	0.32	<0.00005	<0.001	0.001	<0.001	10	<0.0001	<0.0001	0.0047	0.0019	<0.0001	0.0002	0.11	
Bonaparte1 water bore 1	30/08/2017	0.043	0.0003	<0.001	0.019	<0.0001	<0.0001	0.036	0.0002	<0.0005	0.0011	0.001	<0.0001	4.3	<0.005	0.0006	0.0007	0.048	<0.00005	<0.001	0.005	<0.05	9.2	<0.0001	<0.0001	0.0004	0.0007	<0.0001	0.0005	3.2	
Bonaparte2 water bore	28/08/2017	0.027	<0.0001	<0.001	0.018	<0.0001	<0.0001	0.039	0.0006	<0.0005	0.0012	0.0077	<0.0001	0.64	<0.005	0.0024	0.0012	0.81	<0.00005	<0.001	0.003	<0.05	9.4	<0.0001	<0.0001	0.0023	<0.0005	<0.0001</			

Table J3 (continued): Metals chemistry laboratory data obtained from groundwater bores, springs, lakes and rainwater. All units are mg/L, unless otherwise stated

Site	Date	Al	Sb	As	Ba	Be	Bi	B	Cd	Cr	Co	Cu	Ga	Fe	La	Pb	Li	Mn	Hg	Mo	Ni	Se	Si	Ag	Tl	Sn	Ti	U	V	Zn
Oaks Creek	07/09/2017	0.026	<0.0001	<0.001	0.13	<0.0001	<0.0001	0.023	<0.0001	<0.0005	0.0013	0.0012	<0.0001	1.1	<0.005	0.001	0.0062	0.21	<0.00005	<0.001	0.002	<0.05	13	<0.0001	<0.0001	0.0004	<0.0005	<0.0001	<0.0001	0.79
RN029226	13/09/2017	0.023	<0.0001	<0.001	0.055	<0.0001	<0.0001	0.027	<0.0001	<0.0005	0.0002	0.0011	<0.0001	0.18	<0.005	0.0005	0.012	0.01	<0.00005	<0.001	<0.001	<0.05	19	<0.0001	<0.0001	0.0003	<0.0005	<0.0001	<0.0001	0.024
Tanmurra	29/08/2017	0.019	<0.0001	<0.001	0.046	<0.0001	<0.0001	0.023	<0.0001	<0.0005	0.0003	0.0007	<0.0001	0.012	<0.005	0.0001	0.0033	0.041	<0.00005	<0.001	<0.001	<0.05	5.8	<0.0001	<0.0001	0.0001	<0.0005	<0.0001	<0.0001	0.12
WBN5002	28/08/2017	0.013	<0.0001	<0.001	0.032	<0.0001	<0.0001	0.011	<0.0001	<0.0005	<0.0001	0.0003	<0.0001	0.047	<0.005	<0.0001	0.0016	0.009	<0.00005	<0.001	<0.001	<0.05	4.4	<0.0001	<0.0001	0.0004	<0.0005	<0.0001	<0.0001	0.072
WBN5006	17/08/2017	0.04	<0.0001	<0.001	0.036	<0.0001	<0.0001	0.039	0.0001	<0.0005	0.0001	0.0009	<0.0001	0.02	<0.005	0.0004	0.0004	0.017	<0.00005	<0.001	<0.001	<0.05	5.6	<0.0001	0.0003	0.0065	<0.0005	0.0008	0.0004	0.13
Wilson	20/08/2017	0.04	<0.0001	<0.001	0.025	<0.0001	<0.0001	0.016	<0.0001	0.0005	<0.0001	0.0012	<0.0001	0.035	<0.005	0.0004	0.021	0.19	<0.00005	<0.001	<0.001	<0.05	22	<0.0001	<0.0001	0.0043	<0.0005	<0.0001	0.0002	0.039
<b>Springs</b>																														
Bore Spring lower	13/07/2017	0.034	<0.0001	<0.001	0.021	<0.0001	<0.0001	0.11	<0.0001	0.0006	0.0001	0.0008	<0.0001	0.064	<0.005	0.0002	0.0019	0.004	<0.0001	<0.001	<0.001	<0.001	14	<0.0001	<0.0001	<0.0001	<0.0005	0.0001	0.0006	0.025
Bore Spring upper	29/08/2017	0.058	<0.0001	<0.001	0.028	<0.0001	<0.0001	0.09	<0.0001	<0.0005	0.0003	0.003	<0.0001	0.068	<0.005	0.0006	0.0019	0.013	<0.00005	<0.001	<0.001	<0.05	15	<0.0001	<0.0001	0.0008	0.0006	<0.0001	0.0004	0.1
Garimala Creek	09/06/2018	0.016	<0.0001	<0.001	0.023	<0.0001	<0.0001	0.085	<0.0001	<0.0005	0.0002	0.0013	<0.0001	0.31	<0.005	0.0002	0.0022	0.0047	<0.00005	<0.001	<0.001	<0.001	11	<0.0001	<0.0001	0.0008	0.0022	<0.0001	0.0004	0.009
Long Spring	11/09/2017	0.035	<0.0001	<0.001	0.031	<0.0001	<0.0001	0.1	<0.0001	<0.0005	0.0001	0.0012	<0.0001	0.086	<0.005	0.0003	0.001	0.0073	<0.00005	<0.001	<0.001	<0.05	14	<0.0001	<0.0001	<0.0001	0.0009	<0.0001	<0.0001	0.023
New Spring	30/08/2017	0.069	<0.0001	<0.001	0.024	0.0007	<0.0001	0.055	<0.0001	<0.0005	0.0014	0.0013	<0.0001	0.16	<0.005	0.0009	0.0039	0.013	<0.00005	<0.001	0.002	<0.05	14	<0.0001	<0.0001	0.0004	0.0015	0.0005	0.0003	0.043
Oaks Creek	07/09/2017	0.045	<0.0001	<0.001	0.018	<0.0001	<0.0001	0.03	<0.0001	<0.0005	0.0001	0.0012	<0.0001	0.25	<0.005	0.0007	0.0017	0.0096	<0.00005	<0.001	<0.001	<0.05	11	<0.0001	<0.0001	0.0002	0.0006	<0.0001	0.0004	0.034
Tanmurra Creek	11/06/2018	0.015	<0.0001	<0.001	0.056	<0.0001	<0.0001	0.09	<0.0001	<0.0005	<0.0001	0.0018	<0.0001	0.019	<0.005	0.0002	0.0024	0.0066	<0.00005	<0.001	<0.001	<0.001	11	<0.0001	<0.0001	0.001	0.0005	0.0013	0.0009	0.009
Tanmurra Pool	11/06/2018	0.028	<0.0001	<0.001	0.064	<0.0001	<0.0001	0.087	<0.0001	<0.0005	<0.0001	0.0032	<0.0001	0.028	<0.005	0.0004	0.0044	0.0041	<0.00005	<0.001	<0.001	<0.001	6.4	<0.0001	<0.0001	0.0018	0.0012	0.0016	0.0012	0.023
Unnamed creek	10/06/2018	0.016	<0.0001	<0.001	0.09	<0.0001	<0.0001	0.086	<0.0001	<0.0005	0.0004	0.0015	<0.0001	0.024	<0.005	0.0002	0.0026	0.07	<0.00005	<0.001	<0.001	<0.001	8	<0.0001	<0.0001	0.0006	0.0008	0.0007	0.0003	0.008
Yow Spring	19/08/2017	0.042	<0.0001	<0.001	0.0092	<0.0001	<0.0001	0.08	<0.0001	<0.0005	0.0001	0.0003	<0.0001	0.11	<0.005	0.0001	0.0034	0.0074	<0.00005	<0.001	<0.001	<0.05	20	<0.0001	<0.0001	0.0008	<0.0005	<0.0001	0.0003	0.012
<b>Lakes</b>																														
NW Lake	15/08/2017	0.032	<0.0001	<0.001	0.004	<0.0001	<0.0001	0.028	<0.0001	0.0005	0.0001	0.001	<0.0001	0.043	<0.005	0.0002	0.0002	0.0023	<0.00005	<0.001	<0.001	<0.05	1.2	<0.0001	<0.0001	<0.0001	<0.0005	<0.0001	0.0002	0.013
SE Lake	15/08/2017	0.028	<0.0001	<0.001	0.0095	<0.0001	<0.0001	0.019	<0.0001	<0.0005	0.0001	0.0006	<0.0001	0.052	<0.005	0.0002	0.0003	0.0022	<0.00005	<0.001	<0.001	<0.05	2.7	<0.0001	<0.0001	0.0001	<0.0005	<0.0001	0.0002	0.022
<b>Rain</b>																														
Rain 2015–2016 wet season	16/05/2016	0.035	<0.0001	<0.001	0.003	<0.0001	<0.0001	0.009	<0.0001	<0.0005	<0.0001	0.011	<0.0001	0.061	<0.005	0.0023	<0.0001	0.005	<0.00005	<0.001	0.001	<0.001	0.2	<0.0001	<0.0001	0.0001	0.0009	<0.0001	<0.0001	0.12
Rain 2016–2017 wet season1	14/03/2017	0.04	0.0002	<0.001	0.0023	<0.0001	<0.0001	0.005	<0.0001	0.0006	<0.0001	0.0049	<0.0001	0.029	<0.005	0.0018	<0.0001	0.0027	<0.00005	<0.001	<0.001	<0.05	1.7	<0.0001	<0.0001	0.0031	0.0011	<0.0001	0.0006	0.04

Note: Date format is day/month/year

Table J4: Laboratory results for isotope analysis

Site	$\delta^2\text{H}$ (‰)	$\delta^{18}\text{O}$ (‰)	$^3\text{H}$ (TU)	$^3\text{H}$ error (TU)	$\delta^{13}\text{C}$ (‰)	$^{14}\text{C}_{\text{DIC}}$ (pMC)	$^{14}\text{C}$ error (pMC)
<b>Bores</b>							
18BP01D	-52.0	-7.69	ND	ND	-13.00	32.37	0.35
13BP01D	-53.4	-7.83	0.021	0.017	-14.43	70.67	0.27
13BP01PB	-50.5	-7.69	0.043	0.014	-14.50	90.89	0.29
17BP01I	-52.7	-7.86	ND	ND	-18.19	79.88	0.27
17BP01S	-48.8	-7.34	0.850	0.028	-19.64	113.20	0.35
18BP01DD	-52.1	-7.7	ND	ND	-17.40	76.52	0.29
18BP02I	-53.4	-7.9	ND	ND	-18.40	97.32	0.32
17BP02S	-55.5	-8.26	0.627	0.025	-19.27	115.16	0.36
17BP03I	-46.9	-7.02	0.450	0.022	-18.83	112.70	0.35
17BP04I	-53.4	-7.94	ND	ND	-17.41	94.29	0.30
17BP04S	-54.7	-7.94	0.250	0.020	-17.43	93.91	0.30
17BP05I	-52.5	-7.78	ND	ND	-18.15	91.90	0.29
17BP05S	-52.3	-7.95	0.724	0.026	-18.21	112.2	0.34
17BP06I	-53.8	-7.93	ND	ND	-17.40	87.92	0.29
17BP06S	-61.8	-9.02	1.001	0.027	-21.50	109.44	0.34
17BP071	-52.6	-8.00	0.198	0.018	-15.10	86.77	0.28
18BP07D	-53.0	-7.91	ND	ND	-11.40	54.98	0.30
Bonaparte1 water bore 1	-54.8	-8.10	0.542	0.021	-19.62	109.74	0.34
Bonaparte2 water bore	-52.7	-7.85	0.227	0.018	-18.36	100.64	0.32
Brolga	-53.7	-8.04	0.004	0.014	-11.60	25.24	0.34
Calf Spring	-53.0	-7.87	0.013	0.014	-15.60	31.38	0.32
CGDH5 Fishermans	-49.6	-7.58	0.004	0.015	-17.60	87.08	0.28
CGDH6 New Attack	-51.7	-7.83	-0.002	0.016	-17.62	82.67	0.29
CGDH7	-52.4	-7.91	0.014	0.015	-17.87	78.17	0.28
CGDH8 Kemp	-53.6	-7.97	0.011	0.014	-16.45	61.47	0.28
Cleanskin	-51.1	-7.48	0.011	0.015	-15.1	4.16	0.42
Hotplate	-53.7	-8.06	-0.004	0.014	-18.57	93.51	0.30
Lewis	-43.2	-6.65	ND	ND	-11.80	94.44	0.29
No. 8 Paddys	-50.1	-7.44	0.584	0.022	-13.30	89.27	0.28
Oaks Creek	-53.0	-7.98	0.006	0.015	-18.01	60.03	0.29

(continued)

Table J4 (continued): Laboratory results for isotope analysis

Site	$\delta^2\text{H}$ (‰)	$\delta^{18}\text{O}$ (‰)	$^3\text{H}$ (TU)	$^3\text{H}$ error (TU)	$\delta^{13}\text{C}$ (‰)	$^{14}\text{C}_{\text{DIC}}$ (pMC)	$^{14}\text{C}$ error (pMC)
RN029226	-47.9	-7.11	-0.007	0.015	-16.43	45.38	0.30
WBN5002	-44.4	-6.84	ND	ND	-8.61	33.65	0.32
Tanmurra	-44.4	-6.84	0.016	0.014	-7.81	19.52	0.37
WBN5006	-54.9	-8.24	ND	ND	-12.99	96.65	0.31
Wilson	-47.8	-7.14	0.001	0.016	-13.33	18.21	0.37
<b>Springs</b>							
Bore Spring upper	-47.6	-7.11	0.043	0.015	-15.87	94.89	0.31
Long Spring	-48.9	-7.30	0.070	0.016	-18.66	89.11	0.29
New Spring	-49.6	-7.48	0.051	0.015	-18.73	93.29	0.30
Oaks Creek Spring	-44.2	-6.38	0.117	0.019	-15.31	96.29	0.32
Yow Spring	-34.3	-4.31	0.154	0.019	-23.18	98.44	0.31
<b>Rain</b>							
Rain 2015–2016 wet season	-11.3	-3.16	1.723	0.040	ND	ND	ND
Rain 2016–2017 wet season1	-43.2	-7.12	1.441	0.037	ND	ND	ND
Rain 2016–2017 wet season2	-31.3	-5.26	1.528	0.038	ND	ND	ND
Rain 2017 dry season	-2.3	-1.41	1.753	0.048	ND	ND	ND
Rain 2017–2018 wet season	-43.6	-6.99	ND	ND	ND	ND	ND

‰ = parts per thousand;  $\delta^{13}\text{C}$  = ratio normalised to  $\delta^{13}\text{C}$  of -25‰;  $^{13}\text{C}$  = carbon-13, the stable carbon isotope;  $^{14}\text{C}$  = carbon-14, or radiocarbon;  $^{14}\text{C}_{\text{DIC}}$  = dissolved inorganic radiocarbon;  $^{18}\text{O}$  = the stable isotope of oxygen;  $^2\text{H}$  = deuterium;  $^3\text{H}$  = tritium; ND = no data available; pMC = per cent modern carbon; TU = tritium unit, equal to  $^3\text{H}/^1\text{H}$  ratio of  $1 \times 10^{-18}$

Table J5: Laboratory results for sulfur hexafluoride (SF<sub>6</sub>) analysis

Site ID	Sampling date	Measured concentration SF <sub>6</sub> (fmol/kg)	Measured concentration SF <sub>6</sub> error (fmol/kg)	Calculated atmospheric partial pressure SF <sub>6</sub> (pptv)	Calculated atmospheric partial pressure SF <sub>6</sub> error (pptv)	SF <sub>6</sub> temperature (°C)	SF <sub>6</sub> temperature error (°C)	SF <sub>6</sub> excess air (mL/kg)	SF <sub>6</sub> excess air error (mL/kg)	SF <sub>6</sub> piston flow recharge year
<b>Bores</b>										
17BP01S	12/09/2017	1.06	0.08	3.68	1.52	16.9	4.9	-0.3	2.6	1997
17BP02S	20/09/2017	0.53	0.08	0.84	0.19	15.5	3.9	7.2	2.0	1981
17BP03I	19/09/2017	1.22	0.09	2.18	0.23	11.1	1.6	4.1	0.8	1990
17BP04S	18/09/2017	0.21	0.08	0.33	0.13	13.8	2.0	6.7	1.0	1974
17BP05S	10/11/2017	0.50	0.05	1.50	0.40	ND	ND	ND	ND	1986
17BP06S	30/09/2017	0.82	0.09	0.94	0.17	24.7	4.6	14.6	1.9	1982
17BP07I	18/11/2017	1.75	0.06	2.77	0.50	8.9	3.4	5.0	2.2	1993
No. 8 Paddys	05/09/2017	1.51	0.09	3.18	0.39	18.9	2.5	4.4	1.1	1994
<b>Springs</b>										
Bore Spring	29/08/2017	3.10	0.10	10.67	1.41	21.8	2.0	0.9	0.8	contaminated or 2018
Long Spring	11/09/2017	2.77	0.10	8.15	0.73	18.9	1.6	1.4	0.5	2015
New Spring	30/08/2017	0.92	0.07	3.37	0.45	21.6	1.8	0.4	0.6	1995
Oaks Creek	07/09/2017	2.85	0.09	9.64	1.11	19.8	1.8	0.6	0.7	2017–2018
Yow Spring	19/08/2017	2.93	0.10	14.88	1.87	26.9	1.8	-0.4	0.6	contaminated

pptv = parts per trillion of volume; ND = no data for this parameter

Notes:

1. Date format is day/month/year
2. fmol/kg: 1 fmol = 10<sup>-15</sup> moles

Table J6: Laboratory results for chlorofluorocarbon (CFC) analyses

Site	Sampling date	CFC-11 (pmol/kg)	CFC-11 error (pmol/kg)	CFC-12 (pmol/kg)	CFC-12 error (pmol/kg)	CFC-113 (pmol/kg)	CFC-113 error (pmol/kg)	Partial pressure CFC-11 (pptv)	Partial pressure CFC-11 error (pptv)	Partial pressure CFC-12 (pptv)	Partial pressure CFC-12 error (pptv)	Partial pressure CFC-113 (pptv)	Partial pressure CFC-113 error (pptv)	Piston flow recharge year: CFC-11	Piston flow recharge year: CFC-12	Piston flow recharge year: CFC-113
<b>Bores</b>																
17BP01S	12/09/2017	1.34	0.02	1.07	0.04	0.12	0.02	92.3	21.3	274	58	28.5	8.3	1975	1979	1984
17BP02S	20/09/2017	0.91	0.02	0.89	0.03	0.07	0.02	57.4	11.2	198	35	14.8	4.7	1971	1975	1979
17BP03I	19/09/2017	1.71	0.02	1.41	0.04	0.15	0.02	85.9	7.2	265	21	24.1	3.4	1974	1979	1982
17BP04S	18/09/2017	0.23	0.03	0.15	0.02	0.01	0.02	13.1	2.4	32	5	1.6	3.3	1963	1961	1968
17BP05S	18/09/2017	1.15	0.03	0.92	0.03	0.08	0.02	75.4	13.7	225	37	17.0	5.3	1973	1977	1980
17BP06S	30/09/2017	1.38	0.02	1.15	0.03	0.11	0.02	127.0	23.0	326	55	30.4	8.6	1977	1983	1984
17BP07I	18/11/2017	0.88	0.05	0.99	0.03	0.10	0.04	39.2	7.7	167	29	14.5	6.4	1969	1974	1979
Brolga	05/09/2017	0.06	0.03	0.08	0.02	0.02	0.02	5.9	2.7	26	6	5.4	5.2	1958	1959	1973
No. 8 Paddys	05/09/2017	1.06	0.02	1.14	0.03	0.14	0.02	78.5	9.0	299	32	33.3	5.9	1973	1981	1985
<b>Springs</b>																
Long Spring	11/09/2017	0.62	0.49	1.46	0.04	0.09	0.04	46.6	37.3	398	29	23.4	9.1	1970	1987	1982
Bore Spring	29/08/2017	1.94	0.02	1.52	0.04	0.18	0.02	167.0	15.0	470	39	54.2	7.0	1982	1990	1989
New Spring	30/08/2017	0.77	0.02	0.61	0.02	0.07	0.02	66.0	5.3	187	14	20.9	5.1	1972	1975	1981
Oaks Creek Spring	07/09/2017	1.96	0.02	1.56	0.04	0.19	0.02	154.0	12.0	445	34	51.6	6.7	1980	1989	1988
Yow Spring	19/08/2017	1.26	0.05	1.17	0.04	0.13	0.02	135.0	11.0	445	31	48.7	7.2	1978	1989	1988

pptv = parts per trillion of volume

Notes:

1. Date format is day/month/year
2. pmol/kg: 1 pmol = 10<sup>-12</sup> moles



## Appendix K Hydrostratigraphic cross-sections

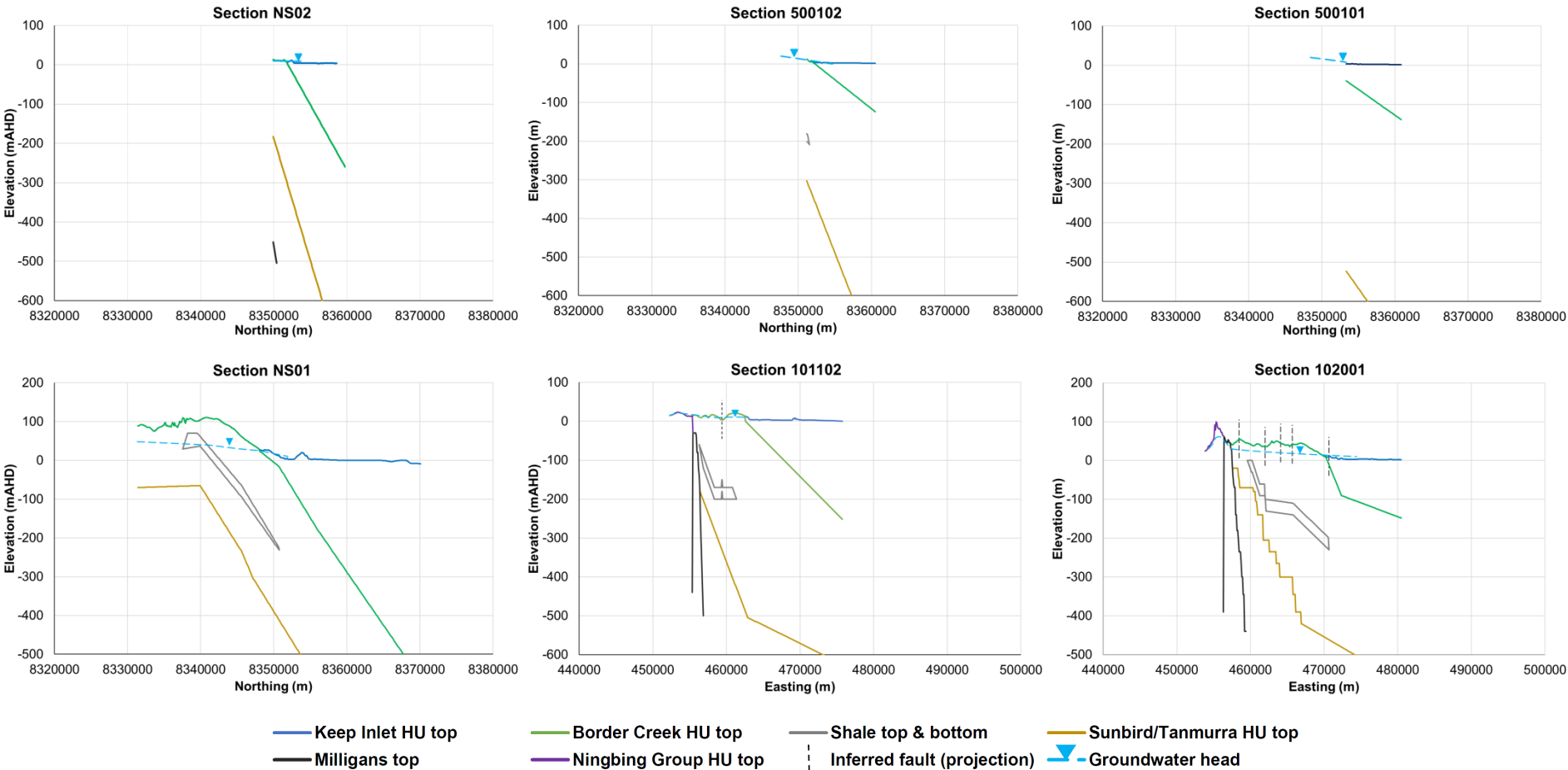


Figure K1: Hydrostratigraphic unit (HU) boundary cross-sections used to develop 3D hydrostratigraphic layers

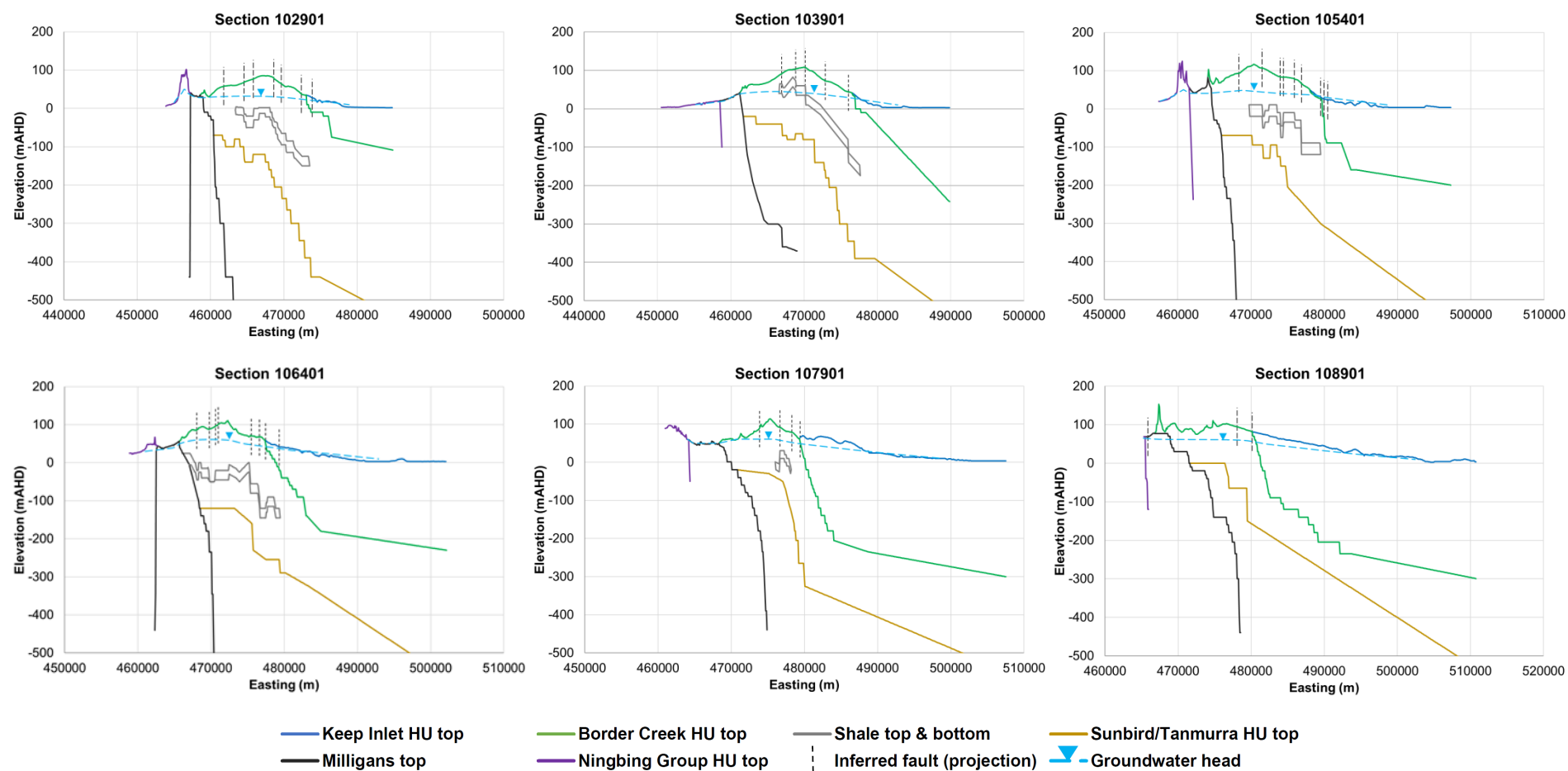


Figure K2: Hydrostratigraphic unit (HU) boundary cross-sections used to develop 3D hydrostratigraphic layer

## Appendix L Pumping cost assumptions

Table L1: Assumptions used for estimating irrigation pumping costs, exclusive of repair and maintenance costs, using diesel power

Parameter	Value
Irrigation system	centre pivot
Pump efficiency (%)	80
Pump derating (%)	75
Diesel use rate (L/kWh)	0.34
Diesel price (\$/L)	1.25–1.75
Flow rate (L/s)	50
Velocity head loss	negligible

Source: C Ham (DPIRD), personal communication, 1 August 2016

Table L2: The effect of total pumping head on pumping cost using the assumptions from Table L1

Total pumping head (m)	Gross diesel power required (kW)	Diesel use (L/h)	Cost of diesel (\$/h)	Pumping cost (\$/ML)
20	13	4.4	5.6–7.8	39–54
30	20	6.7	8.3–11.7	58–81
40	26	8.9	11.1–15.6	77–108
50	33	11.1	13.9–19.4	96–135
60	39	13.3	16.7–23.3	116–162
70	46	15.6	19.4–27.2	135–189
80	52	17.8	22.2–31.1	154–216
90	59	20.0	25.0–35.0	174–243
120	78	26.7	33.3–46.7	231–324

Source: C Ham (DPIRD), personal communication, 1 August 2016

## Shortened forms

Short form	Long form
‰	parts per thousand
<sup>13</sup> C	Carbon-13, the stable carbon isotope
<sup>14</sup> C	Carbon-14, or radiocarbon
<sup>14</sup> C <sub>DIC</sub>	dissolved inorganic radiocarbon
<sup>18</sup> O	the stable isotope of oxygen
<sup>2</sup> H	deuterium
<sup>3</sup> H	tritium
2D, 3D etc.	two-dimensional, three-dimensional
AEM	airborne electromagnetic (survey)
ANSTO	Australian Nuclear Science and Technology Organisation
CFC	chlorofluorocarbon
Cl	chloride
CMB	chlorine mass balance
CRT	constant rate test
DO	dissolved oxygen
DPIRD	Western Australian Department of Primary Industries and Regional Development
DWER	Western Australian Department of Water and Environmental Regulation
EC	specific (electrical) conductivity at 25 °C
FWI	Frank Wise Institute
GDA94 Z52	Geocentric Datum of Australia 1994 Zone 52
GIS	geographical information system
GL	gigalitre
GPS	global positioning system
h	hour
H <sub>2</sub> S	hydrogen sulfide
ha	hectare
HDPE	high-density polyethylene
HU	hydrostratigraphic unit
K	hydraulic conductivity
km; km <sup>2</sup>	kilometre; square kilometre
kW; kWh	kilowatt; kilowatt-hour
L/s	litres per second

(continued)

## Shortened forms (continued)

Short form	Long form
LOR	limit of reporting
m	metre
m/d; m <sup>2</sup> /d	metres per day; square metres per day
m/y	metres per year
mAHD	metres Australian Height Datum
mBGL	metres below ground level
mg/L	milligrams per litre
MJ/m <sup>2</sup>	megajoules per square metre
mL; ML	millilitre; megalitre
mm; mm/d; mm/y	millimetre; millimetres per day; millimetres per year
mRGL	metres relative to ground level
mS/m	millisiemens per metre
mV	millivolt
n	number
NT	Northern Territory
ORP	oxidation–reduction potential
pEt	potential evapotranspiration (FAO Penman-Monteith)
pH	acidity or basicity of a solution
PVC	polyvinyl chloride
SAR	sodium adsorption ratio
s	second
S	storativity
SF <sub>6</sub>	sulfur hexafluoride
SRP	soluble reactive phosphorus
SWI	saltwater interface
SWL	static water level
S <sub>y</sub>	specific yield
T	transmissivity
TDS	total dissolved solids
TN	total nitrogen
TP	total phosphorus
WA	Western Australia
y	year

## References

- Aboriginal Heritage Inquiry System (2021) [Aboriginal Heritage Enquiry System](#), Aboriginal Heritage Inquiry System website, accessed 15 November 2020.
- Allen R, Pereira L, Raes D and Smith M (1998) 'Crop Evapotranspiration: Guidelines for Computing Crop Water Requirements', *FAO Irrigation and Drainage Paper 56*, Food and Agriculture Organisation.
- Allison G and Hughes M (1978), 'Use of environmental chloride and tritium to estimate total recharge to an unconfined aquifer', *Australian Journal of Soil Research*, 16(2):181–95.
- Australia and New Zealand Environment and Conservation Council (ANZECC) and Agriculture and Resource Management Council of Australia and New Zealand (ARMCANZ) (2000) *Australian and New Zealand guidelines for fresh and marine water quality*, available [ANZECC and ARMCANZ \(2000\) guidelines volume 3](#).
- Barnes G and Lee R (1984), *Skull No. 1 Well completion report*, report no. EP-126, Australian Aquitaine Petroleum Pty Ltd.
- Bennett D (2019) 'Investigations of the potential for irrigated agriculture on the Bonaparte Plains: bore completion report', 2nd edition, *Resource management technical report 414*, Department of Primary Industries and Regional Development, Western Australian Government.
- Bennett D and George R (2014) 'Goomig Farmlands development: baseline water quality in the lower Keep River', *Resource management technical report 393*, Department of Agriculture and Food, Western Australia.
- Bennett D and Raper P (unpublished) *Conceptual hydrogeological model: Bonaparte Plains Kulshill Group sandstone aquifers*, Department of Primary Industries and Regional Development, Western Australian Government. Accessed 16 January 2013.
- Bennett D, Donovan L and Palmer D (2015) 'Cockatoo Sands in the Victoria Highway and Carlton Hill areas, East Kimberley: baseline surface water quality', *Resource management technical report 394*, Department of Agriculture and Food Western Australia.
- Bennett D, Simons J, George R and Raper P (2016) 'Cockatoo Sands in the Victoria Highway and Carlton Hill areas, East Kimberley: hydrogeology, aquifer properties and groundwater chemistry', *Resource management technical report 395*, Department of Agriculture and Food Western Australia.
- Bornman J and Doohan K (2016) *Heritage clearance survey report 2016 Department of Agriculture and Food WA (DAFWA) Cockatoo Sands on Bonaparte Plains soil sampling and hydrological survey*, report prepared for the Yawoorroong Miriung Gajerrong Yirrgab Noong Dawang Aboriginal Corporation.
- Bouwer H and Rice R (1976) 'A slug test for determining hydraulic conductivity of unconfined aquifers with completely or partially penetrating wells', *Water Resources Research*, 12(3):423–28.



Butler H and Garnett E (2000) 'Simple procedures for analysis of slug tests in formations of high hydraulic conductivity using spreadsheet and scientific graphics software', *Open-File Rept. 2000-40*, Kansas Geological Survey.

Cane J (1969) *Keep River No. 1 Well Completion Report*, Report no. GS/69/428, Australian Aquitaine Petroleum Pty Ltd.

CSIRO (2009) *Water in the Ord-Bonaparte region of the Timor Sea Drainage Division*, a report to the Australian Government from the CSIRO Northern Australia Sustainable Yields (NASY) project, CSIRO.

DBCA (Department of Biodiversity, Conservation and Attractions) (2020) *Biodiversity survey, mapping, delineation and assessment of selected organic mound springs of the Kimberley region*, DBCA, Western Australian Government.

DBCA (Department of Biodiversity, Conservation and Attractions) (2021) [Threatened ecological communities](#), Threatened ecological communities website, accessed 3 February 2021.

Department of Environment Parks and Water Security (2017) [NR Maps](#), Department of Environment Parks and Water Security website, accessed 4 April 2017.

Department of Mines, Industry Regulation and Safety (2015), [GeoView WA](#), Department of Mines, Industry Regulation and Safety website, accessed 21 April 2015.

Department of Regional Development and Lands (2009) *Ord – East Kimberley development plan*, Western Australian Government.

Department of Water (2010) 'La Grange groundwater allocation plan', *Water Resources Planning and Allocation Series 25*, Department of Water, Western Australian Government.

Department of Water (2013) [Water information reporting system](#), Department of Water website, viewed 21 February 2013.

Garside I (1982), *Ningbing No.1 well completion report*, report no. PG/174/82, Aquitaine Petroleum Pty Ltd.

Geological Survey of Western Australia 2011, *Summary of petroleum prospectivity, Western Australia 2011*, Geological Survey of Western Australia, Perth.

George R, Simons J, Paul B, Raper P, Bennett D and Smith R (2011), 'Weaber Plain hydrogeology: preliminary results', *Resource management technical report 366*, Department of Agriculture and Food, Western Australia, Western Australian Government.

Gorter J, Jones P and Nicoll R (2005) 'A reappraisal of the Carboniferous stratigraphy and the petroleum potential of the south-eastern Bonaparte Basin (Petrel Sub-basin), north-western Australia', *The APPEA Journal*, 45(1):275–296.

Harbaugh A (2005) *MODFLOW-2005, The U.S. Geological Survey modular ground-water model – the ground-water flow process*, Techniques and Methods Book 6, Chapter A16, United States Geological Survey.

IGS (Innovative Groundwater Solutions) (2019) *Water balance model for the Point Spring Sandstone aquifer at Bonaparte Plains, Kimberley*, final report, IGS, Adelaide.

- Langevin C, Thorne D, Dausman A, Sukop M and Guo W (2008) *SEAWAT Version 4 A computer program for simulation of multi-species solute and heat transport*, Techniques and Methods Book 6, Chapter A22, United States Geological Survey.
- LeBlanc M (1964) *Bonaparte No. 1 well completion report*, Alliance Oil Development Australia NL.
- LeBlanc M (1965) *Bonaparte No. 2 well completion report*, Alliance Oil Development Australia NL.
- Meredith K, Hankin S and Priestley S (2018) *Analysis of Bonaparte Plains groundwater chemistry data*, report no. ANSTO/C-1572, Australian Nuclear Science and Technology Organisation.
- MG Corporation (2013) *Bonaparte Plains and Carlton Hill Cockatoo Sand assessment – visit by senior men*, MG Corporation.
- Mory A and Beere G (1988) 'Geology of the onshore Bonaparte and Ord Basins in Western Australia', *Geological Survey of Western Australia bulletin 134*, Department of Mines Western Australia, Western Australian Government.
- NSW Department of Primary Industries (2014), *Farm water quality and treatment*, Primefact 1337, New South Wales Department of Primary Industries, Sydney.
- Nugent O (1989) *Garimala 1 well completion report*, Santos Limited.
- Payne A and Schoknecht N (2011) 'Land Systems of the Kimberley Region, Western Australia', *Technical Bulletin no. 98*, Department of Agriculture and Food Western Australia, Western Australian Government.
- Plumb K and Veevers J (1971) *Cambridge Gulf, WA 1:250,000 Geological series, explanatory notes*, Sheet SD/52-14 International Index, Australia Bureau of Mineral Resources, Geology and Geophysics.
- Pryde J (2017) *Survey of Assemblages of the wetlands with organic mound springs on the tidal mudflats of the Victoria-Bonaparte bioregion Priority 1 ecological community*, Report to the Kimberley Region, Department of Biodiversity, Conservation and Attractions, Western Australian Government.
- Schoknecht N, Payne A and Williams S (2004) *Land unit maps of Carlton Hill and Ivanhoe Stations*, Department of Agriculture, Western Australia.
- SILO (n.d.) [SILO](#), SILO website, accessed 22 February 2019.
- Smolinski H (2019) 'Investigations of the potential for irrigated agriculture on the Bonaparte Plains: land assessment report', *Resource management technical report 410*, Department of Primary Industries and Regional Development, Western Australian Government.
- Smolinski H, Kuswardiyanto K and Laycock J (2010) 'Cockatoo soil survey: assessment of irrigation potential, Kununurra, East Kimberley', *Resource management technical report 264*, Department of Agriculture and Food Western Australia, Western Australian Government.
- Smolinski H, Pathan S, Galloway P, Kuswardiyanto K and Laycock J (2015) 'Cockatoo Sands in the Victoria Highway and Carlton Hill areas, East Kimberley: land capability

assessment for developing irrigated agriculture', *Resource management technical report 391*, Department of Agriculture and Food Western Australia, Western Australian Government.

Speck N, Wright R, Rutherford G, Fitzgerald K, Thomas F, Arnold J, Basinski J, Fitzpatrick E, Lazarides M and Perry R (1964) 'General report on lands of the West Kimberley area, W.A.', *Land Research Series no. 9*, CSIRO, Melbourne.

Stewart G, Perry R, Paterson S, Traves D, Slatyer R, Dunn P, Jones P and Sleeman J (1970) 'Lands of the Ord-Victoria area, Western Australia and Northern Territory', *CSIRO Land Research Series no. 28*, CSIRO.

Symington N, Lawrie K, Brodie R, Tan K, Halas L, Brodie R, Magee J, Bennett D and George R (2016) 'The East Kimberley Ord Bonaparte Project: de-risking investment in agriculture and water infrastructure through airborne and ground geophysical investigations', *Australian Society of Exploration Geophysicists 25th Conference and exhibition*, CSIRO.

Tan K, Harris-Pascal C, Halas L, Symington N, McPherson A, Seiler C, Hostetier S, Clarke J, Smith M, Cathro D, Lawrie K, Christenen N, Brodie R, Halas V and McMillan M (2018) *Ord-Bonaparte Plains groundwater systems investigations*, draft Professional Opinion 2018/xx, Geoscience Australia.

USDA (United States Department of Agriculture) (1954) 'Diagnosis and improvement of saline and alkali soils', *Agriculture handbook no. 60*, USDA.

Van der Kamp G (1976) 'Determining aquifer transmissivity by means of well response tests: the underdamped case', *Water Resources Research*, 12(1):71–77.

Water Quality Australia (2019) [Water quality guidelines](#), Water Quality Australia website, accessed 5 April 2019.

Williams P (1982), *Final report of exploration TR's 8689H–8694H, Cambridge Gulf Western Australia*, Miscellaneous report no. 1104, Utah Development Co.

Zheng C and Wang P (1999) 'MT3DMS: A modular three-dimensional multispecies transport model for simulation of advection, dispersion, and chemical reactions of contaminants in groundwater systems; documentation and user's guide', *American Journal of Roentgenology*, 169:1196–1197.